THE MOMENT CARRYING CAPACITY OF SHORT PILES IN SAND

This thesis is submitted in accordance with the requirements of the University of Liverpool for the degree of Doctor of Philosophy

by

RAMLI BIN NAZIR

Dip.Civ Eng.(UTM), B.Civ.Eng.(Hons.)(UTM)

July 1994

DECLARATION

I declare that no portion of the work referred to in this thesis has been submitted in support of an application for another degree or qualification of this or any other university or institute of learning.

.....

RAMLI BIN NAZIR

Dedicated to

Mak and Abah

My beloved wife Roslina and children

Nurul Farhana, Mohd. Khairil Anwar

Nurul Asyqin, Mohd Khairil Azwar

Nurul Amalina

ABSTRACT

The objective of this research is to investigate various parameters influencing the moment carrying capacity of laterally loaded short pile embedded in sand.

The previous theoretical and experimental research is reviewed. Generally, in the theoretical solutions such as those from Raes(1936), Terzaghi(1943) and Roscoe(1957), an extended analysis of a wall was used to solve the problem concerning the pile. Most of the reports by previous researchers were dedicated to the solution of the flexible pile. Many approaches have been put forward from the simplified classical theories to the finite element method. However, difficulties in choosing the most reliable approach are inevitable since different researchers employ different parameters in solving the problem.

Although work such as those from Shilts et al.(1948), Roscoe(1957), UIC/ORE(1957) and Balfour Beatty(1986, 1988) involved full scale experimental studies, only limited field data are available to verify the analysis of the moment carrying capacity. Time and financial constrain, leads to the scarcity of conducting such field tests.

Solutions based on the conventional tests on small models have rarely taken account of the effect of the low stress level. Overestimation from such conventional tests is very likely since the internal friction angle of the sand increases with a decrease in

stress level reported by Liem(1988). Thus the validity of the solution proposed using the conventional technique based on a small model is questionable.

For the past two decades, the centrifugal modelling technique has been used to replicate prototype behaviour from a small model. In this research full scale prototypes were modelled correctly using this technique. Accordingly, an extensive experimental test program on short rigid pile in both dense and loose sand is carried out using a wide range of centrifugal field force from 7g to 50g, to observe the prototype behaviour of 1m diameter piles at lengths varying from 1m to 5m. Pilot studies performed by Dickin and Wei(1991) on piles up to 3.2m in length showed that the moment carrying capacity is governed by the pile length, diameter and soil unit weight. Pulling height was shown to have a great influence in the range of pulling height ratios e/L<3. Since only limited tests were conducted, no firm conclusion can be made. Tests performed in this project show that the pulling height ratio of greater than 3 still have a significant influence for longer piles.

Broms(1964) and Meyerhof et al.(1981) introduce a shape factor to account for the pile geometry in their solutions. While Meyerhof et al.'s shape factor varies with internal friction and pile length, Broms employs a constant shape factor. Results from single pile tests were compared with the continuous pile tests in this project to obtained an empirical moment shape factor. It was found that the moment shape factor is independent of the pile depth and soil unit weight while pulling height has less significant effect on it.

Apart from the centrifugal test, conventional model tests on various medium size piles of 100mm in diameter were also conducted in reinforced bin to provide a reliable basis for comparison. The centrifugal test results confirm that a scale error exists for conventional tests due to the effect of stress level as explained previously. However the moment shape factor is independent of the scale effect in broad agreement with Leung and Dickin(1984). The moment limit expressed in dimensionless terms as a moment factor decreased with increased pile size. Comparison made from the results based on both technique confirmed that overestimation of predicting values from the conventional tests occurs.

To study the failure mechanism of the test, two dimensional tests were performed in a glass sided box. Dyed layers sand were used to enable the side elevation of failure patterns to be easily studied. Piles in dense sand exhibit behaviour similar to those observed by Broms, while piles in loose sand exhibit local rotational failure patterns as observed by Dembicki et al.(1977).

Finally an empirical relation was developed based on the centrifugal experimental results. This is the compared with existing theoretical and experimental work. Correct triaxial shear strength was applied according to the stress level. Comparison show that for piles embedded in dense sand Broms(1964) and Hansen's(1961) methods show good agreement for the author's result especially with embedment ratio L/D of less than 2. However for L/D>3, Meyerhof et al.'s(1981) value obtained from their solution neglecting interface friction shows good agreement with the centrifugal results for pile in dense sand. Generally Meyerhof et al. give good agreement

with the author's values for piles in both dense and loose packings. No firm conclusion can be made when comparing the author's limiting moment with those of Terzaghi(1943), Roscoe(1957),IRSIA(1950), and UIC/ORE(1957) due to the fact from these methods that no pulling height is involved in assessing the moment capacity. Nevertheless for all range of pulling height encountered in the experimental work, the UIC/ORE gave a close agreement with the author's values.

Generally in most of the tests performed in this project emphasis was placed on the dense packing which is usually encountered in the field. However, it should be borne in mind that this study is not specific to a known field condition and the boundary effects from the container might have affected the results. Nevertheless it is thought that this work is meaningful and identifies the parameters including the geometric factors influencing the pile behaviour.

ACKNOWLEDGEMENTS

I would like to thanks to Dr. E.A Dickin for his invaluable guidance and experience that has been shared with throughout the whole research program. My deepest gratitude and sincere thanks is also due to him for his encouragement in initiating the research program and generous hours of discussion which I received during the course of the present work. His patient and careful evaluation of the manuscript were of invaluable assistance in the preparation of this thesis.

My thanks to Mr. A.J Moorhouse, the Laboratory Manager and the laboratory staff for the preparation and helping to run the centrifugal test throughout the research work in the Geotechnical Centrifugal Laboratory, University of Liverpool.

I am also indebted to Miss Robyna Mitchell for her invaluable guidance and patient in preparing the thesis. Thanks is also due to the Malaysian Government and Universiti Teknologi Malaysia for providing the funding throughout the whole course. Finally I would like to thanks to my wife and children for their continuous encouragement through out the course of this research.

Abstract iv

Acknowledgements viii

Tables of content ix

Notation xvii

CHAPTER ONE

1.0 INTRODUCTION

1.1 Introduction 1

1.2 Scope of research project 3

1.3 Thesis outline 7

CHAPTER TWO

2.0 REVIEW OF PREVIOUS THEORETICAL WORK

2.1 Introduction 11

2.2 Early theoretical solution 12

2.3 Application on the theory of subgrade reaction to laterally loaded pile 15

2.4 Early limit equilibrium analysis 18

2.5 Developments in theoretical solutions 22

2.6 Definition of Shape Factor 30

2.7 Dimensional analysis 32

2.7.1 Buckingham pi-theorem 32

2.8 Summary of previous theoretical analyses 35

CHAPTER THREE

3.0 REVIEW OF PREVIOUS EXPERIMENTAL WORK

3.1 Introduction 38

3.2 Early investigation 38

3.2.1 Shilts et al. field tests 38

3.2.2 The IRSIA tests 41

3.2.3 UIC/ORE field tests 43

3.2.4 McCorkle's method 48

3.3 Recent experimental work 51

3.4 Limitation of the experimental work 54

3.5 Summary of the experimental work 57

CHAPTER FOUR

4.0 COMPARISON OF PREVIOUS THEORETICAL AND EXPERIMENTAL WORK

4.1 Introduction 59

4.2 Moment limit at ground level based on theoretical solutions 60

4.2.1 Terzaghi's method 61

4.2.2 Roscoe's method 62

4.2.3 Hansen's method 62

4.2.4 Broms' method 63

4.2.5 Meyerhof et al.'s method 63

4.2.6 Selection of earth pressure coefficients in analysis 65

4.3 Moment at ground level based on empirical solutions 68

4.3.1 Shilts' et al. studies 68

4.3.2 The IRSIA tests 69

4.3.3 The UIC/ORE formulae 69

4.3.4 McCorkle's formulae 70

4.3.5 Balfour Beatty's formula 70

4.3.6 Dickin and Wei's formula 71

4.4 Limitations of the comparisons 72

4.5 Interpretation of previous theories and experimental work 79

4.5.1 Variation of moment at ground level with embedment ratio 80

4.5.2 Moment value from theories not considering the pulling height effect 82

4.5.3 Variation of moment at ground level with pulling height ratio 83

4.6 A summary of design approaches 85

4.7 General discussion 87

CHAPTER FIVE

5.0 PROPERTIES OF MATERIALS

5.1 Introduction 90

5.2 Properties of Erith sand 90

5.3 Pile materials 93

5.4 Pile rigidity 95

CHAPTER SIX

6.0 CENTRIFUGAL MODEL PILE TESTS

6.1 Introduction 98

6.2 The centrifuge modelling technique 98

6.2.1 Introduction 98

6.2.2 Principle of centrifugal modelling law 99

6.2.3 Applications to centrifugal modelling 102

6.3 Scaling relationships 104

6.3.1 Similarity requirements and percentage error between model and prototype 108

6.3.2 Relationship between rotational speed and scaling factor 116

6.4 Description of centrifugal machine at the University of Liverpool 118

6.5 Centrifugal test package arrangement 120

6.6 Experimental procedures 123

6.6.1 Experimental test program 126

6.6.2 Summary of experimental program 129

6.7 Pile installation in centrifugal experiment 134

CHAPTER SEVEN

7.0 CONVENTIONAL MODEL PILE TEST

7.1 Introduction 136

7.2 Conventional test program 137

7.2.1 Conventional test package arrangement 137

7.2.2 Conventional testing procedure in the reinforced bin 139

7.2.3 Conventional test procedure in centrifugal bucket 142

7.3 Experimental test program 142

7.3.1 Two dimensional failure mechanism tests 144

7.4 Summary of test program 145

7.5 Determinations of test parameters 147

7.6 Moment shape factor 150

CHAPTER EIGHT

8.0 INTERPRETATION OF EXPERIMENTAL RESULTS

8.1 Introduction 151

8.2 Interpretation of centrifugal results 152

8.2.1 Modelling of models 153

8.2.2 Centrifugal test on single short piles 155

8.2.2.1 The effect of pulling height 155

8.2.2.2 The effect of embedment ratio 162

8.2.2.3 The effect of soil density 163

8.2.2.4 The effect of ground surface profile 164

8.2.2.5 The effect of pile diameter 167

8.2.2.6 Pile rotation 170

8.2.3 Centrifugal tests on continuous pile 172

8.2.3.1 Results for continuous piles 175

8.3 Comparison between single and continuous pile 176

8.3.1 Moment shape factor 177

8.4 Results on conventional tests 180

8.4.1 General discussion of conventional test results 181

8.4.2 Piles in flat terrain 181

8.4.3 Piles close to sloping terrain 184

8.4.4 Conventional test in the centrifuge bucket 186

8.5 Comparison between conventional and centrifugal tests 188

8.6 Failure mechanism studies 191

8.6.1 Failure mechanism in loose packing 192

8.6.2 Failure mechanism in dense packing 193

8.6.3 Conclusion 195

8.7 General conclusion 196

CHAPTER NINE

9.0 COMPARISON BETWEEN EXPERIMENTAL WORK AND EXISTING THEORIES

9.1 Introduction 199

9.2 Assumptions made in comparisons with existing theories 200

9.3 Empirical interpretation of experimental results 201

9.3.1 Empirical relationship for continuous pile 202

9.3.2 Empirical relationship for single pile based on continuous pile analysis 204

9.3.3 Empirical expression for a single pile based on Series Two tests 207

9.4 Comparison between observed moment shape factors and the existing theoretical shape factors 209

9.5 Comparison between observed moment factor and predictions from existing theories 209

9.5.1 Moment factor against pulling height ratio 210

9.5.2 Prototype moment with embedment ratio 215

9.6 Pile in close proximity to a slope 216

9.7 Conclusion 217

CHAPTER TEN

10.0 GENERAL CONCLUSION

10.1 Introduction 220

10.2 General conclusion on the research project 220

10.3 Suggestion for future work 224

REFERENCES 225

APPENDIX A

APPENDIX B

APPENDIX C

APPENDIX D

APPENDIX E

NOTATION

a/L : Point of rotation distance ratio

a : Distance of point of rotation below ground surface

A : Shilts et al. average area of soil pressure

A_m : Local acceleration of model

A_o : Terzaghi's coefficient depending on soil density

A_r : Radial acceleration

B_m : Model width of the pile perpendicular to the pulling force

B_p : Prototype width of the pile perpendicular to the pulling force

c : Cohesion of the soil

C_u : Coefficient of uniformity

c_v : Coefficient of consolidation

d/L : Slope distance ratio

d : Distance of the pile from slope crest

D : Diameter of footing(Ovesen) or pile diameter

D/d_g : Ratio of pile diameter with average sand grain size

D_{10} : Effective grain size

d_g : Average grain size

D_m : Model diameter of pile

D_p : Prototype diameter of pile

e : Void ratio

e/L : Pulling height ratio

E : Modulus of elasticity

E_g : Coefficient of elasticity of grain materials

E_h : Horizontal soil modulus of the soil at pile tip

e_m : Model pulling height

e_p : Prototype pulling height

E_{pz} : Hansen's net earth pressure

E_s : Modulus elasticity of the sand

F_m : Model pulling force

F_n : Normal force at the base of the pier

F_o : Horizontal lateral force at ground level

F_p : Prototype pulling force

F_r : Number of revolution per unit time

F_t : Horizontal resisting force at the base of the pier

g : Earth gravity field

G_s : Specific gravity

h : Depth of soil

H_m : Height of model

H_p : Height of prototype

I : Second moment area

I_d : Density index

K : UIC/ORE coefficient accounting for soil geometry

K_a : Coefficient of Rankine active pressure

K_{ar} : Coefficient of active pressure for rough surface

K_b : Net earth pressure coefficient

K_{br} : Net earth pressure coefficient for rough surfaces

K_c : Hansen's net coefficient earth pressure for cohesive soil

k_h : Horizontal coefficient of subgrade reaction

K_o : Coefficient of erath pressure at rest

K_p : Coefficient of Rankine passive pressure

K_{pm} : Model coefficient of Rankine passive pressure

K_{pp} : Prototype coefficient of Rankine passive pressure

K_{pr} : Coefficient of passive pressure for rough surface

K_q : Hansen's net coefficient of earth pressure for cohesionless soil

K_{rs} : Relative stiffness

k_s : Coefficient of subgrade reaction

K_s : Slope factor

K'' : Balfour Beatty's soil pressure constant

K'_a : Coefficient of active pressure at the back of the pile

K'_p : Coefficient of passive pressure at the back of the pile

L/D : Embedment length

L_m : Model pile length

L_p : Prototype pile length

L' : Depth of an unconsolidated layer

M' : Moment factor

M_B : IRSIA moment limit at ground level

M'c : Moment factor for continuous pile

M's : Moment factor for single pile

M_d : Driving moment

M_{ecc} : Moment from a vertical or eccentric load in McCorkle's analysis

M_m : Model moment at ground level

M_p : Prototype moment at ground level

M_{pm} : Permissible/Allowable moment at ground level

M_{pp} : Permissible moment at two third of the pile depth(Balfour Beatty)

M_r : Resisting moment

M'_{pc} : Prototype moment factor for continuous pile

M'_{ps} : Prototype moment factor for single pile

n : Porosity

N : Centrifugal scaling factor

n_h : Constant coefficient of subgrade reaction

n_{max} : Maximum porosity

n_{min} : Minimum porosity

N_l : Linear scaling

N_q : Bearing capacity factor

n_r : Relative porosity

p : Soil pressure

p/A : Shilts et al.'s average pressure

P : Soil resistance

P_1 : Lateral soil resistance

P_2 : Lateral soil resistance

P_a : Rankine active pressure

P_p : Rankine passive pressure

P_u : Ultimate soil resistance

p_z : Soil pressure at depth z

p' : Soil pressure at the back of the pile

q_b , q : Overburden pressure , Total overburden pressure

q_s : Surface load

q_{sp} : Prototype surface load

$\bar{r}$: Optimum scaling radius

r : Radius of a circle

R : Broms' concentrated negative pressure

R_a : Radius of rotating arm

r_b : Moment reduction factor

s : Distance travel along circular path

S_f : Meyerhof's shape factor

S_{fm} : Moment shape factor

S_{fu} : Meyerhof's ultimate shape factor

t : Time travel

t_m : Model time

t_p : Prototype time

T_v : Consolidation time factor

V : Vertical external load

V_r : Radial velocity

V_s : Volume of sand

w : Unit resistance of soil

W : Mass of the pile

w_z : Unit resistance of soil at depth z

x : Eccentric distance between normal force and the centre line of the pier

z : Any distance below ground level

$(EI)_p$: Rigidity of pile section

$(Mr)_p$: Pure overturning moment

$(1\text{-}E_p)$: IRSIA correction factor

α : Inclination angle at the back of the wall

γ : Soil unit weight

$\overline{\gamma}$: Artificial gravity induced by centrifugal forces

γ_m : Model unit weight

γ_p : Prototype unit weight

δ : Interface sand-pile friction angle

Δ_m : Model lateral displacement at ground level

Δ_p : Prototype lateral displacement at ground level

Δ_z : Displacement at depth z

δ' : Interface sand-pile friction angle at the base of pile

ε : Maximum error developed in centrifugal machine

θ : Angle of pile inclination/about centre of rotation

ρ : Soil density

σ_c : Cohesive force between sand grain

σ_g : Crushing strength of grain materials

σ_{vm} : Model vertical stress

σ_{vp} : Prototype vertical stress

τ_f : Shearing stress

ϕ : Soil friction angle

ψ : Slope angle

ω : Angular velocity

Ω : Unit resistivity (Ohms)

RNMM : Modelling of models test

RND : Pile test in dense sand with flat terrain

RNL : Pile test in loose sand with flat terrain

RNSA : Pile test with pulling arm pulls away from the slope

RNST : Pile test with pulling arm pulls towards the slope

RND*G1: Pile test at unit gravity

RNMP : Modelling of prototypes test

RNDCT : Conventional test for pile in dense sand

RNLCT : Conventional test for pile in loose sand

RNDSA : Conventional test for pile pulls away from the slope

RNDST : Conventional test for pile pulls towards the slope

CHAPTER ONE

INTRODUCTION

1.1 INTRODUCTION

Generally piles are used to take advantage of the strong bearing capacity that exists deep below the ground surface or in situations that prohibit the use of shallow foundations. Piles are categorised according to the manner in which loads act upon them. In practice they can be classified into 2 categories:-

a) By the materials from which the pile has been fabricated, such as steel, wood and concrete.

b) By the installation method of the pile itself, which presents a number of examples, such as micro piles, end bearing piles, piers and friction piles.

The commonest function of a pile is to support vertical loads. However, at times, horizontal loads can be more predominant. Structures such as electrification gantries, lamp posts, oil platforms and advertisement posts are subjected to horizontal loads which will induce an overturning moment to their foundations. Since these foundations rely on the lateral support from the neighbouring soil, they have in the past been

termed side-bearing foundations. They are extremely rigid, uniformly circular or square in cross section. The primary resultant external force usually acts well above the ground line, thereby imposing a high external moment at the juncture between foundation and superstructure.

Different approaches have been employed to investigate the moment limit of piles embedded in sand. In the past, the design of laterally loaded piles has been based upon full scale tests or on small models tested in the laboratory at unit gravity. Analyses were simply based on linear relationships and constitutive laws. However in time prediction techniques have been developed and improved. With the development of the computer technology, analyses using the finite element method have been recently used. Many differing solutions have been proposed due to the conflicting ideas and assumptions which have been advanced. As a result different values of limiting moment have been obtained.

A carefully controlled full scale test would probably be the most reliable way to collect useful information for predicting the limiting moment of a laterally loaded pile. Often it is not viable to conduct such a full scale test and, moreover, only a limited number of tests can be done, due to economical and time constraints. However, a test on a small model in the laboratory would involve scaling errors since stress level is an important factor determining the behaviour of the buried structures. Over the past two decades, centrifuge modelling has become one of the most successful geotechnical tools in obtaining solutions for stress-dependent problems. The technique allows a small

model to be subjected to the high stress levels experienced by the prototype under investigation, thereby eliminating the scaling problem. It is not only a low cost technique in comparison with full scale testing, but also provides a greater control over the soil conditions, pile type and loading conditions.

1.2 SCOPE OF RESEARCH PROJECT

In previous literature, the behaviour of short piled or pier foundations embedded in sand and subjected to lateral load was either investigated theoretically, empirically or semi-empirically. Experimental data were obtained from field tests or laboratory tests on a small models. In this project, the behaviour of the laterally loaded pile embedded in sand was investigated. An external load was applied laterally at a distance well above the top of a pile. Attention is given only to short rigid piles with embedment ratio, L/D and pulling height ratio, e/L between 1 and 5.

Although a number of field tests and a small model tests were carried out previously, few attempts were made to compare the results obtained from both types of test. However in studies such as those performed by Shilts et al.(1948) and UIC/ORE(1957), small models were used to obtain the position of the rotation point which then predetermined its position in a full scale test observations. However, Neely et al.(1973), while performing comparison studies on model anchor plates at unit gravity with the full scale tests reported by Smith(1962), observed the existence of a scale error

between the model and the prototype. They attributed this to the variation of the internal friction angle of the soil with the stress level. Values of the friction angle were higher in front of a small model anchor than that at full scale. This was confirmed in the case of Erith sand used in this research by extensive work, accomplished by Liem(1988), showing that the angle of friction reduces with an increase in the stress level. Franke and Muth(1985), reported a study of model scale effects in unit gravity tests on laterally loaded pile and concluded that the scale effects are due to the influence of the elasticity and the crushing strength of the sand grain. However Ovesen (1979), demonstrated that the effect of the sand grain can be neglected if the ratio between the diameter of the foundation and average grain size is greater than 30. Assuming that these findings can also be applied to the case of the geometrically similar short pile, the scale error can also be presumed to exist.

In the past two decades, the centrifugal modelling technique has been widely employed in solving a variety of engineering problems. Problems in soil mechanics such as slope stability and pile foundations are the most popular field where the centrifuge modelling technique has been successfully applied. Generally by using this technique, an artificial gravity is applied to a small model from circular motion at high velocity. At the right speed a model can be made to experience prototype stress levels thus eliminating the scaling errors. Therefore models tested can be considered to behave in similar fashion to prototype. Since, with the exception of the limited pilot study previously reported by Dickin and Wei(1991), relatively little research, in centrifugal modelling of short piles embedded in sand appears to have been carried out to date, it

is of interest to further examine the applicability of the centrifugal modelling technique to this problem in parametric studies. Accordingly, an extensive experimental programme is carried out so that the behaviour of a prototype pile can be simulated under a wide range of centrifugal force fields.

As a basis for comparison, conventional tests were performed in a large reinforced metal bin. Attention was given to the cylindrical piles embedded in different sand unit weights and ground profile. Dimensionless parameters such as the embedment ratio, L/D of the pile, the pulling height ratio, e/L and the rate of loading were made as close as possible to the field situation. The effect on moment limit, due to ground surface profile, was also observed in part of this research work. Piles embedded at various distances from the crest of a slope were pulled either towards or away from it. The effect of the slope on the moment limit was investigated.

Previous theoretical analyses investigate the lateral resistance of a single pile from an extended analysis of a rigid wall, which is essentially a two dimensional problem. This is not the case for a single pile where three dimensional effects are present. Broms(1964) and Meyerhof et al.(1981), attempted to use a 'shape factor' to overcome this limitation. The suggested shape factor was used to convert the result from the analysis of a laterally loaded wall to obtain the limiting value for a single pile. The same approach was adopted in this project where tests on a 'continuous pile wall' were performed. To reduce side friction, the pile was embedded between glass side walls

to which a silicon polish was applied. Test series were conducted conventionally and in the centrifuge. Comparisons were made between data obtained from single and continuous pile studies and a moment shape factor was obtained.

To understand the failure mechanism in the laterally loaded short pile problem, two dimensional model tests were performed in a long narrow glass-sided box. Tests were performed for different sand packings.

Comparisons between the experimental work and existing theoretical and empirical solutions were made. In order for the comparison to be sensible, appropriate values of the soil parameters were used based on the test stress level. Internal friction angles obtained from the triaxial compression test were used in the three dimensional problem single pile.

Generally the research addresses the following questions:-

a) What are the parameters which influence the moment limit?

b) How far do these factors affect the limit and the reliability of the existing formulae in predicting the moment limit?

c) How far do the results using existing formulae depart from the result obtained from the experimental work?

d) Which parameters influenced the moment shape factor?

e) Was the use of the centrifugal modelling successful in achieving the model-prototype simulation of short piles in sand.

It should be emphasised that the tests reported in this study were not specific to a known field subgrade. Nevertheless, it is thought that the research is meaningful and identifies some geometric factors influencing the limiting moment carrying capacity of piles in sand.

1.3 THESIS OUTLINE

Theories from previous researchers are reviewed in Chapter Two with methods of analysis being discussed. Analysis, beginning from Raes(1936) until the most recent analysis available are reviewed. The subgrade reaction approach, based on Terzaghi's evaluation(1955), has been widely employed by most researchers to predict the lateral movement of the pile and basically employs elastic theory in solving the foundation problem. The requirement for a shape factor based on Meyerhof et al.'s(1981) analysis will be discussed. To relate the model to the prototype, dimensional analysis is usually employed. Buckingham's pi-theorem is employed to determine the characteristic of a

physical system by an analytical means where an equation form must be satisfied by the system. Finally a summary of all the theories relating to the short pile problem is presented.

Field tests and laboratory model tests are normally used to study the behaviour in a particular problem. Field studies reported by Shilts et al.(1948) and UIC/ORE(1957), small model studies conducted by the IRSIA(1950), together with the work of McCorkle(1969) and Balfour Beatty(1986, 1988), are discussed in Chapter Three. The parameters from the field and laboratory tests are compared. Development in modelling techniques are also discussed. In the past although results from tests on laboratory models were used to predict the behaviour of the prototype laterally loaded pile, the scale effect was often ignored. Dickin and Wei(1991) performed a pilot study of laterally loaded short piles embedded in sand under the influence of a high stress level in the centrifuge. Using this technique, problems associated with the stress level can be overcome thus eliminating the scaling effect.

In Chapter Four comparisons between the existing theoretical and empirical solutions are made. Solutions obtained from previous researchers discussed in Chapter Two and Three are compared. Although the final criterion in determining the limiting condition differs with each researcher, the moment at ground level is adopted as a limiting value in this research.

Chapter Five discusses the materials used in the tests. Dry Erith sand, generally having a grain sizes between 0.13 and 0.25mm, was used as the embedment medium. Two sand packings were employed i.e dense and loose packing. The same type of sand and packing and pile surface were also used in the conventional tests. Mild steel was used as the pile material. In the centrifugal tests cylindrical piles with diameters ranging from 20mm to 50mm and lengths between 20mm and 100mm and 126mm wide, 20mm thick continuous pile walls ranging from 40mm to 100mm in length, were employed while medium size models with 100mm in diameter and length ranging from 200mm to 500mm were used in conventional test.

Chapter Six addresses the methodology of the centrifuge modelling technique. Theory of centrifuge modelling is discussed in the first part. This chapter also describes the preparation of the centrifuge models and outlines the test series. The selection of appropriate parameters and variables are also mentioned in this chapter.

For comparison purposes, the conventionals tests were performed. In Chapter Seven, similar to Chapter Six, the methodology of conventional test is discussed. Tests on a 100mm diameter pile was performed in a reinforced bin. Two dimensional model tests was also performed to study the failure mechanism in the sand around the short pile. Failure patterns are highlighted using layers of dyed sand.

Chapter Eight contains the interpretation of the experimental results. In the first part, results obtained from centrifuge modelling are presented and discussed. The variation of both model and prototype moment with the embedment ratio L/D and pulling height ratio e/L are considered and a dimensionless moment factor is introduced. The maximum moments, obtained from the two dimensional test using the 'continuous pile wall' are compared with moments obtained from the tests on single piles and a moment shape factor is introduced. Comparisons are also made between the conventional and centrifugal tests.

Chapter Nine includes the derivation of the empirical relationship obtained from the interpretation of the results in Chapter Eight. Empirical relationships for the moment limit at ground level and the moment shape factor are proposed. These moment relationships are compared with existing theoretical and empirical formulae. The proposed shape factor is compared with previous work including that of Meyerhof.

Chapter Ten describes the main the conclusions of the project and suggestions for future work are also outlined.

CHAPTER 2

REVIEW OF PREVIOUS THEORETICAL WORK

2.1 INTRODUCTION

In this chapter, theoretical work and its development in the analysis of a single short pile embedded in sand which experiences lateral force will be discussed.

Most of the literature found (Kubo(1965), Davisson and Sally(1970), Morgenstern and Einsenstein(1970), Reese et al.(1974), Reese and Desai(1977), Georgiadis and Butterfield(1982), Glesser(1984), Abendroth and Greimann(1990)) to name a few, are concerned only with the general solution specifically for a flexible pile experiencing lateral load. However works such as Raes(1936), Shilts et.al(1948), IRSIA(1950), UIC/ORE(1957),Roscoe(1957), Czerniak(1959), Matlock and Reese(1960), Hansen(1961), Broms(1964), Meyerhof(1979), Meyerhof et al.(1981,1983,1988) deal with the ultimate lateral capacity of a rigid pile embedded in sand. Broms(1964a,1964b) and Meyerhof(1981,1983) reported solutions for both flexible and rigid piles embedded in sand and clay while Hansen(1961) introduced a general procedure for determining the ultimate lateral load of a pile. Generally most of the analyses employed either an equilibrium approach (Raes(1936), Czerniak(1957), Hansen(1961), Broms(1964)) or a numerical approach (Palmer and Thompson(1948), Matlock and Reese(1960)). Analysis

using subgrade reaction theory (Terzaghi(1955)) combined with the classical Rankine lateral earth pressure theory is commonly employed by researchers to determine the deflection and the limiting soil resistance.

2.2 EARLY THEORETICAL SOLUTION

In determining the lateral load capacity of piles, numerous methods have been advanced. However two basic requirements need to be satisfied, provision of an adequate safety factor against failure and an acceptable displacement under working load (Poulos and Davis(1980)).

An early report, concerned with laterally loaded piles, was published by Raes(1936) and is based on his static equilibrium solution for the lateral sliding of a small retaining wall founded on vertical concrete piles. He discovered that the method of analysis used was also applicable to a pole embedded in the soil. It was assumed that only soil resistance played an important role in determining the ultimate resistance of the pole while the shape of the pole and its deflection were of lesser significance. Raes assumed this by stating that as movement occurs and the angle of friction is reached, no further increase in resistance occurs.

Palmer and Thompson(1948) proposed a numerical solution which is applicable to any embedment length and type of soil. A differential equation approach was used to solve the problem in computing the lateral earth pressure, the deflection, the shear and the moment at all points throughout the embedment length of both single piles and pile groups.

Czerniak(1957) established a mathematical expression to relate the pile geometry to the failure load. In his assumption, if the pile is absolutely rigid with embedment length ratio L/D<10, it would pivot about a point somewhere along its embedded length. Referring to Figure 2.1(a) the pile subjected to a horizontal load at height 'e' from the ground level would rotate around a pivot point some distance below the ground surface as shown in Figure 2.1(b). The soil modulus is presumed to increase linearly with the depth as shown in Figure 2.1(c). Since the pressure is the product of soil modulus and deflection, at depth z the unit resistance $w_z = wz/L$ and the deflection at ground level, $\Delta = \Delta_z(a-z)/a$ gives soil reaction as;

$$p_z = \frac{wz}{L}.\frac{\Delta_z}{a}(a - z) \tag{2.1}$$

To satisfy horizontal equilibrium

$$F = \int_0^L p_z \, dz \tag{2.2}$$

Substituting equation (2.1) into (2.2) gives;

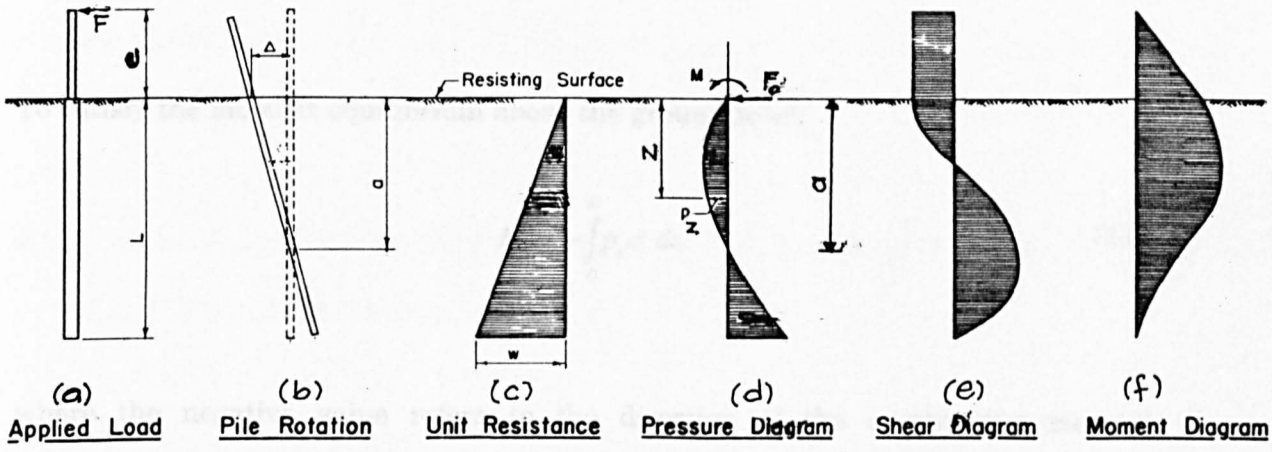

Figure 2.1 Applied load and pile resistance (Czerniak(1957))

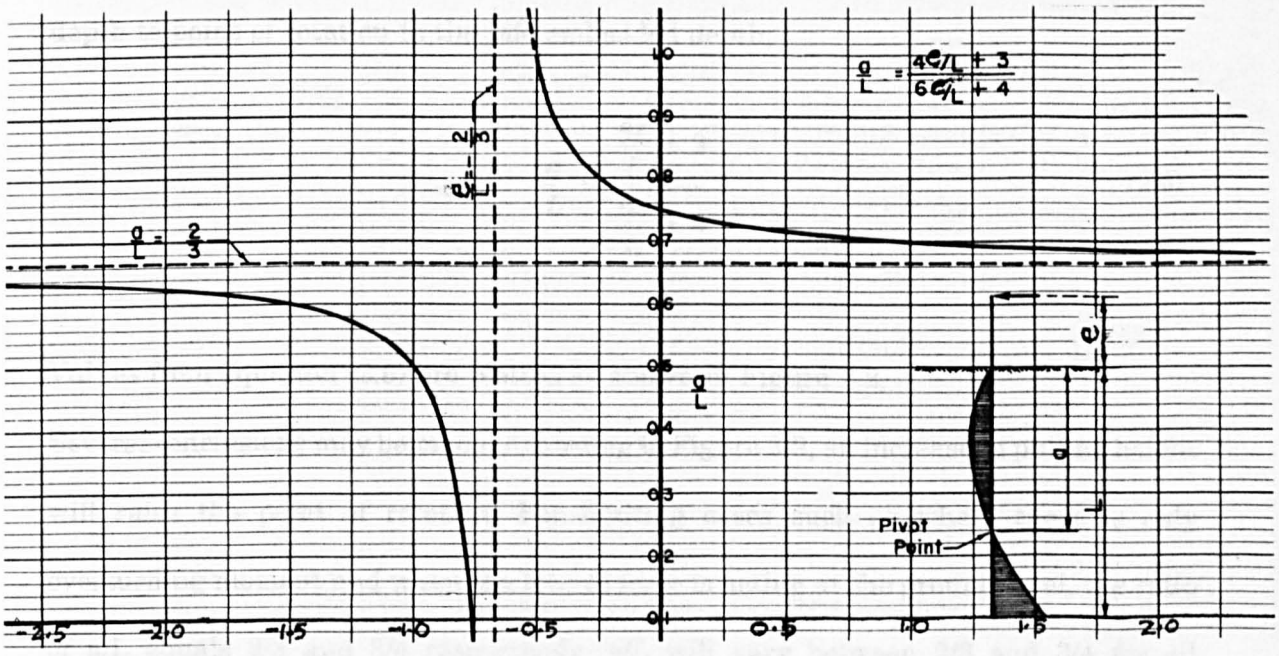

Figure 2.2 Effect of the pulling height on the location of rotation point (Czerniak(1957))

$$F = \frac{w\Delta L}{6a}(3a - 2L) \tag{2.3}$$

To satisfy the moment equilibrium about the ground level;

$$M = -\int_0^L p_z.z\, dz \tag{2.4}$$

where the negative value refers to the direction of the overturning moment. Substituting equation (2.1) into (2.4) gives;

$$M = -\frac{w\Delta L^2}{12a}(4a - 3L) \tag{2.5}$$

However since M = Fe, equation (2.3) and (2.5) can be combined to give the ratio of depth to point of rotation to the pile embedded depth;

$$\frac{a}{L} = \frac{\frac{4e}{L} + 3}{\frac{6e}{L} + 4} \tag{2.6}$$

Values from equation (2.6) are plotted as shown in Figure 2.2.

Several conclusions may be made. According to Figure 2.2, an increase in pulling height will raise the point of rotation. For limiting cases such as where there is only overturning moment and when the lateral force is acting at the ground level, the ratio of a/L equals 2/3 and 3/4 respectively. a/L will vary between 2/3 and 3/4 for all

combinations of moment and lateral force that act on the pile in the same direction. When a/L=0, the lateral resistance of a pile restrained against translation at the soil surface is obtained.

2.3 APPLICATION OF THE THEORY OF SUBGRADE REACTION TO LATERALLY LOADED PILE

Terzaghi(1943), applied the theory of subgrade reaction to obtain approximate solutions to many practical problems such as, the computation of the stresses under a continuous footing acted upon by a concentrated load or piles that are intended to transfer horizontal load to the subgrade. Considering the reaction of an elastic beam on a subgrade, he defined the subgrade reaction as the pressure per unit area of the surface contact between a loaded beam and the subgrade upon which it rests and onto which it transfers its load. Terzaghi(1955), evaluated the theory of subgrade reaction by obtaining the approximate solution applicable to the prediction of a limited resistance of laterally loaded pile. The ratio between the pressure applied on the subgrade and the displacement at which the pressure is produced is termed the coefficient of the subgrade reaction. This coefficient can be written as;

$$k_s = \frac{p}{\Delta} \tag{2.7}$$

In order to compute the limiting lateral resistance of a pile, Terzaghi employed the analysis of a free rigid bulkhead. This method was also utilized by Roscoe(1957) to determine the minimum embedment length of a pier, as explained later in this chapter. Figure 2.3 shows the forces acting on the rigid pile foundation according to Terzaghi(1943). The foundation will be acted upon by the pile weight and the horizontal load above the ground level. The movement of the pile is resisted by the two component forces F_t and F_n at the base of the pile and the lateral soil resistance P_1 and P_2. At any depth below the surface, the elasticity modulus of the sand is equal to;

$$E_s = A_o \gamma z \tag{2.8}$$

where A_0 is a coefficient dependent on the density of the sand ranging from 100 for very loose to 2000 for dense sand. The displacement developed from the horizontal force is due to the deformation of the adjacent medium with the modulus of elasticity E_s. Terzaghi assumed that the pressure acts on the elastic layer, with a thickness of three times the width of the pile perpendicular to the direction of the displacement. This assumes the displacement, at a distance of more than three times the pile width, has no influence on the bending moment of the pile. On this assumption, based on the theory of elasticity, Terzaghi proposed the equation;

$$p = \Delta \frac{E_s}{1.35B} = \Delta \frac{A_o \gamma}{1.35} \frac{z}{B} \tag{2.9}$$

Hence from equation(2.7) using k_h as the coefficient of the horizontal subgrade reaction;

$$k_h = \frac{p}{\Delta} = \frac{A_o \gamma}{1.35} \frac{z}{B} = n_h \frac{z}{B} \qquad (2.10)$$

where n_h is the constant of horizontal subgrade reaction. The values of the constant of horizontal subgrade reaction together with the adopted A_o value are shown in Table 2.1.

Relative packing of sand	Loose	Medium	Dense
Range of values of A_o	100-300	300-1000	1000-2000
Adopted values of A_o	200	600	1500
n_h dry or moist sand	7	21	56
n_h submerged sand	4	14	34

Table 2.1 Values of A_o and n_h (ton/ft^3) for a pile embedded in sand after Terzaghi(1955).

Terzaghi suggested that the n_h value can also be determined experimentally. Figure 2.4 demonstrate the experimental procedure for determining the value of the constant coefficient of the horizontal subgrade reaction by measuring the displacement of the upper end of the rigid pile acted upon by the horizontal load. It consisted of driving a rigid pile, where Terzaghi preferred using a square cross section pile, into the ground then measuring the tilt and the horizontal displacement of the upper end of the pile that was produced by the horizontal force acting on the upper end. Using the

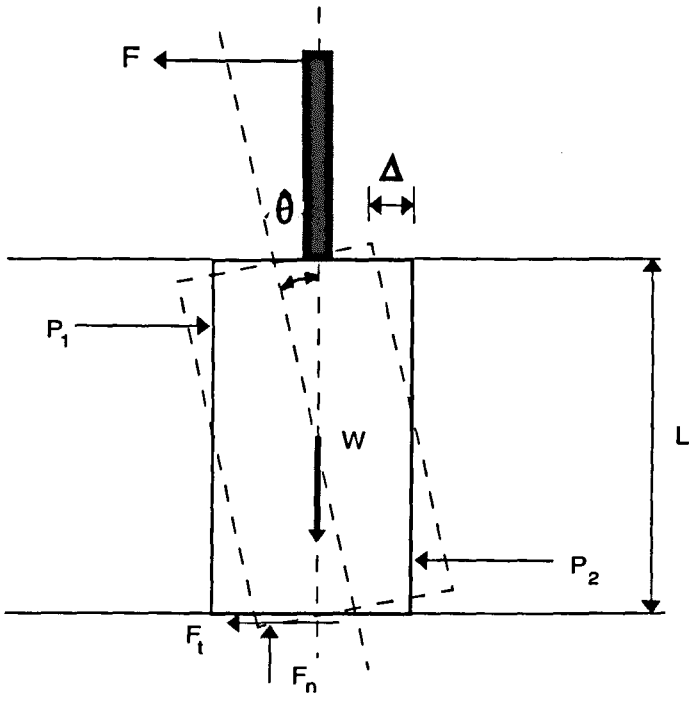

Figure 2.3 Forces acting on the rigid pile according to Terzaghi(1943)

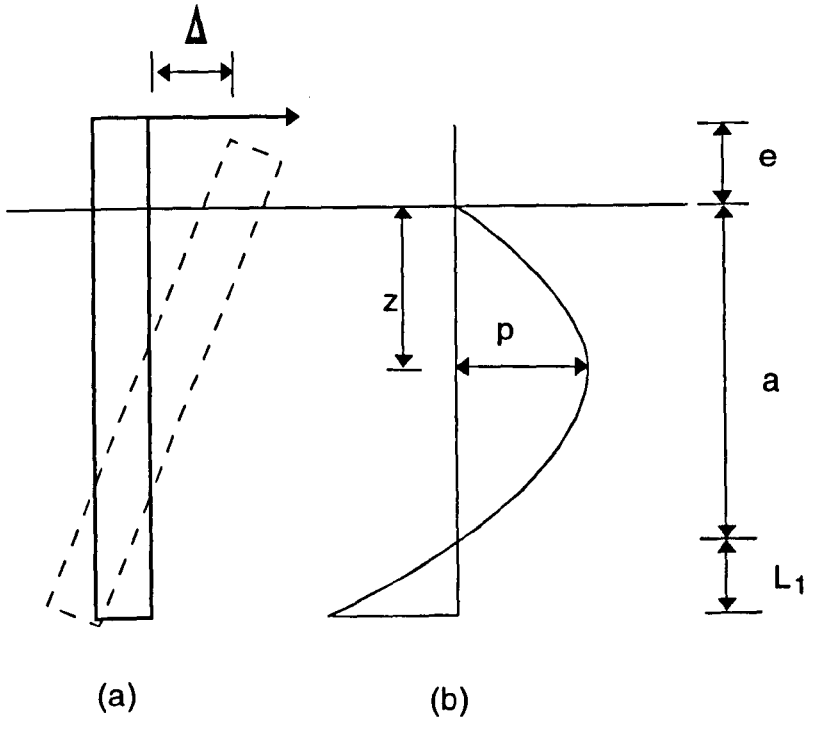

Figure 2.4 Diagram illustrating the experimental procedure to determine the constant coefficient of subgrade reaction n_h after Terzaghi(1955).

relationship in equation(2.9), and from Figure 2.4, he relates the horizontal subgrade reaction p at any depth z for the pile embedded in the sand as;

$$p = \Delta n_h \frac{z}{B} \cdot \frac{a - z}{L_1 + a} \tag{2.11}$$

Though it is simple in definition, however this parameter is difficult to evaluate. This is due to the fact that factors on evaluating the subgrade reaction not only varies with soil type and mechanical properties but also with stress level and pile materials. In the absence of better information, the coefficients of horizontal subgrade reaction based on n_h values in Table 2.1 are acceptable. Because of the influence of stress level and pile geometry, the coefficient of subgrade reaction based on this method must be used with caution.

2.4 EARLY LIMIT EQUILIBRIUM ANALYSIS

An early limit equilibrium analysis of side bearing capacity was first reported by Roscoe(1957). The trial solution was based on the short pier foundation for a single storey portal frame which was tested to collapse. Since the load is sustained before collapse, the upper limit is achieved if the stanchion bases are fixed and the lower limit when pinned. Roscoe then suggested that the frame and the foundation should be designed as a unit. Illustration of the forces acting on the foundation is given in Figure 2.5.

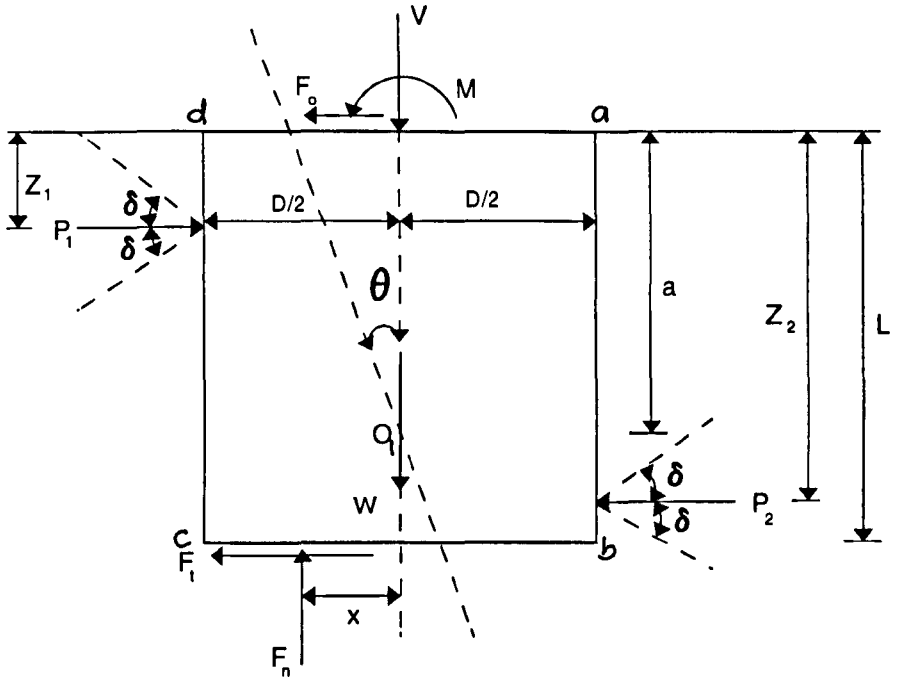

Figure 2.5 Details of forces acting on the short pier foundations by Roscoe(1957).

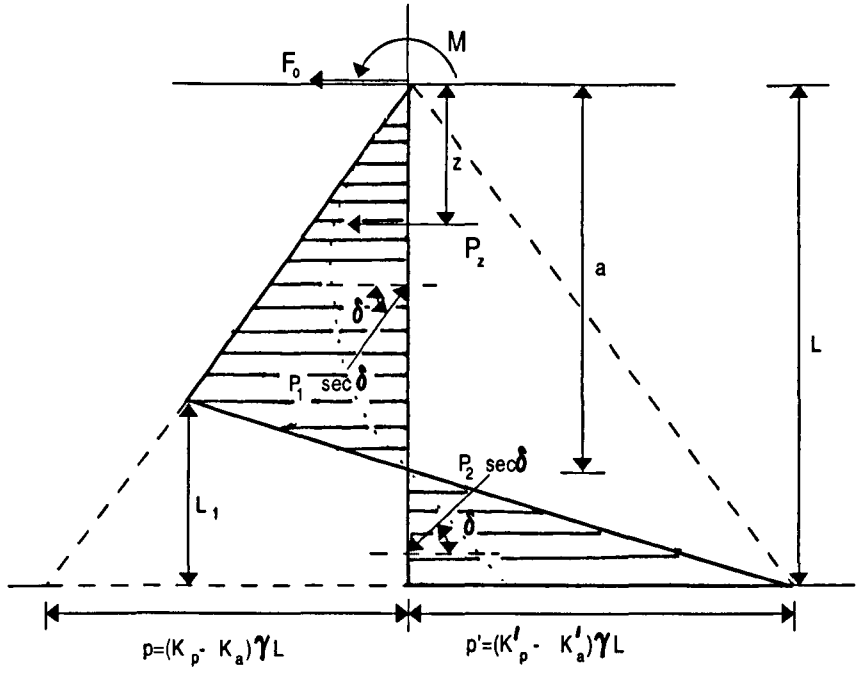

Figure 2.6 Stress distribution at failure of the rigid bulkhead simplified by Terzaghi(1943) based on Krey's idea(1936).

To determine the soil reaction on the pier foundation, Roscoe adopted an analysis by Krey(Terzaghi(1943), Roscoe,(1957)). Krey(1936) suggested that the pressure distribution of the sand at failure is displayed by the hatched triangle as shown in Figure 2.6. Krey's method was simplified by Terzaghi(1943), and applied to the analysis of a rigid bulkhead. Refering to Figure 2.6, Krey assumed that P_1 inclined upwards due to the upward movement of aO_1, which then requires P_2 to incline downwards. However Roscoe argued that, since $P_1 > P_2$ and that additionally W and F_n are present even when V=0, the reactions P_1 and P_2 are inclined at δ. K_p and K_p' are taken to be equal and both correspond to δ and act in an upward direction. Terzaghi assumed that the value of δ=0 in his analysis for the rigid bulkhead and thus K_p is computed from Rankine's coefficient. However Roscoe used the value of δ=20° in his analysis for the sand/concrete interface and adopted the rough coefficient of passive pressure based on CP2(1951).

Resolving forces vertically and horizontally and considering moment equilibrium about the centre of the pier base.

Solving vertically $\Sigma V=0$

$$F_n = V + W - (P_1 + P_2)\tan\delta \tag{2.11}$$

Solving horizontally $\Sigma F=0$

$$F_o = P_1 - P_2 - F_t \tag{2.12}$$

Taking moment about the base centre of the pier $\Sigma M=0$,

$$M + F_o L = P_1(L - Z_1) - P_2(L - Z_2) + \frac{(P_1 - P_2)(D \tan\delta)}{2} + F_n x \tag{2.13}$$

Since $K_{pr} = K_{pr}'$, using similar triangles,

$$a = \frac{2L(L - L_1)}{(2L - L_1)} \tag{2.14}$$

Assuming that $q = (K_{pr} - K_{ar})\gamma B$, therefore the lateral soil resistance with respect to the width of the pier;

$$P_1 = \frac{1}{2} qa(L - L_1) \tag{2.15}$$

and

$$P_2 = \frac{1}{2} qL(L - a) \tag{2.16}$$

Also $F_t = F_n \tan\delta'$

For simplification Roscoe assumed $(P_1 + P_2) = qL^2/2$.

Thus substitution of this value into equation (2.11) gives;

$$F_n = V + W - \frac{1}{2} q \tan\delta L^2 \tag{2.17}$$

Further assumptions applied by Roscoe produced the following approximations to the values L_1 and L;

$$L_1 = \frac{L}{2}(1 + \tan\delta\tan\delta') - \frac{W\tan\delta'}{qL} - \frac{F_o + V\tan\delta'}{qL} \qquad (2.18)$$

and

$$L^4 + \frac{4L^2}{q}(V\tan\delta' - 2F_o) - 12\frac{M}{q}L - \frac{4}{q^2}(F_o + V\tan\delta')^2 = 0 \qquad (2.19)$$

Using these expressions Roscoe postulated that the length of the pile can be found and the value of L_1 can be established from equation (2.18) and the predicted embedment length can be calculated from equation(2.19). Finally the point of rotation can be found mathematically from equation(2.14). Roscoe observed that the centre of rotation of the pier remained steady after the peak moment has been achieved. Roscoe conducted a series of small model tests on rough piers of cross section 2 inches square, 2 inches diameter and √2 inches square. The piers were embedded at a depth of 6 to 9 inches in a dry uniform sand of γ=95lb/ft^3 and ϕ=39.5°. The maximum moment resisted by the 2 inches square pier is 10% times greater than the circular pier of 2 inches diameter.

2.5 DEVELOPMENTS IN THEORETICAL SOLUTIONS

Most of the researchers mentioned above solved the problem of a pile embedded in a specific type of soil. However, Matlock and Reese(1960) and Hansen(1961) developed a general solution which can be used as a design method for a rigid pile embedded in any soil. Matlock and Reese based their solution on dimensional analysis to obtain direct similarity between model and prototype where method of analysis requires access to computer program. The method will not be discussed further since it is outside the scope of this project.

Hansen(1961) developed a solution for laterally loaded piles in either homogeneous or non-homogeneous soil. His general expression for the net earth pressure in front of the pile at depth z is;

$$E_{pz} = q_b K_q + cK_c \qquad (2.20)$$

where q_b is the overburden pressure.

Hansen's net coefficient of earth pressure values of K_q and K_c were established in relation to the depth z and the width B of the square pile and vary with the internal friction angle of the soil as shown in Figure 2.7. Three ranges of K_q and K_c values were derived by Hansen depending on the depth of the soil i.e for pressure at ground surface, at moderate depth and at great depth.

For the pressure at the ground surface which corresponds to the usual plane case, Hansen defined K_q^o as the difference between the passive and active coefficients which is correspond to the rough wall that is being translated horizontally where;

$$K_q^o = e^{\left(\frac{1}{2}\pi + \phi\right)\tan\phi}\cos\phi\tan\left(45^o + \frac{1}{2}\phi\right) - e^{\left(\frac{1}{2}\pi - \phi\right)\tan\phi}\cos\phi\tan\left(45^o - \frac{1}{2}\phi\right)$$

In determining the value of K_c^o, Hansen only included the passive pressure term due to the fact that with the existing of the active pressure it might lead to the negative earth pressure on the active side of the pile. Thus K_c^o is derived as;

$$K_c^o = \left[e^{\left(\frac{1}{2}\pi + \phi\right)\tan\phi}\cos\phi\tan\left(45^o + \frac{1}{2}\right)\phi - 1\right]\cot\phi$$

To determine the increase of earth pressure with a reasonably small depth, Hansen considered the passive Rankine state as shown in Figure 2.8 with an assumed earth wedge bounded by two vertical planes distance D apart. A shearing resistance corresponding to the earth pressure at rest qK_o is derived as;

$$\tau_f = c + (\gamma L + q_s)K_o\tan\phi$$

where q_s is the surcharge load. Refering to Figure 2.8, by considering the width of the plane L and height of the element dL, Hansen assume that the direction of the failure plane is the same as in the plane case,which he considered as sufficiently correct for a reasonable small depth. Based on this assumption, Hansen developed the following simplified expression;

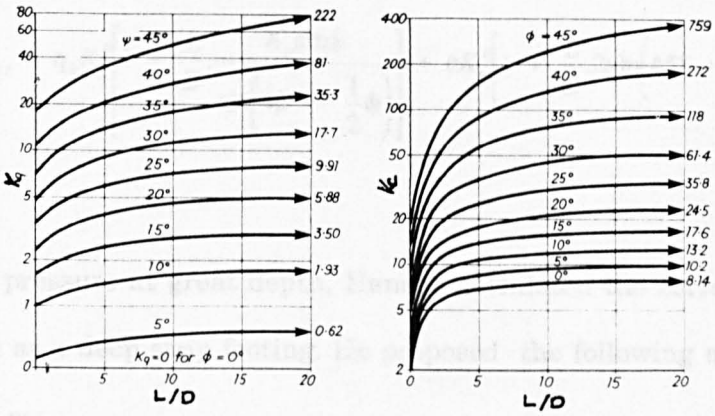

Figure 2.7 Brinch Hansen(1961) coefficients K_q.

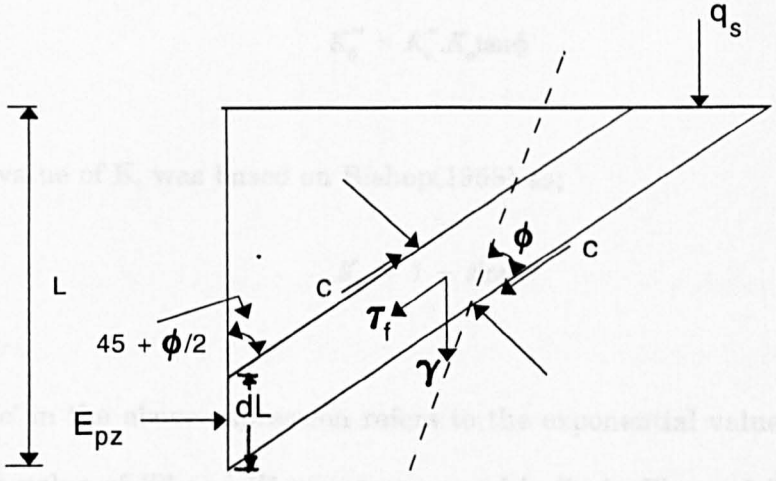

Figure 2.8 Earth wedge in the Rankine case (After Hansen(1961))

$$E_{p\infty} = q_b K_q^o \left[1 + \frac{L}{D}.\frac{K_o \sin\phi}{\sin\left(45^o + \frac{1}{2}\phi\right)}\right] + cK_c^o \left[1 + \frac{L}{D}.2\sin\left(45^o + \frac{1}{2}\phi\right)\right]$$

In the case of pressure at great depth, Hansen calculated the corresponding passive earth pressure as a deep strip footing. He proposed the following net earth pressure at great depth as;

$$E_{p\infty}^{\infty} = q_b K_q^{\infty} + cK_c^{\infty}$$

where

$$K_c^{\infty} = \left[e^{\pi \tan\phi} \tan^2\left(45^o + \frac{1}{2}\phi\right) - 1\right] \cot\phi [1.58 + 4.09\tan^4\phi]$$

and

$$K_q^{\infty} = K_c^{\infty}.K_o \tan\phi$$

where the value of K_0 was based on Bishop(1958) as;

$$K_o = 1 - \sin\phi$$

Note that '*e*' in the above expression refers to the exponential value and not pulling height. The value of K^{∞} and K^{o} are shown graphically in Figure 2.9. For depth L to approach 0, it requires $K \rightarrow K^{o}$ and for $L \rightarrow \infty$, $K \rightarrow K^{\infty}$. Hansen then proposed the net coefficient for the frictional component at an arbitrary depth as;

$$K_q = \frac{K_q^o + K_q^\infty . a_q . \frac{L}{D}}{1 + a_q . \frac{L}{D}}$$

where

$$a_q = \frac{K_q^o}{K_q^\infty - K_q^o} \cdot \frac{K_o \sin\phi}{\sin(45^o + \frac{1}{2}\phi)}$$

and the net coefficient for a cohesive component at an arbitrary depth as;

$$K_c = \frac{K_c^o + K_c^\infty . a_c . \frac{L}{D}}{1 + (a_c . \frac{L}{D})}$$

where

$$a_c = \frac{K_c^o}{K_c^\infty - K_c^o} \cdot 2\sin(45^o + \frac{1}{2}\phi)$$

The value of K_q and K_c are plotted as a function of ϕ and L/D as shown earlier in Figure 2.7. The graph enables a direct determination of the net coefficient of horizontal pressure on the piles to be employed in conjunction with the Hansen's Equation(2.20).In the case of the cohesionless soil, K_c is neglected.

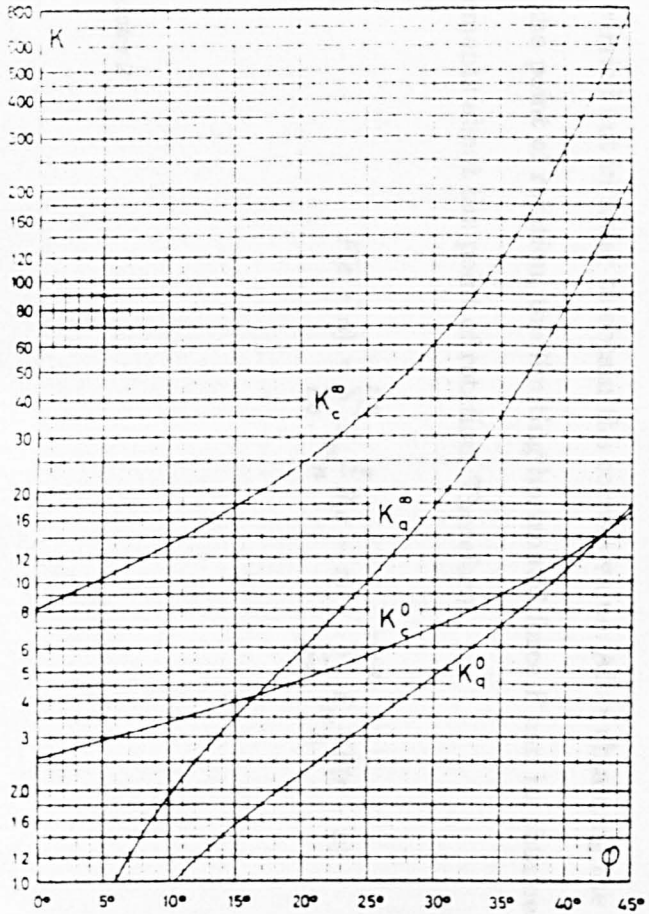

Figure 2.9 Earth pressure coefficients at ground surface and at great depth (After Hansen(1961)

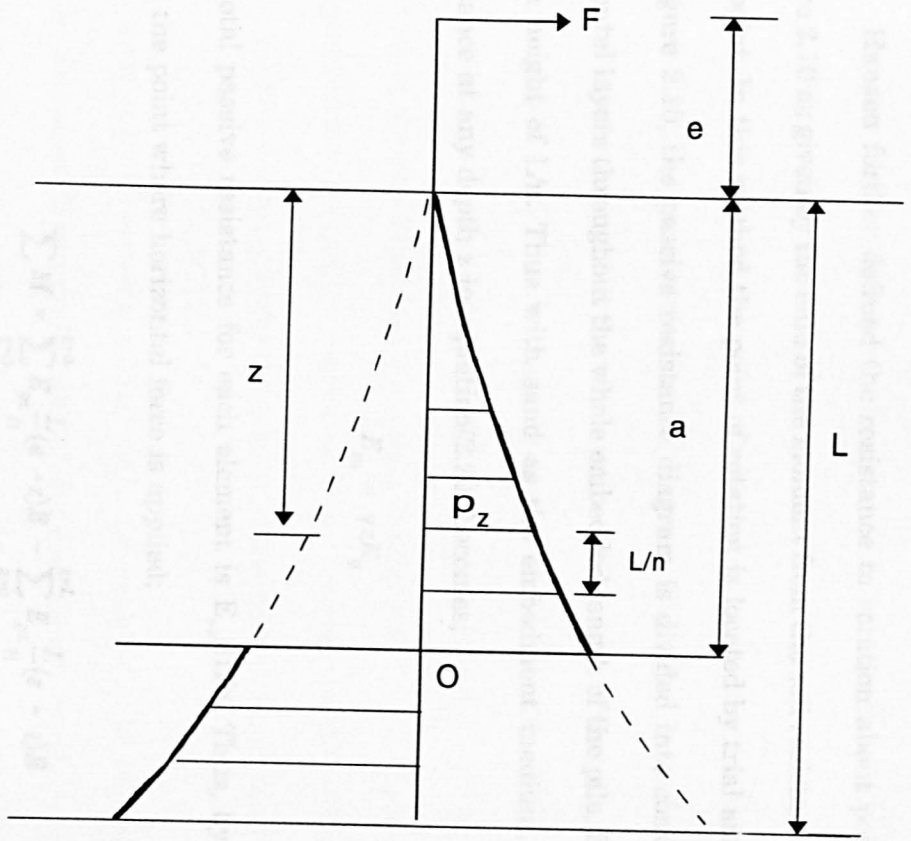

Figure 2.10 Brinch Hansen(1961) earth pressure diagram.

Hansen further defined the resistance to rotation about point X as shown in Figure 2.10 as given by the sum of the moment from the soil resistance above and below this point. In this method the point of rotation is located by trial and error. As shown in Figure 2.10, the passive resistance diagram is divided into convenient horizontal elemental layers throughout the whole embedded length of the pile. Each element thus has a height of L/n. Thus with sand as the embedment medium, the unit passive resistance at any depth z in equation(2.20) becomes;

$$E_{pz} = \gamma z K_q$$

The total passive resistance for each element is $E_{pz}BL/n$. Thus, by taking moments about the point where horizontal force is applied;

$$\sum M = \sum_{z=0}^{z=a} E_{pz}\frac{L}{n}(e + z)B - \sum_{z=a}^{z=L} E_{pz}\frac{L}{n}(e + z)B \qquad (2.21)$$

If $\sum M=0$ the point of rotation is correctly chosen since the moment of passive resistance above the point of rotation balances the one below it. If not, a trial and error procedure is carried out in order to obtain the correct value. After obtaining the correct location of the point of rotation, the limiting horizontal force F can be obtained by taking the moments about the point of rotation. Therefore;

$$F(e + a) = \sum_{z=0}^{z=a} E_{pz}\frac{L}{n}B(a - z) + \sum_{z=a}^{z=a+L} E_{pz}\frac{L}{n}B(z - a) \qquad (2.22)$$

Hansen suggested that a safety factor of 1.5 should be applied to the limiting horizontal force for design purposes. To validate Hansen's theory, Christensen(1961) conducted small model tests. He discovered that in most of the tests no definite maximum value of the horizontal force occured. Therefore he defined the failure load as the load corresponding to a certain deformation. The inclination of the pile relative to its starting position was chosen to represent the deformation. Christensen estimated 11° as a suitable failure rotation. However, when the load decreased with further deformation, the maximum load was taken as the failure point. He concluded that when employing Hansen's approach, results will be a little on the safe side if internal friction angle ϕ is to be taken as that corresponding to a case of plane strain.

Broms'(1964) analysis of the ultimate resistance of the pile was based on Rankine lateral earth pressure while the subgrade reaction theory was used to predict the lateral displacement of the pile. He employed the value of coefficient of subgrade reaction n_h proposed by Terzaghi(1955), shown in Table 2.1, as a function of the lateral deflection of the free headed short pile at the ground surface. Broms expressed the lateral deflection at the ground surface as;

$$\Delta = \frac{18F(1 + 1.33\frac{e}{L})}{L^2 n_h} \tag{2.23}$$

It was pointed out that for a short pile an increase of the embedment length will decrease the lateral deflection at the ground surface. However the stiffness (EI) of the pile does not affect the lateral deflection of a short pile. The mode of failure observed by Broms is shown in Figure 2.11. At failure, the soil in front of the pile moves upwards and the soil behind the pile fills the void created by the movement of the pile. Passive pressures develop in front of the pile while active pressure develops behind it. The high negative pressure which developed at the toe of the pile is replaced by a concentrated load to simplify the analysis. Base on this failure mechanism, Broms assumed that the active pressure is insignificant compared to the passive pressure and thus it was neglected. It was also surmised that the cross section of the pile has little influence on the ultimate resistance of the pile . This evidence was based on the previous work by Shilts et.al.(1948), IRSIA(1950) and Roscoe(1957). In Broms' further assumption, the lateral pressure at failure was taken to be equivalent to three times the Rankine passive pressure. However, according to Poulos and Davis(1980) due to limited empirical evidence from comparison between predicted and observed ultimate loads, this factor of three may be conservative. Broms suggested that the mode of failure depends on the embedment depth and on the degree of end restraint. As shown in Figure 2.11(a), failure takes place when the pile rotates as a unit around the point of rotation beneath the ground surface somewhere along the embedded pile. Based on the above conjecture he assumed the soil reaction at failure per unit length of the pile is;

$$p = 3D\gamma LK_p \tag{2.24}$$

The unit weight γ is equal to the submerged unit weight γ' if the ground water table is

located at or above the ground surface and is equal to the bulk unit weight if the ground water table is below the section considered. K_p is the coefficient of the passive earth pressure which is equal to $\tan^2(45 + \phi/2)$ where the value of friction angle ϕ is determined from drained triaxial or direct shear test. From the equilibrium requirement, the ultimate resistance can be evaluated. The driving moment caused by the external force F with respect to the toe of the pile is;

$$M_d = F(e + L) \tag{2.25}$$

While the corresponding resisting moment, caused by the lateral pressure, neglecting the active earth pressure developed at the back of the pile, will be;

$$M_r = 0.5\gamma DL^3K_p \tag{2.26}$$

At equilibrium the driving moment is equal to the resisting moment. Therefore by combining equation(2.25) and (2.26), the value of the ultimate lateral resistance is;

$$F = \frac{0.5\gamma DL^3K_p}{(e + L)} \tag{2.27}$$

Broms plotted the dimensionless ultimate resistance $F/K_p\gamma D^3$ formulated from equation (2.27) as a function of embedment ratio L/D as shown in Figure 2.12. It shows that the dimensionless ultimate resistance intensified with an increase in the embedded length and a decrease in the pulling height ratio e/L.

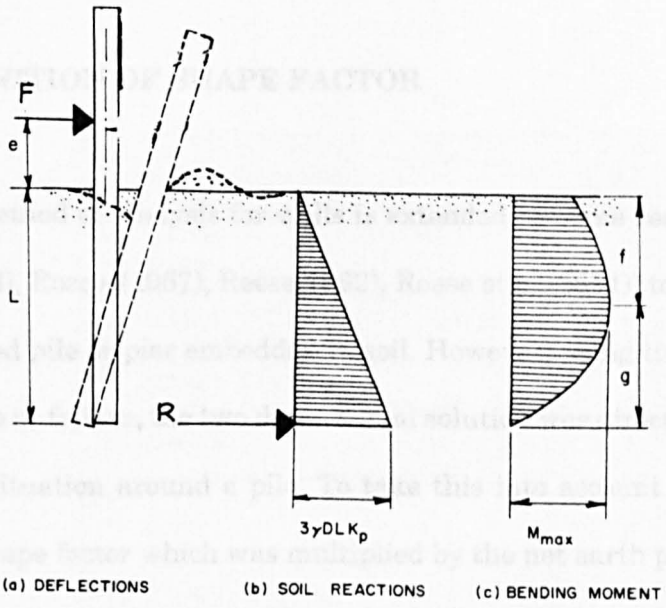

Figure 2.11 Mode of failure for short rigid pile according to Broms(1964)

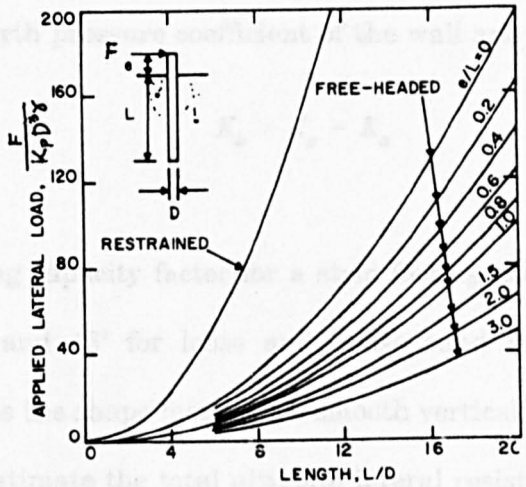

Figure 2.12 Variations of dimensionless applied load with the pile embedment (After Broms (1964)).

2.6 DEFINITION OF SHAPE FACTOR

The method of analysis for walls is extended by some researchers (Raes(1936), Terzaghi(1943), Roscoe(1957), Reese(1962), Reese et al.(1974)) to obtain solutions for a laterally loaded pile or pier embedded in soil. However, using the same distribution of earth pressure at failure, the two dimensional solution was directly applied to the three dimensional situation around a pile. To take this into account Meyerhof et al.(1981) employed a shape factor which was multiplied by the net earth pressure for the wall to obtain a limit resistance for a pile. For a short pile foundation in sand Meyerhof et al.'s shape factor is;

$$S_f = 1 + \sin\phi\left(\frac{L}{D}\right) \leq \frac{K_0 N_q}{K_b} \tag{2.28}$$

where $K_o = 1 - \sin\phi$ is the approximate earth pressure at rest for normally consolidated soil, K_b is the net earth pressure coefficient of the wall and is equal to;

$$K_b = K_p - K_a$$

and N_q is the bearing capacity factor for a strip footing according to Terzaghi(1943). Values of ϕ = 36° and 46° for loose and dense sand respectively. Applying this relationship produces the shape factor for a smooth vertical pile in homogeneous sand, in Figure 2.13. To estimate the total ultimate lateral resistance of the pile, Meyerhof et al. used the value of S_f and experimental data to determine the reduced overall shape

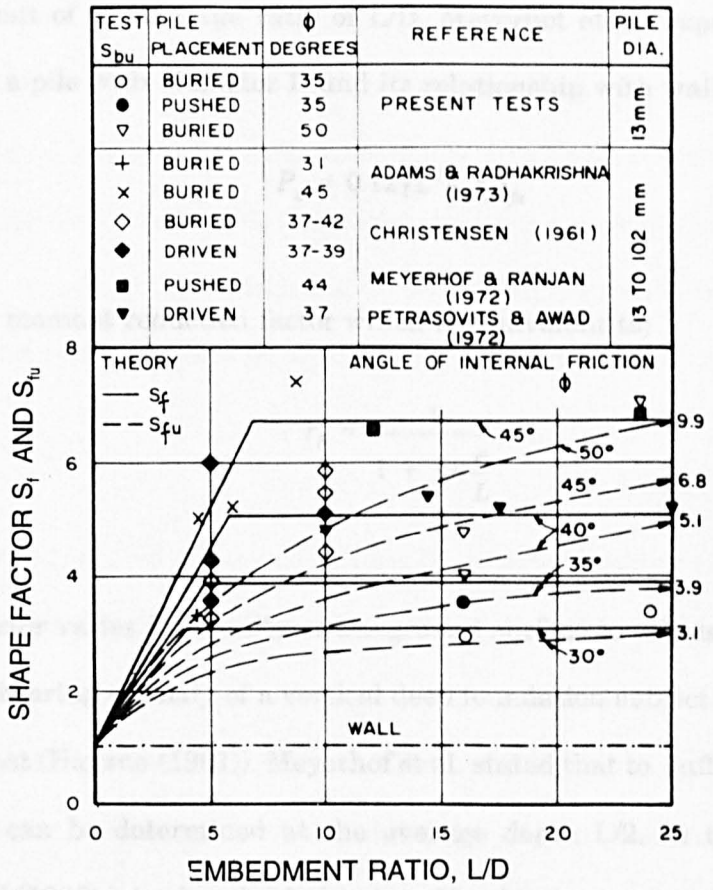

Figure 2.13 Shape factor developed by Meyerhof et al.(1981)

factor S_{fu}. They show that the value of S_{fu} for various embedment ratio L/D approach the upper limit of S_f for large ratio of L/D. Meyerhof et al. expressed the ultimate resistance of a pile with diameter D and its relationship with wall as;

$$P_u = 0.12\gamma L^2 K_b r_b S_{fu} \tag{2.29}$$

where r_b is a moment reduction factor which is equivalent to;

$$r_b = \frac{1}{1 + 1.4\frac{e}{L}}$$

The shape factor varies from unity at the ground surface to values that correspond to the ultimate bearing capacity of a vertical deep foundation subject to the lateral earth pressure at rest (Hansen (1961)). Meyerhof et al. stated that to sufficient accuracy, the shape factor can be determined at the average depth L/2. In their further work, Meyerhof et al.(1988) introduced skin friction of $\delta=\phi/3$ into equation(2.29), thus implying a rough coefficient of net earth pressure. However no shape factor was included in this later equation. No apparent explanation was given by Meyerhof et al. Equation(2.29) is given as;

$$P_u = 0.12\gamma L^2 K_{br} r_b \tag{2.30}$$

where K_{br} is the net coefficient of earth pressure for a rough surface. They also suggested that Equation(2.30) can be applied for pile groups with a spacing of 3 pile diameters when the lateral resistance is governed by the block failure of an equivalent pier, consisting of the pile enclosed soil mass of width B and depth L.

2.7 DIMENSIONAL ANALYSIS

A model can normally be related to a prototype by using the dimensional analysis method. This provides a simple basis for predictions of the behaviour of the full scale prototypes from small model tests. Sets of independent parameters are chosen to build up the complete characteristics of the actual event. However, experimental evidence needs to be established in verifying the significance of these independent parameters.

Dimensionless values are often used for interpreting the prototype value from small model tests. Similarity between model and prototype is attained when the dimensionless quantity has the same value in both model and prototype. It is necessary to decide which factors are likely to be involved in the relationship. This is effected from experience and analysis of the field with which the problem is concerned, along with the factors and laws relating to this field.

2.7.1 BUCKINGHAM PI-THEOREM

To determine the characteristic of a physical system by analytical means, an equation which forms the relation must be satisfied by the system. Relations between the dependent variables and the independent variables relevant to the system will be obtained when this equation is solved mathematically. However, inumerable

associations between both variables can be formed although certain ones of these form a set which are independent of each other.

According to Buckingham's theory(Langhaar(1951)), the dimensionless form is a function of dimensionless numbers that includes all the listed independent parameters. The dimensionless number is known as the Π-product. This leads to Buckingham's pi-theorem which states that a complete dimensional homogeneous equation, relating 'n' physical quantities which are expressible in terms of 'k' fundamental quantities can be reduced to a functional relationship between the 'n-k' dimensionless products. Thus generally it is a process for eliminating extraneous information from the relations between quantities.

Fundamental quantities most commonly employed are based on Newton's second law which states that the rate of change in momentum of a body is proportional to the applied force. This gives,

$$\text{Force} \propto \text{Change of momentum / time}$$

Since

$$\text{momentum} = \text{mass x velocity}$$

and

$$\text{acceleration} = \text{velocity / time}$$

Therefore

$$\text{Force} \propto \text{mass x acceleration}$$

Making unity out of a constant value,

$$\text{Force} = \text{mass x acceleration}$$

The relation above if expressed dimensionally will give,

$$[F] = [M][LT^{-2}]$$

where

[F] dimension of force

[M] dimension of mass

[L] dimension of length

[T] dimension of time

The equation relates four dimensions, [F],[L],[T] and [M]. Therefore while accepting [L] and [T] as fundamental dimensions required for geometry and kinematics, the third fundamental dimension in dynamics can be either force [F] or mass [M]. The choice of these quantities depends upon the measuring system i.e whether to employ the conventional MLT system or the FLT system. However, in this work, since force is the fundamental physical quantity, the latter are employed in deriving the dimensionless value of the equations.

In describing the physical problem, in terms of quantities Q_1, Q_2,.....,Q_n, implies the existence of one or more relationships which pertain to problem of the form,

$$f(Q_1,Q_2,.....,Q_n) = 0 \qquad (2.31)$$

As already stated in the pi-theorem, this relationship can be reduced to the form,

$$\Phi(\Pi_1,\Pi_2,.....,\Pi_{n-k}) = 0 \qquad (2.32)$$

where Π's are dimensionless groups formed by combining any 'k' of the quantities with the remaining 'n-k'. If there are nine physical quantities involved in the relationship of the physical problem and three fundamental physical quantities, six sets of dimensionless groups would be formed. Selection of the physical quantities for a pile embedded in sand, will be discussed later in Chapter 7.

2.8 SUMMARY OF PREVIOUS THEORETICAL ANALYSES

Most of the research reported is devoted to analysis of the limiting soil resistance of a wall. Work such as that of Raes(1936), Terzaghi(1943), Hansen(1961), Meyerhof et al.(1981), extended the theory to the problem of a laterally loaded pile. Analyses were mainly two dimensional due to the difficulties in analysing the three dimensional failure mechanisms. To overcome the problem, a shape factor as used by Meyerhof et al.(1981) and Broms(1964) may then be introduced to multiply the ultimate soil resistance on the wall in order to obtain the ultimate resistance of the soil acting on the pile.

Subgrade reaction theory is mostly employed in determining the horizontal deflection of the pile at ground level. Terzaghi(1955) postulated the effective distance where the pressure acting on the elastic layer is at a distance of three times the pile

width perpendicular to the displacement. Terzaghi also suggested that for simplification in the analysis, the soil modulus increases linearly with depth of the pile.

The method suggested by Hansen(1961), is applicable to use in the general distribution of soil pressure for both sand and clay. He developed a procedure whereby a centre of rotation is established by trial and error. When the centre of rotation is determined , the ultimate lateral resistance can be obtained from horizontal equilibrium.

Broms'(1964) assumption that due to the shape effect, the ultimate lateral resistance is equivalent to three times the passive earth pressure may be somewhat conservative due to limited empirical evidence. However the ultimate resistance at any depth defined by Hansen is equivalent to Broms approach when considering $K_q = 3K_p$ for all depth as mentioned by Poulos and Davis(1980). While others evaluate the limiting resistance of the pile semi empirically, Terzaghi(1943), Czerniak(1957) and Hansen evaluated without any empirical evidence.

Roscoe(1957) adopted the method used by Terzaghi(1943) for a rigid bulkhead with some modifications. Terzaghi assumed that the surface of the pile to be frictionless while Roscoe assume $\delta=20°$ for a sand/concrete interface. Roscoe also found out that the square cross section pier could withstand a moment of about 1.1 times that of a circular cross section pier of the same dimension.

The selection for the friction angle was not mentioned by the majority of researchers except Christensen(1961), Broms(1964) and Meyerhof et al.(1981, 1983). Christensen employed the plane strain test for obtaining the ϕ value. Broms suggested the triaxial compression and direct shear test in obtaining the ϕ value. However the method employed by Meyerhof et al. seems to be more appropriate where ϕ from plane strain is used for analysis of the wall, while ϕ adopted from the triaxial compression test is used for analysis of the single pile.

Dimensional analysis gives a useful hint in determining the various factors involved in the analysis, although one should have sufficient experience dealing with the related problems, since selection of the relevant parameters can be quite difficult.

Generally the ultimate lateral resistance is based on earth pressure theory. The design of the pile will be dependent on satisfying the limiting lateral displacement that may result in the specification of the limiting lateral load or overturning moment. Hansen suggested the safety factor of 1.5 be adopted for his design method while a conservative safety factor of 3 was suggested by Roscoe.

CHAPTER 3

REVIEW OF PREVIOUS EXPERIMENTAL WORK

3.1 INTRODUCTION

Numerous field tests and laboratory work have been done to study the behaviour of a laterally loaded pile. However, there are relatively few papers in the technical literature which deal with a short pile or pier resisting lateral load. Apart from theoretical and semi empirical work carried out for analyzing the limiting capacity of short pile embedded in sand, full scale tests (Shilts et al.(1948), UIC/ORE(1957), McCorkle(1969) and Balfour Beatty(1986, 1988)) and laboratory tests on small models (IRSIA(1950), Christensen(1961) and Dickin and Wei(1991)) were performed in order to obtain an appropriate solution. Most of the model tests were performed under the influence of unit gravity. Dickin and Wei conducted a parametric study of a model short pile under the influence of high gravity in the centrifuge, to simulate the field condition.

3.2 EARLY INVESTIGATION

3.2.1 SHILTS ET AL. FIELD TESTS

An early report by Shilts et al.(1948), describes full scale tests to investigate the stability of posts against a lateral load. Laboratory tests were also conducted to check

and complement the field tests. While field posts were embedded in granular soil and silty clay, the laboratory model posts were tested in a clean fine sand. The laboratory work was designed to check the analysis of the field test results with the location of the point of rotation and the effect of the post shape on resistance to load. In the field testing, thirteen different sizes of post were tested at two different sites. Eight different posts were tested in granular soil and five others were tested in a clay soil. Details of the parameters for the posts tested are shown in Table 3.1. The posts were installed in a straight line 4.7 m apart. Snub posts were installed on a line perpendicular to a test post line at a distance of 6.25m. The snub posts were then anchored against the pull by 13mm diameter screw anchors and cables. Loading was applied with a standard 2-ton hoist fastened to a snub post by a long chain at a maximum value of 9kN and deflection were read when the rate of deflection at ground surface was at an average of 0.025mm/min. A total number of thirteen tests were conducted in the laboratory. Model piles a 1/4 of the size of field posts were embedded in a clean fine sand with an average unit weight of 15.6kN/m^3. Details of the test parameters for the laboratory models are shown in Table 3.2. Shilts et al. observed that from the field test the pull of the lateral load on the post causes the post to rotate in a vertical plane about some point along the embedded portion of the post. This movement will develop a resistance of the soil in opposite directions above and below the point of rotation. In order for the limit resistance of the soil to be achieved, the moment caused by the load is balanced by the moment of the resistance of force in the soil. They pointed out that initially it is necessary to determine the location of the point of rotation to ascertain the distribution of the soil resistance. The point of rotation was found by plotting a length

DEPTH OF EMBEDMENT, WATER CONTENT OF SOIL AND POST TYPE FOR FIELD POSTS			
Post No.	Depth of Embedment Feet	Av. Water Content of Soil, Per Cent 0-4 Ft. Depth	Post Type
	Test SITE NO. 1		
1	5.00	13.5	Olmsted Post
2	5.75	11.1	Olmsted Post set 5.25 ft. in a 6 ft. length of 14 in. dia 10 gauge steel pipe.
2A	7.00	12.5	Olmsted Post set 4 ft. in a 6 ft. length of 14 in. dia. 10 gauge steel pipe.
3	6.00	13.1	Olmsted Post set 3 ft. in a 12 ft. length of 14 in. dia. 10 gauge steel pipe. Concrete collar 1 ft. thick by 3.5 ft. dia. 0.5 ft. underground.
4	5.00	13.1	Olmsted Post with wings 2 ft. x 1.5 ft.
5	5.00	12.4	7 in. steel I-Beam with wings 1.5 ft. x 1.0 ft.
5A	5.00	13.2	7 in. steel I-Beam with wings 2 ft. x 1.5 ft.
6	5.00	13.2	Olmsted Post set in soil-cement 2 ft. dia.
	TEST SITE NO. 2		
9	6.5	22.8	7 in. steel I-Beam set 4.5 ft. in a 6 ft. length of 14 in. dia. 10 gauge steel pipe.
10	5.0	22.6	Olmsted Post set in soil-cement 2 ft. dia.
12	8.0	20.6	8 in. steel I-Beam set 3 ft. in a 12 ft. length of 14 in. dia. 10 gauge steel pipe.
13	5.0	21.3	Olmsted Post with wings 2 ft. x 2 ft.
14	6.0	21.2	10 in. steel I-Beam set 5 ft. in a cast-in place concrete pipe 2 ft. dia.

Table 3.1 Post parameters employed in Shilts et al. field test

DEPTH OF EMBEDMENT, TYPE OF POST AND SAND DENSITY FOR LABORATORY POSTS			
Post No.	Depth of Embedment Inches	Type of Post	Estimated Sand Density Pounds per cu. ft.
17	18	3" Fabridated I-Beam	106
18	24	3" Fabricated I-Beam	106
19	30	3" Fabricated I-Beam	107
20	30	3" Fabricated I-Beam	107
21	30	3" Fabricated I-Beam	102
22	24	3" Fabricated I-Beam	107
23	24	3" Steel Boiler Tube 1/8" Walls	106
24	24	3" Fabricated I-Beam With Wood Wings	108
25	24	3" Square Wood	106
26	18	3" Fabricated I-Beam With Wood Wings	108
27	15	3" Fabricated I-Beam With Wood Wings	108
28	15	3" Square Wood	108
29	18	½ of 3" Dia. Round Wood	108

Table 3.2 Post parameters employed in Shilts et al. laboratory test

of the post against deflection at ground level. A straight line was plotted through every deflection gauge along the post and were projected to a common intersection with the original position of the post. As shown in Figure 3.1, the non linearity of the soil resistance was simplified to an average pressure p/A and is represented by a resultant force P_1 at 0.338 of the depth of embedment below the surface and P_2 at 0.898 of the embedment depth from the surface. Due to the irregular shape of the test post, Shilts et. al proposed that the location of the point of rotation should be based on the vertical cross sectional area of the embedded length of the post perpendicular to the load direction. They found out that the point of rotation is at a depth which includes 0.676 of the vertical post cross sectional area of the post.

In the laboratory tests the stability of square and circular poles was investigated. They reported that, for a small deflection the stability of a round pole of radius r was the same as that of a square pole of side $r\sqrt{2}$., provided that the two sides of the square were parallel to the plane of disturbing forces. It was identified that the point of rotation dropped with increasing of the embedment depth and also with decreasing unit weight of the soil. Finally it was concluded that the movement of the post at ground level and the average pressure caused by the lateral load, may be described by;

$$\frac{p}{A} = P_p \log(1 + 2\Delta^{\tan\phi}) \qquad (3.1)$$

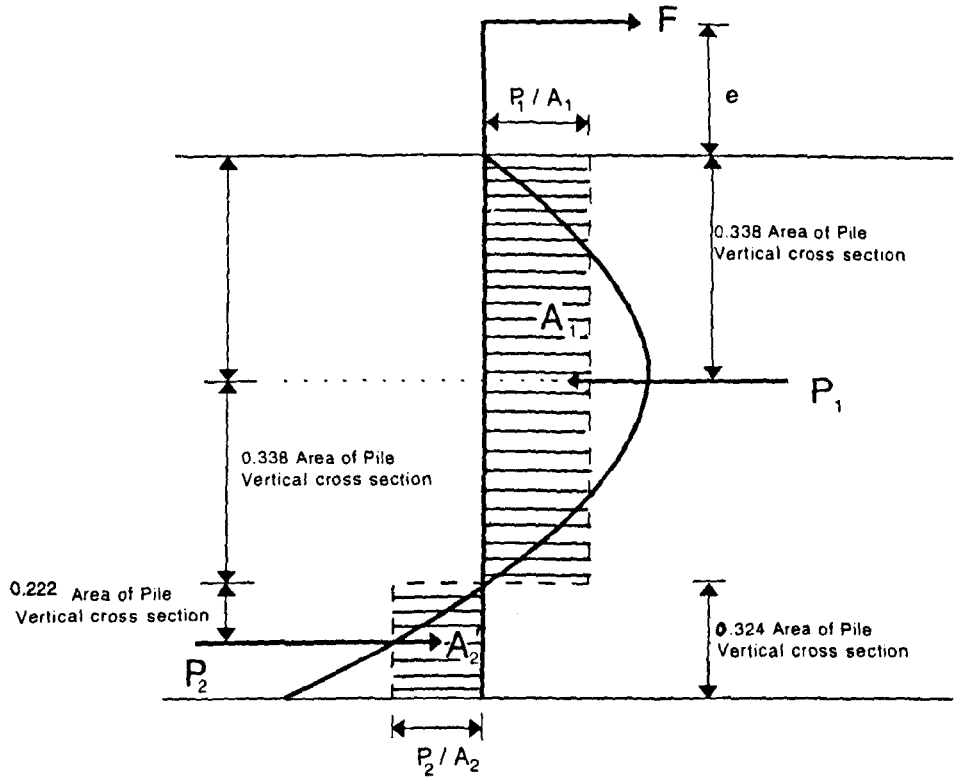

Figure 3.1 Pressure diagram after Shilts et al.(1948)

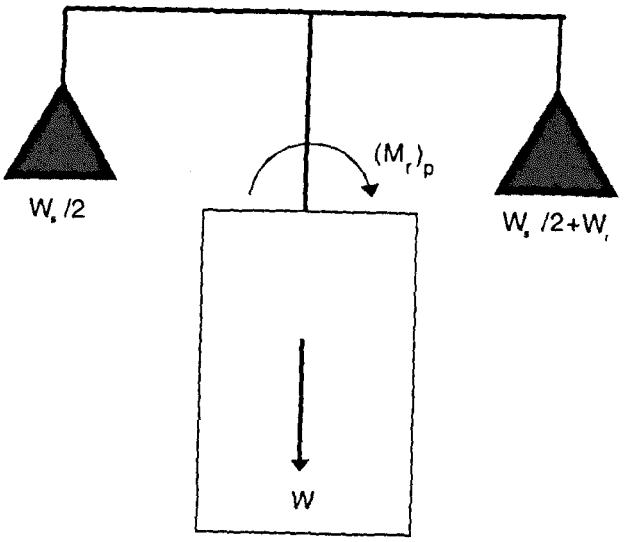

Figure 3.2 Arrangement of the IRSIA test

where

A : Average area of the soil pressure as shown in Figure 3.1

P_p: Rankine passive pressure

ϕ : Internal friction angle of the soil

Δ : Deflection of post at ground surface

Both laboratory and field tests measured the post stability relatively small deflections rather than a complete overturning, while the ϕ value was obtained from a triaxial compression test.

3.2.2 THE IRSIA TESTS

Numerous experiments, on reduced scale models of foundations in cohesionless soil, were carried out by Ramelot and Vandeperre of the IRSIA(1950) (Institut pour l' Encouragement de la Recherche Scientifique dans l' Industrie et l' Agriculture). The tests, more than a thousand in number, on reduced scale models at unit gravity were classified as follows:-

a) Tests on models of driven foundations

b) Tests on models of slab foundations

c) Test on models of block foundations (prismatic or cylindrical)

d) Tests on the models of foundations placed on the surface of the soil

e) Tests on models of foundation implanted at various depths and submitted to centred loads.

Test models had the following dimensions:-

a) Square section, sides ranging from 50mm to 400mm

b) Rectangular section, length 150mm to 300mm and width 100mm to 250mm

c) Circular section of 50mm, 100mm and 200mm in diameter

The sand used in the test had an angle of repose of 34° and was placed at various unit weights between 14.22kN/m^3 and 15.2kN/m^3 according to the degree of compaction. The arrangement for the IRSIA tests was as shown in Figure 3.2. The loading system adopted used a double symmetric balance with the arms carrying two pans containing weights and was mounted on a test block. Initially the loading was balanced in two pans. Overturning was effected by progressively overloading one of the pans. IRSIA introduced a correction term (1 - E_p) to cater for unconsolidated terrain. The value of (1 - E_p)is empirically determined by;

$$(1 - E_p) = 3.44\left(1 + \frac{L'}{L}\right)^3 - 2.44\sqrt{\left[1 + \left(\frac{L'}{L}\right)^2\right]^3} \qquad (3.2)$$

where L′ is the depth of an unconsolidated layer and L is the depth of the embedded length of the pile. The relationship of (1 - E_p) can be plotted graphically as shown in Figure 3.3. Hence the moment limit at ground level according to IRSIA is;

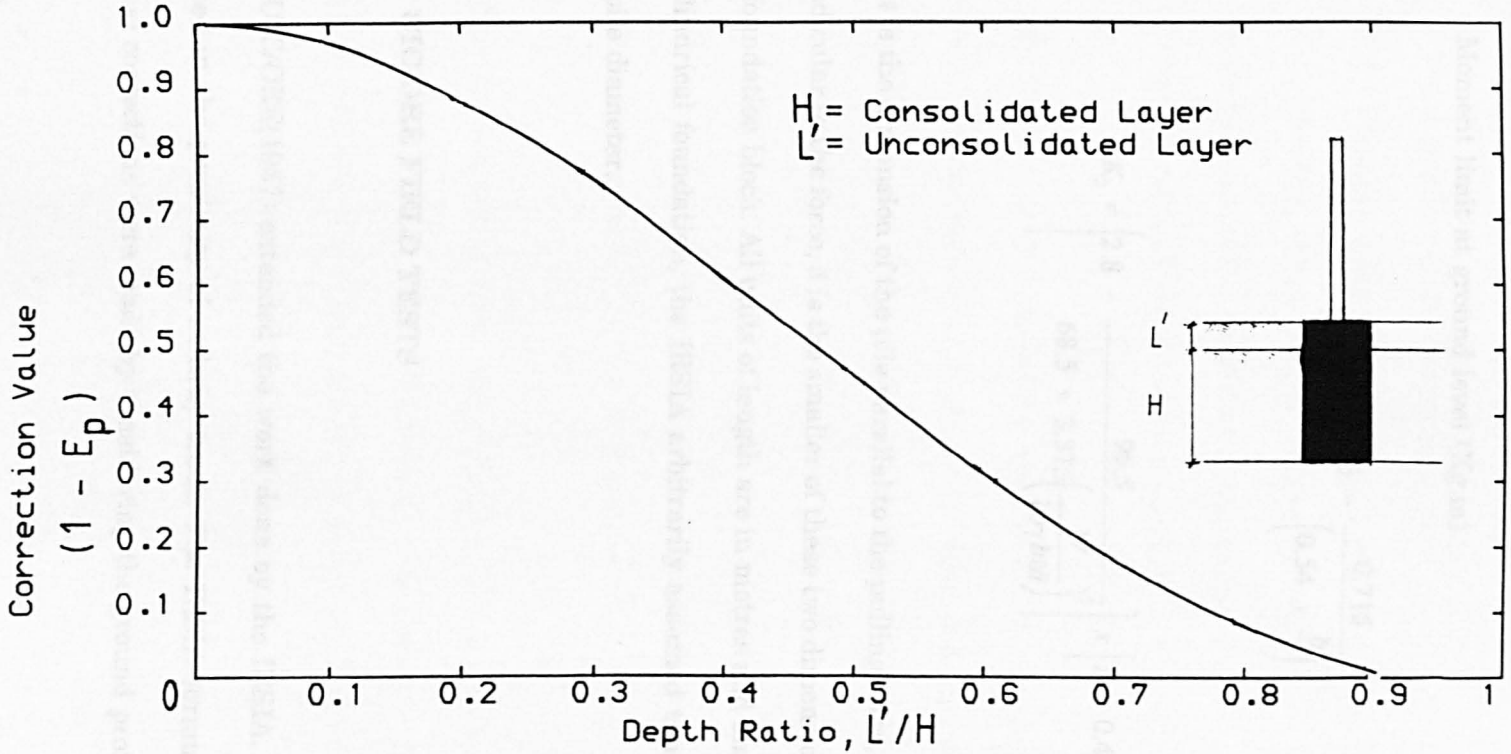

Figure 3.3 Correction factor ($1-E_p$) used in the IRSIA and UIC/ORE formula

$$M_B = (1 - E_p)(M_r)_p \tag{3.3}$$

where $(M_r)_p = K_1 \ell W + K_2 \gamma D L^3$

M_B : Moment limit at ground level (Kg.m)

$$K_1 = 0.5136 - \frac{0.715}{\left(0.54 + \frac{b}{\ell}\right)}$$

and

$$K_2 = \left[2.8 - \frac{96.5}{68.5 + 3.375\left(\frac{W}{10\gamma b \ell ä}\right)^3}\right] x \left[1 + 0.45\left(\frac{\ell}{b}\right)\right]$$

where ℓ is the dimension of the pile parallel to the pulling force, b is the pile dimension perpendicular to the force, ä is the smaller of these two dimensions and W is the weight of the foundation block. All units of length are in metres and mass is in Kg. In the case of a cylindrical foundation, the IRSIA arbitrarily assumed that ℓ=b=ä=0.8D where D is the pile diameter.

3.2.3 UIC/ORE FIELD TESTS

UIC/ORE(1957) extended the work done by the IRSIA. Full scale tests were conducted in the proximity of railway track. The IRSIA formula was evaluated and statistical corrections were made by considering the ground profile and location of the

pile with respect to the track. The UIC/ORE defined the limiting moment of a foundation as a function of:

a) the dimension of the foundation

b) the thickness of the unconsolidated ground

c) the direction of pull with respect to the track

d) the distance of the mass foundation to the track

e) the general configuration of the ground

The full scale tests involved the application of an increasing pulling force(F) at a height 'e' above the foundation as shown in Figure 3.4. This was achieved by pulling adjacent gantries together. UIC/ORE defined the 'Fe-Limit' value which caused the foundation failure as:

"*Failure of a foundation occurs at a moment when there is an increase of strain, the dynamometer measuring the pulling force does not indicate an increase*"

Foundations tested were either circular or rectangular in the cross section. Parameters of the piles tested by UIC/ORE were as shown in Table 3.3. In the case of a cylindrical pile, it was assumed, arbitrarily, from the IRSIA that ℓ=b=ä=0.8D. Three methods of stress application were applied:-

a) Fast overturning: The test was carried out in such a way that the moment limit was reached in approximately 15 minutes.

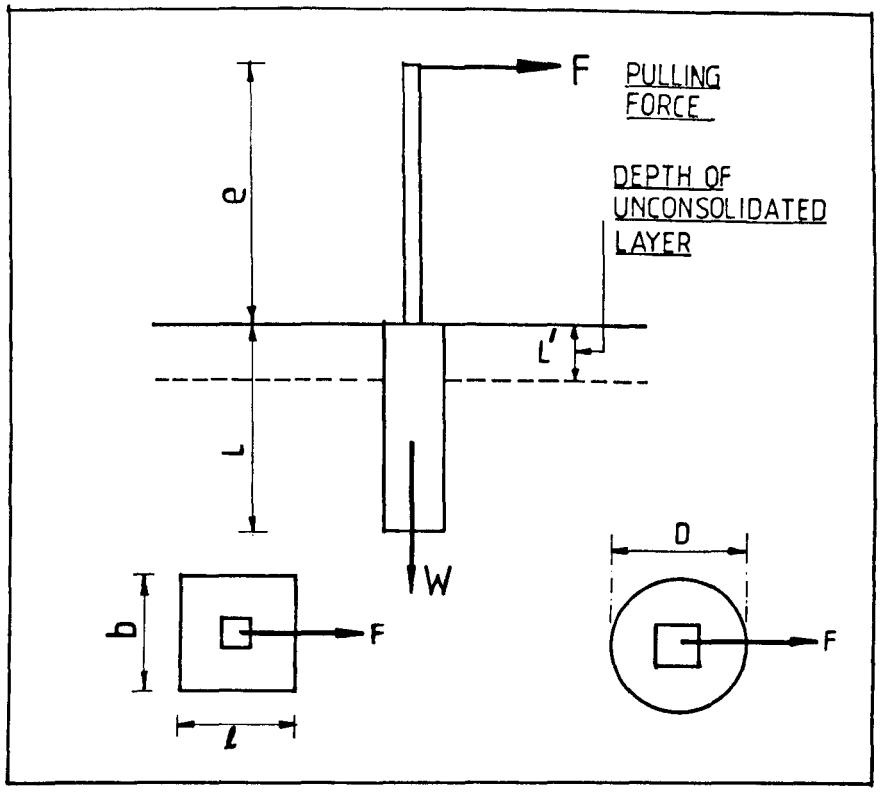

Figure 3.4 The UIC/ORE test arrangement and summary of main geometrical parameters

b) Slow overturning: The test was carried out in such a way that the moment limit was reached after several weeks or months.

c) Mixed overturning: The test consisted of a fast overturning after a slow action stressing.

The emphasis of the full scale tests was on the surface profile, the situation of the foundation on the ground profile and the distance of the foundation and direction of the overturning moment in relation to the railway track. All these elements were taken into consideration when developing their empirical relationships.

Cylindrical	**Pile**	**Prismatic**	**Pile**
Variables	Range	Variables	Range
Diameter, D	0.55m to 1.20m	Width, ℓ	0.6m to 0.9m
ä=0.8D	0.44m to 0.96m	Width, b	1.1m to 1.7m
Depth, L	1.20m to 3.0m	Depth, L	1.5m to 1.9m
Pull. Height, e	6m to 11m	Pull.Height, e	6m to 8.5m
Ratio,e/L	2.0 to 6.7	Ratio, e/L	3.2 to 5.3
Ratio,e/D	5.6 to 14.5		
Ratio,e/ℓ	7.0 to 18.1	Ratio, e/b	4.6 to 7.3
Ratio,L/D	1.5 to 5.5		
Ratio,L/ℓ	1.9 to 6.9	Ratio, L/b	1.3 to 1.5

Table 3.3 Principal dimensions in UIC/ORE field tests

To account for this difference with the IRSIA, a statistical correction was applied to Equation(3.3) giving;

$$Fe\text{-}Limit = 15.75 M_B^{0.72} \tag{3.4}$$

where M_B is derived from Equation(3.3).

Further corrections made by the UIC/ORE aimed to validate the formulae by investigating the influence of particular local factors. The main object of the tests was to verify whether the results obtained would continue to show no significant difference between cohesive and cohesionless soil. From these tests they established several conclusions;

a) the nature of terrain hardly influence the limiting moment value.
b) the correction $(1\text{-}E_p)$ fully allows for unconsolidated terrain.
c) the site configuration and direction of pull play very important roles.

A further series of tests was undertaken in order to investigate the possibility of reducing the depth of the foundation based on the conclusions made above. Seeking a more satisfactory formula for a cohesive soil or for moist granular soil which effectively exhibits cohesion, the final UIC/ORE correction made to Equation(3.4) gives;

$$Fe\text{-}Limit = 27.45 M_B^{0.67} \tag{3.5}$$

To cater for the shape of terrain, UIC/ORE introduced a coefficient K as shown in Table 3.4. They classified the terrain into 3 categories:-

a) normal embankment comprising all the terrains where the transverse slope is greater than 1/3 and less than 1.

b) normal flat terrain where the slope was lower than or equal to 1/3.

c) normal cutting, comprising all types of excavation.

It was suggested that if, d the distance of the pile from the crest of the slope is less than 0.6m, the length of the embedment should be increase by (0.6-d)m. However the slope effect can be neglected if the distance from the crest of the slope to the pile is equivalent to the pile embedment depth.

Shape of Terrain	**Direction of pull**		
	Towards Field	**Towards** i > 2m	**track** i < 2m
Embankment	0.85	0.95	1.5
Level	1	1.3	2
Cutting	1.5	1.8	2

i : The distance of the foundation from the track

Table 3.4 Values of the coefficient K in the UIC/ORE formula.

Based on these classifications, the K coefficients are as shown in Table 3.3. Foundations embedded on these situations were subjected to two directions of pull, either towards or away from the track. Foundations pulled towards the track were embedded in close proximity and also at greater distances from the track. The final definitive formula established by the UIC/ORE tests for dry cohesionless and coherent soil as in Equation(3.4) and (3.5) respectively was then multiplied by the K coefficient in Table 3.4.

During the tests, UIC/ORE measured horizontal displacements in order to locate the point of rotation. They found that the point appeared to be extremely variable, rising and falling, and becoming stationary only during the approach of failure. However they concluded that the final position of the rotation point is a function of the soil resistance and the installation method of the foundation. They did not investigate the influence of pulling height on the limiting moment.

3.2.4 McCORKLE'S METHOD

In deriving the solution for side bearing pier foundations, McCorkle(1969) based his empirical relationship on several assumptions;

a) the pier is considered to be rigid with an embedment ratio L/D of less than 10.

b) the cross section of the pier remains constant.

c) the pier is to be considered free headed.

d) lateral displacement at ground level is to be limited to about 65mm to 130mm for important and less important structures respectively. This design criterion is under working loads without applying safety factor. At this limit the soil was assumed to behave elastically.

e) vertical forces are neglected due to their insignificance when compared to the horizontal force. In conjunction with the working load, McCorkle employed the Rankine passive pressure (P_p) and the coefficient of the subgrade reaction k_h values, as shown in Table 3.5. If ground water exists at a significant distance above the base of the pier, McCorkle suggested that 60% of the tabulated values of P_p and k_h are to be used.

Soil	Description	P_p (ksf)	k_h (kcf)
Sand	Very loose	< 0.6	< 10
Sand	Loose	0.6 - 1.2	10 - 20
Sand	Medium	1.2 - 2.4	20 - 60
Sand	Dense	2.4 - 4.8	60 - 120
Sand	Very dense	> 4.8	> 120

Table 3.5 Soil properties in McCorkle's design formulae.

Based on these assumptions, the formulae giving pier dimensions and lateral movement at ground line, Δ were developed. McCorkle defined his empirical relations in imperial units as;

$$P_p DL^2 - 2.13FL - 3.2(M + M_{ecc}) = 0 \tag{3.6}$$

and

$$\Delta = \frac{216F}{k_h DL^2}\left(1.33\frac{e}{L} + 1\right) \tag{3.7}$$

where P_p : Passive pressure obtained from table 3.4

D : Diameter of pier in ft.

L : Length of pier in ft.

F : Horizontal force in kips

M : Moment at ground level in ft-kips

e : Pulling height distance from ground in ft

M_{ecc}: Moment from the vertical or eccentric load in ft-kips

Δ : lateral displacement at ground level in inches

k_h : coefficient of horizontal subgrade reaction obtained from Table 3.4.

In the case of a laterally loaded foundation, M_{ecc}=0. Consequently the moment limit value at ground level is;

$$M = \frac{P_p DL^2 - 2.13FL}{3.2} \tag{3.8}$$

No allowance was made for the geometry of the ground profile in his empirical formulae.

3.3 RECENT EXPERIMENTAL WORK

In recent years little attention has been given to investigations into the behaviour of the short pile foundations in sand. Only a few researchers have carried out either full scale or a small model laboratory studies.

An internal report by Balfour Beatty(1986) describes the design of the overhead catenary system for the Tuen Muen Light Railway Transit System(LRT). The loading systems as shown in Figure 3.5 are simplified to a vertical force, horizontal force and bending moment. It was suggested that the factors which affect the stability of the foundations are the loading intensity and duration, foundation dimension, properties of the soil, ground geometry, proximity and the depth of the disturbed soil, ground water table and the construction integrity. They proposed a simple design formula for side bearing foundations in sand as;

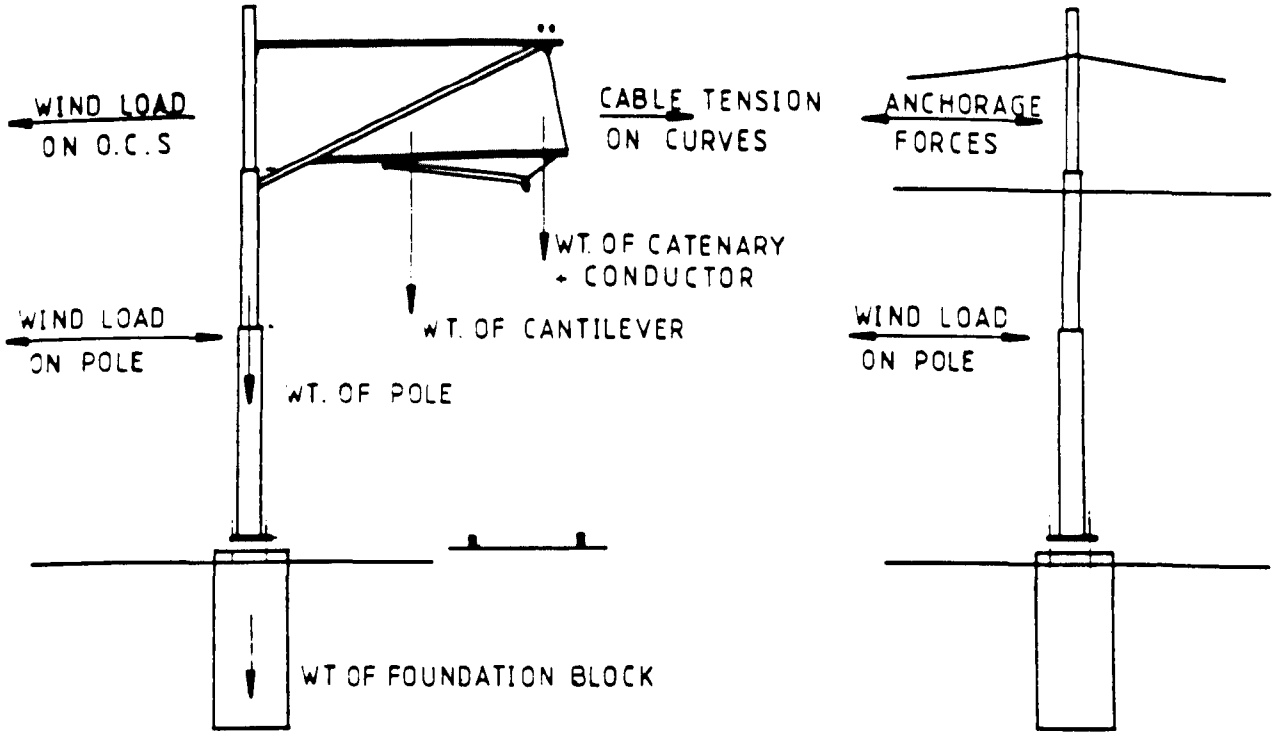

i) FORCES ACTING ON O.C.S. SUPPORT

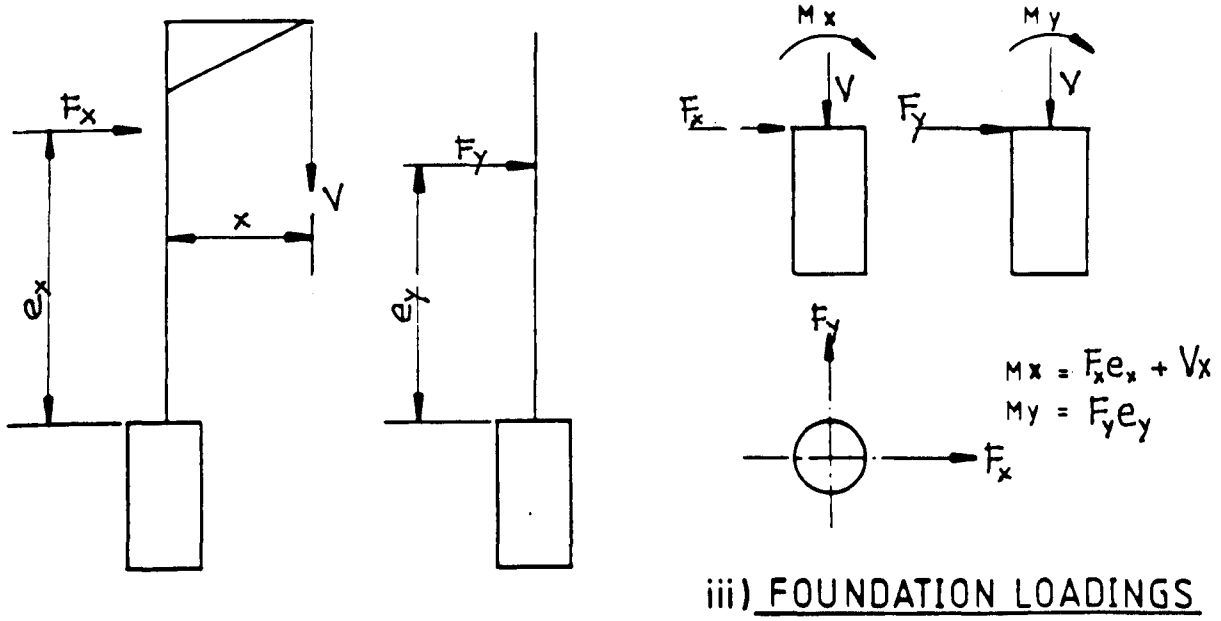

iii) FOUNDATION LOADINGS

ii) SIMPLIFIED SYSTEM OF LOADS.

Figure 3.5 Arrangement of the Balfour Beatty's loading system

$$M_{bb} = \frac{D^3 K'' L}{12} \tag{3.9}$$

where M_{bb} : allowable moment at 2/3 of the effective pile depth(kN.m)

K″ : soil pressure constant ($kN/m^2/m$)

The soil pressure constant K″ was introduced to deal with the varying ground conditions. The specific value of K″ is assessed on site during the installation of the pile and is based upon the experience of design and installation of similar foundations. Balfour Beatty adopted K″ values ranging from 80 to 160$kN/m^2/m$ for loose to dense soil conditions. Empirical factors were proposed to account for the presence of an embankment. It was suggested that for 30° banks, the depth of the foundation should be increased by a factor of 1.25 and for 45° banks it should be increased by a factor of 1.43. The value of K″ should be reduced in the presence of the ground water table. However no specific value was given by Balfour Beatty. A safety factor of three was employed in their design method. In the Balfour Beatty's report comparisons between their empirical relationship and predictions from Czerniak(1957), UIC/ORE(1957), Hansen(1961), Broms(1964) and McCorkle(1969) are made.

In the past most of the model tests conducted ignored the influence of stress level differences between model and prototype. However it is now well recognised that tests on small models usually involve a scale error, as mentioned by several researchers(Ovesen(1979), Leung and Dickin(1984), Franke and Muth(1985),

Steenfelt(1989), Santamarina and Gooding(1989)). Dickin and Wei(1991), reported a pilot study of the moment capacity of short pile foundations employing the centrifugal modelling technique. This limited parametric study was accomplished using small model cylindrical piles 26.7mm in diameter, with lengths ranging from 50mm to 150mm, embedded in a dry clean sand. Two types of sand condition was employed i.e dense and loose. Internal friction angles were obtained from triaxial compression tests and ranged from 46° to 49° and 37° to 40° for dense and loose conditions respectively. The tests were carried out at 37 gravities to simulate the behaviour of prototype piles of 1m diameter. Dickin and Wei found that the moment limit at ground level increased with an increase in pulling height and embedment. However, it was concluded that, at a ratio of pulling height/pile length e/L > 3, the effect of pulling height was less significant. This ratio was considerably less for piles in loose sand. They proposed an empirical formula giving the moment limit at ground level M as;

$$M = \gamma D^3 \frac{L}{K_m}\left(\frac{L}{D} - 1\right) \tag{3.10}$$

where $K_m = 0.24 - 0.08\ln(e/D)$.

However approximation is involved in this relationship which only applies to piles with L/D ratios between 1.9 and 3.2 in the dense sand.

3.4 LIMITATION OF THE EXPERIMENTAL WORK

Different pile and soil parameters were employed by each researcher. Inevitably such a wide range of parameters will contribute to the conflicting conclusions for the moment limit of side bearing foundations. A summary of the parameters employed by previous researchers, is presented in Table 3.5. Shilts et al.(1948) defined their limiting value solely in terms of the soil pressure while others proposed their limiting value in terms of moment limit.

Some of the work reported such as that of UIC/ORE(1957), McCorkle(1969) and Balfour Beatty(1986, 1988) did not include the internal friction angle. Shilts et al.(1948) and Dickin and Wei(1991) obtained their internal friction angle using the triaxial compression test. It is important to select the appropriate value of the internal friction angle, since internal friction angles, vary considerably with stress level (Liem 1988).

Most researchers, testing small models at unit gravity, have not attempted to investigate the effect of stress level. In a small model at unit gravity subjected to a low stress level, an overprediction of the prototype value will result. The centrifugal modelling technique has been used to overcome this error. In a pilot study Dickin and Wei employed the centrifugal modelling technique. This work formed the basis of the present research.

Researchers	Size of pile	Sand		Pile materials	Shape of pile	Depth ranged	Pulling height ranged	Type of test
		γ (kN/m^3)	ϕ					
Shilts et al.	refer T3.1 & 3.2	15.6(lab.test) field test(not mentioned.	not mentioned but obtained from triaxial test	Steel	I beam and gauged steel pipe	380mm - 760mm for lab.test and 1.5m - 2.16m for field test	Not mentioned	Full scale test and laboratory test
Belgian test (IRSIA)	Square 50mm to 400mm. Rectangular 150mm to 300mm length and 100mm to 250mm width. Circular 50mm - 20cm diameter.	14.22 - 15.2	34°	not mentioned	Square, rectangular and circle.	400mm - 700mm	not mentioned	laboratory test

	Circular 0.55m - 1.20m. Prismatic 0.6m - 0.90m width and 1.10m - 1.70m in length	14.71	not mentioned	not mentioned	Cylindrical and prismatic	cylindrical: 1.20m - 3.0m prismatic: 1.5m -1.90m	cylindrical: 6m - 11m prismatic: 6m - 8.5m	Full scale test
McCorkle	not mentioned	not mentioned	not mentioned	not mentioned	Cylindrical pier	L/D < 10	not mentioned	Observation of the full scale test provided by other researchers.
Balfour Beatty	0.6m diameter	Using soil parameters k_h and P as shown in T3.4	not mentioned	Concrete piles	Cylindrical	Maximum length of 2.5m	not mentioned	Full scale observation
Dickin et al.	26.7 mm diameter	14.4 - 16.4	37° - 40° and 46° - 49°	Mild steel coated with sand	Cylindrical	50mm - 150mm	19mm - 150mm	Centrifugal modelling test

Table 3.5 Pile and soil parameters employed by previous researchers

Chapter 3

Empirical factors which are site specific such as the coefficient K to account for soil profile by UIC/ORE, values of P_p and k_h postulated by McCorkle, and the constant soil pressure K″ by Balfour Beatty all question the general application of their formulae.

Limited experimental research has been reported concerning the behaviour of short piles in sand. Thus a comprehensive comparison cannot be made. Due to the present limited data base, the broader application of much of this work is in question.

3.5 SUMMARY OF THE EXPERIMENTAL WORK

Of the research reviewed, Shilts et al.(1948) were concerned mainly with the location of the point of rotation for their field tests. The laboratory tests were designed to investigate pole stability for different vertical cross sectional areas. Due to the variability of pole cross section used, an average of the soil pressure acting on the pole embedded and the location of the pile rotation point were determined in terms of vertical cross section. They also found that the behaviour of a cylindrical pile of radius r is equivalent to that of a square foundation of side $r\sqrt{2}$.

Shilts et al.(1948), IRSIA(1950) and McCorkle(1969) considered only flat ground while UIC/ORE(1957) and Balfour Beatty(1986, 1988) included the influence of the ground profile in their formulation. However, the IRSIA formula does not take into account the shearing force (pulling force F). Only McCorkle proposed predictions for lateral displacement empirically.

Whilst Shilts et al.,IRSIA, UIC/ORE and Dickin and Wei, give the ultimate limiting capacity to which a safety factor must be applied, McCorkle and Balfour Beatty suggested an allowable limiting value where factor of safety was considered in their formulae. However no suggested value of factor of safety was put forward by McCorkle while Balfour Beatty proposed a factor of safety of three in their design method.

Empirical relationships, based on small model tests, have been proven to overpredict prototype behaviour because the friction angle decreases with stress level. The centrifuge modelling technique is the easiest way of predicting prototype behaviour economically, and the results can be used to examine all existing theoretical and empirical relationships for full scale laterally loaded short piles.

CHAPTER FOUR

COMPARISON OF PREVIOUS THEORETICAL AND EXPERIMENTAL WORK

4.1 INTRODUCTION

Most of the research work reported in Chapters Two and Three concerning the overturning resistance of piles in sand leads to either a limiting moment at ground level or a permissible moment at ground level, a limiting soil resistance or a limiting horizontal load. Thus no consistency in determining the limiting value is encountered. Work such as that of Terzaghi(1943), Shilts et al.(1948), and Meyerhof et al.(1981,83,88) offer the limiting soil resistance as a design factor, whereas Broms(1964) and Hansen(1961) define a limiting lateral load. However IRSIA(1950), UIC/ORE(1957) and Dickin and Wei(1991) define their limiting value in terms of moment at ground level while Roscoe(1957), McCorkle(1969) and Balfour Beatty(1986, 1988) employed a permissible moment for their design criteria.

Broms(1964) represents his limit resistance value in terms of non dimensional parameters while others represent it in dimensional form. Due to the diversity in the interpretation of a suitable design criterion, it is difficult to make a direct comparison between all existing formulae. However, in order to achieve a direct comparison, the

value of moment limit at ground level will initially be considered. Calculations are performed for the full range of embedment lengths and for the pulling heights encountered in this research.

4.2 MOMENT LIMIT AT GROUND LEVEL BASED ON THEORETICAL SOLUTIONS

Most of the theoretical solutions are derived in the form of limiting soil resistance. The author will attempt to make a direct comparison wherever possible by converting this value to a moment at ground level. Terzaghi(1943), on analysing a rigid bulkhead, suggested that, in order to obtain the horizontal external force, it is required that the total horizontal soil reaction per unit length of the rigid bulkhead should be equal to the horizontal external force and that the moment at any point should be equal to zero. Assuming Terzaghi's interpretation is valid for a pile embedded in sand which is resisting lateral loading due to the geometrical similarity, the author will assume that the limiting soil resistance will be equivalent to the external force. As proposed by other researchers such as Terzaghi(1943), Czerniak(1957), the soil resistance will be assumed to increase linearly with the embedment length of the pile. Based on McCorkle's(1969) suggestion, the moment at ground level will simply be derived from the product of the external pulling force and the pulling height without adding the

distance from the ground line to the soil reaction which develops from the movement of the pile.

4.2.1 TERZAGHI'S METHOD

The greatest value for the soil pressure p at any depth z that can be assumed is;

$$p_{z\,max} = \gamma z(K_p - K_a)$$

Hence

$$F = D\int_0^L p\,dz$$

and

$$M = D\int_0^L pz\,dz$$

Since p cannot be greater than $p_{z\,max}$, thus maximum moment at ground level will be;

$$M = \frac{\gamma DL^3}{3}(K_p - K_a)$$

where K_p and K_a are the coefficients of Rankine passive and active earth pressure respectively. Note that this is the Author's formula based on a simplification of Terzaghi's approach.

4.2.2 ROSCOE'S METHOD

From equation (2.19), due to the insignificance of the vertical load and self weight when compared to the horizontal load;

$$M_{pm} = \frac{(K_{pr} - K_{ar})\gamma DL^3}{12}$$

where K_{pr} and K_{ar} are the coefficient of the passive and active pressure for a rough surface. Values of K_{pr} and K_{ar} were taken from CP2(1951).

4.2.3 HANSEN'S METHOD

Hansen's method includes a procedure to locate the point of rotation using trial and error. He used equation(2.21) to predict the location of the rotation point, thus equation(2.22) will give the limiting horizontal force. This force will then be multiplied by its distance above the ground surface to obtain the limiting moment at ground level. In this comparison, a back calculation will be performed where the position of the point of rotation obtained from the author's experimental data will be employed to obtain the limiting moment value from Hansen's formulae.

4.2.4 BROMS' METHOD

From equation (2.27)

$$F = \frac{\gamma D L^3 K_p}{2(e + L)}$$

where K_p is coefficient of Rankine passive pressure.

Therefore the moment at ground level will be M = Fe, thus;

$$M = \frac{\gamma D L^3 K_p e}{2(e + L)}$$

Broms proposed using the submerged unit weight in the above equation if the ground water level was close to the surface of the ground.

4.2.5 MEYERHOF ET AL.'S METHOD

From equation(2.29), the ultimate soil resistance for a rigid pile is;

$$P_u = 0.12\gamma L^2(K_p - K_a)r_b S_{fu}$$

where

$$r_b = \frac{1}{1 + 1.4\frac{e}{L}}$$

and S_{fu} is obtain from Figure 2.13.

Considering Terzaghi's(1943) assumption as in section 4.2 earlier, thus $P_u = F$. Since M = Fe, therefore the limiting moment value at ground level will be;

$$M = 0.12\gamma e L^2 r_b S_{fu}(K_p - K_a)$$

However Meyerhof et al.(1988) later revised his earlier equation by neglecting the ultimate shape factor S_{fu} and suggest that interface friction should be taken into account. This gives;

$$M = 0.12\gamma e L^2 r_b (K_{pr} - K_{ar})$$

An interface friction angle $\delta=\phi/3$ was used in determining the coefficients of the earth pressure.

4.2.6 SELECTION OF EARTH PRESSURE COEFFICIENTS IN ANALYSIS

Most of the researchers mentioned previously assumed a perfectly smooth condition between the surface of the pile and the sand and thus generally the coefficient of the earth pressure was computed by smooth Rankine theory. However, such a condition is unrealistic in soils. There will invariably be friction between the surface of the pile and the sand. Roscoe(1957) and Meyerhof et al.(1988) included the effect of the surface friction in their analysis,the former assuming $\delta=20^{\circ}$ for a concrete/sand interface and the latter $\delta=\phi/3$ respectively. CP2(1951) recommended that the maximum value of δ should lie within the range $\phi/2$ to $2\phi/3$. Thus δ is a function of ϕ where its value cannot be greater than ϕ. Design parameters proposed by CP2 for δ are;

a) Timber, steel and precast concrete against sand, $\delta=\phi/2$

b) Cast in situ concrete against sand, $\delta=2\phi/3$

Based on Coulomb's wedge theory, the passive and active earth pressure coefficients for a rough surface respectively are;

$$K_{pr} = \frac{Cos^2\phi}{Cos\delta\left[1-\sqrt{\frac{Sin(\phi-\delta)Sin\phi}{Cos\delta}}\right]^2}$$

and

$$K_{ar} = \frac{Cos^2\phi}{Cos\delta\left[1 + \sqrt{\frac{Sin(\delta + \phi)Sin\phi}{Cos\delta}}\right]^2}$$

When δ increases in the case of passive pressure, Coulomb's computation gives a high value of K_{pr} especially for a high internal friction angle as shown in Table 4.1.

Value of δ	Value of ϕ			
	25	30	35	40
0	2.5	3.0	3.7	4.6
10	3.3	4.1	5.3	6.9
20	4.6	6.1	8.3	11.8
30	-	10.1	15.3	24.9

Table 4.1 Coefficient of passive earth pressure K_{pr} on rough wall based on Coulomb's equation.

This in fact overestimates the passive pressure that the soil can mobilised. Thus CP2 gives the values of K_{pr} shown in Table 4.2 based on curved passive failure surfaces.

Value of δ	Value of ϕ			
	25	30	35	40
0	2.5	3.0	3.7	4.6
10	3.1	4.0	4.8	6.5
20	3.7	4.9	6.0	8.8
30	-	5.8	7.3	11.4

Table 4.2 Coefficient of passive earth pressure K_{pr} on rough wall (CP2 (1951))

CP2 suggested that intermediate values can be found with sufficient accuracy by linear interpolation. Comparison between Coulomb and CP2 values is shown in Figure 4.1.

Value of δ	Value of ϕ				
	25	30	35	40	45
0	0.41	0.33	0.27	0.22	0.17
10	0.37	0.31	0.25	0.20	0.16
20	0.34	0.28	0.23	0.19	0.15
30	-	0.26	0.21	0.19	0.14

Table 4.3 Coefficient of active earth pressure K_{ar} on rough wall (CP2 (1951))

In case of a short pile as in this research, only a small fraction of δ is normally mobilised due to the small weight of the pile and its contact surface area. Smith(1982) argued that when a small amount of friction is developed between the soil and the pile surface, the use of Rankine earth theory is fully justified. Moreover, Leung(1981) calculated that the value of $\delta \geq \phi/2$ and $\phi > 40°$ based on Mueller-Breslau(1906) method for the effect on vertical anchor plate, shows an unrealistically high value of K_{pr}. For comparison purposes the value of K_{pr} and K_{ar} based on CP2 will be employed in both Roscoe's and Meyerhof et al.'s equation.

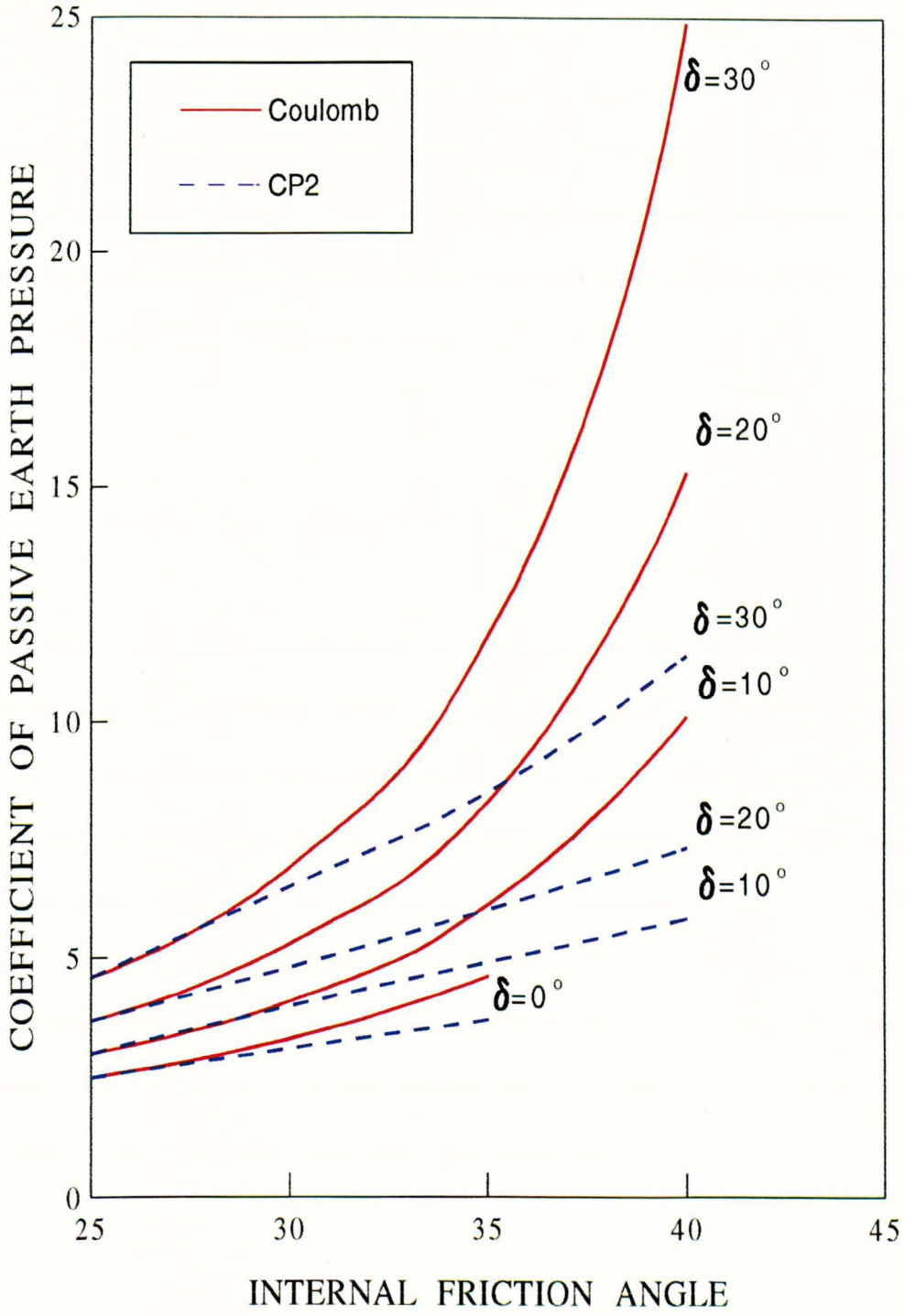

Figure 4.1 Comparison of Coefficient of passive earth pressure between Coulomb and CP2(1951) for rough surface

4.3 MOMENT AT GROUND LEVEL BASED ON EMPIRICAL SOLUTIONS

Due to the complex behaviour of piles embedded in sand, empirical methods may offer a better way of determining the limiting lateral bearing capacity. However, the difference in stress level between small models and the full scale foundation should be considered. Scaling errors will arise in predicting prototype behaviour from small model tests. Empirical expressions for moment, based on both field and small model tests are derived in terms of moment at ground level.

4.3.1 SHILTS' ET AL. STUDIES

Shilts et al. defined the limiting resistance on the post using an average soil pressure. Due to the variability of the cross sectional area of the posts used, they defined the distance of the soil reaction from the ground surface in terms of vertical cross sectional area. Small models were tested in the laboratory to obtain a relationship between the point of rotation and the vertical cross sectional area of the post. It has been noted that the point of rotation is at a distance of 0.324 of the pole vertical cross sectional area from the base of the foundation. Difficulties when compared with other researchers work arise due to the site specific nature of this work. Thus no attempt will be made to compare their work with other research.

4.3.2 THE IRSIA TESTS

As stated in equation(3.3), the IRSIA described the moment at ground level as;

$$M_B = (1 - E_p)(M_r)_p$$

where $(M_r)_p$ is the pure overturning moment without considering the effect of shear resistance and $(1 - E_p)$ is a correction factor which takes into account the depth of unconsolidated soil. Definition of pure overturning moment has been explained earlier in Chapter Three.

4.3.3 THE UIC/ORE FORMULAE

A definitive formula in terms of moment at ground level was described as the Fe-limit. The moment at ground level was based on the IRSIA formula. However after statistical corrections which included the effect of ground geometry and the embedment length, the definitive formula for the moment at ground level for piles in cohesive soil or damp sand which exhibits some cohesion due to capillarity effects;

$$Fe\text{-}Limit = K\left[27.45(M_B^{0.67})\right]$$

However in the case of dry dune sand, the expression was;

$$Fe\text{-}Limit = K\left[15.75(M_B^{0.72})\right]$$

where the value of coefficient K is shown in Table 3.4 and M is in Kg.m.

4.3.4 McCORKLE'S FORMULAE

Equation (3.6) expresses the moment at ground level in imperial units. The values of passive pressure and the subgrade reaction were shown in Table 3.4. For consistency, McCorkle's formula converted into SI units is follows;

$$M_{pm} = \frac{1.4P_pDL^2 - 2.92FL}{4.39}$$

where P_p is in kN/m^2, F is in kN and L,D are in metres. While employing McCorkle's method for comparison work, P_p values of 28.55kN/m^2 and 228.38kN/m^2 will be applied into the calculation for pile embedded in loose and dense sand respectively.

4.3.5 BALFOUR BEATTY'S FORMULA

Balfour Beatty's allowable moment at two thirds of the depth of the embedded length is given by equation (3.9). They adopted a soil pressure constant K" in the computation of the moment at two third of the embedment length. Assuming that the maximum moment varies linearly to zero at the level of the applied horizontal load, the moment at ground level will be;

$$M_{pm} = M_{bb}\left[\frac{e}{e + \frac{2}{3}L}\right]$$

where M_{bb} is the permissible moment at two third of the embedded length. K″ of 80kN/m²/m and 160kN/m²/m will be used for pile in loose and dense sand respectively in the computation based on Balfour Beatty's equations.

4.3.6 DICKIN AND WEI'S FORMULA

A pilot centrifugal study reported by Dickin and Wei(1990), using small model piles which experience a high stress level shows the possibility of predicting behaviour of short piles embedded in sand from small models. An empirical formula for the moment at ground level was proposed as;

$$M = \gamma D^3 \frac{L}{K_m}\left(\frac{L}{D} - 1\right)$$

where

$$K_m = 0.24 - 0.08\ln(\frac{e}{D})$$

Since only a limited number of tests were conducted over a limited range of pulling height, the relationship can only be applied to piles in dense sand where the pile embedment ratio is between 1.9 and 3.

4.4 LIMITATIONS OF THE COMPARISONS

Moments at ground level for a single pile are compared at various embedment ratios, L/D between 1 and 5 and pulling height ratios e/L between 1 and 5 for two different soil densities. Internal friction angles from triaxial compression tests are adopted and comparisons are made in terms of prototype values. Although plane strain friction angles were available for Erith sand(see Figure 5.2), Dickin and Leung(1985) found that the use of these high ϕ values in Rankine analyses considerably overpredicted observation for continuous vertical anchors. Rowe's(1969) progressivity index for passive pressure produces ϕ values very close to those in triaxial compression which, in the case of vertical anchors yielded theoretical values close to observation. Dry unit weights are employed in the formulae since the model study is in dry sand. Values from Hansen's method are based on back-calculation where point of rotation obtained from the author's experiment is used to derive the moment at ground level. Thus there is a possibility where some of the values plot on the comparison graph will not contribute to a smooth connection of points. However for a better presentation, an average curve value of limiting moment at ground level will be plotted in this comparison work.

Values of moment at ground level calculated from the exixting theories are as shown in Table 4.4 and 4.5 for piles embedded in dense and loose sand respectively.

Chapter 4

++CONTINUE

e/L=1		Pp=228.38*	K″=160**				
L/D	Broms	McCorkle	B.Beatty	Meyerhof(δ=0°)	Meyerhof(δ=ϕ/3)	Hansen	Dickin
1	29.33	43.7	4	9.21	7	69.52	
2	234.638	174.959	32	54.7	35.38	345.911	177.731
3	791.903	393.658	108	230.756	87.266	1170.769	646.896
4	1780.775	699.836	256	975.912	162.974	2464.99	
5	3388.952	1093.494	500	1987.531	262.605	4437.833	
e/L=2							
1	39.106	54.656	5	11.628	8.846	48.488	
2	312.851	218.624	40	69.092	40.744	396.388	254.074
3	1055.871	491.904	135	291.482	96.549	1343.304	1018.009
4	2374.366	874.496	320	1232.731	176.333	4238.066	
5	4518.603	1366.4	625	2510.566	280.112	5724.95	

++ CONTINUE

NB: All moment values stated in the table are in kN.m

* : Unit in kN/m^2

**: Unit in $kN/m^2/m$

++CONTINUE

e/L=3		Pp=228.38*	K″=160**				
L/D	Broms	McCorkle	B.Beatty	Meyerhof(δ=0°)	Meyerhof(δ=ϕ/3)	Hansen	Dickin
1	43.995	59.615	5.455	12.746	9.696	71.392	
2	351.957	238.462	43.636	75.735	42.911	402.234	339.336
3	1187.855	536.539	147.273	319.509	100.099		1532.184
4	2671.162	953.847	349.091	1351.263	181.286	2986.383	
5	5083.428	1490.387	681.818	2751.966	286.478	9064.92	
e/L=4							
1	46.928	62.449	5.714	13.39	10.186	61.475	
2	375.421	249.795	45.714	79.56	44.083	426.135	
3	1267.046	562.039	154.286	335.646	101.973	1538.754	
4	2849.239	999.18	365.714	1419.509	183.868	3256.579	
5	5422.323	1561.219	714.286	2890.955	289.771		

++ CONTINUE

NB: All moment values stated in the table are in kN.m

* : Unit in kN/m^2

**: Unit in $kN/m^2/m$

++CONTINUE

e/L=5		Pp=228.38*	K″=160**				
L/D	Broms	McCorkle	B.Beatty	Meyerhof(δ=0°)	Meyerhof(δ=ϕ/3)	Hansen	Dickin
1	48.883	64.282	5.882	13.81	10.504	55.12	
2	391.063	257.127	47.059	82.047	44.818	541.335	
3	1319.839	578.536	158.824	346.134	103.132	1785.464	
4	2967.958	1028.509	376.471	1463.868	185.453		
5	5648.253	1607.045	735.294	2981.297	291.783		

++CONTINUE

L/D	IRSIA	UIC/ORE	Roscoe(δ = 0)	Roscoe(δ=20°)	Terzaghi
1	44.63	66.48	9.589	12.983	38.356
2	257.95	235.1	76.711	103.867	306.845
3	921.06	587.81	258.901	350.55	1035.602
4	2460.02	1192.41	580.9	830.933	2323.601
5	5316.73	2076.88	1104.184	1622.917	4416.74

NB: All moment values stated in the table are in kN.m
* : Unit in kN/m^2
**: Unit in $kN/m^2/m$

Table 4.4 Prototype moment at ground level calculated from the existing theories for pile embedded in dense sand

++CONTINUE

e/L=1		P_p= 28.55*	K″=60**			
L/D	Broms	McCorkle	B.Beatty	Meyerhof(δ=0)	Meyerhof(δ=ϕ/3	Hansen
1	16.184	5.469	3	3.69	4.118	
2	129.476	21.871	24	44.316	20.809	135.64
3	436.981	49.211	81	166.186	51.322	362.548
4	1012.722	87.486	192	461.062	95.846	945.306
5	1977.972	136.696	375	1050.598	154.44	
e/L=2						
1	21.579	6.832	3.75	4.66	5.202	
2	172.634	27.33	30	55.979	23.962	135.244
3	582.461	61.492	101.25	209.918	56.781	464.359
4	1350.296	109.32	240	582.395	103.703	1476.68
5	2637.297	170.812	468.75	1327.07	164.736	
5	3296.621	200.895	551.471	1575.897	171.6	

NB: All moment values stated in the table are in kN.m

* : Unit in kN/m^2

**: Unit in $kN/m^2/m$

++CONTINUE

e/L=3		P_p= 28.55*	K″=60**			
L/D	Broms	McCorkle	B.Beatty	Meyerhof(δ=0)	Meyerhof(δ=ϕ/3	Hansen
1	24.277	7.452	4.091	5.11	5.702	
2	194.214	29.81	32.727	61.361	25.236	142.205
3	655.471	67.072	110.455	230.104	58.869	517.502
4	1519.083	119.239	261.818	614.75	106.616	1346.92
5	2966.959	186.311	511.364	1454.674	168.48	3428.64
e/L=4						
1	25.895	7.807	4.286	5.372	5.99	
2	207.161	31.227	34.286	64.46	25.926	
3	699.169	70.26	115.714	241.726	59.971	669.927
4	1620.355	124.906	274.286	670.64	108.134	1450.203
5	3164.756	195.166	535.714	1528.142	170.417	

NB: All moment values stated in the table are in kN.m

* : Unit in kN/m^2

**: Unit in $kN/m^2/m$

++CONTINUE

e/L=5		P_p= 28.55*	K″=60**			
L/D	Broms	McCorkle	B.Beatty	Meyerhof(δ=0)	Meyerhof(δ=ϕ/3	Hansen
1	26.974	8.036	4.412	5.54	6.178	
2	215.793	32.143	35.294	66.475	26.358	
3	728.301	72.322	119.118	249.28	60.653	698.843
4	1687.87	128.573	282.353	691.594	109.067	
5	3296.621	200.895	551.471	1575.897	171.6	

++CONTINUE

L/D	IRSIA	UIC/ORE	Roscoe(δ=0)	Roscoe(δ=20°)	Terzaghi
1	41.51	63.1	5.129	7.44	20.517
2	235.99	220.51	41.034	59.52	164.135
3	861.54	560.2	138.489	200.88	553.955
4	2313.28	1140.75	320.182	476.16	1280.729
5	4947.33	1971.95	625.356	930	2501.424

NB: All moment values stated in the table are in kN.m
* : Unit in kN/m^2
**: Unit in $kN/m^2/m$

Table 4.5 Prototype moment at ground level calculated from existing theories for pile embedded in loose sand

4.5 INTERPRETATION OF PREVIOUS THEORIES AND EXPERIMENTAL WORK

As mentioned in the previous chapter, the different parameters used in the design methods proposed by different researchers lead to the difficulties in making comparisons. Moreover sufficient information on the strength properties and unit weights of the supporting soil are not always available. For consistency in comparing previous work, parameters based on the author's experimental work are employed. Flat terrain with soil in loose and dense packings are considered. The loose packing unit weight is 14.4kN/m^3 and dense packing is 16.4kN/m^3. The internal friction angle is the drained triaxial compression value which varies from 47.5° to 49° for the dense packing and from 39° to 39.5° for the loose packing depending on the stress level around a particular pile. For the theories of Roscoe(1957) and Meyerhof et al.(1988), coefficients of passive and active pressure for the rough surface based on CP2(1951) from Table 4.2 and 4.3 are employed. Coefficient K_q(see Figure 2.6) is used in computations with Hansen's(1961) theory. Calculations are carried out for a pile with diameter of 1m and embedment length ranging from 1m to 5m and pulling height ratio ranging from 1 to 5 are employed.

4.5.1 VARIATION OF MOMENT AT GROUND LEVEL WITH EMBEDMENT RATIO

For a better comparison between the existing theories, the prototype moment at ground level will be employed. This is due to the fact that difficulties arises in obtaining a consistent line using the dimensionless moment factor.

Variations of moment at ground level and embedment ratio for piles in dense sand for different pulling height ratios are shown in Figures 4.2(a) to 4.2(e). An exponential relationship is generally observed for all design methods considered. Hansen's method exhibits the highest values compared with most other researchers for e/L>2, except Broms which generally gives similar values. However when e/L equals 3 and 4, Hansen's moment value shows a very close agreement with Broms' values. This suggests that Broms' approach is equivalent to assuming that Brinch Hansen's $K_q=3K_p$ for all depths as pointed out by Poulos and Davis(1980). However Broms approach is much simpler than using Hansen's variable factor K_q.

The expression of Meyerhof et al.(1981) employing a shape factor tends to give average values compared to other values for all pulling heights. They showed that the shape factor is dependent on the embedded length and friction angle. However values obtained from their later equation (Meyerhof et al.(1988)) for rough surface where

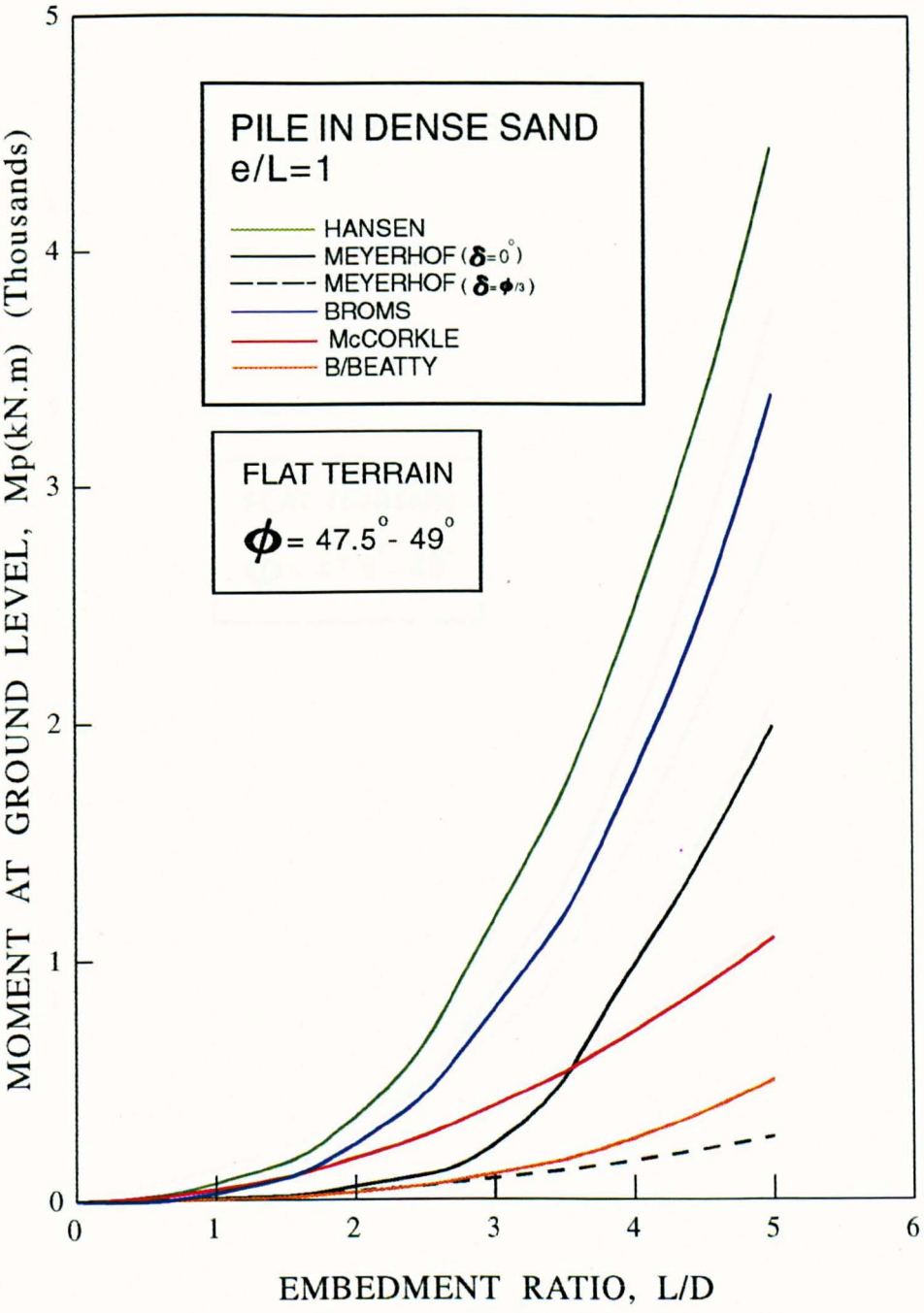

Figure 4.2(a) Variation of prototype moment at ground level with embedment ratio for pile embedded in dense sand.

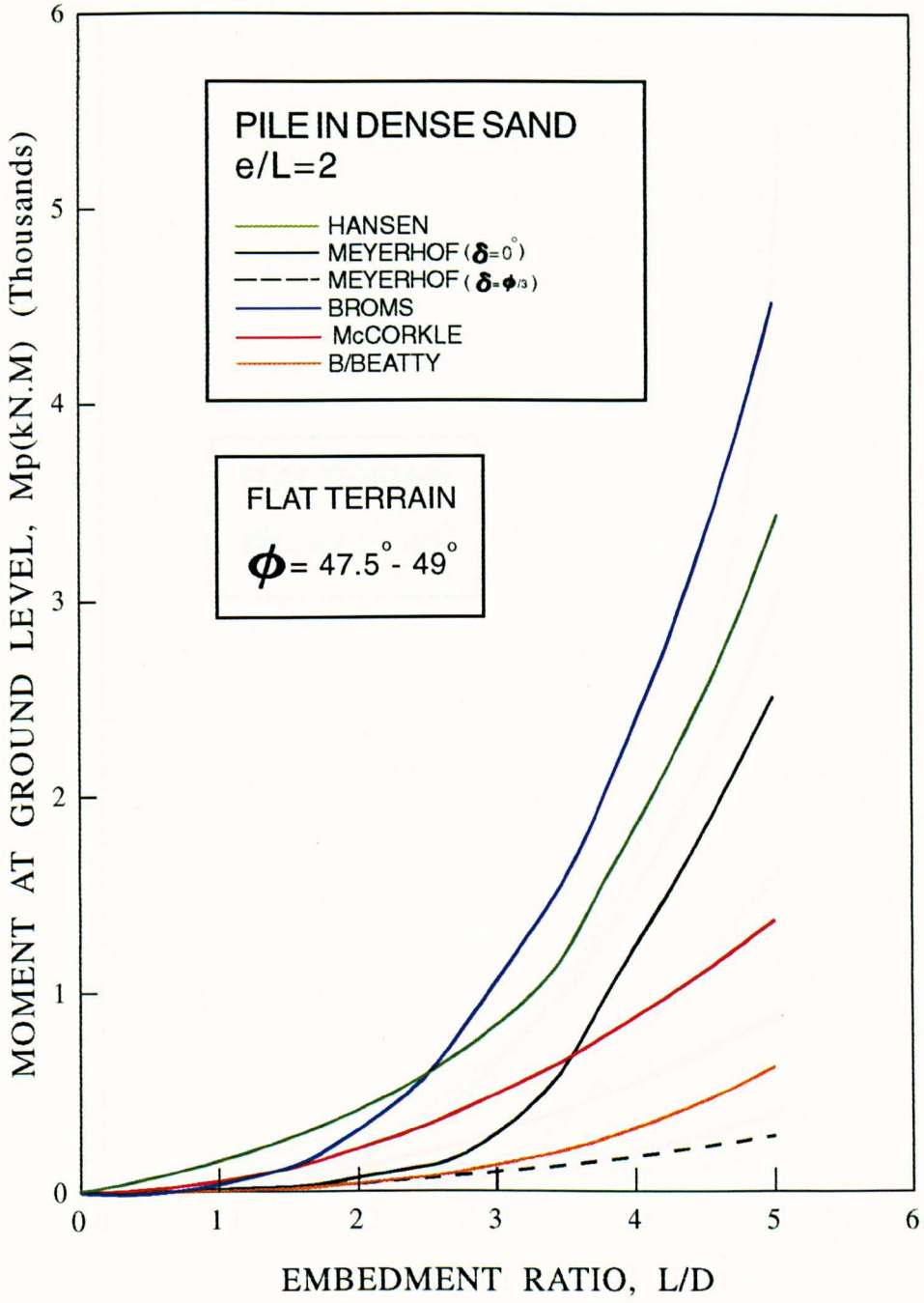

Figure 4.2(b) Variation of prototype moment at ground level with embedment ratio for pile embedded in dense sand.

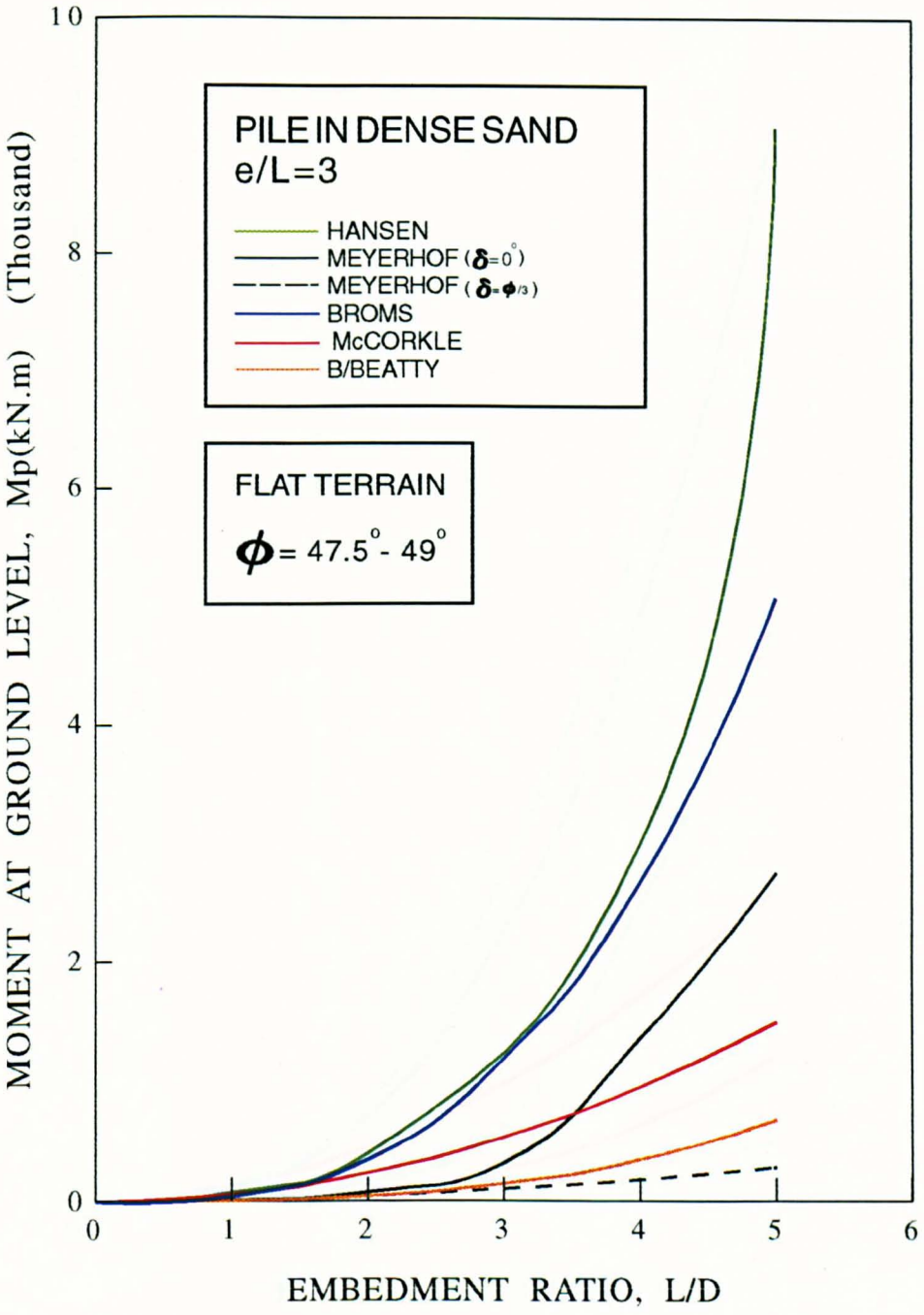

Figure 4.2(c) Variation of prototype moment at ground level with embedment ratio for pile embedded in dense sand.

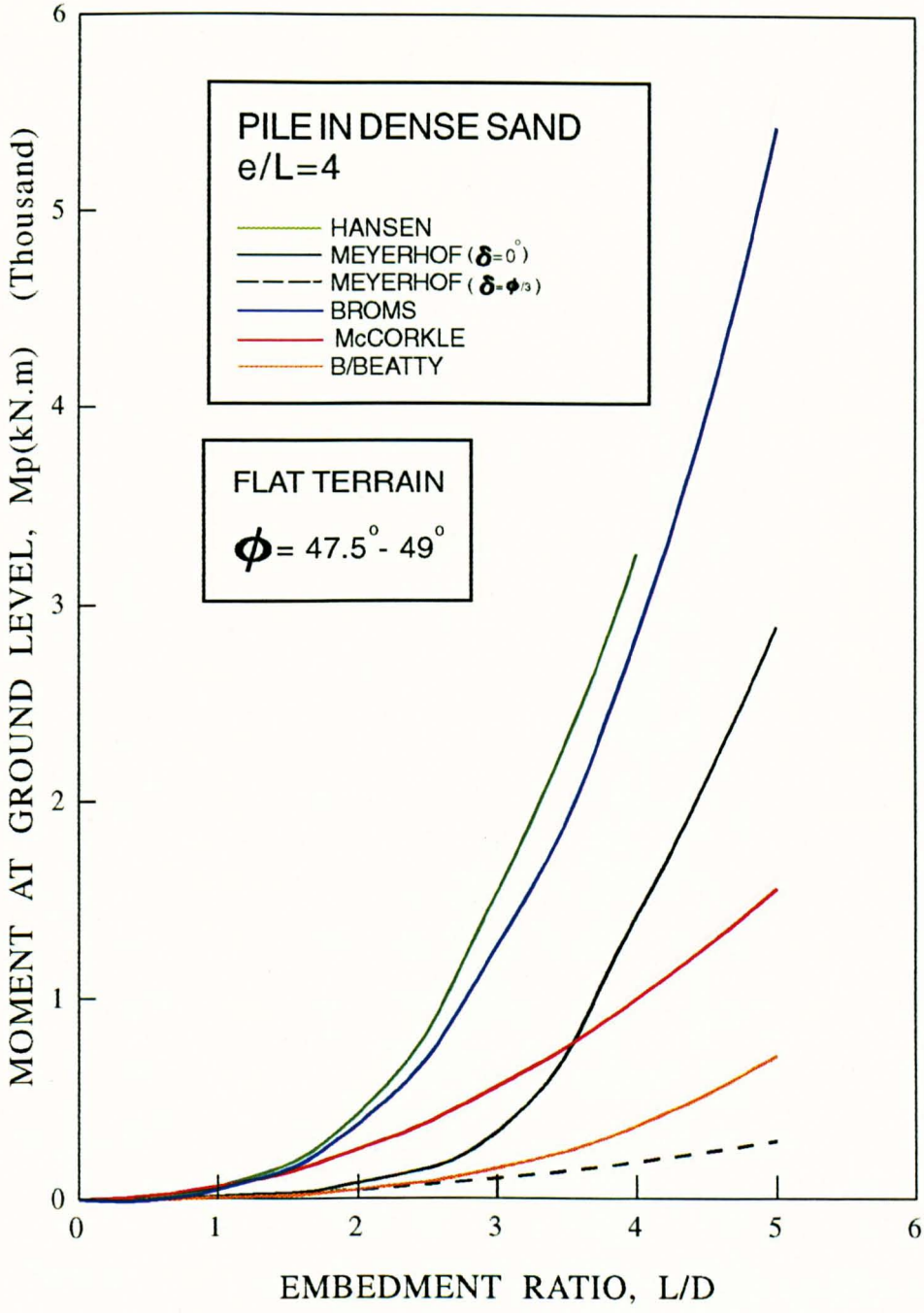

Figure 4.2(d) Variation of prototype moment at ground level with embedment ratio for pile embedded in dense sand.

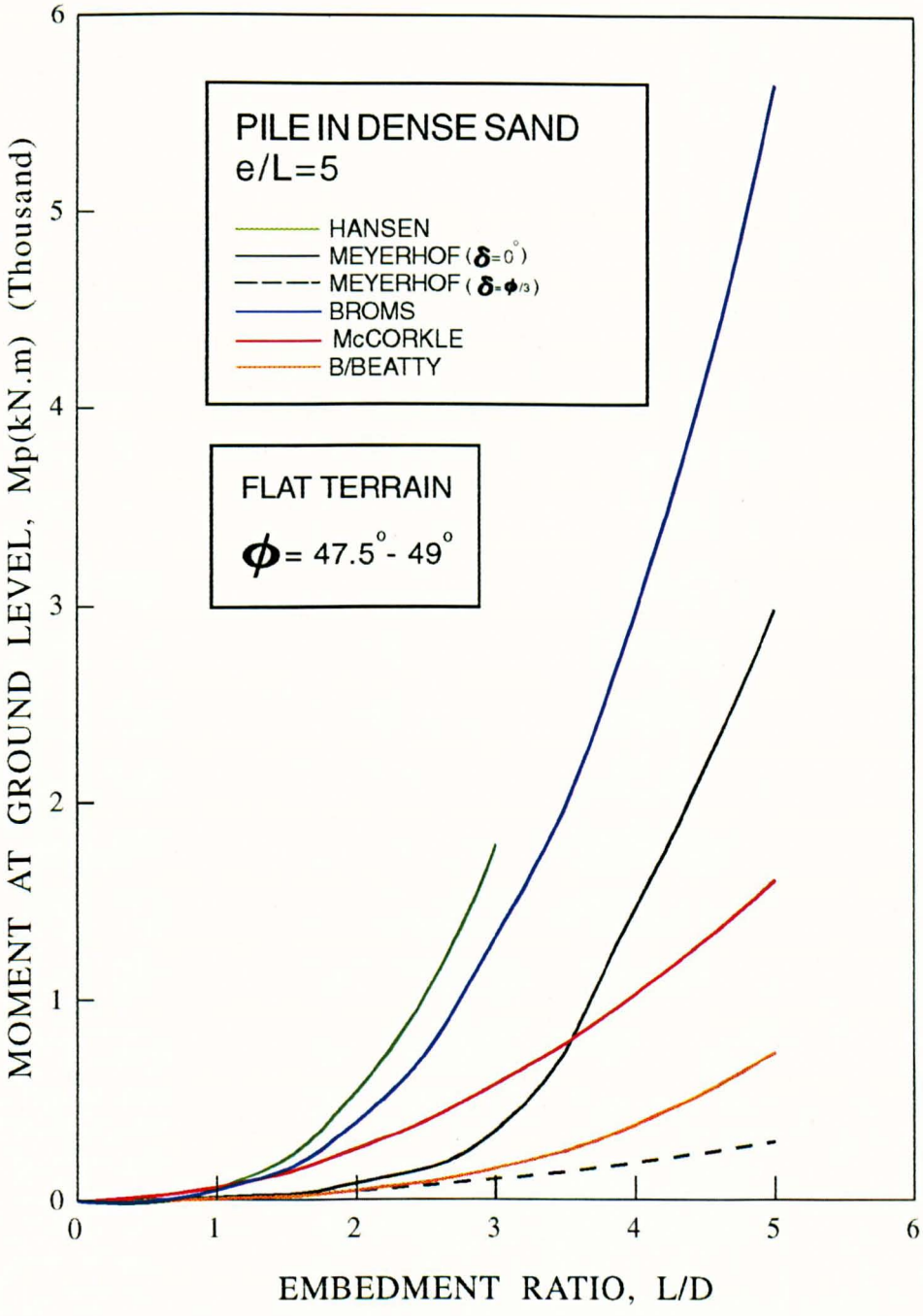

Figure 4.2(e) Variation of prototype moment at ground level with embedment ratio for pile embedded in dense sand.

interface friction was assumed to be equal to $\phi/3$, are conservative compared to other researchers. This would be expected since their later equation does not include a shape factor.

The equations of Balfour Beatty and McCorkle produce allowable moment values. Since the factors such as passive pressure and soil pressure constant involved in the McCorkle and Balfour Beatty formulae respectively vary even for a similar soil packing, maximum values were employed in conjunction with their calculations. Thus in McCorkle's calculation for dense sand, a passive pressure of 228.38kN/m^2 was employed while a soil pressure constant of 160kN/m^2/m was used in the Balfour Beatty computation. Generally Balfour Beatty's allowable moment values give a fairly good agreement with Meyerhof's ultimate moment values for $\delta=\phi/3$, while McCorkle's allowable moment values gives fairly good agreement with Meyerhof's ultimate moment using a shape factor. The McCorkle and Balfour Beatty ultimate values would be higher than those predicted using Meyerhof's method assuming a reasonable safety factor is implicit in their equations. Generally considerable increase in moment at ground level occurs when a pile's embedded length is greater than 3. Meyerhof et al.'s(1981, 1988) values appear to be the most conservative of all the design methods providing a safety factor is used in the McCorkle and Balfour Beatty equations.

Figures 4.2(f) to 4.2(j) shows a similar variation as figure 4.2(a) to 4.2(e) for a pile embedded in loose sand. However lower values than for the dense packing would be expected. No rigid conclusion can be made for Hansen's theory for pile embedded in

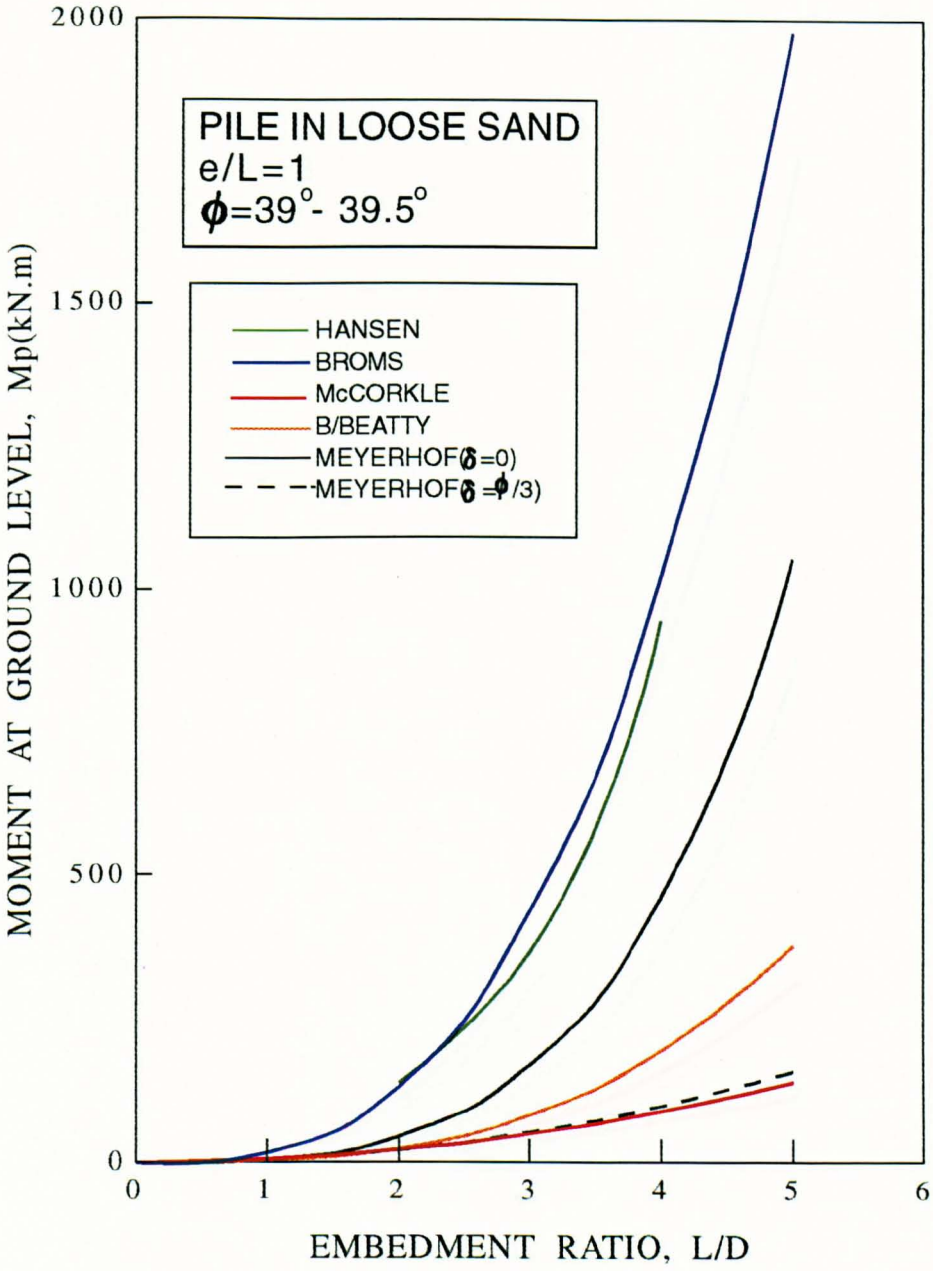

Figure 4.2(f) Variation of prototype moment at ground level with pulling height ratio for pile embedded in loose sand

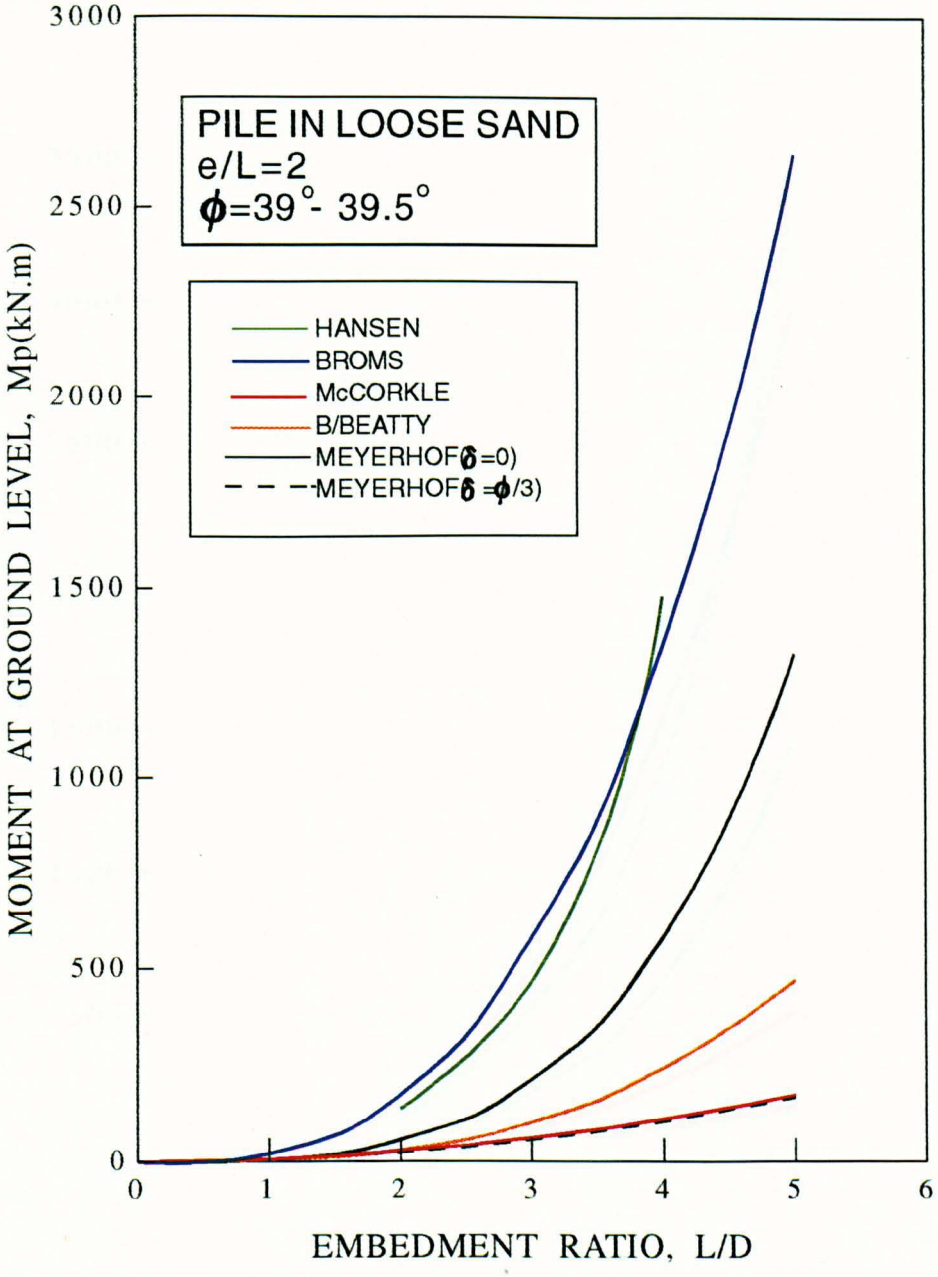

Figure 4.2(g) Variation of prototype moment at ground level with pulling height ratio for pile embedded in loose sand

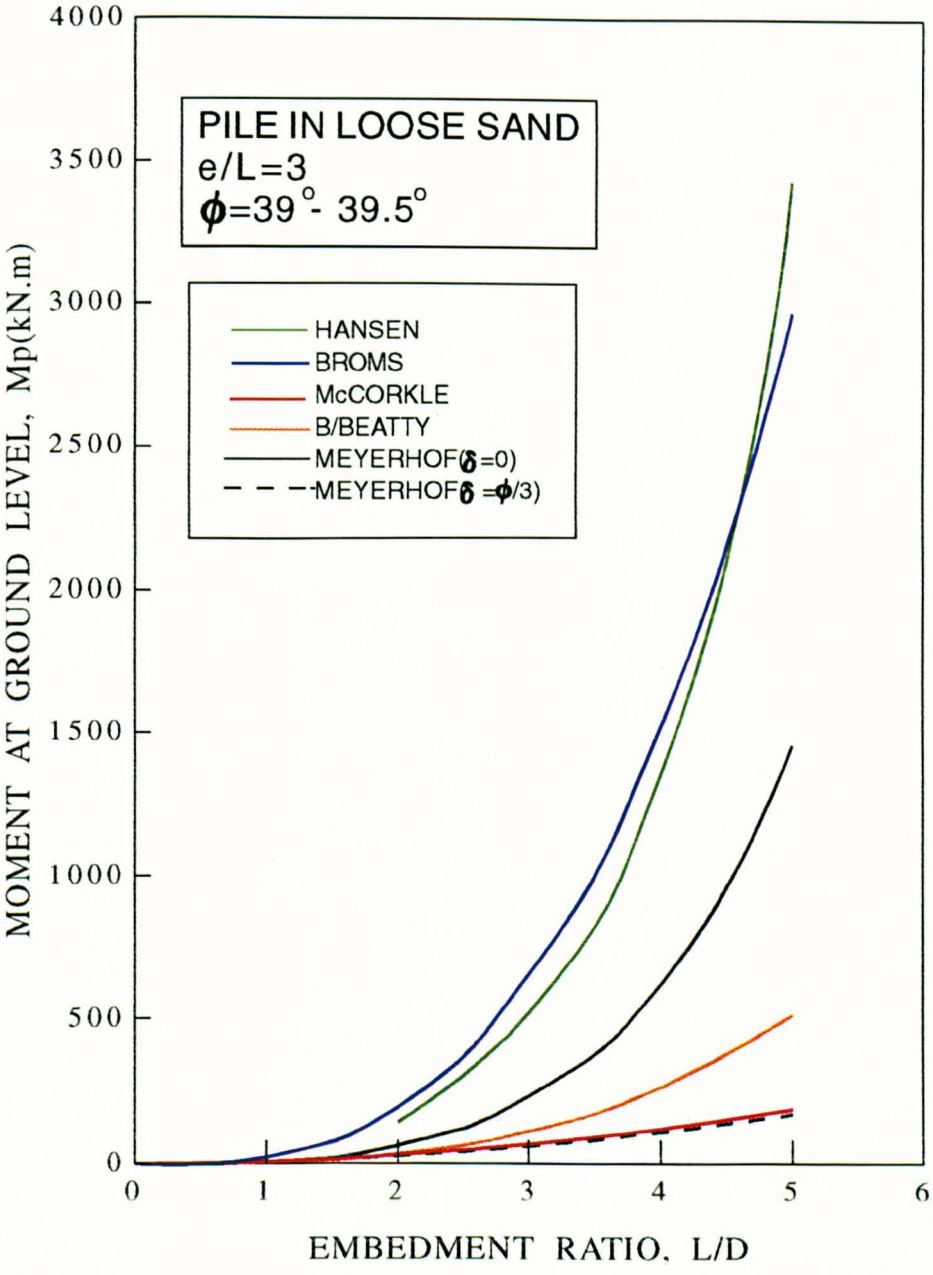

Figure 4.2(h) Variation of prototype moment at ground level with pulling height ratio for pile embedded in loose sand

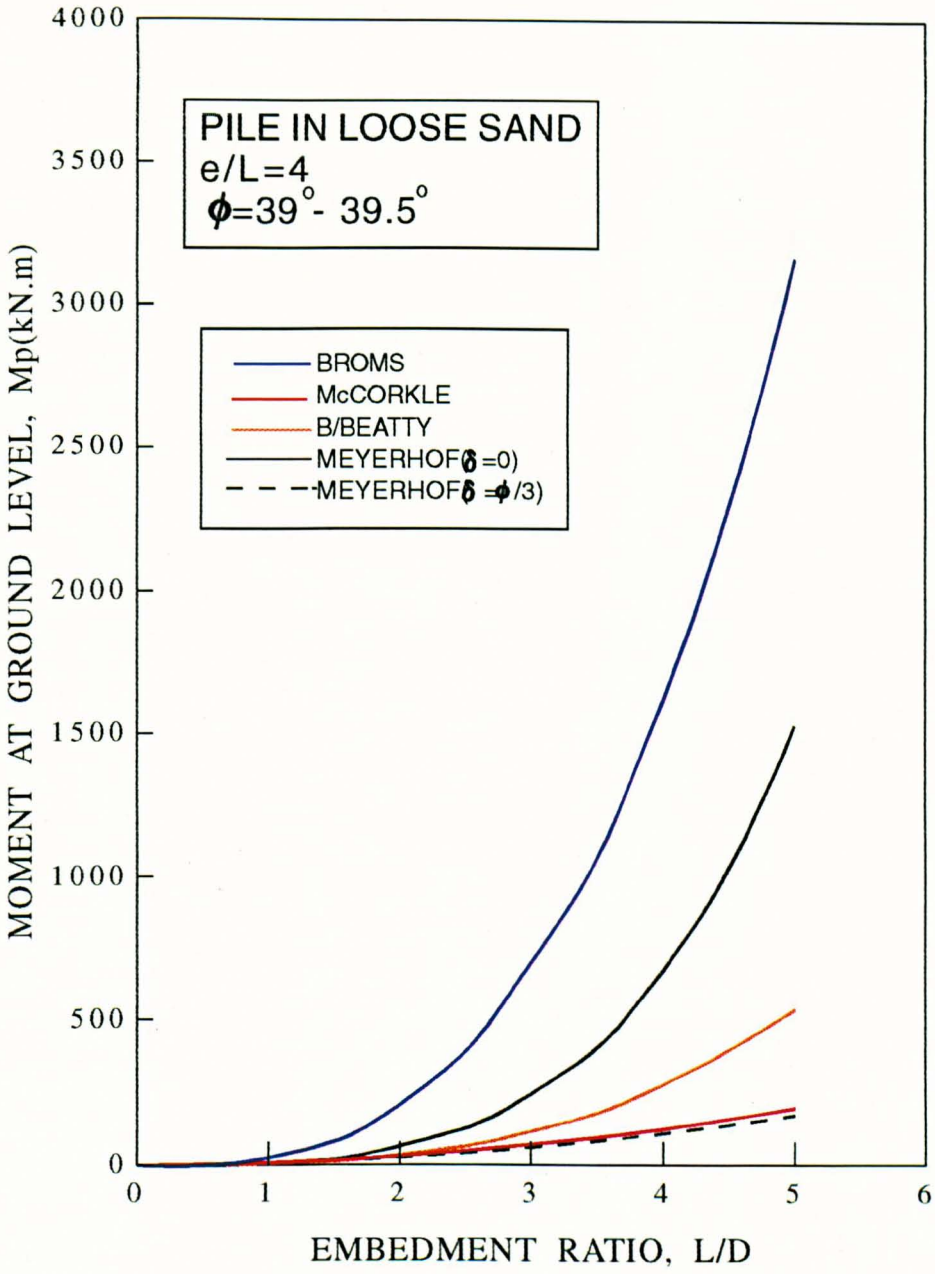

Figure 4.2(i) Variation of prototype moment at ground level with pulling height ratio for pile embedded in loose sand

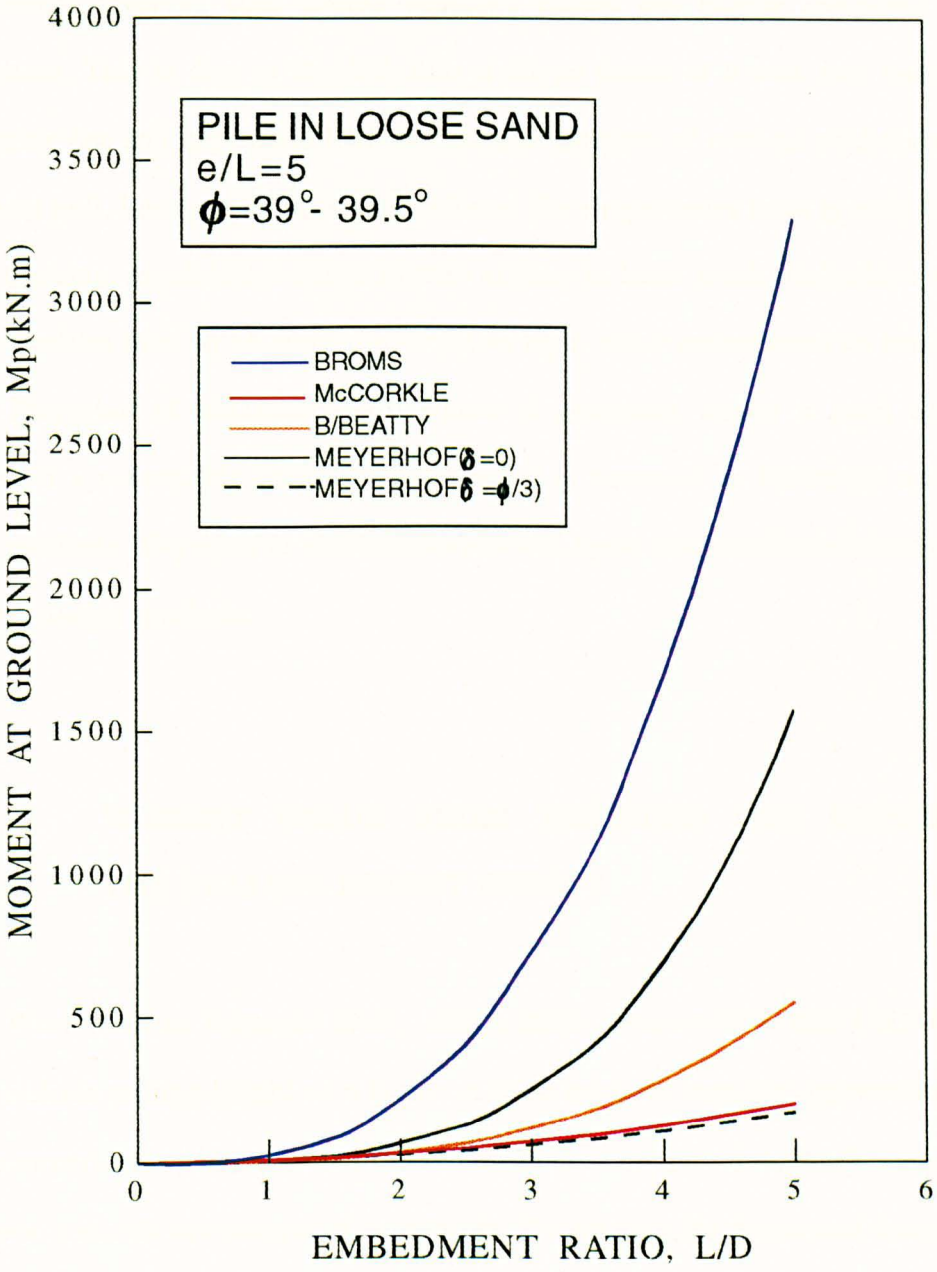

Figure 4.2(j) Variation of prototype moment at ground level with pulling height ratio for pile embedded in loose sand

loose packing since only limited tests were performed by the author for this condition. It is clearly observed that Broms' moment values are higher compared to other researchers. This is due to the fact that a shape factor of 3 was also used without considering the soil unit weight. In the similar problem of vertical anchors subject to horizontal pull, Leung and Dickin(1985) found the shape factor to be greatly influenced by soil packing, much lower shape factors arising in loose sand. McCorkle's allowable moment values tend to be more conservative than other researchers in loose packing except Meyerhof et al.(1988)($\delta=\phi/3$) where it generally shows a good agreement. However if a reasonable safety factor of say 2 is assumed in McCorkle and Balfour Beatty methods, Meyerhof et al.(1988)($\delta=\phi/3$) will again give the lowest moment values of all the design methods.

4.5.2 MOMENT VALUE FROM THEORIES NOT CONSIDERING THE PULLING HEIGHT EFFECT

Work such as Terzaghi(1943), IRSIA(1950), Roscoe(1957) and UIC/ORE(1957) do not include pulling height as a factor in their moment capacity expressions. Thus a direct comparison with the other researchers work is not possible. Predictions based on the above methods are compared separately. Parameters for dense and loose sand are similar to those in section 4.5.1.

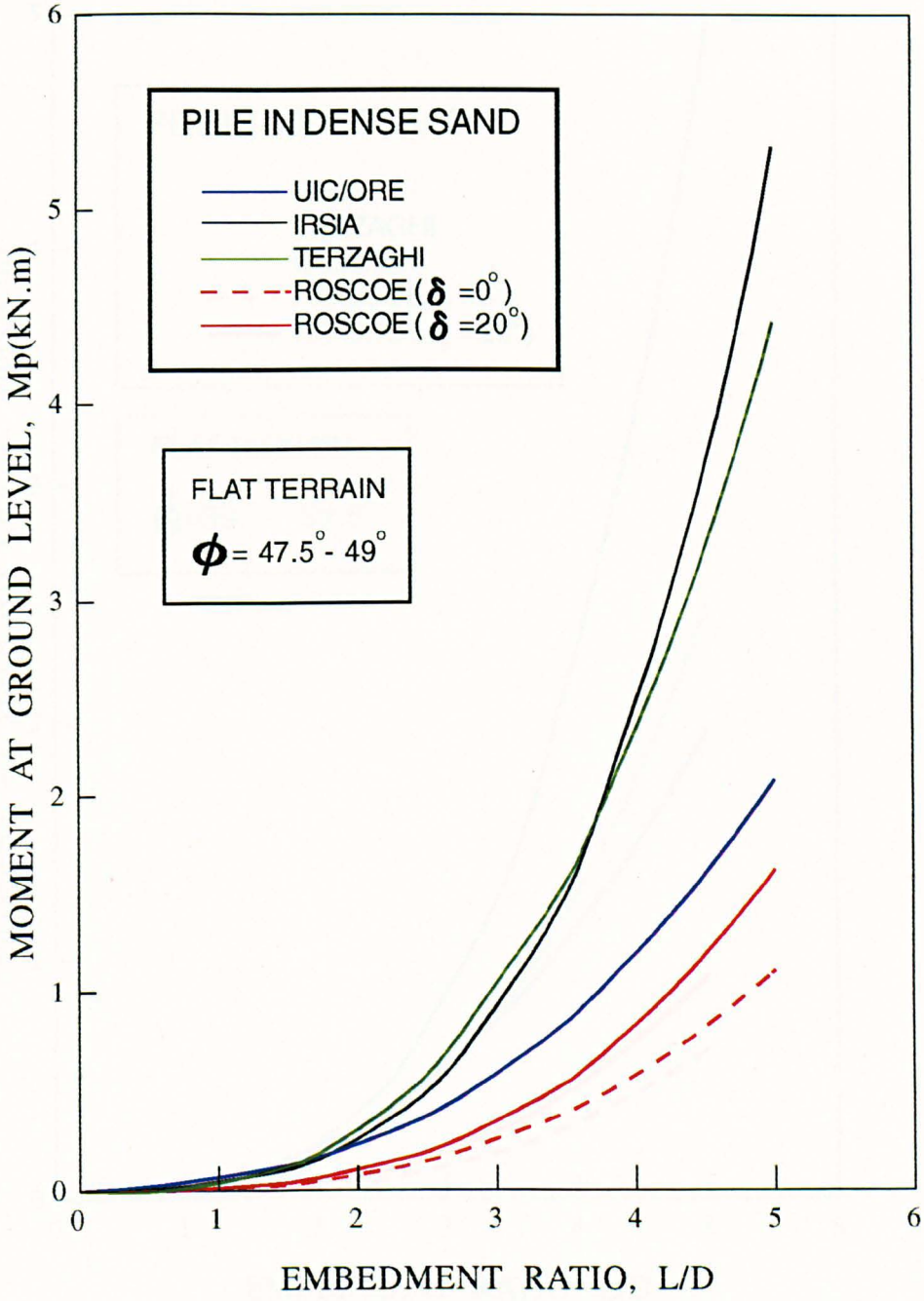

Figure 4.3(a) Variarion of prototype moment at ground level with embedment ratio for pile embedded in dense sand

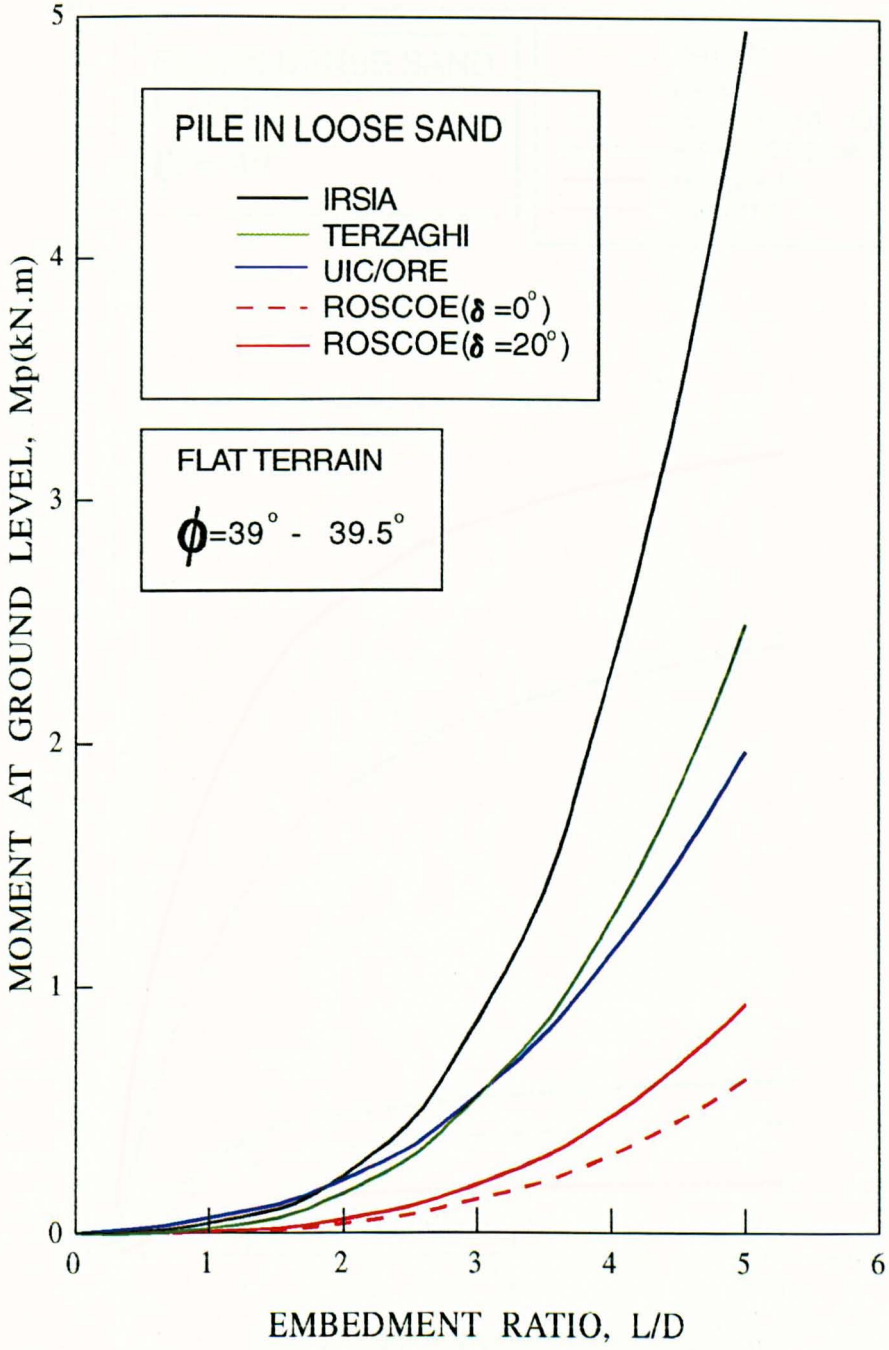

Figure 4.3(b) Variation of prototype moment at ground level with embedment ratio for pile embedded in loose sand

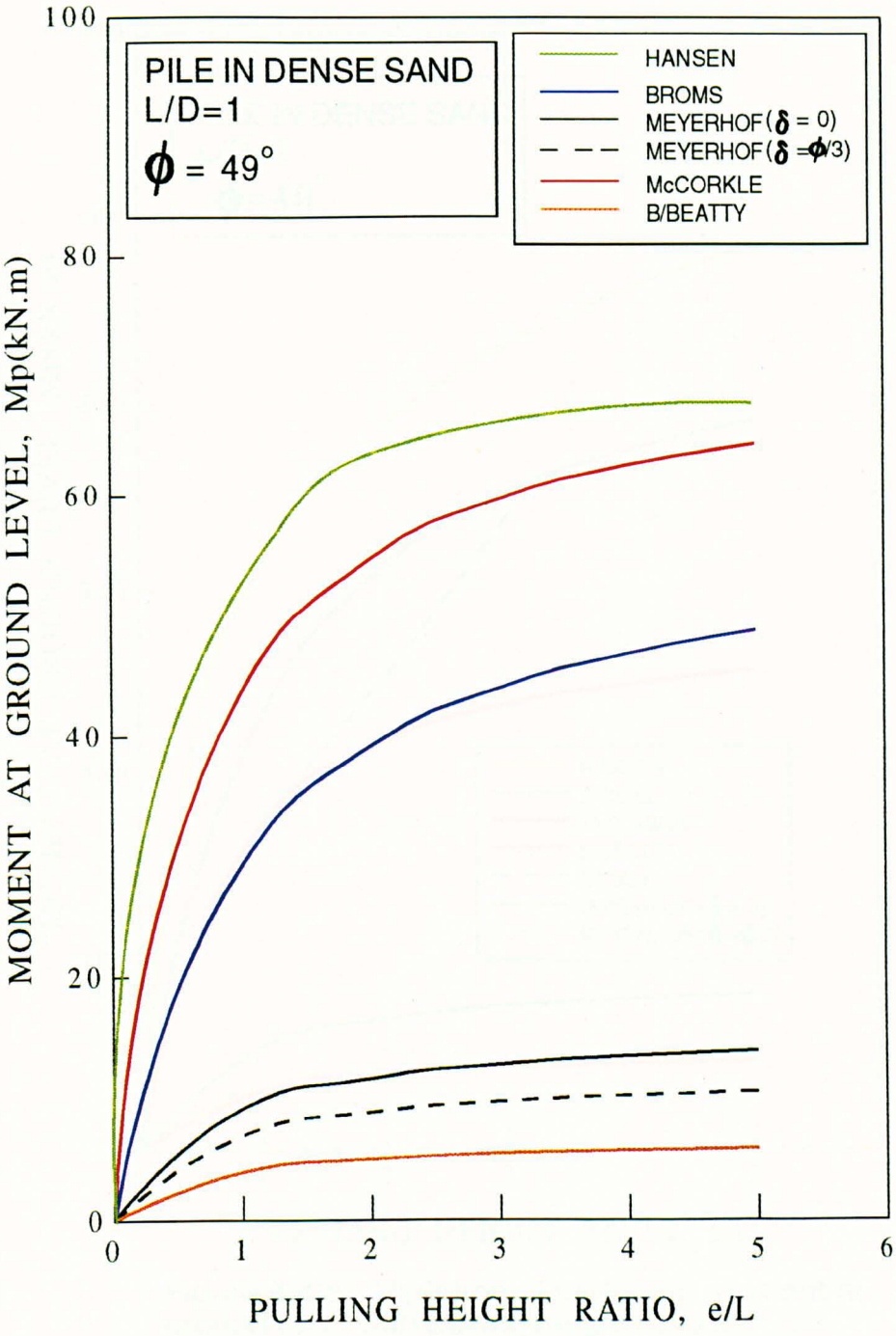

Figure 4.4(a) Variation of prototype moment at ground level with pulling height ratio for pile embedded in dense sand

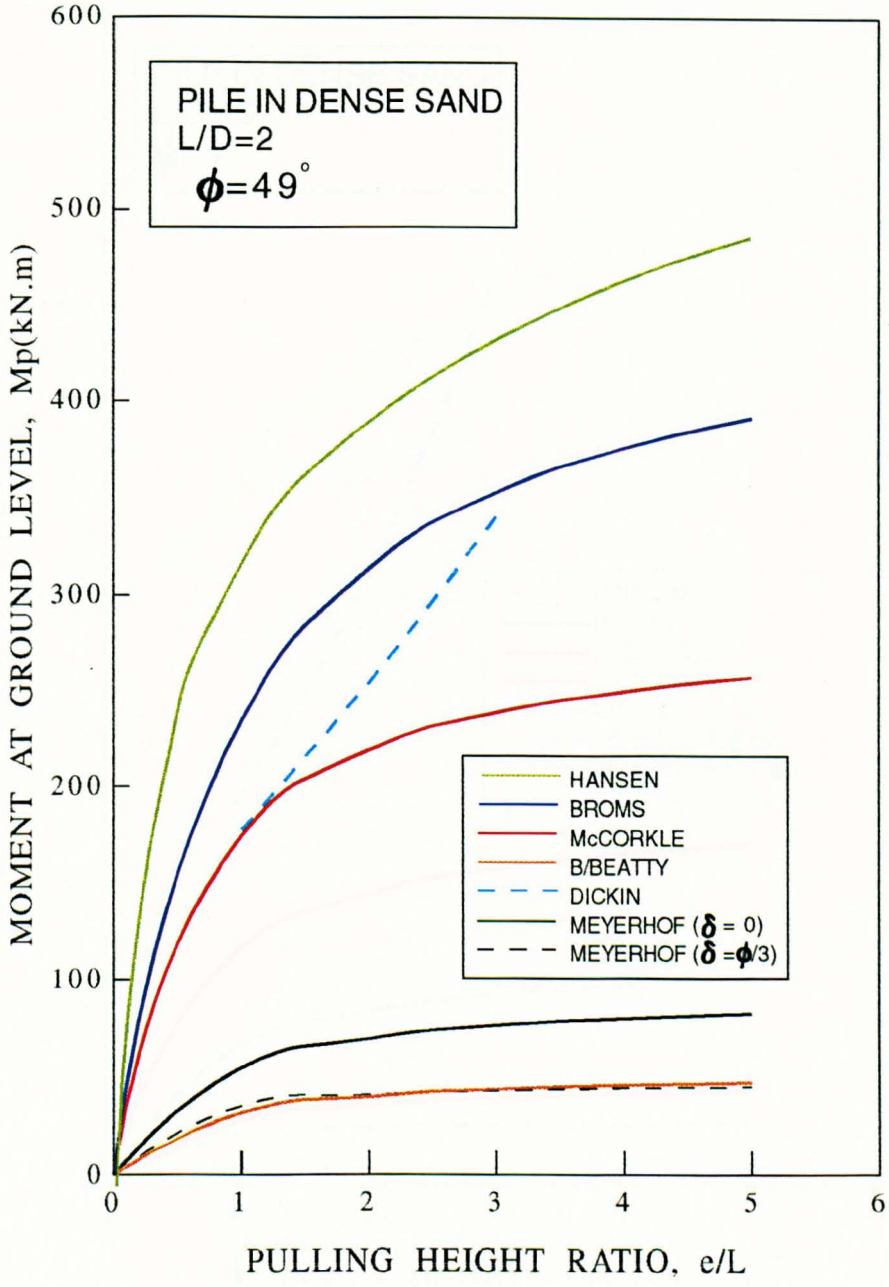

Figure 4.4(b) Variation of prototype moment at ground level with pulling height ratio for pile embedded in dense sand

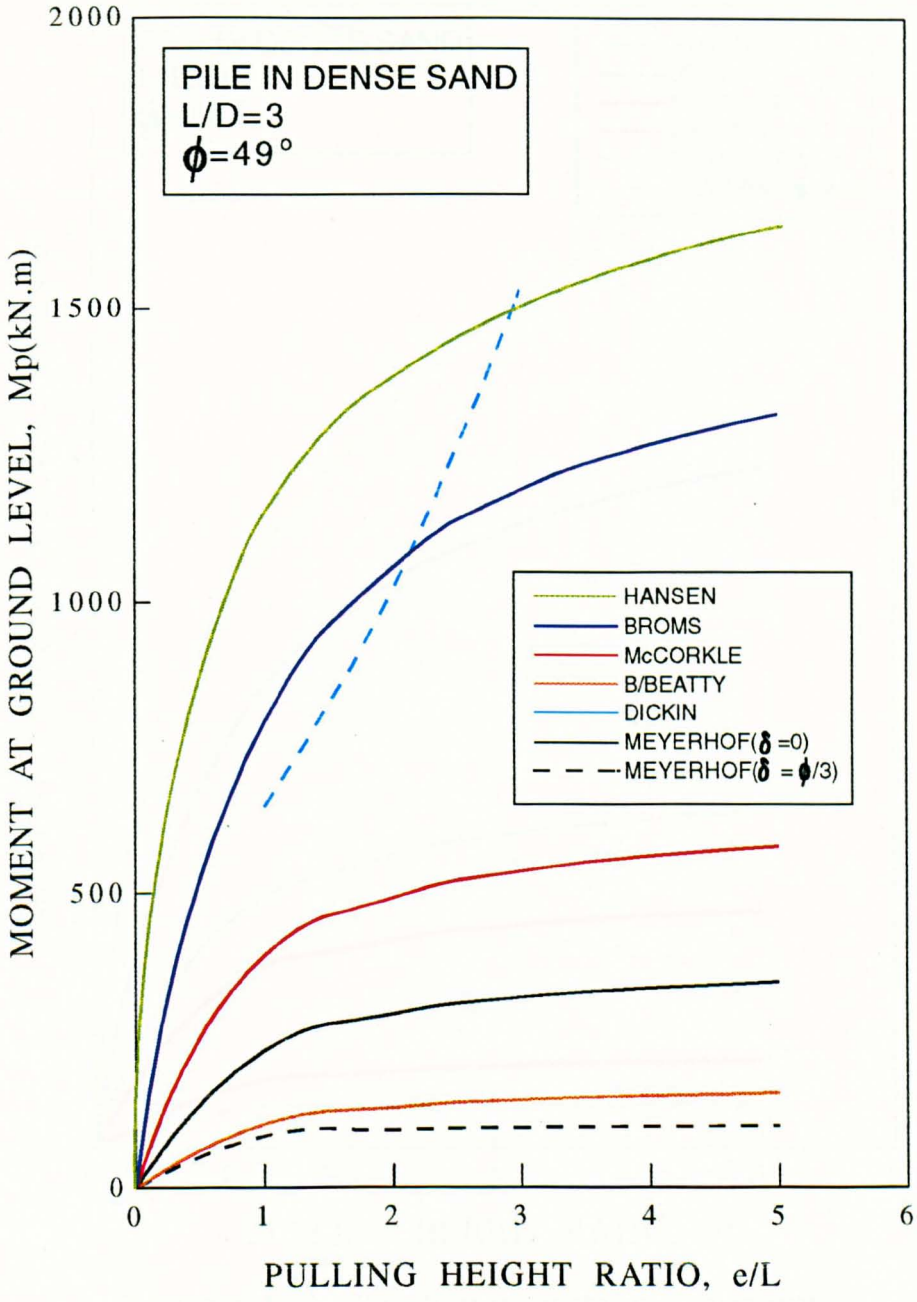

Figure 4.4(c) Variation of prototype moment at ground level with pulling height ratio for pile embedded in dense sand

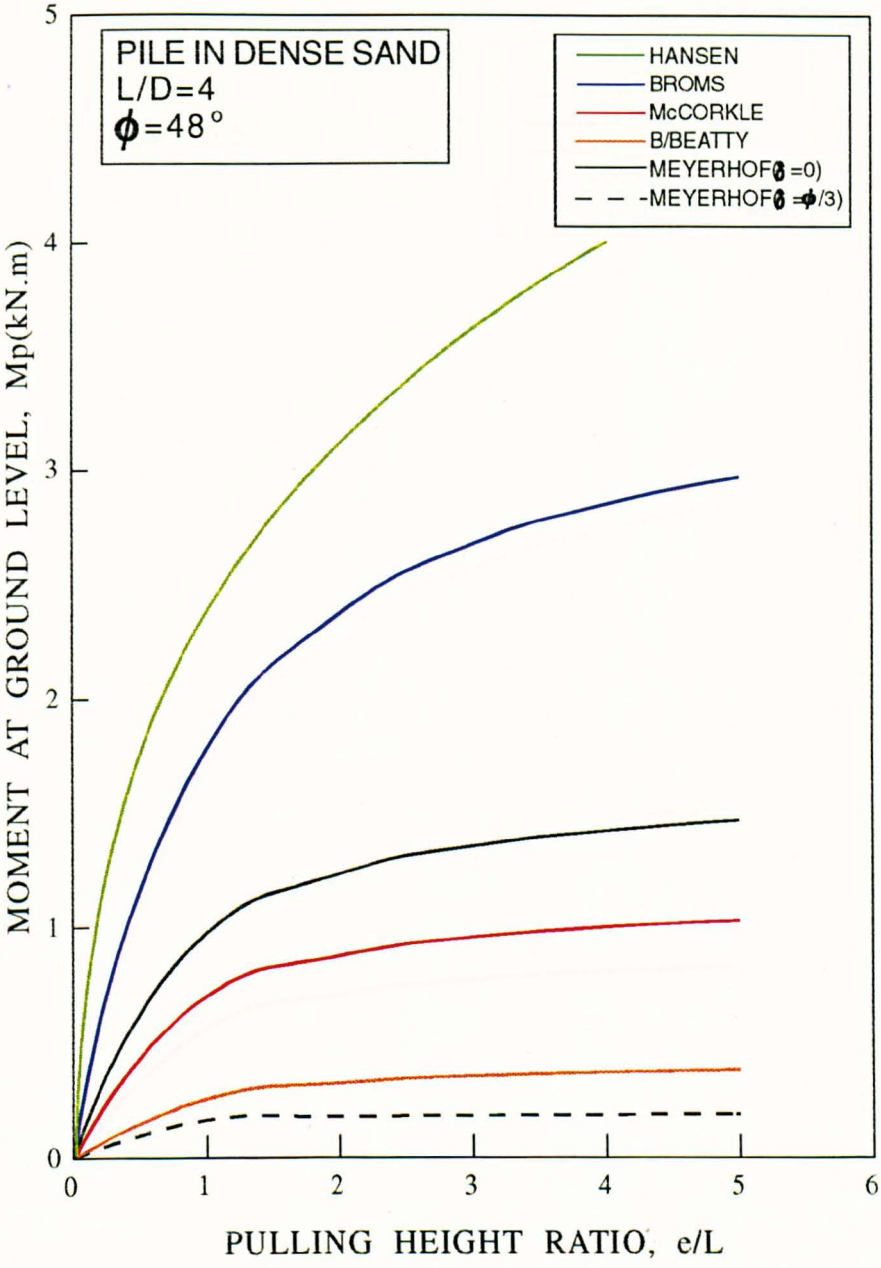

Figure 4.4(d) Variation of prototype moment at ground level with pulling height ratio for pile embedded in dense sand

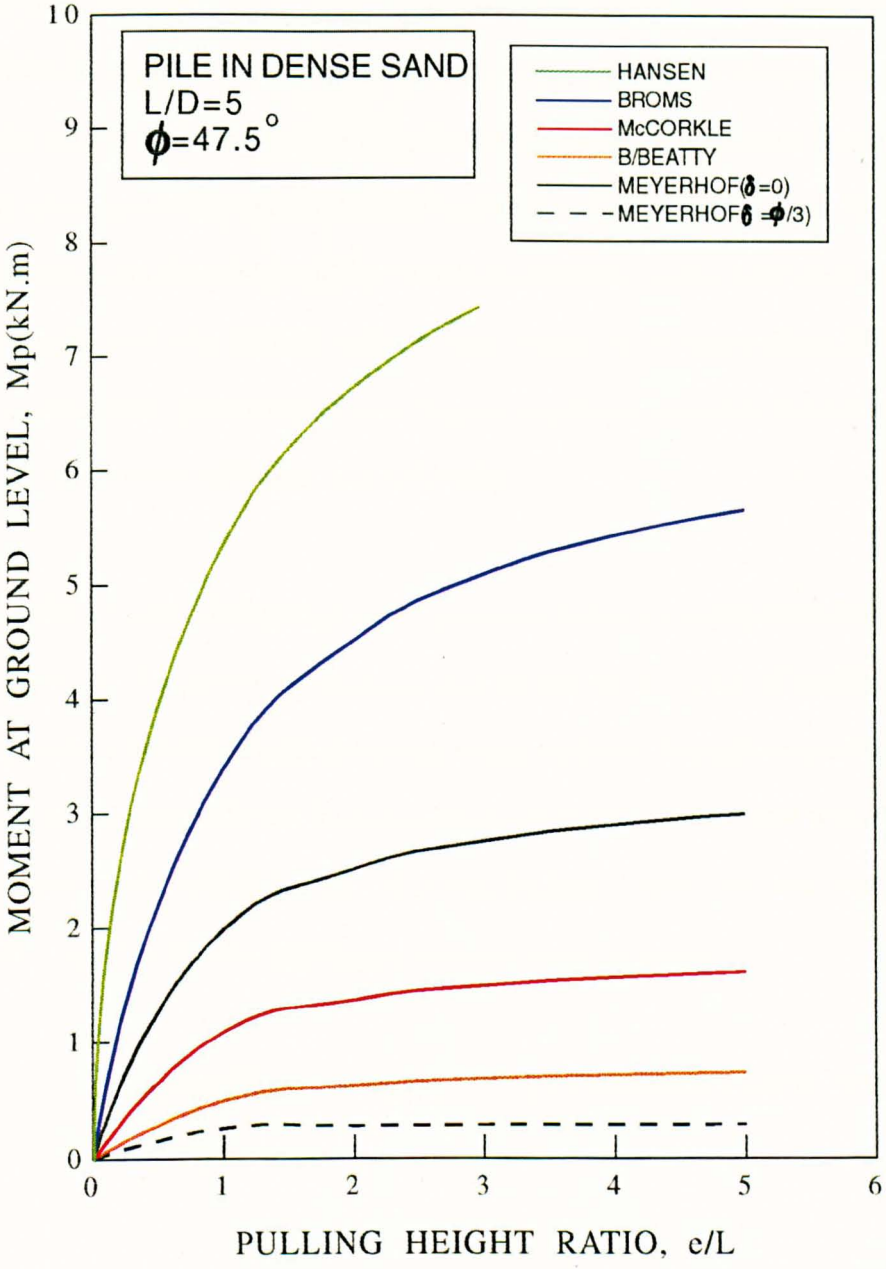

Figure 4.4(e) Variation of prototype moment at ground level with pulling height ratio for pile embedded in dense sand

Figures 4.3(a) 4.3(b) show the variation of moment at ground level with embedment ratio for pile in dense and loose sand packing respectively. The Terzaghi and IRSIA design methods show good agreement and their values are higher compared with the others while Roscoe's method employing surface friction angle of $\delta=20°$ gives a fairly good agreement with UIC/ORE value for piles in dense sand. However for piles in loose sand the Terzaghi and UIC/ORE predictions agree very well while the IRSIA method still gives the highest values. This would be expected since IRSIA conducted small model tests which would give higher predicted moment values compare to the field test conducted by Rosoe and UIC/ORE.

When a smooth Rankine earth pressure value is employed in Roscoe's equation, a lower value of moment is expected due to the lower value of coefficient of passive earth pressure for smooth compared with rough surfaces. Moment capacity obtained from Roscoe's calculation is lower than the others since allowable value was employed in the comparison work. Although the UIC/ORE Fe-limit takes the unit weight of soil into account, its effect on the calculated moment limit is minor.

4.5.3 VARIATION OF MOMENT AT GROUND LEVEL WITH PULLING HEIGHT RATIO

To observe the behaviour of moment capacity at different pulling height predicted by each researcher a series of graphs of moment at ground level with pulling height ratio is plotted in the following figures.

Figures 4.4(a) to 4.4(e) show the effect of moment at ground level with pulling height for various embedded lengths. Generally most of the predictions show a hyperbolic relationship between the moment and pulling height ratio. The effect of pulling height on moment values for all researchers except Dickin and Wei, is considerably less significant for e/L>3. However Broms and Hansen shoes that the effect of pulling height is still significant in excess of e/L>3. Meyerhof et al.'s(1988) method gives conservative results for piles in dense sand for all embedded lengths. McCorkle's method reduces with embedment length in comparison with other researchers work. For L/D=1 his prediction gives higher allowable moment values than others except Hansen. However when the embedment length increases to L/D=5, his values give fairly good agreement with those of Balfour Beatty which are known to be quite conservative compared to most researchers. This might be due to the assumption made in McCorkle's equation which does not recognise the stress dependent strength of cohesionless soil as mentioned by Balfour Beatty. This will result in a higher calculated allowable moments for a lower embedment length which may be unsafe in extreme cases. The relationship from Dickin and Wei tends to diverge from the trend obtained from other researchers.

Figures 4.4(f) to 4.4(j) show the variation of moment at ground level with embedment length for piles in loose sand. Since limited data were available from the author's data, the Hansen moment value could not be plotted. Broms' method shows extremely high values of moment for all embedment lengths due to the application of a similar shape factor as in the dense sand as explained earlier.

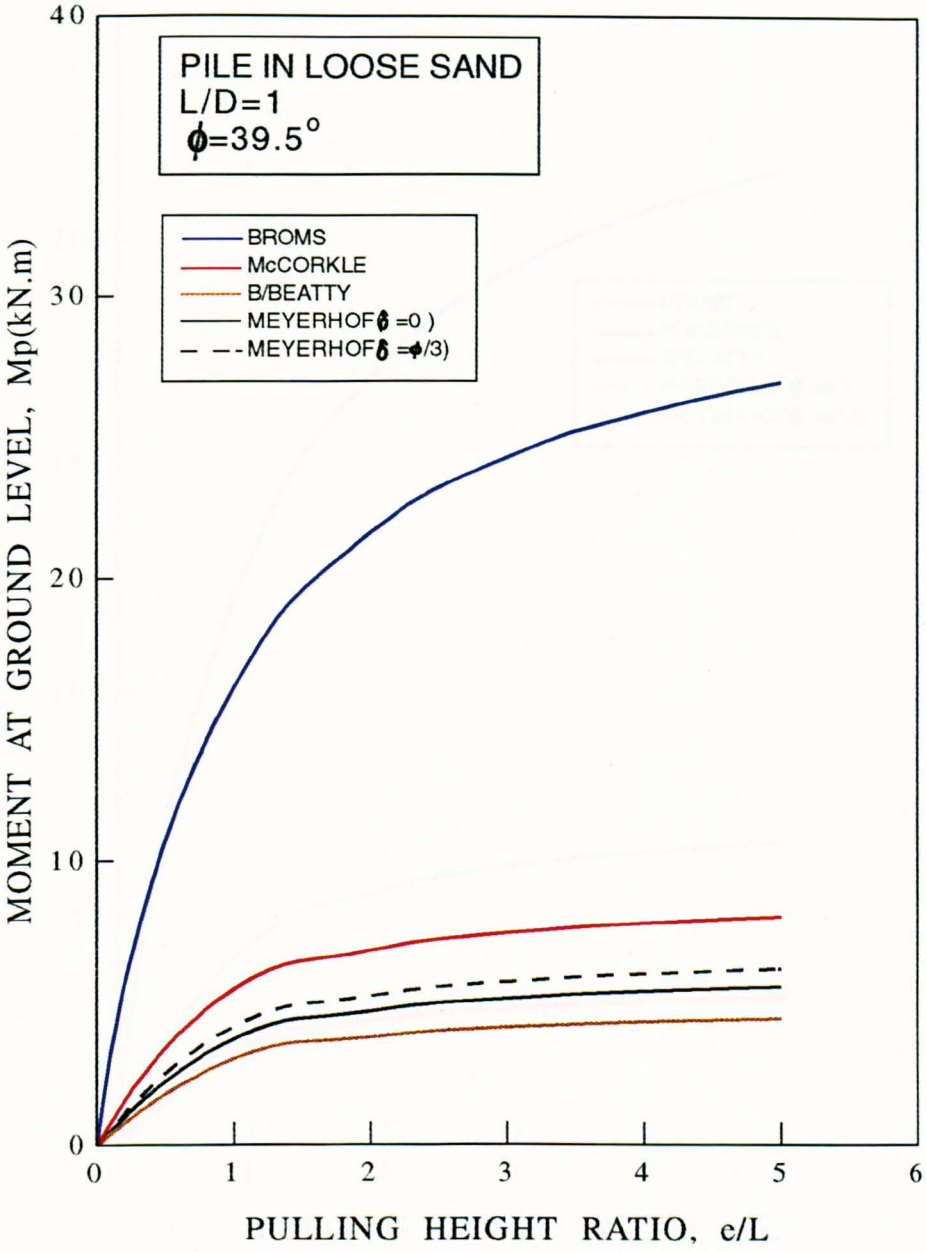

Figure 4.4(f) Variation of prototype moment at ground level with pulling height ratio for pile embedded in loose sand

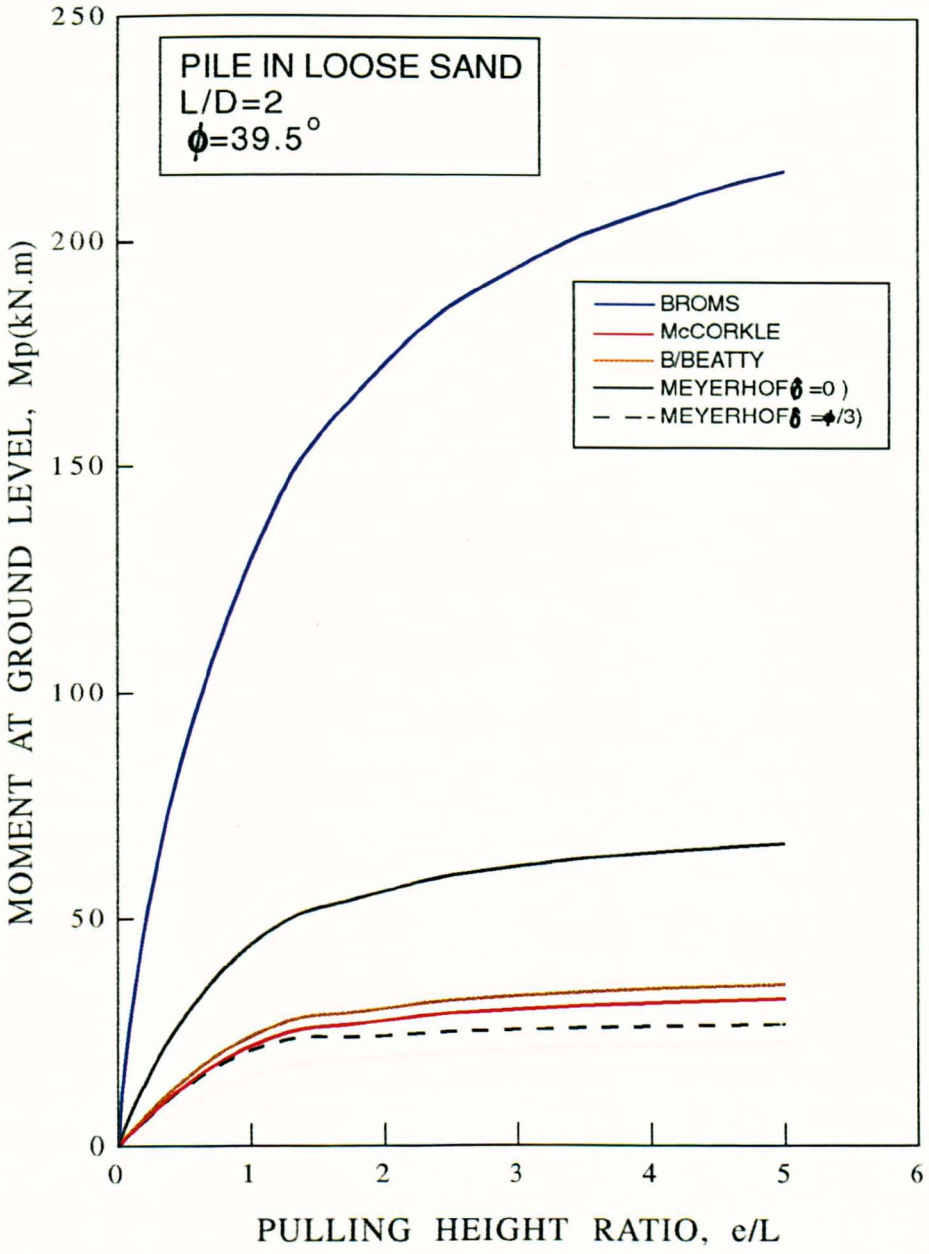

Figure 4.4(g) Variation of prototype moment at ground level with pulling height ratio for pile embedded in loose sand

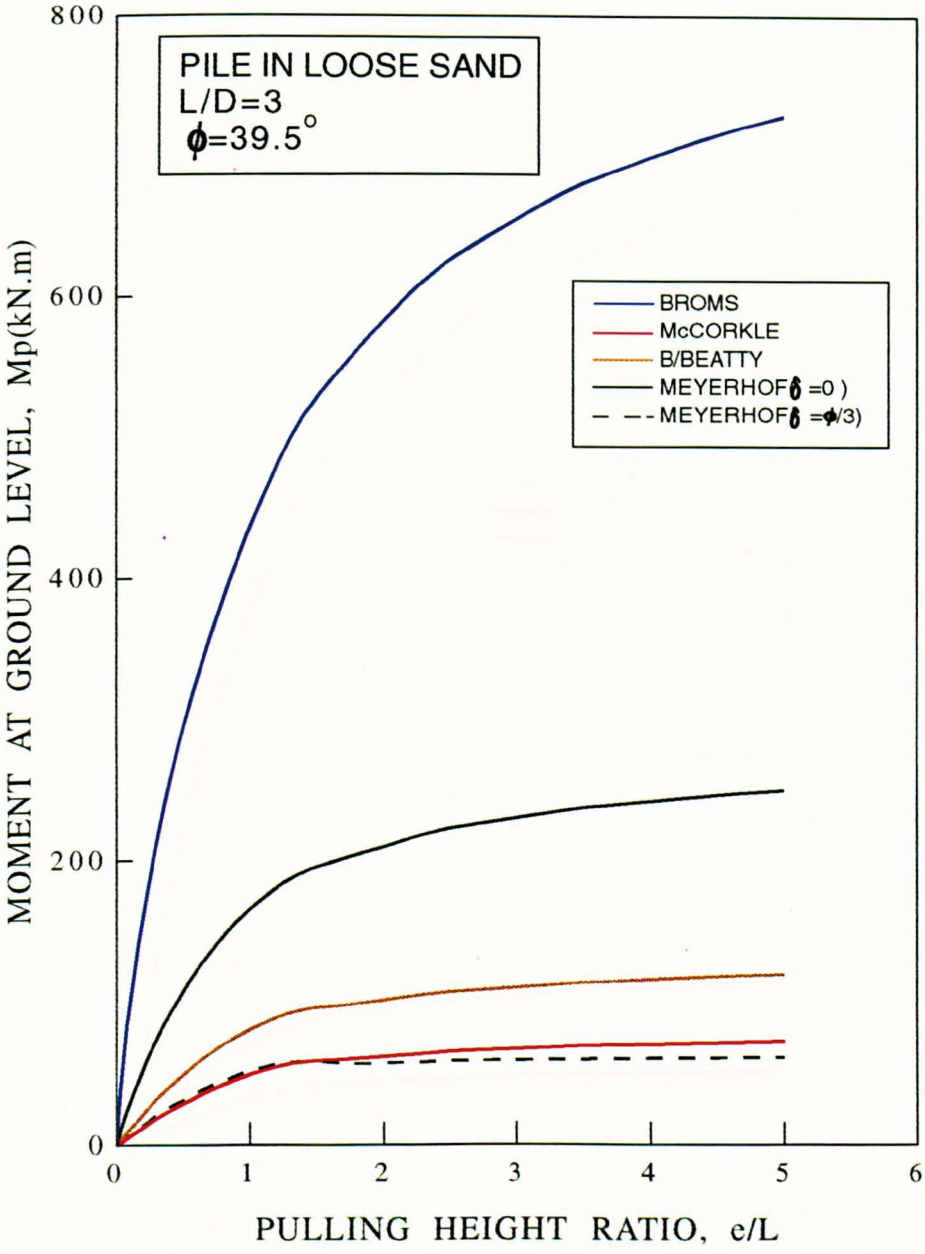

Figure 4.4(h) Variation of prototype moment at ground level with pulling height ratio for pile embedded in loose sand

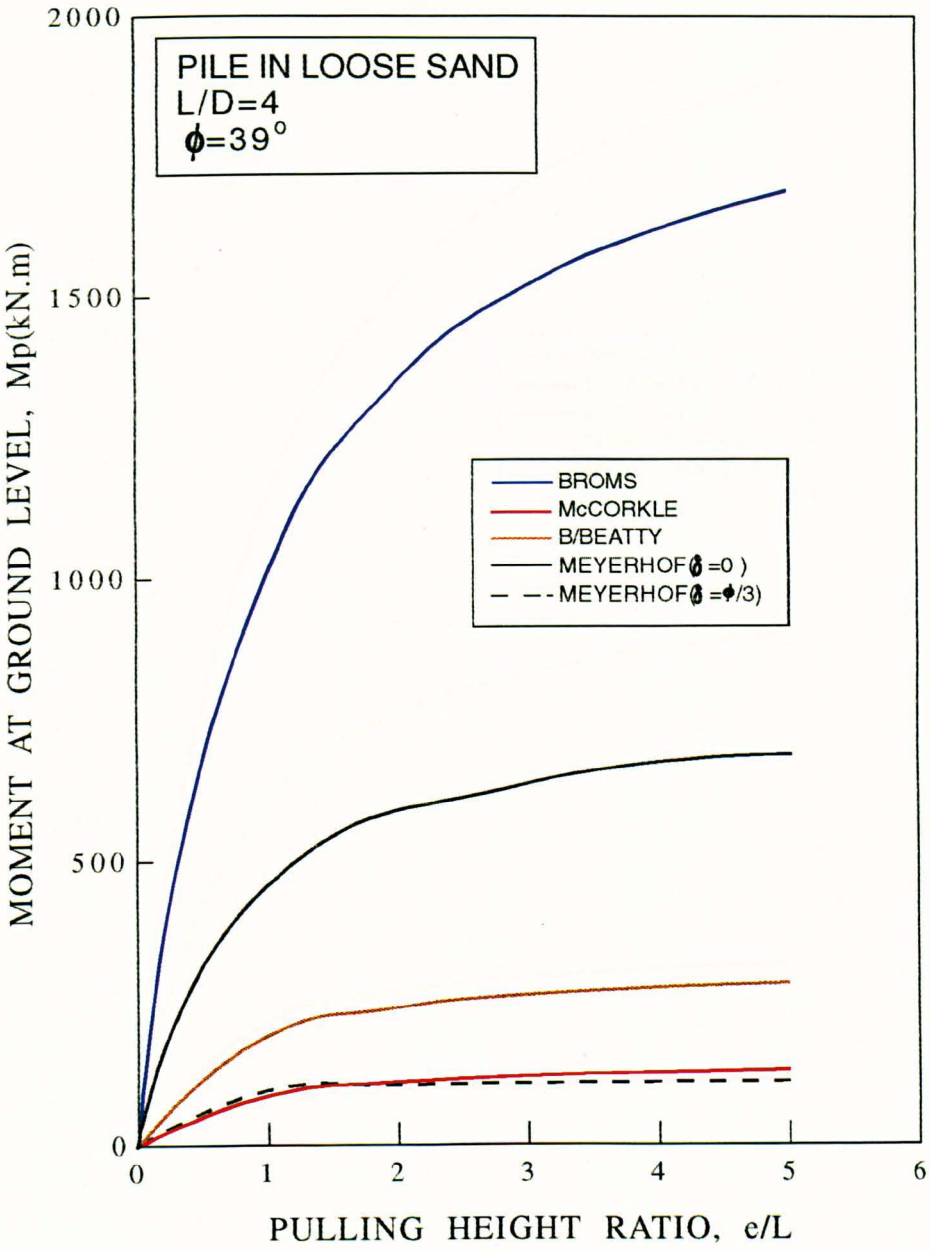

Figure 4.4(i) Variation of prototype moment at ground level with pulling height ratio for pile embedded in loose sand

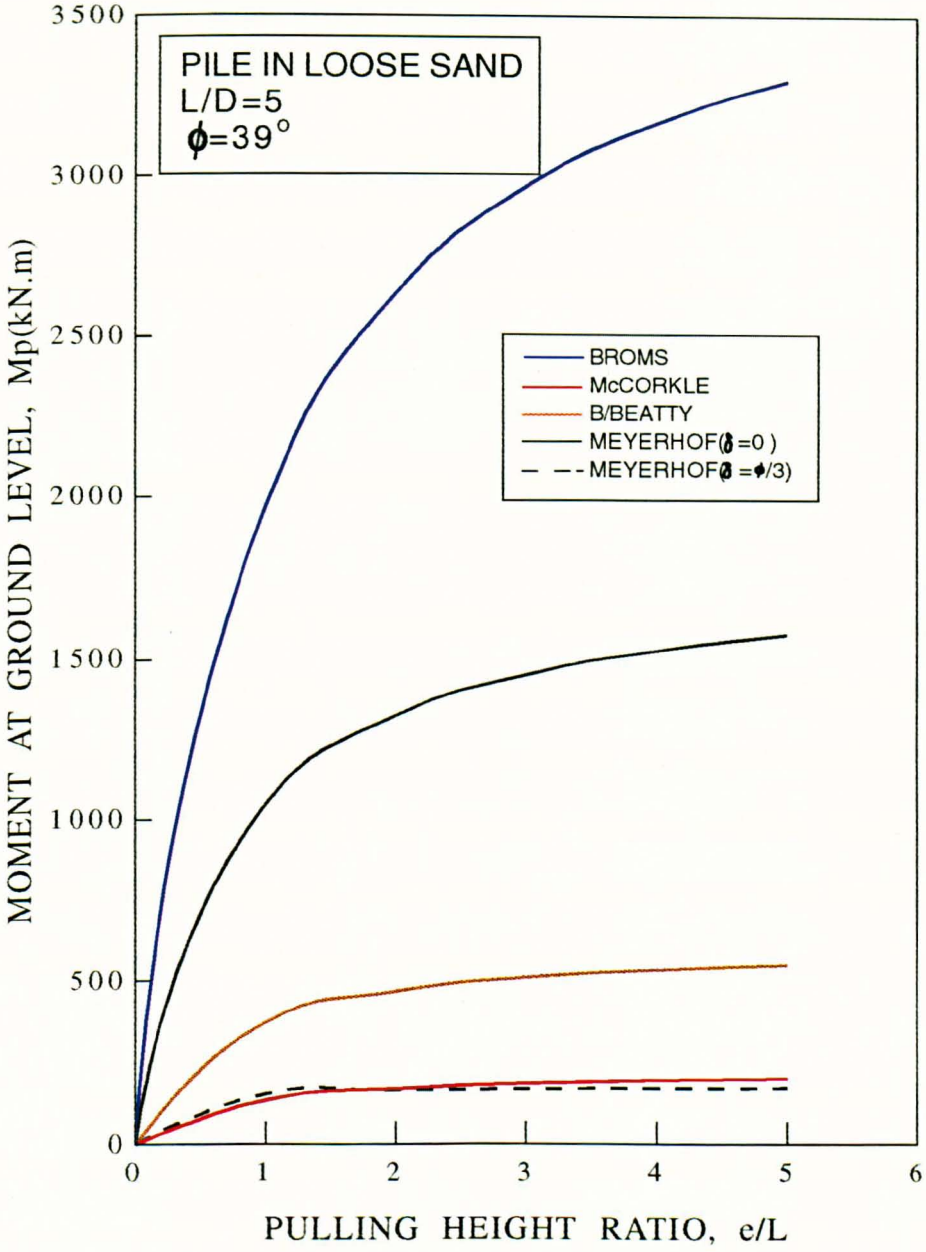

Figure 4.4(j) Variation of prototype moment at ground level with pulling height ratio for pile embedded in loose sand

The effect of the pulling height on moment limit reduces for e/L>2 compared to the pile in dense sand where the effect is still significant even for higher pulling heights. As in the dense sand packing, Meyerhof's et al.(1988) design method tends to be conservative compared to other researchers values. Although Balfour Beatty and McCorkle's theories give considerably lower values but depending on the safety factor their values will gives a fairly good agreement with Broms.

4.6 A SUMMARY OF DESIGN APPROACHES

Terzaghi(1943,55), Roscoe(1957) and Broms(1964), employed subgrade reaction to predict the lateral pile deflection at ground surface. Although McCorkle(1969) established an empirical relationship to predict the displacement of a pile at the ground line it was derived from subgrade reaction methods based on Terzaghi's evaluation. The deflection is considered as a result of long term loading under actual load applied continuously for a period of several years.

Terzaghi, Hansen, Broms, Meyerhof et al. and, Dickin and Wei adopt the ultimate lateral resistance as their failure criterion which requires the use of a factor of safety for design purposes, while Roscoe, Czerniak, McCorkle and Balfour Beatty define the allowable resistance in their formulae. However for consistency throughout the comparison work, the ultimate moment value at ground level has been employed.

Of the design techniques reviewed, although the UIC/ORE considered the influence of the soil consistency, the effect is relatively insignificant. They largely neglected the effect of soil type and thus the theory is only acceptable for a limited range of soil conditions.It was implied that the pulling height has a less significant influence in determining the limiting moment of the pile. In contrast, Dickin and Wei show that the moment at ground level increases significantly with an increase in pulling height. However the pulling height has a less significant effect when the pulling height ratio e/L>3. UIC/ORE and Balfour Beatty made an allowance for the ground surface profile.

Due to the difficulties in analysing the three dimension geometry which a single pile problem involves, a number of the solutions are based on the analysis of a wall. Meyerhof introduced a shape factor to account for the three dimensional condition. The shape factor was used to modify the relationships obtained from his two dimensional analysis to represent the three dimensional behaviour. Table 4.4 shows a summary of the design factors considered by previous researchers.

Although an attempt was made to compare the moment at ground level in dimensionless terms for all the existing theories with different ϕ values, some expressions such as those of IRSIA, UIC/ORE, McCorkle and Balfour Beatty does not considered ϕ as an implicit function. Thus a complete comparison could not be accomplished due to the difficulties in establishing the correct ϕ value for each research investigation.

	1	2	3	4	5	6	7	8	9	10
Soil type	X	X	X	X	X	X	X	X	X	X
Soil consistency	X	X	X	X	X	X	X	X	X	X
Ground geometry			X						X	
Disturbed ground		X	X	X	X	X	X		X	
Water table					X	X	X	X	X	
Surface roughness		X			X			X		
Surface deflection	X	X				X	X			
Ultimate resistance			X		X	X		X		X
Allowable resistance		X		X			X		X	

1: Terzaghi
2: Roscoe
3: UIC/ORE
4: Czerniak
5: Brinch Hansen
6: Broms
7: McCorkle
8: Meyerhof
9: Balfour Beatty
10: Dickin

Table 4.4 Summary of design factors

4.7 GENERAL DISCUSSION

Although moment values obtained by Hansen, Broms and McCorkle show good agreement for certain embedment lengths or pulling heights, relatively large discrepancies occur between various theories which inevitably lead to difficulties in selecting the most reliable design value. The inclusion of surface friction gives no great advantage in the design methods for short piles based on Roscoe's analyses. Although some researchers such as Tschebotarioff(1962), Leung(1981) conclude that it is uneconomical to ignore δ completely, however in cases such as Terzaghi and Broms, and

addition of δ will lead to a higher value of K_p thus leading to a higher moment value which would be unsafe in design consideration. However, Smith(1982) mentioned that for the case of a shallow foundation with a small surface such as those in this project, an application of classic Rankine smooth earth pressure coefficient is fully justified.

In common with those of Dickin and Leung(1985), the shape factors of Meyerhof et al.(1981) are dependent on the internal friction angle and the pile embedded length. It is not clear why the shape factor is disregarded in a later publication(Meyerhof et al.(1988)). However a surface friction angle of $\delta=\phi/3$ is the considered in their equations by way of compensation.

Generally the pulling height has little effect on the moment at ground level at e/L>3 for dense sand and even less for loose sand. Terzaghi, IRSIA, Roscoe and UIC/ORE ignore the contribution of pulling height towards the moment limit at ground level. However Dickin and Wei show that pulling height is a prime factor which affects the moment value for low pulling height ratios. It was speculated that for a higher pulling levels the pulling height is also significant.

Methods proposed by Roscoe, UIC/ORE, McCorkle and Balfour Beatty result in an allowable resistance against overturning. Thus for a direct comparison with the ultimate moment values obtained from other researchers, the allowable resistance needs to be multiplied by a safety factor.

Hansen's formula can be used to determine the moment capacity for a wide range of soils. However a great disadvantage is that, for a shorter pile where failure in translation is dominant, overprediction of the lateral load will be expected. Although his method is theoretically more rigorous than others, it is considerably more difficult to apply since the location of rotation point requires a trial and error approach. However no significant improvement in economy over alternative methods is apparent.

Due to the fact that different parameters were used in determining the relationships between the limiting moment values, a reasoned conclusion is very difficult to make. Previous research shows that a scale error does exist in small model tests, thus questioning the reliability of the ensuing formula. Even though full scale tests give a better insight into the problem, only a limited number of field tests are available, thus making a comprehensive comparison impossible. Furthermore financial and time constraints make extensive full scale testing unattractive.

Pilot studies reported by Dickin and Wei(1991) on the overturning limit of piles embedded in sand using the centrifugal modelling technique demonstrated the possibility of predicting prototype behaviour. Since only limited tests were done, the validity of their equations is restricted to a range of embedment ratios L/D of between 1.9 and 3.2. In this research the same approach is adopted and extended. The results from the extended centrifugal testing programs in this research will be used to examine all the existing theories and empirical relationships applied to the problem of the overturning limit of a short pile in sand.

CHAPTER 5

PROPERTIES OF MATERIALS

5.1 INTRODUCTION

Throughout the experimental programme, sand was used as an embedment medium for the model piles. The majority of the tests were conducted with sand in a dense packing while a few tests in loose sand were also included for comparison purposes. Loose packing tests were of less importance since most of the field work was conducted under dense conditions. Short piles used in both conventional and centrifugal test series were fabricated from the same material and were approximately similar in length/diameter ratios to ensure consistency in the comparative work.

5.2 PROPERTIES OF ERITH SAND

A fine, clean, dry Erith sand was used in the experimental programme. The grain size of 95% of the sand ranged from 0.125mm to 0.355mm, with a mean grain size D_{50} of 0.20mm. Figure 5.1 shows the grain size distribution. The sand was therefore essentially uniform with a coefficient of uniformity C_u of approximately 1.31. Specific gravity G_s obtained by the BS specific gravity bottle method(BS 1377(1975)) was 2.65.

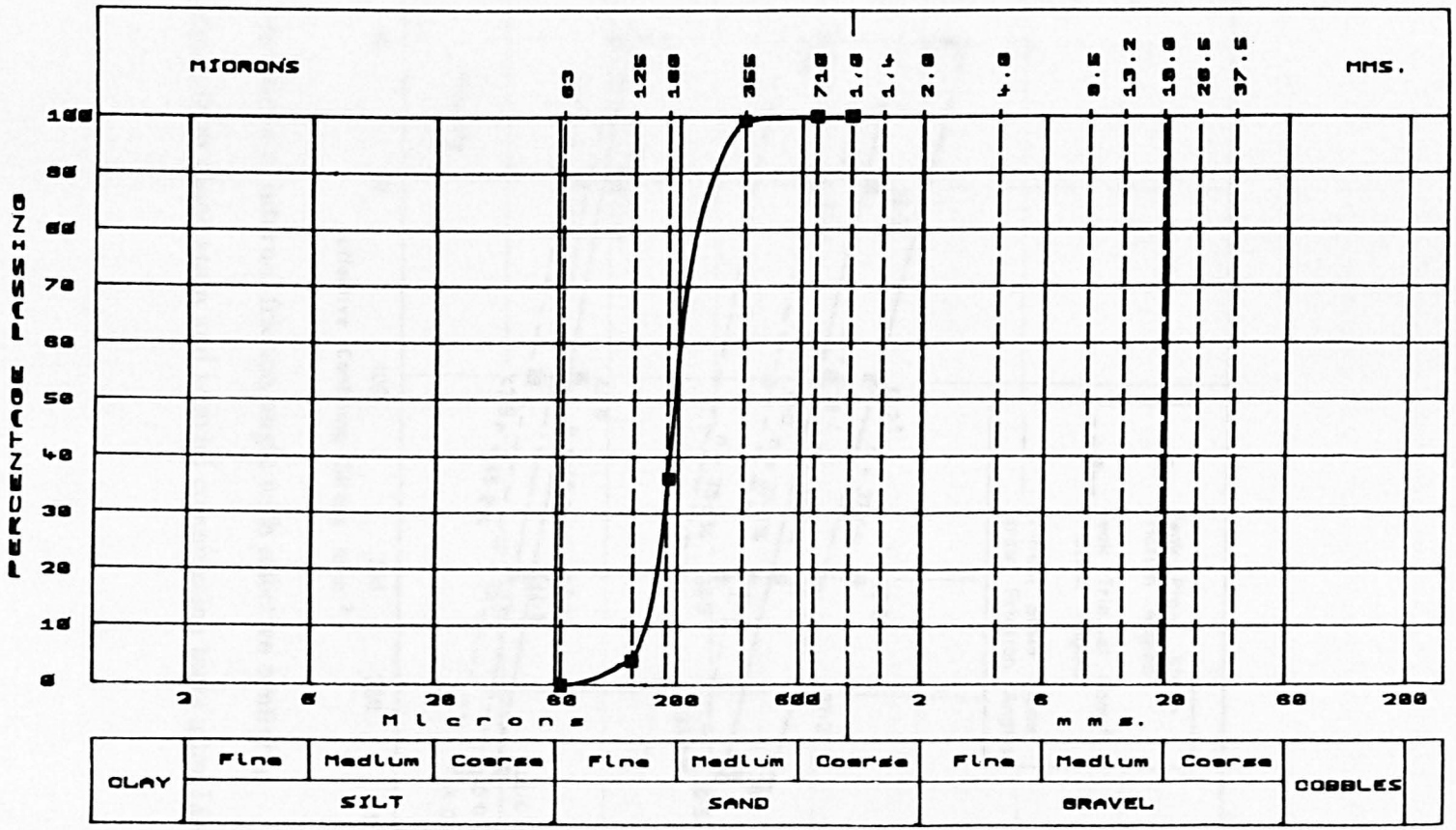

Figure 5.1 Distribution for the size of sand

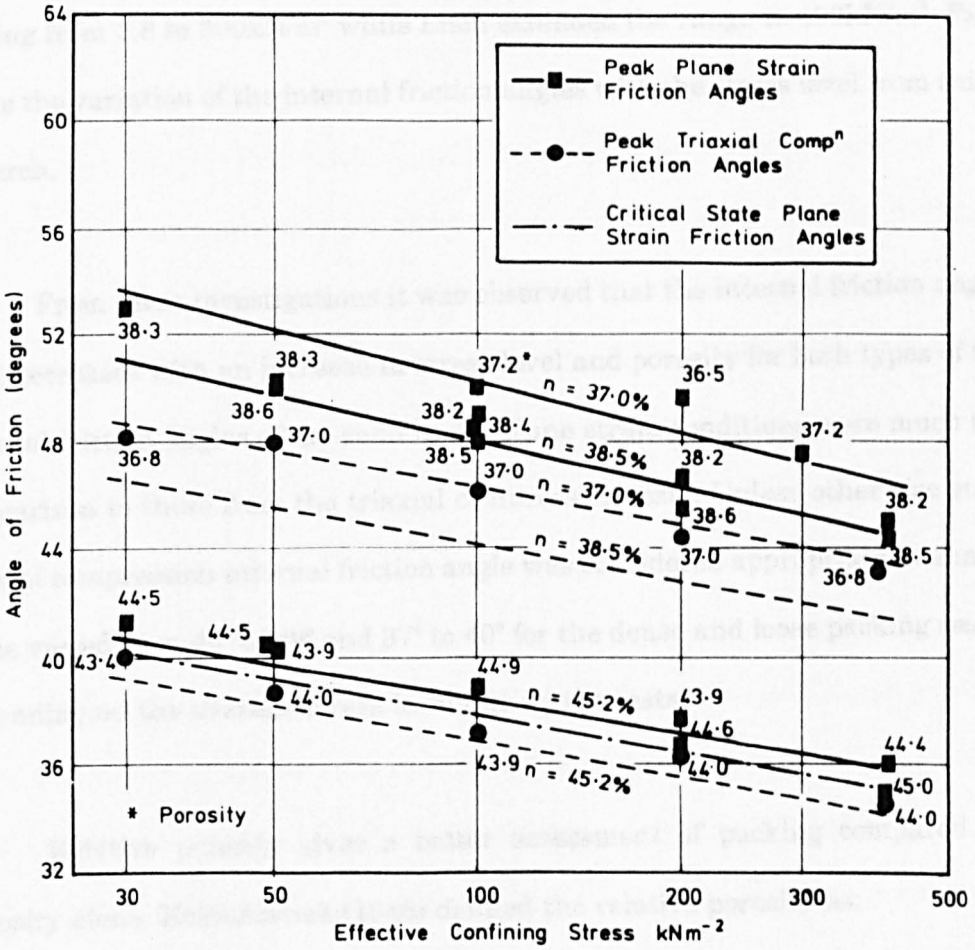

Figure 5.2 Variations of internal friction angle with effective confining stress from plane stain and triaxial compression tests after Liem(1988)

The friction angles for this sand have been well established from extensive research under triaxial and plane strain test conditions by Tang(1979) and Liem(1988). The influence of confining stress level on shear strength was an important finding of this work. Liem shows that the maximum stress ratio (σ_1/σ_3) and dilation characteristics reduce with increased confining stress level. Tang carried out tests at confining stresses ranging from 2.8 to 200kN/m^2 while Liem extended the range to 400kN/m^2. Figure 5.2 shows the variation of the internal friction angles with the stress level from this earlier research.

From these investigations it was observed that the internal friction angle of the sand decreases with an increase in stress level and porosity for both types of test. The internal friction angles of the sand under plane strain conditions were much higher in comparison to those from the triaxial compression tests. Unless otherwise stated, the triaxial compression internal friction angle was considered appropriate in analyses. Its value varied from 46° to 49° and 37° to 40° for the dense and loose packing respectively depending on the average stress level during the tests.

Relative porosity gives a better assessment of packing compared with the porosity alone. Kolbuszewski(1948) defined the relative porosity as;

$$n_r = \frac{n_{max} - n}{n_{max} - n_{min}}$$

where n_{max} and n_{min} are the limiting porosities obtained from standard procedures to produce very loose and dense packings and n is the actual porosity. Apart from relative porosity, density index I_d is also used to describe the packing of the sand. It can be written as;

$$I_d = \frac{e_{max} - e}{e_{max} - e_{min}}$$

where e_{max} and e_{min} are the limiting void ratios and e is the actual void ratio.
The determination of limiting porosities was carried out by Leung(1981) for Erith sand. The maximum porosity was determined from the method suggested by Kolbuszewski(1948). This was accomplished by settling 1000g of sand through water in a 2 litre measuring cylinder. The maximum porosity was given by;

$$n_{max} = 1 - \frac{1000}{VG_s}$$

The minimum porosity was that of a very dense triaxial test specimen, 100mm high and 100mm diameter prepared by mechanical vibration as suggested by Smith(1965). Using both methods described above, Leung(1981) obtained maximum and minimum porosities of 49.5% and 34% respectively. Equivalent porosities in this research were 37.1% for dense packing and 44.8% for loose packing. Density indices, I_d were 85% and 37% for dense and loose packings respectively. Detailed calculations of the sand packing during the pile tests are shown in Appendix B. In the centrifugal and the conventional test series, unit weights of 16.4kN/m^3 and 14.4kN/m^3 were

achieved for the dense and loose packings respectively. The method of obtaining the dense and loose packings is explained in detail in Chapters 6 and 7 for centrifugal and conventional tests respectively.

In the two dimensional glass box tests, a small amount of sand was coloured with a dye. The colouring of the sand was accomplished by mixing the sand with a green crystal dye in water. The sand was then oven dried. It was assumed that the colouring did not alter any of its physical properties. The colouring sand enabled the failure pattern to be appreciated.

5.3 PILE MATERIALS

Single cylindrical and continuous piles, as shown in Plate 5.1, were used in the test programs. Work done by previous researchers such as Shilts et al(1948), Roscoe(1957) and Broms(1964) shows that the shape of cross section of a single pile plays a relatively minor role in contributing towards the limiting value of the overturning resistance.

Piles tested in the centrifuge were made from mild steel with a range of effective diameters, lengths and mass shown in Table 5.1. The geometric parameters for the pile use in this research project are shown in Figure 5.3. The surface of the piles was coated with sand using epoxy resin to ensure that the surface in contact with the surrounding

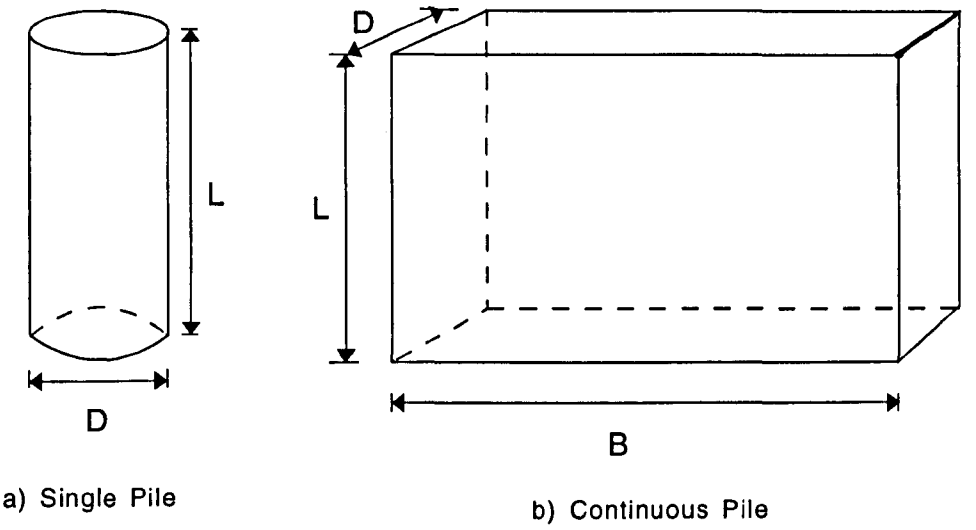

Figure 5.3 Geometrical dimension for single and continuous pile.

sand approximates to the field condition for a concrete pile. Similar material was used for the continuous piles in the two dimensional tests.

In conventional tests at medium scale a hollow mild steel section of 100mm diameter was used as a model pile shown in Plate 5.2. The hollow section tube was

TEST MODELS	L(mm)	D(mm)	W(kg)
CENTRIFUGAL MODELS SINGLE PILE	100	50	1.450
	100	20	0.2067
	80	40	0.727
	80	20	0.1652
	60	30	0.297
	60	20	0.1223
	50	50	0.7082
	50	25	0.166
	40	20	0.0792
CONVENTIONAL MODELS SINGLE PILE	500	100	40.8
	400	100	38.55
	300	100	35.35
	200	100	32.95

TEST MODELS	L(mm)	B(mm)	D(mm)	W(kg)
CONTINUOUS PILES	100	126	20	1.856
	80	126	20	1.501
	40	126	20	0.747

Table 5.1 Geometrical parameters for pile tested conventionally and in centrifuge

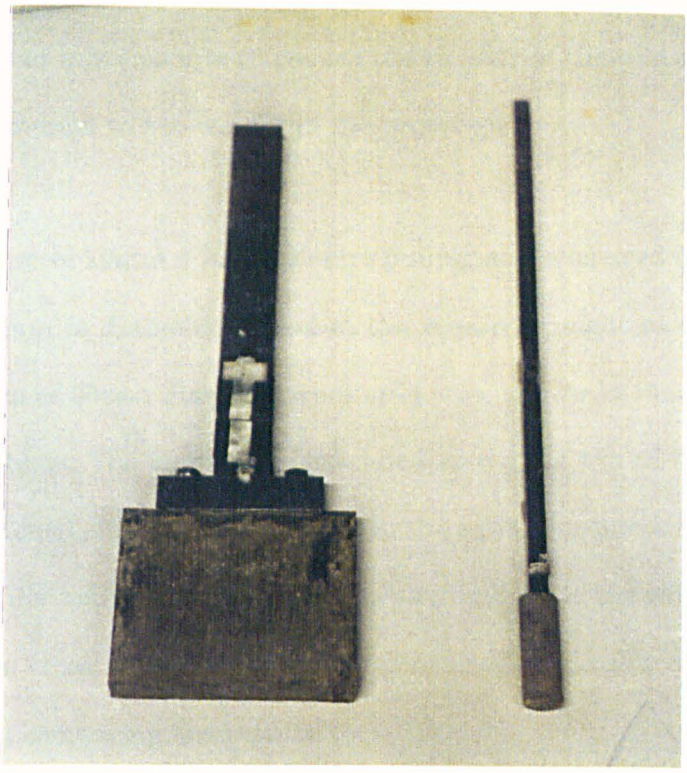

Plate 5.1 Single and continuous pile used in centrifugal test

Plate 5.2 Single cylindrical pile used in conventional test

filled with a lean mix concrete to ensure the rigidity of the pile section and to achieve a fair approximation to the weight of the prototype.

A mild steel 10mm x 10mm square pulling arm was used in the centrifugal tests with a hole 5mm in diameter drilled at the required height as shown in Plate 5.3. A cylindrical arm of 50mm diameter from mild steel shown in Plate 5.4 was used in the conventional tests. The arms were extended above the top of the pile and a loading cable was attached either through a hole in the square arm or by using a clamp for the circular arm. For both conventional and centrifugal tests, the ratio of pile cross section to pulling arm cross sectional area was maintained at a value of approximately 2, for consistency in comparing the results.

5.4 PILE RIGIDITY

Piles can be classified as either flexible or rigid. Several suggestions have been brought forward to define the rigidity of a pile. Czerniak(1957) and McCorkle(1969) considered that a pile with an embedment ratio L/D<10 while Williams and Parry(1979) considered a pile with L/D<20 can be classified as a rigid pile. Broms(1964) and Tomlinson(1986) relate the rigidity of a pile to the subgrade properties. Based on Terzaghi's(1955) evaluation of the coefficient of subgrade reaction, it was considered that a pile with $\eta L < 2$ is rigid, where the value of η is equivalent to;

Plate 5.3 Square pulling arm for centrifugal test

Plate 5.4 Circular cross section pulling arm used in conventional test

$$\eta = \sqrt[5]{\frac{n_h}{(EI)_p}}$$

where n_h is the constant coefficient of subgrade value as shown in Table 2.1 and $(EI)_p$ is the stiffness of the pile cross section.

Poulos and Davis(1980), Vallabhan et al.(1982) and Meyerhof et al.(1983) suggested that laterally loaded piles can be considered rigid for practical purposes if their relative stiffness K_{rs} is greater than about 0.1 to 0.01 depending on the degree of fixity at the pile head. The value of K_{rs} is given by;

$$K_{rs} = \frac{(EI)_p}{E_h L^4}$$

E_h is a horizontal soil modulus of the sand at the pile tip while L is the embedment length of the pile. According to Terzaghi(1955), $E_h = \gamma L A_o$ where A_o is the coefficient which is dependent on the packing of the soil, ranging from a value of 100 for very loose sand to a value of 2000 for a very dense sand.

Considering that the largest pile embedment ratio in this project is L/D=5, comparison made in Table 5.2 shows that all piles are rigid since this value lies within the range suggested by the previous researchers. Since only the method of installation is the essential difference between a short pile and a pier, the short pile, for analysis purposes, will be assumed to behave as a rigid pier.

Researchers	Limiting values of pile rigidity	Longest pile used in the project
Czerniak(1957)	L/D<10	L/D=5
Broms(1964) and Tomlinson(1986)	L/D<15(dense) L/D<23(loose)	L/D=5(dense) L/D=4(loose)
McCorkle(1969)	L/D<10	L/D=5
Williams and Parry(1979)	L/D<20	L/D<5
Poulos and Davis(1980), Vallabhan et al.(1982), Meyerhof et al.(1983)	Krs > 0.01 to 0.001	K_{rs} = 6.6(dense) Krs = 56(loose)

Table 5.2 Limiting values for pile rigidity classification

CHAPTER 6

CENTRIFUGAL MODEL PILE TESTS

6.1 INTRODUCTION

Modelling was previously done either by small or full scale conventional tests. Although a small model scale test is relatively economical, in terms of finance and time, compared with a full scale test, it is not reliable in predicting the actual prototype behaviour due to the differences in stress levels surrounding the model and prototype respectively. For this reason the centrifugal modelling technique has become increasingly used. In this chapter an extensive study of the behaviour of short piles embedded in sand is described. All models were tested using a medium sized centrifugal accelerator which will be mentioned in section 6.4.

6.2 THE CENTRIFUGE MODELLING TECHNIQUE

6.2.1 INTRODUCTION

As early as 1869, Edouard Phillips, a French Engineer proposed the first idea of centrifuge modelling as mentioned by Craig(1989). Not until the early 1930's was the

idea brought to fruition in America and the USSR. The earliest study was used to replicate the effect of body forces in a scaled model of an earth structure which was done by Bucky et al.(1935) in the USA and Pokrovsky and Fedorov(1936) in the USSR independently. In late 1960's, Schofield initiated the use of centrifuge modelling in the United Kingdom. Ever since, the centrifuge modelling technique has been recognized as an important geotechnical research tool by which a physical model of soil can be made to satisfy the requirements of similarity. The two most popular fields of study in geotechnical engineering, are the various aspects of slope stability and pile behaviour.

6.2.2 PRINCIPLE OF CENTRIFUGAL MODELLING LAW

Soil behaviour mainly depends upon the 'stress-strain' relationships which are commonly dependent upon stress level. By making the model stress equal to prototype stress the behaviour of the model under test will simulate the behaviour of the prototype. Based on this principle the idea of modelling using the centrifugal technique was developed.

Assuming an element is free to move, a force exerted on the element would be the product of its local acceleration and its mass. The force acting on the element would determine the weight of the element itself. In view of this, the element is moved radially at radius r and at a velocity of V_r as shown in Figure 6.1. If the element was not fixed at the centre of the circle O, element of A and B would tend to move out of the

curved path into a straight line in the directions of V and T respectively. Since the element is fixed relative to the centre of rotation, the angular velocity ω defined as the change of angle per second is created from the circular motion of the element.

Therefore

$$\omega = \frac{\theta}{t_\omega} \qquad (6.1)$$

where θ = Angle about centre of rotation

t_ω = Time travel about θ

The tangential speed V_r which developed due to the movement along the circular path is defined as:

$$V_r = \frac{s}{t} \qquad (6.2)$$

Where s = Distance travelled along the path

t = time taken to travelled at distance s

Since $t = t_\omega$

Then by substituting equations (6.1) and (6.2)

$$V_r = \frac{s\omega}{\theta} \qquad (6.3)$$

Assuming $\theta \rightarrow 0$ Tan $\theta = \theta$

Hence

$$r = \frac{s}{\theta}$$

Therefore the velocity of an element in the circular path is:

$$V_r = r\omega \qquad (6.4)$$

Although the speed of the element moving in the circular motion has the same value such that $V_A = V_B$ as shown in Figure 6.2, however the magnitude is different at all time. The direction of motion of an element differs at every point of the circular track as shown in Figure 6.2 . Due to this change, radial acceleration A_r has occurred. The radial acceleration is defined as change of velocity with respect to the change of time.

$$A_r = V_r \frac{\partial\theta}{\partial t} \qquad (6.5)$$

In the limit where $\partial t \rightarrow 0$,

$$\frac{\partial\theta}{\partial t} = \frac{d\theta}{dt} = \omega$$

Since $V_r = r\omega$

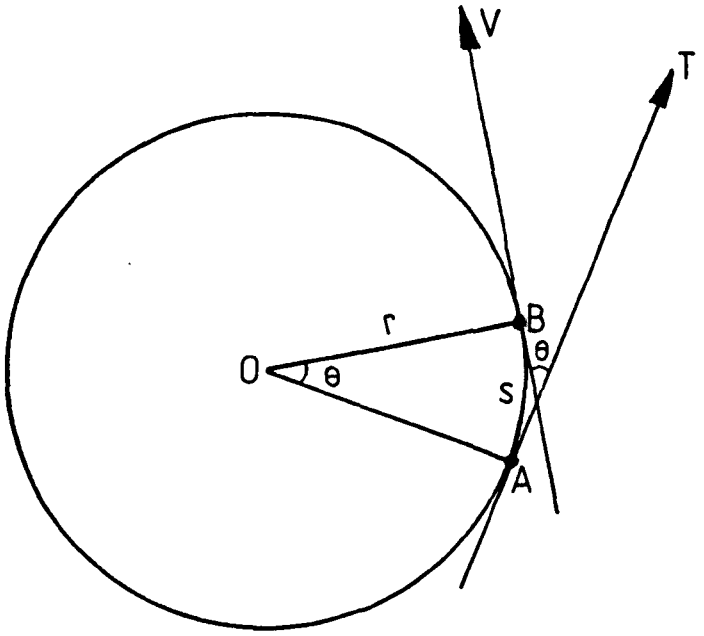

Figure 6.1 Angular velocity of an element in a circular path

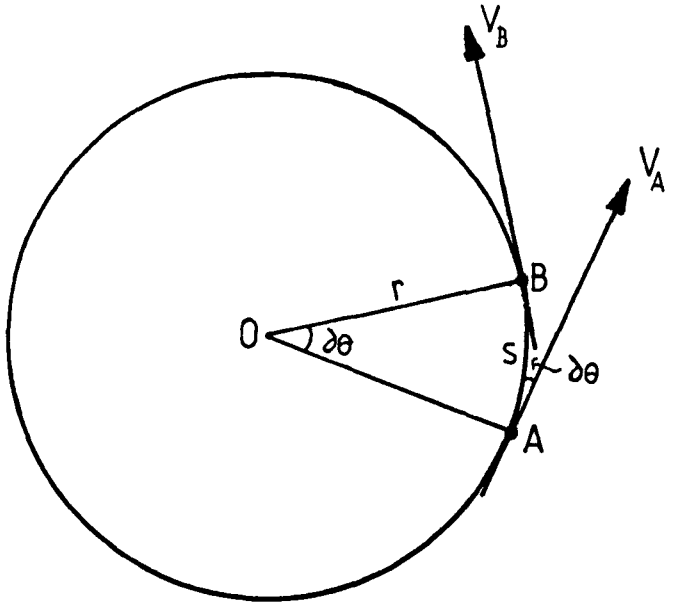

Figure 6.2 Element in a circular motion moving in different direction

$$A_r = r\omega^2 \qquad (6.6(i))$$

or

$$A_r = \frac{V_r^2}{r} \qquad (6.6(ii))$$

Therefore the radial acceleration A_r imposed on the element pulled from its straight movement is $r\omega^2$.

6.2.3 APPLICATIONS TO CENTRIFUGAL MODELLING

An object at rest in static equilibrium experiencesan inertial force commonly known as body-weight. The force is a product of the mass of the object and the local acceleration namely the gravity force. When an object is rotated at a fixed radius, it experiences an inertial force acting towards the centre of its body. Apart from the body-weight of the object at rest, the object now experiences an increase in body-weight which is equivalent to the radial acceleration of the centrifuge.

Suppose the mass of an object at rest is ρ, when this object is rotated it would tend to move from its circular path to a straight path at an instantaneous rate of $A_m=V_r^2/r$. However, since it was held at the centre of the rotation to restrained it from moving into a straight path, the inertial force acting on the object would now be

equivalent to the product of the acceleration induced by the centrifugal action and the mass of the object.Therefore the weight of the object increased from ρg to ρA_m.

Since $A_m = V_r^2/r$

Therefore $\rho A_m = \rho . V_r^2/r$

then multiplying ρ by g/g gives,

$$\rho A_m \frac{g}{g} = \gamma \frac{V^2}{rg} \qquad (6.7(i))$$

Assuming N to be a scaling factor which is equivalent to V_r^2/rg, equation (6.7(i)) can be simplified to

$$\overline{\gamma} = \gamma N \qquad (6.7(ii))$$

Thus it can be seen that, an object having a unit weight of γ will increase its unit weight to γN when it is rotated. The behaviour of prototype structures can be simulated from that of a small model by increasing its unit weight so that the same stress level will be experienced at a corresponding points in model and prototype. So the fundamental action of the centrifuge is to increase the unit weight γ at rest to γN at speed.

If the model is made from the same material as the prototype and tested under the same boundary conditions, the model with linear scaling of 1/N will experience the same stresses as the prototype at the corresponding points if it experiences the local acceleration of N times the earth gravity. Results of such a test accurately represent the behaviour of the prototype thus eliminating the scale errors.

6.3 SCALING RELATIONSHIPS

Avgherinos and Schofield(1969), explained the scaling laws with reference to two basic problems in soil mechanics, i.e slope stability and consolidation. The geometrical relationship is primarily based on slope stability while time scale factor is based on the primary consolidation process.

In a slope stability analysis, a dimensionless coefficient, the stability number, is expressed in terms of dimensionless value $c/\gamma H$ and ϕ. Assuming that the models used the same materials and maintained the same boundary conditions as the prototype, values of c and ϕ are identical in the model and prototype. Equating both prototype and model stability equations gives;

$$\frac{(c)_m}{(c)_p} = \frac{\gamma_m H_m}{\gamma_p H_p} \qquad (6.8)$$

Since $(c)_m = (c)_p$

Therefore

$$\frac{\gamma_m}{\gamma_p} = \frac{H_p}{H_m} \qquad (6.9)$$

Assuming that the model is scaled down to 1/N and is spun at N times earth's gravity, the unit weight of the soil is increased from γ to $N\gamma$. Thus according to Avgherinos and Schofield giving equation (6.9) as

$$N = \frac{\gamma_m}{\gamma_p}$$

Similarly for the ratio of height of model and prototype,

$$N = \frac{H_p}{H_m}$$

Therefore the condition of the scaling ratio is that,

$$N = \frac{\gamma_m}{\gamma_p} = \frac{H_p}{H_m} \qquad (6.10)$$

Avgherinos and Schofield derived equation (6.10) from the requirement that the body-forces of the corresponding elements, in model and prototype, should be in the same ratio as their surface area.

Time factor T_v in the primary consolidation process introduced by Terzaghi was used to determine the scaling relationship which is dependent on the time in the centrifuge. In the model law of consolidation, it was stated that if the same layer of soil, having a different drainage length, is acted upon by the same pressure increases and reaches the same degree of consolidation at its own time, the coefficient of consolidation c_v and the time factor T_v are then theoretically identical.

Considering the basic relationship for primary consolidation ,

$$T_v = \frac{c_v\, t}{H^2} \qquad (6.11)$$

Therefore

$$\left(\frac{T_v}{c_v}\right)_m = \left(\frac{T_v}{c_v}\right)_p$$

$$\frac{t_m}{H_m^2} = \frac{t_p}{H_p^2}$$

$$\frac{t_m}{t_p} = \frac{H_m^2}{H_p^2}$$

But

$$\frac{H_m^2}{H_p^2} = \frac{1}{N^2}$$

Therefore

QUANTITY	Scale:model at Ng
Length	1 : 1/N
Acceleration(gravitational,inertial)	1 : N
Area	1 : $1/N^2$
Volume	1 : $1/N^3$
Density	1 : 1
Mass	1 : $1/N^3$
Force	1 : $1/N^2$
Stress	1 : 1
Strain	1 : 1
Displacement	1 : 1/N
Frequency of loading	1 : N
Time	
Creep, viscous phenomena	1 : 1
Inertial effects	1 : 1/N
Fluid flow, diffusion phenomena	1 : $1/N^2$

Table 6.1 Fundamental scaling relationship for centrifuge modelling after Craig(1983)

$$t_p = N^2 t_m \qquad (6.12)$$

In all scaling involving time factors, generally a 1/N scale model will experience N^2 times faster than they occur in the prototype. Craig(1983) summarises the principal scaling relationships assuming that the same soil is used in the model and prototype shown in Table 6.1.

6.3.1 SIMILARITY REQUIREMENTS AND PERCENTAGE ERROR BETWEEN MODEL AND PROTOTYPE

Generally when a model is scaled down to 1/N of a prototype size, it must then be subjected to a force of N times earth's gravity in order to simulate the prototype behaviour. However, in certain tests prototype soil parameters are used, such as the size of soil particles and the soil density. It can be argued that both of these parameters should be similarly reduced. Because of this Ovesen(1979), considered the scaling law relationship based on dimensional analysis. This methodology was demonstrated by determining the bearing capacity of a circular footing on a dry sand. To apply this methodology two essential requirements should be satisfied.

- The complete set of similarity requirement must be established by means of dimensional analysis.

- Any similarity differences must be justified by secondary experimental evidence.

Ovesen conducted centrifugal and conventional tests to investigate the deviation from similarity between model and prototype. Eight independent quantities shown in Figure 6.3(a) and 6.3(b) were listed as potential influences on the load-settlement curve:

γ	N/m^3	Unit weight of sand
D	m	Diameter of footing
e	-	Void ratio of sand
ϕ	-	Internal friction angle of sand
σ_c	N/m^2	Cohesive force between sand grains
σ_g	N/m^2	Crushing strength of grain material
E_g	N/m^2	Coefficient of elasticity of grain material
d_g	m	Average grain size

Taking γ and D as basic units, Ovesen expressed the peak value of surface load q_s in dimensionless form as a function of six independent dimensionless products;

$$\frac{q_s}{\gamma D} = F\left(e, \phi, \frac{\sigma_c}{\gamma D}, \frac{\sigma_g}{\gamma D}, \frac{E_g}{\gamma D}, \frac{d_g}{D}\right)$$

For complete similarities, these six dimensionless quantities should have the same values for both models and prototypes. Table 6.2 summarises six the similarity

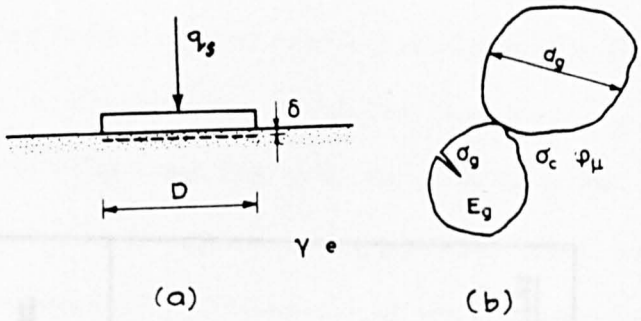

Figure 6.3 Parameters of circular footing resting on a dry sand surface and the dimension of a sand grain. (Ovesen, 1979)

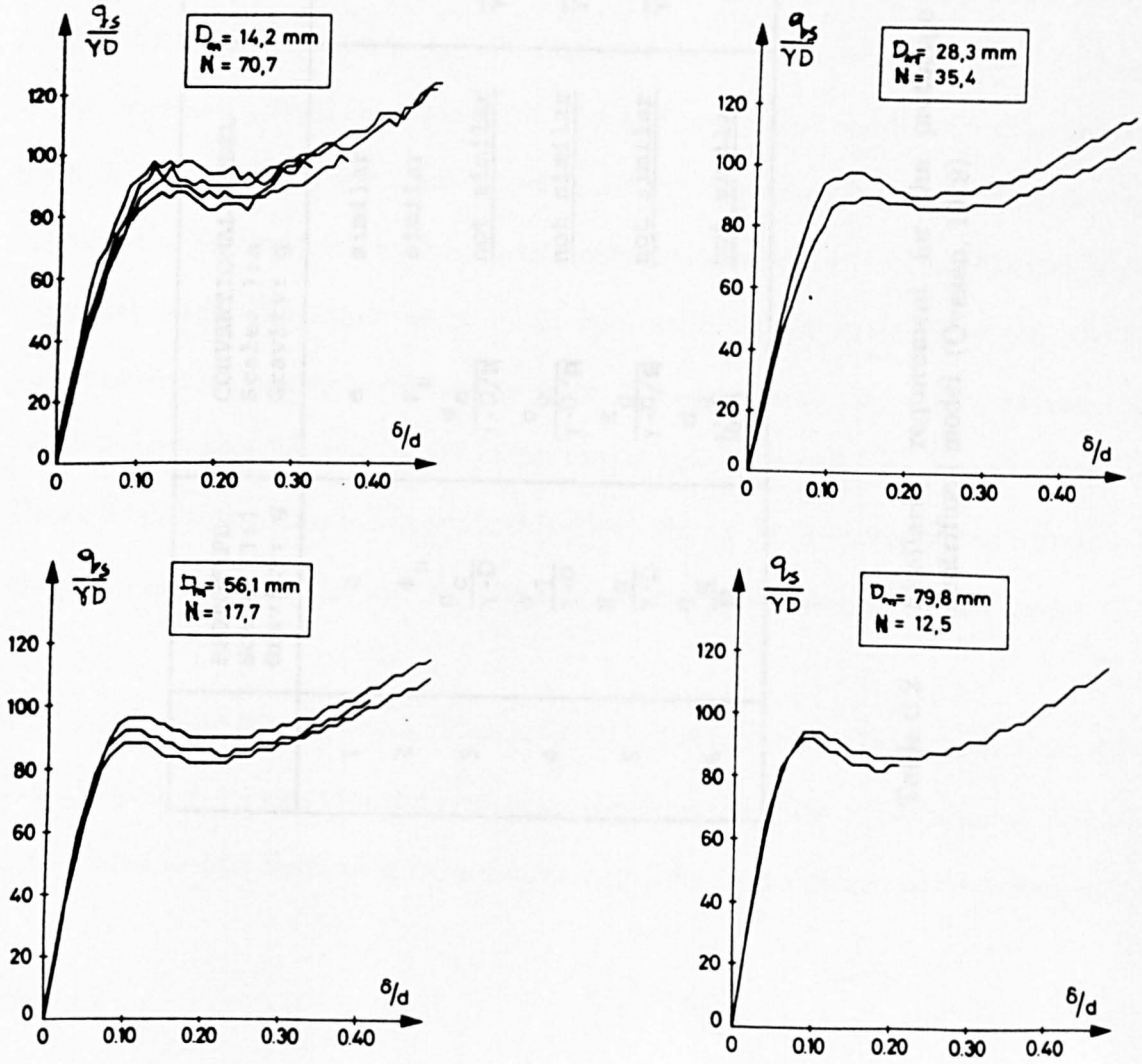

Figure 6.4 Dimensionless load-settlement curves for test corresponding to a 1m diameter prototype footing. (Ovesen, 1979)

	PROTOTYPE Scale: 1:1 Gravity: g	CONVENTIONAL MODEL Scale: 1:n Gravity: g		CENTRIFUGAL MODEL Scale: 1:n Gravity: n·g	
1	e	e	similar	e	**similar**
2	ϕ_μ	ϕ_μ	similar	ϕ_μ	**similar**
3	$\frac{\sigma_c}{\gamma \cdot D}$	$\frac{\sigma_c}{\gamma \cdot D/N}$	not similar	$\frac{\sigma_c}{\gamma N \cdot D/N}$	**similar**
4	$\frac{\sigma_g}{\gamma \cdot D}$	$\frac{\sigma_g}{\gamma \cdot D/N}$	not similar	$\frac{\sigma_g}{\gamma N \cdot D/N}$	**similar**
5	$\frac{E_g}{\gamma \cdot D}$	$\frac{E_g}{\gamma \cdot D/N}$	not similar	$\frac{E_g}{\gamma N \cdot D/N}$	**similar**
6	$\frac{d_g}{D}$	$\frac{d_g}{D/N}$	not similar	$\frac{d_g}{D/N}$	**not similar**

Table 6.2 Similarity requirement for the prototype in conventional and centrifugal model (Ovesen, 1979)

requirements for both conventional and centrifugal models. In the conventional test, the model departs considerably from complete similarity with the prototype, in that four of the similarity requirements are not fulfilled. However five similarity requirements are fulfilled in a centrifugal test. Due to the fact that the prototype sand is usually used in the model, the similarity requirement on grain size is not complied with. To check this departure from similarity, Ovesen carried out a series of centrifuge tests on model footings.

Figure 6.4 shows results obtained from Ovesen's centrifugal tests in which all models simulated a 1m diameter prototype footing. Various sizes of model footing, ranging from d_m = 14.2mm to d_m = 79.8mm and acceleration ratios from N = 70.7 to N = 12.5 were used. From these graphs it is clear that all peak values are identical. The peak values from Figure 6.4 are summarised in Figure 6.5. It appears that no scale effects were observed for models having diameters from 14.2mm to 79.8mm which represent model diameter/average grain size ratios ranging from 30 to 180. Ovesen observed that a minor scale effect occurred for two cases, i.e the model diameter/average grain size of about 15, and for the larger model footing diameter in a small container. Hence he proposed that, to eliminate this effect, the model diameter/average grain size should be greater than 30 and the container size/footing diameter should exceed 5.

Normally the prototype is under earth's gravity field where the radius of the earth is infinite compared to the prototype size. Thus the earth's gravitational field will act parallel and be uniform in direction at all points in the prototype. However in the

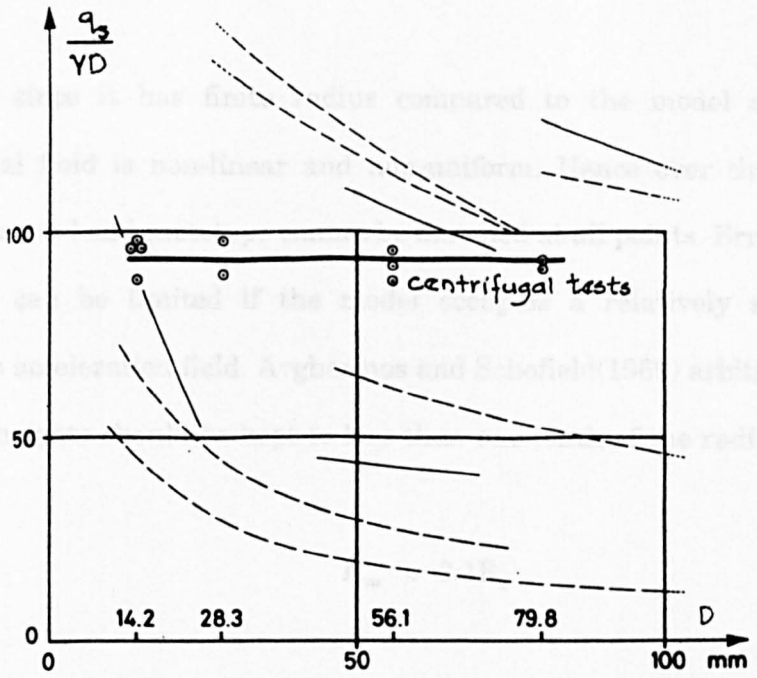

Figure 6.5 Summary of a peak values obtained from centrifugal test and a conventional test. (Ovesen, 1979)

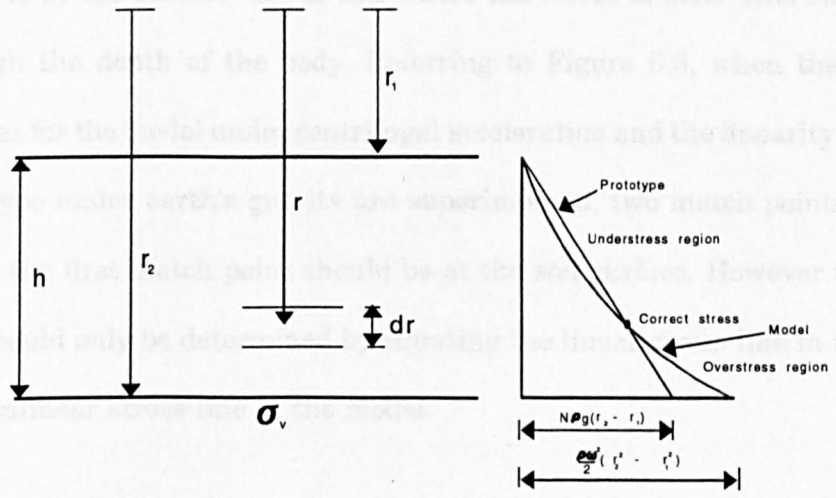

Figure 6.6 Stress distribution in centrifuge modelling

centrifuge, since it has finite radius compared to the model size, the artificial gravitational field is non-linear and non-uniform. Hence over the depth of model, stresses in model and prototype cannot be matched at all points. Error caused by these differences can be limited if the model occupies a relatively small part of the centrifuge's acceleration field. Avgherinos and Schofield(1969) arbitrarily decided that the model heights should be kept to less than one tenth of the radius of rotating arm R_a.

$$H_m < 0.1R_a$$

However, Schofield(1980) presented a more systematic way to determine the percentage error in differences between model and prototype. Schofield suggested that an integration is required to calculate this error which was caused by the difference between the uniform acceleration in a prototype and radially varying acceleration in the centrifuge. According to Newton's gravity law, the force acting at the centre of mass of each atom will affect the self weight of the body. In this case the upper surface of the body is not affected by the stress. Thus the first match point between prototype and model is at the surface of the soil where the stress is zero. This stress will build up through the depth of the body. Referring to Figure 6.6, when the non linearity of stresses for the model under centrifugal acceleration and the linearity of stresses for the prototype under earth's gravity are superimposed, two match points can be obtained where the first match point should be at the soil surface. However the second match point could only be determined by equating the linear stress line in the prototype and the nonlinear stress line in the model.

Assuming r is to be the effective radius of the model, the vertical stresses at r need to be integrated from the surface r_1 to the depth defined by radius r.

Therefore,

$$\sigma_{vm} = \int_{r_1}^{r} \rho\omega^2 r \, dr$$

$$= \frac{\rho\omega^2}{2}(r^2 - r_1^2) \qquad (6.13)$$

Assuming that the second match point is at $r = r_o$

Therefore

$$\sigma_{vm} \text{ at } r_o = \frac{\rho\omega^2}{2}(r_o^2 - r_1^2)$$

and

$$\sigma_{vp} \text{ at } r_o = N\rho g(r_o - r_1)$$

Since $\sigma_{vm} = \sigma_{vp}$

Therefore

$$\frac{\rho\omega^2}{2}(r_o^2 - r_1^2) = N\rho g(r_o - r_1)$$

$$\omega^2 = \frac{2Ng}{(r_o + r_1)} \qquad (6.14)$$

At any other position in the understress region, the error developed is,

$$\varepsilon = N\rho g(r-r_1) - \frac{\rho\omega^2}{2}(r^2 - r_1^2)$$
$$= N\rho g(r - r_1) - N\rho g\frac{(r^2 - r_1^2)}{r_o + r_1} \qquad (6.15)$$

At maximum error mathematically

$$\frac{d\varepsilon}{dr} = 0$$

$$\frac{d\varepsilon}{dr} = N\rho g - \frac{2N\rho gr}{r_o + r_1}$$
$$0 = N\rho g - \frac{2N\rho gr}{r_o + r_1}$$

which gives

$$r = \frac{r_o + r_1}{2} \qquad (6.16)$$

Substituting the value of r into equation (6.15) then the maximum error is

$$= \frac{\frac{r_o}{2} - \frac{r_1}{2}}{r_o + r_1} \qquad (6.17)$$

Practically the maximum error will occur at the point r = r_2(i.e point in overstress region).

Therefore error at r = r_2

$$= N\rho g\frac{(r_2^2 - r_1^2)}{(r_o + r_1)} - N\rho g(r_2 - r_1) \qquad (6.18)$$

Maximum error is

$$= \frac{(r_2^2 - r_1^2)}{(r_o + r_1)} - 1$$

$$= \frac{r_2 + r_1}{r_o + r_1} - 1 \qquad (6.19)$$

By equating both maximum error from equation (6.17) and (6.19) gives,

$$\frac{\frac{r_o}{2} - \frac{r_1}{2}}{r_o + r_1} = \frac{r_2 - r_o}{r_o + r_1}$$

$$r_o = r_1 + \frac{2}{3}(r_2 - r_1)$$

$$r_o = r_1 + \frac{2}{3}h \qquad (6.20)$$

Therefore the value of r_o is at one third of the depth up from the base.

Since the optimum speed is calculated as

$$\overline{r}\,\overline{\omega}^2 = Ng$$
$$\overline{r} = \frac{Ng}{\overline{\omega}^2}$$

Taking the value of ω^2 from equation (6.14),therefore

$$\bar{r} = \frac{r_o + r_1}{2} \qquad (6.21)$$

Substituting r_o from equation (6.20) into equation (6.21) gives,

$$\bar{r} = \frac{r_1 + \frac{2}{3}h + r_1}{2}$$

$$= r_1 + \frac{h}{3} \qquad (6.22)$$

The optimum scaling radius is therefore at one third of the depth from the surface of the soil. Taking the maximum error from equation (6.19)

$$\varepsilon = \frac{r_2 - r_1}{r_o + r_1} - 1$$

and by substituting r_o from equation (6.20) into it gives

$$\varepsilon = \frac{r_2 - r_1 - \frac{2}{3}h}{r_1 + \frac{2}{3}h + r_1}$$

$$= \frac{h - \frac{2}{3}h}{\frac{2}{3}h + 2r_1}$$

$$= \frac{\frac{h}{3}}{2(r_1 + \frac{h}{3})}$$

$$\varepsilon = \frac{h}{6r} \qquad (6.23)$$

For the centrifugal machine, at the University of Liverpool with an optimum scaling radius of 1.07m and the model of maximum depth of 0.23m, the maximum deviation between prototype and model in percentage terms will be 3.6%. This error is relatively small and can be ignored if the height of model is maintained at minimum possible.

6.3.2 RELATIONSHIP BETWEEN ROTATIONAL SPEED AND SCALING FACTOR

Scaling factor N is not recorded directly from the instrumentation of the centrifugal machine. However it can be related to the rotational speed. Angular velocity ω in equation 6.4 can also be expressed as

$$\omega = 2\pi F_r \qquad (6.24)$$

where F_r is the number of revolution/sec.

Substituting equation 6.4 into equation 6.24, the tangential velocity V_r in term of number of revolution/sec F_r can be written as

$$V = 2\pi F_r r \qquad (6.25)$$

Since $A_r = V^2/r = Ng$

Therefore

$$Ng = \frac{(2\pi F_r r)^2}{r}$$

$$F_r = \sqrt{\frac{Ng}{4\pi^2 r}}$$

$$= \frac{1}{2\pi}\sqrt{\frac{Ng}{r}} \qquad (6.26)$$

However if F_r is quoted in revolution/minute (rpm) then,

$$F_r = \frac{1}{2\pi}\sqrt{\frac{Ng.60^2}{r}}$$

$$= \frac{30}{\pi}\sqrt{\frac{Ng}{r}} \qquad (6.27)$$

For example if r = 1.097m and a scaling factor N = 50 is needed to model the desired prototype, therefore the value of speed of rotation needed is 201.9 rpm.

6.4 DESCRIPTION OF CENTRIFUGAL MACHINE AT THE UNIVERSITY OF LIVERPOOL

The research programme was carried using the facility in the Geotechnical Centrifuge Laboratory at the University of Liverpool. The facility is a medium size model G-380-3A centrifuge machine supplied by Triotech California. The machine is ideally suited for modelling problems which involve interaction between soil and buried structures under conditions of static equilibrium. It was originally designed to carry a maximum of 13g-tonnes up to 100g or 68 kg test package or less up to a maximum of 200g. Its medium size has facilitated numerous parametric studies, many involving the behaviour of piled foundations. Investigations into the response of pile to lateral load were reported by King et al.(1984), King and Fulthorpe(1986) and by Lyndon and Pearson(1988). Interaction studies between piles in group subjected to lateral loading were presented by Kulkarni et al.(1985). Subsequent research investigating the uplift capacity of piled foundations with enlarged bases was published by Dickin and Leung(1990,1992) and Leung and Dickin(1991). Preliminary work on the behaviour of short piled foundations subjected to large moments was reported by Dickin and Wei(1991) which has been extended in this project. At present, a research is being conducted by Laman to investigate the behaviour of short square pier embedded in clay.

The equipment consists of a cylindrical steel housing which contains a 20 h.p drive motor, drive shaft, rotor arm and bucket (see Plate 6.1 and Figure 6.7). The buckets, which are attached to both ends of the rotating arm are interchangeable, a

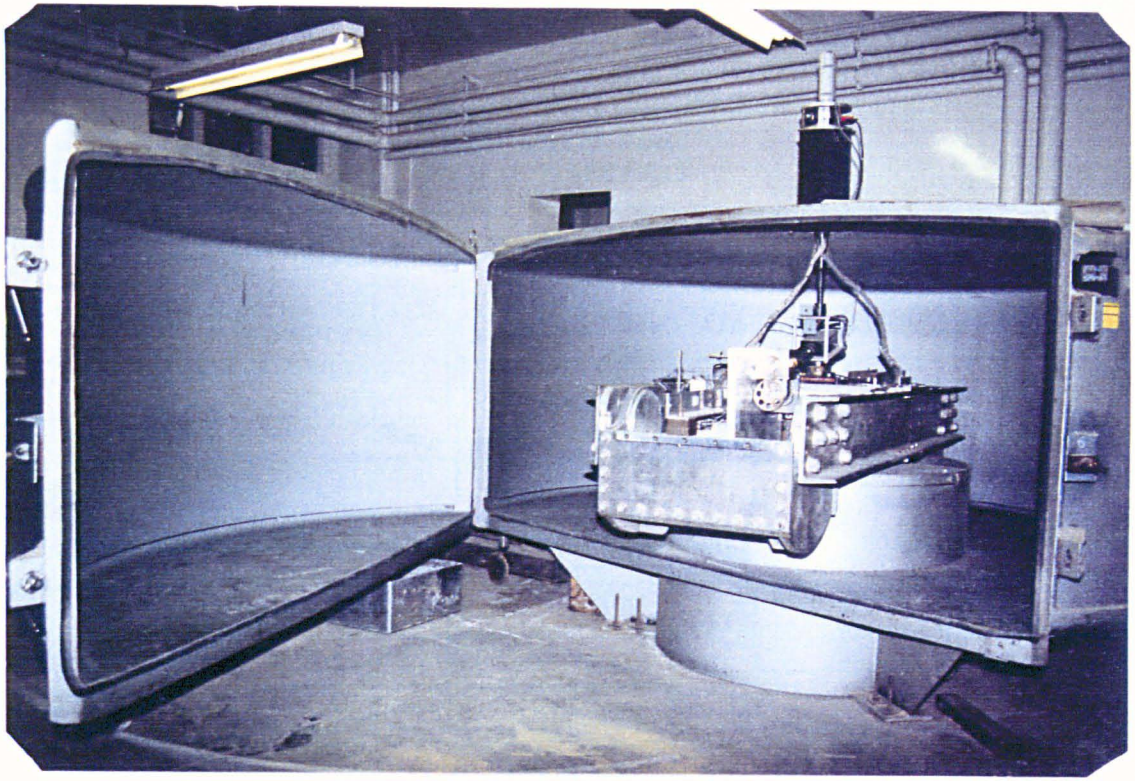

Plate 6.1 Centrifuge at the University of Liverpool

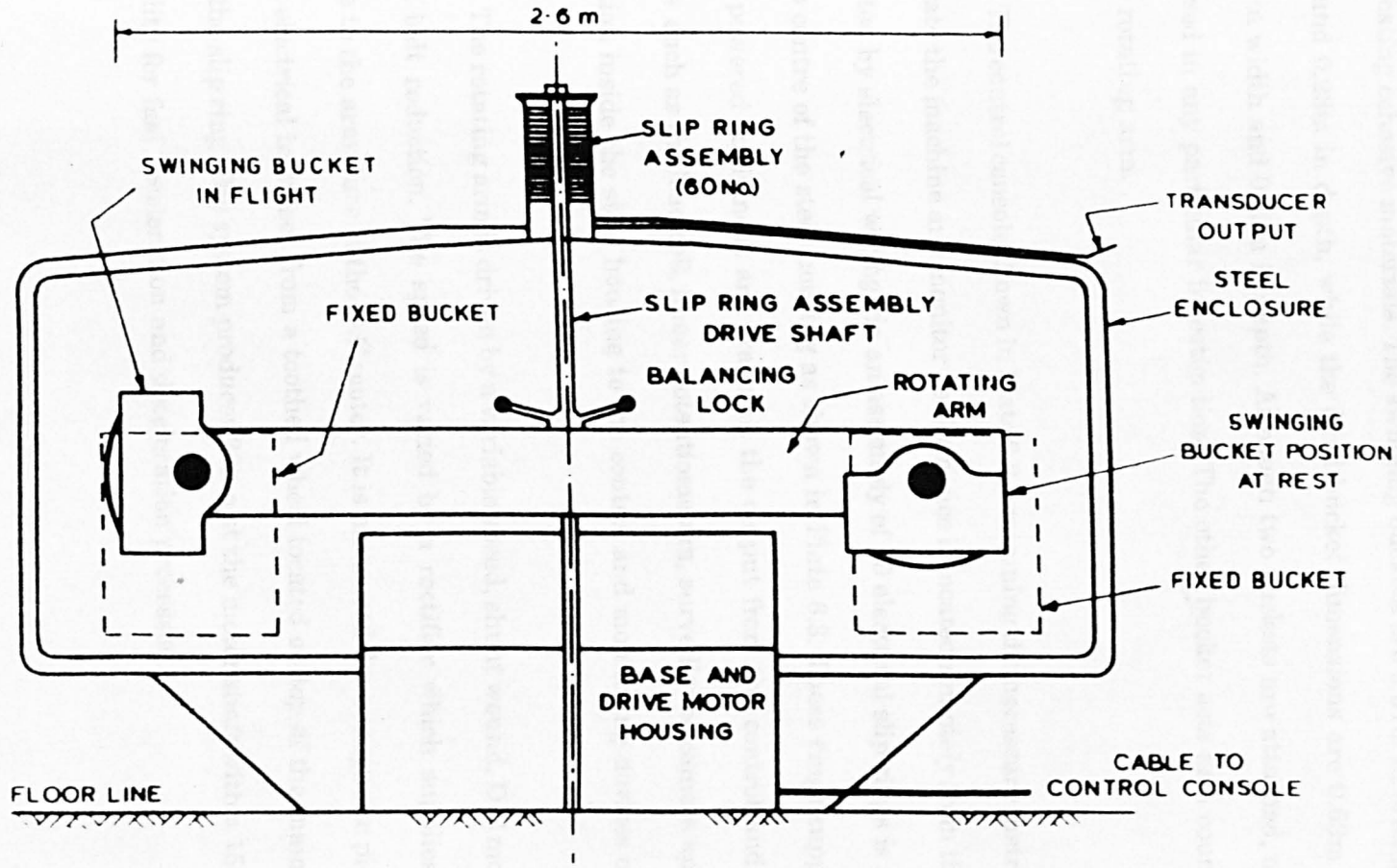

Figure 6.7 Schematic diagram of centrifuge facilities at the University of Liverpool

swinging or fixed arrangement being available. The swinging bucket is particularly advantageous when testing cohesionless material while the fixed bucket has been used when testing cohesive materials. The swinging buckets are 0.57m in breadth, 0.46m in width and 0.23m in depth, while the fixed bucket dimensions are 0.63m in breadth, 0.47m in width and 0.52m in depth. Although two buckets are attached, only one has been used in any particular investigation. The other bucket acts as a counter balance for the rotating arm.

The control console shown in Plate 6.2, containing the necessary instrumentation to operate the machine and monitor performance is located remotely from the enclosure connected by electrical wiring via an assembly of 60 electrical slip rings is mounted on the top centre of the steel housing as shown in Plate 6.3. These rings supply power to mains powered equipment and transmit the output from the control and monitoring devices such as the load cell, linear potentiometers, surveillance camera and the motor activation inside the steel housing to the control and monitoring devices outside.

The rotating arm is driven by a variable speed, shunt wound, D.C motor through cogged belt reduction. The speed is varied by a rectifier which supplies a variable voltage to the armature of the D.C motor. It is measured by a magnetic pick-up which senses electrical impulses from a toothed wheel located on top of the main drive shaft below the slip ring. The system produces 20h.p at the motor shaft with a 150% overload capability for fast acceleration and deceleration processes.

Plate 6.2 Centrifuge control console

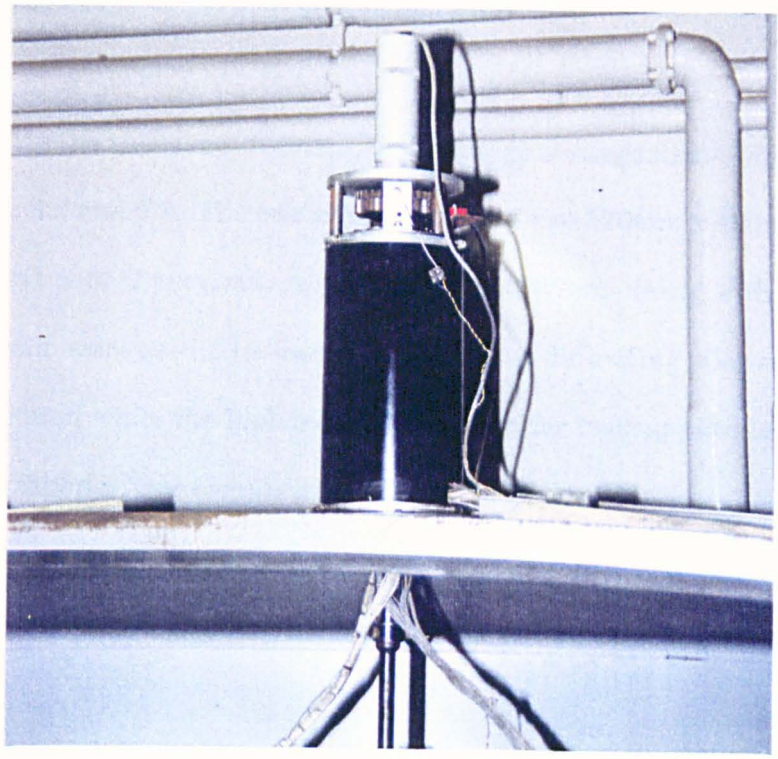

Plate 6.3 Slip ring assembly mounted on top of a steel housing

The rotating arm 2.6m long, 0.86m wide and 0.26m deep fabricated from a steel channel section was locked onto the drive shaft which is connected to the drive motor by a cogged belt and pulley located in the lower portion of the assembly. The rotating arm contains a horizontal pivot shaft and special locking and unlocking mechanism for balancing the arm. Imbalance of the arm will result in vibration. An excess vibration indicator is provided to warn of excessive vibration caused by an imbalance of 750g-lbs or more.

6.5 CENTRIFUGAL TEST PACKAGE ARRANGEMENT

Before setting up the testing package, careful consideration has to be given to the limitations of the centrifugal machine capacity. The arrangement was designed to make optimum use of the space available in the centrifuge.

Considering the above requirement, test package arrangements were adopted as shown in Figures 6.8 and 6.9. The centrifuge bucket of size 570mm x 460mm x 230mm depth was divided into 2 sections. Aluminium walls 20mm thick with a height of 300mm and 500mm were used. The lower wall was used for testing piles with a pulling arm less than 200mm while the higher wall was used for testing piles with a pulling arm greater than 200mm. One compartment 380mm x 460mm x 230mm deep, was filled with sand in order to embed the pile. The adjacent compartment housed the motor and gearing arrangement which was mounted on the wall at various heights as required.

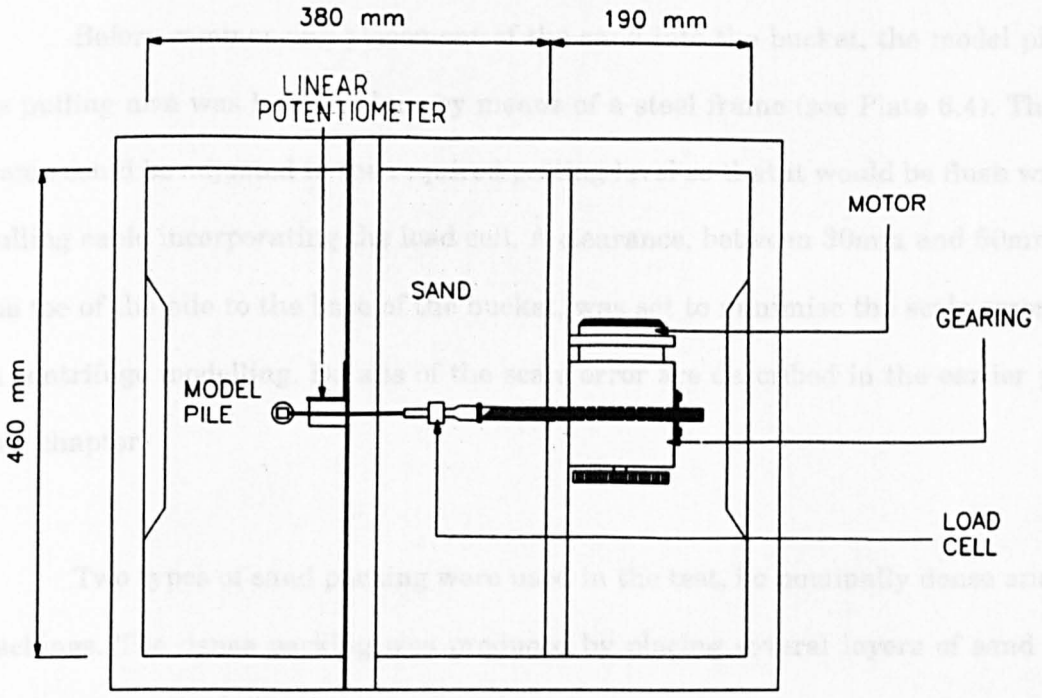

Figure 6.8 Plan view of package arrangement of a single pile embedded in flat terrain

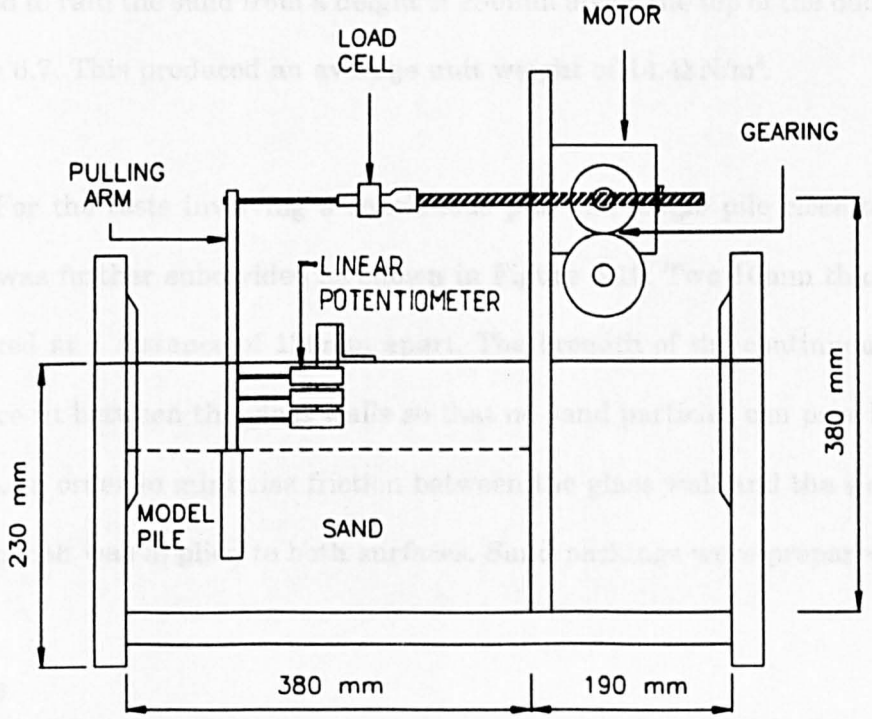

Figure 6.9 Side elevation of a package arrangement of a single pile embedded in flat terrain

Before commencing placement of the sand into the bucket, the model pile and its pulling arm was held in place by means of a steel frame (see Plate 6.4). The steel frame could be adjusted to the required pulling level so that it would be flush with the pulling cable incorporating the load cell. A clearance, between 30mm and 50mm from the toe of the pile to the base of the bucket, was set to minimise the scale error effect in centrifuge modelling. Details of the scale error are described in the earlier part of this chapter.

Two types of sand packing were used in the test, i.e nominally dense and loose packings. The dense packing was produced by placing several layers of sand in the bucket at an interval of less than 25mm. Each layer was compacted using a hand vibrator (see Plate 6.5). An average unit weight of 16.4kN/m^3 was achieved using this method. A sand raining method was used for the preparation of a loose packing. A baffle with 4mm diameter holes at 20mm spacing in a rectangular pattern(see Plate 6.6) was used to rain the sand from a height of 250mm above the top of the bucket as shown in Plate 6.7. This produced an average unit weight of 14.4kN/m^3.

For the tests involving a continuous pile and single pile close to a slope the bucket was further subdivided as shown in Figure 6.10. Two 10mm thick glass walls were fixed at a distance of 126mm apart. The breadth of the continuous pile gave a clearance fit between the glass walls so that no sand particles can pass by the side of the pile. In order to minimise friction between the glass wall and the side of the pile, silicon polish was applied to both surfaces. Sand packings were prepared similarly to

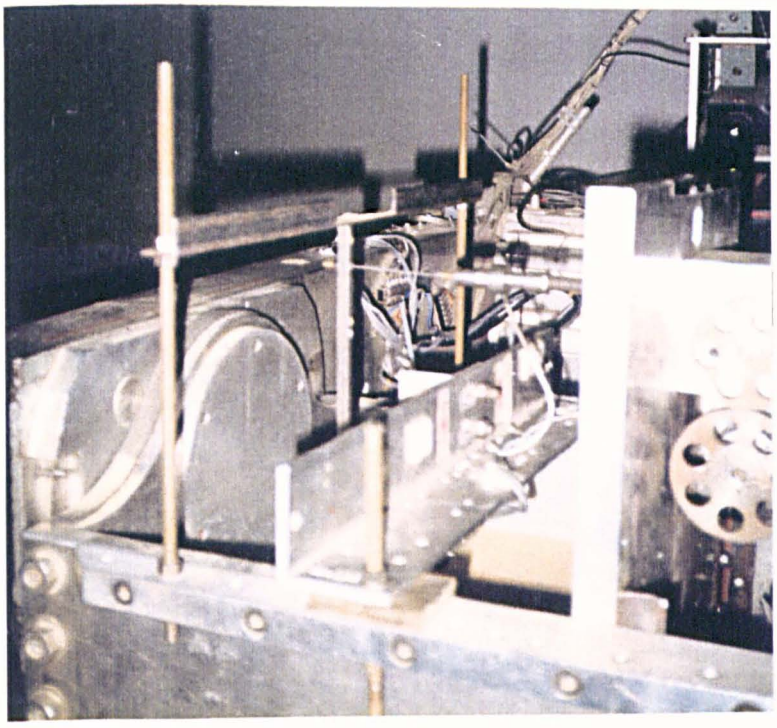

Plate 6.4 Pile supported on steel frame during sand placement

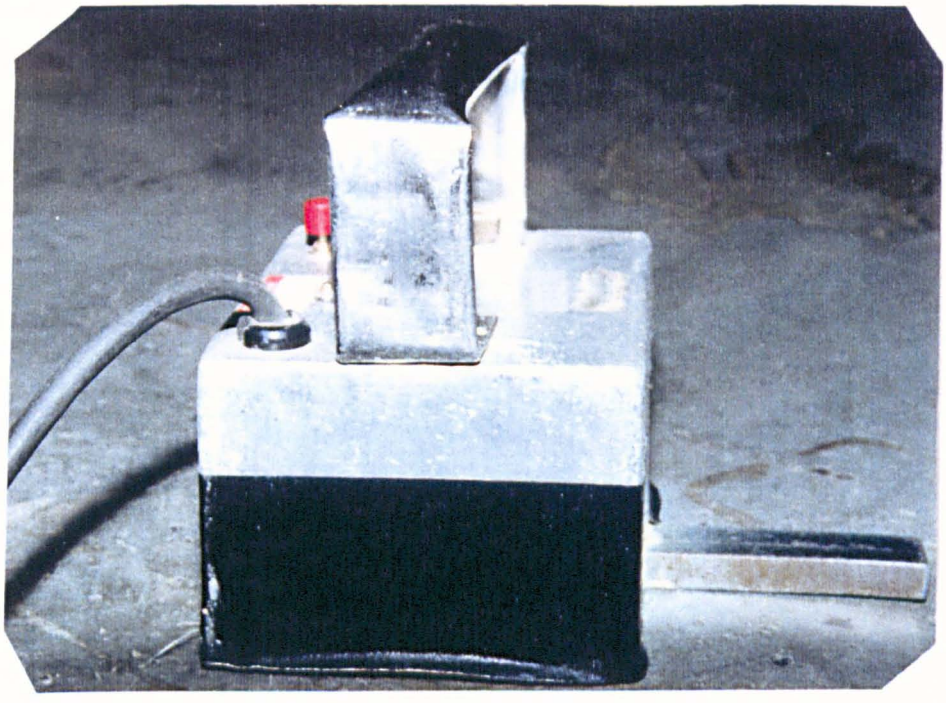

Plate 6.5 Small hand vibrator used in preparation for dense packing

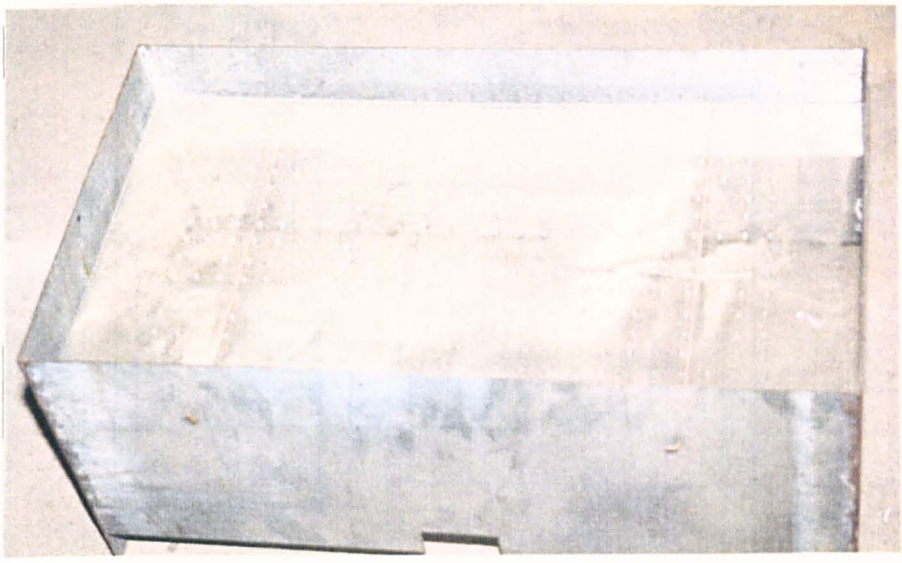

Plate 6.6 Baffle used for sand raining in preparation of loose packing

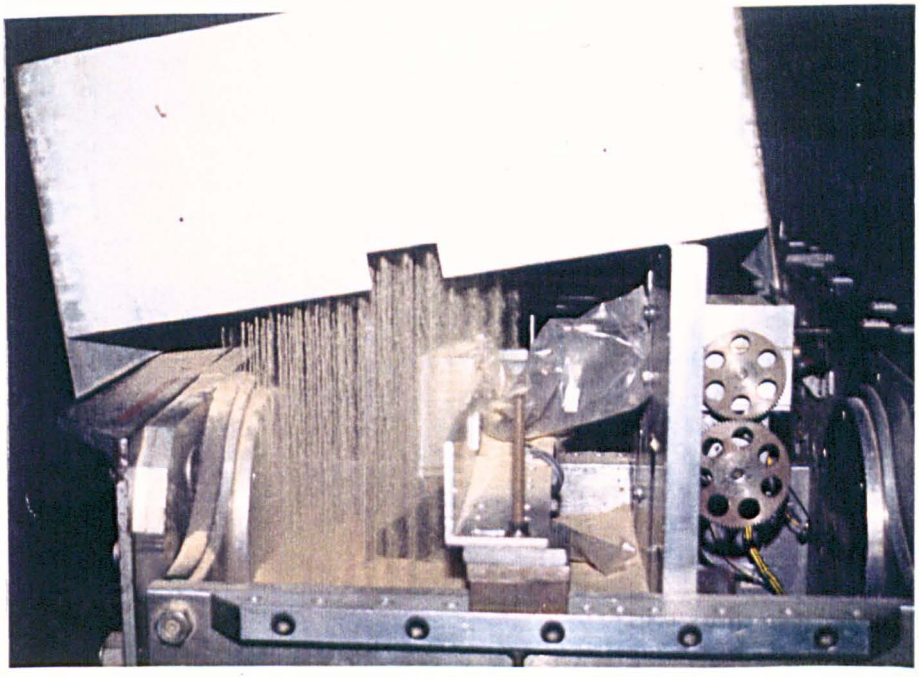

Plate 6.7 Sand raining method

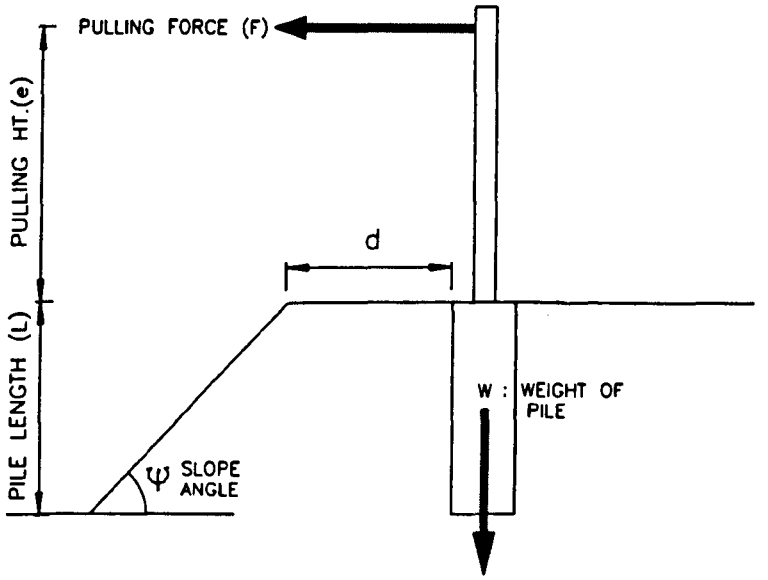

Figure 6.12 Side view of a lateral force pulling towards a slope

those for the single pile arrangement. However, in a 'slope' test, a dense sand layer was prepared up to the top of the pile. The slope was cut at the desired distance from the top of the pile. An average angle of 36° being formed. Lateral force was applied towards or away from the slope and the effect of the slope distance ratio, d/L is observed. Figures 6.11 and 6.12 show the orientation of the lateral force applied with respect to the slope.

Once the sand level was slightly above the top of the pile, surplus sand was skimmed off using a rectangular aluminium plate, to obtain a flat surface. A 3mm thick pulling cable, incorporating the appropriate load cell, was fixed through a hole at the required height(see Plate 6.8). Three SAKAI conductive plastic linear potentiometers capable of monitoring a horizontal movement of up to 25mm were placed directly in front of the pulling arm. The spindle was extended from the potentiometer to the surface of the pulling arm. To ensure a contact between the spindle of the linear potentiometers and the surface of the pulling arm was maintained, double-sided adhesive tape was stuck to the arm. The calibration of the linear potentiometers is shown in Appendix C.

A horizontal load was applied by a PARVALUX model 21SIS geared motor, linked to a custom built worm to worm mechanism to increase pulling power, attached to the dividing wall as shown in Plate 6.9. The rate of movement was achieved by the selection of appropriate gears linking the motor and gear box. A loading rate of 0.4mm/s was use throughout the program. The rotational movement of the motor gives a linear

at a constant displacement of

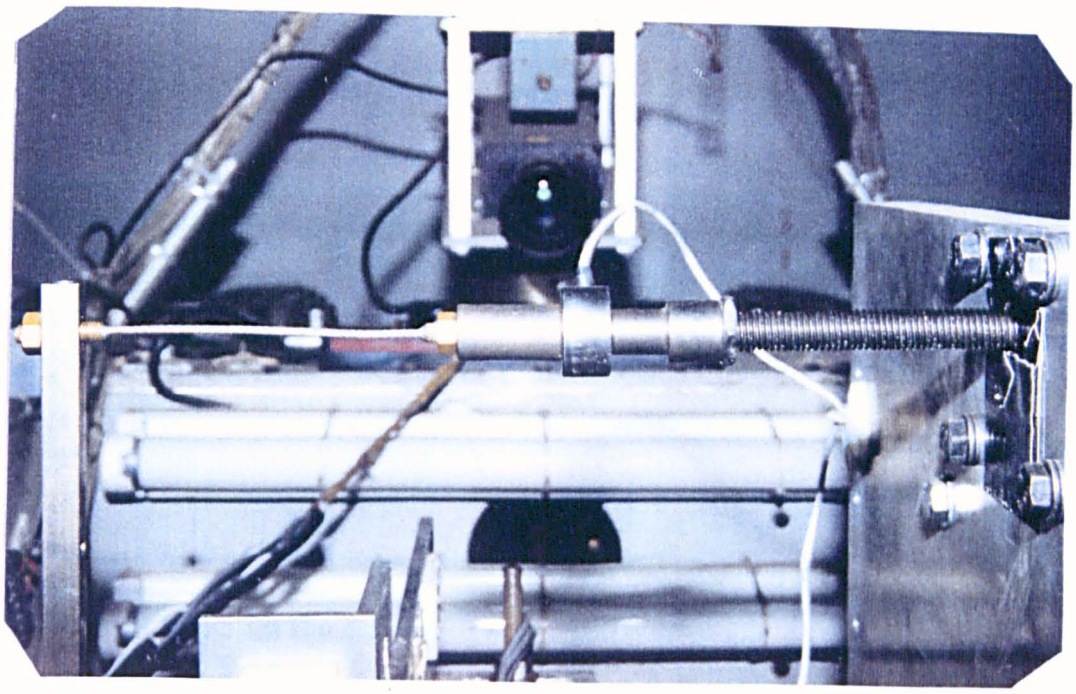

Plate 6.8 Pulling cable and load cell fixed to the pulling arm

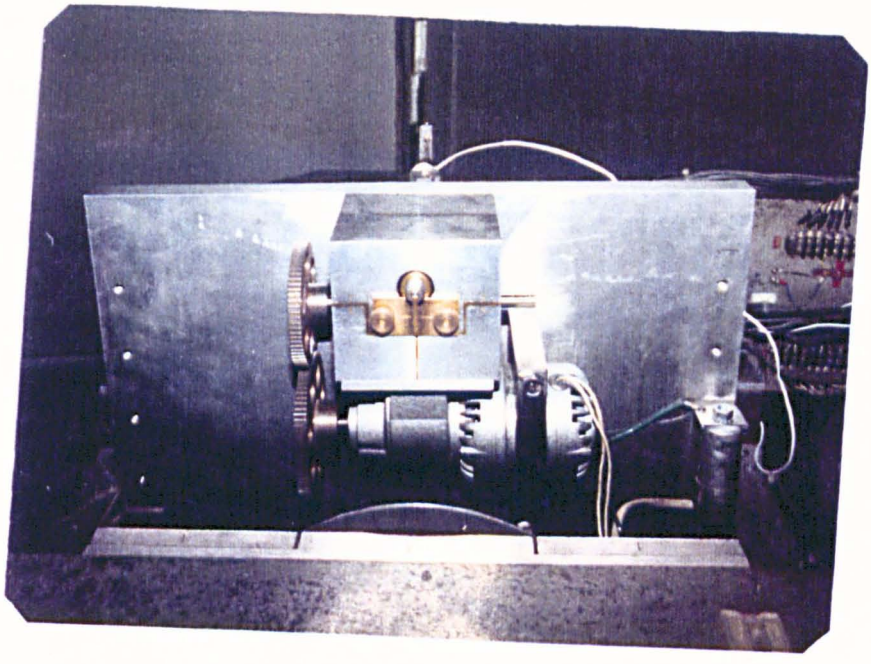

Plate 6.9 High torque geared motor and gear box attached to the partition wall

motion of the threaded gearbox shaft which was attached to the load cell. Two ranges of load cell were used in the test program depending on the requirements of the test. A load cell with a capacity of 2000 lb, was used in a continuous pile test series while the test on a single pile used a 250 lb load cell capacity. Calibration of the load cells are shown in Appendix C.

Signal wires from the monitoring devices attached to the test package were connected to the data logger through the slip ring system. A remote switch box connected to the PARVALUX motor was mounted on the side of the steel housing. The switch box is used to control the movement of the motor from outside the steel housing. Raw data obtained from the ORION data logger was read by a BBC computer (see Plate 6.10) using the program "READ" written by A.J Moorhouse, shown in Appendix D. It was then converted into ASCII format using the program "MODEL" written by Kueh(1989), in the same Appendix. Data was then transferred to IBM format using the available software BDOS. Data was mostly analyzed using the University's UNIX system facilities. Graph plotting was done using a UNIRAS subroutine which was written into the programs name "LOAD" and "MOMENT", as shown in Appendix D.

6.6 EXPERIMENTAL PROCEDURES

Prior to the commencement of the test, a safety check had to be completed. After finishing setting up the test package, balancing of the rotating arm was accomplished.

Plate 6.10 Computer facilities for data capture

As has been explained earlier in section 6.5, the other swinging bucket was used as a counterweight to obtain a balanced rotor arm. During the placing of the 'dummy' load in the bucket, the locking mechanism was unlocked leaving the arm to balance on the knife-edge. The load was added until the rotor arm was in the horizontal position. As soon as this was achieved, the locking mechanism was locked. If vibration occurs, due to the imbalance of the package during the test operation, it will be detected by a warning light on the control console. Electrical and signal wiring from the monitoring devices in the enclosure was tied carefully and firmly along the top of the bucket. Since the bucket will swing into the horizontal position, sufficient length of untied wiring has to be allowed between the bucket and the rotating arm. The untied wiring was held by a rubber band attached to the centre of the rotating arm to ensure that it could not be ripped off during the movement of the bucket into its 'in flight' position.

All test items such as the aluminium partition wall, the angle holding the linear potentiometers, the motor and the gearing were securely mounted using a sufficient number of high tensile bolts. The rotor arm was then checked for it smooth movement by rotating it once by hand before running the actual test.

The radial distance extending from the axis of the centrifuge to a position of one third of the depth of the embedded pile was measured to obtain the required acceleration. Theoretically the optimum scaling radii were calculated to the one third depth of the pile rather than the full soil depth, since in this particular research the contribution to overturning resistance from the sand below the pile was considered

minor. Observations from the two dimensional tests, performed in the glass box (See Chapter Eight) show that the sand layer below the tip of the pile has not been significantly affected during the rotational movement of the pile. The clearance between the tip of the pile and the base of the bucket was kept between 30mm and 50mm to ensure that the increase of scaling radius is minimised. The radial distance and acceleration were used to calculate the rotational speed using equation (6.27) shown earlier in this chapter.

After completing the above task, the steel housing door was then closed and locked by a single key which will operate the centrifugal machine. The key had been designed and installed as an additional safety measure in view of the danger of opening the door by mistake during the test operation. The machine can only be started when the single key is fully locked in a box near the console and will only be released the rotor is static.

The program "READ" was run to read the data from the data logger which was fed by the load cell and linear potentiometers. A "start" button was depressed and the digital display representing the rotational speed of the rotating arm in revolution per minute was displayed to the nearest 0.1 rev/min. The speed control knob was adjusted over an interval of 1 minute to ensure a smooth increase in rotational speed. After reaching the desired value, the speed was maintained for at least 2 minutes before initial readings of load and displacement were taken. A remote switch, located by the side of the steel housing which controls the movement of the motor, was used to

activate the loading mechanism linked to the model pile. The test was then continued until the output from the load cell had clearly reduced, or the applied load showed no significant change with the increase inclination of the model pile. When neither of these features occurred as was usually in the case of longer piles, a pile inclination of 8° was chosen as a failure criterion and the test was stopped. Inclinations of this magnitude have obviously exceeded the serviceability limits of any civil engineering construction. Once the failure value had been reached, the motor was switched off and the variable speed control knob turned back to a zero reading. The rotor arm then decelerates steadily. At a speed of less than 160 rev/min, the "stop" button was depressed to provide a dynamic braking and bring the machine to a fast, sure and controlled stop.

Throughout the test, constant surveillance was maintained by a video camera mounted on top of the rotor arm close to the axis of the machine. The camera was connected to a monochrome TV monitor (See plate 6.11 and 6.12). This has proved invaluable in establishing whether a drive mechanism was functioning correctly and providing a visual check on the test package. Each test took between 30 - 45 minutes to complete.

6.6.1 EXPERIMENTAL TEST PROGRAM

The test program carried out using the centrifugal machine comprised 5 main series as shown in Tables 6.3 to 6.7. Most of the tests simulated the behaviour of 1m

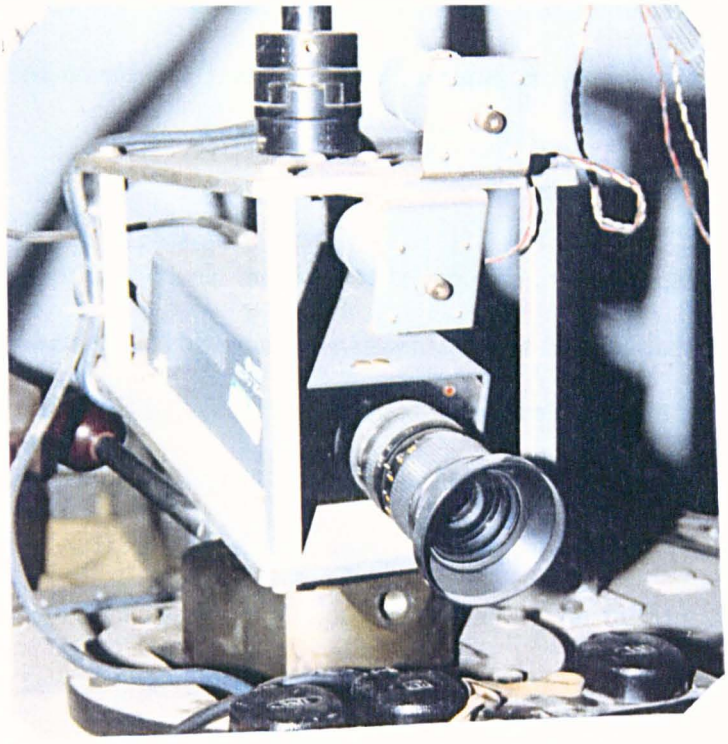

Plate 6.11 Video camera for internal surveillance

Plate 6.12 A 550mm monochrome TV monitor for visual checking

diameter prototype piles embedded in either dense or loose sand. Due to the restriction of space in the centrifuge bucket, pulling height ratios and embedment ratios of were 5 or less.

To provide a check on the centrifuge model testing and validate the scale relations, modelling of the models is essential and was performed in Series 1. Models of different sizes and accelerations were selected to simulate behaviour of a prototype of diameter 1m. Model lengths between 40mm $\leq L_m \leq$ 100mm with diameters varying between 20mm $\leq D_m \leq$ 50mm were tested under the appropriate acceleration value of between 20g $\leq N \leq$ 50g. An embedment ratio of 2 and pulling height ratio of 3 were used in this test series.

Series 2 was sub-divided into 4 sub-series. A 1m diameter prototype was simulated in Series 2A by spinning a 20mm diameter at 50g in dense packing to observe the effect of the pulling height and the pile length contributing toward the ultimate moment capacity of the pile. Series 2B had a similar packet arrangement to Series 2A. However the model piles were embedded in a loose sand. The effect of sand condition was observed apart from the pulling height and pile length. Practical difficulties arose in maintaining the stability of very short model piles with the embedment ratio of 1, especially for a 20mm diameter model pile in dense sand and embedment ratio of 2 in loose sand. To overcome this in Series 2C and 2D, the acceleration value was decreased to 20g and 33.3g and the pile diameter was increased to 50mm and 30mm respectively to obtain the same prototype diameter as in Series 2A

and 2B. Essentially tests in series 2 modelled the prototype length of $1m \leq L_p \leq 5m$ and the pulling height of $1m \leq e_p \leq 16m$ for a single prototype diameter of 1m. Arrangement of pile in this series is a shown in Figure 6.8 and 6.9.

Tests on models in dense sand in close proximity to a slopes were performed in Series 3. Series 3A investigated the effect of a pile pulled away from a slope as shown in Figure 6.11. Series 3B examines the effect when the pile was pulled towards the slope as shown in Figure 6.12. A slope factor K_s was introduced to show the effect on the moment limit of the pile embedded at a distance of $0 \leq d/L \leq 1.5$ from the top of the slope.

Series 4 involved tests on a 20mm diameter single model piles with embedment ratios between 2 and 5 and a pulling height ratio of 3, spun at different accelerations between 7g and 50g. Data for piles less than 0.2 m diameter were obtained using conventional unit gravity tests. The effect of pile diameter on the moment, expressed in both dimensional and dimensionless form, was observed.

In series 5, two dimensional tests were done on continuous model piles. Series 5A involved tests in dense sand. Embedment ratio of 2,4 and 5 were chosen with pulling height ratios ranging between $1 \leq e/L \leq 4$. An empirical moment shape factor (S_{fm}) could then be introduced based on the data obtained for single and continuous piles. Also in series 5B, a continuous pile was tested in a loose sand condition. The package arrangement was as shown in Figure 6.10.

6.6.2 SUMMARY OF EXPERIMENTAL PROGRAM

The tables below summarise test in the centrifuge.

i) Series 1

TEST	N	L(mm)	D(mm)	e(mm)	L/D	e/L
RND19	50	40	20	120	2	3
RNMM2	40	50	25	150	2	3
RNMM3	33.3	60	30	180	2	3
RNMM4	25	80	40	240	2	3
RNMM5	20	100	50	300	2	3

Table 6.3 Summary of modelling of model test

ii) Series 2A

TEST	N	L(mm)	D(mm)	e(mm)	L/D	e/L
RND1	50	100	20	320	5	3.2
RND2	50	100	20	300	5	3
RND3	50	100	20	240	5	2.4
RND4	50	100	20	200	5	2
RND5	50	100	20	100	5	1
RND6	50	80	20	320	4	4
RND7	50	80	20	240	4	3
RND8	50	80	20	200	4	2.5
RND9	50	80	20	160	4	2
RND10	50	80	20	120	4	1.5

RND11	50	80	20	80	4	1
RND12	50	60	20	300	3	5
RND13	50	60	20	240	3	4
RND14	50	60	20	180	3	3
RND15	50	60	20	120	3	2
RND16	50	60	20	60	3	1
RND17	50	40	20	200	2	5
RND18	50	40	20	160	2	4
RND19	50	40	20	120	2	3
RND20	50	40	20	80	2	2
RND21	50	40	20	40	2	1

ii) Series 2B

TEST	N	L(mm)	D(mm)	e(mm)	L/D	e/L
RNL1	50	80	20	320	4	4
RNL2	50	80	20	240	4	3
RNL3	50	80	20	200	4	2.5
RNL4	50	80	20	160	4	2
RNL5	50	80	20	120	4	1.5
RNL6	50	80	20	80	4	1
RNL7	50	60	20	300	3	5
RNL8	50	60	20	240	3	4
RNL9	50	60	20	180	3	3
RNL10	50	60	20	120	3	2
RNL11	50	60	20	60	3	1

iii) Series 2C

TEST	N	L(mm)	D(mm)	e(mm)	L/D	e/L
RND22	20	50	50	250	1	5
RND23	20	50	50	200	1	4
RND24	20	50	50	150	1	3
RND25	20	50	50	100	1	2
RND26	20	50	50	50	1	1

iv) Series 2D

TEST	N	L(mm)	D(mm)	e(mm)	L/D	e/L
RNL12	33.3	60	30	240	2	4
RNL13	33.3	60	30	180	2	3
RNL14	33.3	60	30	120	2	2

Table 6.4 Summaries of tests in series two

v) Series 3A

TEST	N	L(mm)	D(mm)	e(mm)	d/L	L/D	e/L
RNSA0	50	80	20	240	0	4	3
RNSA1	50	80	20	240	0.4	4	3
RNSA2	50	80	20	240	0.6	4	3
RNSA3	50	80	20	240	0.8	4	3
RNSA4	50	80	20	240	1.0	4	3
RNSA5	50	80	20	240	1.5	4	3

vi) Series 3B

TEST	N	L(mm)	D(mm)	e(mm)	d/L	L/D	e/L
RNST0	50	80	20	240	0	4	3
RNST1	50	80	20	240	0.4	4	3
RNST2	50	80	20	240	0.6	4	3
RNST3	50	80	20	240	0.8	4	3
RNST4	50	80	20	240	1.0	4	3
RNST5	50	80	20	240	1.5	4	3

Table 6.5 Summaries of tests for pile embedded within slope proximity

vii) Series 4

TEST	N	L(mm)	D(mm)	e(mm)	L/D	e/L
RN1G	1	100	20	300	5	3
RN12G	12	100	20	300	5	3
RN25G	25	100	20	300	5	3
RND2	50	100	20	300	5	3
RNDCT1	1	500	100	1500	5	3
RNMM2	40	50	25	150	2	3
RNMP2	13	80	40	240	2	3
RNMP3	7	80	40	240	2	3
RNMP4	1	80	40	240	2	3
RNDCT1	1	200	100	600	2	3

Table 6.6 Summary of test for prototype pile with different diameter

viii) Series 5A

TEST	N	L(mm)	D(mm)	B(mm)	e(mm)	L/D	e/L
SFD1	50	100	20	126	300	5	3
SFD2	50	100	20	126	240	5	2.4
SFD3	50	100	20	126	200	5	2
SFD4	50	100	20	126	100	5	1
SFD5	50	80	20	126	320	4	4
SFD6	50	80	20	126	240	4	3
SFD7	50	80	20	126	160	4	2
SFD8	50	80	20	126	80	4	1
SFD9	50	40	20	126	160	2	4
SFD10	50	40	20	126	120	2	3
SFD11	50	40	20	126	80	2	2
SFD12	50	40	20	126	40	2	1

ix) Series 5B

TEST	N	L(mm)	D(mm)	B(mm)	e(mm)	L/D	e/L
SFL1	50	80	20	126	320	4	4
SFL2	50	80	20	126	240	4	3
SFL3	50	80	20	126	200	4	2
SFL4	50	80	20	126	100	4	1

Table 6.7 Summaries of continuous pile tests

6.7 PILE INSTALLATION IN CENTRIFUGAL EXPERIMENT

Most of the research dealing with centrifugal model studies has been concerned with the simulation of the field conditions, many of which have involved the testing of piles. However the installation of the model has usually been carried out at a unit gravity. For example Avgherinos and Schofield(1969), Scott(1981), Leung(1981) and Liem(1988) prepared their models in this way. Attempts have been made to install a model piles at high acceleration thereby simulating the field condition. Craig(1985) highlighted the need for such preparation,if a centrifugal model test was to simulate realistic field conditions. Cook and Lewis(1979) appear to be the first to report the installation of a pile 'in flight'. Oldham(1984) reported the installation of 19mm diameter model piles 'in flight'. However, the installation process caused damage to the externally mounted strain gauges near the base of the piles. Subsequently cyclic horizontal loading was applied to the pile. Results obtained from Oldham shows that there is a little difference in the behaviour of piles installed at unit gravity and at high acceleration.

Craig concluded that the effect of lack in similarity during installation is not crucial under a static or cyclic lateral loading. However a pile experiencing axial load will be most affected if installation had been done under unit gravity. The reasonsfor these are:-

1. For a pile experiencing lateral loading, the behaviour of the pile is dominated by soil reactions in the upper region, where stress differences due to the installation of the pile are lowest.

2. The nature of the pile loading modifies the stress regime around the pile to a greater extent than for axial loading.

Based on this reasoning, the author considers that pile installation 'in flight' for piles experiencing quasi-static lateral loading is less crucial and can be disregarded. Moreover due to the limitation of the centrifugal bucket size, the installation of the driving mechanism would consume large spaces. This would constrain the installation of the pile itself. Moreover as discussed in Chapter One, this project aims to identify some geometric factors influencing the pile behaviour and is not specific to a known field subgrade.

CHAPTER 7

CONVENTIONAL MODEL PILE TEST

7.1 INTRODUCTION

Most of the previous work done in establishing the moment carrying capacity of short pile foundations was based on conventional testing either at full scale or on small models. Research such as that of Shilts et al.(1948), Roscoe(1957), and UIC/ORE(1957) was at full scale, investigating the resistance of piles to lateral stresses, while work reported by Raes(1936), IRSIA(1950) and Czerniak(1957) was mainly based on small models tested in the laboratory. A direct comparison of results obtained from past research is difficult, since each investigator employed different test parameters. However in the present study, conventional tests performed in a reinforced bin on medium scale model piles were included to provide a basis for comparison with the centrifugal test data. Small scale model tests were also performed at unit gravity in the centrifugal bucket as a further comparison between conventional and centrifugal modelling. Consideration is given to the selection of suitable parameters for comparing conventional and centrifugal tests at the end of the chapter.

7.2 CONVENTIONAL TEST PROGRAM

As mentioned above, two main series of conventional tests were undertaken. Medium sized models of short piles 100mm in diameter, were tested in a large reinforced bin, at a scale of $1/10^{th}$ of a typical prototype size of 1m diameter, while a small model 20mm in diameter and 100mm in length was used in a unit gravity test in the centrifugal bucket. Thirty conventional tests were done. Details of the model parameters are shown later in sections 7.4

7.2.1 CONVENTIONAL TEST PACKAGE ARRANGEMENT

The conventional medium scale model tests were carried out in the test apparatus previously used by Dickin and Leung(1983) for testing anchor plates. A few modifications in particular to enable the lateral pull to be applied at various levels above the sand surface, were made to conform with the pile testing procedure. Generally, the test apparatus employed in the conventional test arrangement consisted of the reinforced bin, electrically motorised winch, a team of free running pulleys, displacement transducers, load cell, switch box and digital display.

Details of the reinforced bin, measuring 1.36m in length, 1.22m in width and 0.84m in depth, fabricated from 10mm thick steel plate are shown in Figures 7.1(a) and 7.1(b). An internal formica finish was used to reduce the friction between the side walls and the sand during testing. Two slotted 20mm x 20mm mild steel angles, were attached vertically to the outer surface of one side of the reinforced bin,

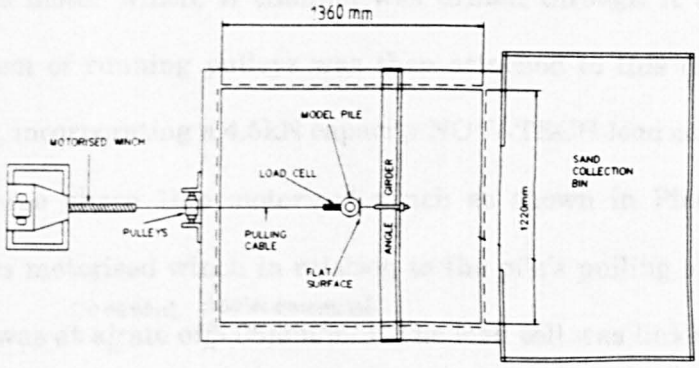

Figure 7.1(a) Plan arrangement for conventional test in reinforced bin

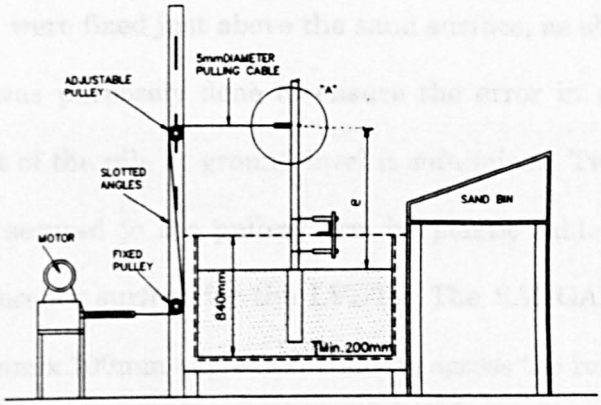

Figure 7.1(b) Side elevation for conventional test in reinforced bin

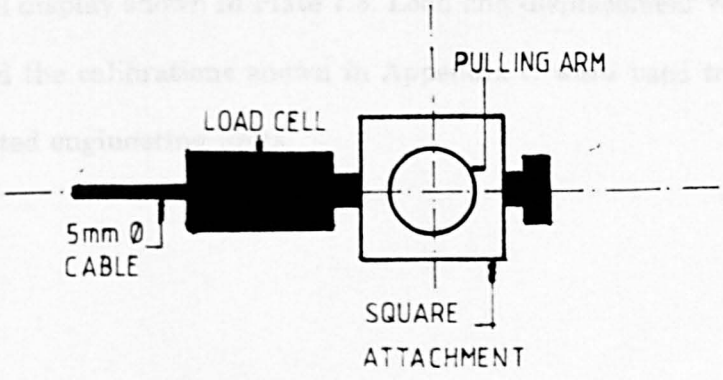

Figure 7.1(c) Detail of section 'A' from attachment of pulling cable to pulling arm

adjacent to the motor winch. A channel was drilled through it at the required height. A system of running pulleys was then attached to this channel. A 5mm diameter cable, incorporating a 4.5kN capacity NOVATECH load cell, was attached to a geared three phase 1h.p motorised winch as shown in Plate 7.1. Loading imposed by this motorised winch in relation to the pile's pulling arm through the pulley system was at a constant displacement of rate of 5.05mm/min. The load cell was linked to the pulling arm through a square attachment which could be raised or lowered and pinched to the arm surface at the required level. Details of the attachment are shown in Figure 7.1(c).

Two SANGAMO LVDT's, capable of measuring a horizontal movement to a maximum of 50mm, were fixed just above the sand surface, as shown in Plate 7.2. This arrangement was purposely done to ensure the error in calculating of the lateral displacement of the pile at ground level is minimised. Two 50mm x 50mm square plates were secured to the pulling arm by plastic cable ties, providing a smooth and flat reference surface for the LVDT's. The SANGAMO LVDT's were clamped onto a 100mm x 100mm angle iron running across the reinforced bin. They were fixed vertically at a distance of 205mm apart.

Readings from the LVDT's and load cell were monitored by an isolated switch box and a digital display shown in Plate 7.3. Load and displacement were recorded in millivolts and the calibrations shown in Appendix C were used to convert the readings to related engineering units.

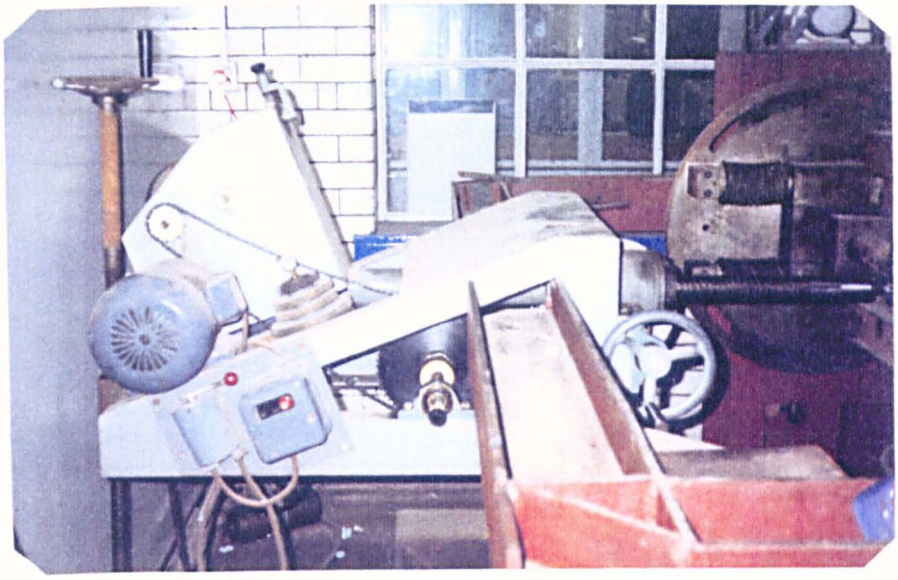

Plate 7.1 Three phase 1h.p geared motorised winch

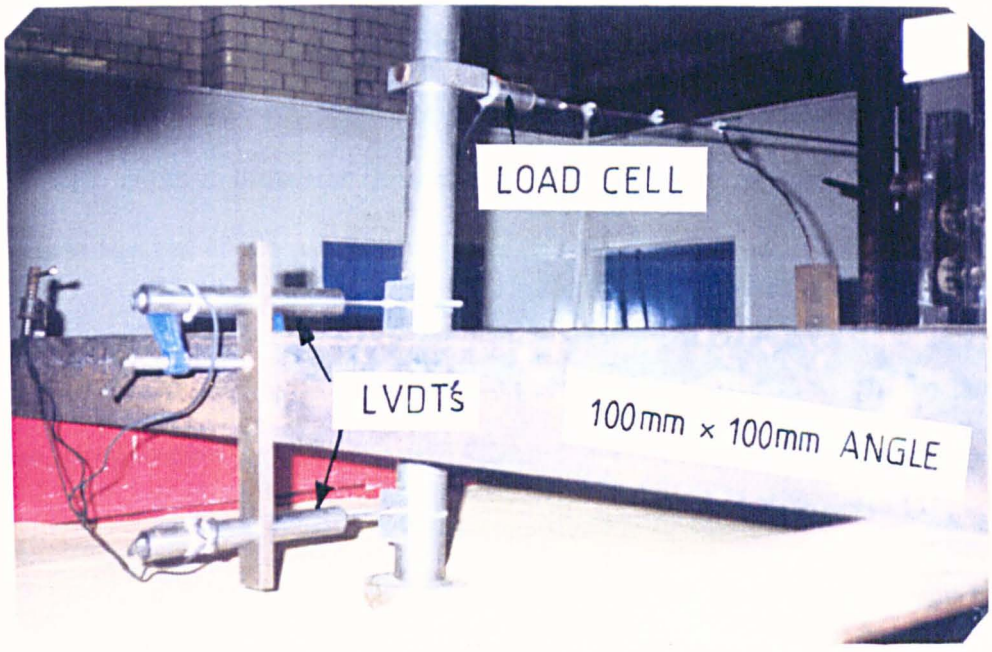

Plate 7.2 Arrangement of LVDT's and load cell in test

The test arrangement for a unit gravity test in the centrifuge bucket is identical to that explained previously in Chapter 6, Section 6.5 for the centrifugal test program.

7.2.2 CONVENTIONAL TESTING PROCEDURE IN THE REINFORCED BIN

The same Erith sand was used in the conventional test and in the centrifugal tests. Model piles used in the reinforced bin were made from mild steel casing and filled with a lean mix concrete to give a fair approximation to the weight of the prototype piles and to maintain their rigidity. The piles were 100mm in diameter with lengths of 500mm, 400mm, 300mm and 200mm. Except for the natural roughness of the steel casing, no other roughening method such as that for the centrifugal model piles were used. A circular pulling arm 1.7m long and 50mm in diameter with a 12mm diameter threaded head was used in all tests. The arm was screwed into the top of the pile by means of this threaded head.

Two types of sand packing were employed in these tests i.e nominally dense and loose. Preparation procedures were selected so that the unit weights achieved would be similar to those obtained in the centrifuge package. A dense packing was achieved by compacting in 100mm thick layers with an electrical vibrator type AV/ARV/1 shown in Plate 7.4. An average unit weight of $\gamma = 16.4 kN/m^3$ was attained using this method. Detailed calculations are shown in Appendix B. A loose packing was produced by raining the sand from a height of about 250mm to 300mm through

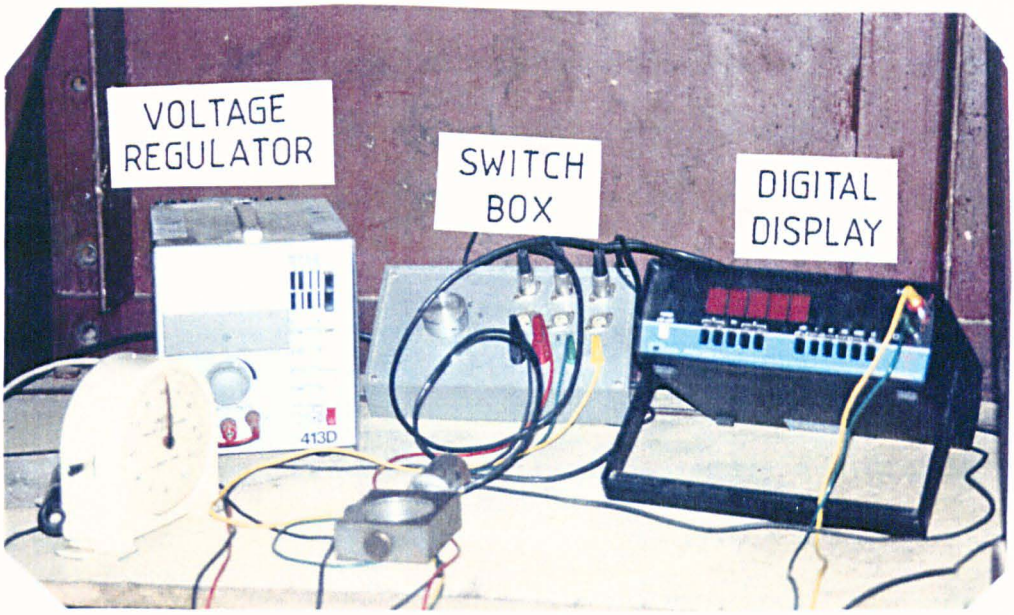

Plate 7.3 Monitoring devices used in the conventional test

Plate 7.4 Electrical vibrator type AV/ARV/1

a sieve mesh No. 200 with holes 425μm in diameter in a rectangular grid. Raining of the sand was done in a rectangular pattern to ensure that the sand was spread evenly. Through this method an average unit weight of $\gamma = 14.4 kN/m^3$ was achieved. Details of the equivalent soil parameters such as porosities, density indices and void ratios are explained in detail in Chapter 5.

Before placing a model pile inside the reinforced bin, a layer of dry Erith sand was placed at the base of the bin to a height of 200mm. A pile was then placed in the centre of the bin and the vertical position was maintained by eye judgement. Backfill preparation up to the top of the pile was achieved by placing sand layers every 100mm then compacting thoroughly with the electrical vibrator. When the sand covered half the pile depth, the pulling arm was screwed into the top of the pile. To ensure the vertical position was maintained, the pulling arm was clamped against the 100mm x 100mm cross angle which in turn was clamped to the top of the bin. Verticality was checked against a reference line above the side of the bin.

When the sand level was flush with the top of the pile, the load cell and LVDT's were placed in position as shown in Plate 7.5. The loading point was adjusted to the appropriate height on the pulling arm by using the square attachment described earlier. Pulling height levels ranging from 400mm to 1500mm were used in the tests. The movable pulley height was adjusted to the appropriate pulling load point level. A 5mm diameter cable, incorporating the 4.5kN capacity load cell, connected the loading gear to the loading arm.

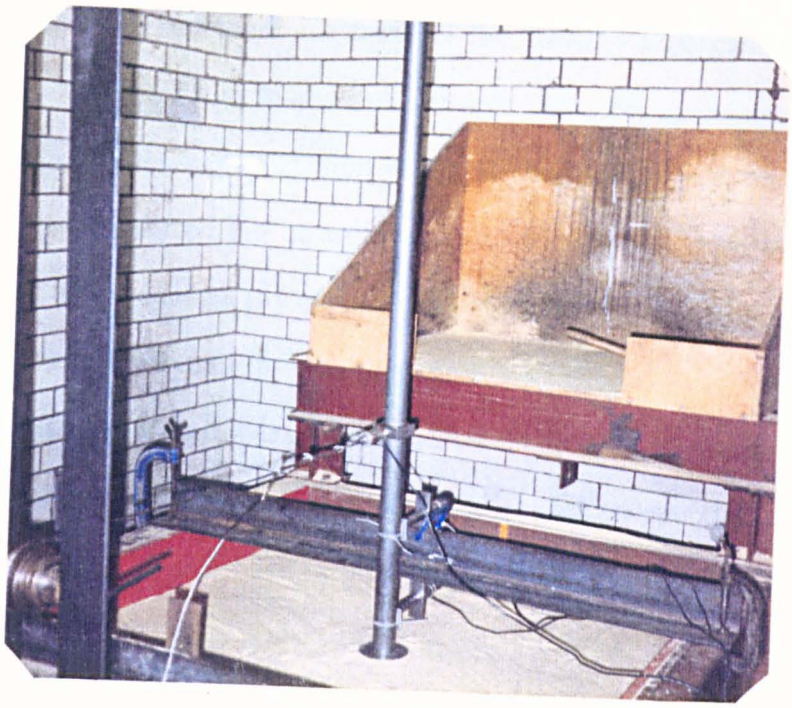

Plate 7.5 Final arrangement before commencing the test

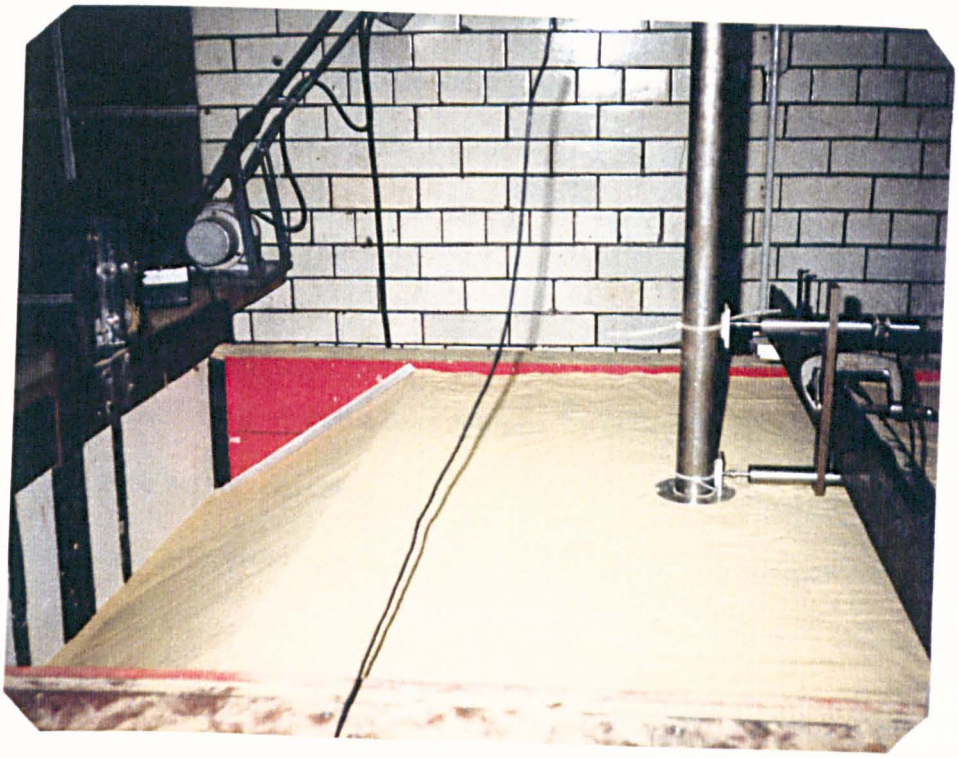

Plate 7.6 Arrangement for pile test in a slope terrain

The same arrangement for tests in flat terrain was also used for a pile embedded in close proximity to a slope . However, in order to construct the slope a 10mm x 10mm metal angle of 500mm in length, was fixed to the inner face of the side wall of the reinforced bin at an inclination of 35° to the horizontal. A 12mm thick plywood was placed on top of the metal angle during the sand placement and compaction. When the sand level was flush with the top of the pile, the plywood was then removed and the sand was allowed to flow freely until it stopped. On average a slope inclination obtained using this method was 33° to 35°. A typical test arrangement for a pile embedded in proximity to sloping terrain is shown in Plate 7.6.

Since a pulling arm of circular section was used, flat reference plates had to be fixed to the arm at the appropriate levels to ensure the spindles of the LVDT's do not slip during the movement of the pile. To ensure accuracy in measuring ground level lateral displacement of the piles, the LVDT's were attached as close to sand level as possible. The LVDT's were clamped in position to the angle girder at a vertical interval of 205mm.

Monitoring devices such as the six channel switch box and digital display multimeter were connected to the load cell and LVDT's. The load cell was connected to channel One while channels Two and Three were linked to the LVDT's. Thereafter power was provided via a voltage regulator. The gearing mechanism was wound back manually and the initial reading was recorded on a digital display multimeter. Horizontal load was applied when the gearing mechanism was engaged using a dog clutch and a timer was started simultaneously. Loading was applied to

the pile loading arm at a constant rate of 5.05mm/min. Readings were taken every 60 seconds and continued until just beyond the peak load value. Generally each pile test was completed in about 25 to 30 minutes.

7.2.3 CONVENTIONAL TEST PROCEDURE IN CENTRIFUGAL BUCKET

In common with the centrifugal testing program, tests was set up for two types of model piles, single and continuous. Glass side walls were included for tests in continuous piles to minimise side friction during the rotation of the model. A silicon polish was used on the surface of the glass to further reduce friction. All attachment and monitoring devices used in the centrifugal program were employed in these conventional tests. A single pile 20mm in diameter and a continuous pile 126mm in width, 20mm in thickess and 100mm in length with an embedment ratio of 5 were employed . Pulling height ratios between 1 and 3 and a dense sand packing $\gamma = 16.4 kN/m^3$ were used throughout these tests.

7.3 EXPERIMENTAL TEST PROGRAM

A total of 4 series of tests were done either in the centrifugal bucket or the reinforced bin. Results from tests in reinforced bin and unit gravity in centrifugal bucket are mainly used for comparison with the centrifuge result and to investigate the scaling effect.

Series 1 comprises two sets of tests. In series 1A pile lengths ranging from 200mm to 500mm for a 100mm diameter pile were employed. Pulling height ratios ranging from 1 to 4 were used in the tests. Tests were performed in a dense sand condition.

Series 1B involved tests similar to those in Series 1A but performed in a loose sand packing. Essentially comparisons with Series 1A were made to observe the effect of sand condition apart from that of embedment and pulling height ratio.

The effect of ground slope on the moment carrying capacity of a pile was investigated in Series 2. Slope distance ratio, d/L of between 0.8 and 1.5 were employed. Series 2A and 2B involved test for pile pulling towards and away from the slope respectively. A pile with embedment ratio of 4 with pulling height ratio of 3 was used. Results from this test series were used as a comparison for the slope test in the centrifuge.

While tests in Series 1 and 2 were conducted in the reinforced bin, tests in Series 3 were run under unit gravity in the centrifuge bucket and employed a 20mm diameter single pile with an embedment ratio of 5. The pulling height ratio used ranged from 1 to 3 with the pile embedded in dense sand throughout the whole test series.

Series 4 involved tests on a continuous pile performed under unit gravity conditions in the centrifugal bucket. In common with Series 3, an embedment length of 5 and pulling height ratios between 1 and 3 were employed in dense sand.

7.3.1 TWO DIMENSIONAL FAILURE MECHANISM TESTS

The purpose of the two dimensional tests was to observe the failure mechanism in the sand around the pile as it rotated. The tests were carried out in a large narrow glass box 600mm long x 175mm wide x 445mm deep. The ends of the box was made from 25mm thick plywood while the sides comprised two 10mm thick glass walls 155mm apart. Figures 7.2(a) and 7.2(b) show the dimensions of the glass box in plan and side elevation respectively. Only the effect on the extreme pulling height and embedment ratios were observed in this test. Pulling height ratios of 1 and 3 using embedment ratio of 5 were employed.

Densification was applied using identical methods to those in the centrifugal test preparation, where an average unit weight of 16.4kN/m^3 and 14.4 kN/m^3 was obtained for dense and loose packings respectively. At 15mm vertical intervals, 3mm depths of dyed sand were placed at the front face of the box. The original position of the pile was marked with a black tape on the outside of the glass surface. Load was applied by a simple horizontal screw rod attached on the angle at the end of the box. By winding the nut manually, load was applied to the lever arm the end of the box. The failure pattern was noted during the test. The pile was made to rotate until a maximum distance well above failure to ensure the failure pattern is clearly visible. The final failure pattern was photographed. Typical results from the two dimensional tests are presented and discussed in Chapter 8.

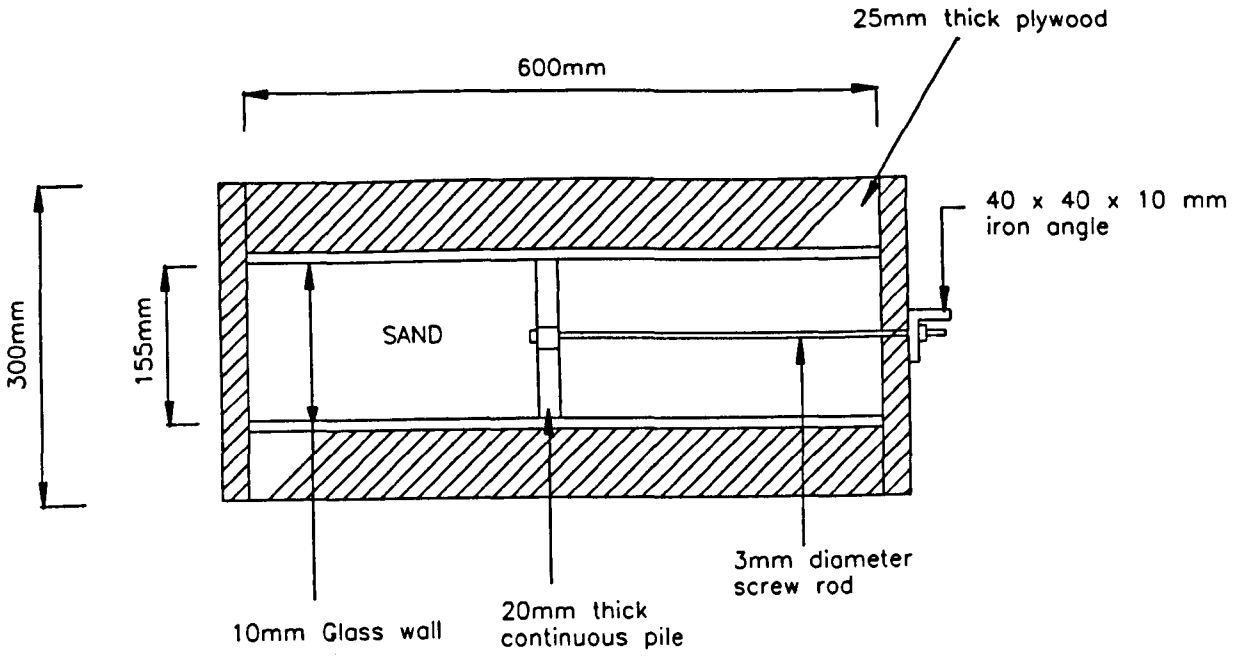

Figure 7.2(a) Plan arrangement for two dimensional testing in glass sided box

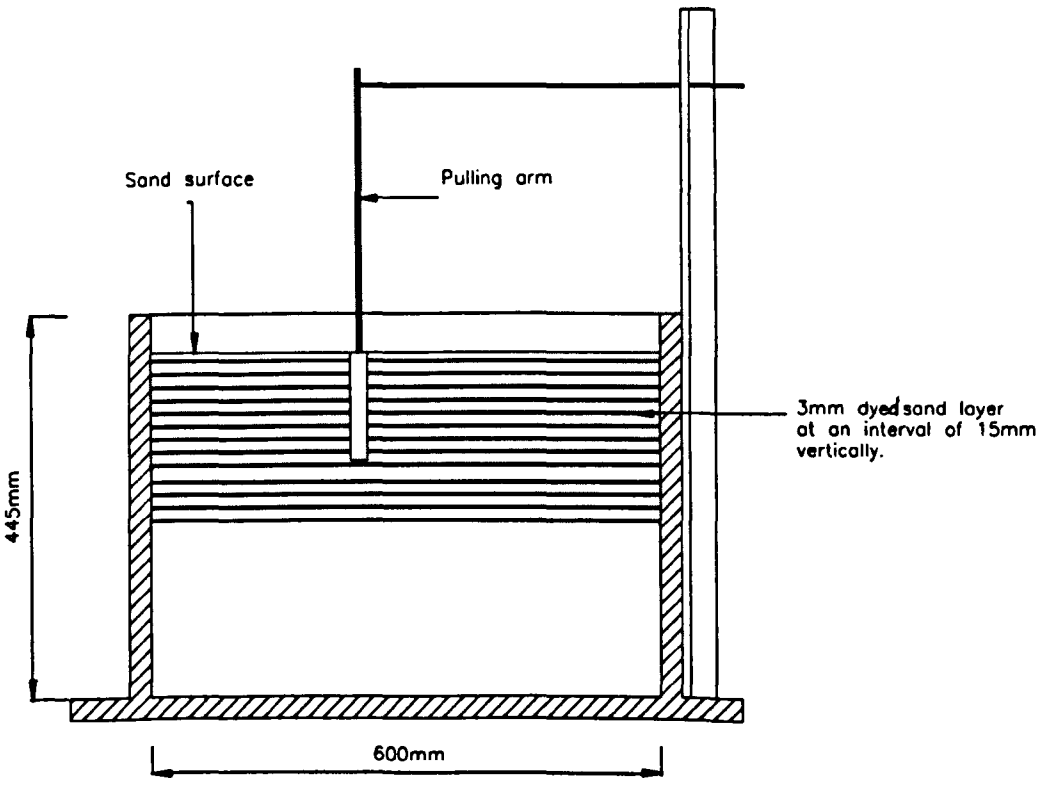

Figure 7.2(b) Side elevation for two dimensional testing in glass sided box

7.4 SUMMARY OF TEST PROGRAM

The summaries of conventional tests are given below;

i) Series 1A

	L(mm)	D(mm)	e(mm)	L/D	e/L
RNDCT1	500	100	1500	5	3
RNDCT2	500	100	1000	5	2
RNDCT3	500	100	500	5	1
RNDCT4	400	100	1200	4	3
RNDCT5	400	100	800	4	2
RNDCT6	400	100	400	4	1
RNDCT7	300	100	900	3	4
RNDCT8	300	100	600	3	3
RNDCT9	300	100	300	3	2
RNDCT10	200	100	800	2	4
RNDCT11	200	100	600	2	3
RNDCT12	200	100	400	2	2

ii) Series 1B

TEST	L(mm)	D(mm)	e(mm)	L/D	e/L
RNLCT1	300	100	600	3	2
RNLCT2	300	100	900	3	3
RNLCT3	300	100	1200	3	4

iii) Series 2A

TEST	L(mm)	D(mm)	e(mm)	d/L	L/D	e/L
RNDST1	400	100	1200	0.8	4	3
RNDST2	400	100	1200	1.0	4	3
RNDST3	400	100	1200	1.2	4	3

iv) Series 2B

TEST	L(mm)	D(mm)	e(mm)	d/L	L/D	e/L
RNDSA1	400	100	1200	0.6	4	3
RNDSA2	400	100	1200	0.8	4	3
RNDSA3	400	100	1200	1.0	4	3
RNDSA4	400	100	1200	1.5	4	3

v) Series 3

TEST	L(mm)	D(mm)	e(mm)	L/D	e/L
RND1G1	100	20	300	5	3
RND2G1	100	20	240	5	2.4
RND3G1	100	20	200	5	2
RND4G1	100	20	100	5	1

vi) Series 4

TEST	L(mm)	D(mm)	B(mm)	e(mm)	L/D	e/L
SFD1G1	100	20	126	300	5	3
SFD2G1	100	20	126	240	5	2.4
SFD3G1	100	20	126	200	5	2
SFD4G1	100	20	126	100	5	1

7.5 DETERMINATIONS OF TEST PARAMETERS

In determining the physical quantities for the overturning resistance of a short pile in sand, the author assumed both conventional and centrifugal model tests are similar without involving the gravity factor. Table 7.1 describes the physical quantities involved. From table 7.1 there are nine physical quantities and two fundamental quantities involved in the relationship. It is also assumed that the same factor applied to the continuous pile, except that diameter D is change to width B or thickness t of the continuous pile, depends on the relationship when comparing it with the single pile.

Materials properties	**Symbol**	**Units**	**Fundamentals Quantities**
Pile			
Pulling Height	e	m	L
Diameter	D	m	L
Length	L	m	L
Weight	W	kN	F
Lateral Load	F	kN	F
Sand			
Bulk Unit weight	γ	kN/m^3	FL^{-3}
Porosity	n	-	-
Internal friction Angle	ϕ	-	-
Density Index	I_d	-	-

Table 7.1 Physical quantities assumed to be involved in determining the limiting moment carrying capacity of laterally loaded pile

Therefore by appropriate manipulation of the physical quantities, seven sets of dimensionless products can be developed.

$\Pi_1 = F/\gamma DL^2$ $\Pi_5 = I_d$

$\Pi_2 = L/D$ $\Pi_6 = \phi$

$\Pi_3 = e/L$ $\Pi_7 = n$

$\Pi_4 = W/\gamma DL^2$

From equation (7.2), the set of Π term can be expressed in the following functional relation,

$$\frac{F}{\gamma DL^2} = f\left(\frac{L}{D}, \frac{e}{L}, \frac{W}{\gamma DL^2}, I_d, \phi, n\right) \qquad (7.3)$$

The piles experience a much greater horizontal force compared to vertical ones, therefore the weight of the pile in contributing towards resistance is assumed to be very small and can be disregarded. Therefore the dimensionless terms of $W/\gamma DL^2$ can be eliminated from the sets of dimensionless parameters in equation (7.3). Where the same type of sand was used throughout the study parameters I_d, ϕ and n were kept constant, thus its effect can be minimised. In the continuous pile, as explained above, the pile diameter does not exist, thus further algebraic transformations need to be done. Therefore the continuous pile of thickness t and width B and the Π terms can be transformed as:-

$F/\gamma DL^2 \rightarrow F/\gamma BL^2$

$L/D \rightarrow L/t$

Therefore equation (7.3) can be reduced to,

$$\frac{F}{\gamma DL^2} = g_1\left(\frac{L}{D}, \frac{e}{L}\right) \qquad (7.4(i))$$

and for continuous pile the functional relations are,

$$\frac{F}{\gamma BL^2} = g_2\left(\frac{L}{t}, \frac{e}{L}\right) \qquad (7.4(ii))$$

Dimensionless terms of $F/\gamma DL^2$ and $F/\gamma BL^2$ can be further simplified in terms of moment. By multiplying the dimensionless values by e/L, the dimensionless terms will be $M/\gamma DL^3$ and $M/\gamma BL^3$. Introducing $M'_s=M/\gamma DL^3$ and $M'_c=M/\gamma BL^3$ as moment factors for single and continuous piles respectively, equation (7.4(i)) and (7.4(ii)) can be written as,

$$M'_s = g_1\left(\frac{L}{D}, e/L\right) \qquad (7.5(i))$$

and

$$M'_c = g_2\left(\frac{L}{t}, \frac{e}{L}\right) \qquad (7.5(ii))$$

Thus it is clear that the moment factor is a function of embedment ratio L/D, L/t and the pulling height ratio e/L. However for simplicity the pile thickness t, is refered as the diameter of the single pile D since the continuous pile is essentially a series of single piles arranged in a row. These relations are determined from the experimental results which will be comprehensively discussed in the following chapter.

7.6 MOMENT SHAPE FACTOR (S_{fm})

Analyses provided by Raes(1936), Terzaghi(1943), IRSIA(1950), Roscoe(1957) and many others are mainly based on a two dimensional analysis. However, the problem of a laterally loaded single pile is essentially three dimensional, suitable factors must be applied to 'two dimensional' theoretical moments.

A moment shape factor can be defined as the ratio between the moment capacity of a single pile and the moment capacity of a continuous pile with the same values of L/D and e/L. Mathematically the relationship can be written as:-

$$S_{fm} = \frac{M'_s}{M'_c} \qquad (7.6)$$

Moment shape factors derived from the centrifugal and conventional tests will be compared in order to investigate the influence of scale on this factor.

CHAPTER EIGHT

INTERPRETATION OF EXPERIMENTAL RESULTS

8.1 INTRODUCTION

Interpretation of the results obtained from the experimental work will be discussed in two sections. The first section will deal with the results obtained from the centrifugal tests while conventional test results are discussed in section two.

Data collected from every test are presented in graphical form as shown in Appendix A. The variation of moment at ground level with pile rotation and applied lateral force with displacement at ground level were plotted. The maximum value of moment at ground level or lateral force is taken from the peak point of the graph. In some cases where no peak point was observed, the failure lateral force or moment at ground level is determined when the lateral force or moment ceased to increase significantly for a considerable pile movement. This method was adopted by Leung(1981) to determine the failure of the soil resistance due to anchor movement. Christensen(1961), however predetermined the failure of the pile as 11° rotation.

8.2 INTERPRETATION OF CENTRIFUGAL RESULTS

Most of the tests conducted simulated of a 1m diameter cylindrical short pile. The relations between moment at ground level and pile rotation and lateral force and pile displacement at ground level are shown in Appendix A. Values plotted in Appendix A are subjected to a small correction. As shown in Figure 8.1, data obtained without correction shows a small negative displacement during the initial stages of applying horizontal load to the pile. The negative displacement shown was either due to an error in the initial reading of the linear potentiometers or from a slackening of the attachment mechanism on the pulling arm. The origin is then translated to the peak negative displacement value. The correction to the displacement will not affect the lateral force value.

Generally the force-displacement and moment-rotation graphs show an approximately hyperbolic shape. However it is apparent that the lateral force and the moment increased in an irregular manner exhibiting a 'stick-slip' effect. This effect was due to the progressive failure during the movement of the pile. During this mobilisation, the sand in front of the pile is sheared. When this zone has reached its ultimate value, another mass which is still intact is now mobilised. This offers an increase in resisting force. The progressive shearing of the soil continues until in some cases a maximum value of total resisting force is obtained. It may be noted that in the

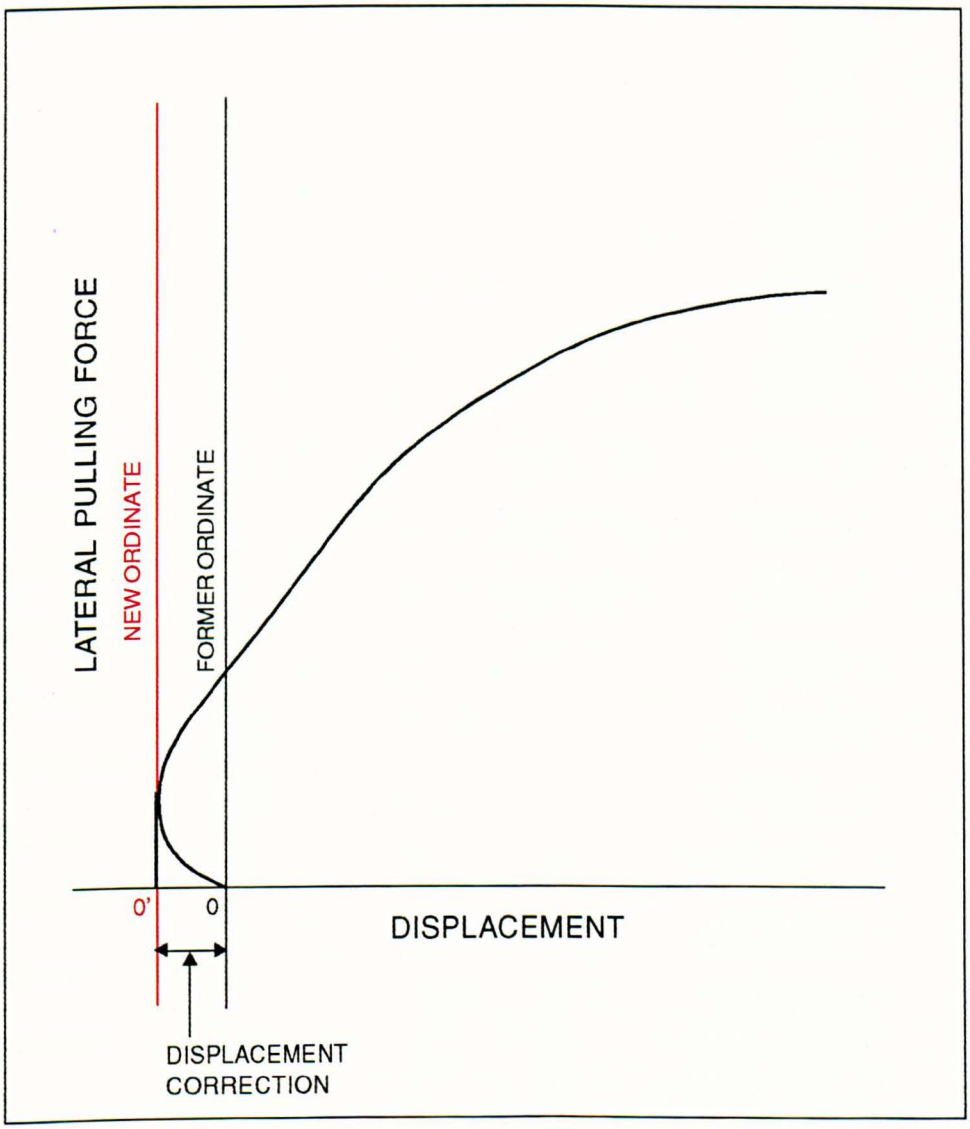

Figure 8.1 Example of correction made to the pile displacement value due to the slackening of the cable and pulling arm connection.

case of pile in dense sand with L/D=5 and in loose test, a maximum resistance was not observed and the failure value determined as described by Leung(1981) in preference to a criterion based on a particular rotation.

8.2.1 MODELLING OF MODELS

To verify the scaling relationship in centrifuge modelling tests need to be performed where models of different sizes are tested at different gravity values. The concept is known as 'modelling of models' has been demonstrated by many researchers involved in centrifuge modelling such as Bassett and Horner(1979), Dickin and Leung(1983), Ko(1988), Craig et al.(1988), Fulsgang and Ovesen(1988) and Steenfelt(1989). This concept has evolved to provide a check on the internal consistency of the centrifugal model testing scheme and to validate the scaling relationships. However the important criterion in modelling of models is to attain the same values for model and prototype in dimensionless terms. The model and prototype are then said to be completely similar.

Tests were performed by employing a pile with embedment ratio of 2 and pulling height ratio of 3. Table 8.1 shows the results obtained from the modelling of models tests. Prototype moment values were transformed into dimensionless moment factor, $M'_p=M_p/\gamma D_p L_p^3$. Figure 8.2 compares the results shown in Table 8.1. The values of

prototype moment factor M_p' of the models having the same prototype dimension agree reasonably well. Slight discrepancy however does occur due to the fact that complete consistency in preparing every specimen is not possible. In fact moment limits in Series 1 tests in Table 8.1 were within ±3% of the mean value.

EMBEDMENT LENGTH RATIO, L/D = 2

PULLING HEIGHT RATIO, e/L = 3

TEST	N	F_m(kN)	M_m(kN.m)	F_p(kN)	θ°	M_p(kN.m)	M'_{ps}
RND19	50	0.027	0.0032	67.50	4.0	400.00	3.05
RNMM2	40	0.0421	0.0063	67.36	6.1	403.20	3.07
RNMM3	33.3	0.0622	0.0112	68.97	6.2	413.57	3.15
RNMM4	25	0.1046	0.0251	65.38	4.1	392.19	2.99
RNMM5	20	0.1646	0.0494	65.84	3.9	395.20	3.01

** m and p subscript denotes model and prototype respectively.*

Table 8.1 Summary for modelling of model results

The prototype moment factors conform to the similarity requirements provided by Ovesen(1979). With an average size D_{50} of the sand equivalent to 0.2mm and the smallest pile circumference of 62mm gives the ratio between pile circumference and average grain size in excess of 300. This value is well above the critical value of 40 where grain size effects have been previously identified by Ovesen. These tests confirm the validity of the centrifugal test technique to the problems related to laterally loaded short piles in sand.

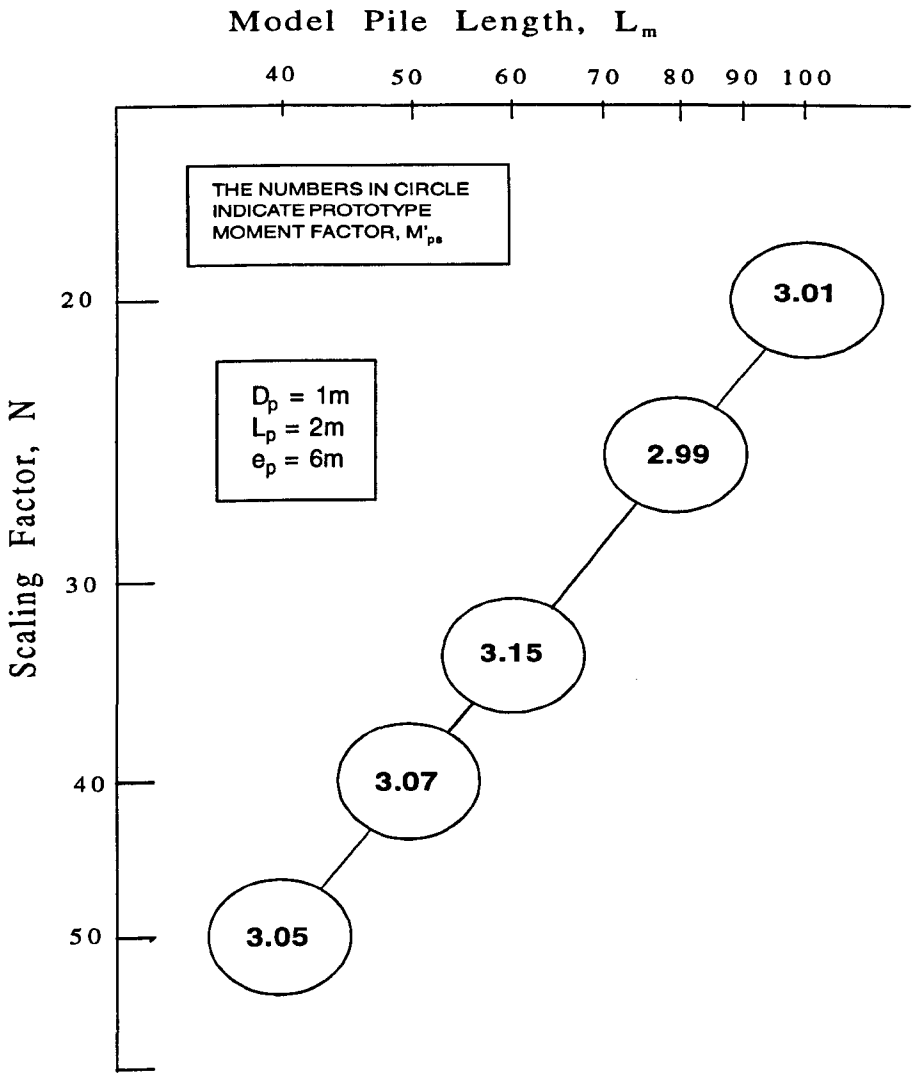

Figure 8.2 Summary of modelling of model test for pile in dense sand.

8.2.2 CENTRIFUGAL TESTS ON SINGLE SHORT PILES

Tests on a single pile were designed to investigate the effect of pulling height, embedment length, soil unit weight, ground profile and pile diameter on the moment limit at ground level. In series 2, model piles with D_m=20mm were tested at N=50, simulating the conditions around a 1m diameter prototype pile. However in some cases, to achieve pile stability during the preparation of the package, larger model piles were used. In this case, model piles with D_m=50 and 30mm were spun at 20g and 33.3g respectively. In Series 3 the effect of ground profile for a pile embedded close to a slope was investigated, while Series 4 examined the effect of pile diameter on the moment limit.

8.2.2.1 THE EFFECT OF PULLING HEIGHT

Summaries of results in Series 2 are shown in Figures 8.3 to 8.12 based on failure values shown in Table 8.2. Tables 8.2(a) and 8.2(b) represent values for piles embedded in dense and loose packing respectively. The maximum lateral force and maximum moment at ground level in terms of model and prototype were plotted against pulling height ratio for various embedment ratios. Figures 8.3 ,8.4 and Figures 8.5, 8.6 exhibit the variation of lateral pulling force in model and prototype terms for piles embedded in dense and loose sand packings respectively. Generally the maximum lateral force values decrease with an increase in pulling height ratio. It can be seen in

Figure 8.3 and 8.4, that piles pulled from lower pulling heights in dense sand show a sudden increase in lateral force values especially for e/L<2 and L/D>2 while an increase in pulling height reduces the maximum lateral force until at almost a constant value for e/L>3 and L/D<3 is attained. Similar trends were observed for loose sand packing as shown in Figures 8.5 and 8.6.

Due to the difficulties in preparation, data for piles with L/D=1 were obtained by testing a 50mm diameter model at 20g and for L/D=2 using a 30mm diameter model pile tested at 33.3g for dense and loose sands respectively. It may be noted that in Figure 8.3 the model value of lateral force exceeds for L/D=1 that for a test at 50g on a 20mm diameter pile of L/D=2 in dense sand. Similarly in Figure 8.5 the model value for L/D=2 exceed that for a test at 50g on a 20mm diameter pile of L/D=3 in loose sand. However when the lateral force values are expressed in prototype terms as shown in Figures 8.4 and 8.6, the results for the 20g and 33.3g tests are consistent with an increase in the embedment ratio for both dense and loose sand packing respectively.

The variation of moment at ground level in model and prototype terms with pulling height ratio for piles in dense and loose sand packing is shown in Figures 8.7 to 8.10. In contrast with the lateral force relationship,the moment at ground level increases significantly with an increase in pulling height ratio and embedment ratio. Figures 8.7 and 8.8 summarise the effects of pulling height on model and prototype moment limit for piles in dense sand respectively, while the effects of pulling height on the moment limit in terms of model and prototype in loose sand are shown in Figures

8.9 and 8.10 respectively. For piles in dense sand with L/D<3 the effect of pulling height is minor especially when the pulling height ratio is greater than 3 in broad agreement with Dickin and Wei(1991). However for piles with longer embedment ratios of L/D=4 and 5, there is some evidence that pulling height ratio is still significant since further increase in the moment at ground level is clearly evident. This could only be confirmed by testing longer piles. However, due to the space restriction in the centrifuge package, tests on piles with embedment ratios greater than 5 and with pulling height ratios greater than 4 cannot be accomplished. Similarly moments at ground level for piles in loose sand increase with an increase in pulling height ratio and embedment ratio. Figures 8.9 and 8.10 show that piles embedded in loose sand still show a significant effect of pulling height on moment at ground level even for e/L>3 and L/D>4. Limited tests (e/L<3) could be performed for L/D=2 since applying the modelling of models using a larger model was limited by the space in the centrifuge package. However by extrapolation the effect of the pulling height on moment limit is still significant. The results for piles in loose sand were rather scattered compared to those in the dense packing due to non-homogeneity during package preparation.

As explained earlier results obtained for L/D=1 and L/D=2 for piles in dense and loose sand respectively give a higher model moment value compare with L/D=2 in dense sand and L/D=3 in loose sand since larger models were used in the tests. However consistent values can be seen when the results are expressed in prototype terms.

TEST	N	F_m(kN)	M_m(kN.m)	Δ_m(mm)	F_p(kN)	M_p(kN.m)	Δ_p(mm)	θ°	L/D	e/L	M'_{ps}
RND1	50	0.0927	0.0297	3.94	231.75	3712.50	197.00	3.59	5	3.2	1.81
RND2	50	0.0938	0.0281	3.65	234.50	3512.50	182.50	4.30	5	3	1.71
RND3	50	0.1061	0.0255	6.28	265.25	3187.50	314.00	5.47	5	2.4	1.55
RND4	50	0.1336	0.0267	6.43	334.00	3337.50	321.50	5.85	5	2	1.63
RND5	50	0.2415	0.0242	7.72	603.75	3025.00	386.00	6.84	5	1	1.48
RND6	50	0.0500	0.0160	5.88	125.00	2000.00	294.00	5.97	4	4	1.91
RND7	50	0.0621	0.0149	6.48	155.25	1862.50	324.00	6.23	4	3	1.77
RND8	50	0.0698	0.0140	5.79	174.50	1750.00	289.50	6.48	4	2.5	1.67
RND9	50	0.0776	0.0124	3.12	194.00	1550.00	156.00	4.23	4	2	1.48
RND10	50	0.1054	0.0127	4.45	263.50	1587.50	222.50	4.44	4	1.5	1.51
RND11	50	0.1389	0.0111	5.98	347.25	1387.50	299.00	6.51	4	1	1.32
RND12	50	0.0230	0.0069	3.32	57.50	862.50	166.00	5.08	3	5	1.95
RND13	50	0.0272	0.0065	3.86	68.00	812.50	193.00	5.30	3	4	1.83
RND14	50	0.0337	0.0067	2.12	84.25	837.50	106.00	3.31	3	3.3	1.89
RND15	50	0.0500	0.0060	2.70	125.00	750.00	135.00	3.72	3	2	1.69
RND16	50	0.0944	0.0057	5.17	236.00	712.50	258.50	7.60	3	1	1.61

Chapter 8

Chapter 8

RND17	50	0.0175	0.0035	0.61	43.75	437.50	30.50	1.47	2	5	3.33
RND18	50	0.0206	0.0033	1.10	51.50	412.50	55.00	1.95	2	4	3.14
RND19	50	0.0270	0.0032	2.09	67.50	400.00	104.5	4.00	2	3	3.05
RND20	50	0.0285	0.0023	3.21	71.25	287.50	160.50	6.80	2	2	2.19
RND21	50	0.0328	0.0013	3.50	82.00	162.50	175.00	7.79	2	1	1.24
RND22	20	0.0295	0.0074	1.03	11.80	59.20	20.60	1.71	1	5	3.61
RND23	20	0.0299	0.0060	0.86	11.96	48.00	17.20	1.62	1	4	2.93
RND24	20	0.0426	0.0064	1.28	17.04	51.20	25.60	2.77	1	3	3.12
RND25	20	0.0585	0.0059	1.53	23.40	47.20	30.60	1.98	1	2	2.88
RND26	20	0.1000	0.0050	0.72	40.00	40.00	14.40	1.82	1	1	2.44

** Subscript p and m denote prototype and model respectively.*

Table 8.2(a) Summary of centrifugal test results for pile embedded in dense sand.

TEST	N	F_m(kN)	M_m(kN.m)	Δ_m(mm)	F_p(kN)	M_p(kN.m)	Δ_p(mm)	θ°	L/D	e/L	M'_{ps}
RNL1	50	0.0299	0.0095	2.74	74.5	1187.50	137.00	2.94	4	4	1.29
RNL2	50	0.0354	0.0085	2.77	88.50	1062.50	138.50	2.78	4	3	1.15
RNL3	50	0.0348	0.0070	2.67	87.00	875.00	133.50	2.97	4	2.5	0.95
RNL4	50	0.0469	0.0075	4.73	117.25	937.50	236.50	5.52	4	2	1.02
RNL5	50	0.0736	0.0088	5.52	184.00	1100.00	276 "	5.32	4	1.5	1.19
RNL6	50	0.0889	0.0071	7.22	222.25	887.50	361.00	6.97	4	1	0.96
RNL7	50	0.0186	0.0056	3.02	46.50	700.00	151.00	3.10	3	5	1.80
RNL8	50	0.0219	0.0053	4.39	54.75	662.50	219.50	4.51	3	4	1.70
RNL9	50	0.0272	0.0049	4.92	68.00	612.50	246.00	5.82	3	3	1.58
RNL10	50	0.0342	0.0041	4.62	85.50	512.50	231.00	5.71	3	2	1.32
RNL11	50	0.0411	0.0025	4.21	102.78	312.50	210.50	5.10	3	1	0.80
RNL12	33.3	0.0331	0.0060	3.78	36.67	219.71	125.87	4.98	2	3	1.91
RNL13	33.3	0.0533	0.0064	5.36	59.09	235.96	178.49	5.97	2	2	2.05
RNL14	33.3	0.0727	0.0044	2.97	80.56	161.00	98.90	4.89	2	1	1.40

** Subscript p and m denote prototype and model respectively*

Table 8.2(b) Summary of centrifugal test results for pile embedded in loose sand

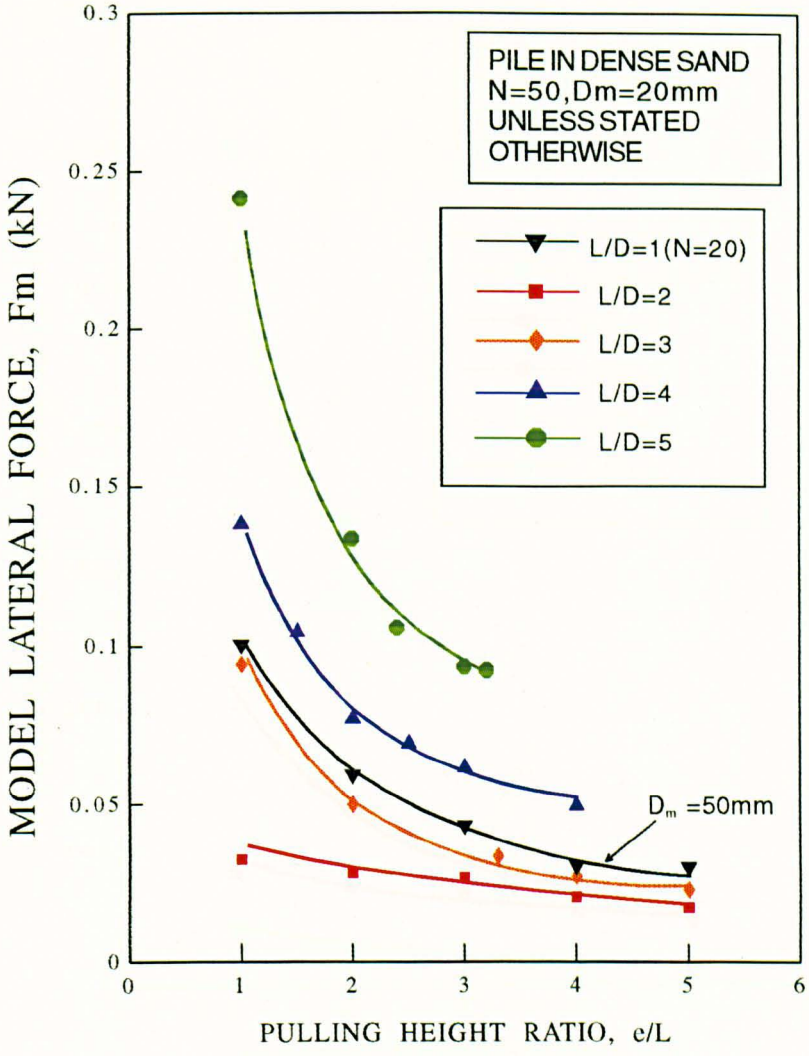

Figure 8.3 Variation of model lateral force with pulling height ratio for 1m diameter prototype piles in dense sand.

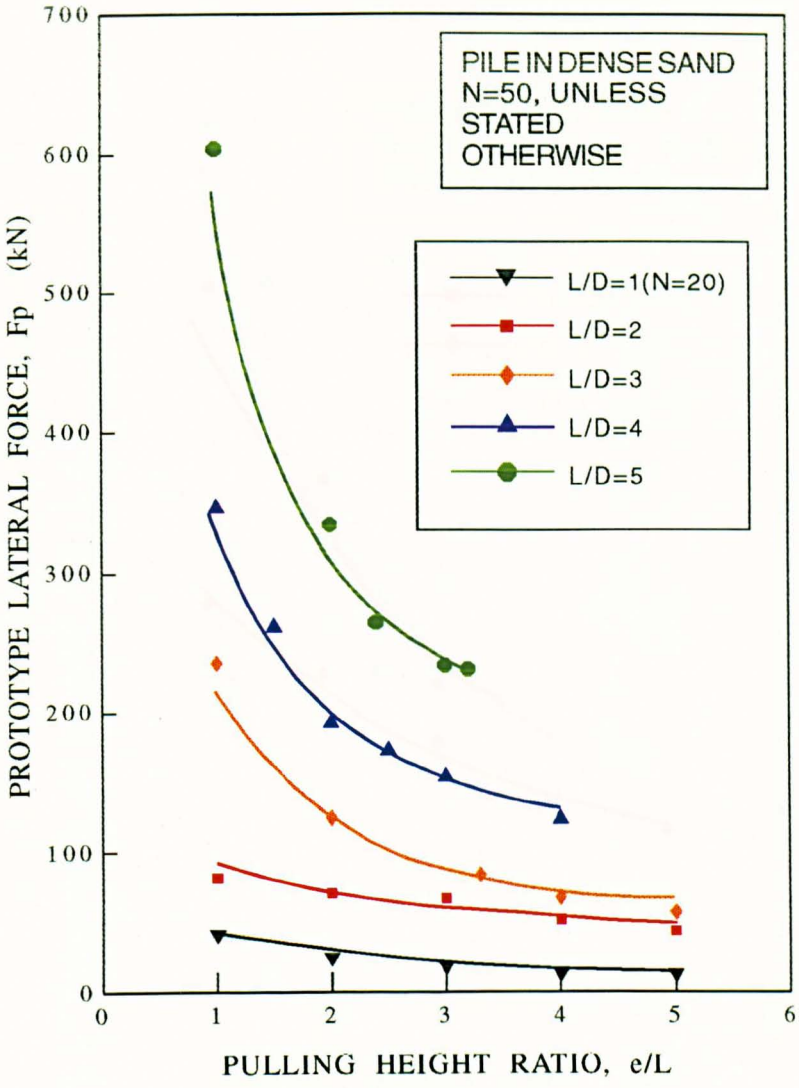

Figure 8.4 Variation of prototype lateral force with pulling height ratio for 1m diameter piles in dense sand.

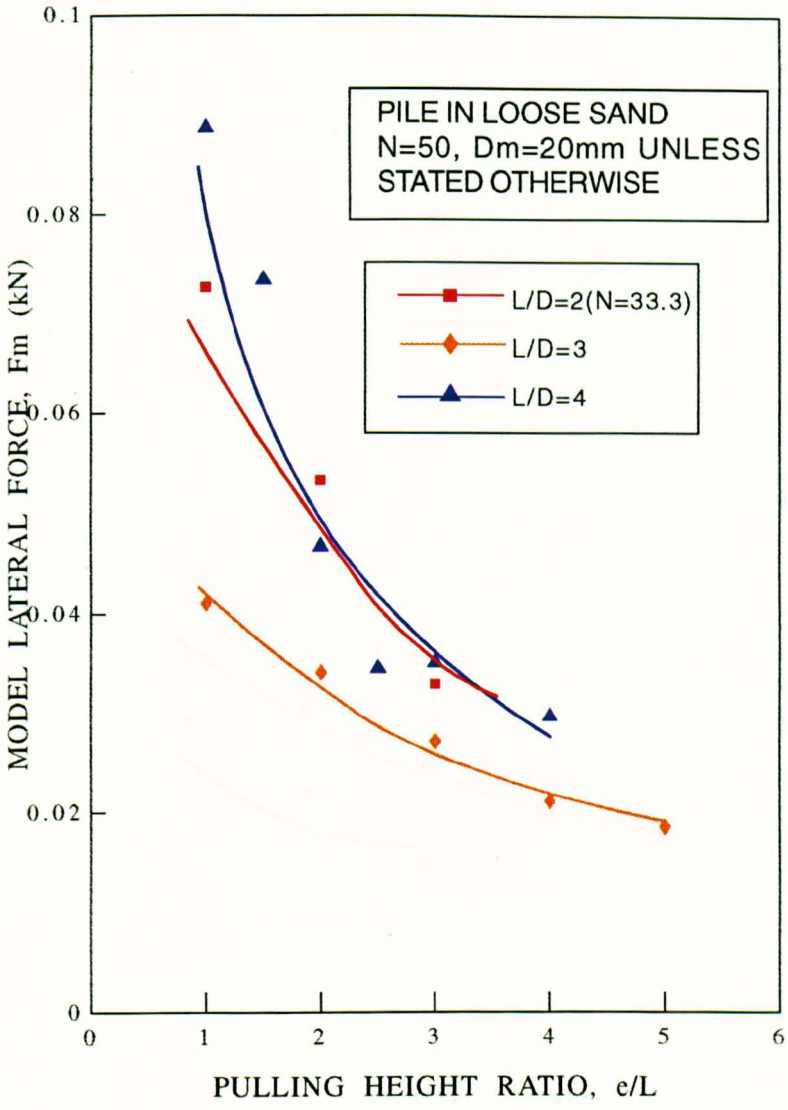

Figure 8.5 Variation of model lateral force with pulling height ratio for 1m diameter prototype piles in loose sand.

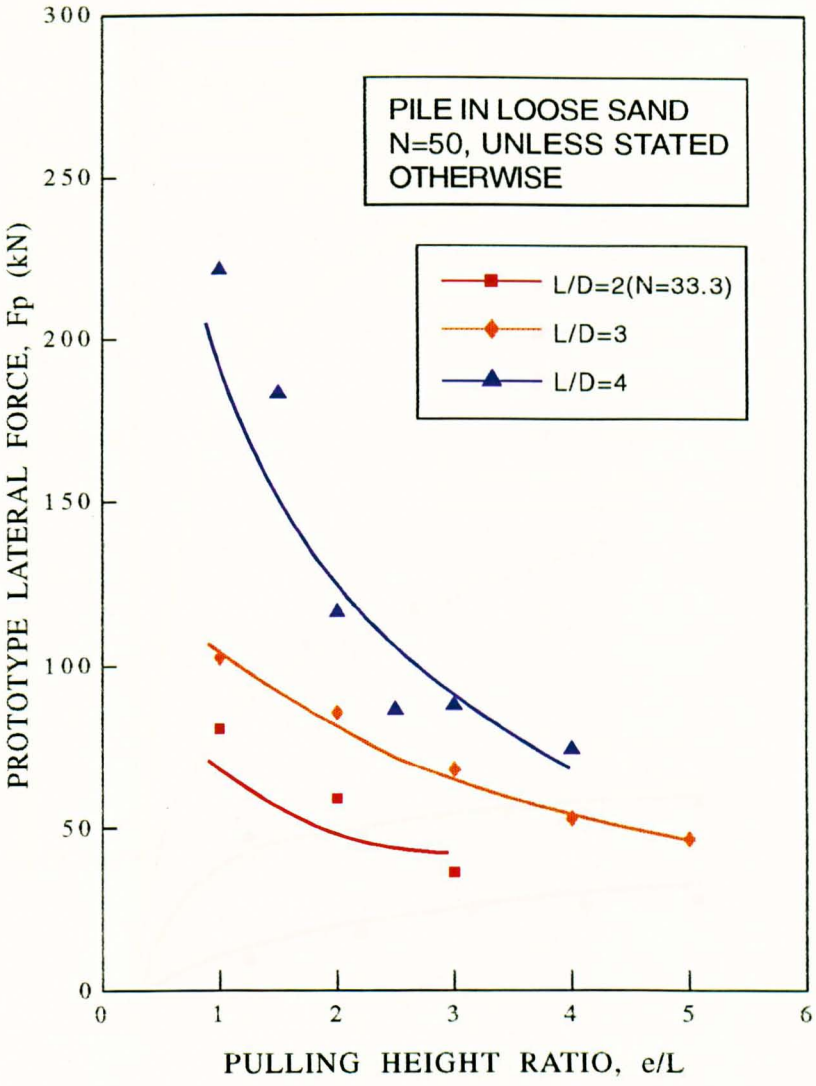

Figure 8.6 Variation of prototype lateral force with pulling height ratio for 1m diameter piles in loose sand.

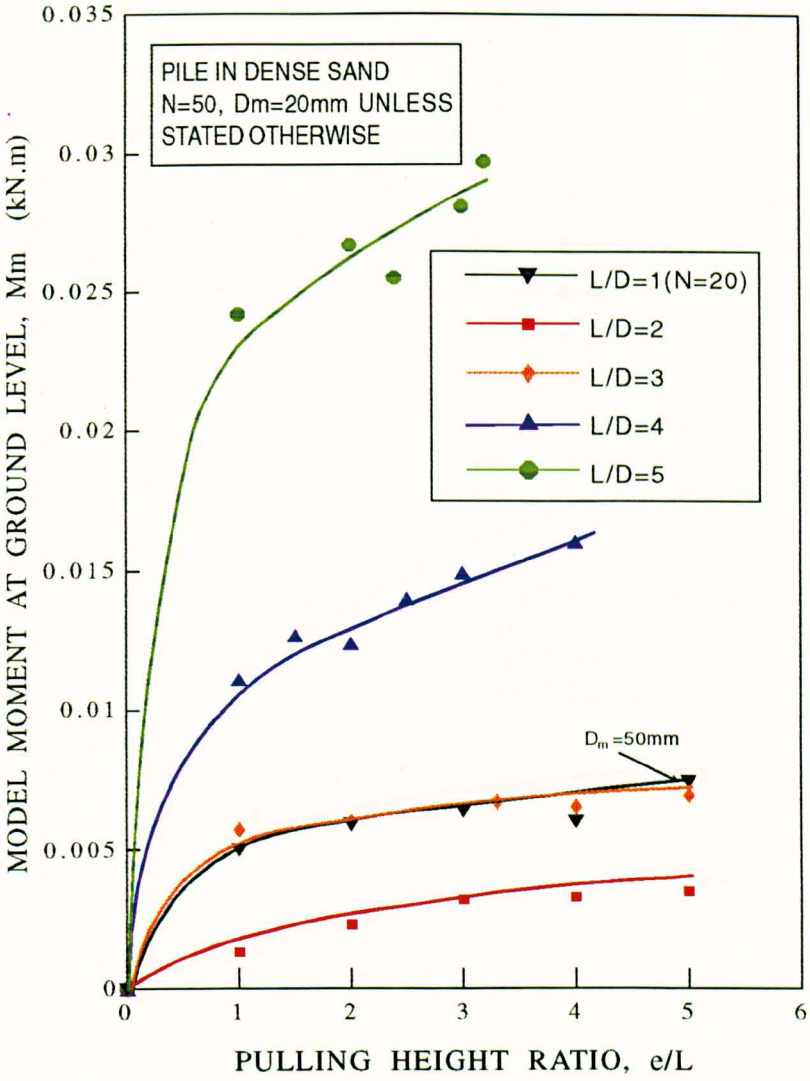

Figure 8.7 Variation of model moment at ground level with pulling height ratio for 1m diameter prototype piles in dense sand.

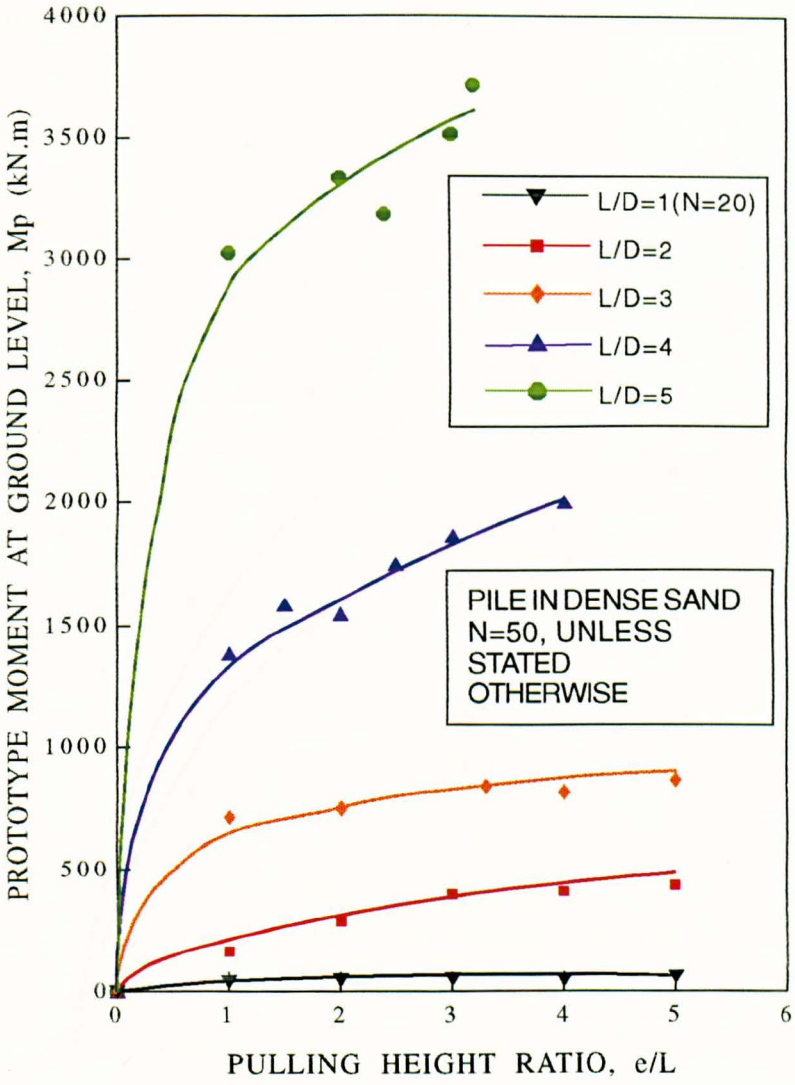

Figure 8.8 Variation of prototype moment at ground level with pulling height ratio for 1m diameter piles in dense sand.

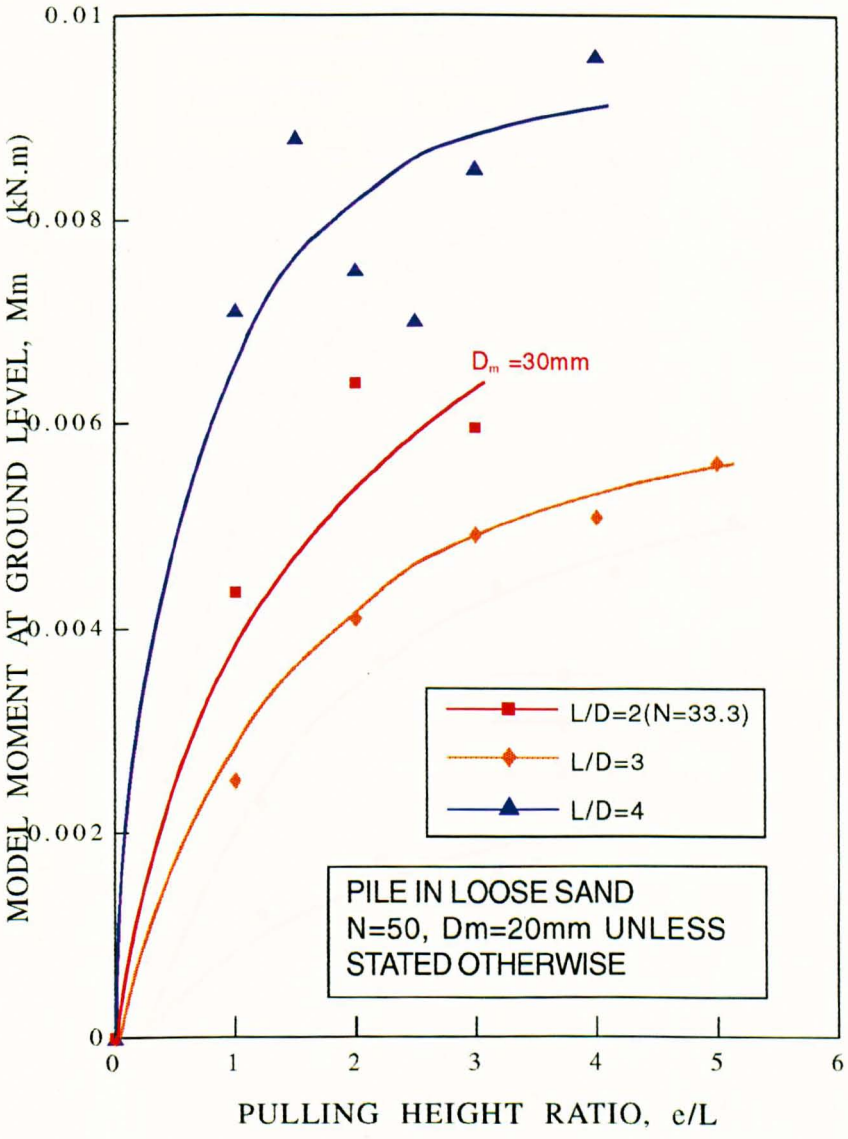

Figure 8.9 Variation of model moment at ground level with pulling height ratio for 1m diameter prototype piles in loose sand.

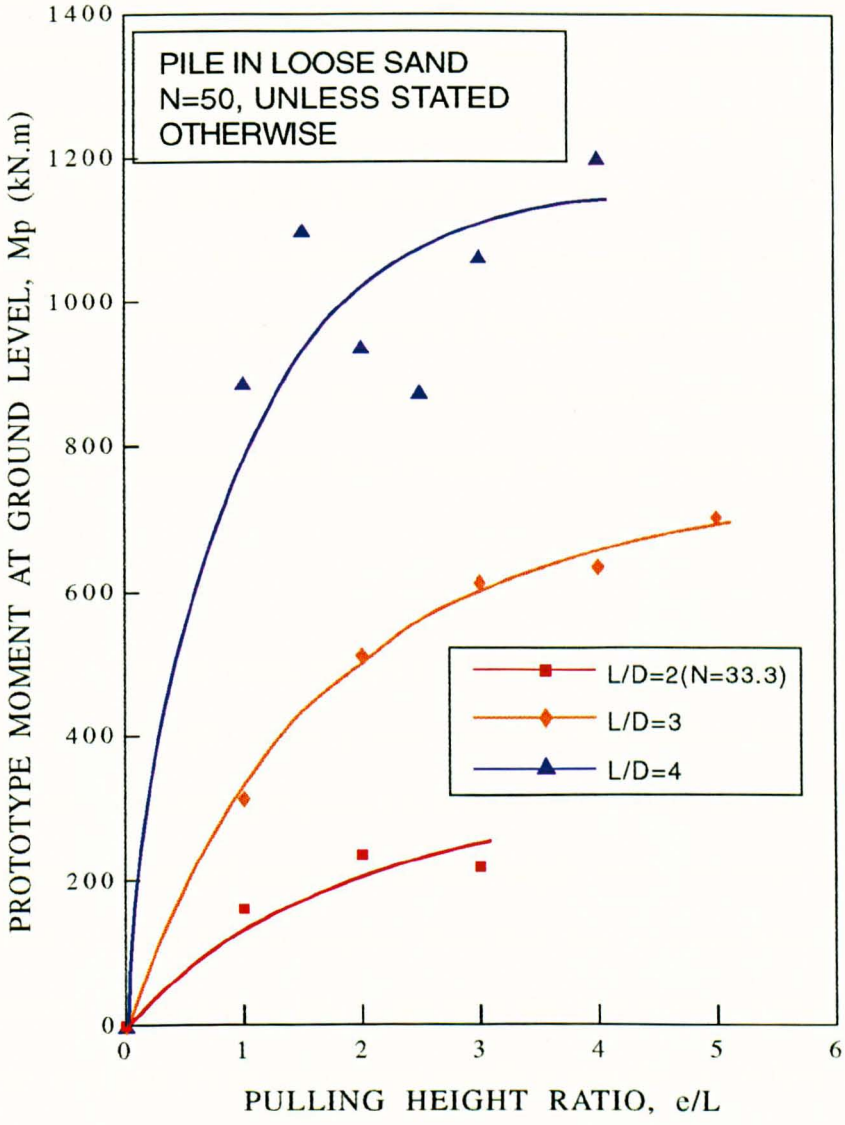

Figure 8.10 Variation of prototype moment at ground level with pulling height ratio for 1m diameter piles in loose sand.

Figures 8.11 and 8.12, show the variation of prototype moment factor M_p' with pulling height ratio for dense and loose sand respectively. It is noticeable that the prototype moment factor decreases with an increase in embedment ratio. However results for an embedment ratio of 5, clearly depart from the general trend. Thus it was suspected that for an embedment ratio of greater than 5, piles could no more be considered as short pile. As mentioned earlier, confirmation by testing longer piles would clarify this. However with a diameter of 1m, the embedment ratio of 5 is outside the range usually encountered in the field for side bearing foundations Such a test would also require a greater depth than available in the package for a model of 20mm diameter.

Generally moment limits increase with an increase in pulling height ratio contrary to UIC/ORE(1957) where it was concluded that pulling height was of only minor importance. Comparing Figures 8.3 to 8.10 which relate the variation of lateral force and moment at ground level with pulling height ratio, the value of lateral force with pull from a higher level is smaller than that from a lower level. However the resulting limiting moment for a pile pulled from the higher level is greater than that for the lower level pull. At an embedment length of less than 3, pulling height ratios of greater than 3 have a less significant effect on the moment limit. However for longer embedment length, there is some evidence of a significant increase in moment limit with an increase of pulling height ratio.

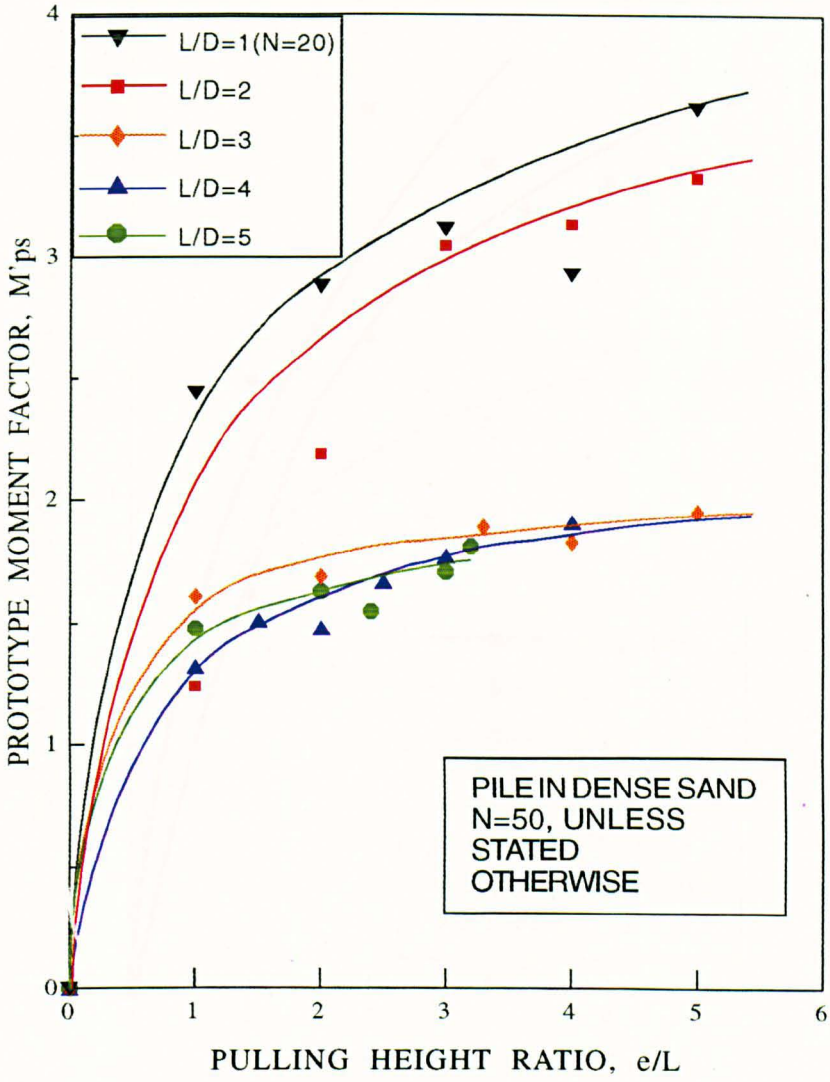

Figure 8.11 Variation of prototype moment factor with pulling height ratio for 1m diameter prototype piles in dense sand.

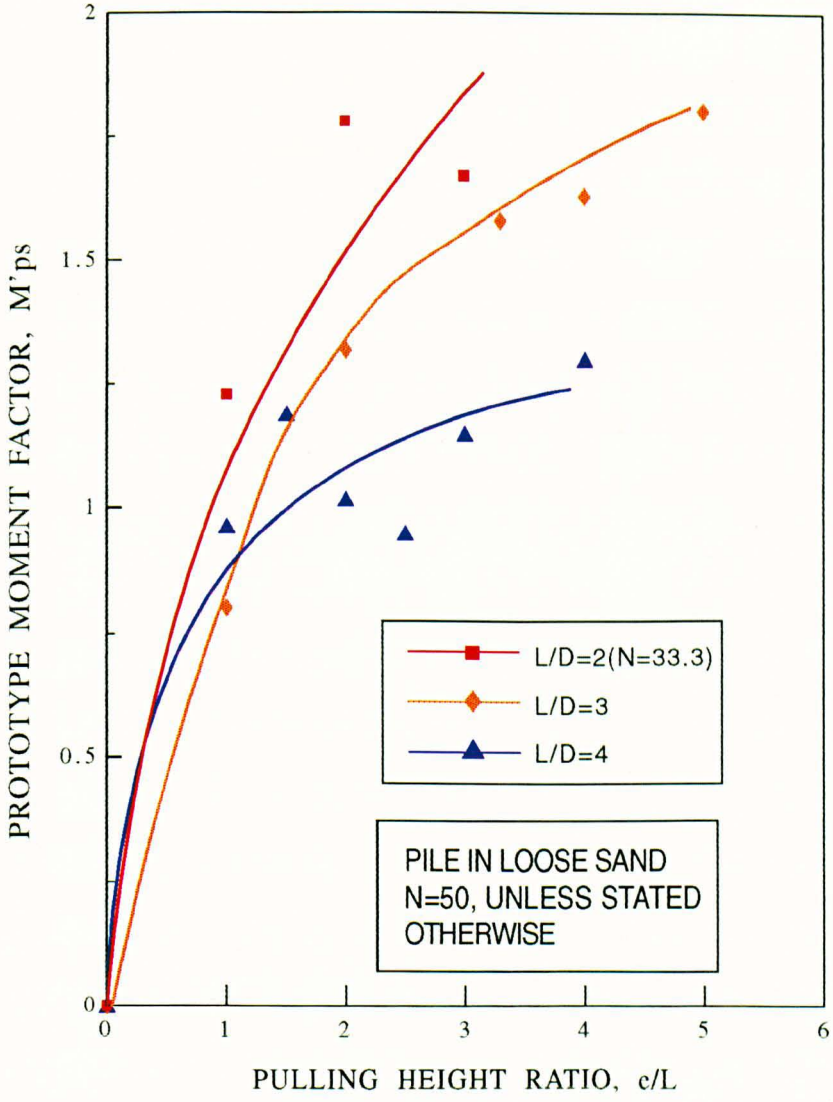

Figure 8.12 Variation of prototype moment factor with pulling height ratio for 1m diameter prototype piles in loose sand.

8.2.2.2 THE EFFECT OF EMBEDMENT RATIO

The influence of embedment can be seen in the preceding section. This section further discusses the effect of embedment ratio with respect to the moment limit at ground level. This effect is shown in Figures 8.13 to 8.22 from Table 8.2. It is evident that the embedment ratio is one of the factors which predominantly affects the limiting moment values. The results obtained are plotted in prototype terms in Figures 8.14, 8.16, 8.18, and 8.20 since different accelerations were employed for piles with embedment ratio of L/D=1 and L/D=2 for dense and loose sand respectively.

Figures 8.13 and 8.15 show the variation of model lateral force with embedment ratio for piles in dense and loose packings respectively. As explained in the preceding section, lateral force values from L/D=1 and L/D=2 for dense and loose packings were tested using bigger model pile diameters and results obtained are therefore higher than those which would have been obtained for D_m=20mm. Similar situations can also be seen in Figures 8.17 and 8.19 where model moment is plotted against embedment ratio for piles in dense and loose sand packing. However these values regain consistency when plotted in prototype terms.

It is noticeable that, from Figures 8.13 and 8.16, for a decrease in pulling height ratio, the rate of increase of lateral load increases with an increase in embedment ratio for both dense and loose packings. The moment limit shows a considerable increase with embedment and pulling height ratios as shown in Figures 8.17 and 8.20.

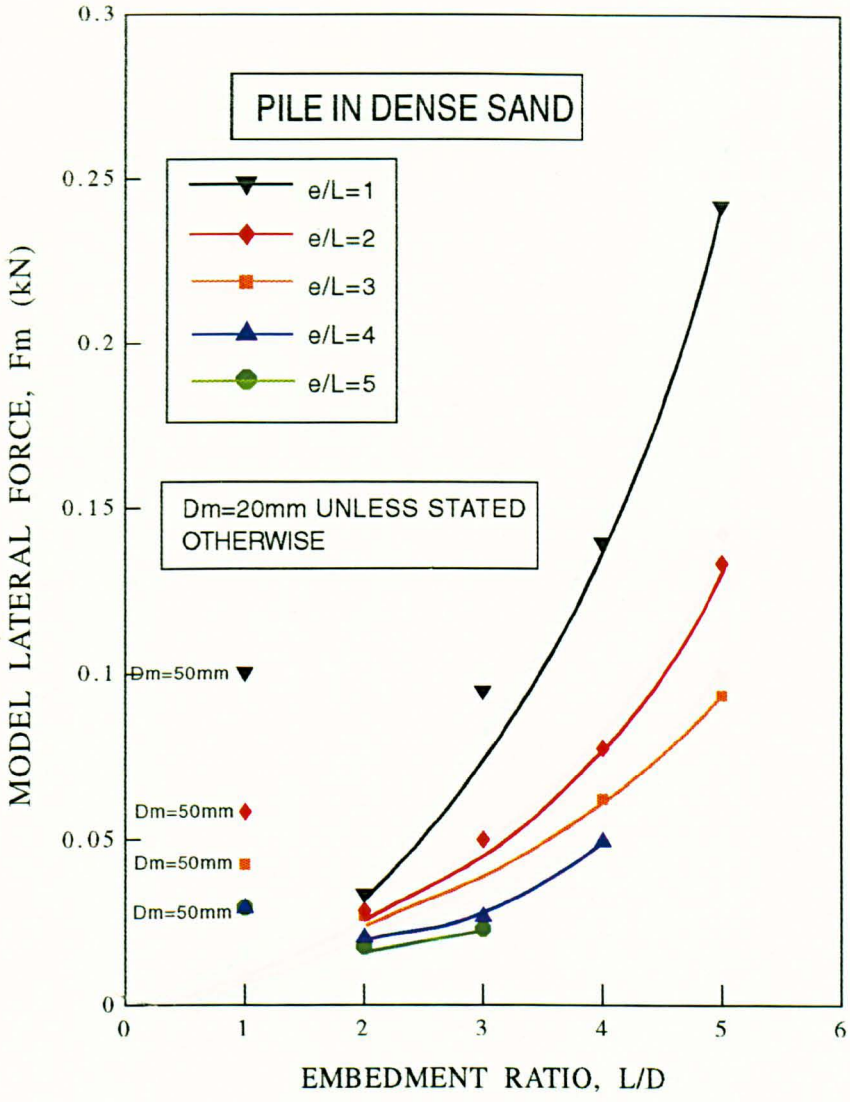

Figure 8.13 Variation of model lateral force with embedment ratio for 1m diameter prototype piles in dense sand.

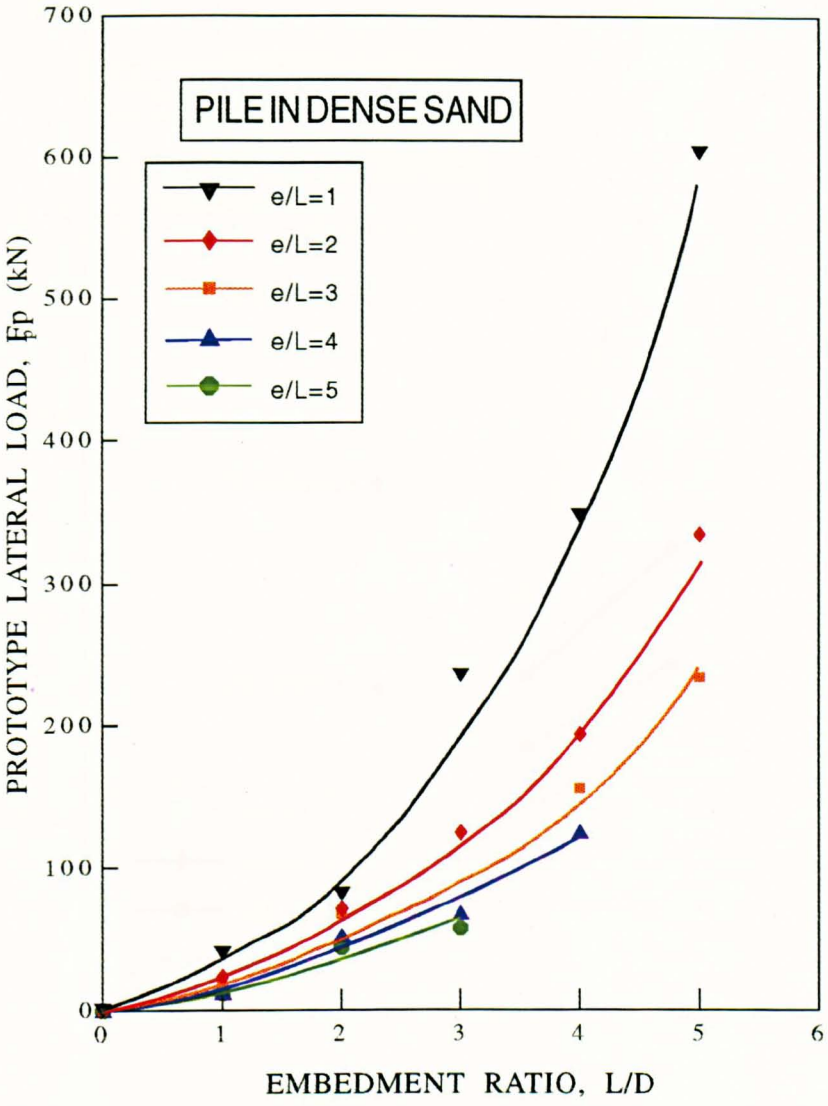

Figure 8.14 Variation of prototype lateral force with embedment ratio for 1m diameter piles in dense sand.

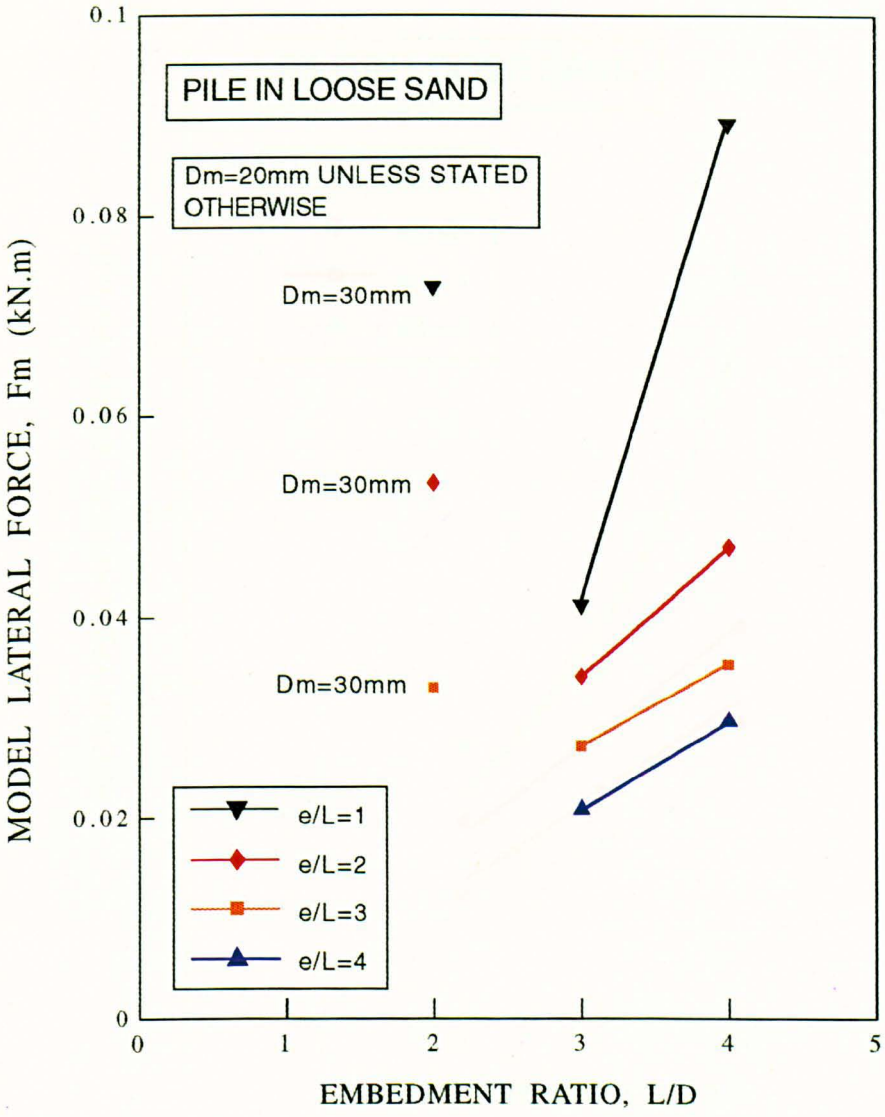

Figure 8.15 Variation of model lateral force with embedment ratio for 1m diameter prototype piles in loose sand.

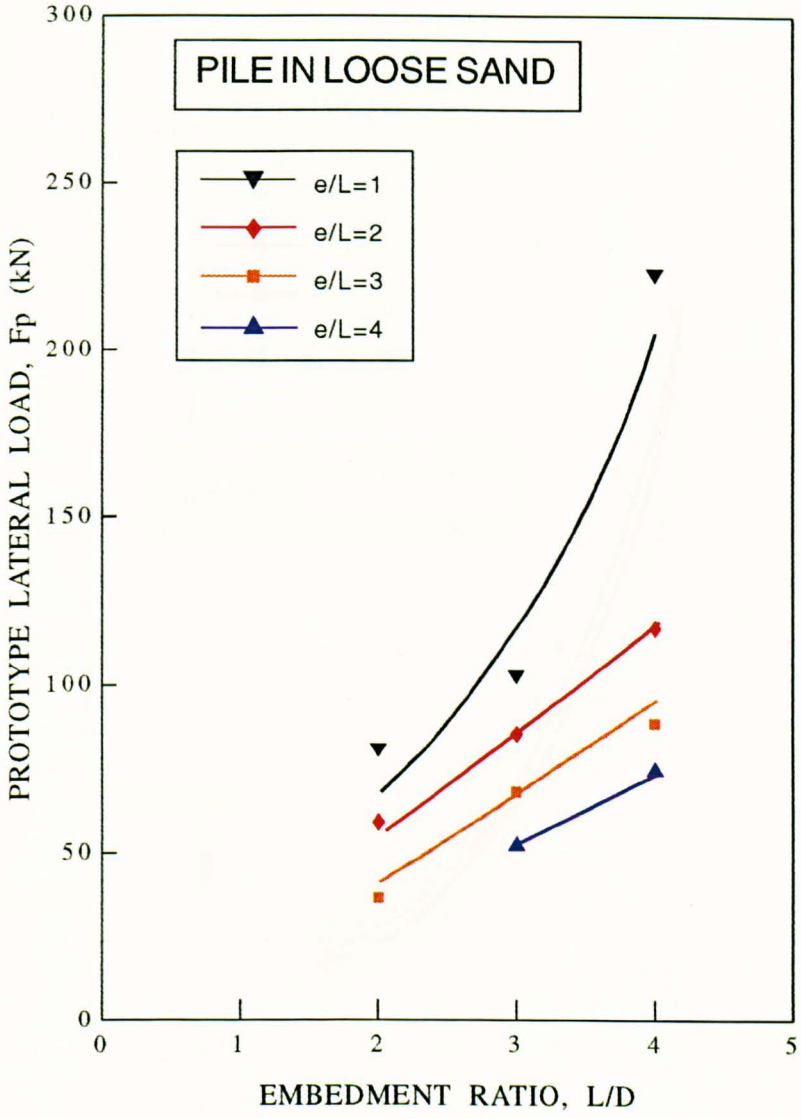

Figure 8.16 Variation of prototype lateral force with embedment ratio for 1m diameter piles in loose sand.

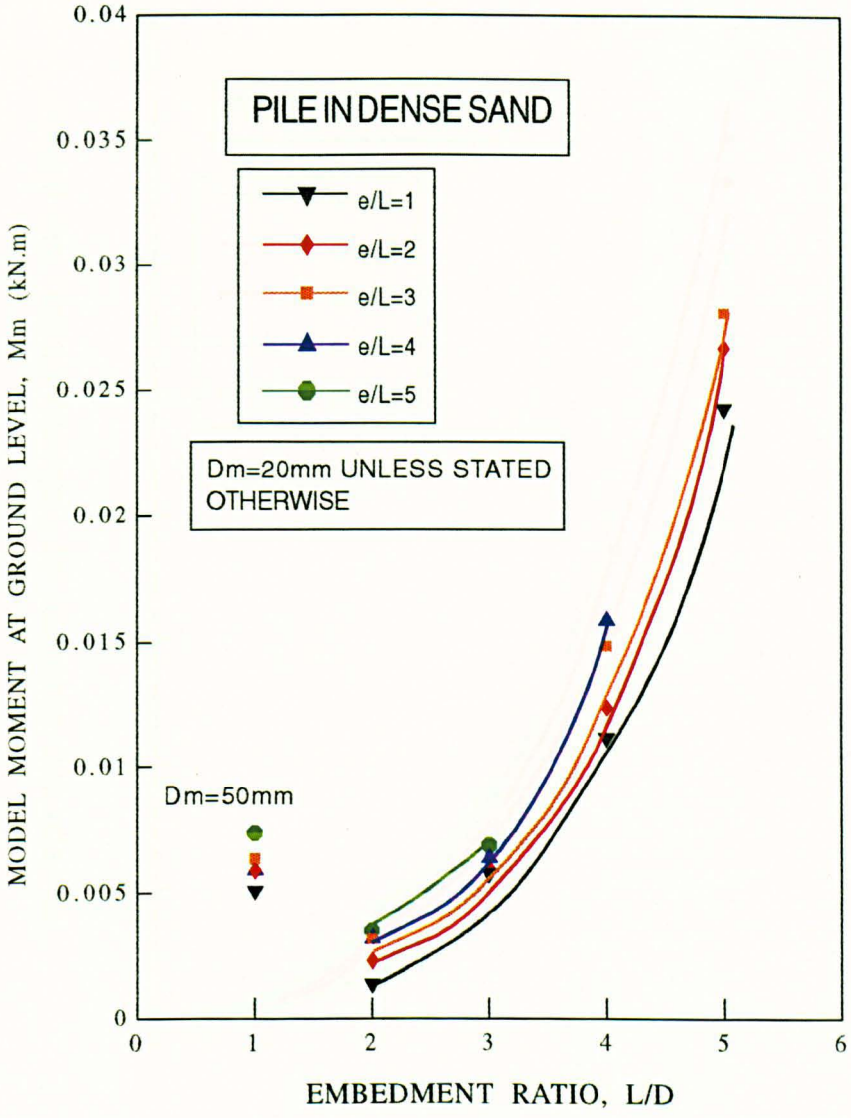

Figure 8.17 Variation of model moment at ground level with embedment ratio for 1m diameter prototype pile in dense sand.

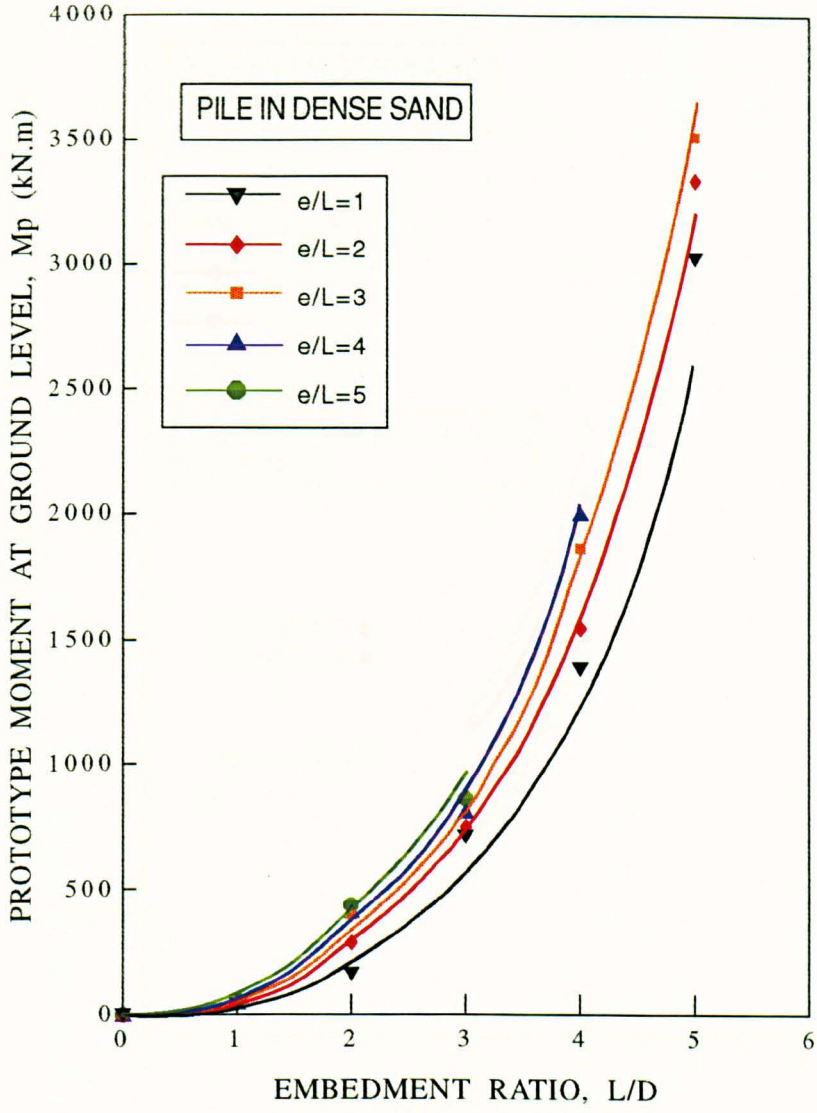

Figure 8.18 Variation of prototype moment at ground level with embedment ratio for 1m diameter piles in dense sand.

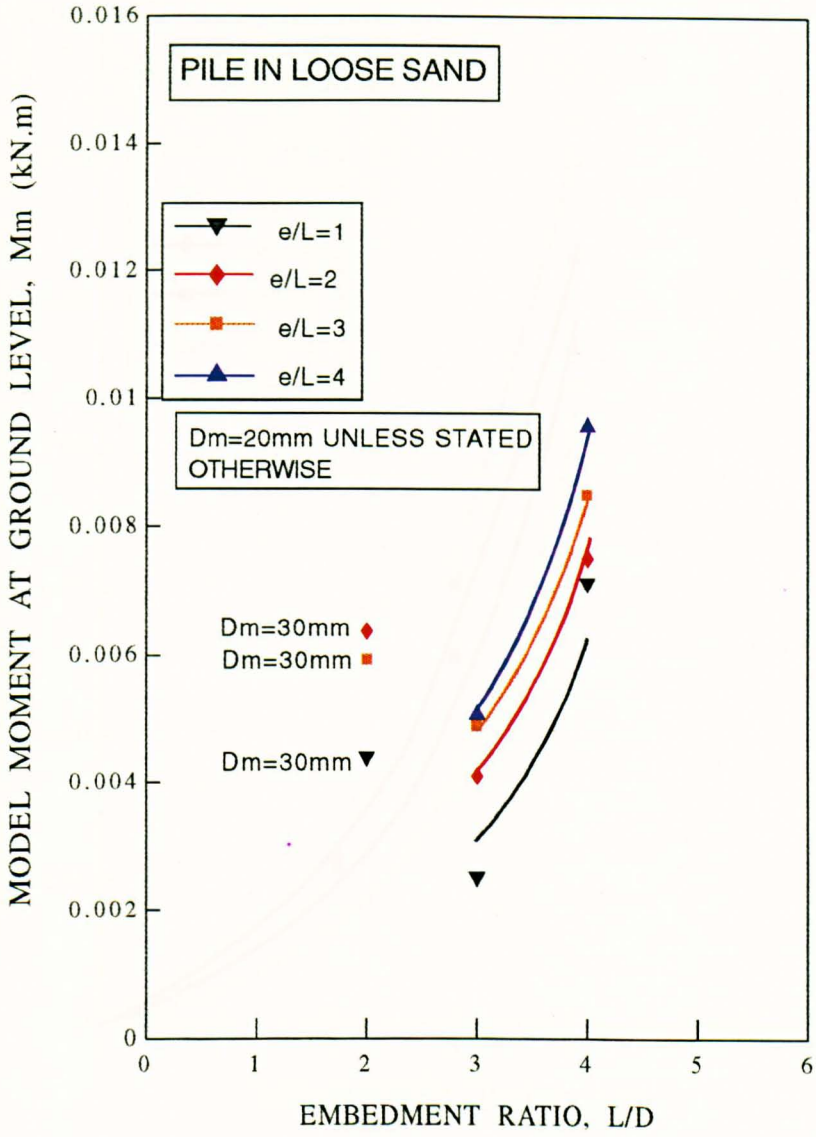

Figure 8.19 Variation of model moment at ground level with embedment ratio for 1m diameter prototype piles in loose sand.

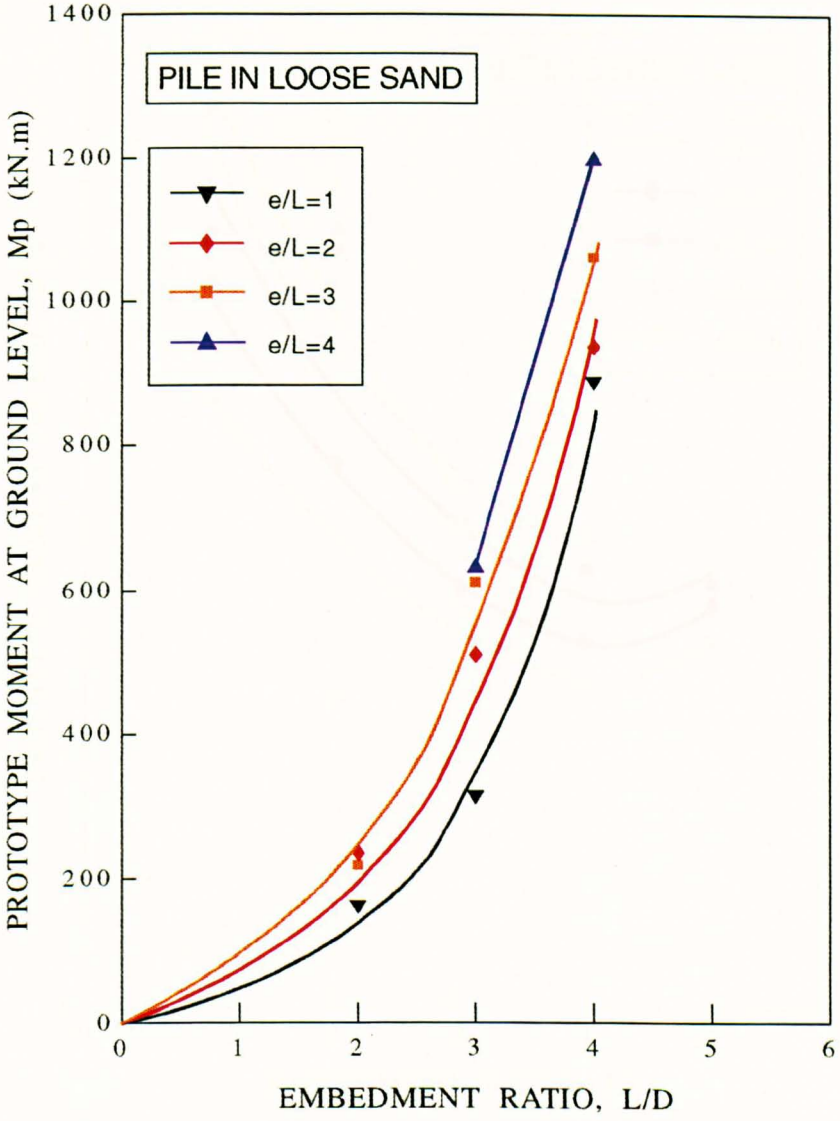

Figure 8.20 Variation of prototype moment at ground level with embedment ratio for 1m diameter piles in loose sand.

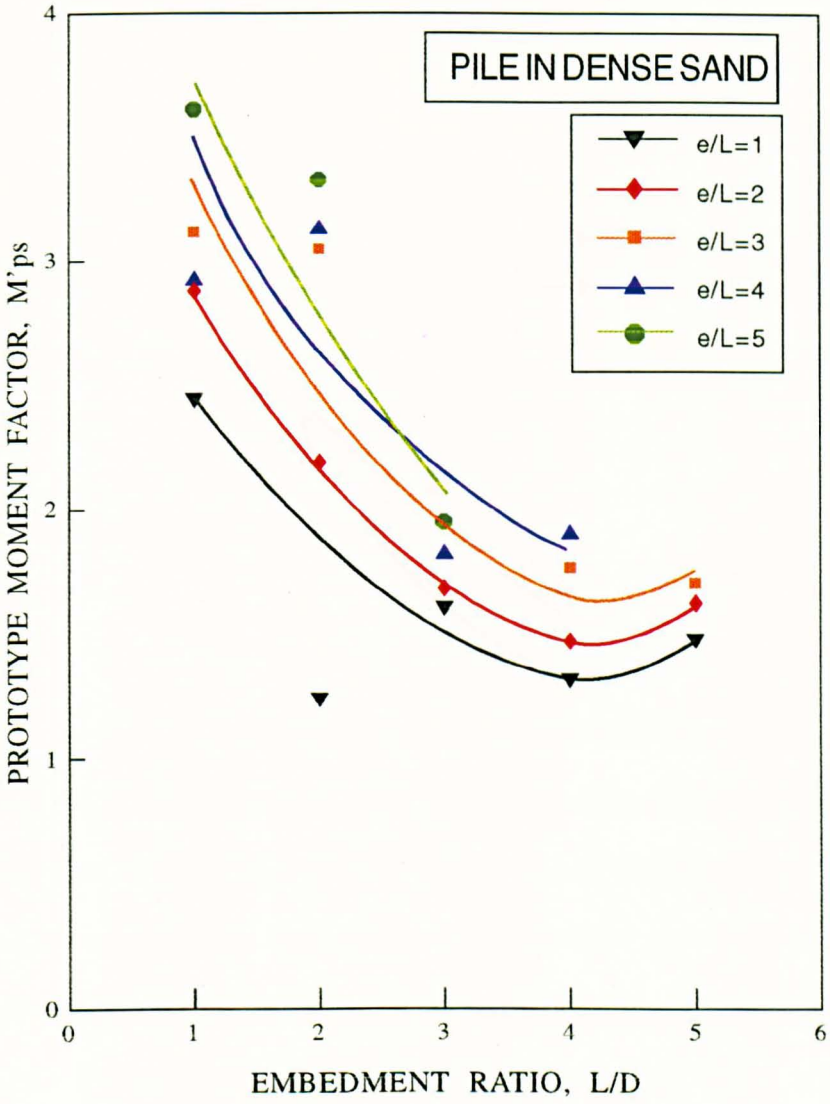

Figure 8.21 Variation of prototype moment factor with embedment ratio for 1m diameter pile in dense sand.

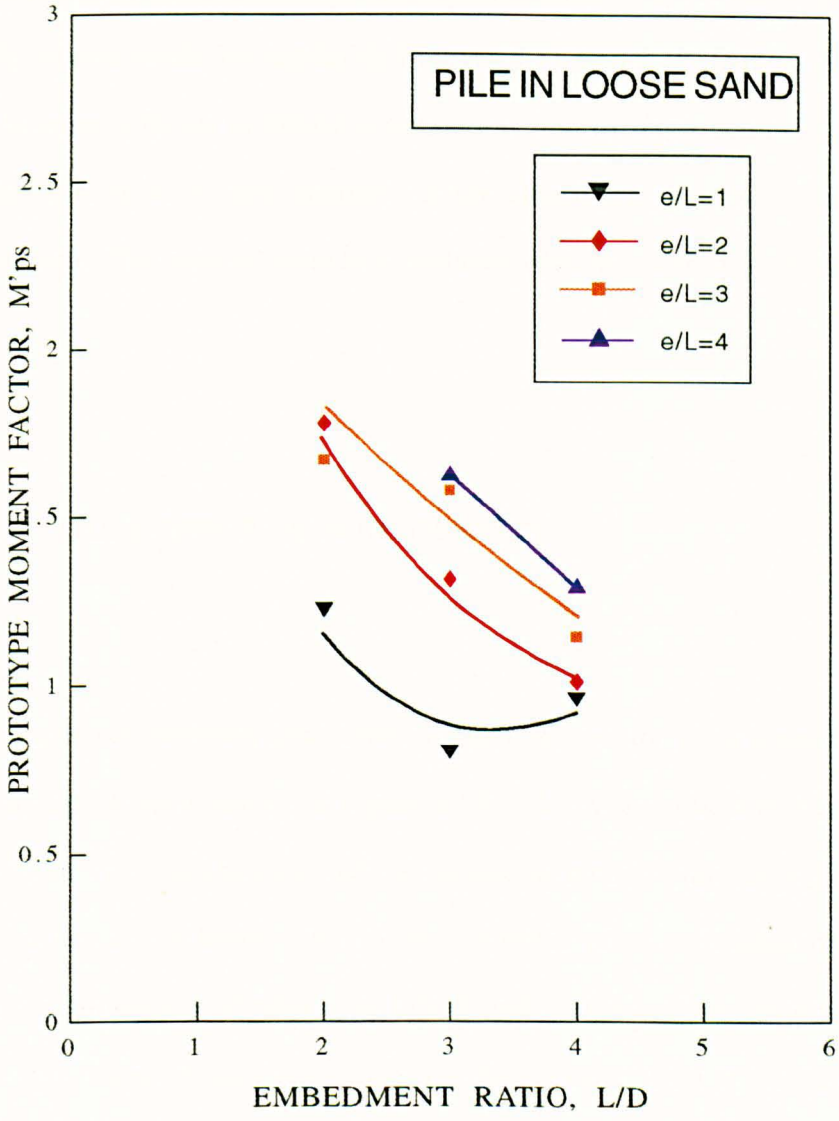

Figure 8.22 Variation of prototype moment factor with embedment ratio for 1m diameter piles in loose sand.

Figures 8.21 and 8.22 show the variation of prototype moment factor with embedment ratio for piles in dense and loose sand respectively. It was expected that the relationship shown would be similar to Figures 8.11 and 8.12. Due to the presence of scatter, it is quite difficult to obtain a consistent line through points of equal pulling height ratio. Nonetheless the moment factor clearly reduces with an increase in embedment ratio. The rate of reduction, reduces with increase in embedment ratio.

8.2.2.3 THE EFFECT OF SOIL DENSITY

A comparison between prototype moment factors for piles embedded in dense and loose sand packing is shown in Figure 8.23. Piles with embedment ratios of 3 and 4 were employed. As would be expected, the prototype moment factors of piles embedded in loose sand are much lower than those of similar piles embedded in dense sand. Prototype moment factors of piles with L/D=3 and L/D=4 in loose sand are 30% lower on average than those of their equivalents in dense sand. This is due to the fact that the lateral soil resistance, dominantly passive, which determines the limiting moment value is dependent on the density index of the soil. On the contrary, although UIC/ORE has taken soil unit weight into account in their formula, its effect is relatively insignificant.

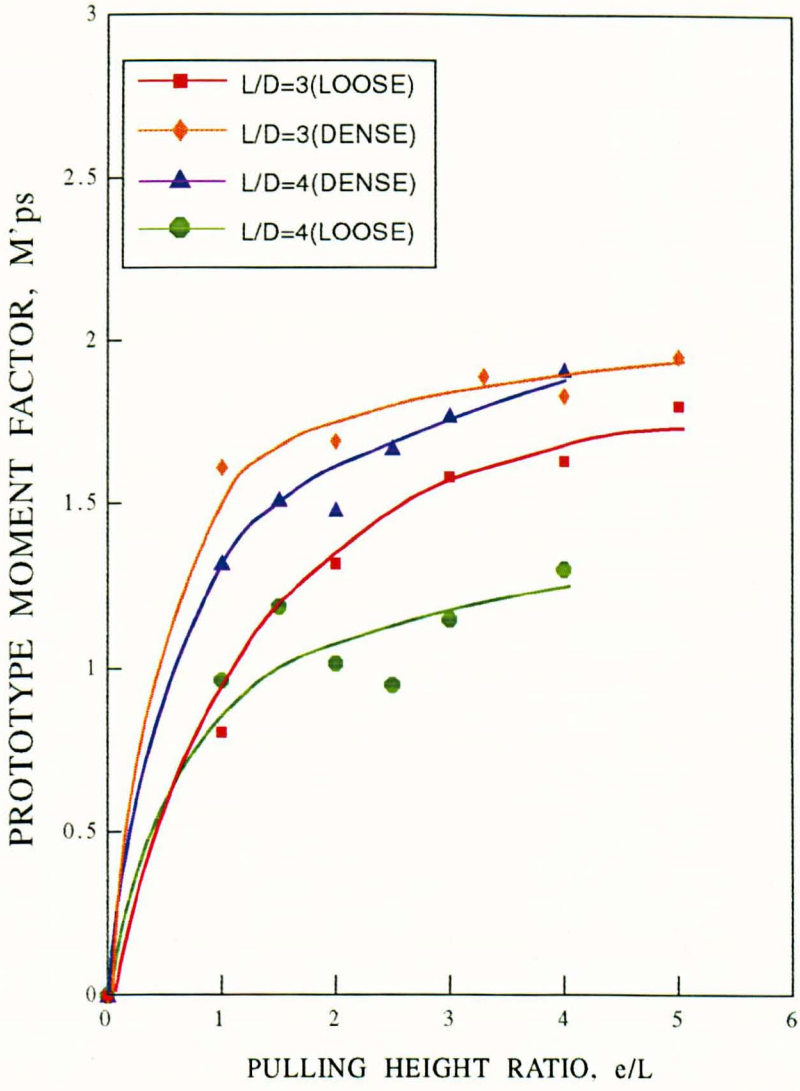

Figure 8.23 Comparison of prototype moment factor with pulling height ratio for 1m diameter pile in dense and loose sand packing.

Although in practice, loose materials would seldom exist around a pile, nevertheless, the tests conducted here serve to identify the potential variation in the moment carrying capacity due to soil packing.

8.2.2.4 THE EFFECT OF GROUND SURFACE PROFILE

It is common for that the electrification gantries supported by side bearing foundations to be located close to either a cutting or an embankment. Thus the influence of the slope proximity was investigated in Series 3. A model with L/D=4 and e/L=3 employed in the tests. A pile embedded on top of the slope was pulled either towards or away from it. The slope was cut in dense sand at an average of 36° from horizontal as explained earlier.

Tables 8.3(a) and 8.3(b) shows the results obtained from these tests. Figure 8.24 shows the variation of model moment at ground level with the slope distance ratio, d/L for a pile pulled away or towards the slope respectively. It can be seen that, on this limited evidence, a pile located very close to the slope and pulled towards it gives a lower moment value than a pile pulled away from the slope. However when the slope distance ratio exceeds 0.5, a pile pulled towards the slope shows an increase in its moment limit value compared with a pile pulled away from the slope. The moment limit values generally show an increase as the distance from the slope increases. For a slope

distance ratio greater than 1.5 it may be speculated that the moment limit would reach an almost constant value. This would define a distance limit beyond which any influence of slope is negligible.

a) PILE PULLED AWAY FROM A SLOPE IN DENSE SAND

(L/D=4, e/L=3)

TEST	N	d/L	F_m(kN)	M_m(kN.m)	Δ_m(mm)	θ°	K_s
RNSA0	50	0	0.0286	0.0069	1.75	2.00	0.46
RNSA1	50	0.4	0.0364	0.0087	1.75	2.14	0.58
RNSA2	50	0.6	0.0434	0.0104	2.37	3.24	0.70
RNSA3	50	0.8	0.0431	0.0103	3.53	4.11	0.69
RNSA4	50	1	0.0434	0.0104	3.67	4.34	0.70
RNSA5	50	1.5	0.0491	0.0118	3.38	4.71	0.79

Table 8.3(a) Summary of results for a pile pulled away from a slope.

b) PILE PULLED TOWARDS A SLOPE IN DENSE SAND

(L/D=4, e/L=3)

TEST	N	d/L	F_m(kN)	M_m(kN.m)	Δ_m(mm)	θ°	K_s
RNST0	50	0	0.0146	0.0035	3.46	2.86	0.23
RNST1	50	0.4	0.0353	0.0085	2.46	2.63	0.57
RNST2	50	0.6	0.039	0.0094	2.72	3.37	0.63
RNST3	50	0.8	0.0559	0.0134	3.1	4.21	0.90
RNST4	50	1	0.0533	0.0128	2.4	3.08	0.86
RNST5	50	1.5	0.06	0.0144	3.22	3.99	0.97

* *Subscript p and m denote prototype and model.*

Table 8.3(b) Summary of results for a pile pulled towards a slope.

For convenience in observing the influence of the slope on limiting moment values, data obtained from this test series is compared with that for the pile embedded in flat terrain having a similar parameters. A slope factor K_s, defined as the ratio of the moment limit at ground level for sloping terrain to the moment at ground level for flat terrain, was introduced. Figure 8.25 illustrate the variation of slope factor K_s with slope distance ratio, d/L. It was observed that at a d/L value of greater than 1.5 for a pile pulled towards the slope, the effect of the slope is negligible. However, at that point, when pull is away from the slope, the pile can only develop approximately 75% of its full moment carrying capacity. An extended series of sloping terrain tests for different L/D and e/L values would be required to substantiate these findings.

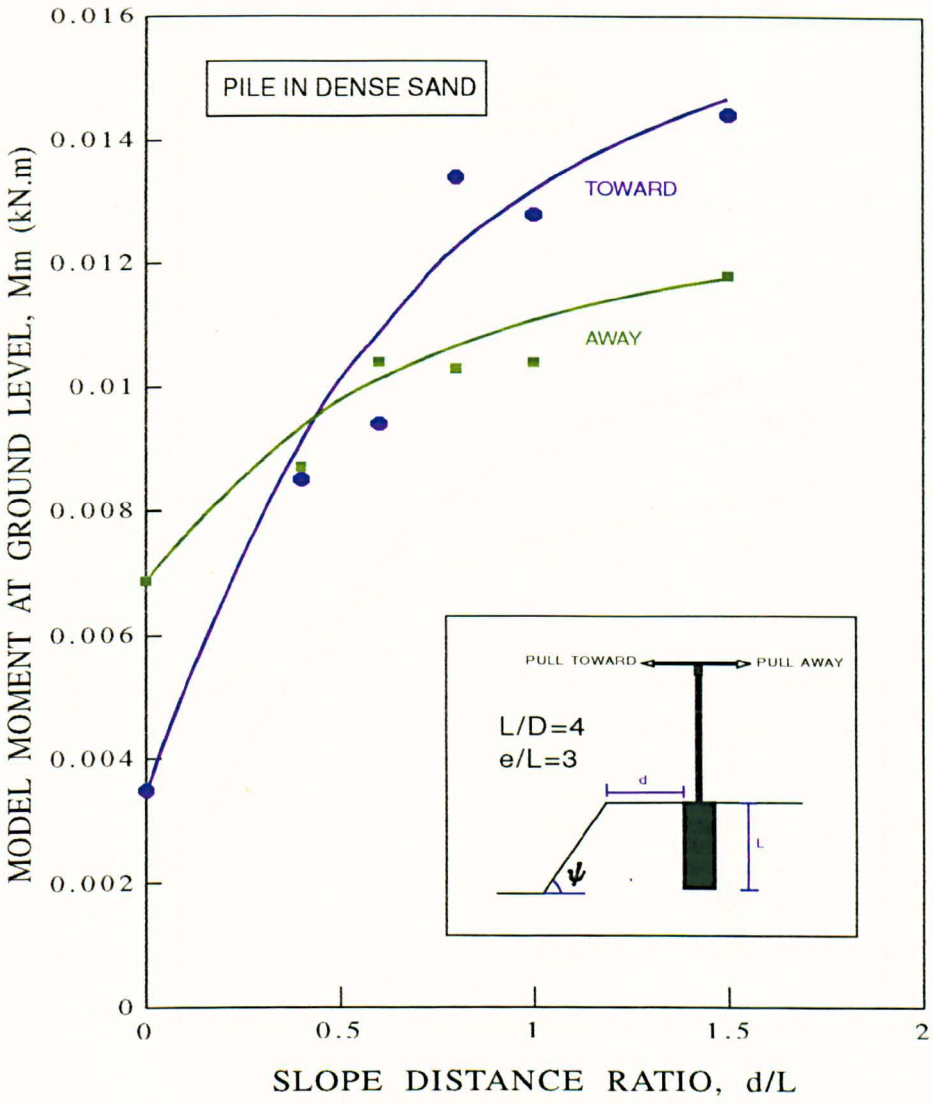

Figure 8.24 Variation of model moment at ground level for pile embedded within proximity of a slope

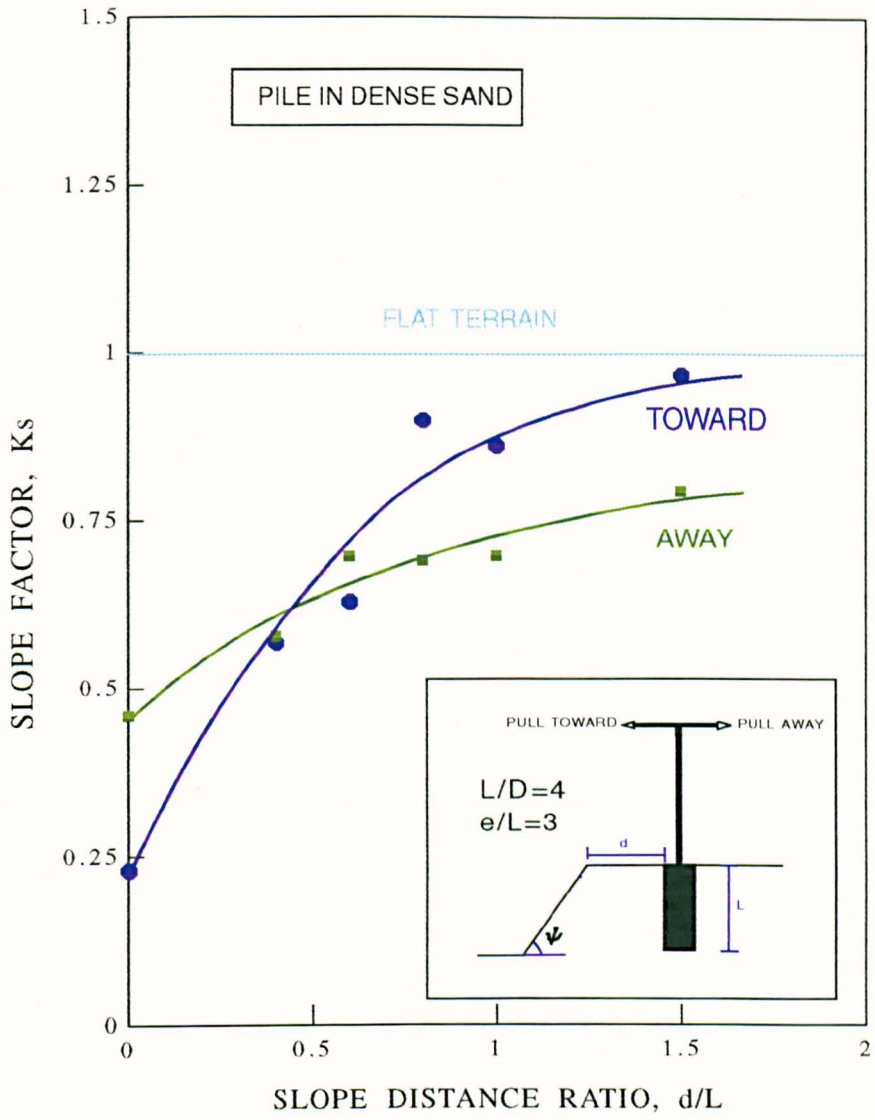

Figure 8.25 Variation of slope factor Ks for pile embedded within the proximity of a slope

8.2.2.5 THE EFFECT OF PILE DIAMETER

Tests in Series 4 were performed to investigate the influence of pile diameter on the limiting moment. Results from Series 4 are presented in model terms in Table 8.4(a) includes prototype values. Embedment ratios, L/D=2 and L/D=5 and a pulling height ratio e/L=3 were employed. Model diameters ranging from 20mm to 40mm were tested at different accelerations, are shown in Figure 8.26 and 8.27.

Figure 8.26 shows the variation of moment at ground level with pile diameter plotted logarithmically in prototype terms. While limiting moments increase considerably with pile diameter, they also increase with embedment ratio. Discrepancies occur with the limiting moment value adopted from pilot tests by Kueh(1989) test using similar equipment. This has to be expected, since it is difficult to obtain similar test parameters even though the same materials were used. Moreover, handling technique in conducting the test varies from one study to another. Generally a similar trend to that found by Kueh was observed. The moment factor plotted against pile diameter in prototype terms are shown in Figure 8.27. While the moment at ground level increases greatly with an increase in pile diameter,the moment factor reduces significantly and is inclined to reach a constant value at a diameter of 1m. Thus the effect of pile diameter on moment limit is less significant for pile with bigger diameter. However in this circumstance, a pad or strip footing can be considered, where the foundation is solely depending on the vertical rather than lateral bearing capacity.

Chapter 8

TEST	N	D_m(mm)	L_m(mm)	F_m(kN)	M_m(kN.m)	Δ_m(mm)	L/D	e/L	θ^o
RND1G	1	20	100	0.0043	0.0013	3.32	5	3	2.41
RND12G	12	20	100	0.0319	0.0096	5.76	5	3	5.33
RND25G	25	20	100	0.0554	0.0166	4.62	5	3	5.32
RND2	50	20	100	0.0938	0.0281	3.65	5	3	3.65
RNDCT1	1	100	500	0.613	0.92	16.68	5	3	3.62
RNMM2	40	25	50	0.0421	0.0063	3.72	2	3	6.05
RNMP2	13	40	80	0.0562	0.0135	3.36	2	3	3.65
RNMP3	7	40	80	0.0319	0.0077	2.58	2	3	2.81
RNMP4	1	40	80	0.0066	0.0016	2.01	2	3	1.58
RNDCT11	1	100	200	0.084	0.05	5.13	2	3	1.6

Table 8.4(a) Summary for Series Four presented in terms of model values

TEST	D_p(m)	L_p(m)	F_p(kN)	M_p(kN.m)	Δ_p(mm)	M'_{ps}
RND1G	0.02	0.1	0.0043	0.0013	3.32	3.96
RND12G	0.24	1.2	4.59	16.59	69.12	2.44
RND25G	0.5	2.5	34.63	259.38	134.75	2.02
RND2	1	5	234.50	3512.50	182.50	1.71
RNDCT1	0.1	0.5	0.6130	0.9200	16.68	4.49
RNMM2	1	2	67.36	403.20	148.80	3.07
RNMP2	0.52	1.04	9.50	29.66	43.68	3.09
RNMP3	0.28	0.56	1.56	2.64	18.06	3.28
RNMP4	0.04	0.08	0.0066	0.0016	2.01	4.76
RNDCT11	0.1	0.2	0.084	0.05	5.13	3.81

Table 8.4(b) Summary for Series 4 presented in terms of prototype values

Results obtained from a 100mm pile diameter tested in the reinforced bin attained a moment factor value about 12% higher than a 20mm diameter pile tested in the centrifuge bucket at unit gravity. This higher moment factor value for 100mm diameter piles was attributable to the boundary effect since the failure zone is constrained by the size of the bin. Since the pile was situated in the middle of the bin, the distance from pile to the side of the bin is 630mm (see chapter 7 for details of bin size). The result of the slope test series(8.2.2.4) indicates the limit of influence of a boundary within the failure zone as d/L=1.5. Thus for a 500mm pile, the edge distance required is, 1.5 x 500mm = 750mm.

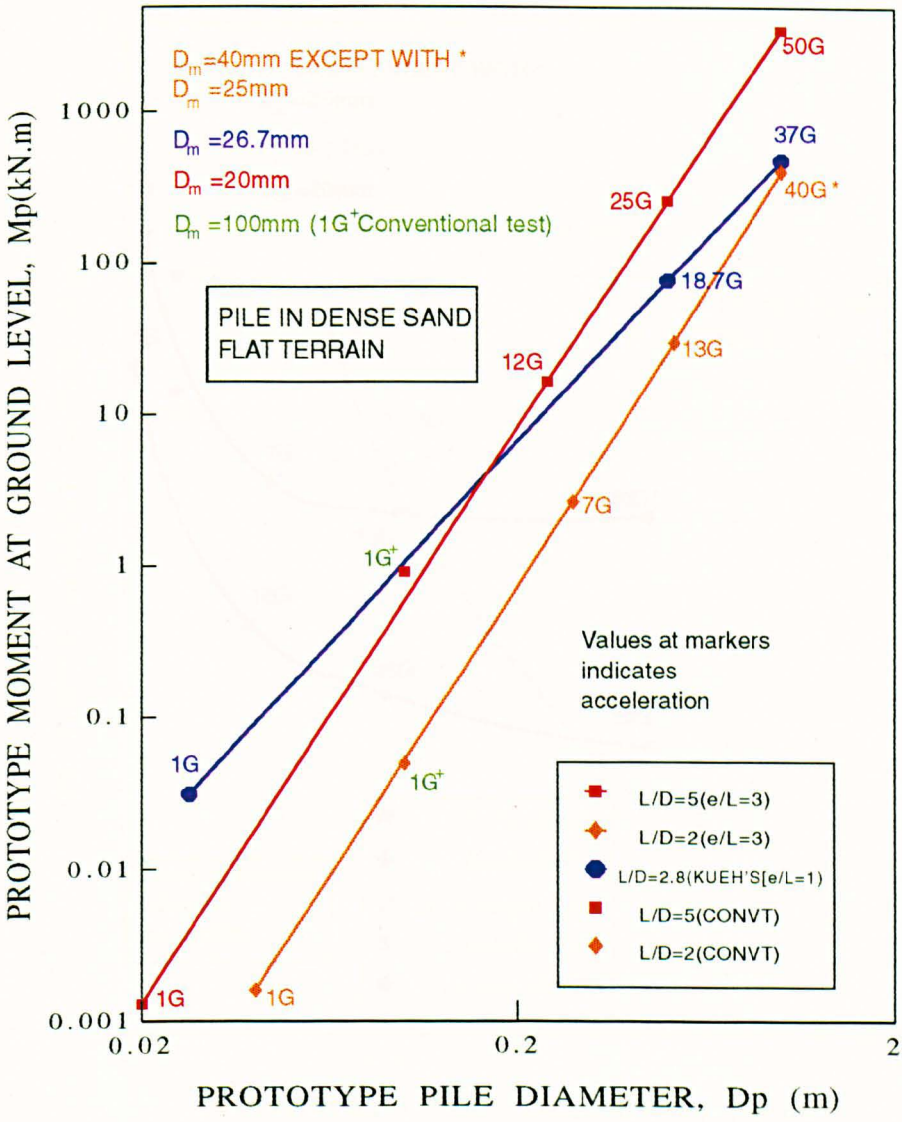

Figure 8.26 Variation of prototype moment at ground level with prototype pile diameter.

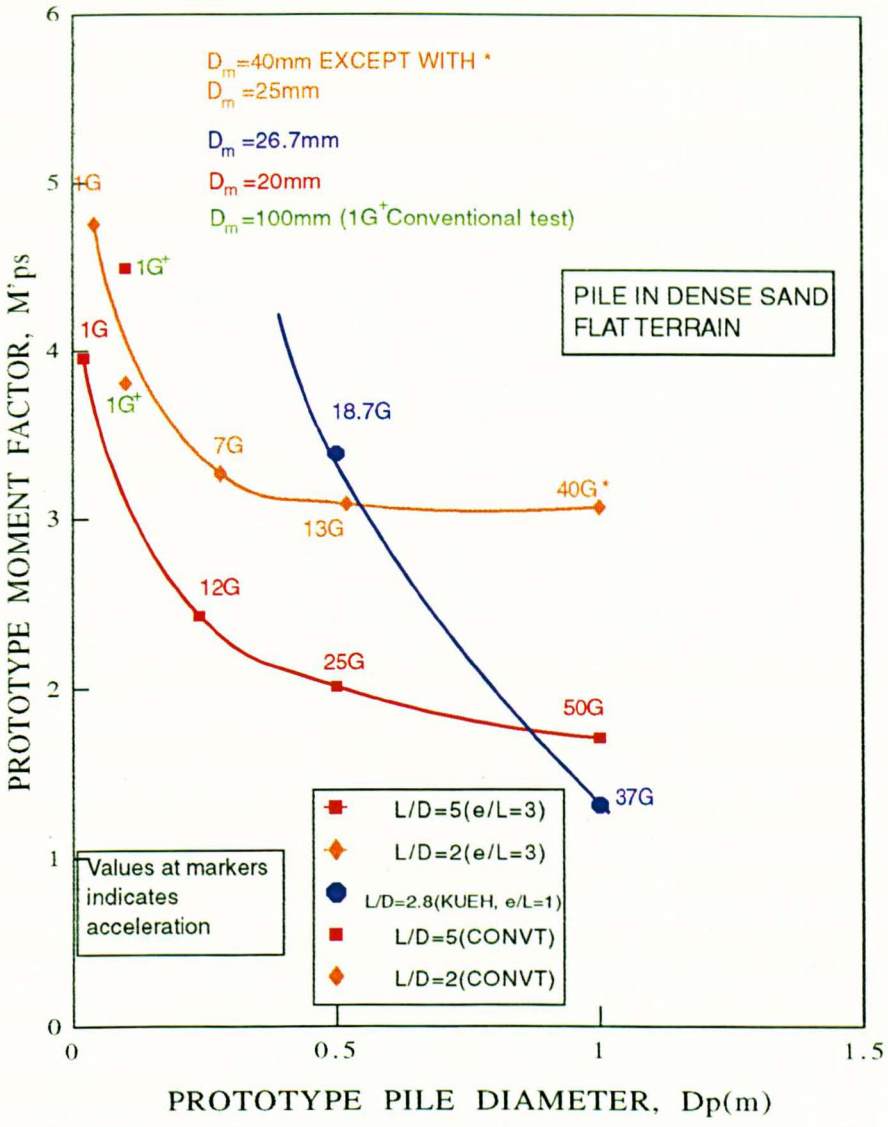

Figure 8.27 Variation of prototype moment factor M'ps with prototype pile diameter

Since the distance between the pile and the side of the bin is only 630mm, the results are like to be affected. However results obtained from a conventional test for L/D=2 show a slightly lower moment factor value along with the other larger pile diameters. The problem is probably associated with the eccentricity of the pulling arm weight which will be explained later in conventional test section.

8.2.2.6 PILE ROTATION

Variation of pile rotation at failure with pulling height and embedment ratio for dense sand are shown in Figures 8.28 and 8.29 respectively. The points shown are considerably scattered. It should also be noted that 'failure' for the piles with L/D=5 was not determined in the same way as for the shorter piles. It is difficult to determine the trend of pile rotation with respect to the pulling height or embedment ratio. However for convenience, lines enclosing the points were plotted to show the general behaviour of the rotation at failure.

As shown in Figure 8.28, the value of pile rotation decreases with an increase in pulling height ratio and ranged from 2° to 8°. A pile pulled nearer to ground level required a higher rotation before failure compared to a pile pulled at higher level. A pile

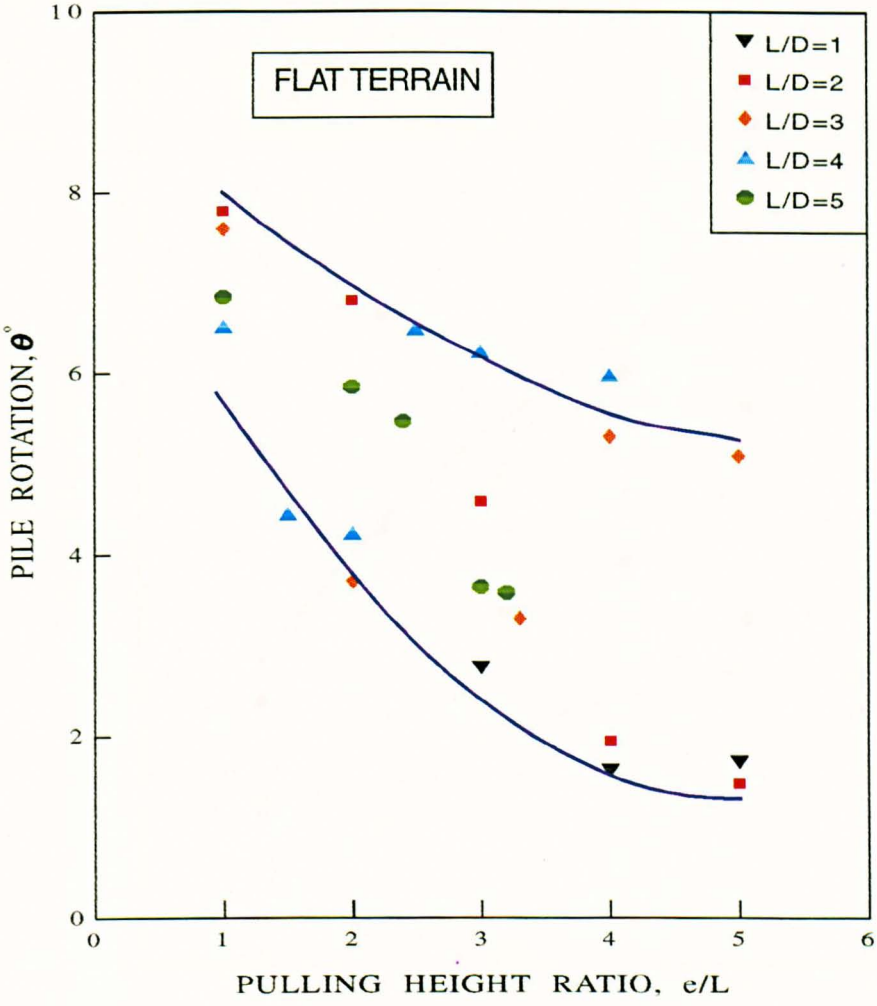

Figure 8.28 Variation of pile rotation with pulling height ratio for 1m diameter prototype pile in dense sand in flat terrain.

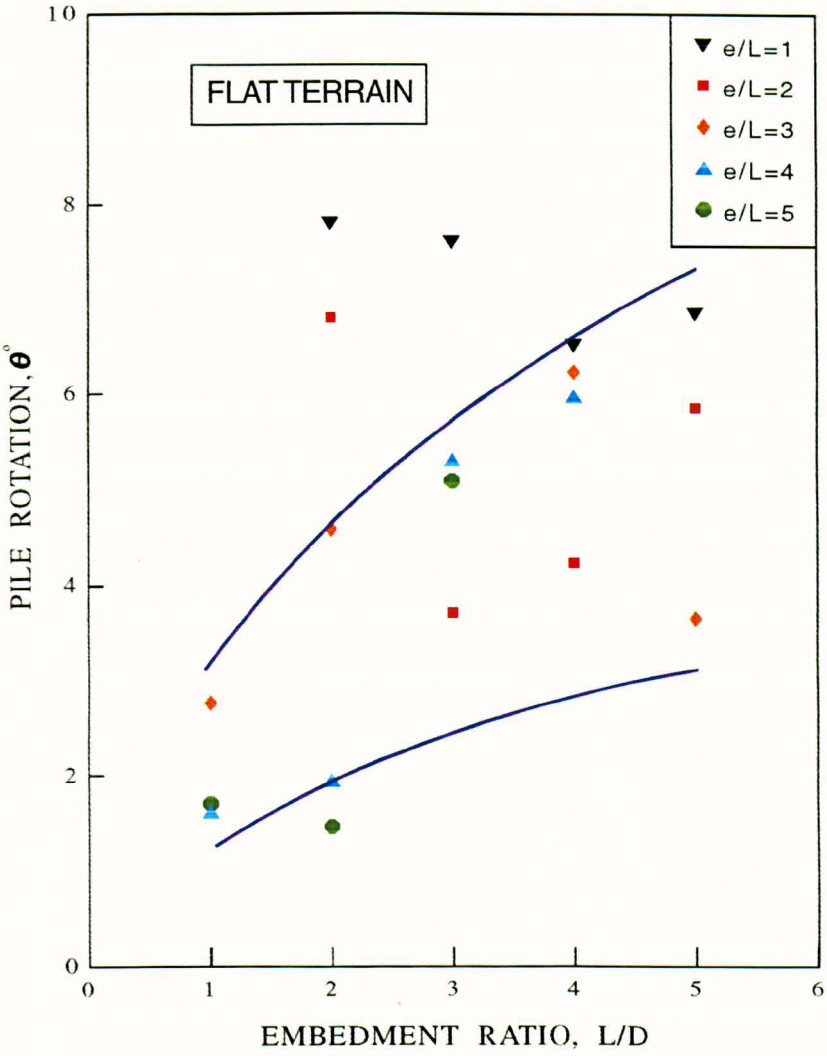

Figure 8.29 Variation of pile rotation with embedment ratio for 1m diameter prototype pile in dense sand in flat terrain.

with a longer embedded length required a larger rotation to mobilise full moment resistance as shown in Figure 8.29. Thus for longer piles loaded at low level a design approach based on allowable rotation rather than one applying a suitable safety factor to the moment limit value, would probably be more appropriate.

Figures 8.30(A) to 8.30(D) shows the position of the centre of rotation during pile rotation. Extreme values were selected for piles with longest embedment length(L/D=5) and shortest embedment length(L/D=1). The pulling height ratios selected were between 1 and 5. It is difficult to determine whether the pile undergoes rotation or translation at the initial stage of the test. Assumption was made that just before failure, the pile was purely under rotation. The apparent centre of pile rotation was calculated from the intersection of the axis of the inclined foundation with the initial axis with the foundation unloaded. It is clearly seen that the centre of rotation varied during the progression of the tests.

Results for piles pulled from relatively high levels are shown in Figures 8.30(A) and 8.30(C). It is noticeable that the location of the point of rotation quickly falls below the mid depth of the pile. As the test proceeds, the point of rotation increases and continues to fluctuate until it reaches a steady value of between 2/3 and 3/4 of the pile depth, which in this case gives broad agreement with Czerniak(1957).

Figures 8.30(B) and 8.30(D), show the behaviour of piles pulled at lower levels. In Figure 8.30(B) for a long pile, the point of rotation was initially located above the

mid depth of the pile. With further movement, the location of the point of rotation steadily dropped to a point at about 2/3 of the pile depth reaching a similar position to that for the same pile subjected to high level pull. However this was not the case for the short pile in Figure 8.30(D). The point of rotation dropped well below the base of the pile showing that translation is governing the initial movement of the pile. At a rotation of 0.25° the point of rotation tends to move upwards. The translation process reduces when the pile has rotated to an angle of 1.5°. Thereafter the point of rotation increases until it reaches a steady value around 2/3 of the pile depth. It can be inferred that for the shortest piles pulled at low level, the location of the point of rotation is lower with respect to ground surface compared to the pile pulled at higher level where rotation is dominating the later stage of the pile movement.

8.2.3 CENTRIFUGAL TESTS ON CONTINUOUS PILE

Most of the analyses provided by previous researchers such as Terzaghi(1943), Hansen(1961), Broms(1964), Meyerhof(1981,83,88) and many others, derived their formulation based on two dimensional geometry. It is no surprise that these methods of solution are most popularly employed since a much easier analysis results compared to the three dimensional alternative.

Broms(1964) and Meyerhof et al.(1981) attempt to relate the three dimensional problem to their two dimensional computations by introducing a shape factor. As

Chapter 8

TEST	N	F_m(kN)	M_m(kN.m)	Δ_m(mm)	F_p(kN)	M_p(kN.m)	Δ_p(mm)	θ°	B_p(m)	L/D	e/L	M'_{pc}
SFD1	50	0.2665	0.0853	3.95	666.25	10662.50	197.50	2.99	6.3	5	3	0.83
SFD2	50	0.3328	0.0799	4.77	832.00	9987.50	238.50	3.61	6.3	5	2.4	0.77
SFD3	50	0.4152	0.0830	6.76	1038.00	10375.00	338.00	5.36	6.3	5	2	0.80
SFD4	50	0.7981	0.0798	5.19	1995.25	9975.00	259.50	4.23	6.3	5	1	0.77
SFD5	50	0.1728	0.0553	3.06	432.00	6912.50	153.00	3.21	6.3	4	4	1.05
SFD6	50	0.2104	0.0505	2.63	526.00	6312.50	131.50	2.88	6.3	4	3	0.95
SFD7	50	0.3165	0.0506	3.78	791.25	6325.00	189.00	3.49	6.3	4	2	0.96
SFD8	50	0.5700	0.0456	5.05	1425.00	5700.00	252.50	5.54	6.3	4	1	0.86
SFD9	50	0.0742	0.0119	1.03	185.48	1483.75	51.50	5.08	6.3	2	4	1.80
SFD10	50	0.0978	0.0117	0.99	244.50	1462.50	49.50	5.30	6.3	2	3	1.77
SFD11	50	0.1417	0.0113	1.34	354.25	1412.50	67.00	3.31	6.3	2	2	1.71
SFD12	50	0.1914	0.0077	2.23	478.50	962.50	111.50	3.72	6.3	2	1	1.16

** Subscript p and m denote prototype and model respectively.*

Table 8.5(a) Summary of centrifugal test results for continuous pile embedded in dense sand.

Chapter 8

TEST	N	F_m(kN)	M_m(kN.m)	Δ_m(mm)	F_p(kN)	M_p(kN.m)	Δ_p(mm)	θ°	B_p(m)	L/D	e/L	M'_{pc}
SFL1	50	0.1217	0.0389	2.84	304.25	4862.50	142.00	1.47	6.3	4	4	0.84
SFL2	50	0.1274	0.0306	3.10	318.50	3825.00	155.00	1.95	6.3	4	3	0.66
SFL3	50	0.2451	0.0310	6.65	612.75	3875.00	332.50	4.58	6.3	4	2	0.67
SFL4	50	0.3642	0.0291	5.39	910.50	3637.50	269.50	6.80	6.3	4	1	0.63

* *Subscript p and m denote prototype and model*

Table 8.5(b) Summary of centrifugal test results for continuous pile embedded in loose sand.

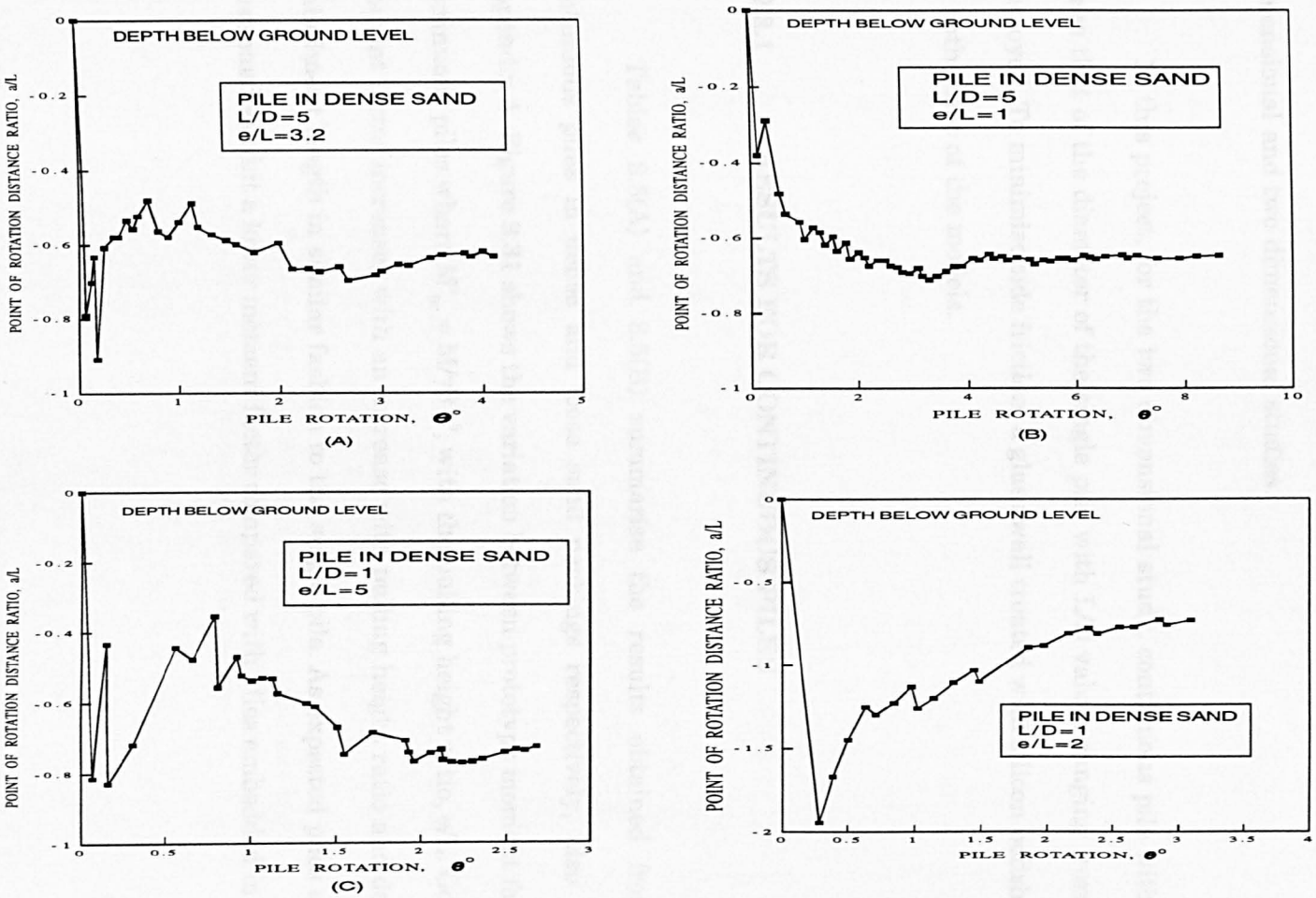

Figure 8.30 Variations of point of rotation distance ratio with pile rotation at various embedment pulling height ratio.

explained in Chapters Two and Four, the shape factor is used to convert the result obtained from the analysis of a wall to a final result which predicts the soil resistance for a single pile. Although it is not irrefutable, since the shape factor depends on the soil and pile geometry, nevertheless it provides a rational way of relating three dimensional and two dimensional studies.

In this project, for the two dimensional study, continuous pile with widths 6.3 times that of the diameter of the single pile with L/D values ranging from 2 to 5 was employed. To minimise side friction, a glass wall treated with silicon polish was placed on both sides of the models.

8.2.3.1 RESULTS FOR CONTINUOUS PILES

Tables 8.5(A) and 8.5(B) summarise the results obtained from tests on continuous piles in dense and loose sand packings respectively, also included in Appendix A. Figure 8.31 shows the variation between prototype moment factor M'_{pc} for continuous piles where $M'_{pc} = M/\gamma BL^3$, with the pulling height ratio, e/L. Generally, the moment factor increases with an increase with pulling height ratio and decrease with embedment length in similar fashion to the single pile. As expected piles embedded in loose sand exhibit a lower moment factor compared with piles embedded in dense sand.

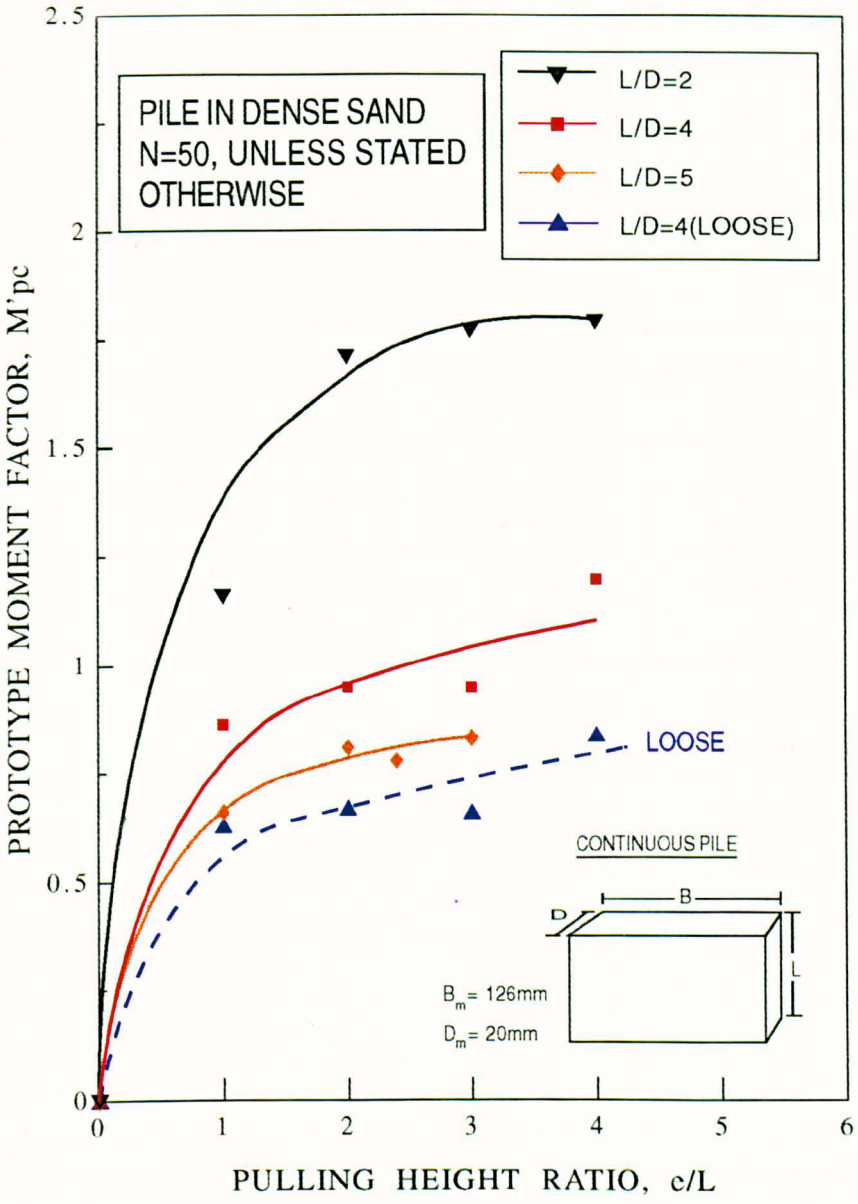

Figure 8.31 Variation of prototype moment factor with pulling height ratio for 1m width continuous prototype pile in dense and loose sand

To observe the side friction effect, tests with and without side walls were carried out at unit gravity in the centrifuge bucket. A summary of the results is shown in Table 8.6. Figure 8.32 shows that the moment factor for a pile without the glass side walls exhibits an average of 7% higher moment factor compared to a pile tested with glass side wall. This justifies the use of glass side wall in the main testing program.

TEST	N	B_m(mm)	L/D	e/L	F_m(kN)	M_m(kN.m)	Δ_m(mm)	θ°
SFD1W	1	126	5	3	0.0138	0.0043	2.33	1.87
SFD2W	1	126	5	2.4	0.0172	0.0041	1.43	1.08
SFD3W	1	126	5	2	0.0190	0.0038	1.38	1.02
SFD4W	1	126	5	1	0.0334	0.0033	1.43	1.14
SFD1G1	1	126	5	3	0.0134	0.0040	0.90	0.92
SFD2G1	1	126	5	2.4	0.0163	0.0039	1.43	1.07
SFD3G1	1	126	5	2	0.0185	0.0037	1.33	1.10
SFD4G1	1	126	5	1	0.0260	0.0026	0.98	0.81

Table 8.6 Comparison of results between continuous pile with and without glass side wall

8.3 COMPARISON BETWEEN SINGLE AND CONTINUOUS PILE

Comparing Figures 8.11 and 8.12 with Figure 8.31, the moment factor value for a single pile is always higher than that for the equivalent continuous pile, while failure displacements were generally similar. This clearly demonstrates the difference which

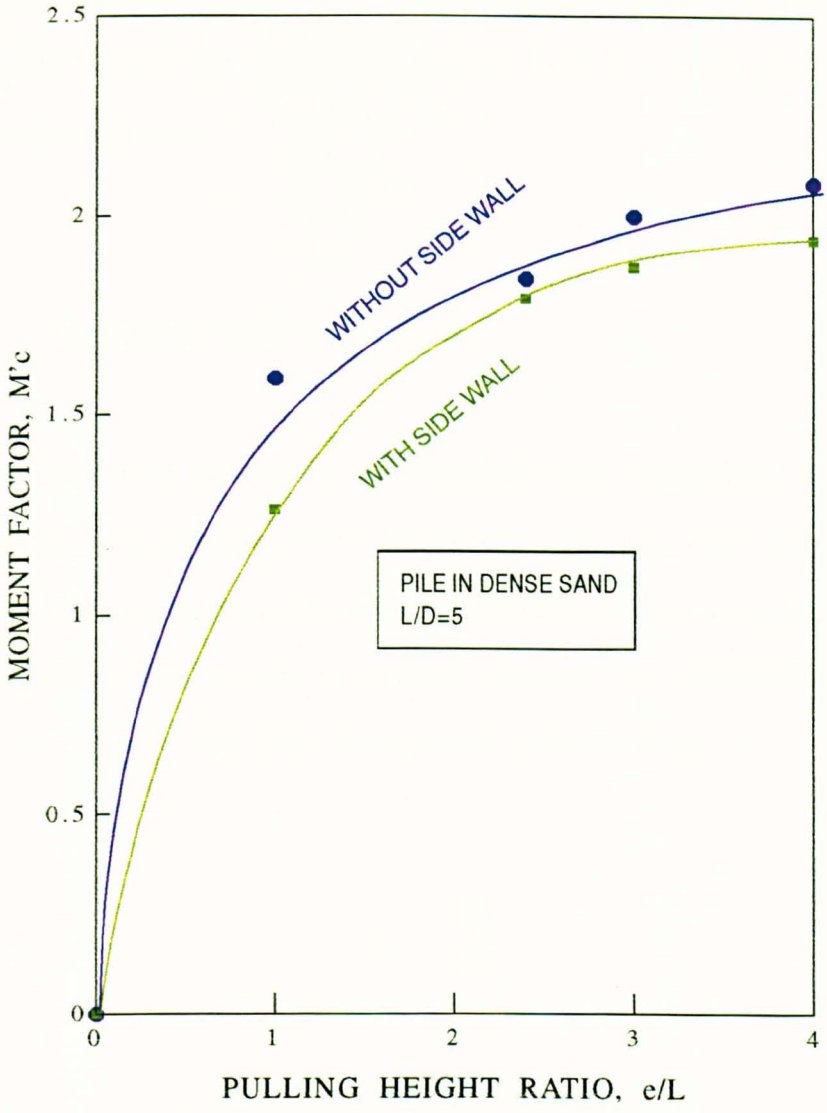

Figure 8.32 Comparison of moment factor for continuous pile in dense sand with and without side wall

exists between the plane strain and triaxial condition. For higher embedment ratios the deviation is more significant. Thus a limiting moment value predicted from the analysis of a wall would not strictly apply to the moment limit of a single pile particularly for higher embedment ratios.

8.3.1 MOMENT SHAPE FACTOR

In an attempt to account for the essentially three dimensional behaviour of the laterally loaded short pile, the author introduced a suitable shape factor to relate the effect of the three dimensional case to the two dimensional analyses. Since the limiting moment at ground level is used as a design criterion, the empirical moment shape factor, S_{fm} was adopted. This may be expressed mathematically as;

$$S_{fm} = \frac{M'_{ps}}{M'_{pc}}$$

Comparative values of moment factor for continuous and single piles are summarised in Table 8.7 together with values of S_{fm} from the above equation. Figure 8.33 exhibits the variation of moment shape factor with pulling height ratio. Although the plot gives a general indication of the variation of moment shape factor with pulling height ratio, it is noticeable that the pulling height ratio has a limited effect on it. Readings were scattered due to the combined scatter of the two test series. However the

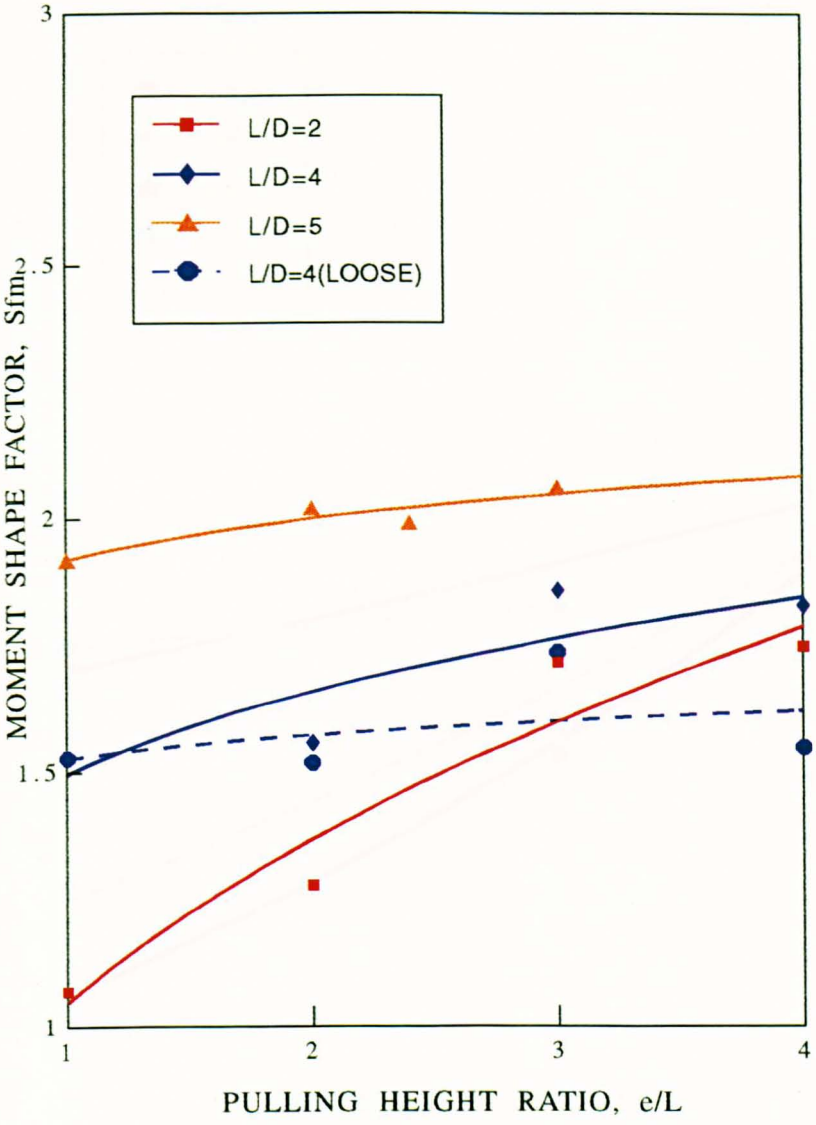

Figure 8.33 Variation of dimensionless moment shape factor with pulling height ratio for pile in dense and loose sand

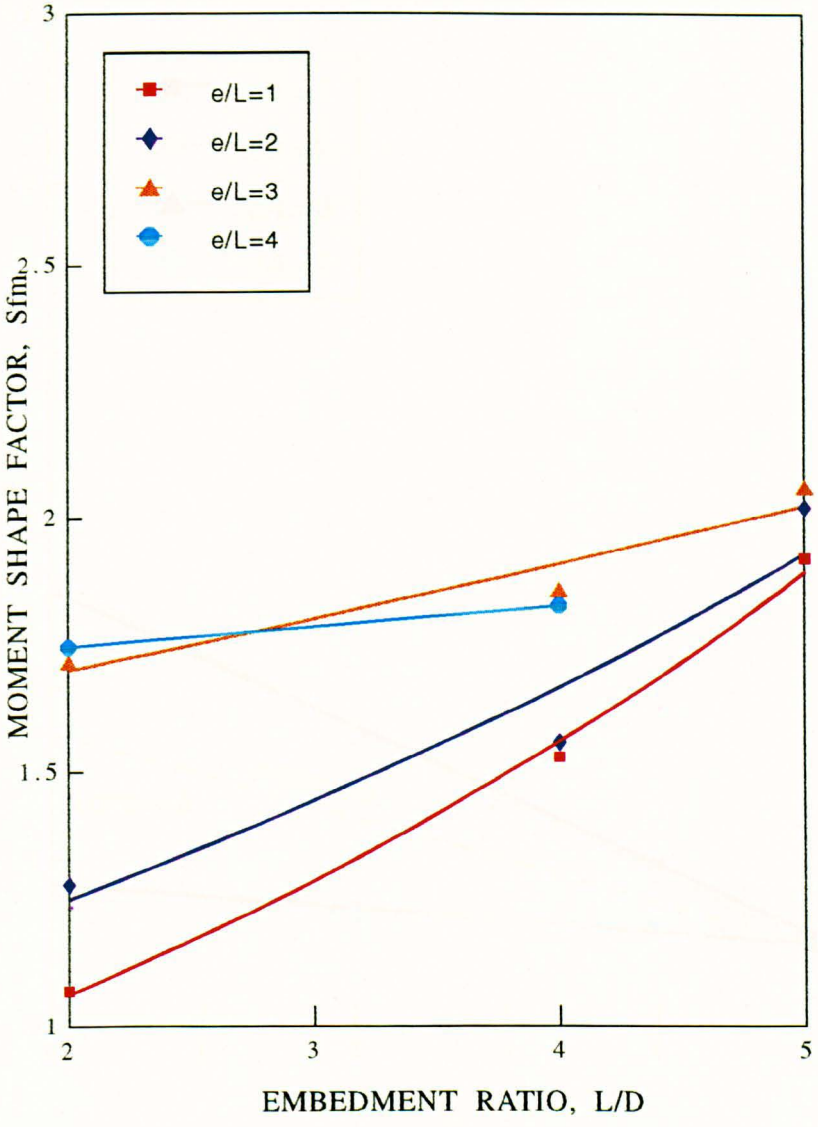

Figure 8.34 Variation of dimensionless moment shape factor with embedment ratio for piles in dense sand

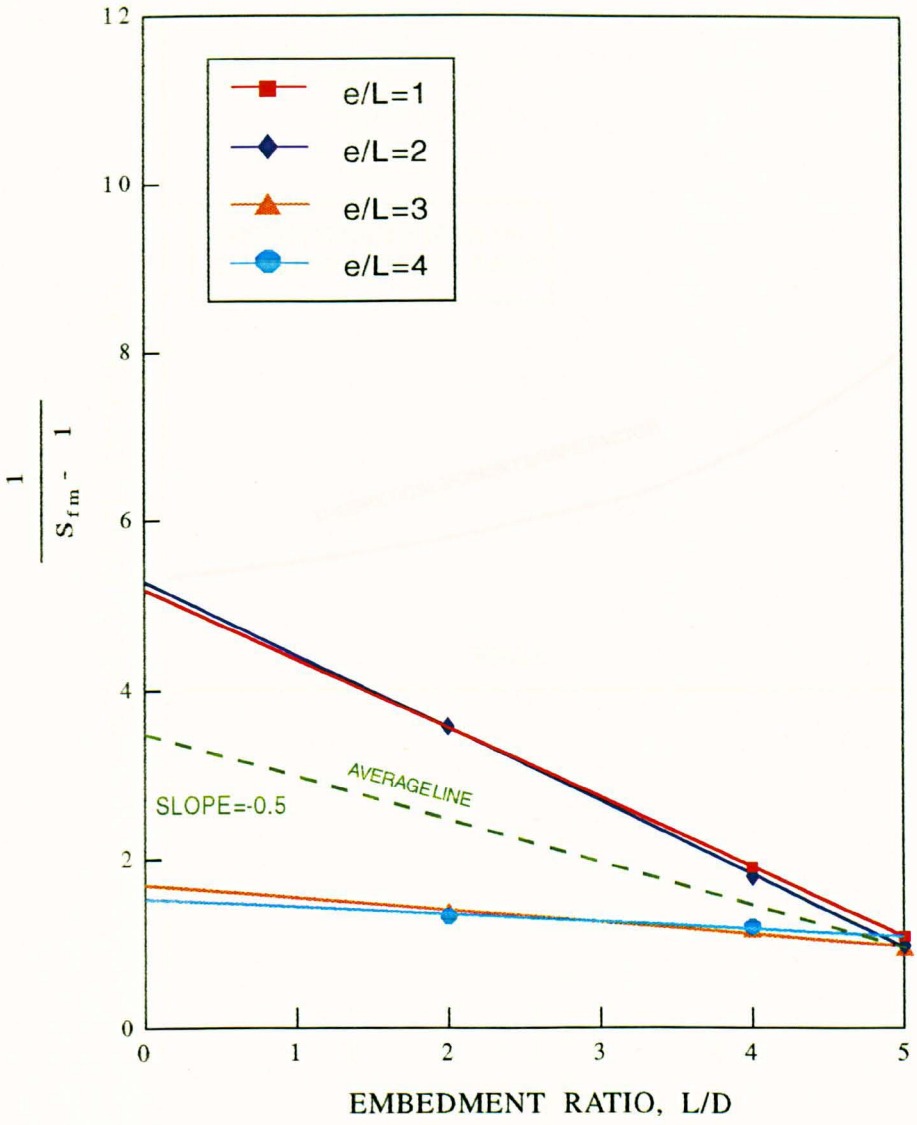

Figure 8.35 Variation of dimensionless moment shape factor with embedment ratio for pile in dense sand

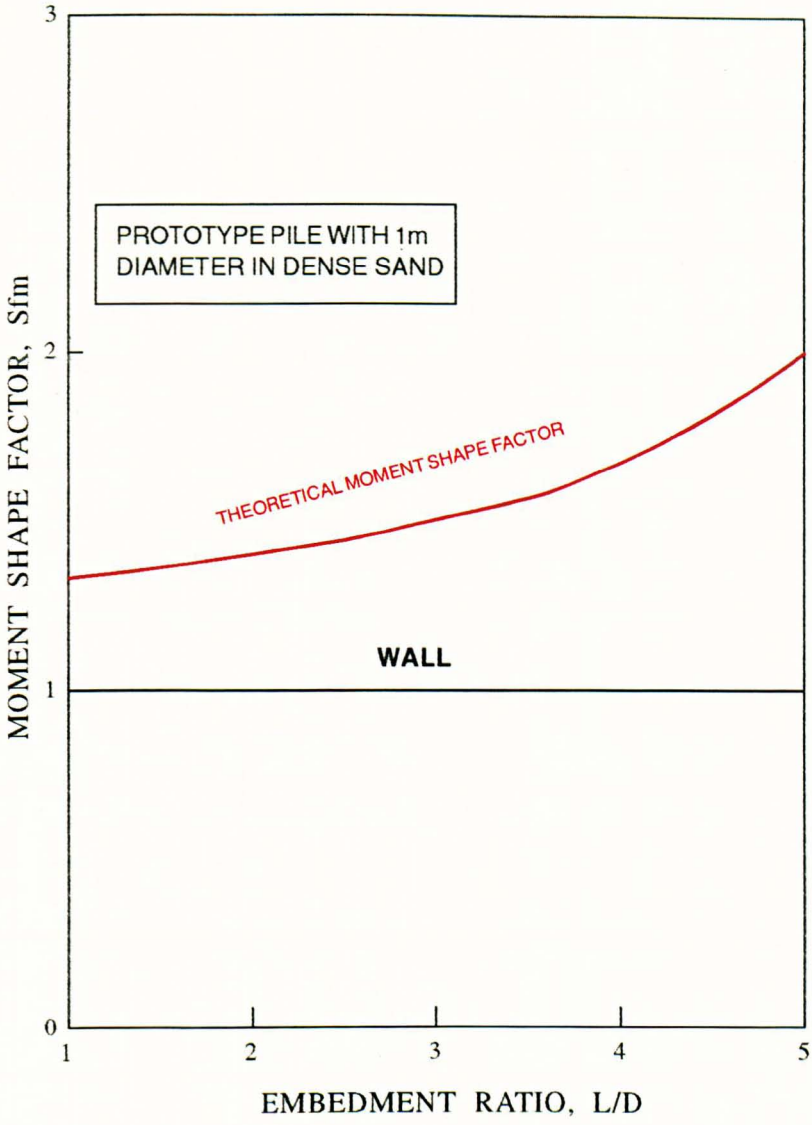

Figure 8.36 Variation of dimensionless moment shape factor with embedment ratio for pile in dense sand

TEST	M_p(kN.m)	M'_{ps}	TEST	M_p(kN.m)	M'_{pc}	L/D	e/L	S_{fm}	$1/S_{fm}$-1
RND2	3512.50	1.71	SFD1	10662.50	0.83	5	3	2.06	0.94
RND3	3187.50	1.55	SFD2	9987.50	0.77	5	2.4	2.01	0.99
RND4	3337.50	1.63	SFD3	10375.00	0.80	5	2	2.04	0.96
RND5	3025.00	1.48	SFD4	9975.00	0.77	5	1	1.92	1.08
RND6	2000.00	1.91	SFD5	6912.50	1.05	4	4	1.82	1.22
RND7	1862.50	1.77	SFD6	6312.50	0.95	4	3	1.86	1.16
RND9	1550.00	1.48	SFD7	6325.00	0.96	4	2	1.54	1.85
RND11	1387.50	1.32	SFD8	5700.00	0.86	4	1	1.53	1.87
RND18	412.50	3.14	SFD9	1483.75	1.80	2	4	1.74	1.34
RND19	400.00	3.05	SFD10	1462.50	1.77	2	3	1.72	1.38
RND20	287.50	2.19	SFD11	1412.50	1.71	2	2	1.28	3.56
RND21	162.50	1.24	SFD12	962.50	1.16	2	1	1.07	14.50
RNL1	1200.00	1.30	SFL1	4862.50	0.84	4	4	1.55	1.83
RNL2	1062.50	1.15	SFL2	3825.00	0.66	4	3	1.74	1.35
RNL4	937.50	1.02	SFL3	3875.00	0.67	4	2	1.52	1.91
RNL6	887.50	0.96	SFL4	3637.50	0.63	4	1	1.52	1.91

Table 8.7 Summary of the moment shape factor results

general trends clearly show that embedment ratio and soil unit weight influence the moment shape factor in broad agreement with Meyerhof et al.(1981) but in contrast with Broms who adopted a constant shape factor. Figure 8.34 shows more clearly how the moment shape factor increases with an increase in embedment ratio. A general empirical expression for the variation of moment shape factor with embedment ratio may thus be derived. Figure 8.35 was replotted using the reciprocal of the moment shape factor, with ratio origin at (0,0) for simplification purposes. Figure 8.35 shows that the variation of $1/(S_{fm}-1)$ with embedment ratio gives a linear relationship for $0<L/D<5$.

From Figure 8.35, the average line gives the following relationship;

$$\frac{1}{S_{fm}-1} = 3.5 - 0.5\frac{L}{D} \tag{8.1}$$

From further manipulation of Equation(8.1), a general expression for the moment shape factor for short rigid piles embedded in dense sand is;

$$S_{fm} = \frac{2}{(7 - \frac{L}{D})} + 1 \tag{8.2}$$

Figure 8.36 shows the moment shape factors based on Equation (8.2).It must be borne in mind that, due to the limited number of tests, equation(8.2) is only applicable for a pile with $1<L/D<5$ in dense sand.

Values of S_{fm} from Equation (8.2) may be used to derive the limiting moment at ground level using a two dimensional result as a basis computation. In this research the moment shape factors obtain from this empirical relationship will be used in conjunction with the continuous pile values to compare with single pile results. Comparison of the moment limit of single piles obtained in this way will be compared with existing design methods in Chapter Nine.

8.4 RESULTS OF CONVENTIONAL TESTS

As a basis for comparison with the results from the centrifugal tests, conventional tests were performed by Desta(1992) under the author's supervision. Medium size model piles, $1/10^{th}$ scale of the 1m prototype diameter, with lengths ranging from 200 to 500mm were employed in the test series. Parameters involved in the tests were chosen as close as possible to those in the centrifuge package so that direct comparisons could be achieved. Details of the conventional test package were discussed in detail in Chapter Seven. Apart from the conventional tests performed in the reinforced bin, unit gravity tests conducted in the centrifuge bucket were performed.

8.4.1 GENERAL DISCUSSION OF CONVENTIONAL TEST RESULTS

The first part of this section section will deal with pile testing on flat terrain. Piles embedded close to the top of a slope will then be considered. The unit gravity tests in the centrifuge bucket will also be discussed.

8.4.2 PILES IN FLAT TERRAIN

A summary of results in Series 1 of the conventional tests is shown in Table 8.8 for dense and loose sand packing. Figure 8.37 shows the variation of model lateral pulling force F_m with pulling height ratio. The pulling force increases with an increase in embedment ratio but decreases with an increase in pulling height ratio as expected. Figure 8.38 shows the variation of model moment at ground level M_m with pulling height ratio. It is significant that the pile with L/D=5 exhibits a higher moment value than expected. This is due to the boundary effect of the bin as explained earlier in this Chapter. Piles with embedment ratios of 3 and 4 show reasonable results. The lower value for the pile with L/D=2 is probably due to the error which arises from the use of the same pulling arm for all pile lengths in these tests. During the rotation of the pile, the weight of the pulling arm was suspected to contribute the moment carried by the pile due to its eccentricity. This adverse effect is clearly seen in Figure 8.39 where the variation of moment factor is plotted against pulling height ratio. The values for a pile with L/D=5 and L/D=2 give a fallacious indication on the behaviour of pile. A correction

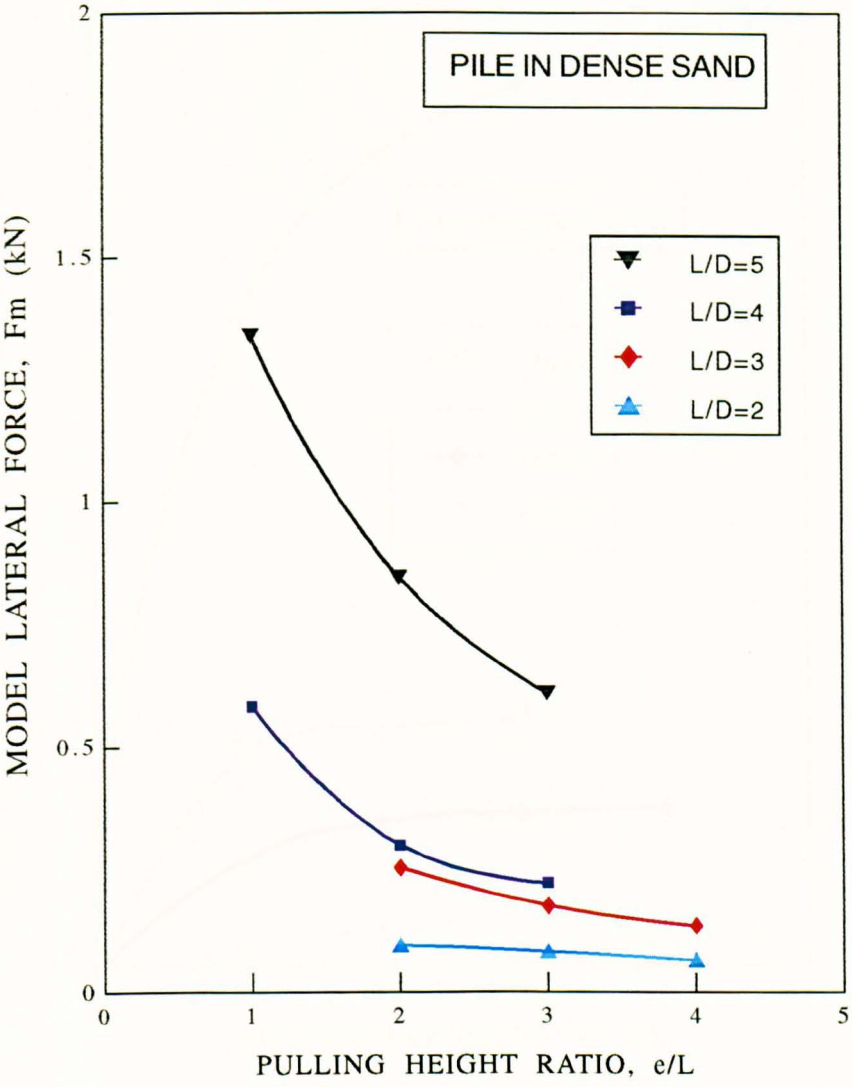

Figure 8.37 Variation of model lateral force with pulling height ratio for 100mm diameter pile in dense sand in conventional test.

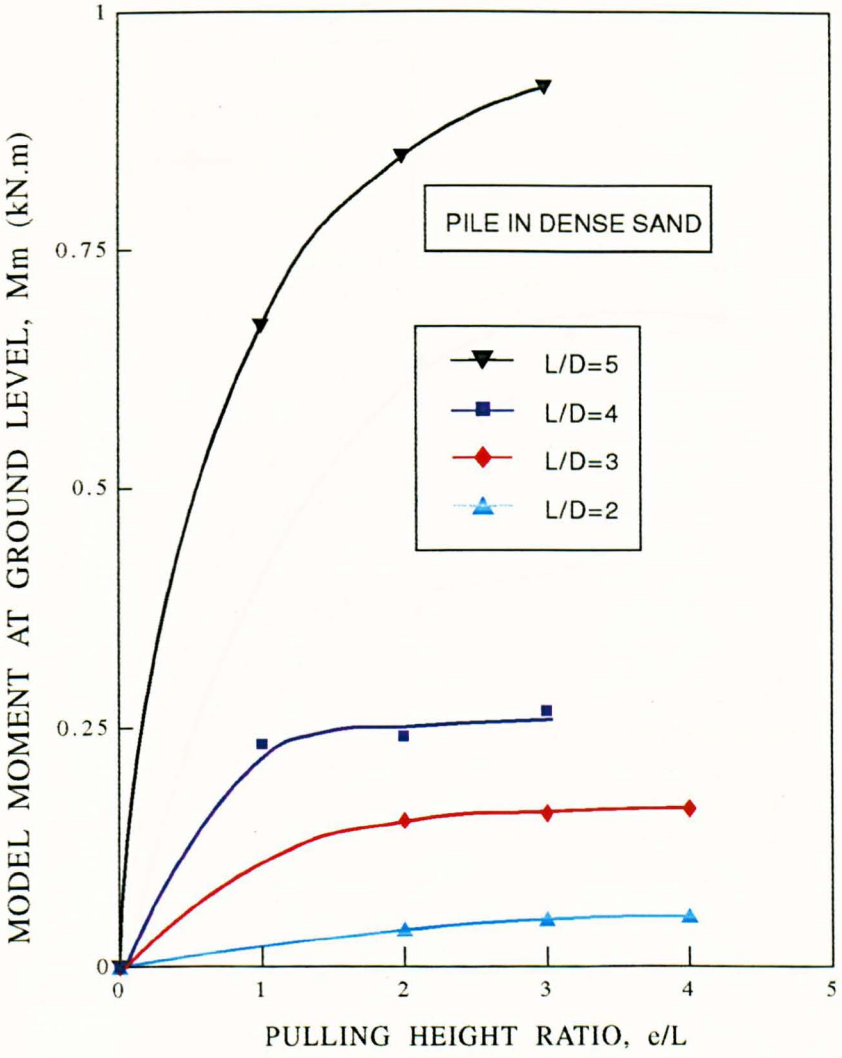

Figure 8.38 Variation of model moment at ground level with pulling height ratio for 100mm diameter pile in dense sand in conventional test.

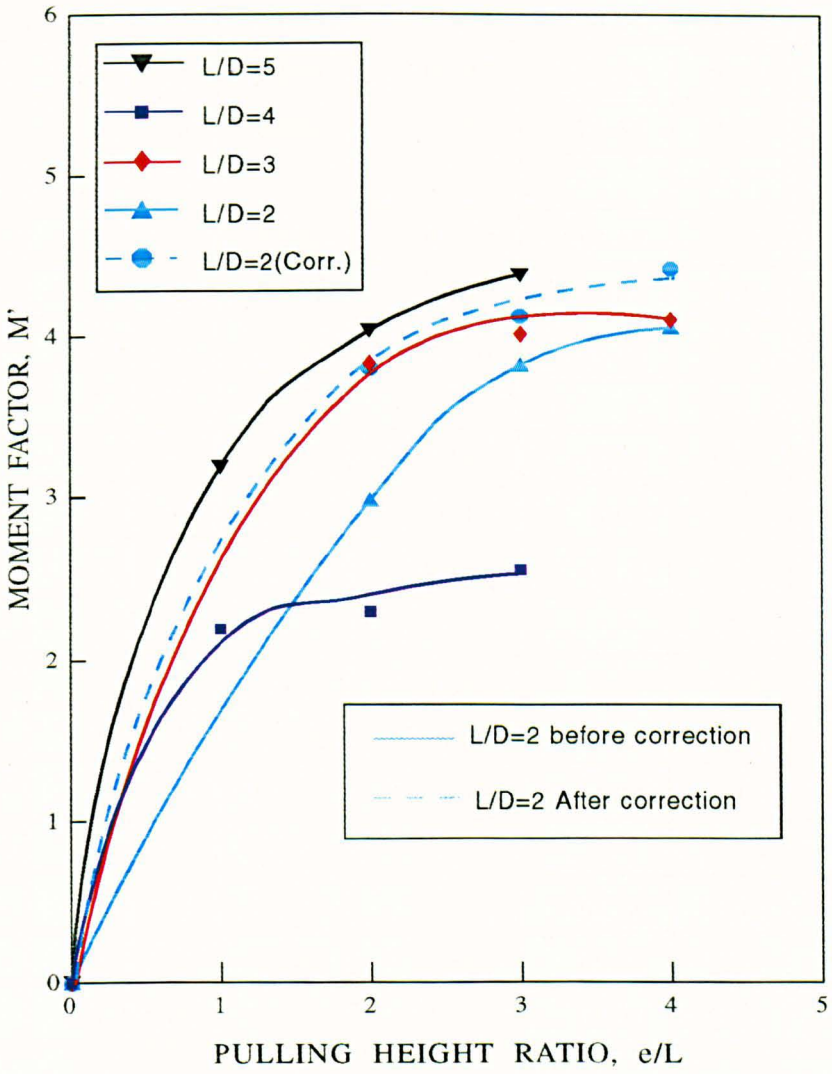

Figure 8.39 Variation of model moment factor with pulling height ratio for a 100mm diameter pile in dense sand in conventional test.

TEST	L/D	E/L	F(kN)	M(kN.m)	Δ(mm)	θ°	M′
RNDCT1	5	1	1.34	0.67	23.34	4.63	3.19
RNDCT2	5	2	0.847	0.847	21.87	3.98	4.03
RNDCT3	5	3	0.613	0.92	16.68	3.62	4.38
RNDCT4	4	1	0.584	0.233	17.49	3.55	2.22
RNDCT5	4	2	0.301	0.241	15.51	3.72	2.30
RNDCT6	4	3	0.224	0.268	17.12	3.86	2.55
RNDCT7	3	2	0.255	0.153	6.92	1.91	3.83
RNDCT8	3	3	0.178	0.16	9.59	2.29	4.00
RNDCT9	3	4	0.137	0.164	13.2	2.41	4.10
RNDCT10	2	2	0.097	0.039	4.68	1.9	2.98
RNDCT11	2	3	0.084	0.05	5.13	1.6	3.82
RNDCT12	2	4	0.066	0.053	4.92	1.46	4.05
RNLCT1	3	2	0.054	0.032	10.24	2.02	0.72
RNLCT2	3	3	0.039	0.035	11.68	2.54	0.79
RNLCT3	3	4	0.032	0.039	13.01	2.51	0.88

Table 8.8 Summary of results from medium size pile in conventional test.

was made to compensate the effect of the pulling arm weight towards the limiting moment value of pile with L/D=2. The calculation is shown in Appendix E. The lower pulling height ratio of e/L=2 is the most critical where allowance for effect of the pulling

arm weight has increase the actual limiting moment by about 27%. However for a higher pulling level, the error on average is about 9%. After plotting corrected values for L/D=2 as shown in Figure 8.39, they are still lower than expected. Since the embedded length is 200mm, it is difficult to obtain a consistent unit weight surrounding the pile during compaction which will also tend to give to a lower limiting moment value apart from the effect of pulling arm weight. No attempt was made to correct the limiting moment values from the centrifugal tests since a series of pulling arms proportional to the pile length were employed.

Values for L/D=3 and L/D=4 were assumed to represent a truer picture of the behaviour of a medium size pile in the conventional tests. Thus further comparisons between the conventional and centrifugal test will be based on the embedment lengths of L/D=3 and 4.

Figure 8.40 compares the effect of soil density on the limiting moment. Only a single value of embedment ratio L/D=3 was employed which is sufficient to show the typical effect. An average percentage difference of about 60% is seen between the loose and dense packing. Thus soil unit weight clearly has a significant effect on the limiting moment of a short laterally loaded pile.

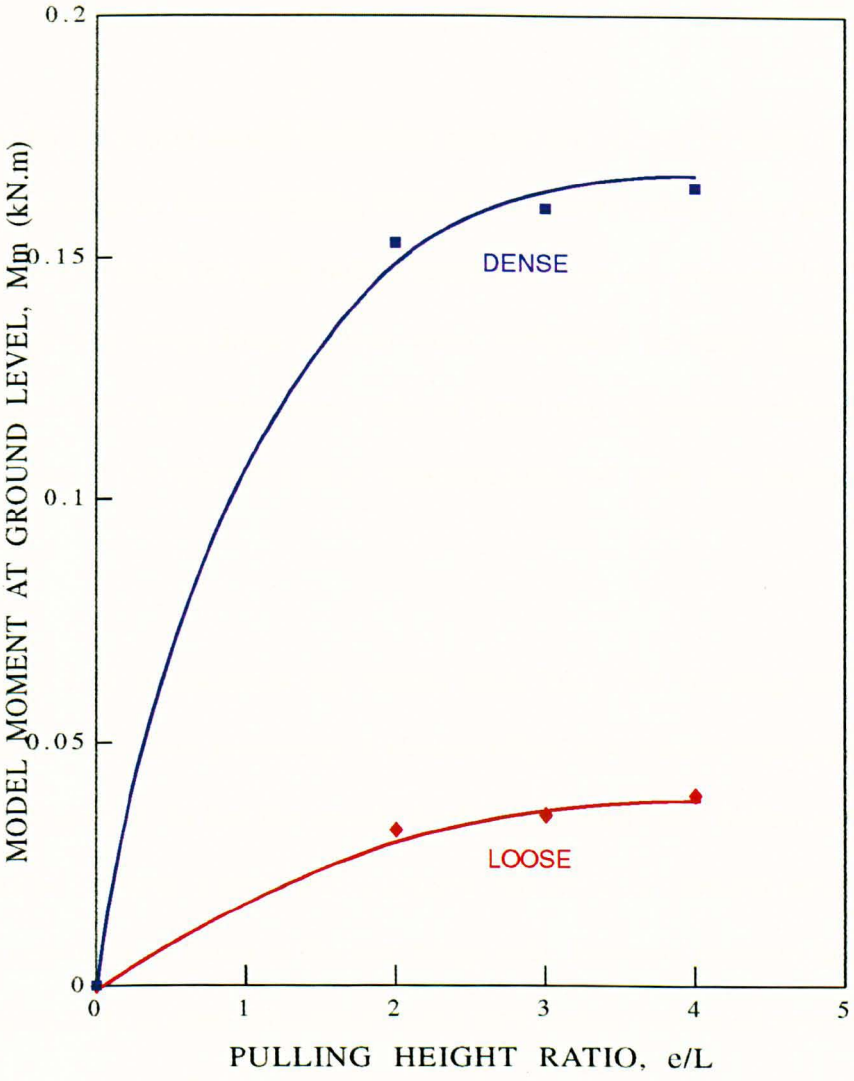

Figure 8.40 Variation of model moment at ground level with pulling height ratio for pile with L/D=3 in dense and loose packing in conventional test

8.4.3 PILES CLOSE TO SLOPING TERRAIN

Results for a pile tested in sloping terrain are shown in Table 8.9. In similar manner to the tests in the centrifuge, Table 8.9(a) shows values for a pile pulled away from a slope while those for a pile pulled towards a slope are presented in Table 8.9(b). Tests towards and away from a slope were performed for slope distance ratios of $0.6<d/L<1.5$. A pile with embedment ratio of 4 and pulling height ratio of 3 was used, embedded close to the crest of a slope approximately 35° from the horizontal.

Figure 8.41 summarises the results from Table 8.9 showing the variation of moment factor with slope proximity. A similar effect would have been expected to that in the centrifugal test. In fact the results do show comparatively higher moment factors for piles pulled towards a slope and a general reduction in moment carrying capacity with slope proximity as found in the centrifuge tests. However moment factors for piles constructed close to a slope fallaciously gave 20% higher values on average compared to the pile embedded in flat terrain. This could be again attributed to the restriction of the sides in the reinforced bin, the piles were erected close to the side of the bin to allow for the slope construction. Thus during the load application, apart from the soil resistance, the confining influence of the side of the bin would contribute to a higher pulling force value. The method of compaction could also contribute to the error. Due to the erratic values from this unsuccessful attempt to obtain data from a slope test, no

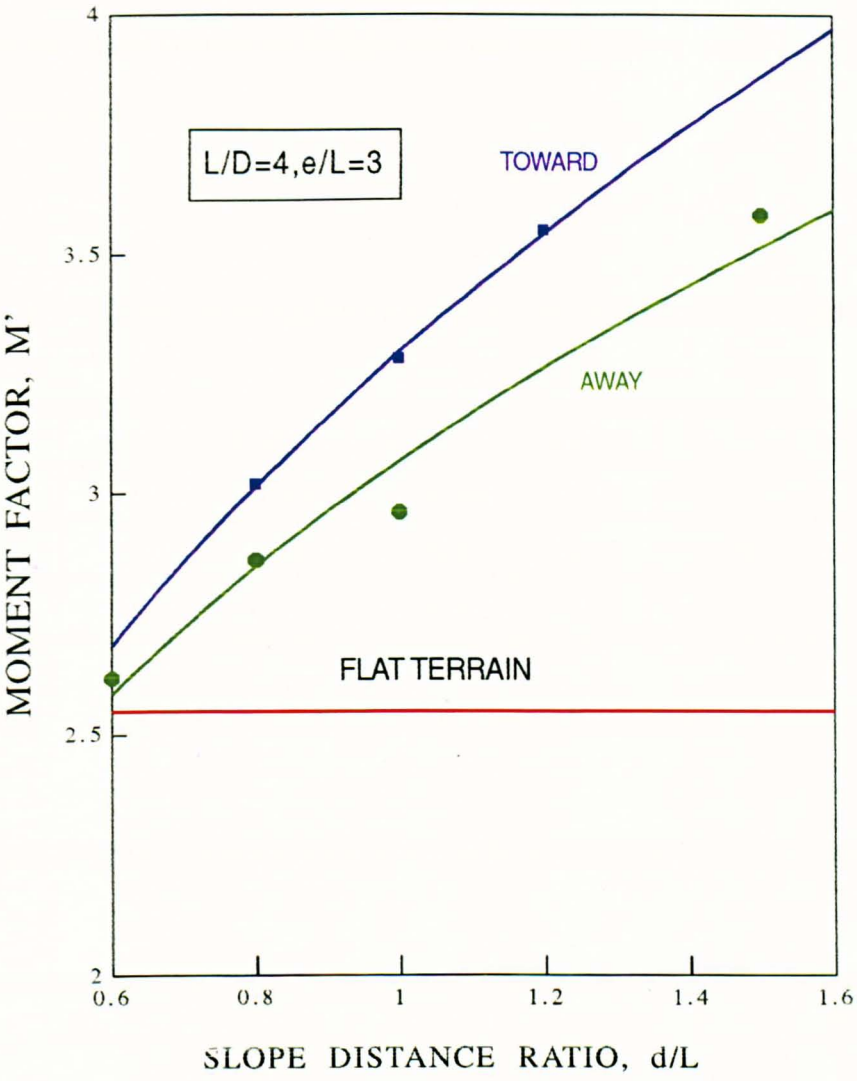

Figure 8.41 Variation of moment factor with slope distance ratio for model pile in conventional test

reasonable conclusion can be made. Thus comparison with the centrifugal test results is not possible. Nevertheless an insight into the behaviour of a pile embedded close to a slope is achieved.

a) **PILE PULLED TOWARDS SLOPE (CONVENTIONAL TEST)**

TEST	d/L	F(kN)	M(kN.m)	Δ(mm)	θ°	M′
RNDST1	0.8	0.264	0.3168	21.5	5.07	3.02
RNDST2	1	0.287	0.3444	24.4	6.29	3.28
RNDST3	1.2	0.311	0.3732	17.7	4.21	3.55

Table 8.9(a) Summary of pile pulled away from slope

b) **PILE PULLED AWAY FROM SLOPE (CONVENTIONAL TEST)**

TEST	d/L	F(kN)	M(kN.m)	Δ(mm)	θ°	M′
RNDSA1	0.6	0.232	0.278	3.722	1.15	2.65
RNDSA2	0.8	0.251	0.301	14.37	3.45	2.87
RNDSA3	1	0.259	0.311	9.8	2.46	2.96
RNDSA4	1.5	0.307	0.368	27.47	6.60	3.50

Table 8.9(b) Summary of pile pull toward the slope.

8.4.4 CONVENTIONAL TEST IN THE CENTRIFUGE BUCKET

Due to the difficulties in fabricating a medium size wall compatible with the medium size single pile, a test was performed in the centrifuge bucket with the machine static. The purpose of the test was to observe the effect of scale on the moment shape factor.

Table 8.10 shows a summary of results obtained from unit gravity tests for both single and continuous piles with L/D=5, while Table 8.11 gives the moment shape factor calculated from Table 8.10. Figure 8.42 shows a comparison between moment factor and pulling height ratio for single and continuous piles embedded in dense sand. As expected values of moment factor for a continuous pile are lower than those of a single pile due to the plane strain conditions around the former. A difference of 50% on average was observed.

Comparison of shape factors from centrifugal and unit gravity tests is shown in Figure 8.43. Using L/D=5 as a basis of comparison, moment shape factor of L/D=5 for pile tested in centrifugal and unit gravity tests on average agree fairly well. This further suggests that pile size is of minor significance on the moment shape factor. The finding is in broad agreement with the shape factor for anchors where Dickin and Leung(1983) concluded that the anchor shape factor is not greatly influenced by the anchor size.

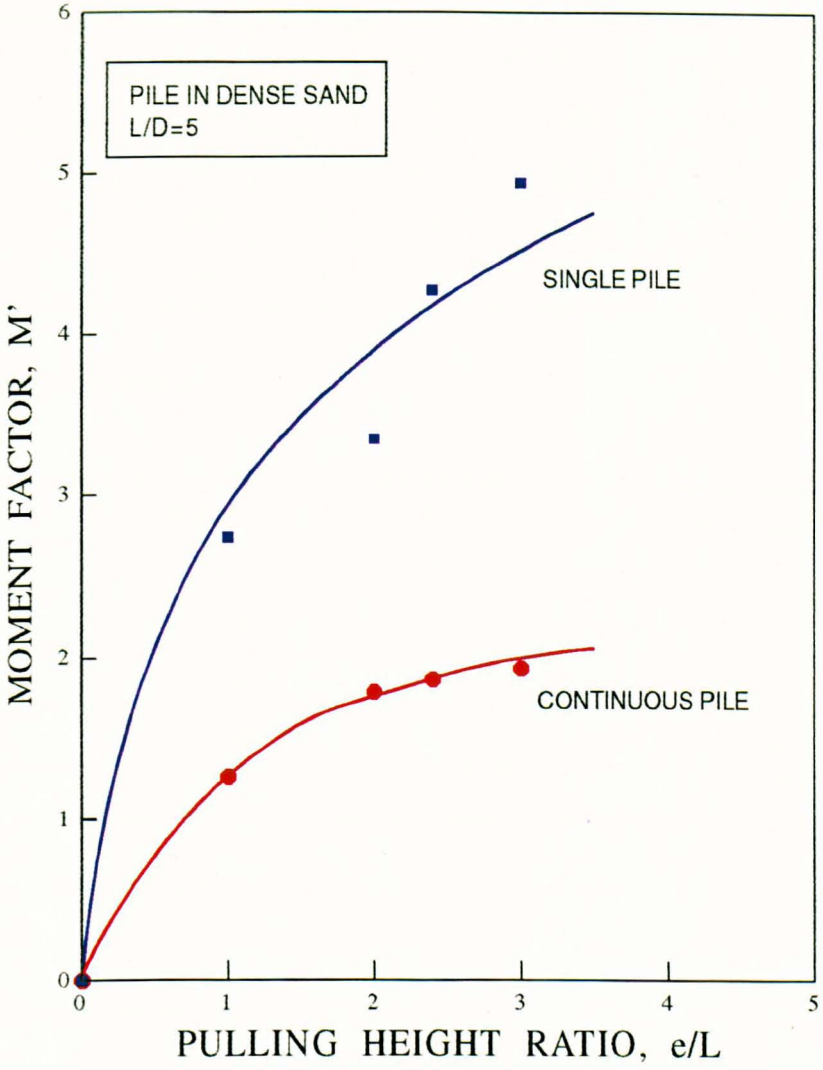

Figure 8.42 Comparison between moment factor and pulling height ratio for 100mm diameter single and continuous piles embedded in dense sand at unit gravity

a) **SINGLE PILE**

TEST	N	L(mm)	L/D	e/L	F(kN)	M(kN.m)	Δ(mm)	θ°
RND1G1	1	100	5	3	0.0054	0.0016	4.47	3.42
RND2G1	1	100	5	2.4	0.0060	0.0014	2.73	2.07
RND3G1	1	100	5	2	0.0053	0.0011	3.35	2.18
RND4G1	1	100	5	1	0.0088	0.0009	3.13	2.07

b) **CONTINUOUS PILE**

TEST	N	B(mm)	L/D	e/L	F(kN)	M(kN.m)	Δ(mm)	θ°
SFD1G1	1	126	5	3	0.0134	0.0040	0.90	0.92
SFD2G1	1	126	5	2.4	0.0163	0.0039	1.43	1.07
SFD3G1	1	126	5	2	0.0185	0.0037	1.33	1.10
SFD4G1	1	126	5	1	0.0260	0.0026	0.98	0.81

Table 8.10 Summary of results from unit gravity tests in centrifuge bucket for single and continuous piles

c) **MOMENT SHAPE FACTOR**

TEST	M(kN.m)	M'_{ps}	TEST	M(kN.m)	M'_{pc}	L/D	e/L	S_{fm}
RND1G1	0.0016	4.88	SFD1G1	0.0040	1.94	5	3	2.52
RND2G1	0.0014	4.27	SFD2G1	0.0039	1.89	5	2.4	2.26
RND3G1	0.0011	3.35	SFD3G1	0.0037	1.79	5	2	1.87
RND4G1	0.0009	2.74	SFD4G1	0.0026	1.26	5	1	2.18

Table 8.11 Summary of the moment shape factors for unit gravity tests

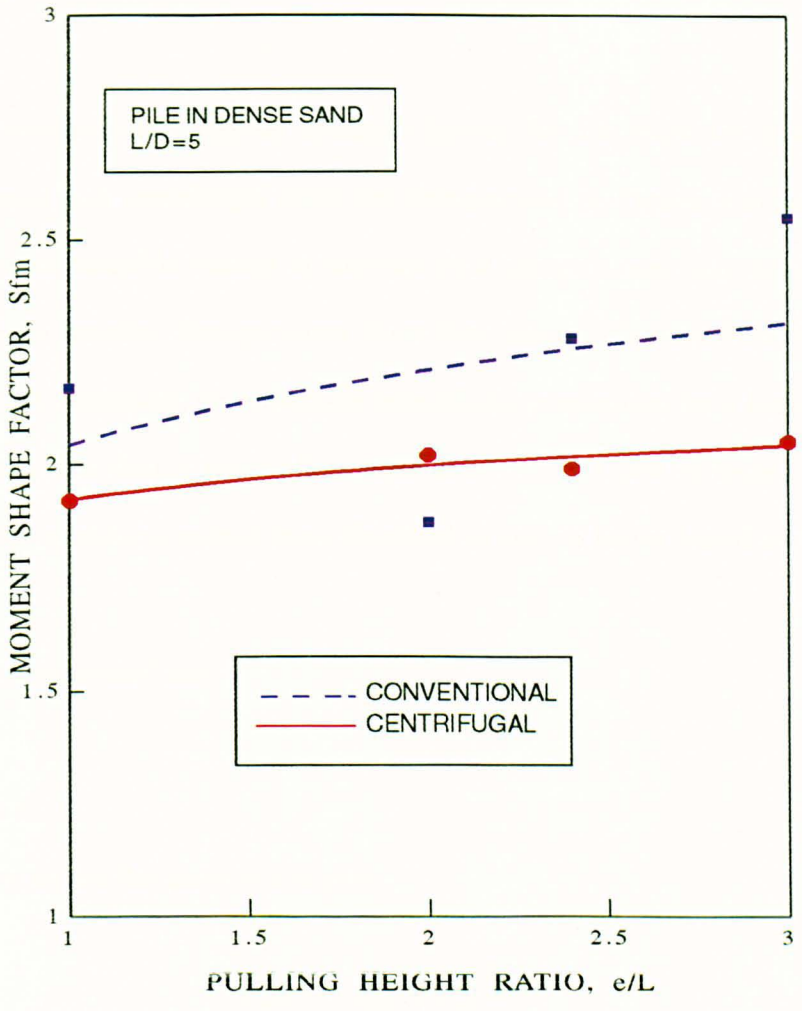

Figure 8.43 Comparison of moment shape factor between centrifugal and unit gravity test for pile in dense sand

8.5 COMPARISON BETWEEN CONVENTIONAL AND CENTRIFUGAL TESTS

Direct comparisons between moment factors for 1m diameter piles predicted from conventional and centrifugal tests are summarised in Figure 8.44 for piles with L/D=3 and 4 since sensible values of conventional medium size pile behaviour were obtained for these lengths. Comparisons show that moment factors from conventional tests by direct extrapolation, overestimate centrifugal predictions by a factor of at least 2. This demonstrates that a scale effect does exist when a pile is tested at different stress levels. The prototype values were obtained as shown below based on Figure 8.45.

a) Scaling in conventional test

From Figure 8.45,

Taking moment about the base of the pile

$$F_m(e_m + L_m) = P_m(\frac{L_m}{3})$$

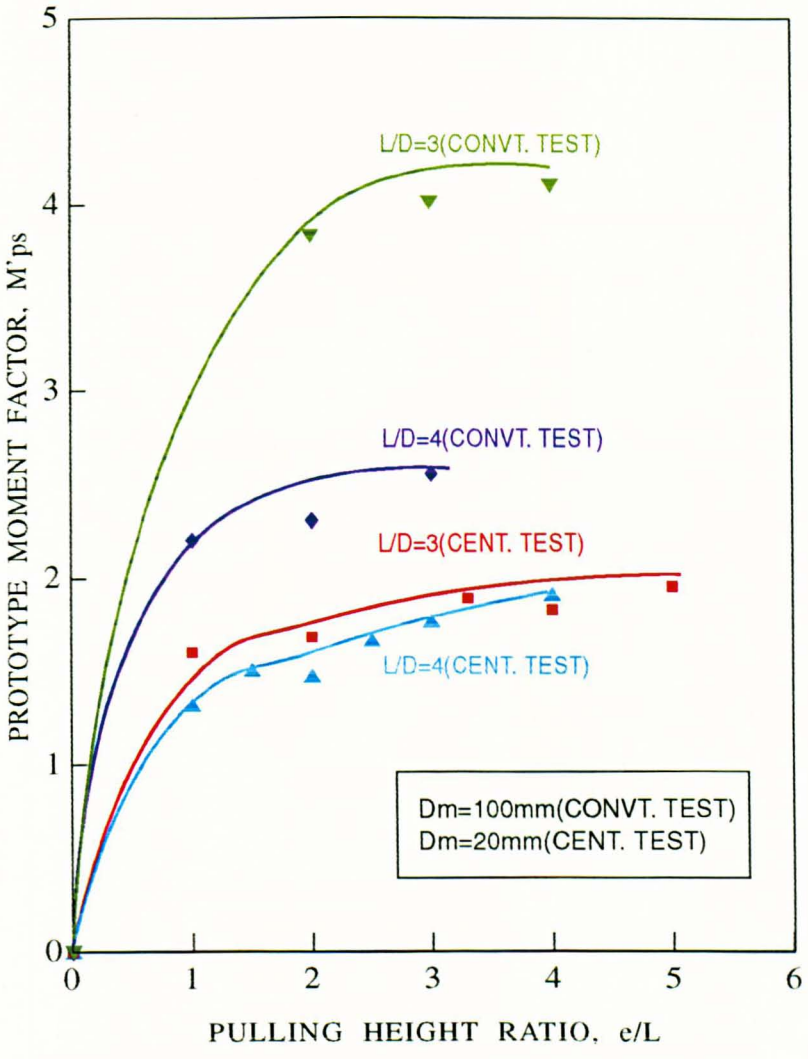

Figure 8.44 Comparison between conventional test and centrifugal test for 1m diameter prototype piles in dense sand

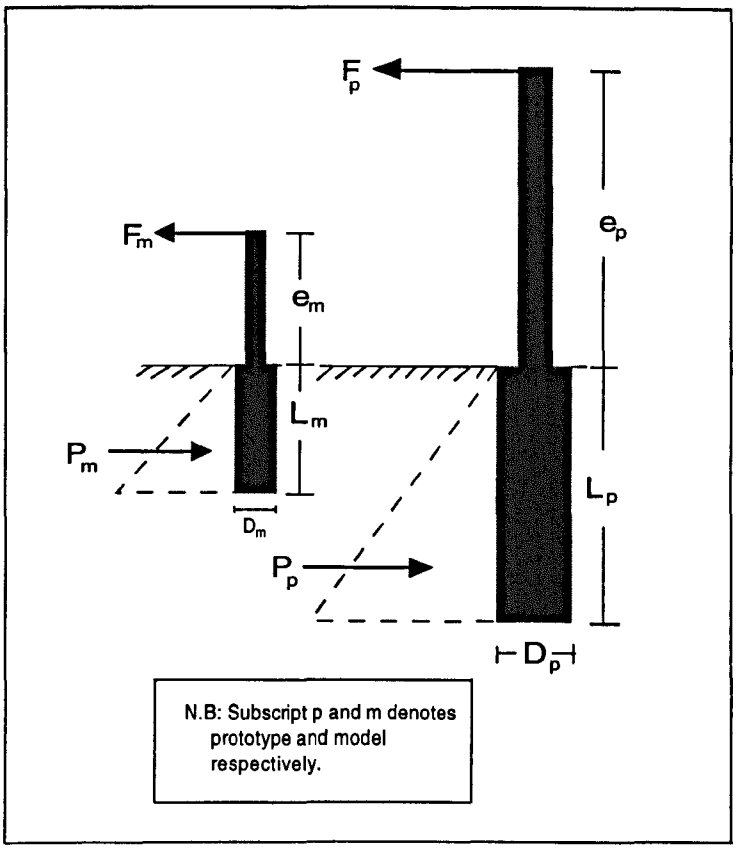

Figure 8.45 Relative comparison between model and prototype geometry.

$$F_m = \frac{P_m L_m}{3(e_m + L_m)} = \frac{P_m}{3\left(\frac{e_m}{L_m} + 1\right)}$$

If prototype and model are geometrically similar,

$$F_p = \frac{P_p}{3\left(\frac{e_p}{L_p} + 1\right)}$$

Since $P_p = 0.5K_{pp}\gamma L_p^2 D_p$ and $P_m = 0.5K_{pm}\gamma L_m^2 D_m$

Assuming $K_{pp} \approx K_{pm}$, and that $L_p = L_m N_l$ and $D_p = D_m N_l$

where N_l is the linear scaling factor, thus giving

$$P_p = N_l^3 P_m$$

Hence

$$F_p = N_l^3 \frac{P_m}{3\left(\frac{e_m}{L_m} + 1\right)}$$

$$F_p = N_l^3 F_m$$

However $M_p = F_p \times e_p$

$= N_l^3 F_m \times e_m N_l$

which gives $M_p = N_l^4 M_m$

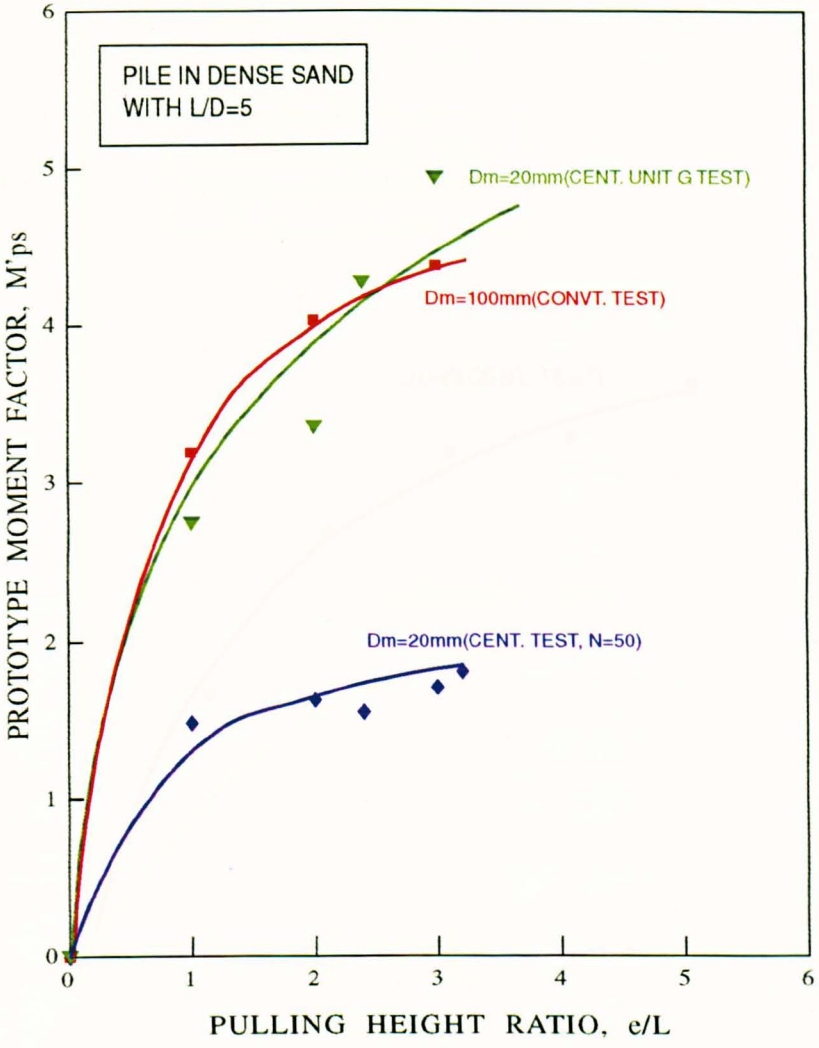

Figure 8.46 Comparison between conventional test and centrifugal test for 1m diameter prototype pile in dense sand

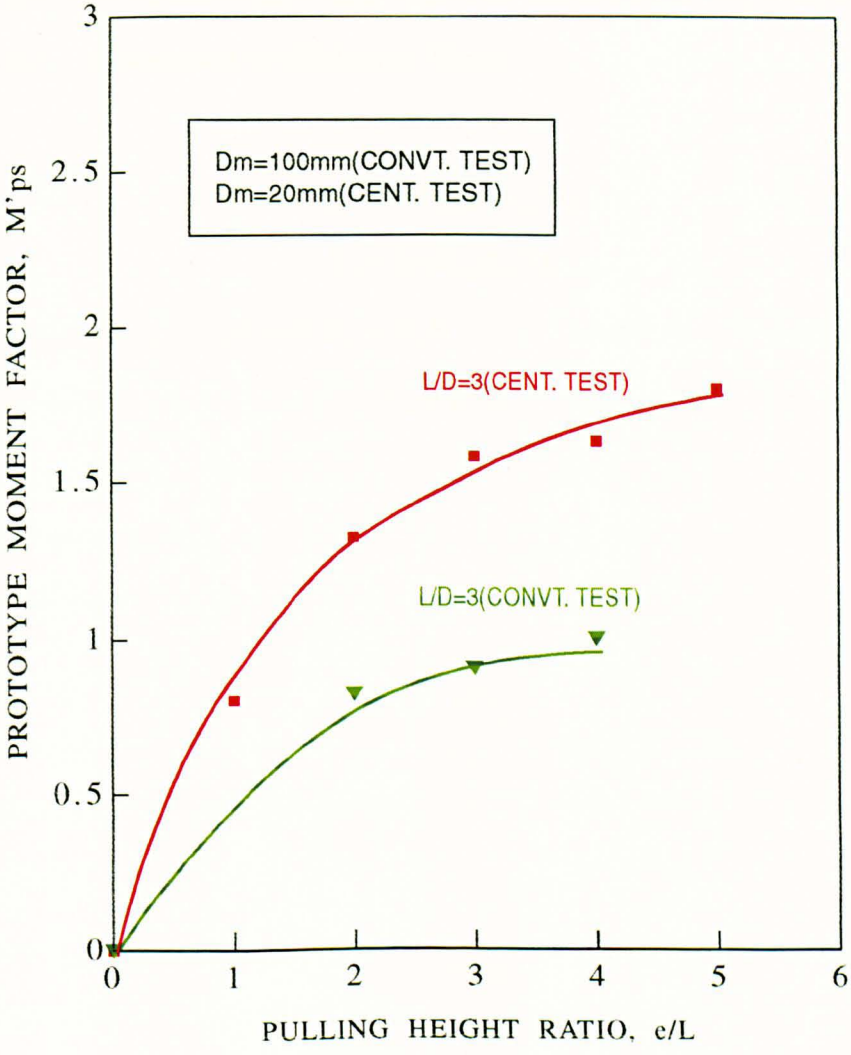

Figure 8.47 Comparison between conventional test and centrifugal test for 1m diameter prototype pile in loose sand

b) Centrifugal test

In the case of centrifugal test, based on fundamental requirements, the unit weight of soil γ is increased to γN during 'flight'.

Therefore $$P_m = 0.5K_{pm}\gamma N L_m^2 D_m$$

and $$P_p = 0.5K_{pp}\gamma L_p^2 D_p$$

but $K_{pp} = K_{pm}$ and $L_p = L_m N$ and $D_p = D_m N$

Giving $$P_m = N^2 P_p$$

Hence

$$F_p = \frac{N^2 P_m}{3\left(\frac{e_m}{L_m} + 1\right)}$$

$$F_p = N^2 F_m$$

Giving $$M_p = N^3 M_m$$

Further comparisons are shown in Figure 8.46 for L/D=5 based on the calculations shown in (a) and (b). Although the medium size pile with L/D=5 and D_m=100mm was slightly affected by boundary conditions mentioned earlier, the comparison shows the influence of size on the pile behaviour. It was expected that a pile with embedment ratio of 3 in conventional test for loose packing would show a higher moment factor value compared to the centrifugal results as seen in Figure 8.47. However the reverse

occurs. Problems in identifying peak moment values and non-homogeneities in test beds could be the main reason for this.

8.6 FAILURE MECHANISM STUDIES

Two-dimensional tests were carried out in a glass sided box to scrutinise the failure mechanism around short rigid pile(continuous). The model was prepared with layers of coloured parent sand against the glass wall. Horizontal load was applied using a screw-nut operated by hand. The original position of the pile is marked with a black tape. The method of placing the sand was similar to that in the centrifugal test for the dense packing using the small hand vibrator, while the loose packing was prepared by direct pouring into the glass sided box. By means of photography, the failure planes denoted by the coloured sand were recorded. Plates 8.1 to 8.26 show the failure mechanism around a pile with L/D=5 for pulling height ratios e/L=3.2 and e/L≤1 embedded in dense and loose sand packing. A pile with L/D=5 was chosen since it requires sufficient layers of the coloured sand to be observed. Test rotations of greater than 15°, well beyond those associated with failure in the main tests, were required to enable the failure planes to be observed clearly. Typical deformation patterns around the pile shows the existence of both rotational and linear shear planes.

8.6.1 FAILURE MECHANISM IN LOOSE PACKING

Plates 8.1 and 8.6 show the failure mechanism around a pile embedded in a loose sand packing with lateral pull at e/L=3.2. Initially with the rotation of the pile, an active plane develops at the back of the pile. The ground level in front of the pile starts to raise due to the compression of the surrounding soil in front of the pile as seen in Plate 8.3. Further movement resulted in the development of a primary passive plane in front of the pile. At this stage the active plane became more pronounced as seen in Plate 8.4. A local rotational plane immediately developed as the passive plane started to generate. At this stage the observed point of rotation becomes constant at a distance of slightly greater than two-thirds of the embedment length. Further movement of the pile as shown in Plate 8.5 and 8.6 did not result in significant changes in the failure pattern, except that the development of the secondary passive plane and the former planes become more prominent. Figure 8.48 illustrate the schematic diagram of the failure zones based on Plate 8.6.

Plates 8.7 to 8.12 describes the failure mechanism of a pile in loose sand pulled at a height of e/L=1. Similar failure patterns were observed as for the pile pulled at higher level except that the rotational pattern is much more prominent compared to other patterns. In the case of the lower pulling height, the rotational plane develops earlier than the passive plane as seen in plates 8.8 and 8.9. Further movement will then generate the passive plane as shown in Plate 8.10, where at this stage the centre of rotation was deemed to reach a constant value of approximately two-thirds of the

Plate 8.1 to Plate 8.6 : Pile in loose sand with L/D=5 and e/L=3.2

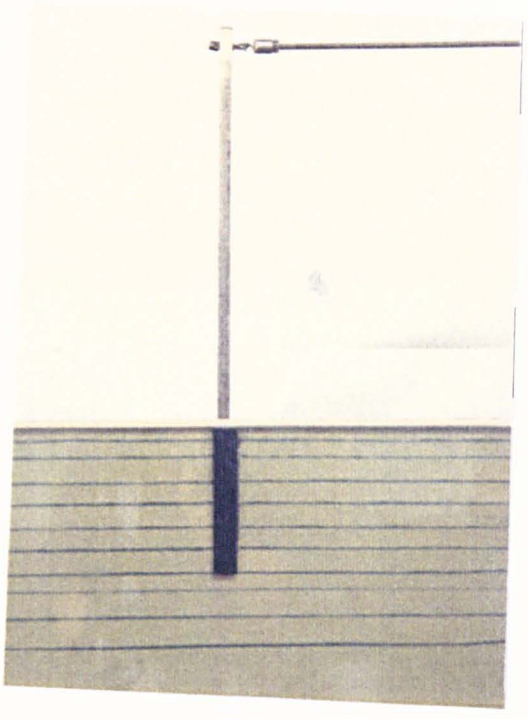

Plate 8.1

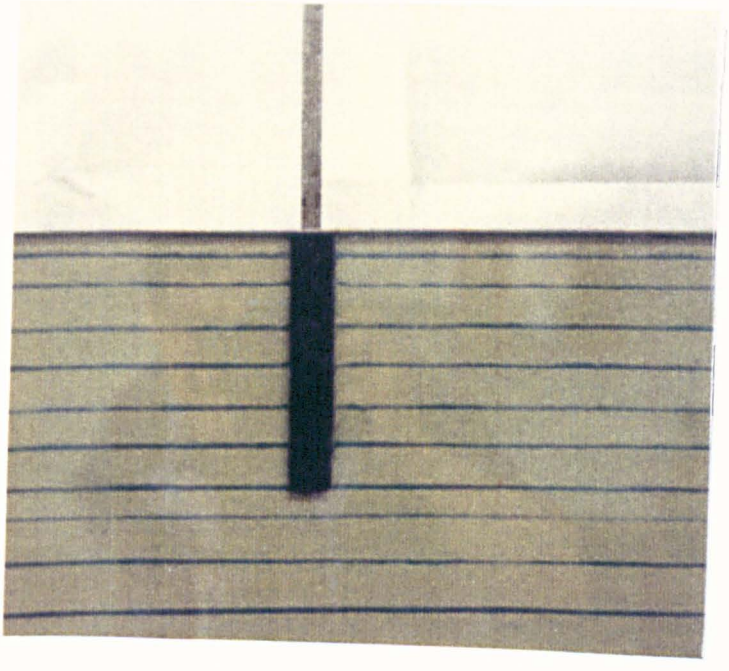

Plate 8.2

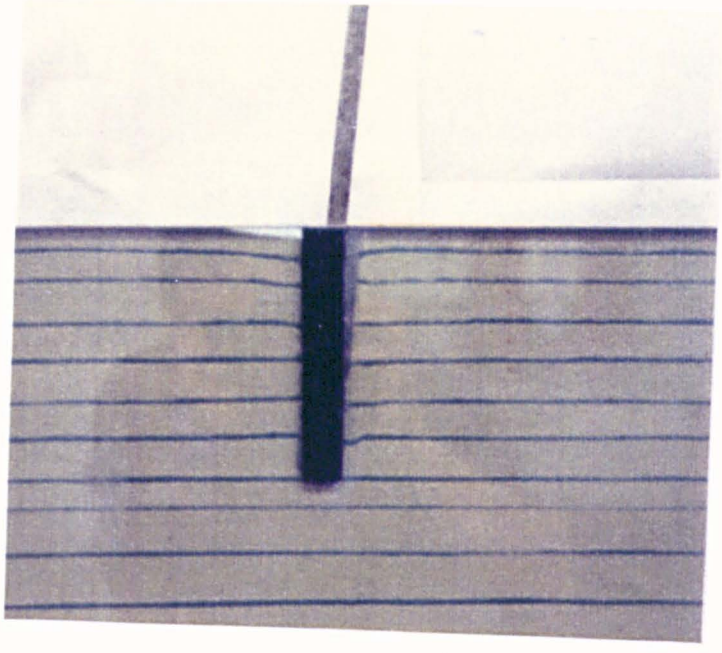

Plate 8.3

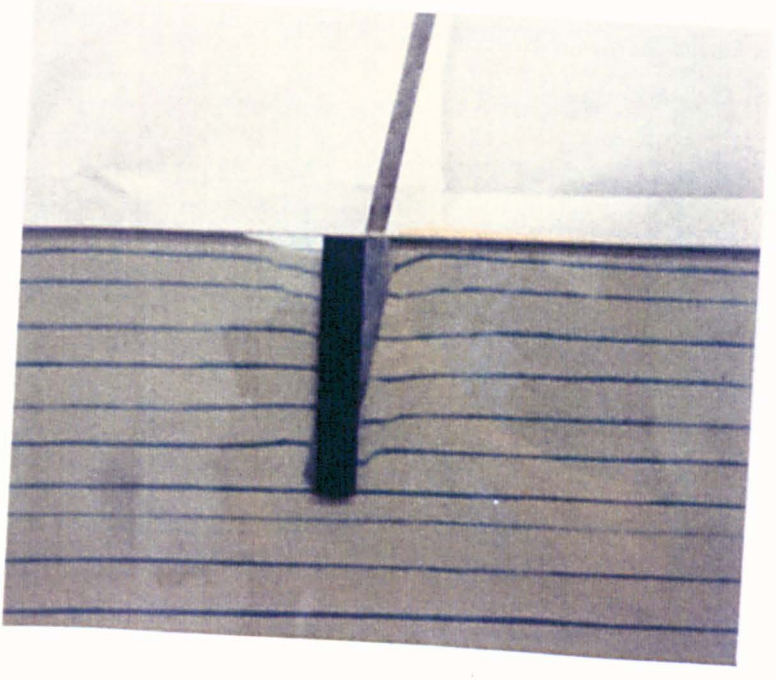

Plate 8.4

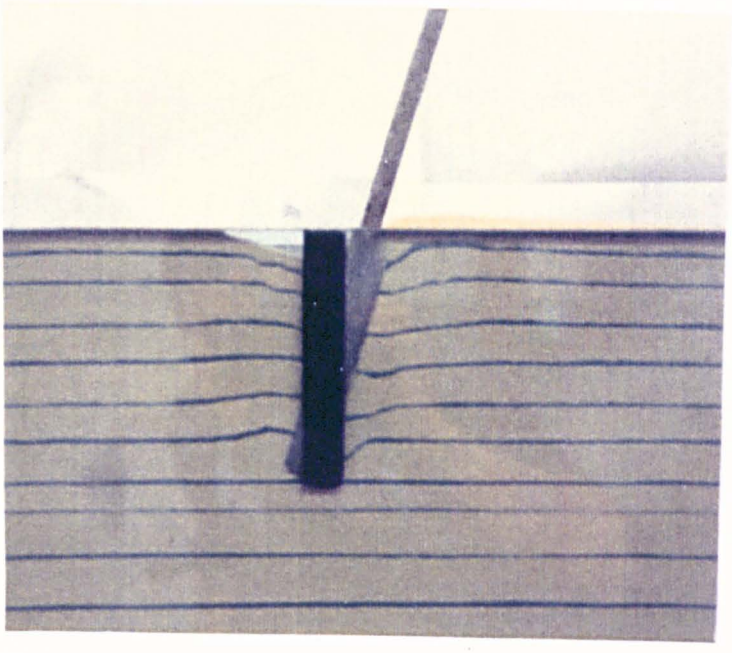

Plate 8.5

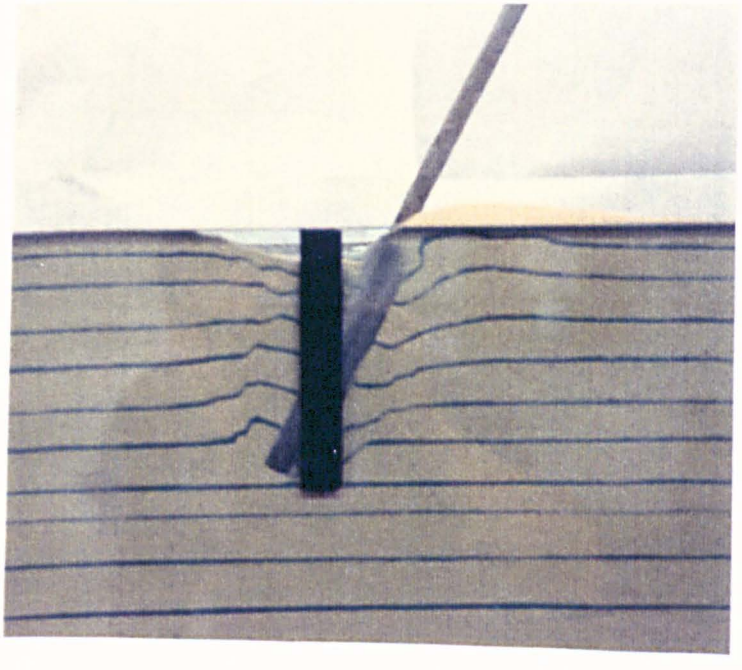

Plate 8.6

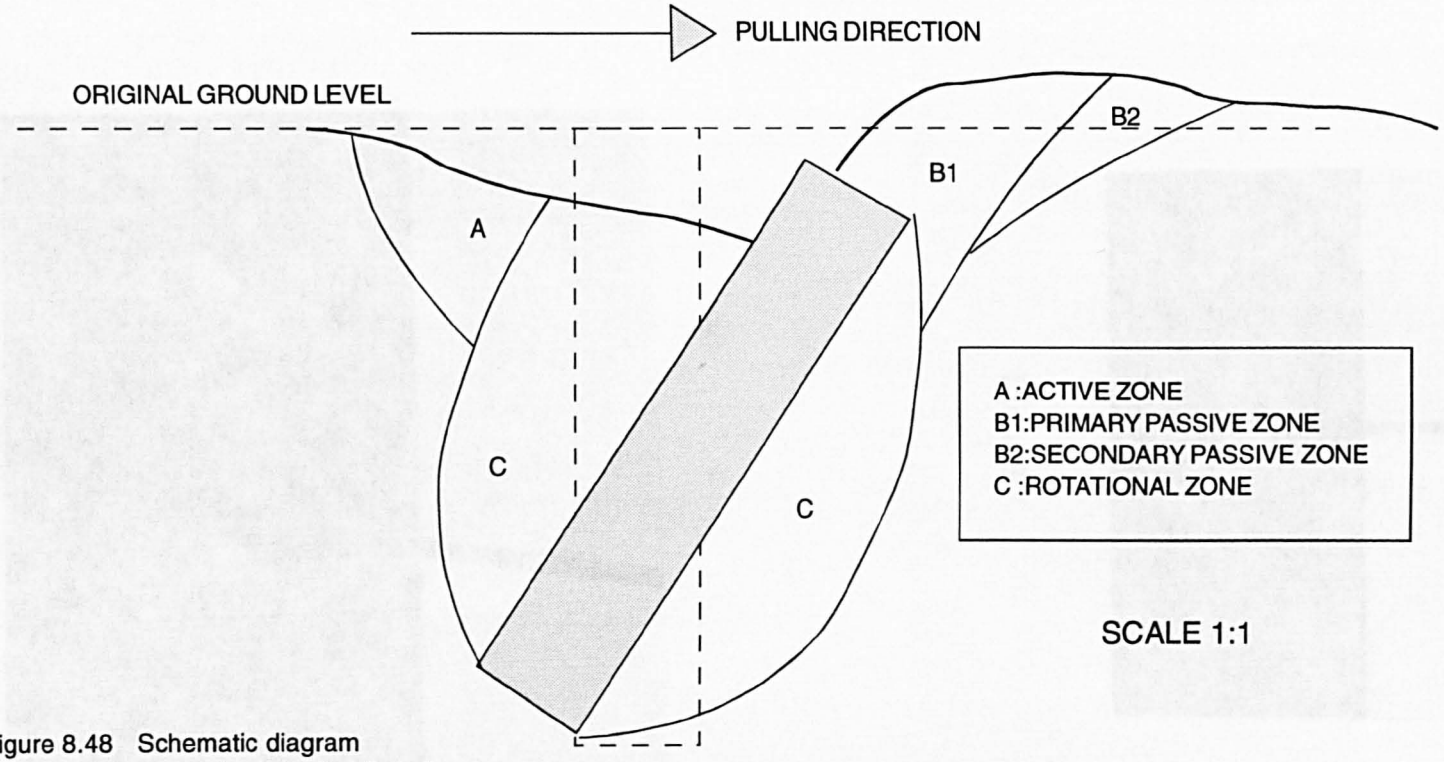

Figure 8.48 Schematic diagram showing failure mechanism developed during pile movement for L/D=5 and e/L=3.2 in loose sand

Plate 8.7 to Plate 8.12 : Pile in loose sand with L/D=5 and e/L=1

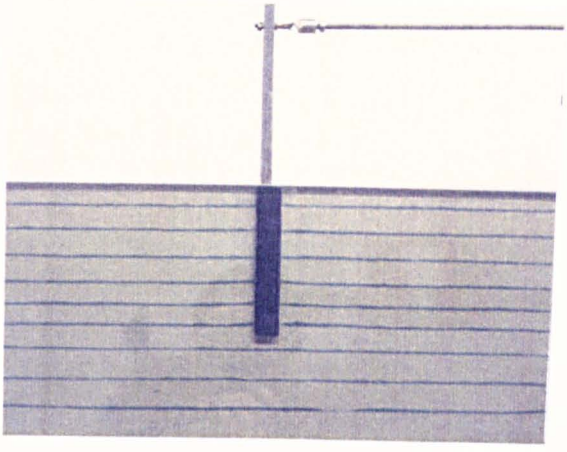

Plate 8.7

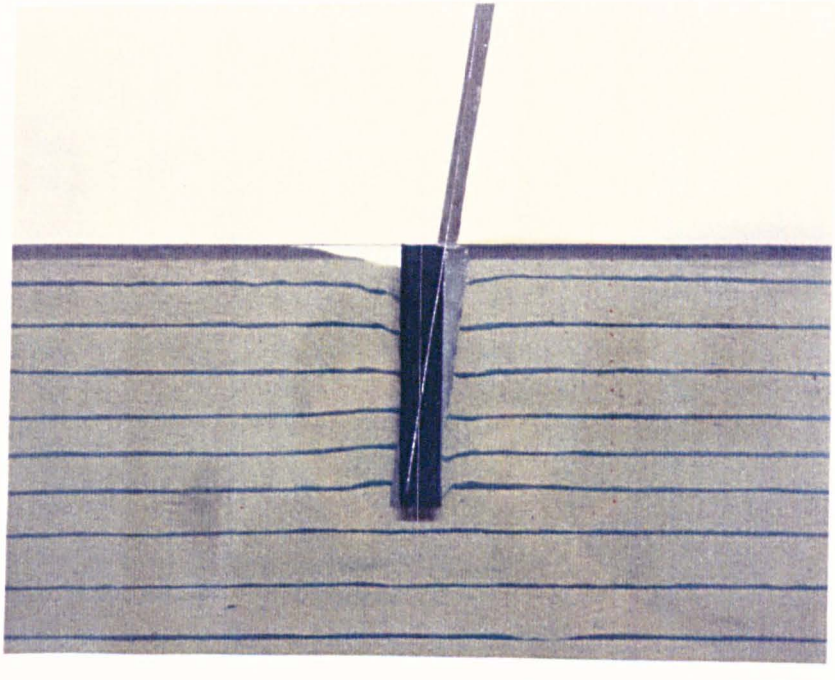

Plate 8.8

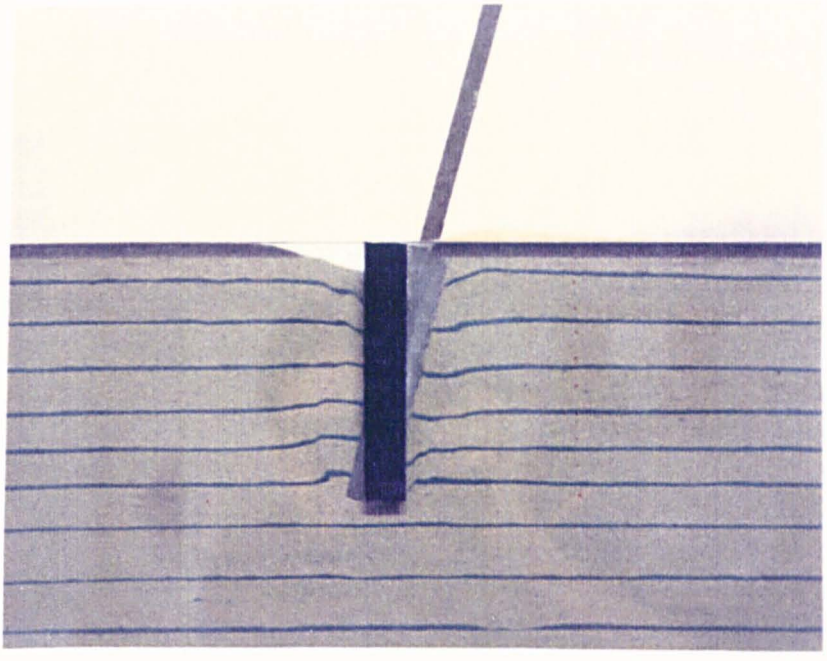

Plate 8.9

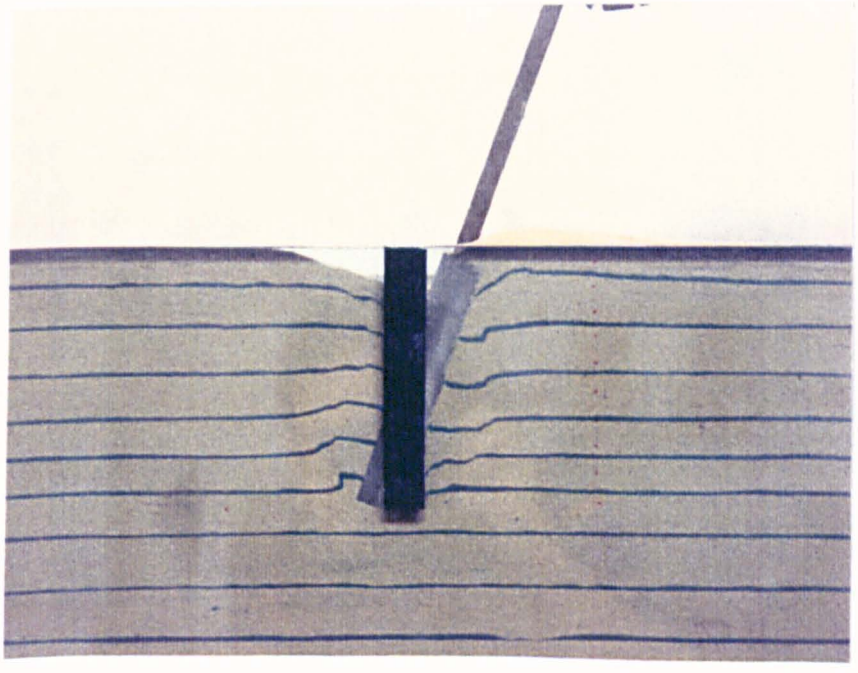

Plate 8.10

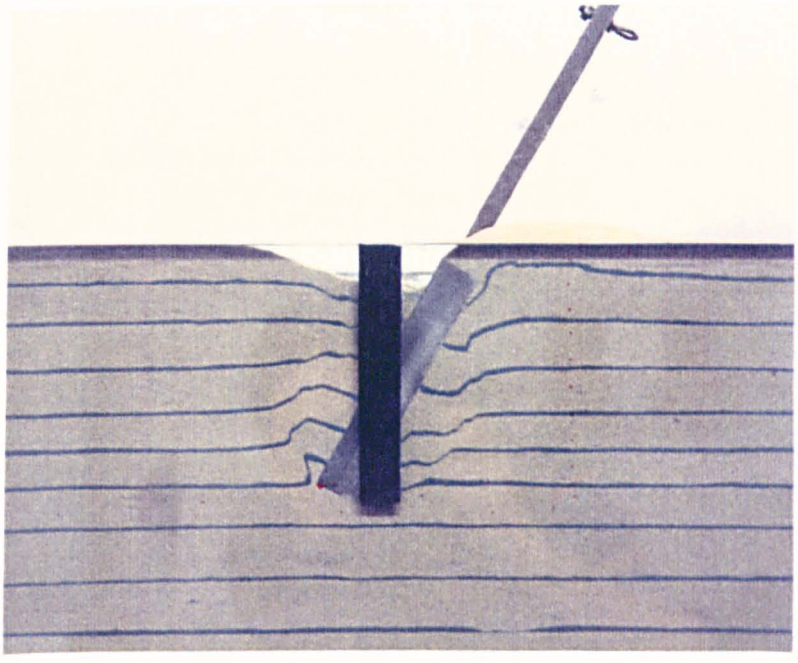

Plate 8.11

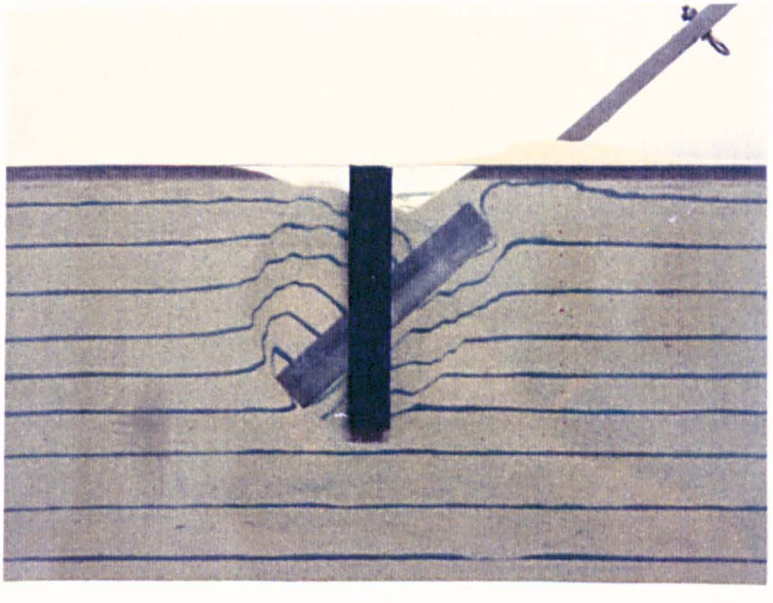

Plate 8.12

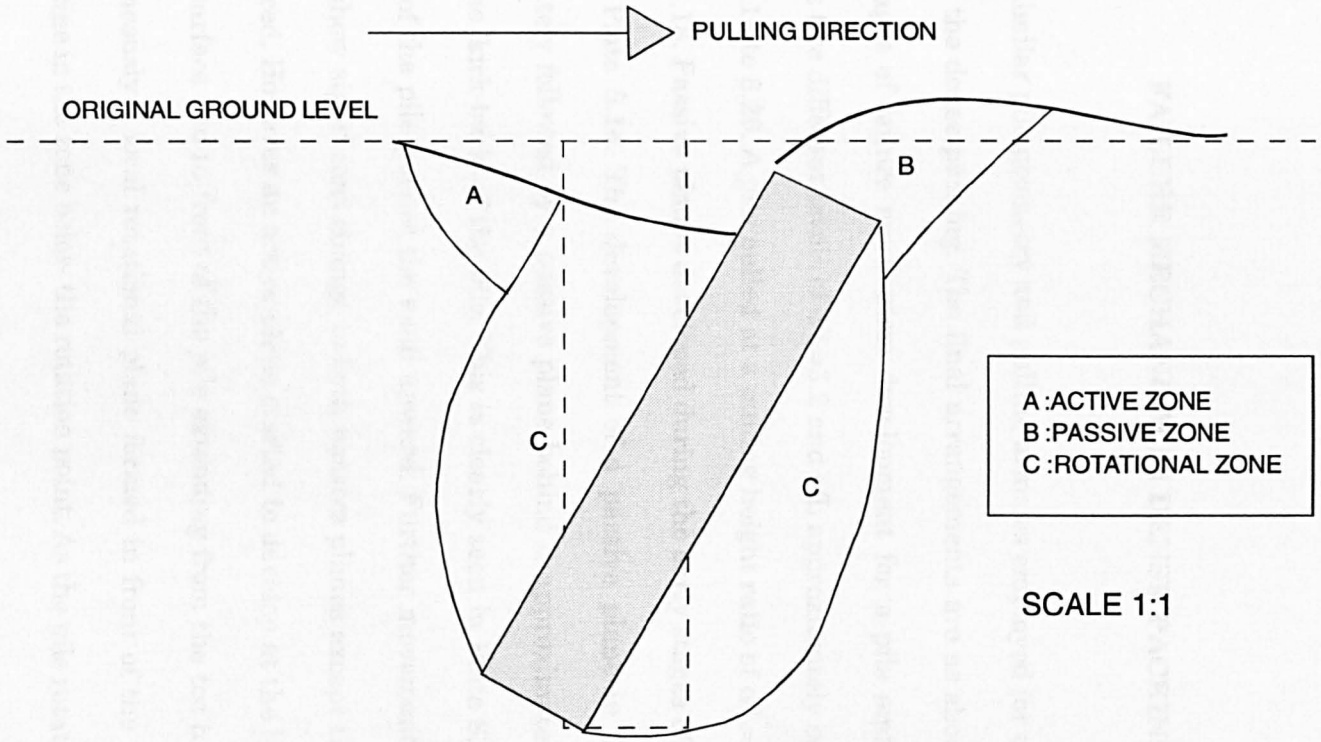

Figure 8.49 Schematic diagram showing failure mechanism developed during pile movement for L/D=5 and e/L=1in loose sand

embedment length. Plate 8.11 illustrated in Figure 8.49 and Plate 8.12 illustrates the rotation, which is well beyond the failure value, showing that local rotational plane governs the failure of the pile pulled at lower levels.

8.6.2 FAILURE MECHANISM IN DENSE PACKING

Similar pile geometry and pulling arms as employed for the loose packing were used for the dense packing. The final arrangements are as shown in Plates 8.13 and 8.19. Stages of failure mechanism development for a pile embedded in dense sand pulled at two different levels of e/L=3.2 and e/L approximately equal to 1 are shown in Plates 8.13 to 8.26. A pile pulled at a pulling height ratio of e/L=3.2 is shown in Plates 8.13 to 8.18. Passive planes developed during the early stages of the pile movement as seen in Plate 8.14. The development of a passive plane in front of the pile, was immediately followed by a passive plane behind it approximately 40° from horizontal due to the 'kick-back' of the pile. This is clearly seen in Plate 8.15. The passive plane in front of the pile pushes the sand upward. Further movement as seen in Plate 8.16 did not show significant change to both passive planes except that they became more pronounced. However an active plane started to develop at the back of the pile near to ground surface and in front of the pile extending from the toe to the point of rotation. Simultaneously a local rotational plane formed in front of the pile and obscured the active plane in the zone below the rotation point. As the pile rotates further a secondary

Plate 8.13 to Plate 8.18 : Pile in dense sand with L/D=5 and e/L=3.2

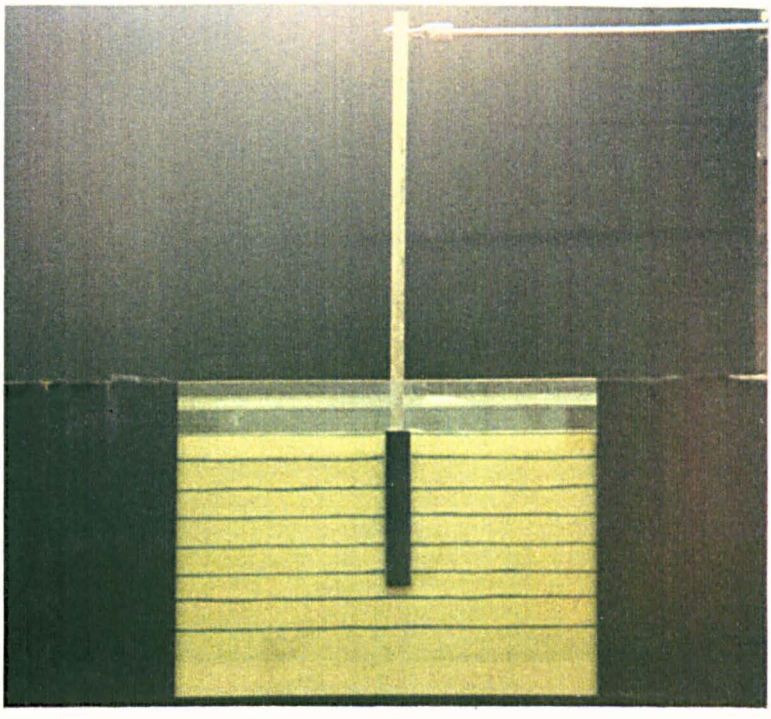

Plate 8.13

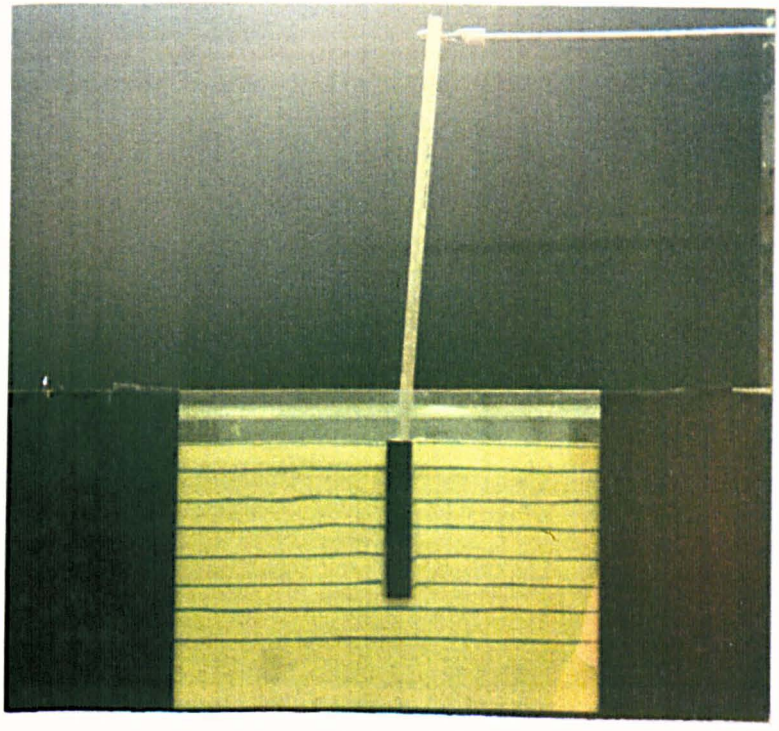

Plate 8.14

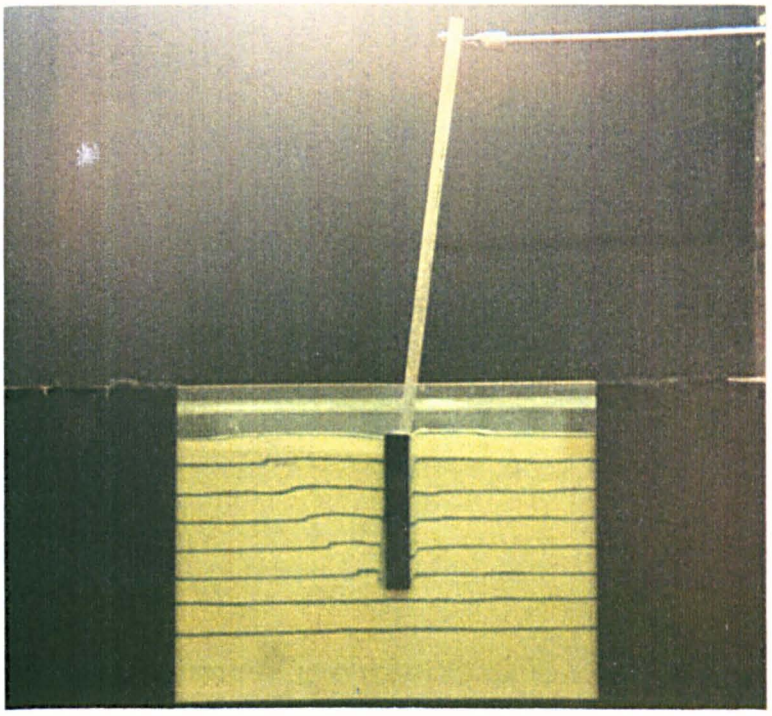

Plate 8.15

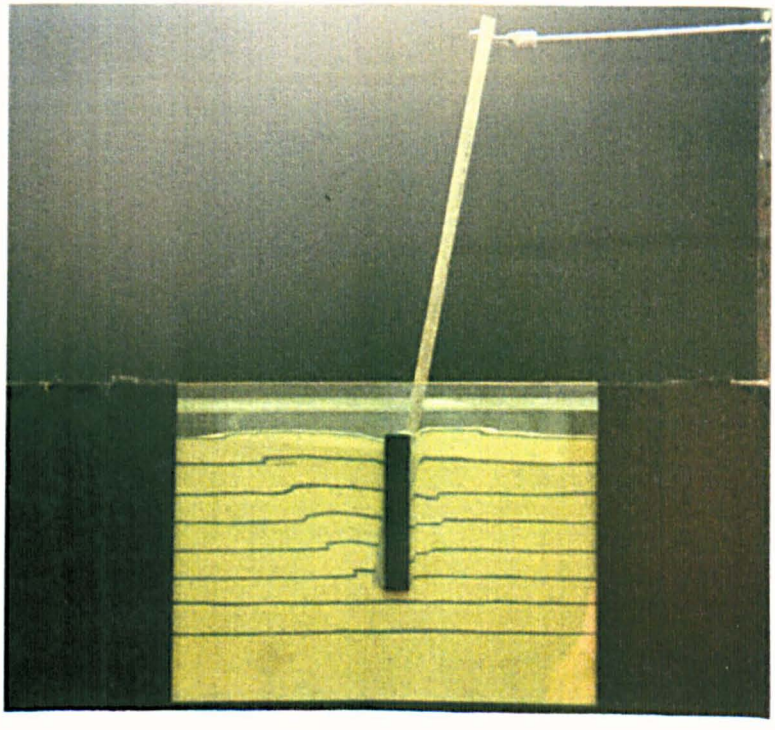

Plate 8.16

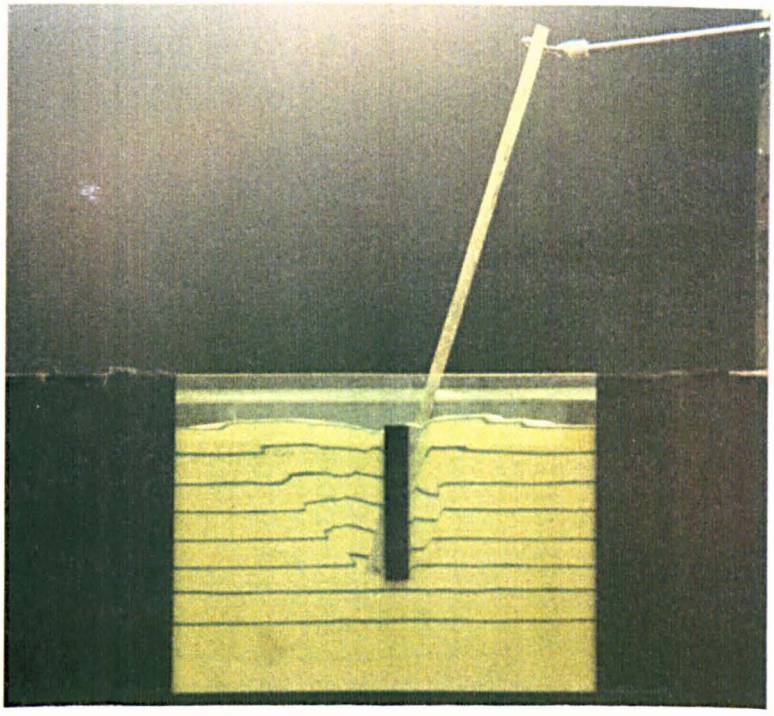

Plate 8.17

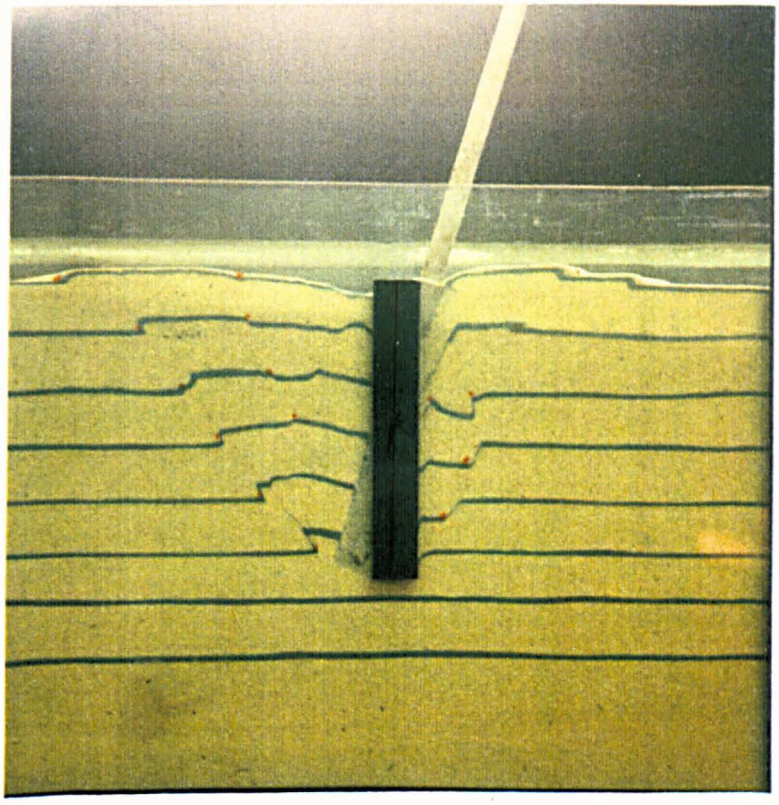

Plate 8.18

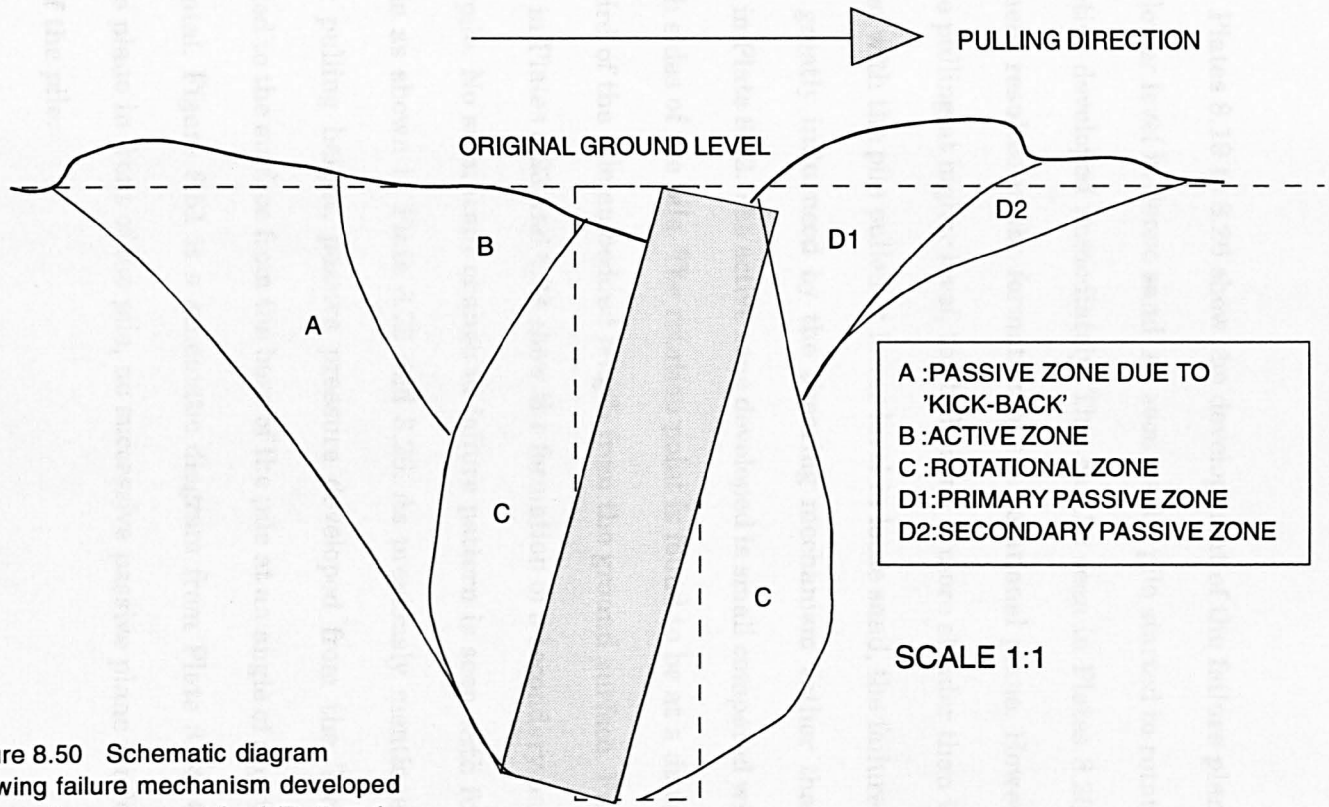

Figure 8.50 Schematic diagram showing failure mechanism developed during pile movement for L/D=5 and e/L=3.2 in dense sand

passive plane developed as seen in Plates 8.17 and 8.18. All failure planes become more pronounced without any changes occurring to the failure pattern. A schematic diagram of Plate 8.18 is shown in Figure 8.50. The rotation point developed halfway down the embedment length.

Plates 8.19 to 8.26 show the development of the failure planes for a pile pulled at the lower level in dense sand. As soon as the pile started to rotate the passive plane and active developed immediately. This can be seen in Plates 8.20 and 8.21. Further movement resulted in the formation of the rotational plane. However, compared with the pile pulling at higher level, the bulb zone is more slender than in the latter test. In contrast with the pile pulled at lower level in loose sand, the failure of the surrounding soil is greatly influenced by the shearing mechanism rather than rotation. This is shown in Plate 8.22. The active zone developed is small compared with the passive zone on both sides of the pile. The rotation point is found to be at a distance approximately two-third of the pile embedded length from the ground surface. Further movement as shown in Plates 8.23 and 8.24 show the formation of a secondary passive plane in front of the pile. No significant change in failure pattern is seen with further movement of the pile as shown in Plate 8.25 and 8.26. As previously mentioned for the pile with higher pulling height, passive pressure developed from the 'kick-back' of the pile extended to the surface from the base of the pile at an angle of approximately 40° to the horizontal. Figure 8.51 is a schematic diagram from Plate 8.24. Compared with the passive plane in front of the pile, no successive passive plane tended to develop at the back of the pile.

Plate 8.19 to Plate 8.26 : Pile in dense sand with L/D=5 and e/L<1

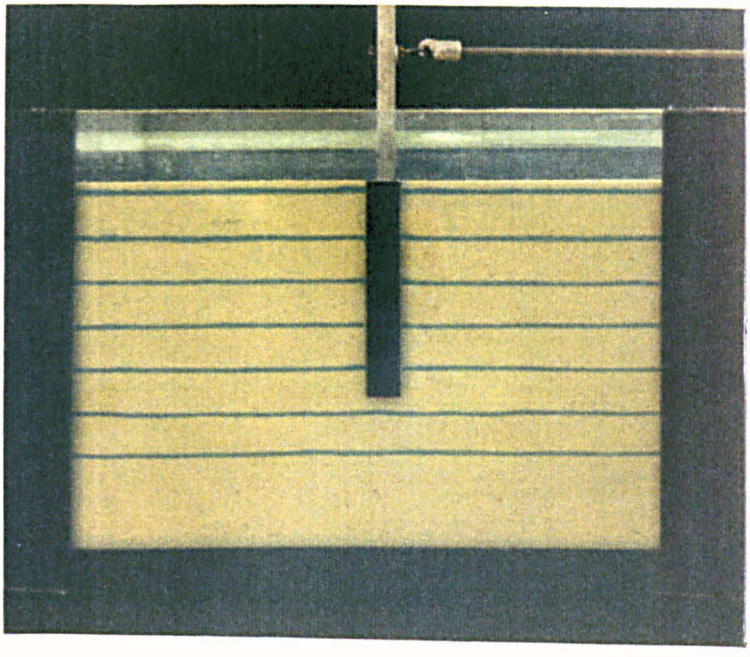

Plate 8.19

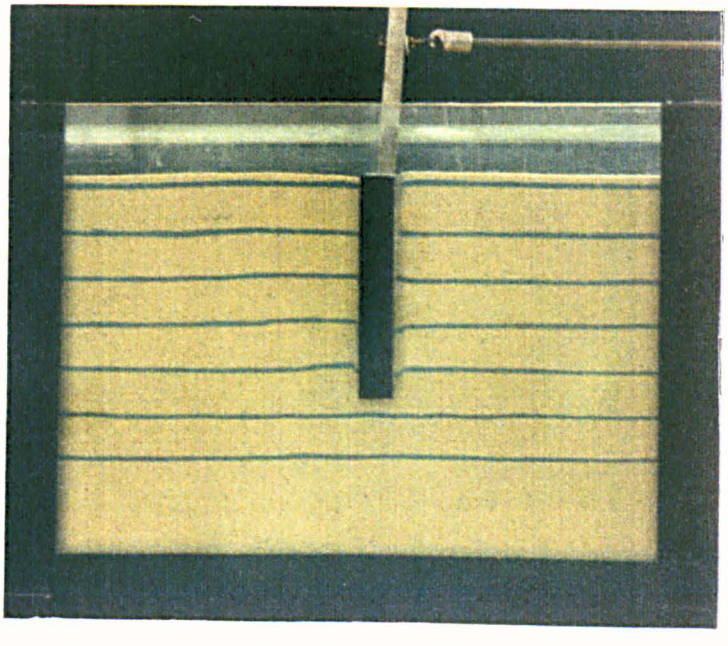

Plate 8.20

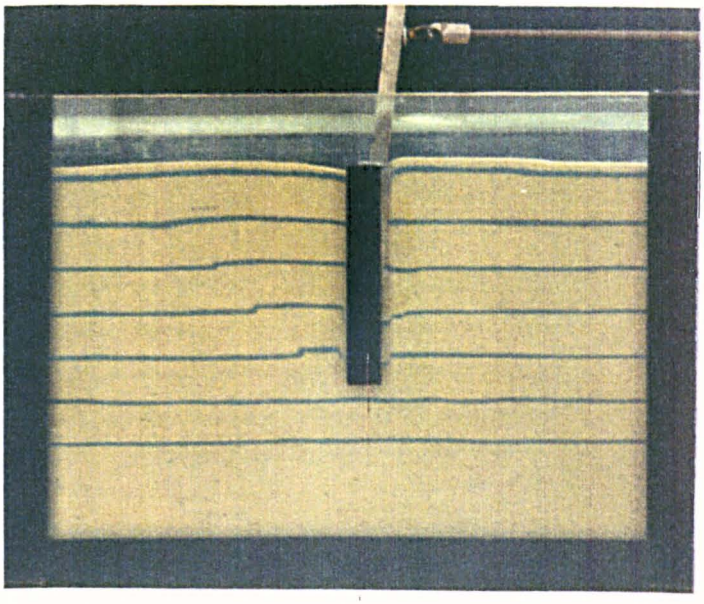

Plate 8.21

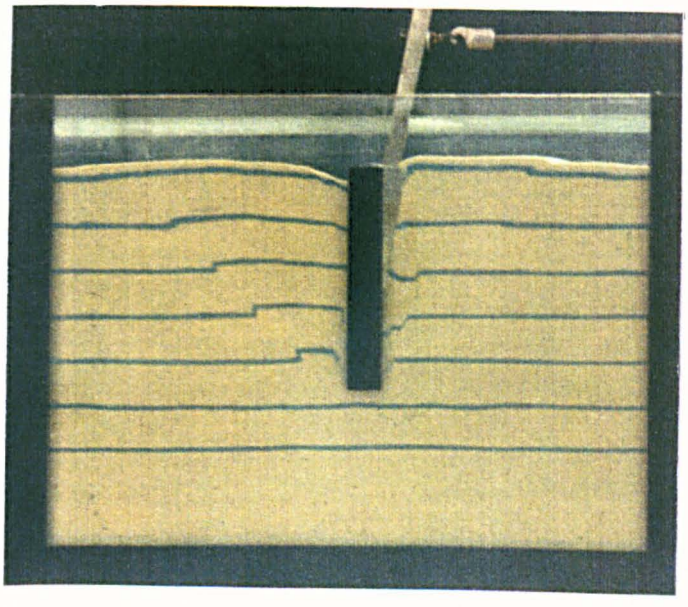

Plate 8.22

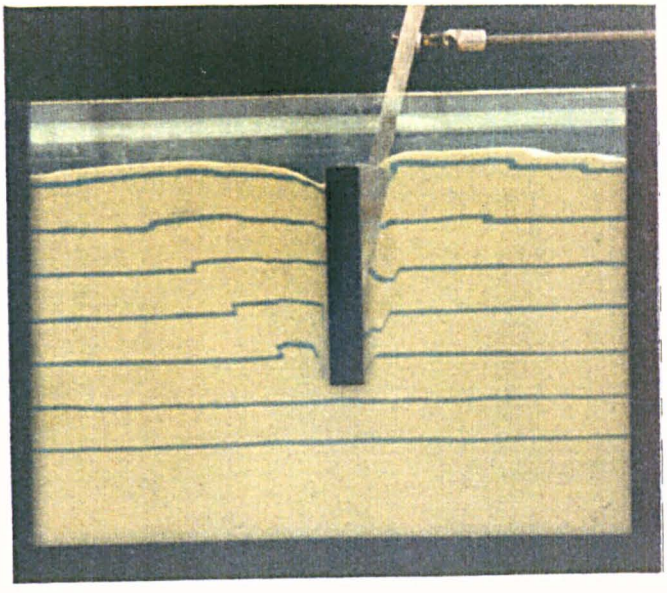

Plate 8.23

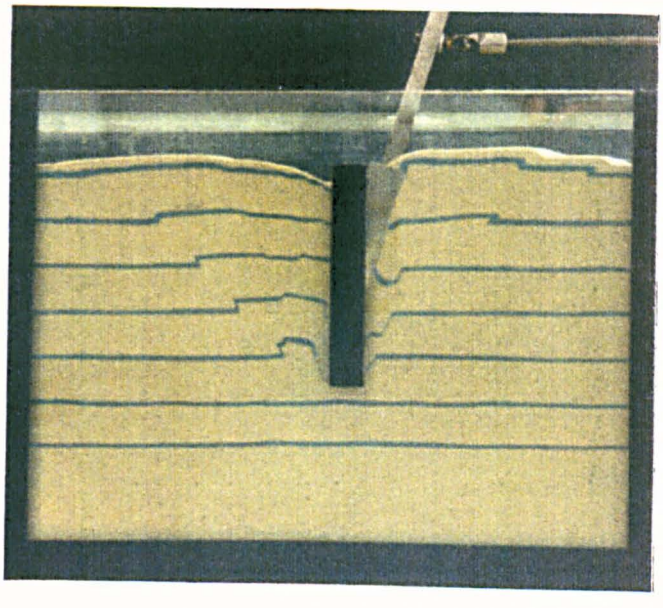

Plate 8.24

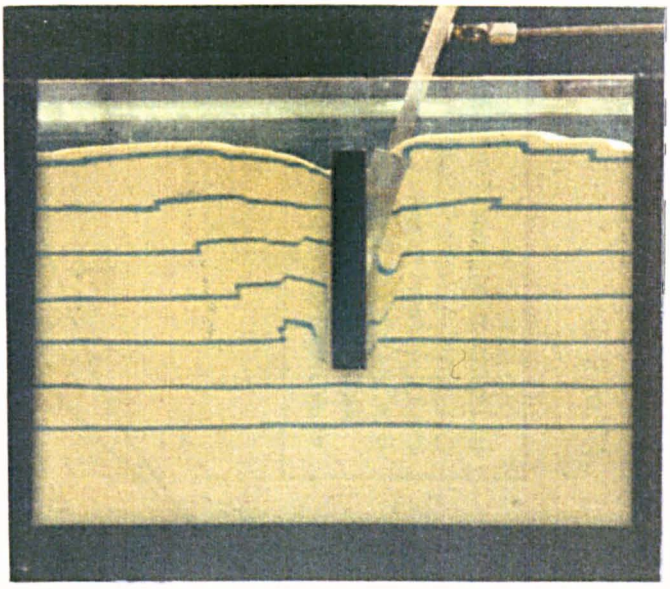

Plate 8.25

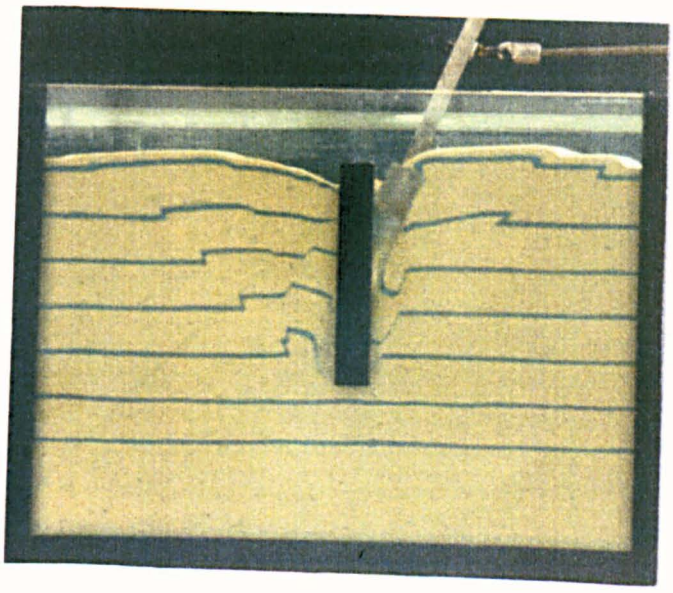

Plate 8.26

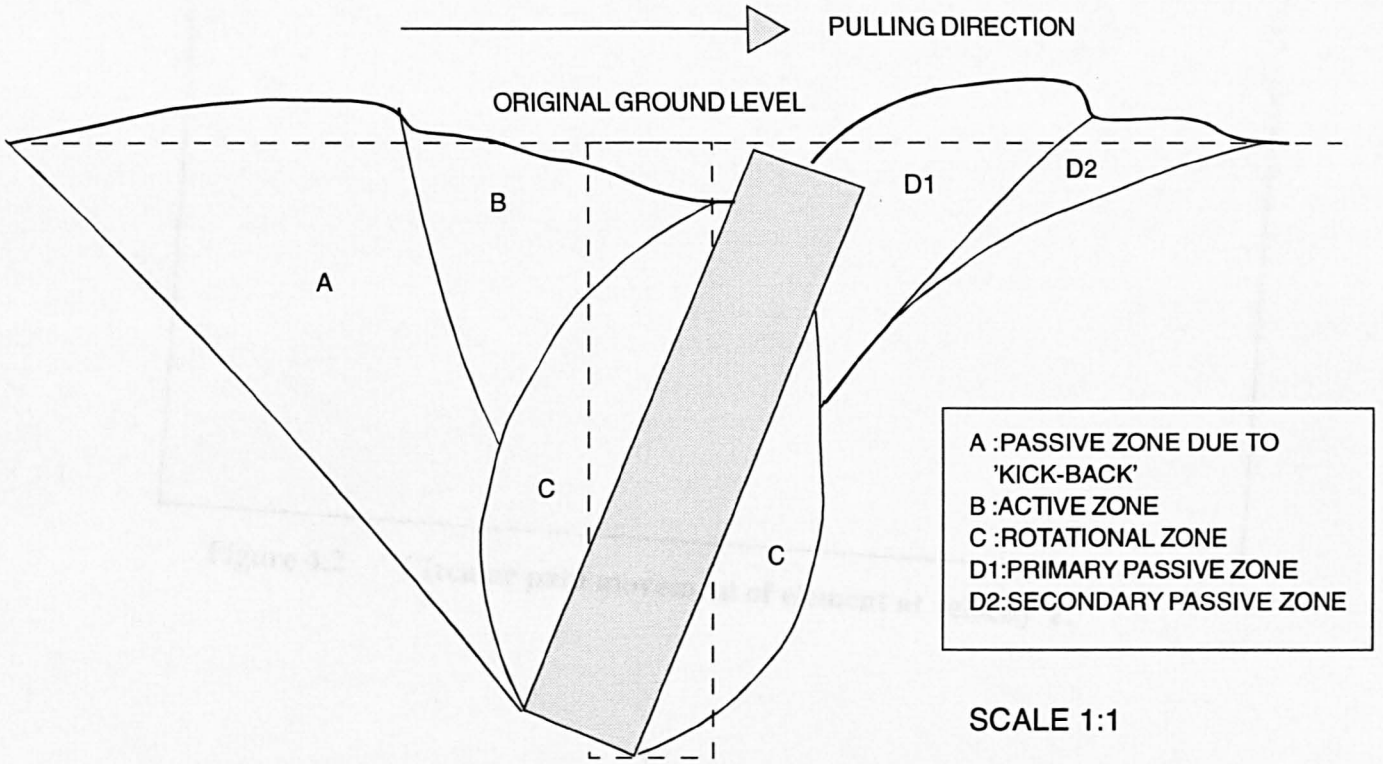

Figure 8.51 Schematic diagram showing failure mechanism developed during pile movement for L/D=5 and e/L<1 in dense sand

8.6.3 CONCLUSION

The pulling height of pile in loose and dense sand has no great influence in determining the failure pattern. It was observed that the failure planes develop progressively in a loose packing whereas in dense packing the failure planes developed almost instantaneously for the whole soil mass. The layer beneath the toe of the pile shows no significant disturbance due to the movement of the pile. Thus friction at the base of the pile is so small that, for simplification, it can be ignored without affecting the limiting resistance of the pile.

Generally for a pile embedded in loose sand significant rotational failure is exhibited while for a pile in dense sand a shear plane is developed which is more pronounced than the rotational mechanism especially for a pile pulled at a lower level. The point of rotation tends to develop below the midpoint of the pile embedment length. The findings tend to deviate from Broms(1964) and Reese(1962) where no rotational pattern was included in their analyses. However Dembicki et al.(1977) made an attempt to include rotational failure in their analyses. Broms assumptions on the failure pattern agree fairly well with the author's observations for a pile embedded in dense sand. For simplification, Broms introduced a concentrated load in his analyses to account for the high passive pressure which develops at the back of the pile.

8.7 GENERAL CONCLUSION

Modelling of models provides an internal check on the consistency of the centrifugal modelling application and in validating the scaling relationships. Results confirm the validity of the centrifugal modelling technique to the short rigid pile problem. No attempt was made to observe the minimum acceleration which could be used to obtained reliable prototype results. However tests conducted as low as 7g still gave reasonable values as shown in Figure 8.27.

The results plotted show that the moment limit is greatly affected by several factors such as, pulling height, embedment ratio, pile diameter and soil unit weight. Apart from these factors, ground profile inevitably affects the moment limit to a certain extent. The slope proximity was shown to affect the moment limit at distance closer than 1.5 times the pile length for a pile pulled towards a slope. Piles pulled away from the slope could only attain approximately 75% of the total moment limit at this distance. Balfour Beatty suggested that, for a slope distance ratio d/L=1.2, a pile can be considered as embedded in flat terrain. Due to limited work done to investigate the behaviour of piles embedded within the vicinity of slope, the value obtained from the experimental work could not be proven conclusively.

Broms and Meyerhof employed a shape factor to predict the soil resistance based on two dimensional analyses. Using the moment at ground level as the design factor, the author introduced a moment shape factor to account for pile geometry. The

moment shape factor is defined as a ratio between moment factors of a single and equivalent continuous pile. Results show that moment shape factor is influenced by the embedment ratio. However pulling height has a less significant effect. It is also noticeable that the scale effect has no significant influence on the moment shape factor. Although not proven conclusively in this research since only one pile with L/D=5 was employed, Dickin and Leung(1983) had proved that in the case of vertical anchors pulled horizontally that the shape factor is not greatly affected by scale.

Apparently 100mm diameter piles tested in conventional tests show similar behaviour to that in centrifugal tests. Unfortunately fallacious values were obtained for piles with L/D=5(flat terrain) and L/D=4(sloping terrain) due to the boundary effect of the bin. A pile with L/D=2 tends to give a lower value of limiting moment than expected since the same 1.7m long pulling arm was used for all pile lengths. The weight of the arm was suspected to contribute to this apparently low value. However piles with L/D=3 and 4 seem to give reasonable limiting moment values. Thus direct comparison between conventional and centrifugal tests was based on them. The centrifugal test results further confirm the inaccuracy of conventional test on small model in predicting prototype behaviour. Moment factors increase with a decrease in pile size. Any overestimation of the prototype behaviour could lead to a potentially unstable design.

The two dimensional tests performed in a glass sided box give a useful insight into the failure mechanisms around a pile subjected to horizontal force. Failure of piles in loose sand is generally governed by local rotational failure especially for piles pulled

at lower level. Although passive and active zones were seen, they were relatively small compared to the rotational zone. In contrast failure patterns for piles in dense sand show a significant influence of passive resistance during the rotation of the pile. The passive plane which was seen to develop behind the pile due to kick back was taken into account by the introducing of a concentrated load at the pile toe by Broms(1964). However the active plane which develops behind the pile is ignored in Broms' assumptions. Pulling height has no great influence in determining the failure pattern around the pile. However piles pulled at lower pulling height exhibit a greater rotation compare to those pulled at higher level. Thus for a lower pulling height value, piles should be designed on the limiting movement at ground level rather than by employing a safety factor as mentioned earlier. The local rotational planes exhibited in the failure mechanisms of the piles tested confirm the assumption made earlier that the piles experience local rotational failure before ultimate failure is reached.

CHAPTER NINE

COMPARISON BETWEEN EXPERIMENTAL WORK AND EXISTING THEORIES

9.1 INTRODUCTION

It has already been demonstrated in preceeding chapters that centrifuge modelling is a successful method of simulating full scale behaviour. Scaling errors which emanate from small scale modelling can be eliminated if the correct acceleration is chosen to generate the prototype stress level.

Difficulty in making a direct comparison with other theories are inevitable since different parameters are involved in the work of each individual researcher. In fact the classification of the short rigid pile differs according to different researchers as shown in Table 5.1 in Chapter Five. Comparisons made show that the piles used in this project were definitely rigid. Because of the difference in moment-rotation relationship shown in Appendix A in that no pronounced peak was observed in the relationship it was suspected that pile the with embedment ratio L/D=5 is no longer a short pile. However, further tests on longer piles need to be performed to clarify the situation. This in fact would consume greater space than available in the existing centrifugal package. Moreover deeper piles are considered outside the scope of this project.

Most of the theories proposed which involved either two or three dimensional analyses, aim to provide a solution associated with flexible rather than rigid piles. With the evolution of the computer technology, finite difference and element methods are employed in solving the three dimensional problem of a laterally loaded pile. Work such as that of Matlock and Reese(1960), Kubo(1965), Reese and Desai(1977), Fulthorpe(1986) involved the use of computer programming to solve the related problems. Of course this sophisticated method can only be readily understood by researchers who are familiar with such method. One of the main objectives of this project is to investigate the factors which affect the moment carrying capacity of a short pile embedded in sand and to produce a simple empirical relationship which may readily be employed by most designers. Most of the tests were performed in sand in a dense packing since this condition is usually encountered on site. Moreover, it is easier to assess since data is less scattered than for a loose packing due to the non-homogeneity of the latter.

9.2 ASSUMPTIONS MADE IN COMPARISONS WITH EXISTING THEORIES

Since direct comparison could not possibly be done, several assumptions will be made for convenience.

a) The piles are assumed to be short and rigid with L/D between 1 and 5 and pulling heights ranging from 1 to 5.

b) Parameters such as unit weight, internal friction angle of the soil and distance of point of rotation from ground surface obtained from the experimental work will be adopted in computing predictions from the existing theories.

c) The moment at ground level will be considered as a limiting factor.

d) Where existing theories employed soil resistance as their design factor, these values will be transformed into moment at ground level where, based on Terzaghi(1943), the soil resistance acting on the pile should be equivalent to the external force acting on it.

e) Due to the uncertainties in the factors of safety involved, allowable values such as those of Roscoe(1957), McCorkle(1969) and Balfour Beatty(1986, 1988) will be directly compared with the other limiting values.

9.3 EMPIRICAL INTERPRETATION OF EXPERIMENTAL RESULTS

For a better comparison between moment factors from the present tests and existing theories, it is preferable to derive an empirical relationship from the data available. The rationale of the analysis is to derive empirical equations for a single short pile based on the empirical expression for the continuous pile employing the

moment shape factor determined in Chapter Eight. Moment values obtained from the calculation using the empirical method will be compared with data obtained from centrifugal tests on single piles in dense sand.

9.3.1 EMPIRICAL RELATIONSHIP FOR CONTINUOUS PILE

Based on Figure 8.31 , the variation of prototype moment factor with pulling height ratio is replotted. As shown in Figure 9.1, the ratio of (e/L)/M'_{pc} is plotted against pulling height ratio e/L giving straight line relationships. Since no significant difference in intercept values at the y axis is observed, therefore for simplicity an average value of 0.25 is adopted. This enables the following empirical relationship to be derived;

$$\frac{e}{LM'_{pc}} = m\left(\frac{e}{L}\right) + 0.25 \qquad (9.1)$$

where m is the gradient obtained for every line plotted. Values of m are plotted against embedment ratio in Figure 9.2 which shows the best fit straight line. The relationship between m and L/D is;

$$m = 0.23\frac{L}{D} \qquad (9.2)$$

Combining equation(9.1) and (9.2) gives;

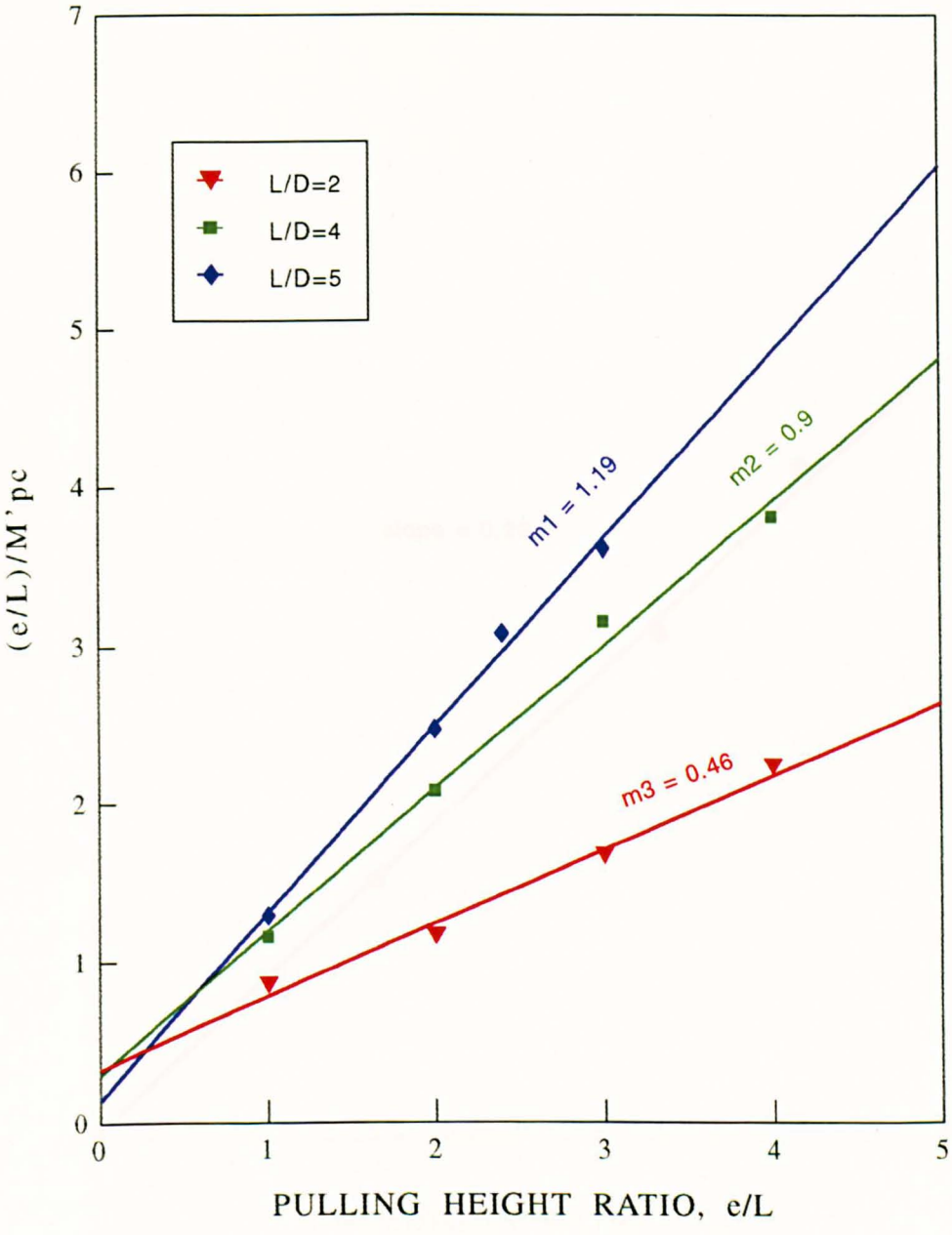

Figure 9.1 Variation of (e/L)/M'pc with pulling height ratio for continuous pile embedded in dense sand

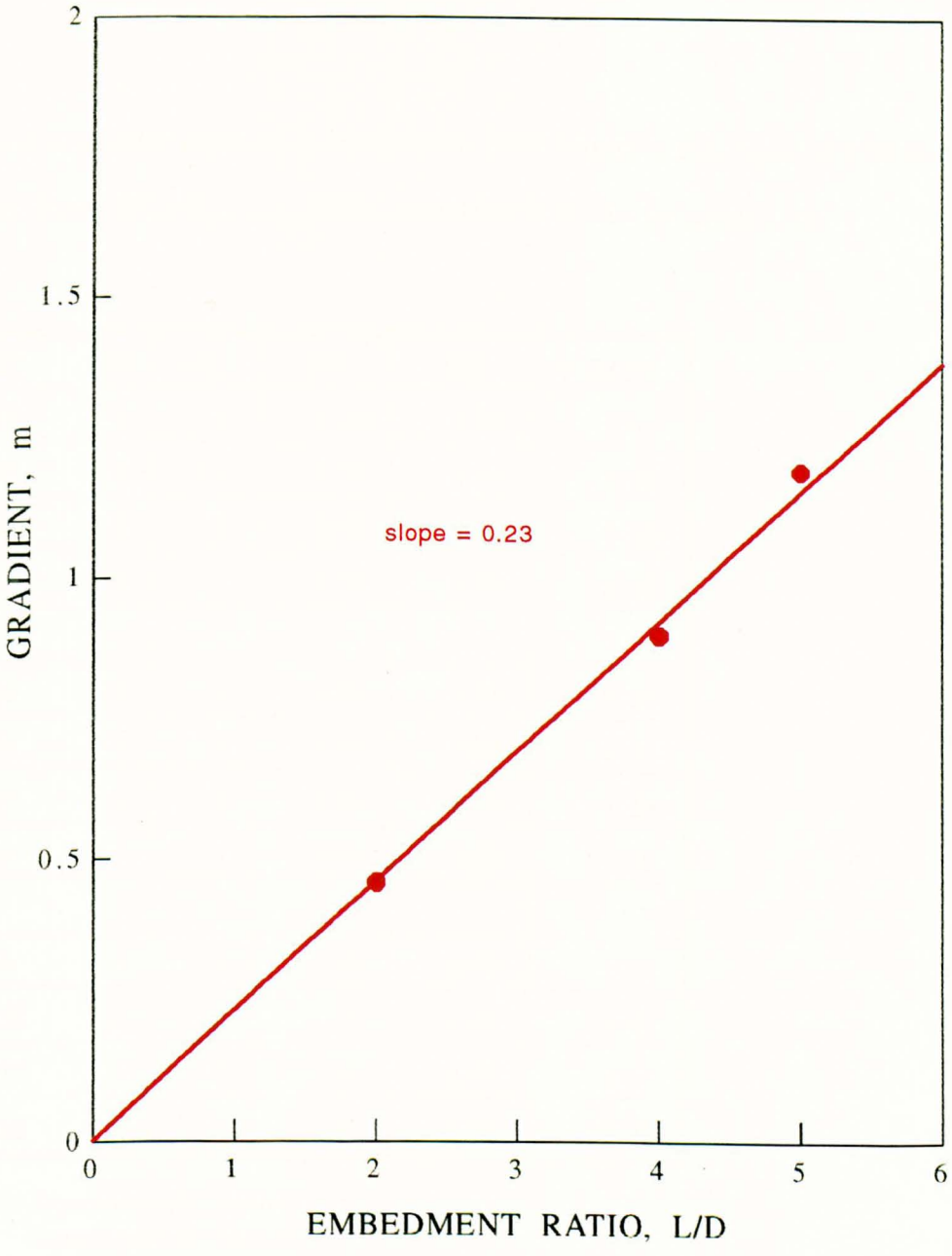

Figure 9.2 Variation of gradient m with embedment ratio for continuous pile in dense sand

$$\frac{e}{LM'_{pc}} = 0.23\frac{e}{D} + 0.25 \qquad (9.3)$$

However a simpler expression in equation (9.3) results if the value of 0.23 is replaced by 0.25. Since $M'_{pc}=M_{p(continuous)}/\gamma BL^3$, equation (9.3) can be written as;

TEST	L/D	e/L	ER	EM	% DIFF
SFD1	5	3	0.83	0.75	9.64
SFD2	5	2.4	0.77	0.74	4.16
SFD3	5	2	0.80	0.73	9.13
SFD4	5	1	0.77	0.67	13.38
SFD5	4	4	1.05	0.94	10.38
SFD6	4	3	0.95	0.92	2.84
SFD7	4	2	0.96	0.89	7.40
SFD8	4	1	0.86	0.80	6.98
SFD9	2	4	1.80	1.78	1.22
SFD10	2	3	1.77	1.71	3.16
SFD11	2	2	1.71	1.60	6.43
SFD12	2	1	1.61	1.33	17.20

ER : Experimental values
EM : Equation(9.4) values

Table 9.1 Percentage difference between experimental values and the values obtained from the author's empirical expression for continuous piles

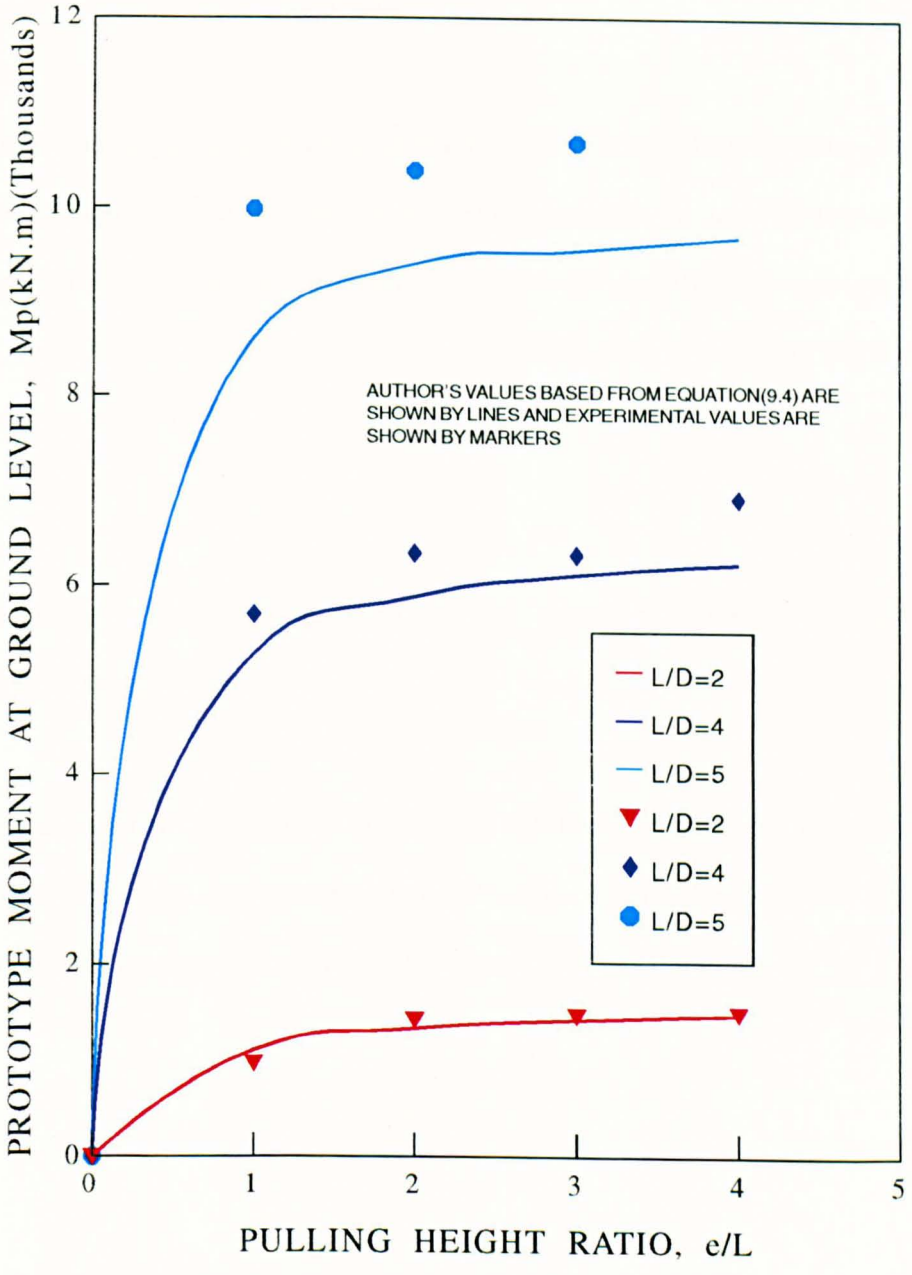

Figure 9.3 Variation of empirical prototype moment at ground level with pulling height for 1m diameter continuous pile in dense sand

$$M_{p(continuous)} = \frac{4e\gamma BL^2D}{(e + D)} \tag{9.4}$$

Figure 9.3 shows a comparison between moment factor with pulling height ratio based on the empirical expression(Equation 9.4) and the experimental data. Values obtained from the empirical expression compares with experimental results are on average of 8% higher than experimental results due to the approximation involved in deriving the formula as shown in Table 9.1.

9.3.2 EMPIRICAL RELATIONSHIP FOR SINGLE PILE BASED ON CONTINUOUS PILE ANALYSIS

It is of interest in this project to estimate the limiting moment at ground level of a single short pile based on a two dimensional values in combination with a moment shape factor. Since the moment shape factor $S_{fm}=M'_{ps}/M'_{pc}$, this gives;

$$S_{fm} = \frac{M_{p(single)}}{M_{p(continuous)}} \cdot \frac{B}{D} \tag{9.5}$$

where $M'_{ps} = M_{p(single)}/\gamma DL^3$

Substituting Equation (9.5) into (9.4) gives;

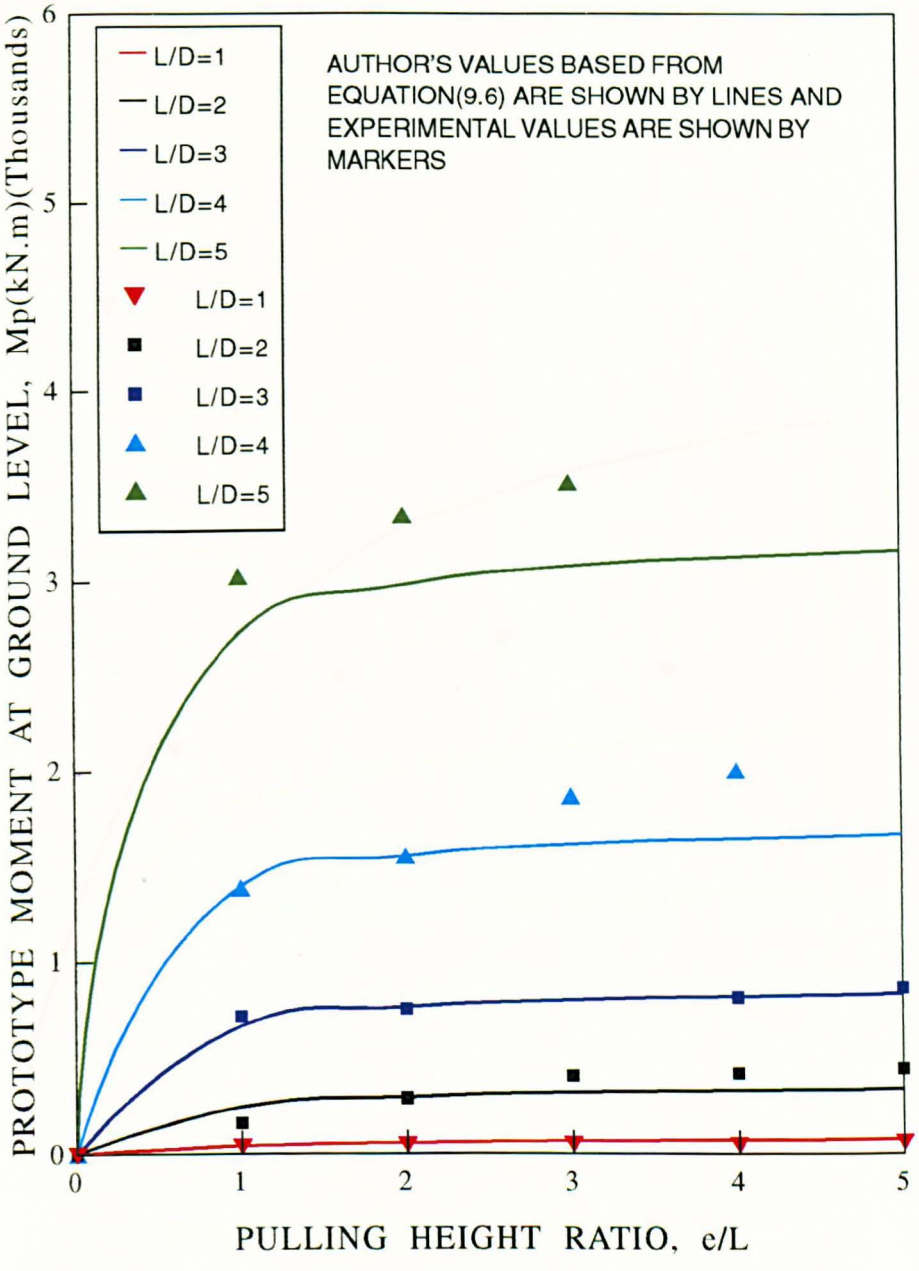

Figure 9.4 Variation of empirical prototype moment at ground level with pulling height for 1m diameter single pile in dense sand

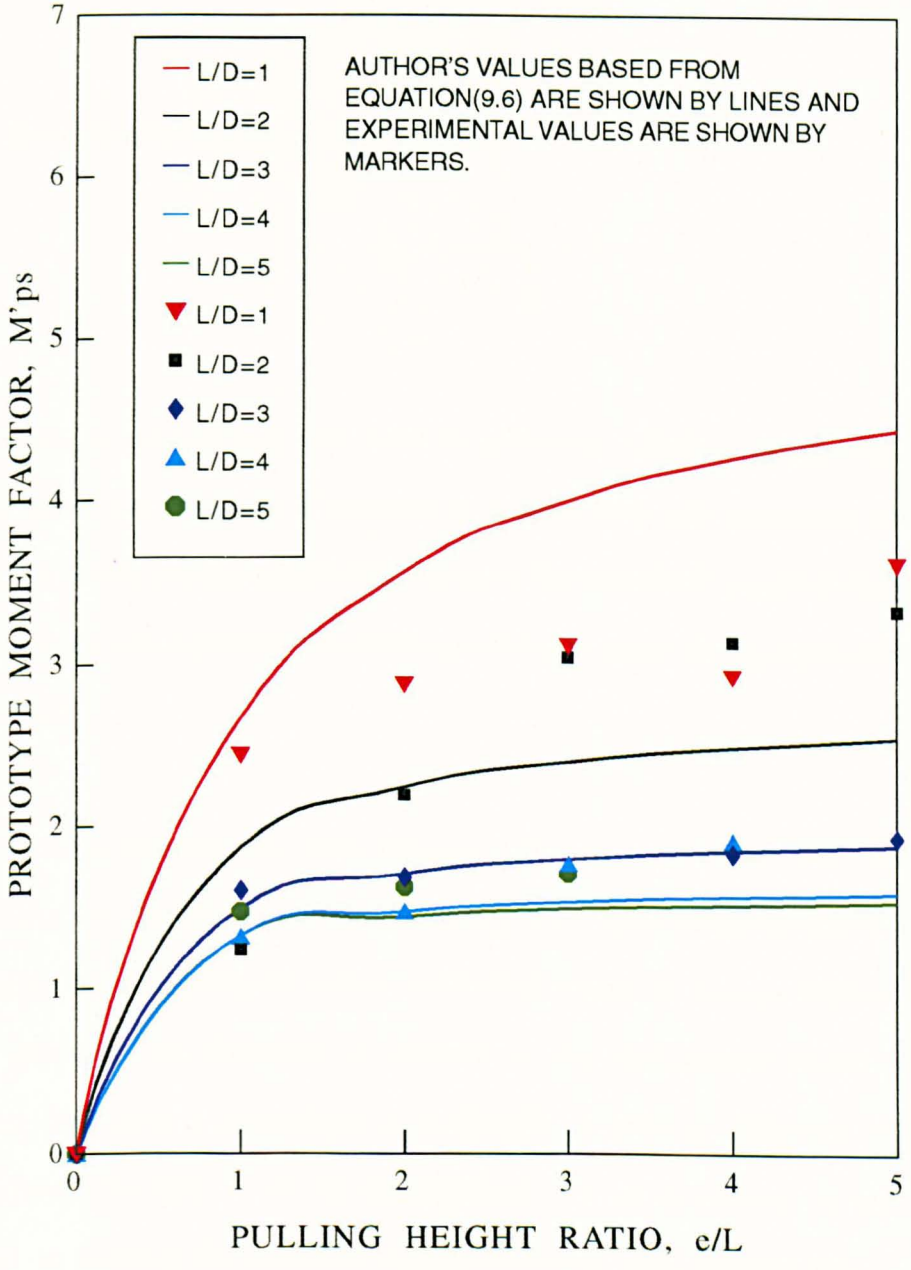

Figure 9.5 Variation of empirical prototype moment factor with pulling height for 1m diameter single pile in dense sand

$$M_{p(single)} = \frac{4e\gamma L^2 D^2 S_{fm}}{(e + D)} \tag{9.6}$$

where from Chapter Eight in Equation(8.2)

$$S_{fm} = \frac{2}{7 - \frac{L}{D}} + 1$$

This empirical expression is only valid for piles with L/D<5 in dense sand. Figures 9.4 and 9.5 show the variation of moment at ground level and prototype moment factor respectively with pulling height ratio based on Equation(9.6) together with values from the experimentals. A general relationship similar to those obtained from the centrifugal tests results.

A close examination from Figures 8.11 and 9.5 reveals that the expression generally gives slightly higher values of M'_{ps} than observation as shown in Table 9.2 and Figure 9.6, especially for L/D=1 and L/D=2 where an average difference of 20% is found. However the difference is reduced as the embedment length is increased. Equation (9.6) gives a particularly good fit with an average difference of 2% for piles with L/D=3. The lack of fit for other values can be attributed to approximations involved in deriving the equation and the scattered experimental data.

As explained earlier, no attempt was made to determine the limiting value of embedment ratio for which a pile can be considered as short. However the empirical

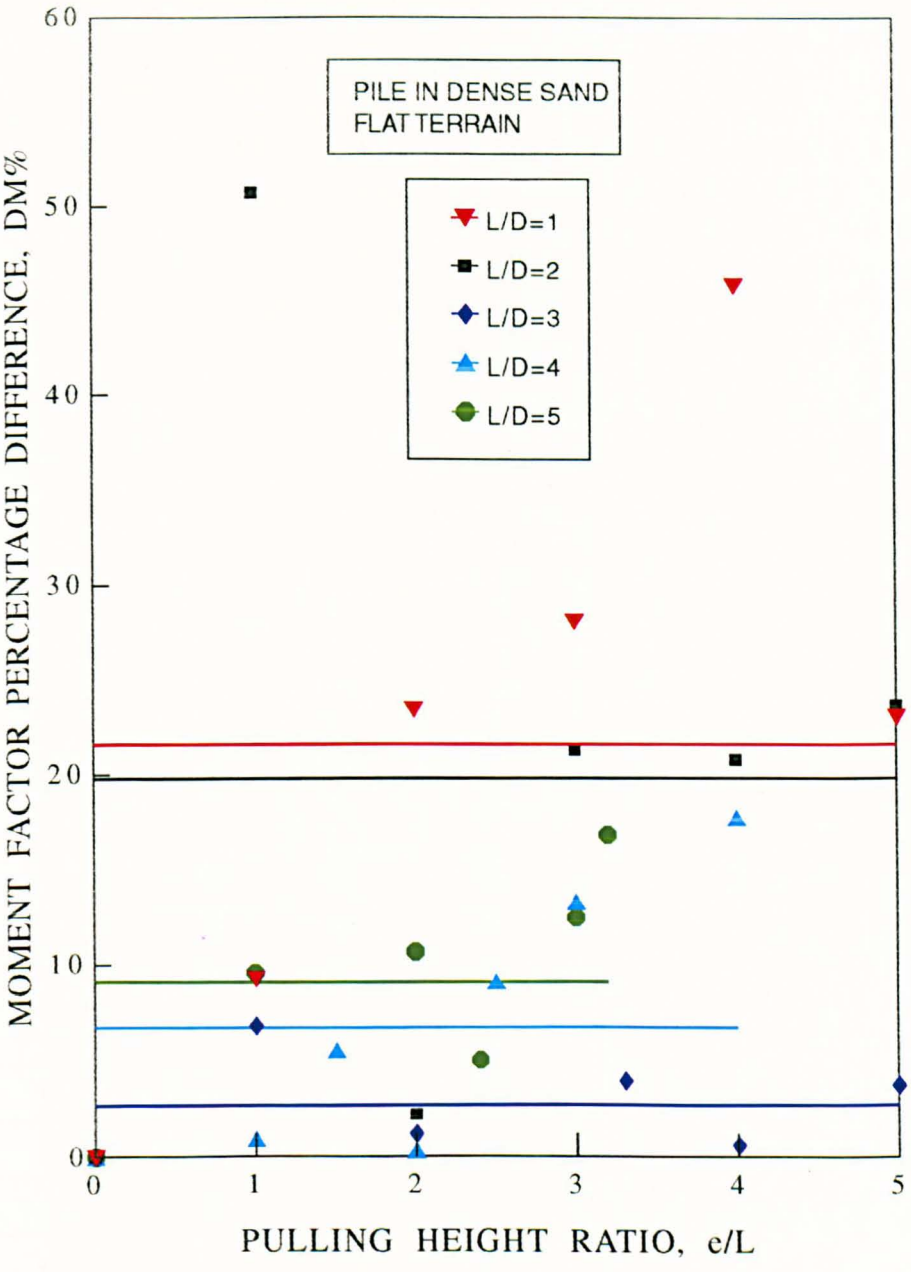

Figure 9.6 Comparison of an average percentage difference of moment factor with pulling height ratio with different embedment ratio

expression for moment shape factor shown in Equation(8.2), gives increasingly high values for L/D<6 which confirms the limitations of employing Equation (9.6). Since

TEST	L/D	e/L	ER	EM	% DIFF.
RND1	5	3.2	1.81	1.51	16.57
RND2	5	3	1.71	1.50	12.28
RND3	5	2.4	1.55	1.48	4.71
RND4	5	2	1.63	1.46	10.74
RND5	5	1	1.48	1.33	9.93
RND6	4	4	1.91	1.57	17.85
RND7	4	3	1.77	1.54	13.11
RND8	4	2.5	1.67	1.52	9.28
RND9	4	2	1.48	1.48	0.07
RND10	4	1.5	1.51	1.43	5.36
RND11	4	1	1.32	1.33	0.98
RND12	3	5	1.95	1.88	3.85
RND13	3	4	1.83	1.85	0.87
RND14	3	3.3	1.89	1.82	3.86
RND15	3	2	1.69	1.71	1.42
RND16	3	1	1.61	1.50	6.83
RND17	2	5	3.33	2.55	23.57
RND18	2	4	3.14	2.49	20.73
RND19	2	3	3.05	2.40	21.31
RND20	2	2	2.19	2.24	2.28
RND21	2	1	1.24	1.87	50.56

++

++ continue

TEST	L/D	E/L	ER	EM	% DIFF.
RND22	1	5	3.61	4.44	23.10
RND23	1	4	2.93	4.27	45.63
RND24	1	3	3.12	4.00	28.21
RND25	1	2	2.88	3.56	23.47
RND26	1	1	2.44	2.67	9.30

++ continue

ER : Experimental values
EM : Equation(9.6) values

Table 9.2 Percentage difference between experimental values and the values obtained from the author's empirical expression for single pile

the moment obtained from this equation is the ultimate value, a safety factor would be introduced during the design stage. The prototype moment factor, M'_{ps} values obtained from Equation (9.6) are compared with those obtained from existing theoretical and empirical relationships in section 9.5.

9.3.3 EMPIRICAL EXPRESSION FOR A SINGLE PILE BASED ON SERIES TWO TESTS

As an alternative procedure, an empirical expression for limiting moment of a single pile can also be derived from Figure 8.11. Similar procedures to those used in

deriving the empirical expression for the continuous pile are employed in deriving this alternative expression. Figure 9.7, shows a plot of $(e/L)/M'_{ps}$ against e/L which gives a straight line in a form of;

$$\frac{\left(\frac{e}{L}\right)}{M_{ps}} = m\left(\frac{e}{L}\right) + 0.3 \tag{9.7}$$

where m is the gradient of the lines shown. Plotting m against L/D as shown in Figure 9.8 gives;

$$m = 0.12\left(\frac{L}{D}\right) \tag{9.8}$$

Combining Equation(9.7) and Equation(9.8) gives the alternative expression for a single pile as;

$$M_s = \frac{eD^2\gamma L^2}{0.3(0.4e + D)} \tag{9.9}$$

However, Equation(9.9) will not be discussed in comparison with the existing theories.

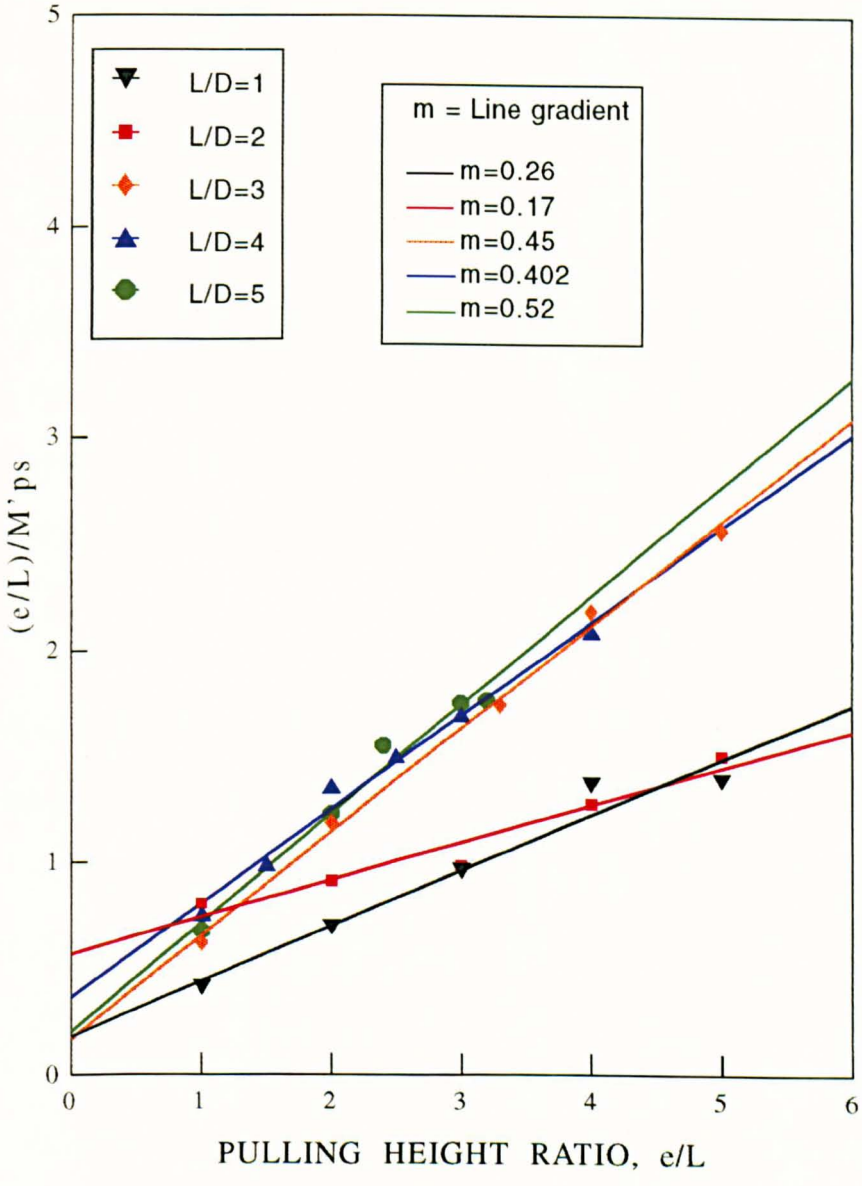

Figure 9.7 Variation of (e/L)/M'ps with pulling height ratio for 1m diameter prototype pile in dense sand

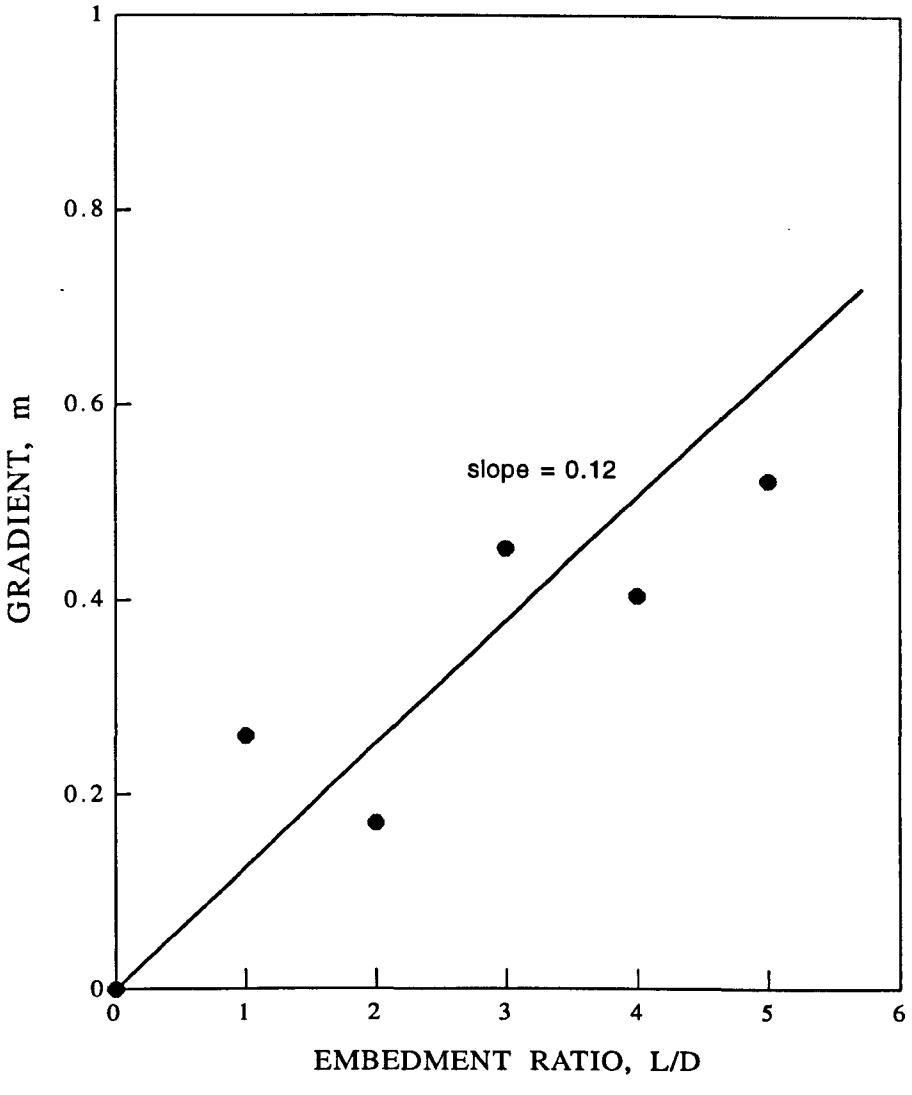

Figure 9.8 Variation of gradient m with embedment ratio for 1m diameter prototype single pile in dense sand

9.4 COMPARISON BETWEEN OBSERVED MOMENT SHAPE FACTORS AND THE EXISTING THEORETICAL SHAPE FACTORS

Figure 9.9 shows a comparison between shape factors established by Broms(1964) and Meyerhof et al.(1981) with the author's empirical moment shape factor. Broms' shape factor is constant for all embedment lengths. However the author's moment shape factor S_{fm} and Meyerhof's ultimate shape factor S_{fu} are both dependent on embedment ratio although different trends are observed. For an embedment length of 5, the values of shape factor and moment shape factor tends to approach 3, which in fact agrees with Broms' shape factor.

9.5 COMPARISON BETWEEN OBSERVED MOMENT FACTOR AND PREDICTIONS FROM EXISTING THEORIES

The aim of this section is to compare M'_{ps} values obtained from the author's empirical expression (Equation (9.6)) with those derived from the existing theories. For values which were back-calculated such as those from Hansen's theory, the point of rotation obtained from the author's centrifugal test results will be employed. Test parameters from the centrifugal testing will be input to the existing theories. These were evaluated for the appropriate stress level. M'_{ps} values obtained from the author's empirical expression(Equation(9.6)) are also included on the appropriate graphs. Comparisons are made in terms of prototype moment factor of a single pile, M'_{ps} as shown in Table 9.3 below.

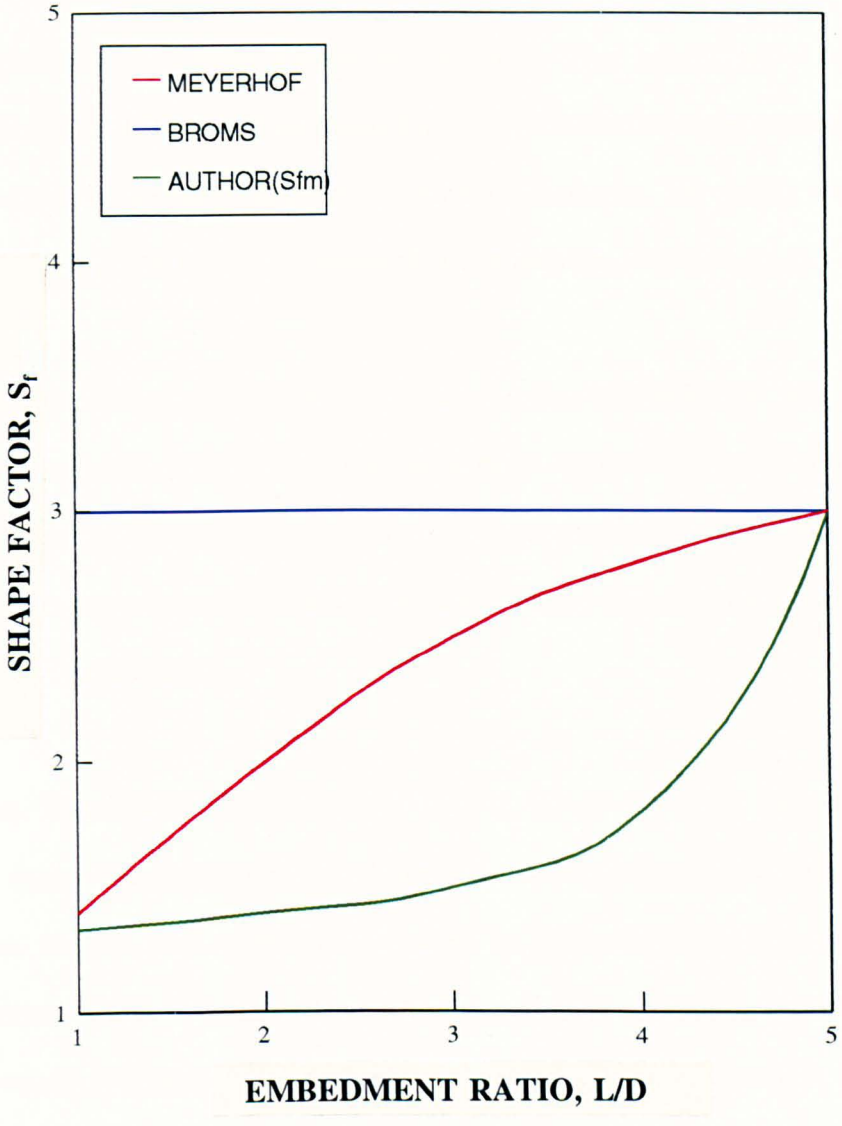

Figure 9.9 Comparison of shape factor from Equation(8.2) with existing theories

9.5.1 MOMENT FACTOR AGAINST PULLING HEIGHT RATIO

Comparison of moment factors for various pulling height ratios are shown in Figures 9.10 and 9.14. It should be noted that since Hansen's values were derived from back calculation, scattered points were obtained. However, the points were fitted to produce a smooth curve so that a reasonable comparison could be made.

An upper limit of passive pressure with a value of 228 kN/m^2 was employed in McCorkle's calculation while a soil constant with an upper limit value of 160 kN/m^2/m was used in Balfour Beatty's computation for dense sand. The McCorkle and Balfour Beatty's methods produce an allowable moment factor and include a safety factor in their empirical relationships.

From Figure 9.10, for piles with L/D=1, values from the author's empirical expression show close agreement with those of Hansen and Broms. Although McCorkle's values seem to give good agreement it must be borne in mind that his values are allowable ones. Thus it is likely that ultimate prototype moment factor values from McCorkle would overestimate the author's postulation. Both Meyerhof's relationships using $\delta=0$(Meyerhof et al.(1981) and $\delta=\phi/3$(Meyerhof et al.(1988)) exhibit lower values than the author's results. Values for $\delta=\phi/3$ are lower than those with $\delta=0$ since a shape factor is not included in Equation(2.30). No apparent reason was given for this omission in the latter expression. Balfour Beatty's values were conservative as expected since they are allowable moment factors. Figure 9.11 for a pile with L/D=2 exhibits a similar behaviour in comparison with the existing theories. Values calculated from the

++

e/L=1			P_p=228 kN/m^2	K″=160kN/m^2/m			
L/D	Author	Broms	McCorkle	B.Beatty	Meyerhof(δ=0)	Meyerhof(δ=ϕ/3)	Hansen
1	2.67	1.79	2.66	0.24	0.56	0.43	4.24
2	1.87	1.79	1.33	0.24	0.42	0.27	2.64
3	1.50	1.79	0.89	0.24	0.52	0.20	2.64
4	1.33	1.70	0.67	0.24	0.93	0.16	2.35
5	1.33	1.65	0.53	0.24	0.97	0.13	2.16
e/L=2							
1	3.56	2.38	3.33	0.30	0.71	0.54	2.96
2	2.24	2.38	1.67	0.30	0.53	0.31	3.02
3	1.71	2.38	1.11	0.30	0.66	0.22	3.03
4	1.48	2.26	0.83	0.30	1.17	0.17	4.04
5	1.45	2.20	0.67	0.30	1.22	0.14	2.79
e/L=3							
1	4.00	2.68	3.64	0.33	0.78	0.59	4.35
2	2.40	2.68	1.82	0.33	0.58	0.33	3.07
3	1.80	2.68	1.21	0.33	0.72	0.23	NA

4	1.54	2.54	0.91	0.33	1.29	0.17	2.85
5	1.50	2.48	0.73	0.33	1.34	0.14	4.42
e/L=4							
1	4.27	2.86	3.81	0.35	0.82	0.62	3.75
2	2.49	2.86	1.90	0.35	0.61	0.34	3.25
3	1.85	2.86	1.27	0.35	0.76	0.23	3.48
4	1.57	2.71	0.95	0.35	1.35	0.18	3.10
5	1.52	2.65	0.76	0.35	1.41	0.14	NA
e/L=5							
1	4.44	2.98	3.92	0.36	0.84	0.64	3.36
2	2.55	2.98	1.96	0.36	0.63	0.34	4.13
3	1.88	2.98	1.31	0.36	0.78	0.23	4.03
4	1.59	2.83	0.98	0.36	1.39	0.18	NA
5	1.54	2.76	0.78	0.36	1.45	0.14	NA

++ *Continue*

++

e/L=1							
L/D	Author	IRSIA	UIC/ORE	Roscoe(δ=0)	Roscoe(δ=20°)	Terzaghi	Dickin
1	2.67	2.72	4.05	0.58	0.79	2.34	NA
2	1.87	1.97	1.79	0.58	0.79	2.34	1.35
3	1.50	2.08	1.33	0.58	0.79	2.34	1.46
4	1.33	2.34	1.14	0.55	0.79	2.21	NA
5	1.33	2.59	1.01	0.54	0.79	2.15	NA
e/L=2							
1	3.56	2.72	4.05	0.58	0.79	2.34	NA
2	2.24	1.97	1.79	0.58	0.79	2.34	1.94
3	1.71	2.08	1.33	0.58	0.79	2.34	2.30
4	1.48	2.34	1.14	0.55	0.79	2.21	NA
5	1.45	2.59	1.01	0.54	0.79	2.15	NA
e/L=3							NA
1	4.00	2.72	4.05	0.58	0.79	2.34	NA
2	2.40	1.97	1.79	0.58	0.79	2.34	2.59
3	1.80	2.08	1.33	0.58	0.79	2.34	3.46

4	1.54	2.34	1.14	0.55	0.79	2.21	NA
5	1.50	2.59	1.01	0.54	0.79	2.15	NA
e/L=4							
1	4.27	2.72	4.05	0.58	0.79	2.34	NA
2	2.49	1.97	1.79	0.58	0.79	2.34	NA
3	1.85	2.08	1.33	0.58	0.79	2.34	NA
4	1.57	2.34	1.14	0.55	0.79	2.21	NA
5	1.52	2.59	1.01	0.54	0.79	2.15	NA
e/L=5							
1	4.44	2.72	4.05	0.58	0.79	2.34	NA
2	2.55	1.97	1.79	0.58	0.79	2.34	NA
3	1.88	2.08	1.33	0.58	0.79	2.34	NA
4	1.59	2.34	1.14	0.55	0.79	2.21	NA
5	1.54	2.59	1.01	0.54	0.79	2.15	NA

NA :not applicable

Table 9.3 Comparison of prototype moment factor from various existing theories for pile in dense sand.

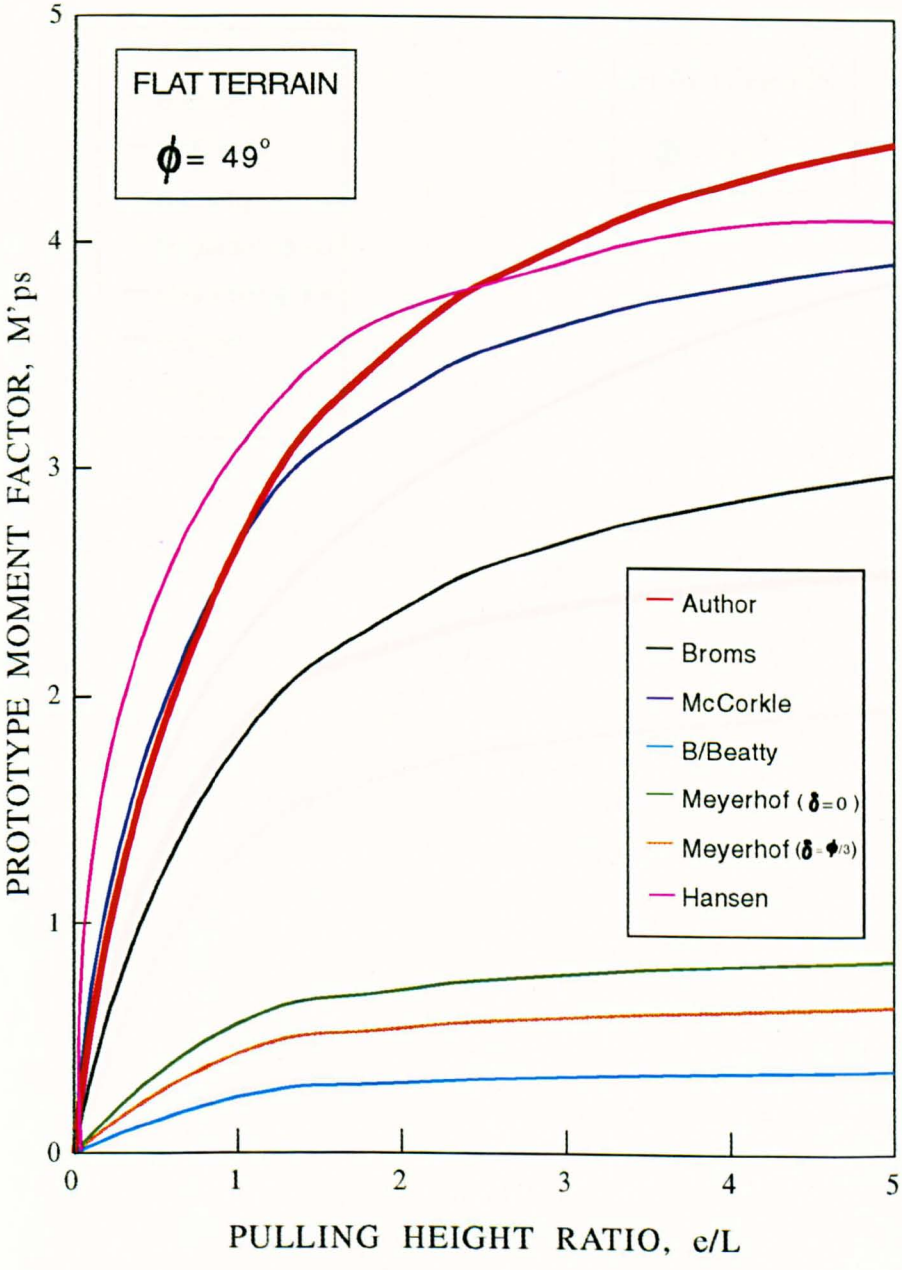

Figure 9.10 Variation of empirical prototype moment factor with pulling height for 1m diameter single pile of L/D=1 in dense sand

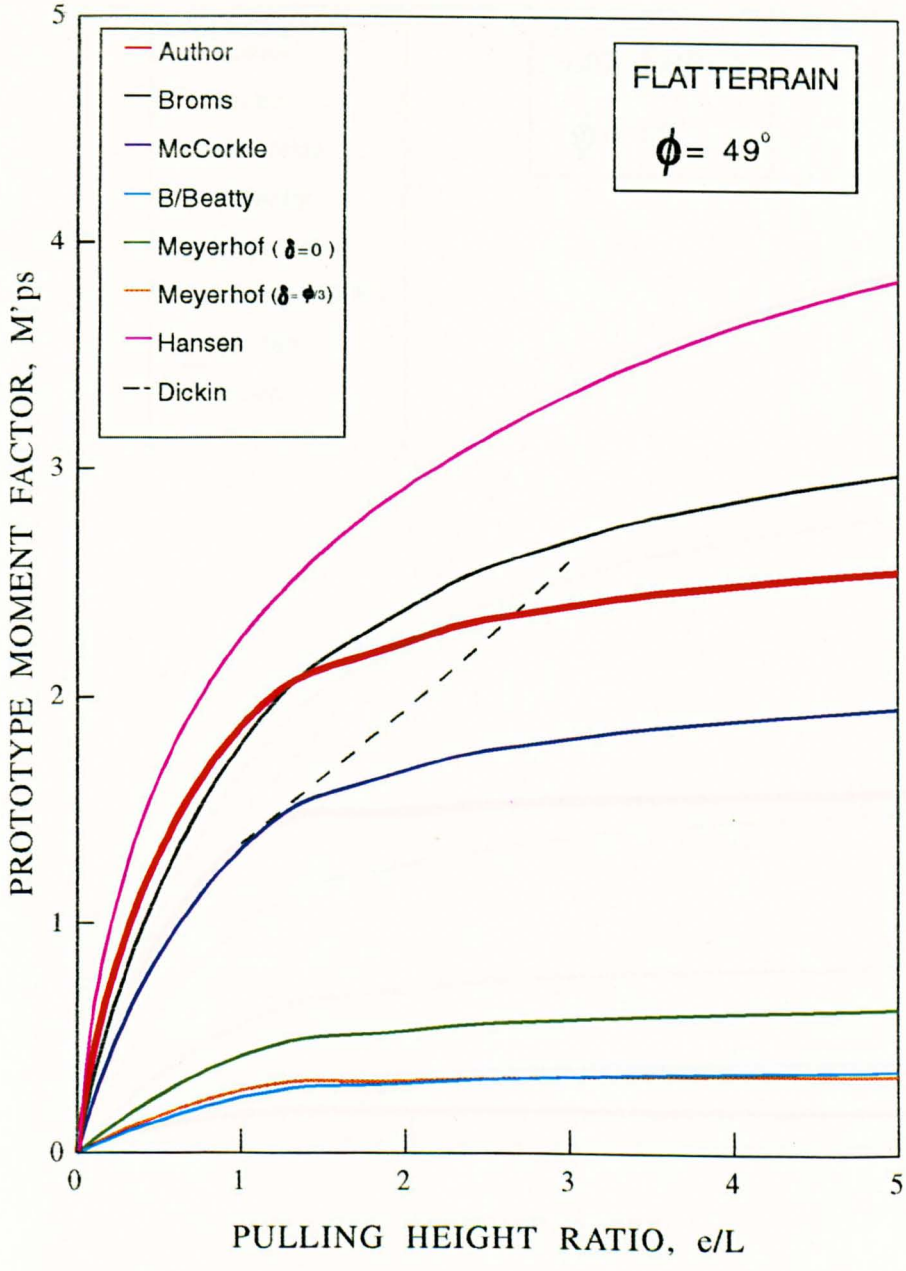

Figure 9.11 Variation of empirical prototype moment factor with pulling height for 1m diameter single pile of L/D=2 in dense sand

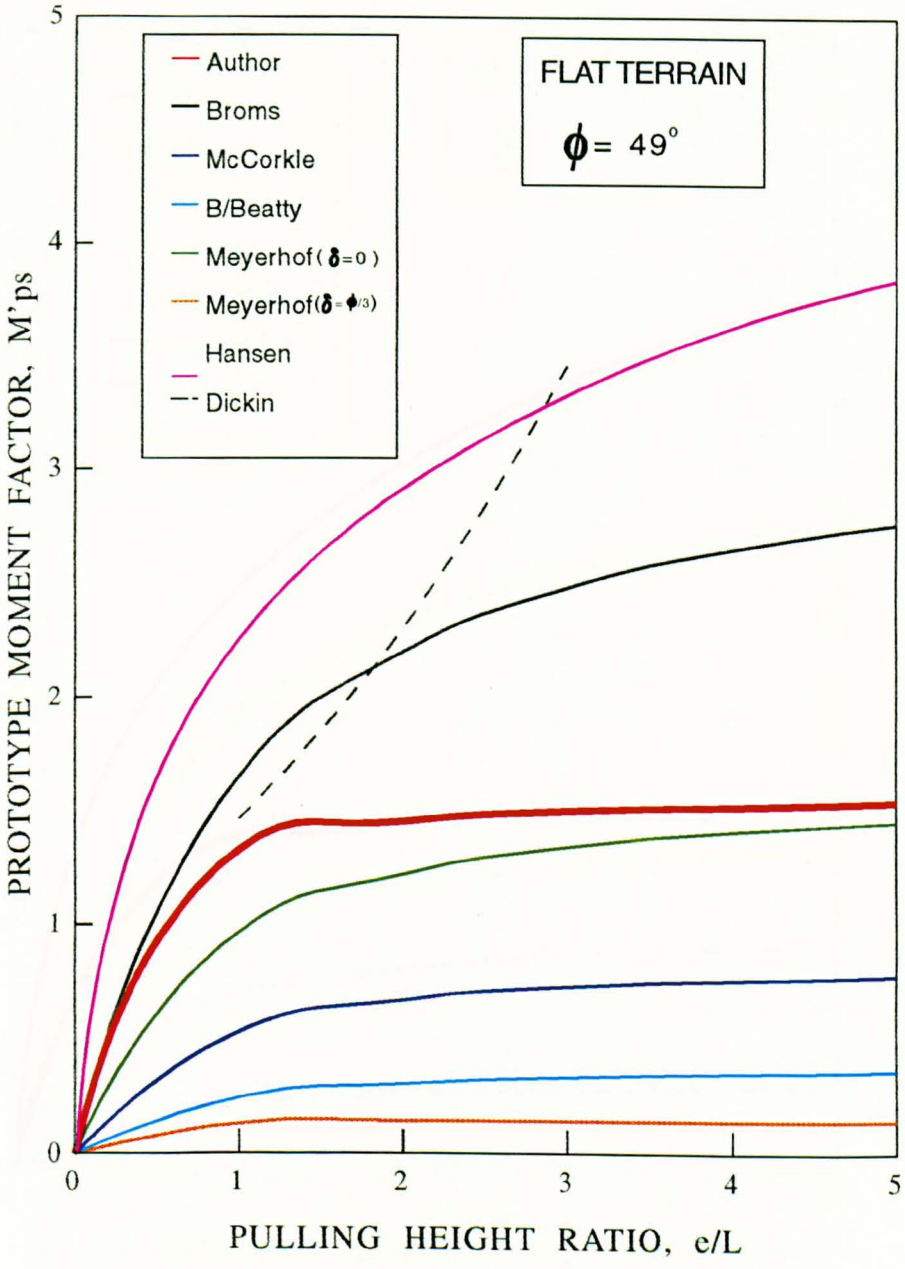

Figure 9.12 Variation of empirical prototype moment factor with pulling height for 1m diameter single pile of L/D=3 in dense sand

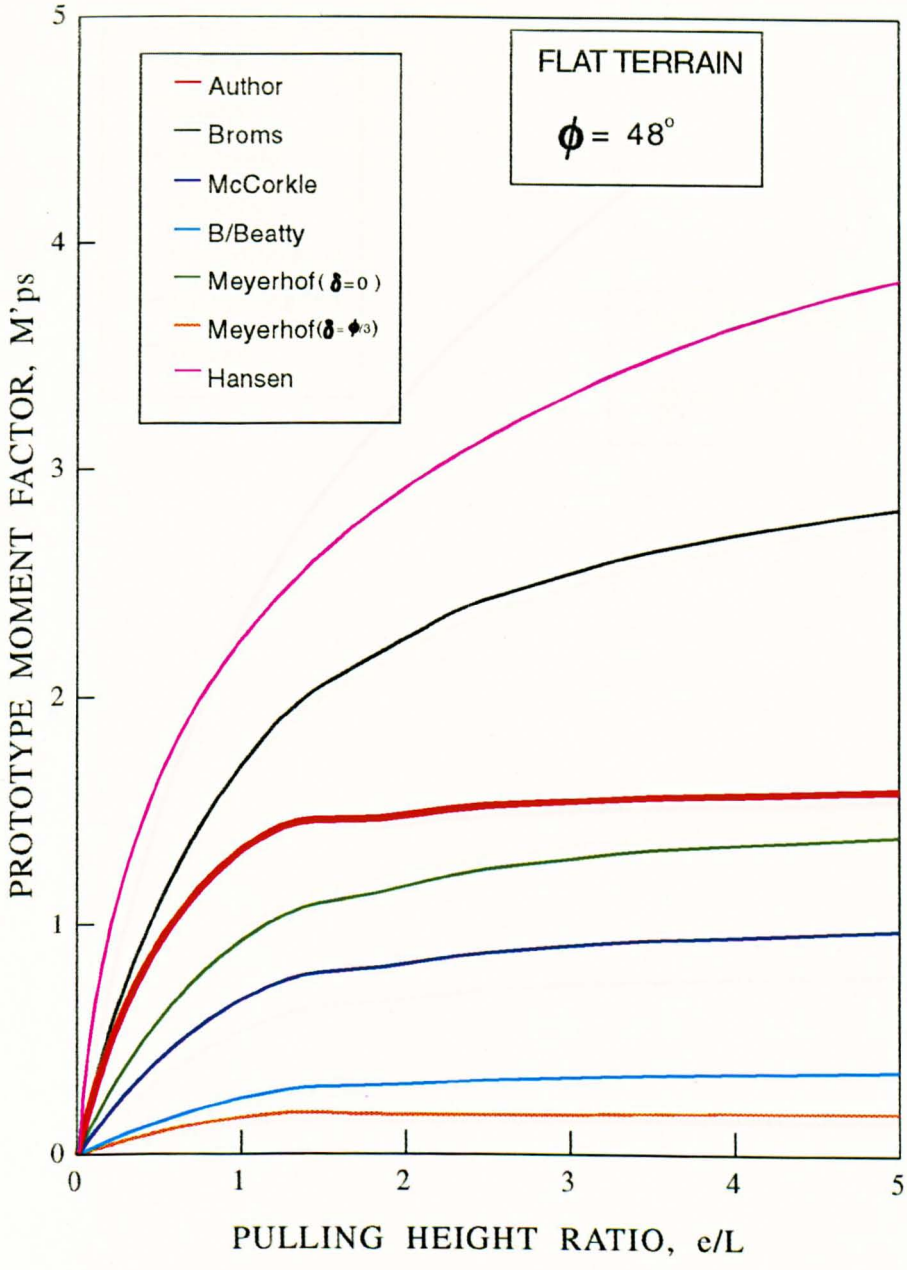

Figure 9.13 Variation of empirical prototype moment factor with pulling height for 1m diameter single pile of L/D=4 in dense sand

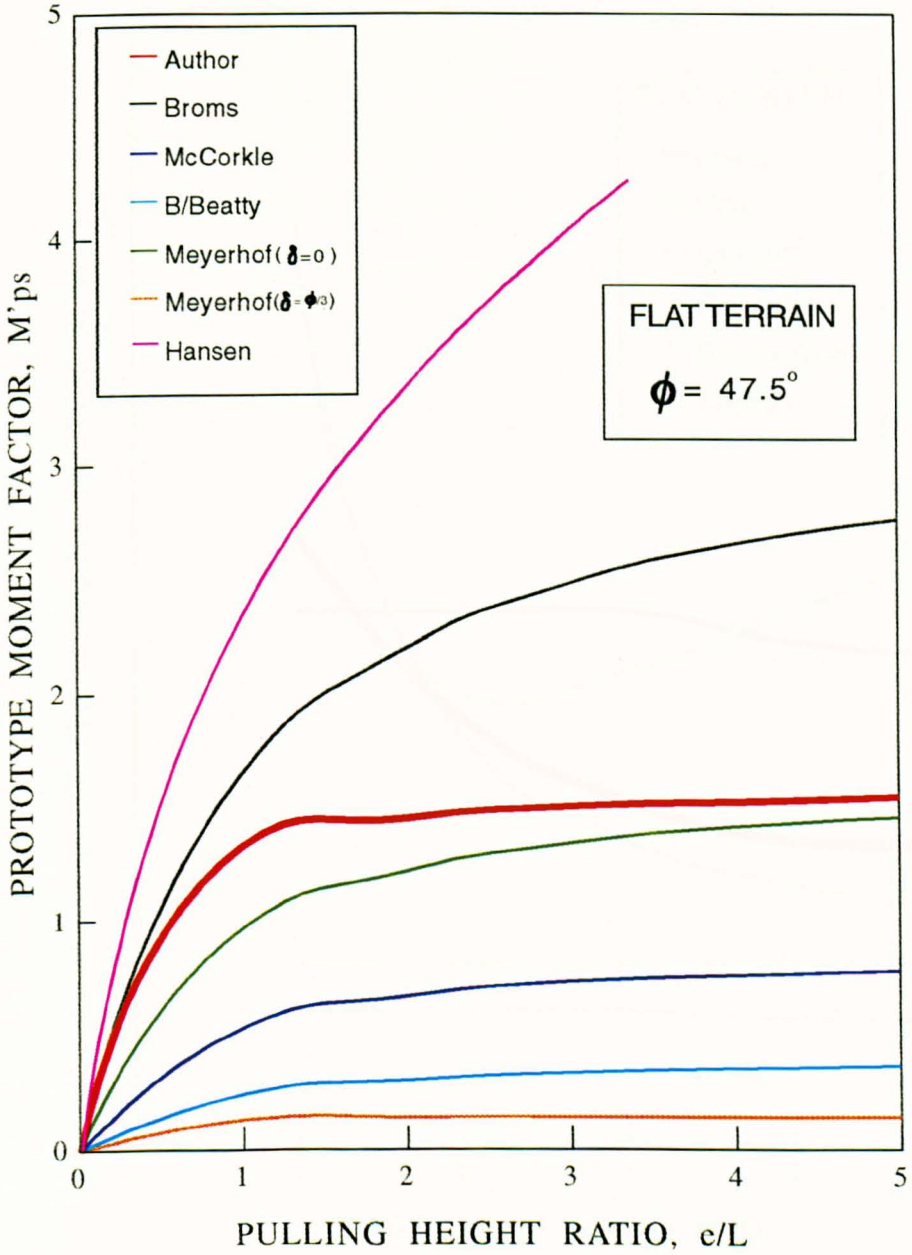

Figure 9.14 Variation of empirical prototype moment factor with pulling height for 1m diameter single pile of L/D=5 in dense sand

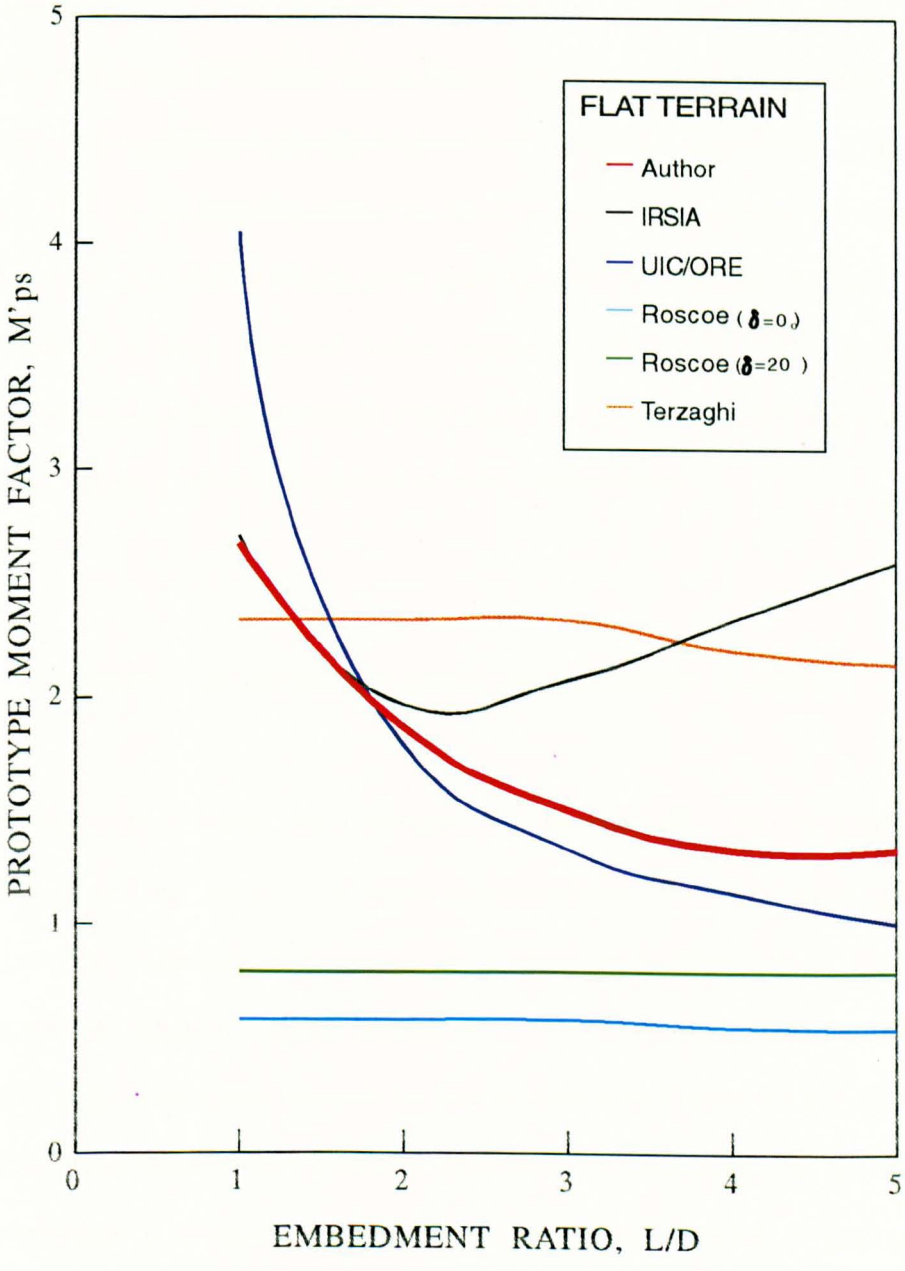

Figure 9.15 Variation of prototype moment factor with embedment ratio for 1m diameter single pile of e/L=1 in dense sand

empirical expression of Dickin and Wei(1991) are included. Since limited tests were performed, their formulae only applies to a small range of embedment and pulling height ratios as explained in Chapter Three. Broms' values show close agreement while McCorkle gives lower values compared to the author's empirical expression. Figure 9.12 for piles with L/D=3 shows that disparities in values for most expressions are consistent except for Meyerhof et al.(1981) which gives good agreement with the author's values. Figures 9.13 and 9.14 show moment factor values for piles with L/D=4 and L/D=5 respectively. The moment factor obtained from Meyerhof et al.(1981) again gives closest agreement with author's values compared to other researchers.

9.5.2 PROTOTYPE MOMENT WITH EMBEDMENT RATIO

Values based on Terzaghi(1943), IRSIA(1950), Roscoe(1957) and UIC/ORE(1957), show no effect of pulling height. To avoid complications in comparisons with the author's values, the variation of moment values with embedment ratio L/D will be employed for all the range of pulling heights encountered in the experimental work. Attempts were made to compare moment factors as shown in Figure 9.15. However, no consistent trend was seen which produced difficulties in assessing the theories. An improved comparison is obtained by plotting the prototype moment at ground level against embedment ratio. Figure 9.16 to 9.20 show this comparison. Apparently, the UIC/ORE method gives fairly good agreement with author's moment values for the whole range of pulling heights. Roscoe's values for $\delta=0°$ and $\delta=20°$ are lower since the allowable moment values are produced. However close agreement with the author's

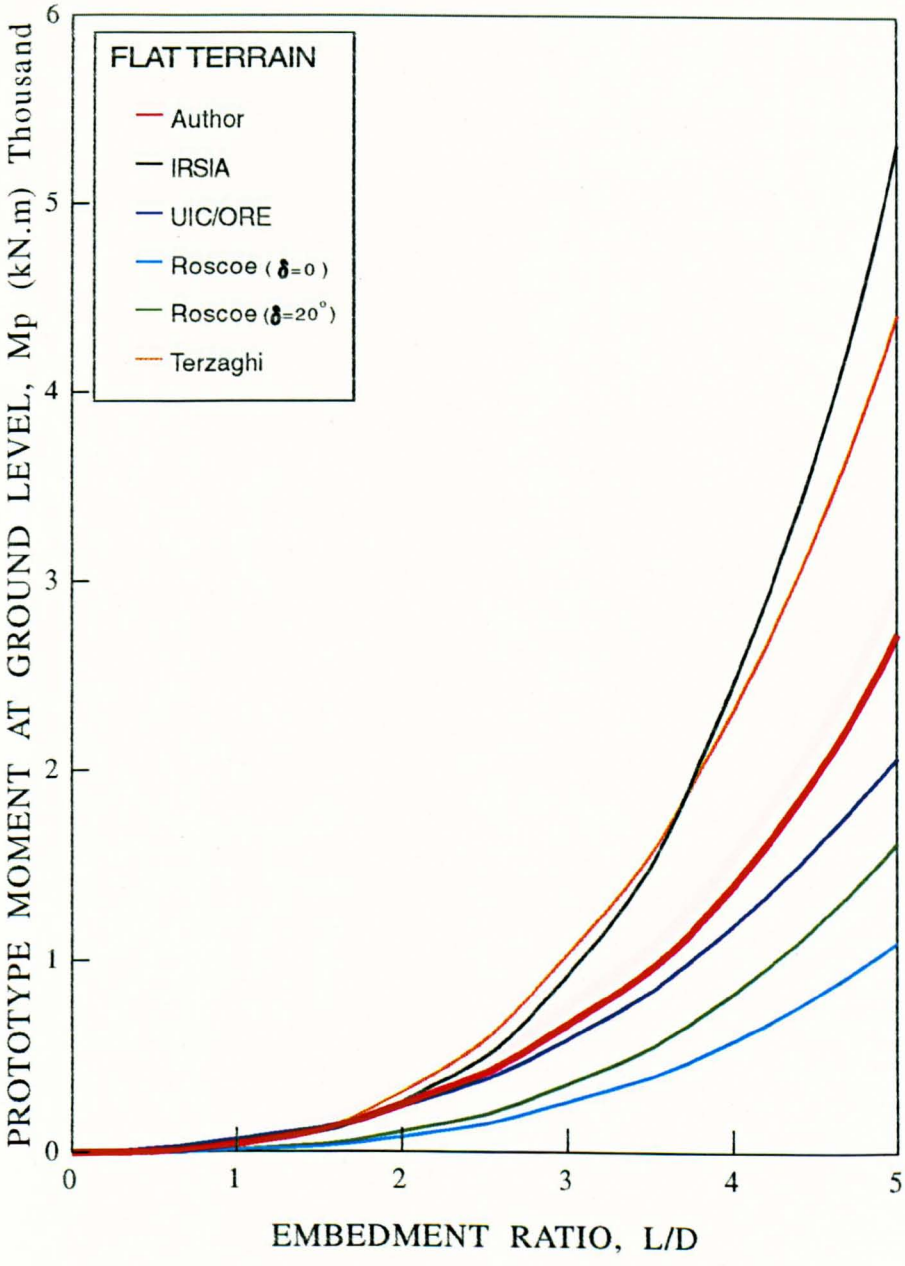

Figure 9.16 Variation of prototype moment at ground level with embedment ratio for 1m diameter single pile of e/L=1 in dense sand

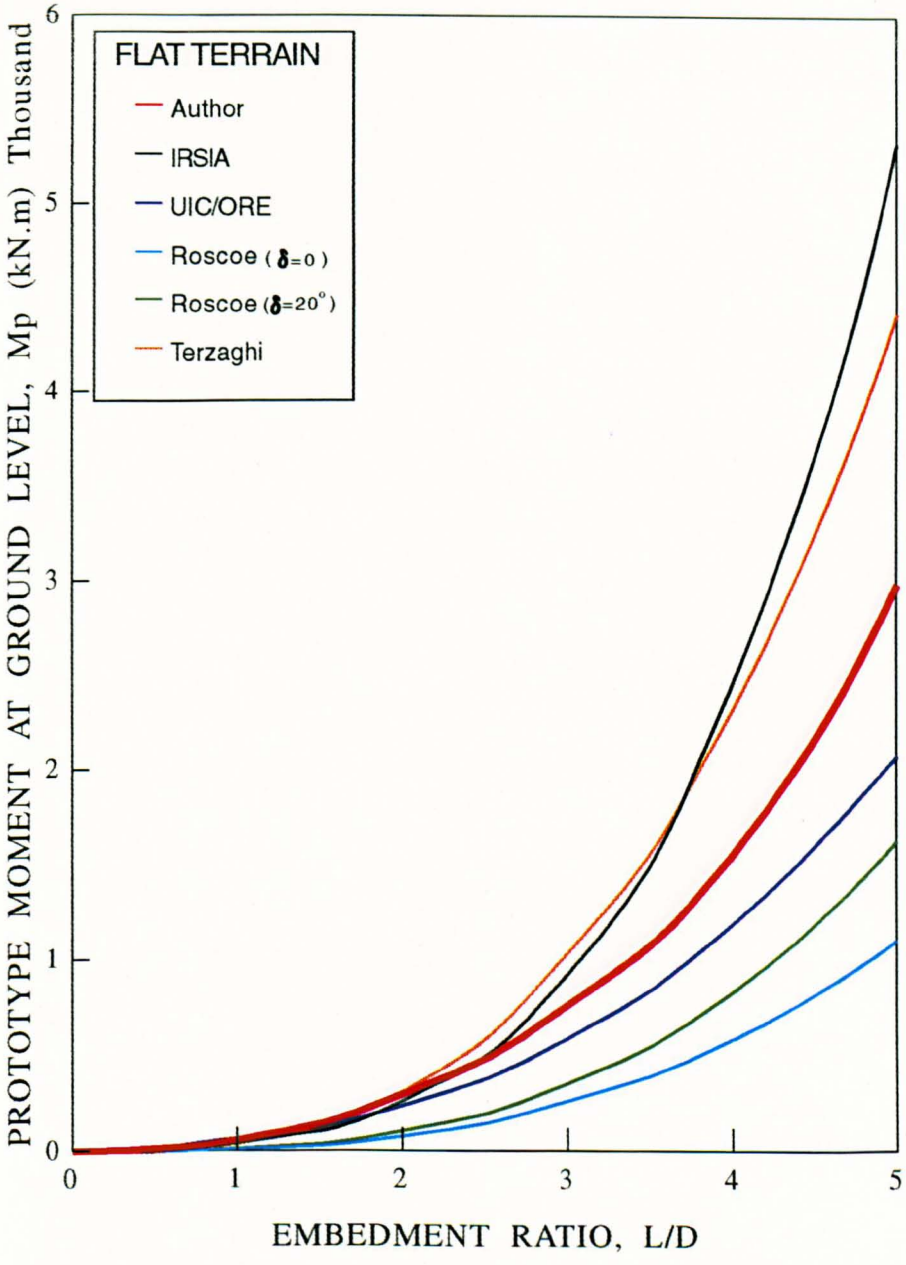

Figure 9.17 Variation of prototype moment at ground level with embedment ratio for 1m diameter single pile of e/L=2 in dense sand

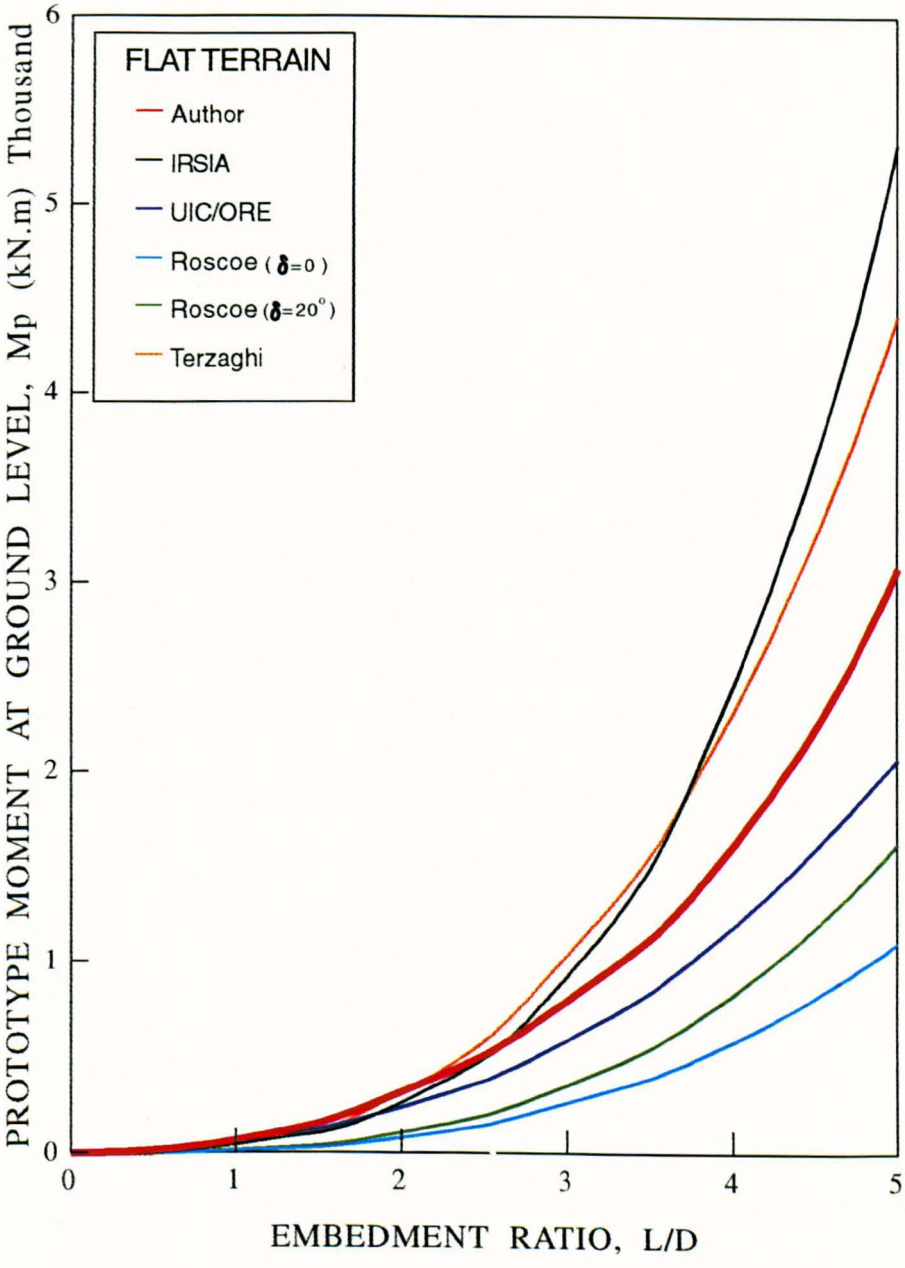

Figure 9.18 Variation of prototype moment at ground level with embedment ratio for 1m diameter single pile of e/L=3 in dense sand

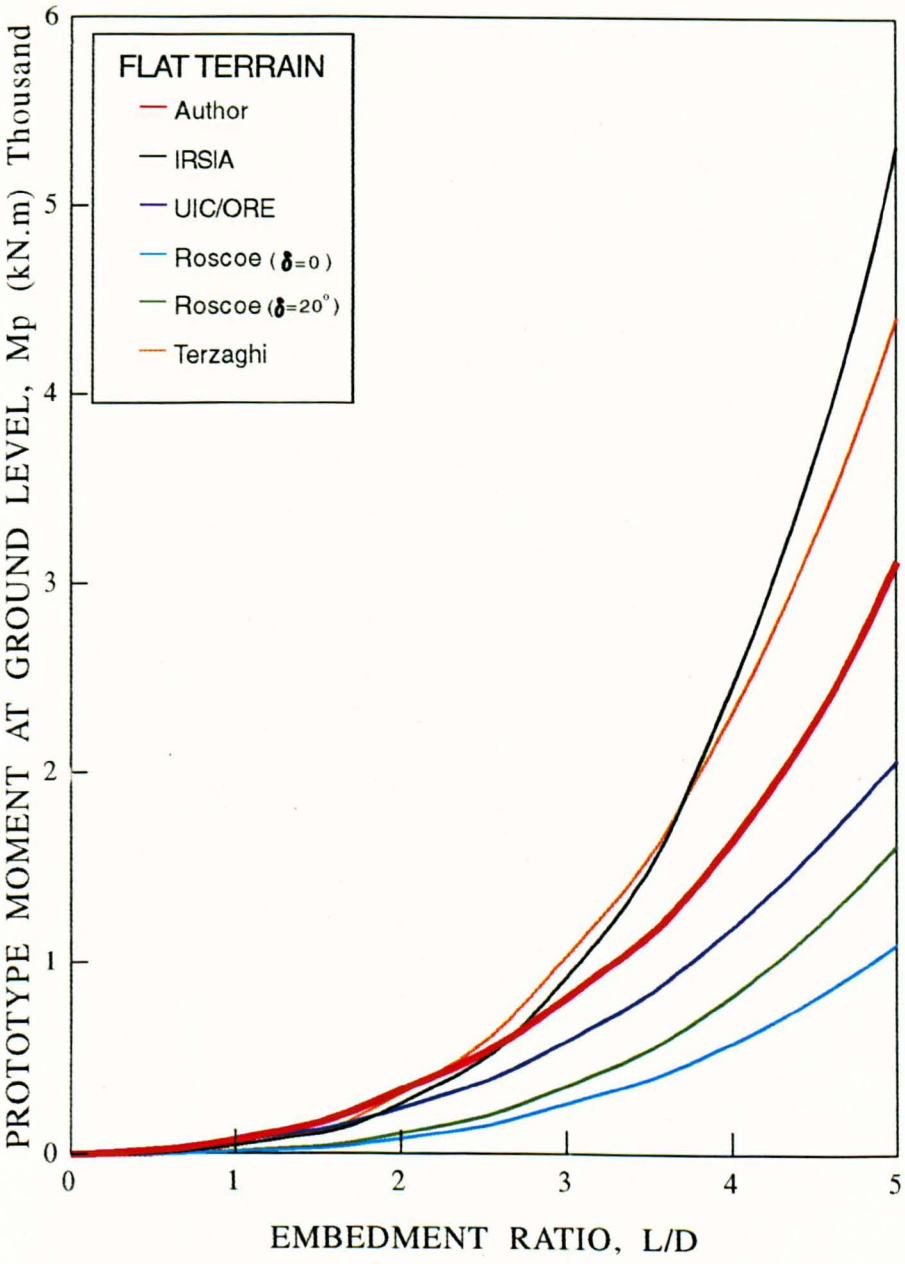

Figure 9.19 Variation of prototype moment at ground level with embedment ratio for 1m diameter single pile of e/L=4 in dense sand

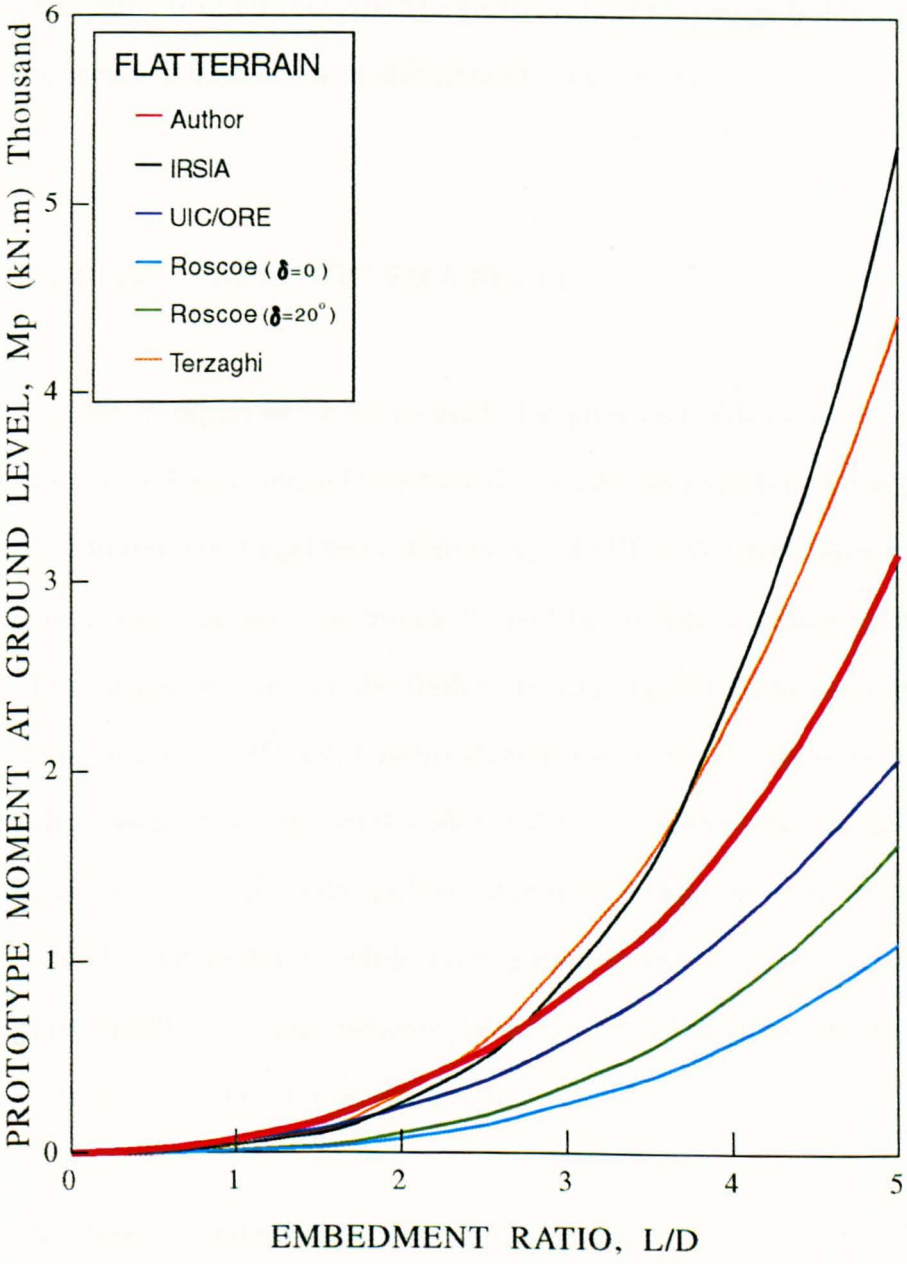

Figure 9.20 Variation of prototype moment at ground level with embedment ratio for 1m diameter single pile of e/L=5 in dense sand

values would result for a factor safety of 1.5 to 2. IRSIA together with Terzaghi give higher values compared to other theories. The IRSIA values were expected to be higher since they were obtained from small model tests at unit gravity.

9.6 PILE IN CLOSE PROXIMITY TO A SLOPE

No exhaustive comparison could be made for piles embedded close to a slope since limited tests were done using only a pile with embedment ratio L/D=4 and pulling height ratio e/L=3 in the centrifugal tests. Moreover, only UIC/ORE and Balfour Beatty produce recommendations for such conditions. While UIC/ORE gave a constant K value (see Table 3.3) to account for soil profile, Balfour Beatty suggest an increasing factor such that for slopes of 30° and 45°, pile lengths should be increased by factor of 1.25 and 1.43 respectively. However experimental evidence shows that the moment factor also varies with slope proximity. Also piles pulled away from a slope develop only 75% of their full mobilised moment factor while piles pulled towards a slope exhibit full moment carrying capacity at a slope distance ratio d/L of 1.5. For simplicity, as shown in Figure 9.21, an average slope factor was plotted.

Table 9.4 shows a comparison of the slope factors from previous work. Moment factors obtained a pile embedded in flat terrain should be multiplied by the slope factor at the design stage if a slope is to be constructed within the vicinity of the pile. Due to restriction of space in the centrifugal package, slope distance ratios greater than 1.5L could not be examined.

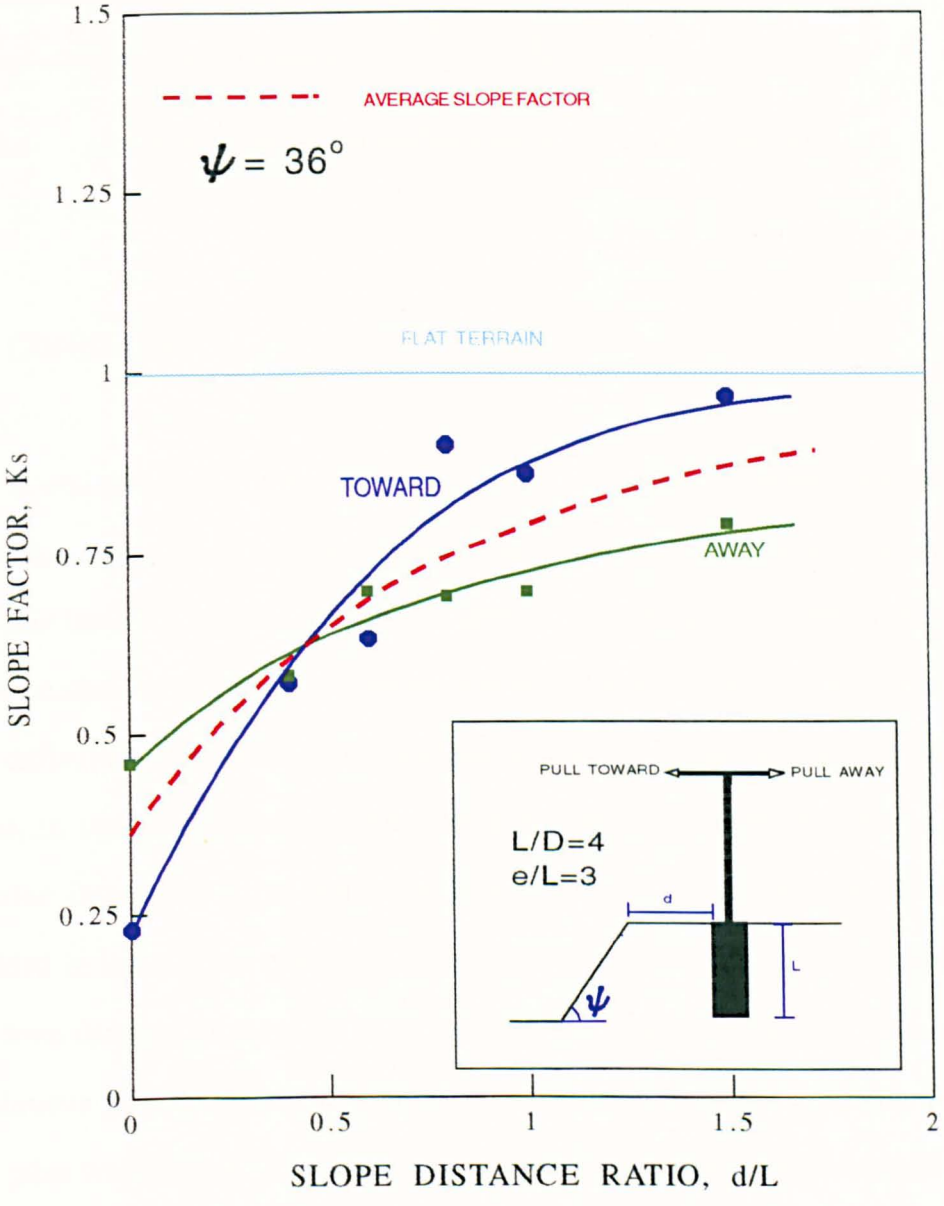

Figure 9.21 Variation of slope factor Ks for pile embedded within the slope proximity

d/L	Author (ψ=36°)	UIC/ORE (Towards)	UIC/ORE (Away)	B/Beatty (ψ=45°)	B/Beatty (ψ=30°)
0.5	0.6	0.95	0.85	1.43L	1.25L
1.0	0.8	1.0	1.0	1.43L	1.25L
1.5	0.9	1.0	1.0	1.0L	1.0L

Table 9.4 Factors for piles embedded within the slope proximity.

9.7 CONCLUSION

It was possible to develope convenient empirical relationships from the author's results. An empirical relationship was developed from two dimensional continuous model pile tests. To account for the pile geometry, an empirical moment shape factor was introduced. No empirical expression was established for pile in a loose packing, due to the difficulties in obtaining a consistent values due to non-homogeneity of the soil. Besides, in practice, such soil conditions are seldom encountered. Thus it is not of particular interest to this project to investigate in detail the behaviour of piles embedded in loose sand, except for comparison purposes in terms of soil unit weight. Apart from deriving moment carrying capacity of a single pile based on the analyses of a continuous pile, an alternative empirical expression from the centrifugal testing of single piles was derived. However no comparisons were made between this empirical expression and the existing theoretical values since in this research the author is mainly concerned with prediction of the behaviour in a three dimensional problem based on a plane strain condition together with a moment shape factor.

No overall agreement was found between the author's results and existing theories which include the effect of pulling height. Close agreement with previous exists theories for particular embedment ratios. Hence for lower embedment ratios such as L/D<2, Hansen(1961) and Broms(1964) give close agreement with the author's values. McCorkle(1969) also gives close agreement for lower embedment ratios. However since this is only an allowable moment value, overprediction of the ultimate values is likely. Meyerhof et al's.(1981) method using $\delta=0$ gives a close agreement with the author's expression for the higher embedment ratio of L/D>4. However the alternative approach(Meyerhof et al.(1988)) with $\delta=\phi/3$, the prototype moment factor tends to be conservative.

No rigid conclusion can be made in comparing the author's expression and that of Dickin and Wei(1991) due to the limited range of tests used in establishing their empirical expression. The final computation of moment factor values for single piles from the author's empirical expressions provide fairly good agreement with those formulae employing shape factors such as Meyerhof et al.(1981) and Broms(1964). Although simple in principle care must be taken in establishing the empirical moment shape factor, to ensure that sand and pile properties are similar in both continuous and single pile studies. However since the moment shape factor appears to be essentially independent of scale, values can be derived from simple conventional model tests for the corresponding soil unit weights. Values of moment factor for continuous and single piles differs from the author's expressions on average by 8% and between 3% to 20% respectively due to the approximations made in deriving the formulae and the scatter of the experimental data.

Slope factors were established to facilitate the design of piles embedded in proximity to a slope. The increasing effect of slope with closer slope distance ratio was confirmed. No further conclusion could be made since limited comparisons were performed with only one slope angle ψ used.

The author feels that the simplest way of predicting the prototype moment carrying capacity of a single short pile accurately is by employing a two dimensional solution in association with a moment shape factor. The centrifugal modelling technique further improves the accuracy of prediction by providing the stress level experienced by the prototype. Values from the author's empirical expression(Equation(9.6)) would be subjected to a safety factor since the ultimate moment value is derived from the calculation. The expression is limited to a dense packing and to piles with $L/D<6$. Although conventionally a safety factor of 2 is employed in the design stage, it can be reduced significantly if sound experimental apparatus is available.

CHAPTER TEN

GENERAL CONCLUSION

10.1 INTRODUCTION

Reese et al.(1974), Meyerhof et al.(1983,88) suggested that a semi-empirical approach offers the best way to solve the problems associated with laterally loaded piles in cohesionless soil. However since stress level has a significant influence on the behaviour of such soil, Neely et al.(1973), Ovesen(1979), Dickin and Leung(1983), Leung and Dickin(1984), Franke and Muth(1985), have shown that scaling errors do exist when results from conventional tests on small models are used to predict prototype behaviour. Closest physical modelling requires full or large scale testing which is obviously uneconomical and time consuming. Consequently only a limited number of tests are usually be performed. The centrifugal modelling technique has proved very useful in overcoming the model-prototype scaling effect and enables prototype behaviour to be simulated relatively cheaply.

10.2 GENERAL CONCLUSION ON THE RESEARCH PROJECT

Two dimensional model studies in a glass sided box show that the failure mechanism around a pile pulled at low level is similar to that postulated by Broms, in

that the soil resistance dominates. Active zones, although present, are small compared with the passive zones. 'Negative pressure' at the back of the pile as described by Broms is pronounced especially for the dense packing. This deviates from the soil wedge assumption made by Reese(1962), Reese et al.(1974) where soil moves as a mass in front of the pile without considering passive pressure at the back of it. A pile pulled at higher level exhibits a significant local rotational failure. The local rotational failure is more significant in the loose packing for both pulling heights. No passive plane or 'negative pressure' was observed at the back of the pile at failure.

Tests performed in the centrifuge and at unit gravity show that embedment length, pile diameter and soil density governed the limiting moment capacity of the pile. However pulling height also greatly affects the moment carrying capacity of the piles. Results obtained for L/D=5 in the dense sand packing tend to depart from the normal trend observed for shorter piles. It was suspected that pile with L/D=5 could no more to be considered as a short pile although Czerniak(1957), Broms(1964), McCorkle(1969) and Meyerhof et al.(1983) show that the value of L/D=5 still well within the rigid limit. No firm conclusion can be made since the testing of longer piles of 20mm diameter would need a larger space in the centrifuge carriage than is currently available.

As the internal friction angle ϕ varies with stress level as well as soil porosity, it is evident that earlier existing theories based on small scale unit gravity testing will involve a scaling error which would normally tend to overpredict the prototype values. This error would lead to potentially unstable design. Thus a higher safety factor is

needed which will inevitably lead to overdesign. Only a full scale test carried out on a specific site would justify the method. However this is quite difficult to implement. Thus for a safer and more economic means of predicting prototype behaviour based on small model tests, the study is best performed in the centrifuge.

Most of the available theories providing solutions for laterally loaded single piles are based on an extended two dimensional analysis of a wall. The solution for a wall, essentially experiencing plane strain conditions, is much easier than that for a three dimensional solution of a single pile. However theoretical predictions for a pile based on this method are quite problematical due to the fact that the value of internal friction angle based on plane strain is typically 10% higher than the triaxial equivalent. This point was taken into account only by Broms(1964) and Meyerhof et al.(1981). The author introduced an empirical moment shape factor in this project. The moment capacity of a single pile can be computed from calculations for a continuous pile which are factored by the moment shape factor. Although limited experiments were performed, there is strong evidence that this shape factor is independent of scale and pulling height. However the shape factor increases with an increase in embedment length, in contrast with Broms.

Empirical expressions developed by the author give slightly higher values than

observation. The difference varies from 3% to 20% depending on the embedment ratio. This effect is due to the approximations made in deriving overall empirical expressions for continuous piles and shape factors.

The empirical expression developed from the centrifugal tests was compared with existing theories. The appropriate shear strength of the soil was selected according to the pile embedment length, L/D. Results show that for lower embedment ratios, Broms'(1964) and Hansen's(1961) methods provide close agreement, for higher embedment ratios L/D>3, Broms and Meyerhof et al.(1981) give close agreement. Values calculated from the UIC/ORE formulae, which does not consider the effect of pulling height, show close agreement with the author's empirical equation(9.6). Values calculated from Roscoe((1957), McCorkle(1969) and Balfour Beatty(1986, 1988) generally give lower values since an allowable moment is calculated. However a close agreement could be attained if a safety factor of between 1.5 and 2 were to be used.

From the author's point of view, it was convenient to predict the moment at ground level for a single pile based on two dimensional analysis with the incorporation of a moment shape factor from extended testing. Moment shape factors could be developed for different soil types which would lead to a complete design chart or empirical relationship for a single pile base on two dimensional analysis.

10.3 SUGGESTION FOR FUTURE WORK

Further suggestions are put forward relating with this project.

1. A more appropriate replica of a typical prototype such as a concrete model should be used instead of one of mild steel as tested here.

2. Tests at embedment ratios greater than 5 are recommended to observe the critical depth for a short pile. This would require smaller diameter model piles to be tested at higher accelerations.

3. Various slope angles should used to obtain a wide range of slope factors to be employed with the empirical expression for flat terrain.

4. Tests on piles with the pulling arm and pile as single unit are recommended to avoid potential weakness at the top of the pile.

5. Further experimental work should be carried out on continuous piles to obtain a wide range of shape factors in various soil packings to enable a more comprehensive empirical relationship for a single pile to be developed.

REFERENCES

Abendroth, R.E and Greimann, L.F (1990)

"Pile behaviour established from model test", Journal of Geotechnical Engineering, Proc. of the ASCE, No.4, Vol.116, pp 571-588.

Avgherinos, P.J and Schofield, A.N (1969)

"Drawdown failures of Centrifuge Models", Proc. of the 7th. ICSMFE Mexico, Vol.2, pp 497-505.

Balfour Beatty Const. Ltd (1986)

"Report on foundation design for overhead catenary system", Tuen Mun LRT Interim report, BBPCL.

Balfour Beatty Construction Ltd. (1988)

"Report on design calculation of ORE foundation design method".

Banerjee, P.K and Davies, T.J (1978)

"The behaviour of axially and laterally loaded single piles embedded in non-homogeneous soils", GEOTECHNIQUE, The Institution of Civil Engineers, London, Vol. 28, pp 309-326.

Bassett, R.H and Horner, J (1979)

"Prototype deformations from centrifugal model tests", Design parameters in Geotechnical Engineering, BGS London, Vol.2, pp 1-9.

Bassett, R.H and Craig, W.H (1988)

"The development of geotechnical centrifuge in U.K 1965-1985", Centrifuges in Soil Mechanics - ed. Craig, W.H, James, R.G and Schofield, A.N. Balkema, Rotterdam, pp 35-60.

Bishop, A.W (1958)

"Test requirements for measuring the coefficient of earth pressure at rest", Proc. Conf. Earth Pressure, Vol.I, Brussels.

Bloomquist, D.G, Davidson, J.L and Townsend, F.C (1984)

"Platform orientation and start-up time during centrifuge testing", Geotechnical Testing Journal, No.4, Vol.7, pp 195-199.

Broms, B.B (1964)

"Lateral resistance of piles in cohesionless soils", Journal of Soil Mechanics and Foundation Division, Proc. of the ASCE, No. SM3, Vol.90, pp 79-99.

Broms, B.B (1981)

"Precast piling practice", Thomas Telford Ltd. London, pp 68-79.

Broms, B.B (1965)

"Design of laterally loaded piles", Journal of the Soil Mechanics and Foundations Division, Proc. of the ASCE, No. SM3, Vol.91, pp 79-99.

BS 1377 (1975)

"Method of testing soils for Civil Engineering purposes", British Standard Institution, London.

Bucky, P.B, Solakian, A.G, Baldin, L.S (1935)

"Centrifugal method of testing models", Civil Engineering, Vol.5, pp 287-290.

Caquot, A and Kerisel, J (1948)

"Tables for the calculation of passive pressure, active pressure and bearing capacity of foundations", Gauthier-Villars, Paris.

Czerniak, E, (1957)

"Resistance to overturning of single short piles", Journal of Structural Division, Proc. of the ASCE, No. ST2, Vol. 83, pp 1-25.

Chari, T.R and Meyerhof, G.G (1983)

"Ultimate capacity of rigid single piles under inclined loads in sand", Canadian Geotechnical Journal, Vol.20, pp 849-854.

Christensen, N.H (1961)

"Model tests with transversally loaded rigid piles in sand", The Danish Geotechnical Institute, Bulletin No.12, Copenhagen, pp 10-16

Civil Engineering Code of Practice (1951)

No.2 "Earth retaining structures", Institute of Structural Engineers, London.

Cook, D and Lewis, R.T (1980)

"Discussion: The use of physical models in design", Pro. 7th. European Conference on Soil Mechanics and Foundation Engineering, Brighton, Vol.14, pp 349-353.

Craig, W.H,(1983)

"Simulation of foundations for offshore structure using centrifuge modelling", Development in Soil Mechanics and Foundation Engineering, Model Studies: ed.Banerjee, P.K and Butterfield, R, Vol.1, pp. 1-25

Craig, W.H, (1985)

"Modelling pile installation in centrifuge experiments", Proc. of the 11th. ICSMFE San Francisco, Vol.2, pp 1101-1104.

Craig, W.H, (1985)

"Installation studies for model piles", Proc. Symposium on application of centrifuge modelling to geotechnical design, University of Manchester, pp. 440-445.

Craig, W.H (1988)

"Introduction to geotechnical centrifuge modelling principles", Centrifuges in Soil Mechanics - ed. Craig, W.H, James, R.G and Schofield, A.N. Balkema, Rotterdam, pp 1-8

Craig, W.H, (1989)

"The use of Centrifuge in Geotechnical Engineering Education", Geotechnical Testing Journal, No.4, Vol.12, pp 288-291.

Davisson, M.T and Sally, J.R (1970)

"Model study of laterally loaded piles", Journal of the Soil Mechanics and Foundation Division, Proc. of the ASCE, No. SM5, Vol.96, pp 1605-1627.

Dembicki, E, Odrobinski, W and Cichy, W (1977)

"Stabilité Des Fondations Des Poteaux, Soumis A Des Moments", Annales de L'institut technique du Batiment et des Travaux Publics.(In France).

Desta, M, (1992)

"Moment carrying capacity of laterally loaded short pile foundation in sand", MSc.(Eng) Dissertation, University of Liverpool.

Dickin, E.A (1973)

"Influence of grain shape and size upon the limiting porosities of sands", Evaluation of relative density and its role in geotechnical projects involving cohesionless soils, American Society of Testing Materials, pp. 113-120.

Dickin, E.A and King, G.J.W (1982)

"The behaviour of hyperbolic stress-strain models in triaxial and plane strain compression", International Symposium on Numerical Models in Geomechanics, Zurich - ed. Dungar, R, Pande, G.N and Studer, J.A, Numerical models in Geomechanics, Balkema, Rotterdam, pp 303-312.

Dickin, E.A and Leung, C.F (1983)

"Centrifugal model tests on vertical anchor plates", Journal of Geotechnical Engineering, Proc. of the ASCE, No.GT12, Vol.109, pp 1503-1525.

Dickin, E.A and Leung, C.F(1985)

"Evaluation of design methods for vertical anchor plates", Journal of Geotechnical Engineering, Proc. of the ASCE, No.4, Vol.111, pp 500-520.

Dickin, E.A and Leung, C.F (1990)

"Performance of piles with enlarged bases in sand", Canadian Geotechnical Journal, No.5, Vol.27, pp 546-556

Dickin, E.A and Leung, C.F (1992)

"The influence of foundation geometry on the uplift behaviour of piles with enlarged bases in sand", Canadian Geotechnical Journal, No.3, Vol.29, pp 498-505.

Dickin, E.A and Nazir, R (1992)

"Overturning resistance of short piled foundations in sand", GEOTROPIKA '92, International Conference on Geotechnical Engineering, Malaysia.

Dickin, E.A and Nazir, R (1993)

"Centrifugal modelling of side-bearing foundations in sand", Dept. of Civil Engineering, University of Liverpool, Report No. CE/26/93.

Dickin E.A and Nazir, R (1994)

"Appraisal of design methods for laterally loaded short piles in sand", Accepted for GEOTROPIKA '94, International Conference on Geotechnical Engineering, Malaysia.

Dickin, E.A and Nazir,R (1994)

"Geometric factors influencing the behaviour of side-bearing foundations in sand", Accepted for International Conference Centrifuge '94, Singapore.

Dickin, E.A and Wei, M.J (1991)

"Moment carrying capacity of short piles in sand", Centrifuge 91, Proc. International Conference Geotechnical Centrifuge Modelling, Paris, Balkema, Rotterdam.

Duncan, J.M and Chang, C.Y (1970)

"Nonlinear analysis of stress and strain in soils", Journal of the Soil Mechanics and Foundations Division, Proc. of the ASCE, No. SM5, Vol.96, pp 1629-1653.

Fordham, A.A (1944)

"The lateral pressure of earth against footing subject to overturning moment", The Structural Engineer, London, England, No.22, pp 297-308.

Franke, E and Muth, G (1985)

"Scale effect in 1-g model tests on horizontally loaded piles", Proc. of the 11th. ICSMFE San Francisco, Vol.2, pp 1011-1014.

Fuglsang, L.D and Ovesen, N.K (1988)

"The application of the theory of modelling to centrifuge studies", Centrifuge in Soil Mechanics - ed. Craig, W.H, James, R.G and Schofield, A.N, Balkema, Rotterdam, pp 119-138

Fulthorpe, J.N (1986)

"The response of vertical piles to lateral loading and moment", Ph.D Thesis, University of Liverpool.

Gabr, M.A and Borden, R.H (1990)

"Laterally analysis of piers constructed on slopes", Journal of Geotechnical Engineering, Proc. of the ASCE, No.12, Vol.116, pp 1831-1850.

Georgiadis, M and Butterfield, R (1982)

"Laterally loaded pile behaviour", Journal of the Geotechnical Engineering Division, Proc. of the ASCE, No. GT1, Vol.108, pp 155-165.

Georgiadis, M, Anagnostopoulos, C and Saflekou, S (1991)

"Centrifugal testing of laterally loaded piles in sand", Canadian Geotechnical Journal, No.2, Vol.29, pp 208-216.

Glesser, S.M (1984)

"Generalised behaviour of laterally loaded vertical piles", Laterally loaded deep foundations: Analysis and performance, ASTM STP835 - ed. Langer, J.A, Mosley, E.T and Thompson, C.D, American Society for Testing and Materials, pp 72-96.

Hansen, J.B (1961)

"The ultimate resistance of rigid piles against transversal forces", The Danish Geotechnical Institute, Bulletin No.12, Copenhagen, pp 1-9

Hoadley, P.J, Barton, Y.O and Parry, R.H.G (1981)

"Cyclic lateral load on model pile in a centrifuge", Proc. of the 10th. ICSMFE, Vol.1, pp 621-625.

IRSIA (1950)

Report of research of IRSIA, No.2, Ramelot and Vandeperre.

Jewel, R.A (1989)

"Direct shear test on sand", GEOTECHNIQUE, The Institution of Civil Engineers, London, No.2, Vol.39, pp 309-322.

Johnson, W.C (1944)

"Mathematical and physical principles of engineering analysis", Mc Graw Hill Book Company Inc. New York and London.

King, G.J.W and Fulthorpe, J.N (1986)

"Centrifuge model tests on laterally loaded single piles", Proc. 3rd Indian Conference on Ocean Engineering, Bombay, pp BB1-BB11.

King, G.J.W, Dickin, E.A and Lyndon, A (1984)

"The development of a medium size centrifugal testing facility", Symposium of applications of Centrifuge Modelling in geotechnical design", Manchester, pp 25-46.

Ko, H.Y (1988)

"Summary of the state-of-the-art in centrifuge model testing"; Centrifuge 88, Proc. International Conference Geotechnical Centrifuge Modelling, Paris, Balkema, Rotterdam.

Kolbuszewski, J.J (1948)

"An experimental study of the maximum and minimum porosities of sand", Proc. of the 2nd. ICSMFE, Rotterdam, Vol.1, pp 158-165

Krey, H (1936)

Erddruck, Erdwiderstand und Tragfähigkeit des Baugrundes, 5th. ed. Berlin, pp 207-210.

Kubo, K (1965)

"Experimental study of the behaviour of laterally loaded piles", Proc. of the 6th. ICSMFE, Montreal, Vol.2, pp 275-279.

Kueh, G.C, (1989)

"The design of foundation subjected to large moments", MSc.(Eng) Dissertation, University of Liverpool.

Kulkarni, K.R, Chandrasekaran, V.S and King, G.J.W (1985)

"Centrifugal model studies on laterally loaded pile groups in sand", Proc. of the 11th, ICSMFE, San Francisco.

Laman, M

In preparation for Ph.D Thesis, University of Liverpool.

Langhaar, H.L (1951)

"Dimensional analysis and theory of models", John Wiley and Sons Inc. New York.

Leung, C.F (1981)

"The effect of shape, size and embedment on the load displacement behaviour of vertical anchor in sand", Ph.D Thesis, University of Liverpool.

Leung, C.F and Dickin, E.A (1984)

"Scale error of conventional model test", Proc. Int. Symposium on Geotechnical Centrifuge Model Testing, Japanese Soc. for Soil Mechanic and Foundation Engineering, pp 133-138.

Leung, C.F and Dickin, E.A (1991)

"Uplift capacity of foundations", Recent Advances in Geotechnical Engineering III, Singapore, pp 20-24.

Liem, D.H.W (1988)

"Appraisal of Lade's elasto-plastic soil models and their application to vertical anchor in sand", Ph.D Thesis, University of Liverpool.

Lyndon, A and Pearson, R.A (1988)

"Skin friction effects on laterally loaded large diameter piles in sand", Centrifuge 88 -ed. Corté, J.F, Balkema, Rotterdam, pp 363-369.

Lyndon, A, Turner, N.G and Wei, M.J(1991)

"Centrifugal modelling of stress-reducing piled foundations on sand", Proc. Int. Conf. on Piling and Deep foundations, ed. Deep Foundations Institute, Balkema, Rotterdam, pp 611-616

Matlock, H and Reese, L.C (1960)

"Generalised solutions for laterally loaded piles", Journal of the Soil Mechanics and Foundation Division, Proc. of the ASCE, No. SM5, Vol.86, pp 63-91.

McCorkle, B.L (1969)

"Side-bearing pier foundations", Civil Engineering - Proc. of the ASCE, pp 65-66.

Mc Nutty, J.F (1956)

"Thrust loading on piles", Journal of Soil Mechanics and Foundations Division, Proc. of the ASCE, No. SM2, Vol.82, pp 940-965.

Meyerhof, G.G (1979)

"Pile foundations with special reference to bridges" Proc. Seminar on the International Association for Bridge and Structural Engineering, Madras, Vol.1, pp. 1-16.

Meyerhof, G.G, Mathur, S.K and Valsangkar A.J (1981)

"Lateral resistance and deflection of rigid walls and piles in layered soils", Canadian Geotechnical Journal, Vol. 18, pp. 159-170.

Meyerhof, G.G, Yalcin, A.S and Mathur, S.K (1983)

"Ultimate pile capacity for eccentric incline load", Journal of Geotechnical Engineering Division, Proc. of the ASCE, Vol. 109, pp 408-423.

Meyerhof, G.G, Sastry, V.V.R.N and Yalcin, A.S (1988)

"Lateral resistance and deflection of flexible piles", Canadian Geotechnical Journal, Vol.25, pp 511-521.

Morgenstern, N.R and Einsenstein, Z (1970)

"Methods of estimating lateral loads and deformation", Lateral stresses in the ground and design of earth retaining structures: Soil Mechanics and Foundation Division, Proc. of the ASCE - Special Conference, pp 51-97.

Mueller-Breslau, H.F.B (1906)

"Erddruck Aut Stuetzmauern"

Alfred-Kroner-Verlag, Stuttgart, 2nd. Ed. 1947

Neely, W.J, Stuart, J.G and Graham, J (1973)

"Failure loads of vertical anchor plates in sand", Journal of Soil Mechanics and Foundation Div., Proc. of the ASCE, No. SM9, Vol.99, pp 669-685.

Oldham, D.C.E (1984)

"Experiments with lateral loading on single piles in sand", Proc. Symposium on application of centrifuge modelling to Geotechnical Design, University of Manchester, pp 122-142.

Ovesen, N.K (1979)

"The use of physical models in design: the scaling law relationship", Proc. 7th. European Conference Soil Mechanics and Foundation Engineering, Brighton, Vol.4, pp. 318-323.

Palmer, L.A and Thompson, J.B (1948)

"The earth pressure and deflection along the embedded length of piles subjected to lateral thrust", Proc. of the 2nd. ICSMFE Rotterdam, Vol.5, pp 156-161.

Pise, P.J (1984)

"Lateral response of free-head pile", Journal of Geotechnical Engineering, Proc. of the ASCE, No.12, Vol.110, pp 1805-1809.

Pokrovsky , G.Y and Fedorov, I.S (1936)

"Studies of soil pressures and soil deformations by means of a centrifuge". Proc. of the 1st. ICSMFE, Harvard University, Vol.1, pp 70.

Poulos, H.G (1971)

"Behaviour of laterally loaded piles: I. Single piles", Journal of Soil Mechanics and Foundations Division, Proc. of the ASCE, No. SM5, Vol. 97, pp 711-731.

Poulos, H.G (1973)

"Analysis of piles in soil undergoing lateral movement", Journal of Soil Mechanics and Foundations Division, Proc. of the ASCE, No. SM5, Vol.99, pp 391-407.

Poulos, H.G and Davis, E.H (1980)

"Pile foundation analysis and design", John Wiley and Son Inc. New York.

Pyke, R and Beikae, M (1984)

"A new solutions for the resistance of single piles to lateral loading", Laterally loaded deep foundations: Analysis and performance, ASTM STP835 -ed. Langer, J.A, Mosley, E.T and Thompson, C.D, American Society for Testing Materials, pp 497-505.

Raes, P.E (1936)

"Theory of lateral bearing capacity of piles", Proc. of the 1st ICSMFE Harvard University, Vol.3, pp 166-169.

Reese, L.C (1962)

"Ultimate resistance against a rigid cylinder moving laterally in a cohesionless soil", Journal society of Petroleum Engineers, pp 355-359.

Reese, L.C and Desai, C.S (1977)

"Laterally loaded pile", Numerical methods in Geotechnical Engineering -ed. Desai, C.S and John, T.C, Mc Graw Hill Book Company, London and New York.

Reese, L.C and Grubbs, B.R (1974)

"Field testing of laterally loaded piles in sand", Proc. of the 6th. Offshore Tech. Conf. Houston, Paper OTC 2079, pp 459-472.

Reese, L.C, Cox, W.R and Koop, F.D (1974)

"Analysis of laterally loaded piles in sand", Proc. of the 6th. Offshore Tech. Conf. Houston, Paper OTC 2080, pp 473-483.

Roscoe, K.H (1957)

"A comparison of tied and free pier foundations", Proc. of the 4th. ICSMFE London, Vol.1, pp 419-423.

Roscoe, K.H and Schofield, A.N (1956)

"The stability of short pier foundations in sand", Symposium on the Plastic Theory of Structures, Cambridge, British Welding Journal, No.8, Vol.3, pp 343-354.

Rowe, P.W (1969)

"Progressive failure and strength of a sand mass", Proc. of the 7th. ICSMFE, Mexico, Vol.1, pp 341-349.

Rowe, P.W (1956)

"The single pile subject to horizontal force", GEOTECHNIQUE, The Institution of Civil Engineers, London, No.2, Vol.6, pp 70-85.

Santamarina, J.C and Goodings, D.J (1989)

"Centrifuge modelling: A study of similarity", Geotechnical Testing Journal, GTJODJ, No.2, Vol.12, pp 163-166.

Schofield, A.N (1980)

"Cambridge Geotechnical Centrifuge operations", GEOTECHNIQUE, The Institution of Civil Engineers, London, No.4, Vol.30, pp 227-268.

Schofield, A.N (1988)

"An introduction to centrifuge modelling", Centrifuge in Soil Mechanics - ed. Craig, W.H, James, R.G and Schofield, A.N, Balkema, Rotterdam, pp 1-9.

Scott, R.F (1981)

"Pile testing in centrifuge", Proc of the 10th. ICSMFE Stockholm, Vol.2, pp 839-842.

Shilts, W.L, Graves, L.D and Driscoll, C.G (1948)

"A report of field and laboratory tests on the stability of posts against lateral load", Proc. of the 2nd. ICSMFE Rotterdam, Vol.5, pp 107-112.

Smith, G.N (1982)

"Element of Soil Mechanics", Granada Publishing.

Smith, D (1965)

"The influence on particle shape on the limiting porosities and shear strength of sand", M.E Thesis, University of Liverpool.

Smith, J.E (1962)

"Deadman anchorages in sand", Technical report, R199, United States Naval Civil Engineering Laboratory.

Sokolovski, V.V (1965)

"Statics of soil media", Butterworths Scientific Publications, London.

Spillers, W.R and Stoll, R.D (1964)

"Lateral response of piles", Journal of Soil Mechanics and Foundations Division, Proc. of the ASCE, No. SM6, Vol.90, pp 1-9.

Steenfelt, J.S (1989)

"Centrifuge modelling and limit analysis - Reciprocity or adversity?", Proc. of the 12th. ICSMFE Rio de Janerio, Vol.2, pp 987-990.

Stroud, K.A (1982)

"Engineering Mathematics", The Macmillan Press Ltd. London.

Tang, Y.K (1979)

"Stress-strain modelling of dense sand in triaxial and plane strain compression", M.Eng. thesis, University of Liverpool.

Terashi, M, Kitazume, M and Kawabata, K (1989)

"Centrifuge modelling of a laterally loaded pile", Proc of the 12th. ICSMFE Rio de Jenerio, Vol.2, pp 991-994.

Terzaghi, K (1943)

"Theoretical Soil Mechanics", John Wiley and Sons, New York.

Terzaghi, K (1955)

"The evaluation of coefficients of subgrade reaction", GEOTECHNIQUE, The Institution of Civil Engineers, London, No.3, Vol.5, pp 297-326.

Ting, J.M (1987)

"Full-scale cyclic dynamic lateral load responses", Journal of Geotechnical Engineering, Proc. of the ASCE, No.1, Vol.113, pp 30-45.

Tomlinson, M.J (1986)

"Foundation design and construction - 5th.ed.", John Wiley and Sons Inc. New York.

Tschebotarioff, G.P (1962)

"Retaining structures", Foundation Engineering ed. Leornards, G.A, McGraw-Hill, New York, pp. 438-524.

UIC/ORE (1957)

"Calculation of catenary masts and foundations", Interim report No.1, International Union of Railways/Office for Research and Experiments, Utrecth.

Vallabhan, C.V.G and Alikhanlou, F (1982)

"Short rigid piers in clay", Journal of the Geotechnical Engineering Division, Proc. of the ASCE, No. GT10, Vol.108, pp 1255-1271.

William, D.J and Parry, R.H.G (1979)

"Model pile tests in dense normally consolidated sand", Offshore Structures: The use of physical models in their design, ed. Armer, G.S.T and Garas, F.K, The Construction Press Ltd. pp 281-287.

Woodward, R.J, Gardner, W.S and Greer, D.M (1972)

"Drilled pier foundations", Mc Graw Hill Book Company, London and New York.

Yukio, Y (1986)

"Prediction of horizontal behaviour of pier foundations", Proc. of the International Symposium on Computer and Physical Modelling in Geotechnical Engineering, Bangkok, pp 149-159.

APPENDIX A

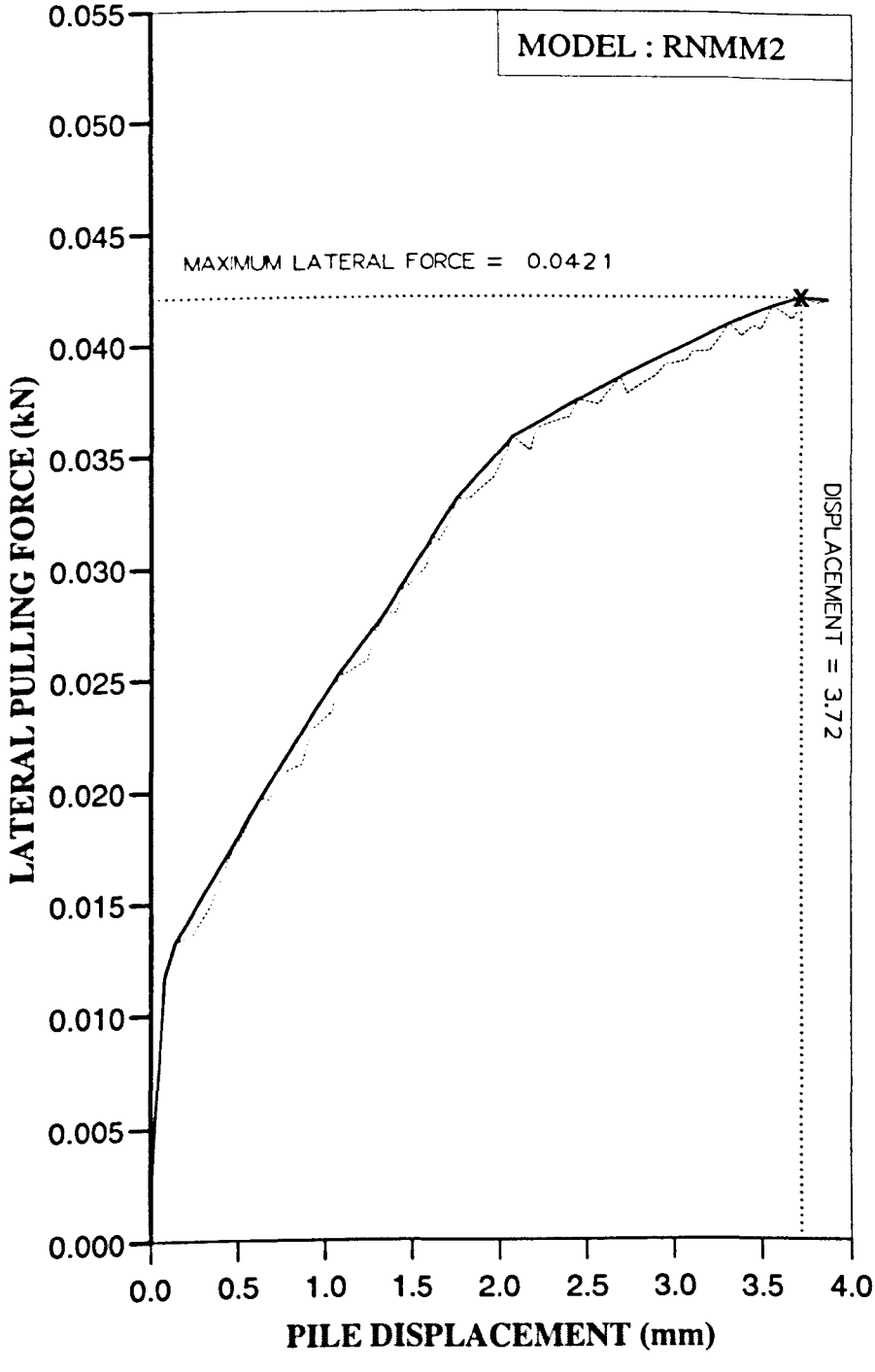

Figure AL1 Variation of lateral force with displacement at ground level for Series 1 test.

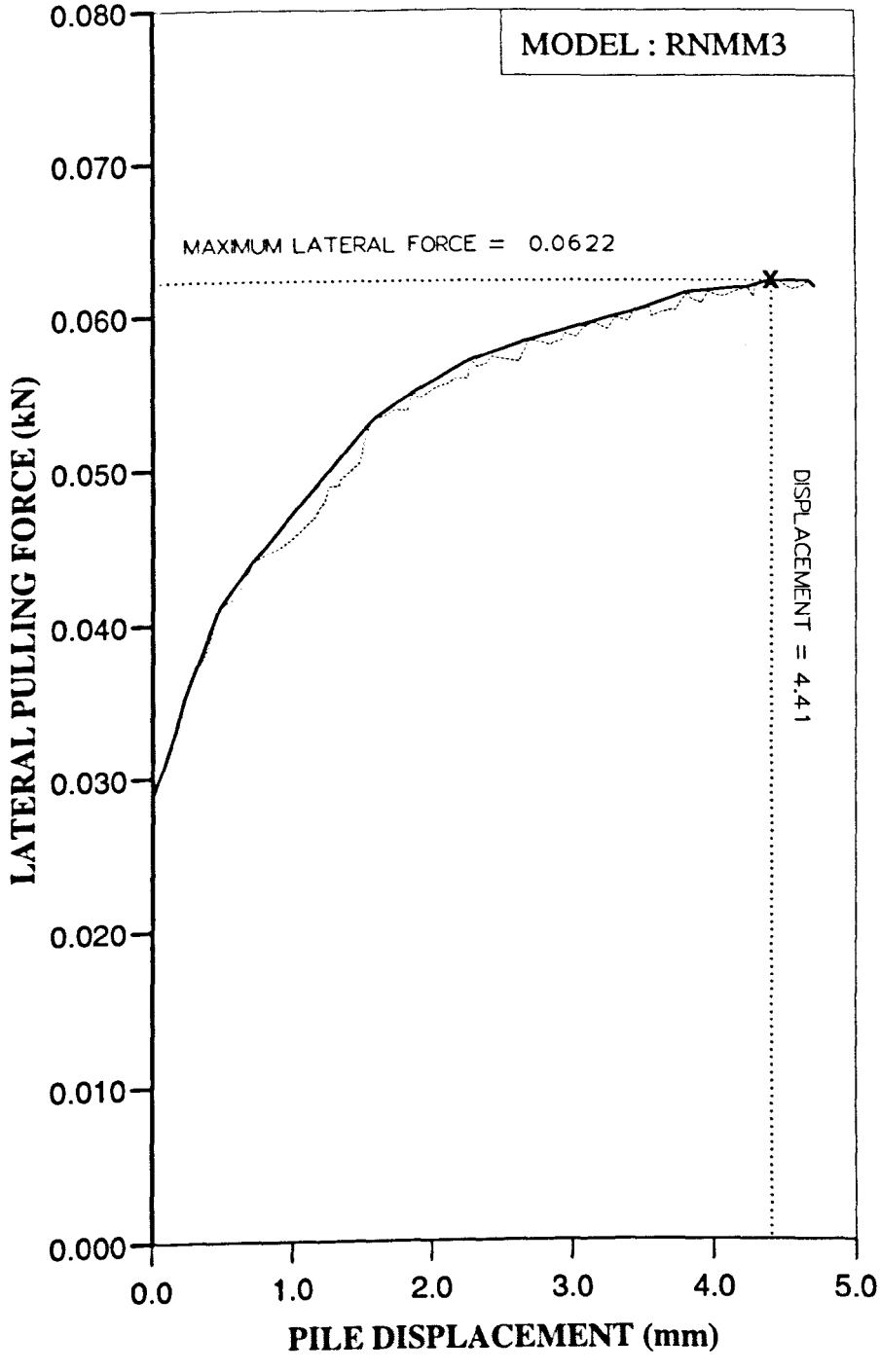

Figure AL2 Variation of lateral force with displacement at ground level for Series 1 test.

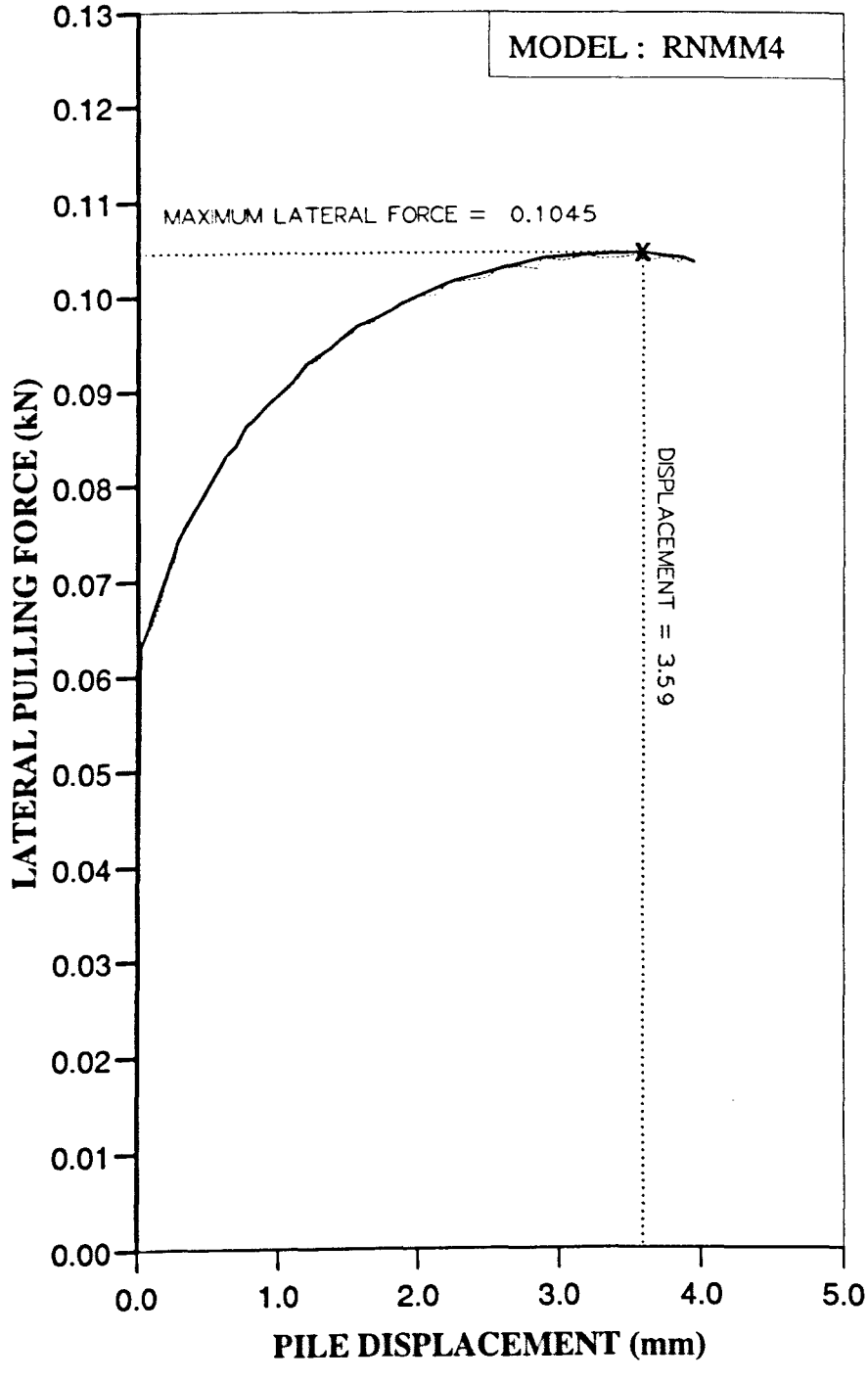

Figure AL3 Variation of lateral force with displacement at ground level for Series 1 test.

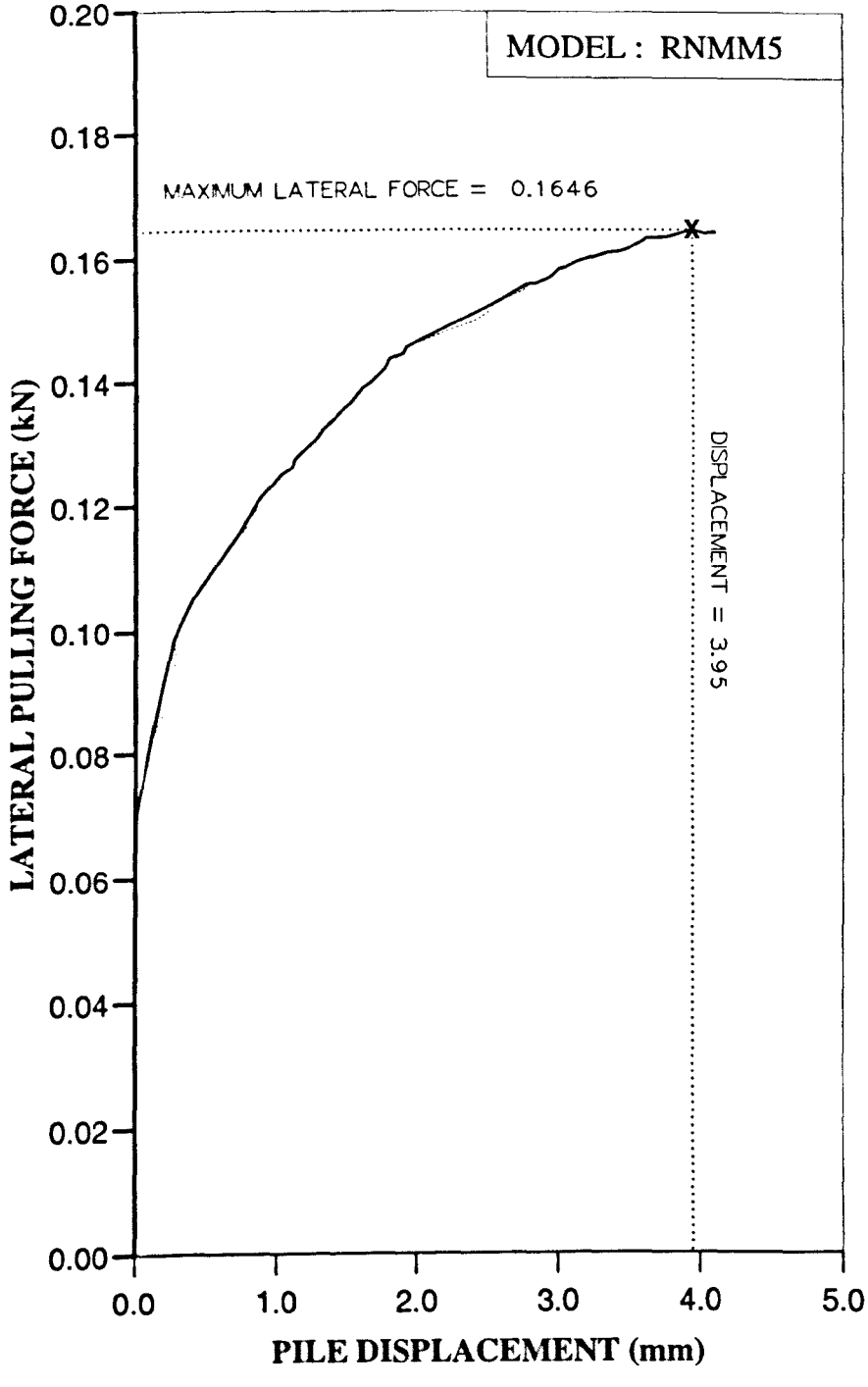

Figure AL4 Variation of lateral force with displacement at ground level for Series 1 test.

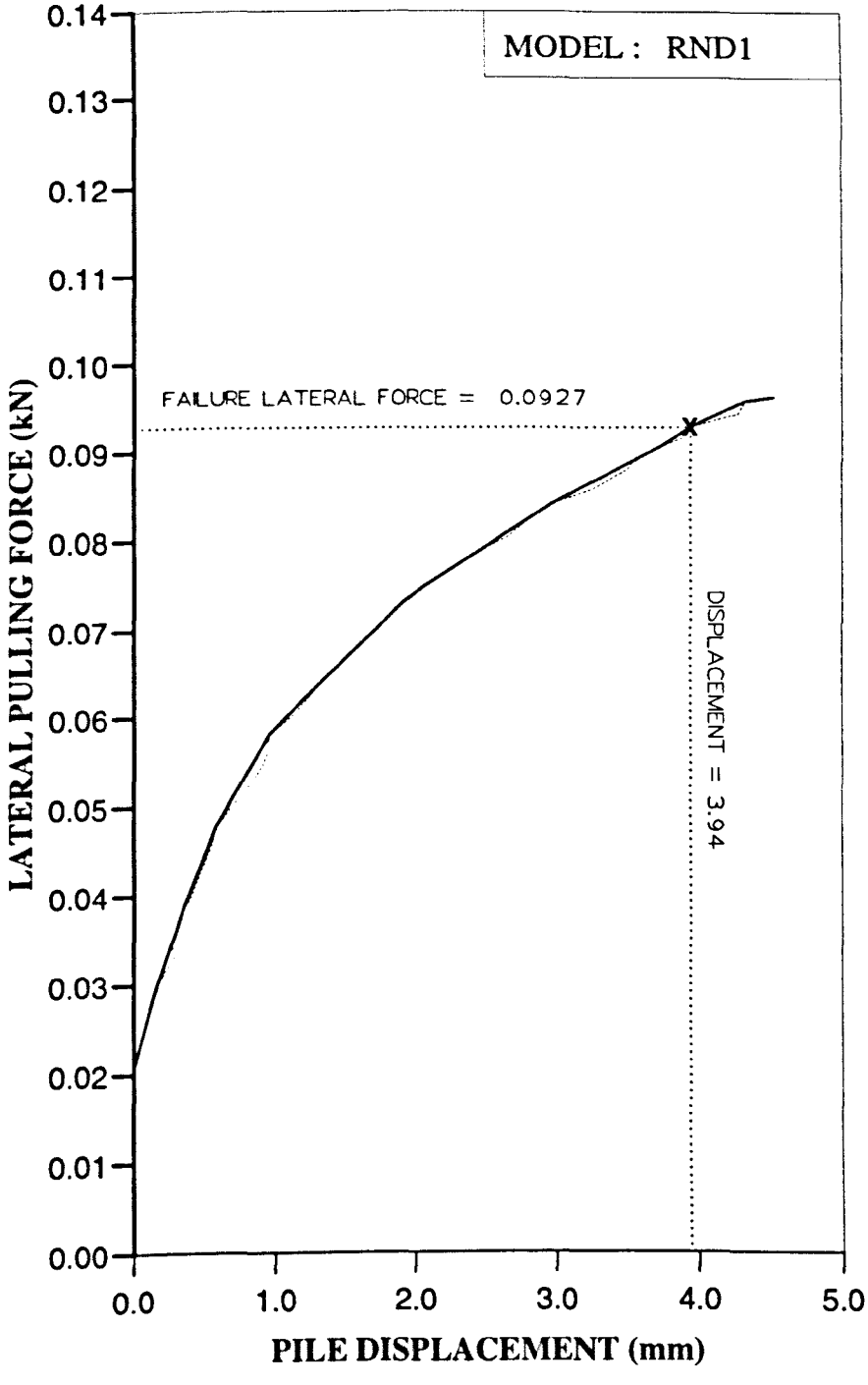

Figure AL5 Variation of lateral force with displacement at ground level for Series 2 test.

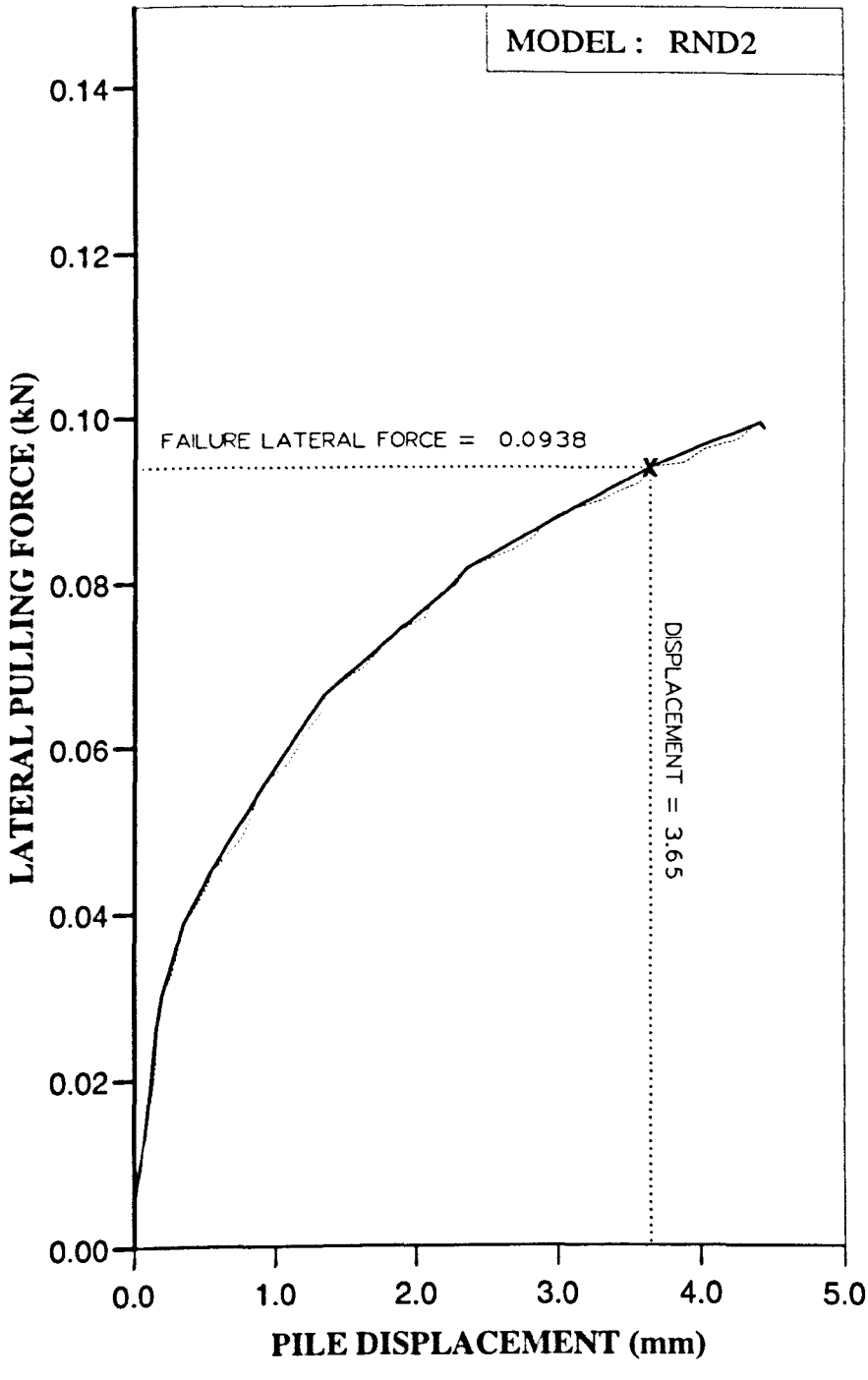

Figure AL6 Variation of lateral force with displacement at ground level for Series 2 test.

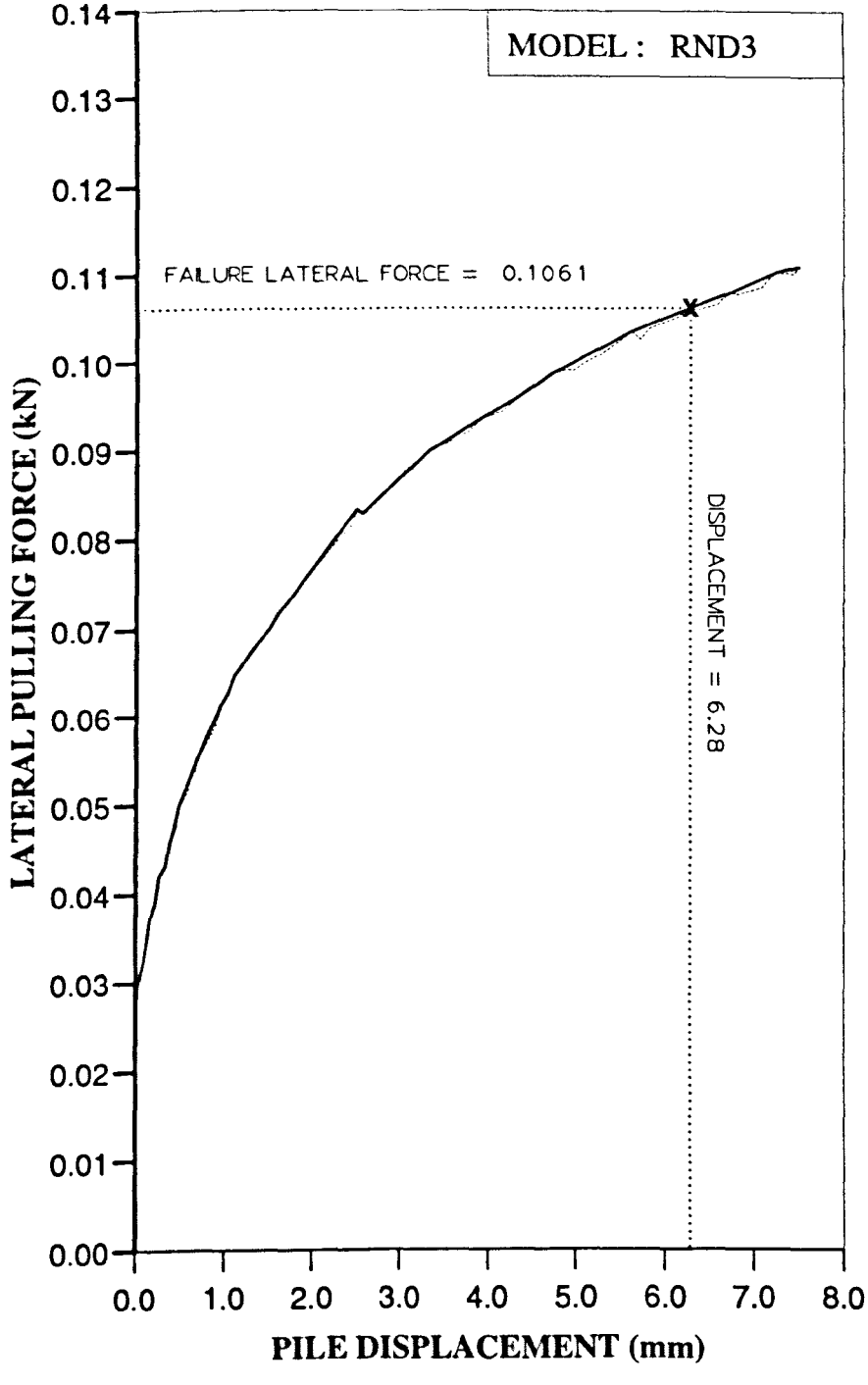

Figure AL7 Variation of lateral force with displacement at ground level for Series 2 test.

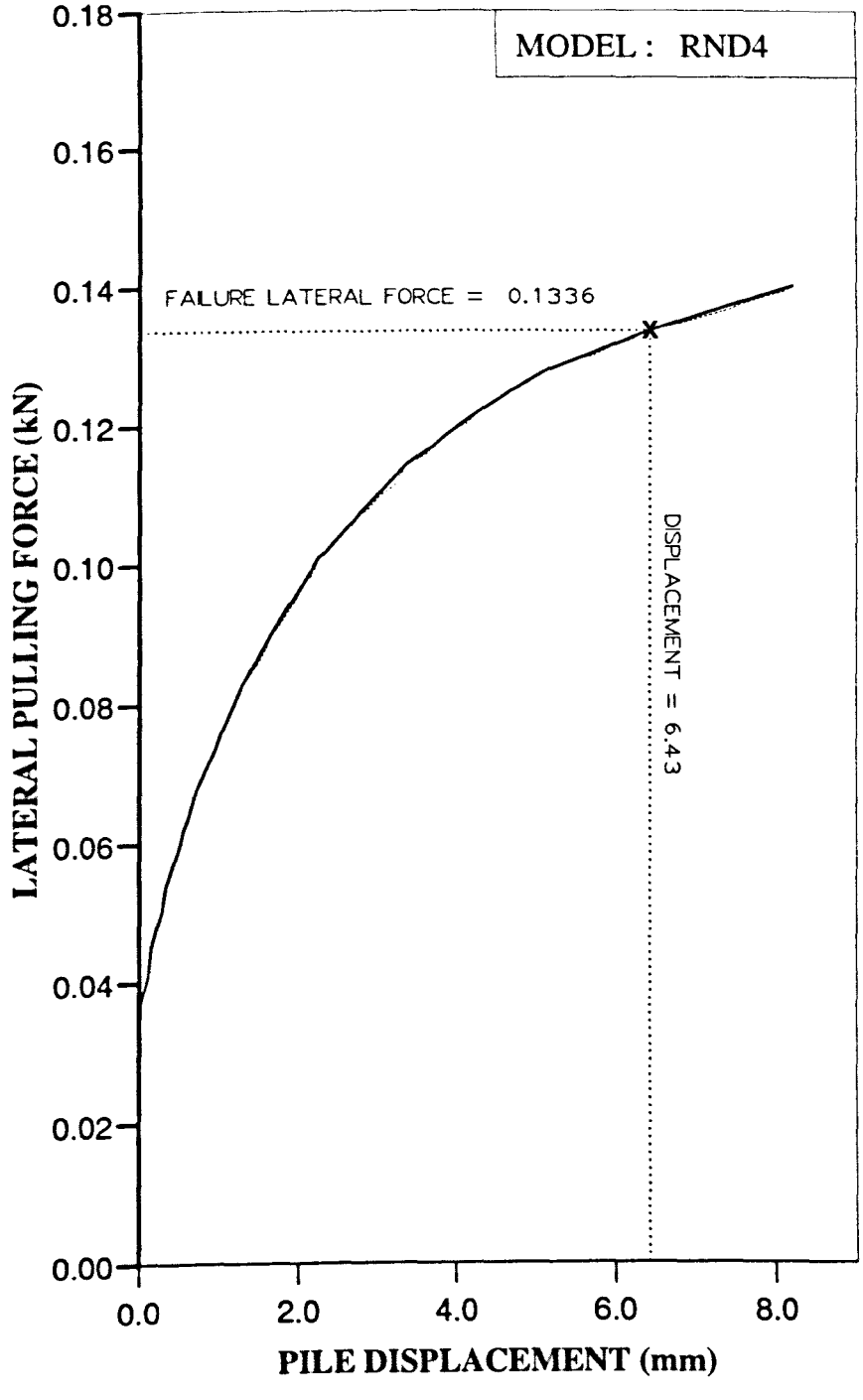

Figure AL8 Variation of lateral force with displacement at ground level for Series 2 test.

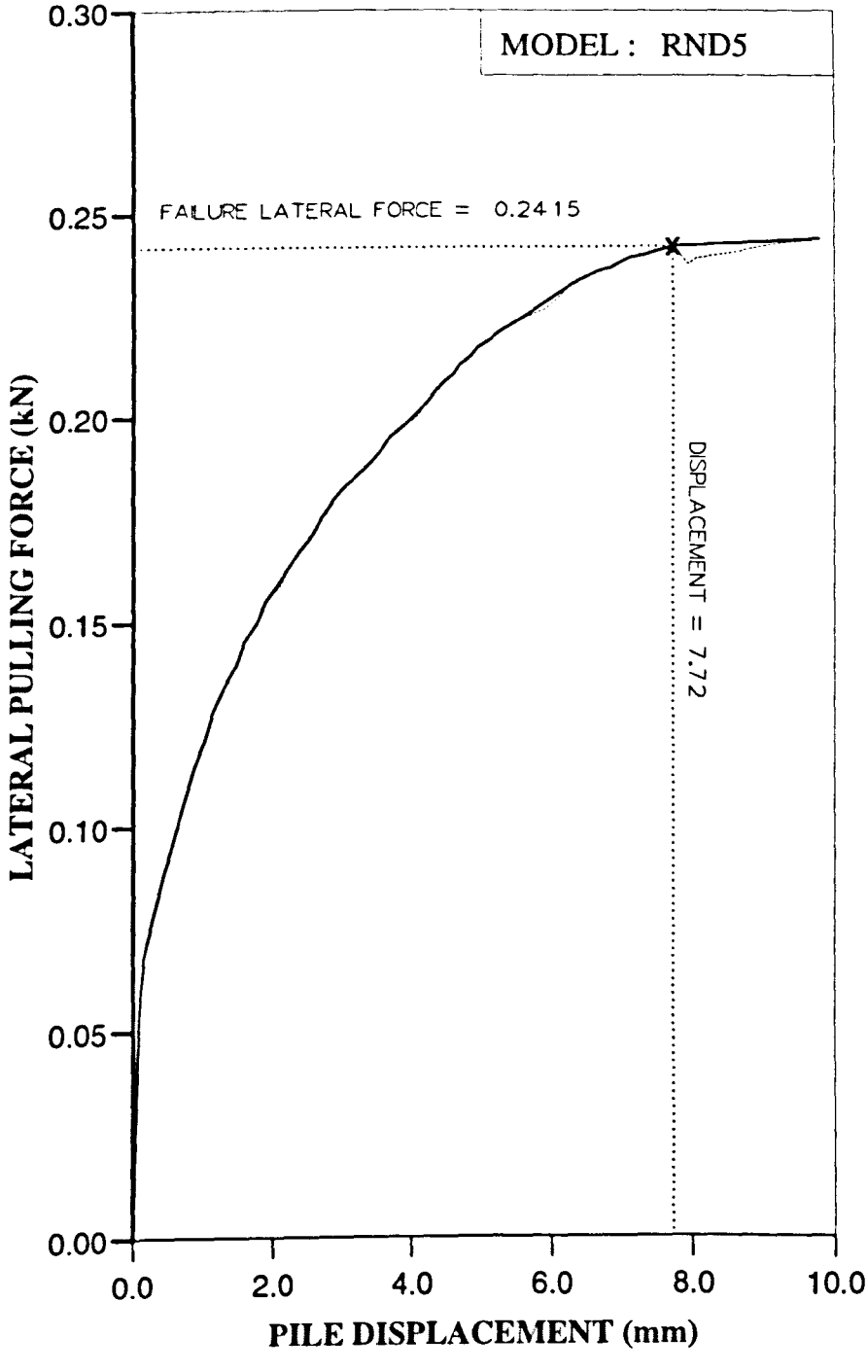

Figure AL9 Variation of lateral force with displacement at ground level for Series 1 test.

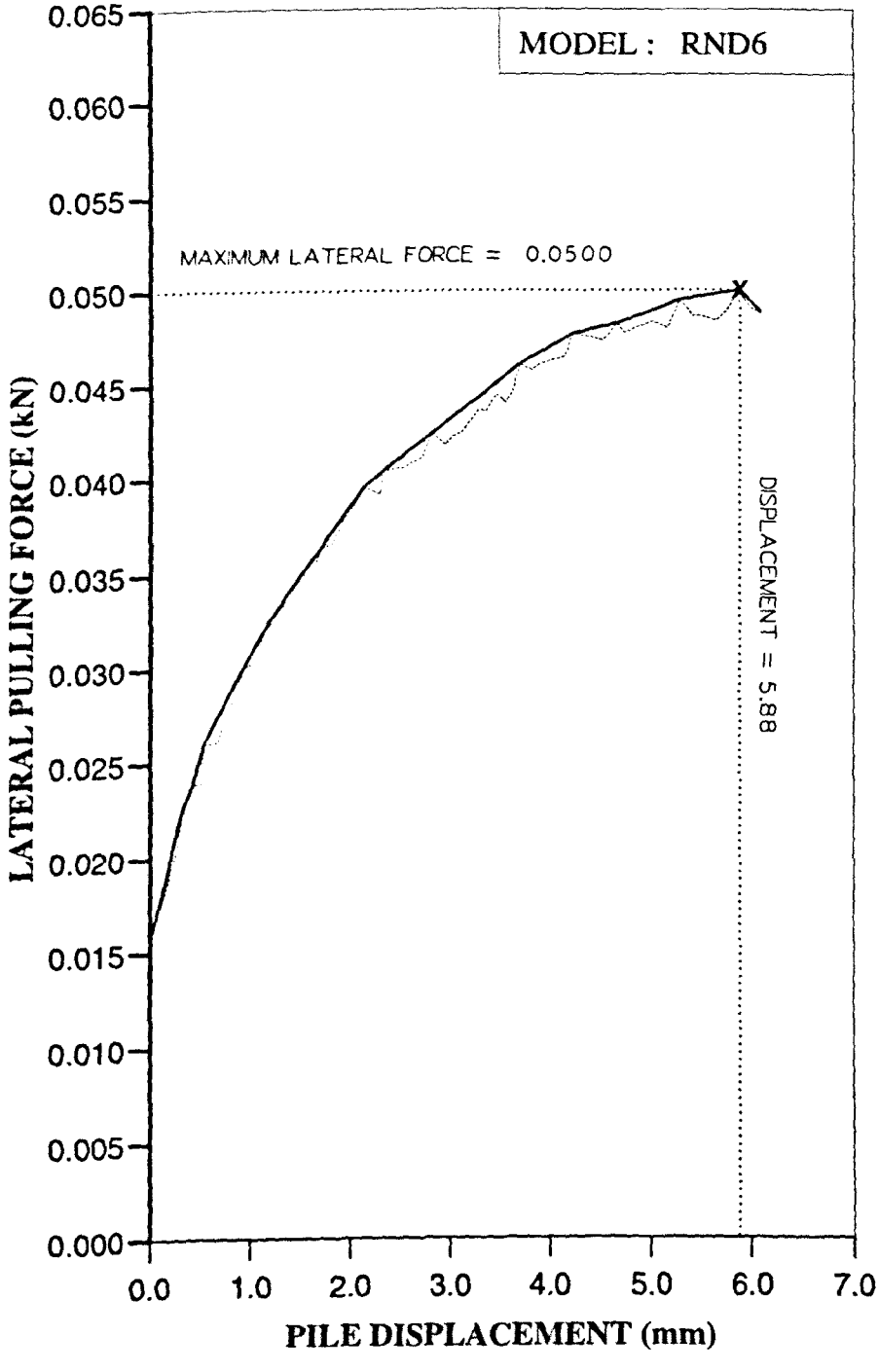

Figure AL10 Variation of lateral force with displacement at ground level for Series 1 test.

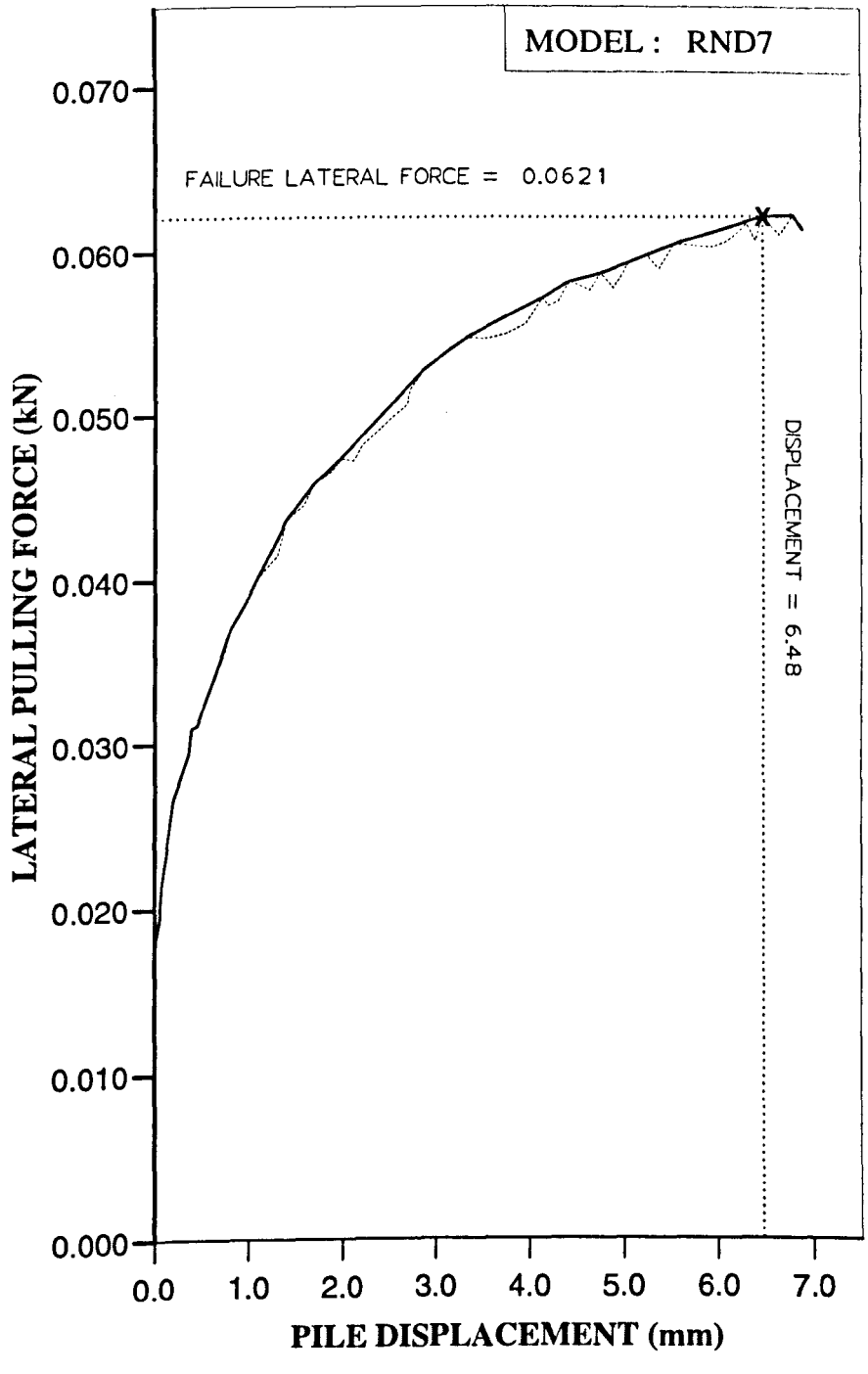

Figure AL11 Variation of lateral force with displacement at ground level for Series 1 test.

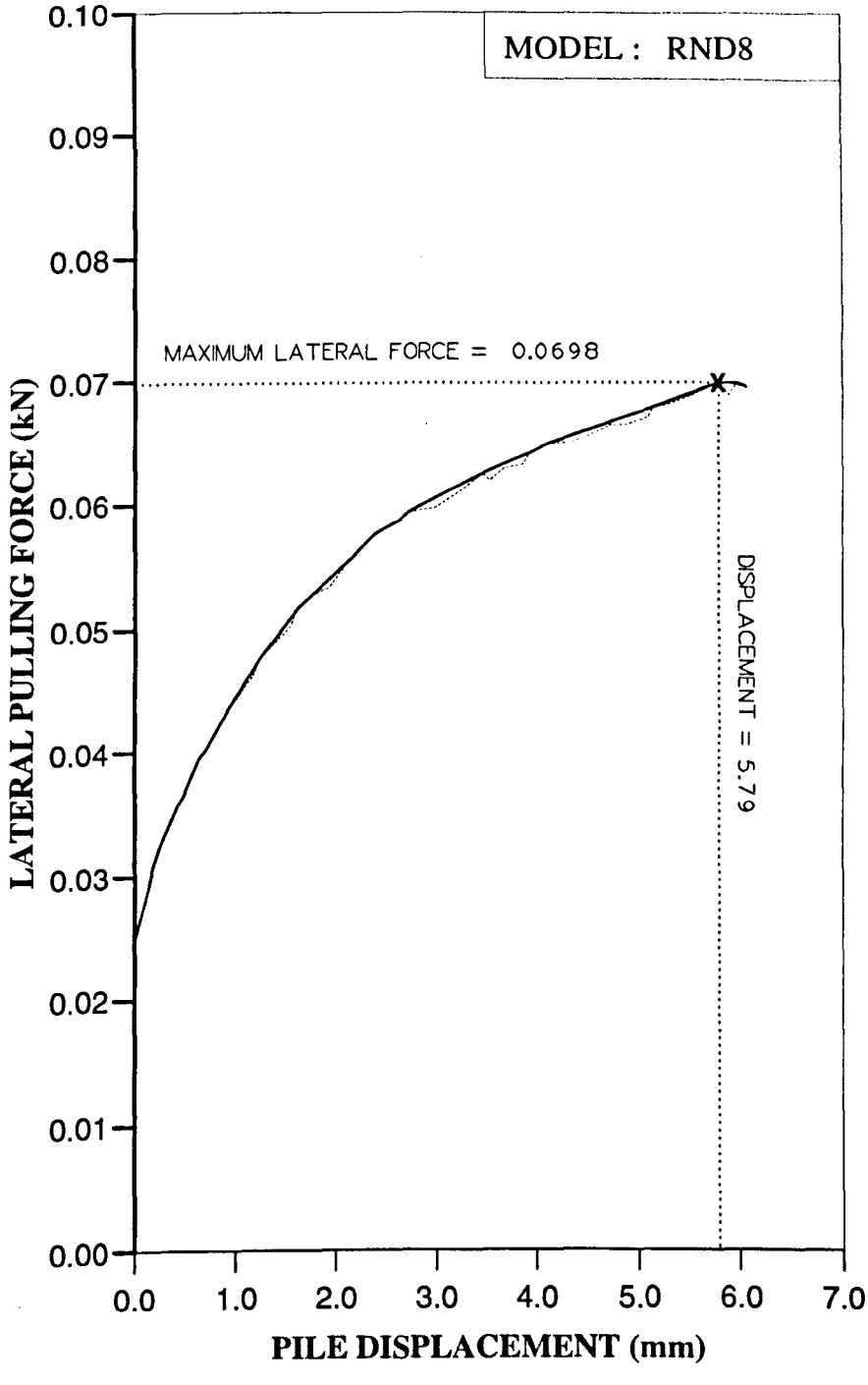

Figure AL12 Variation of lateral force with displacement at ground level for Series 1 test.

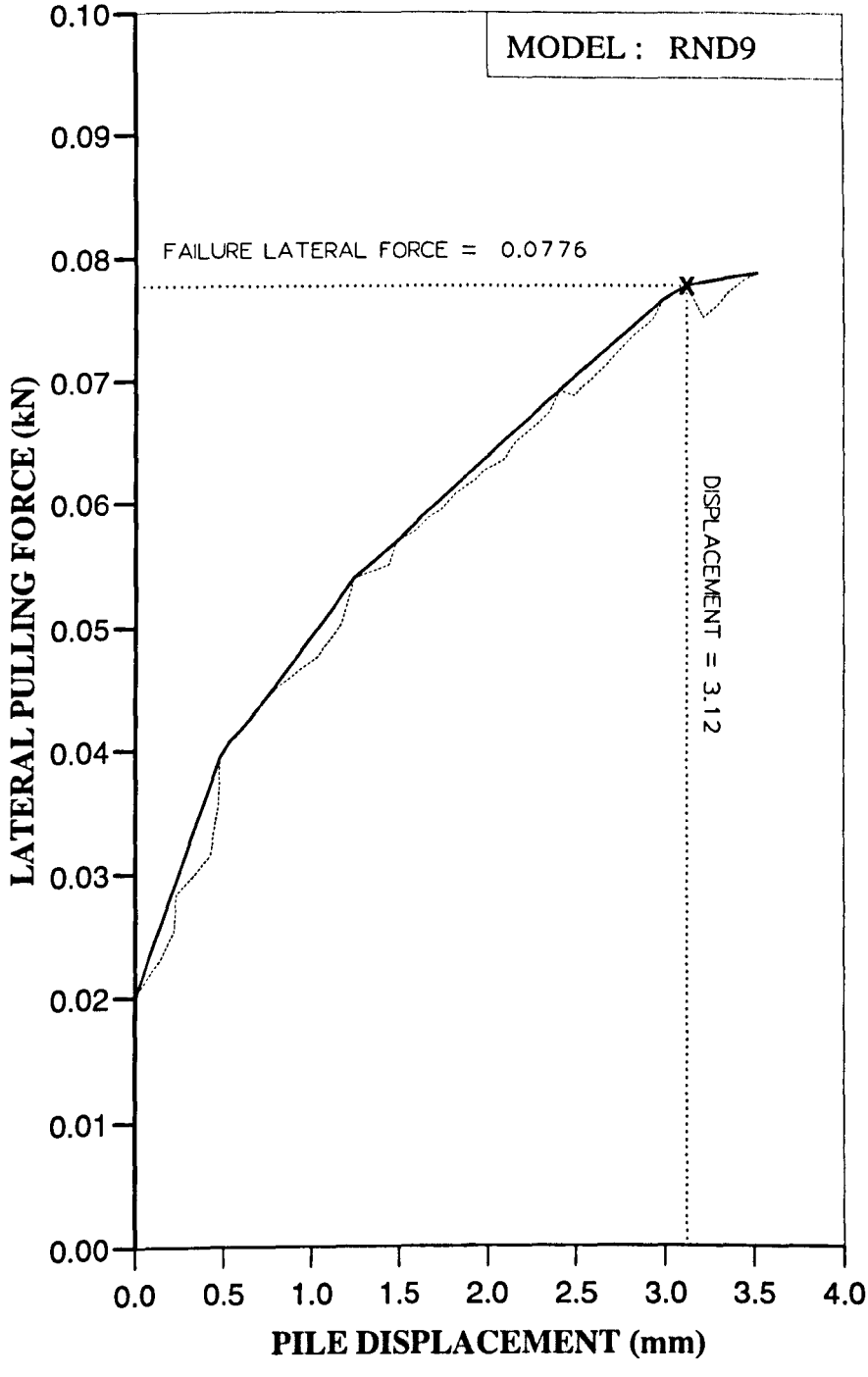

Figure AL13 Variation of lateral force with displacement at ground level for Series 2 test.

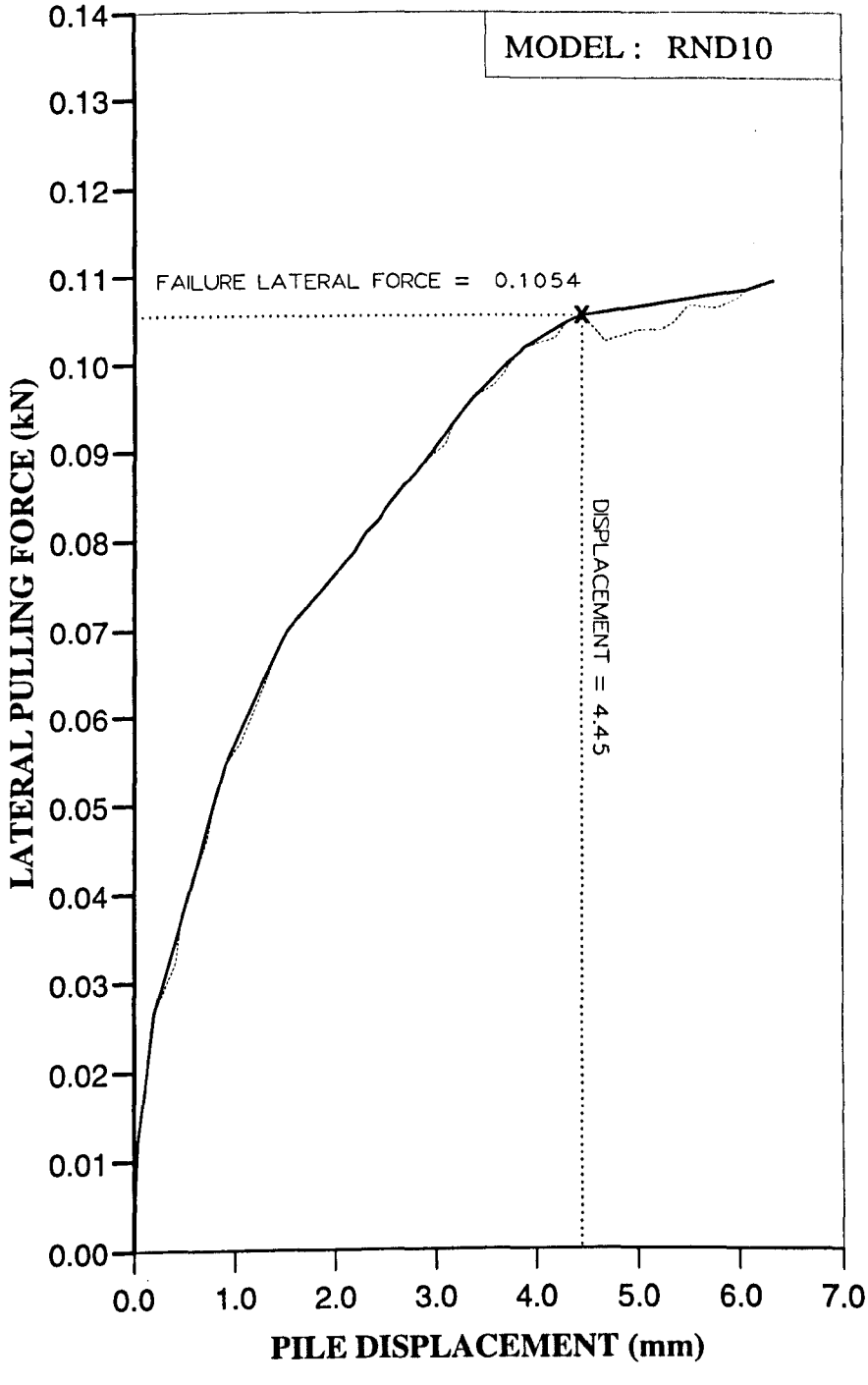

Figure AL14 Variation of lateral force with displacement at ground level for Series 2 test.

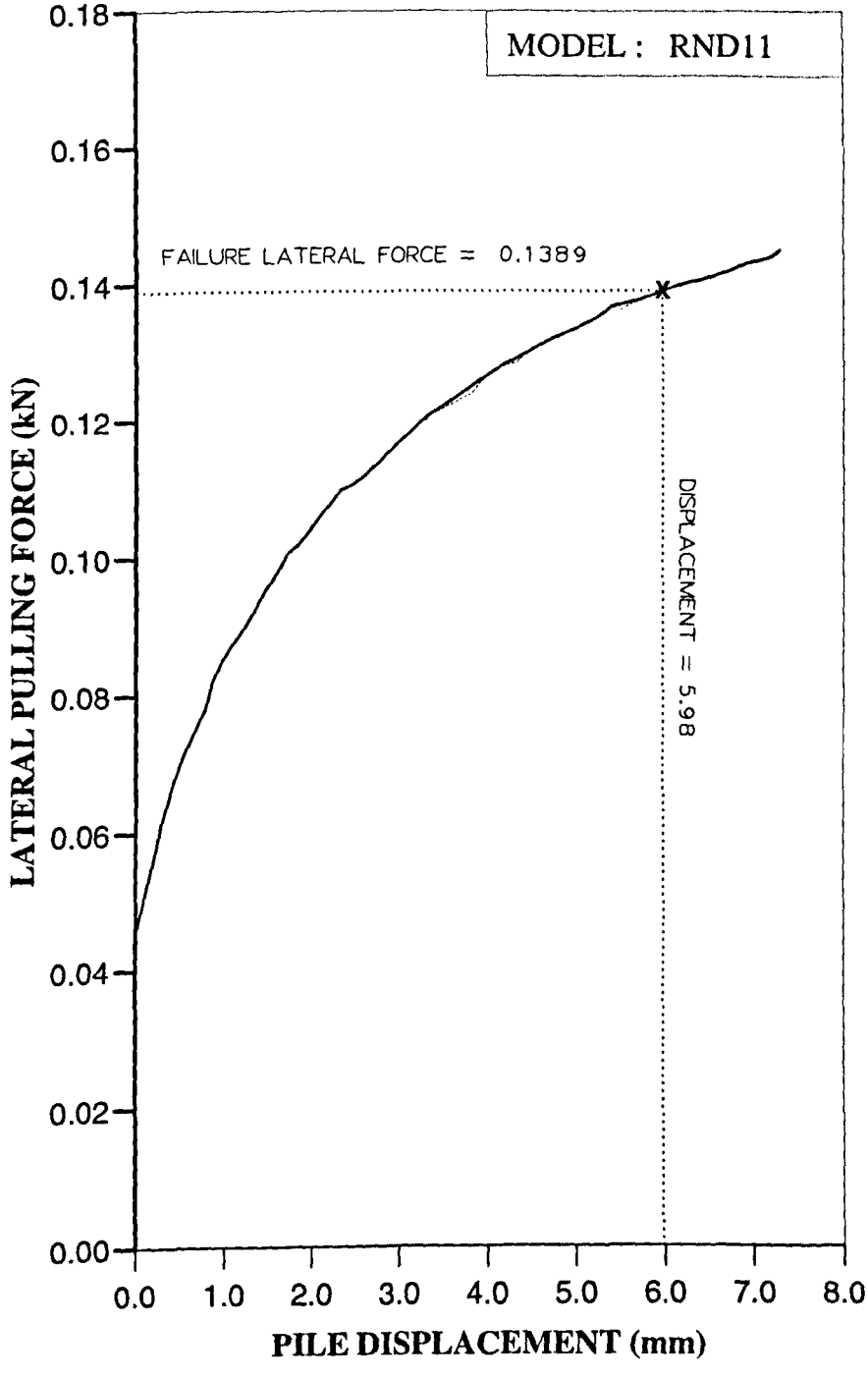

Figure AL15 Variation of lateral force with displacement at ground level for Series 2 test.

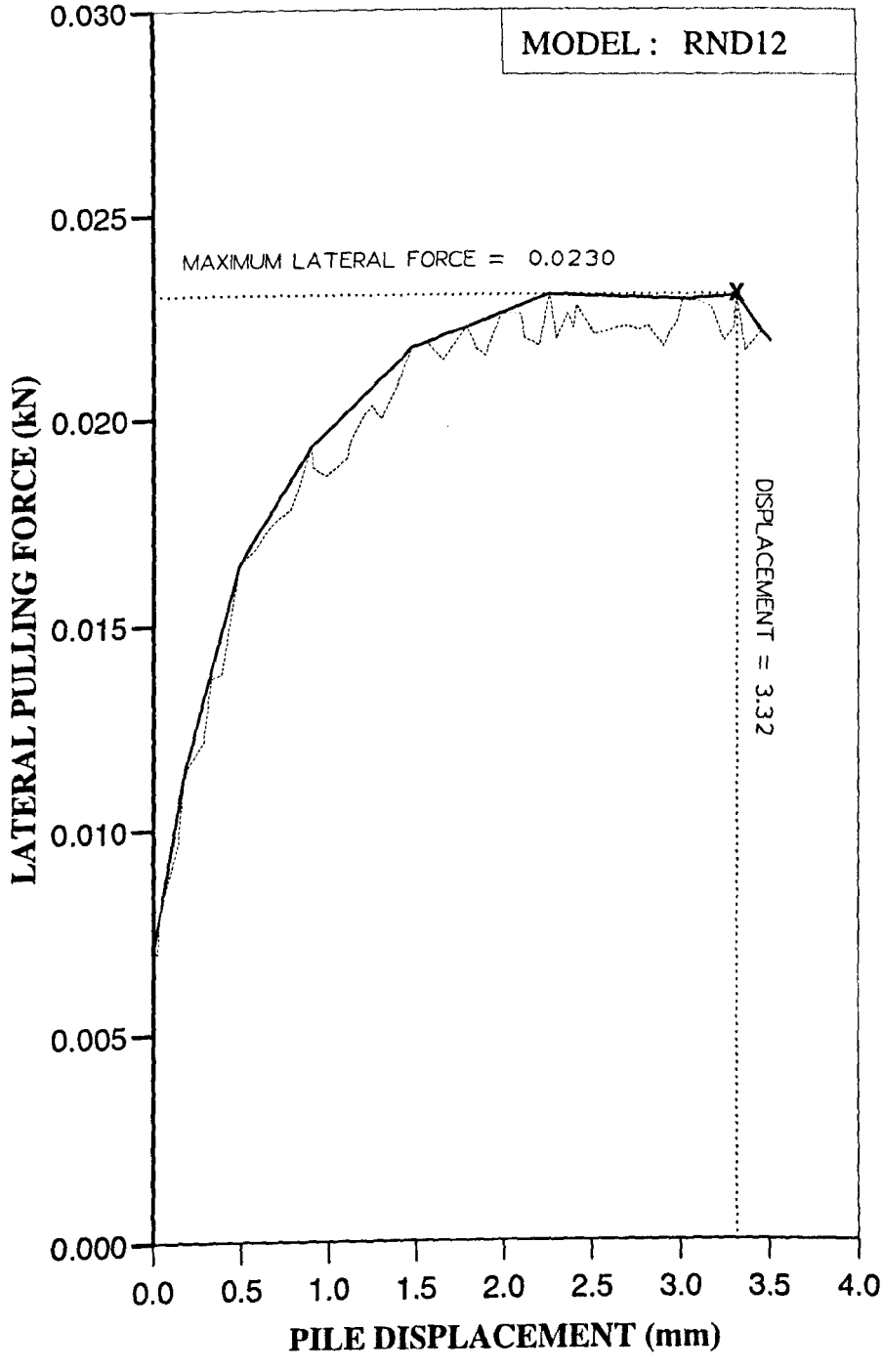

Figure AL16 Variation of lateral force with displacement at ground level for Series 2 test.

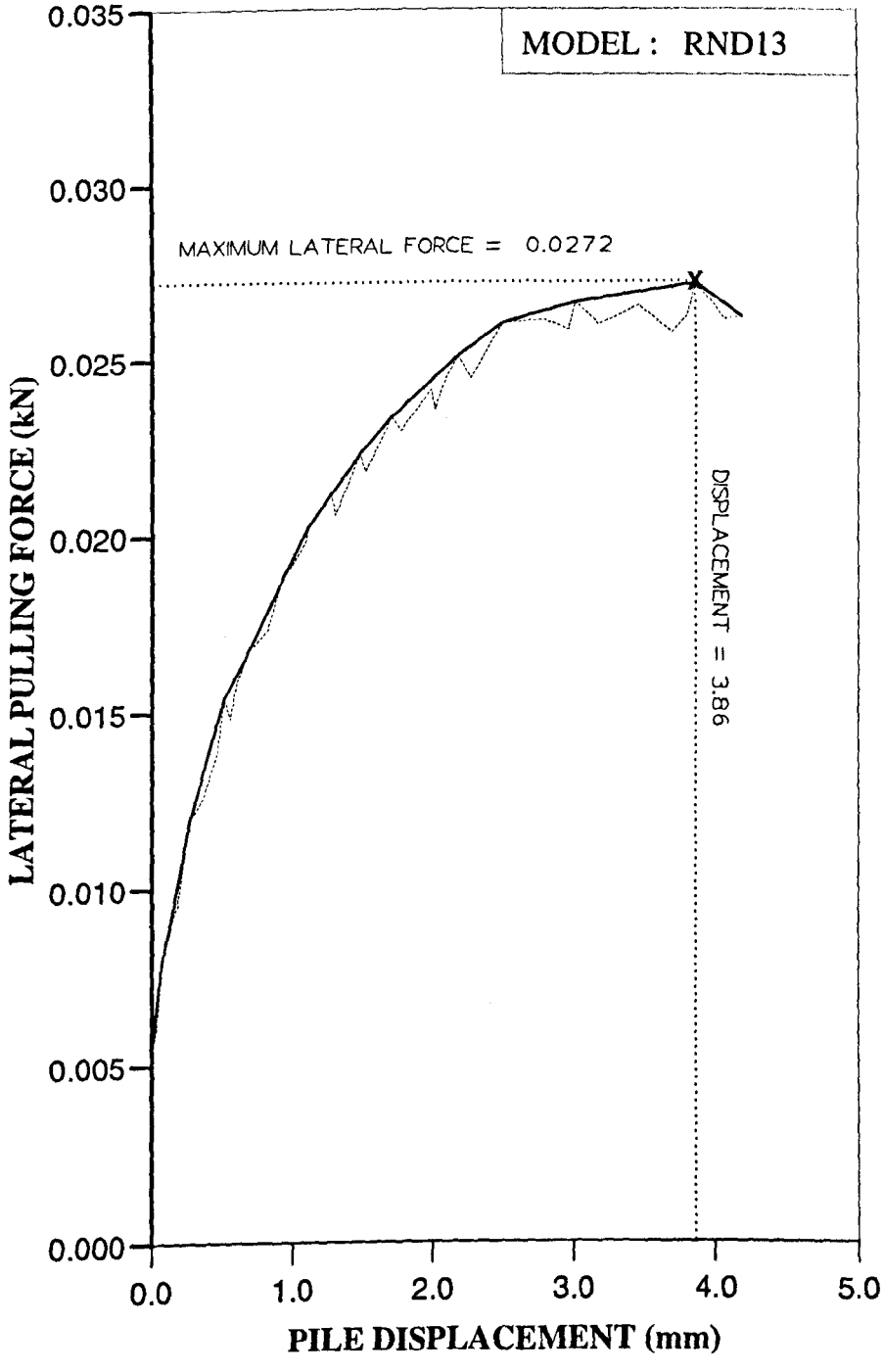

Figure AL17 Variation of lateral force with displacement at ground level for Series 2 test.

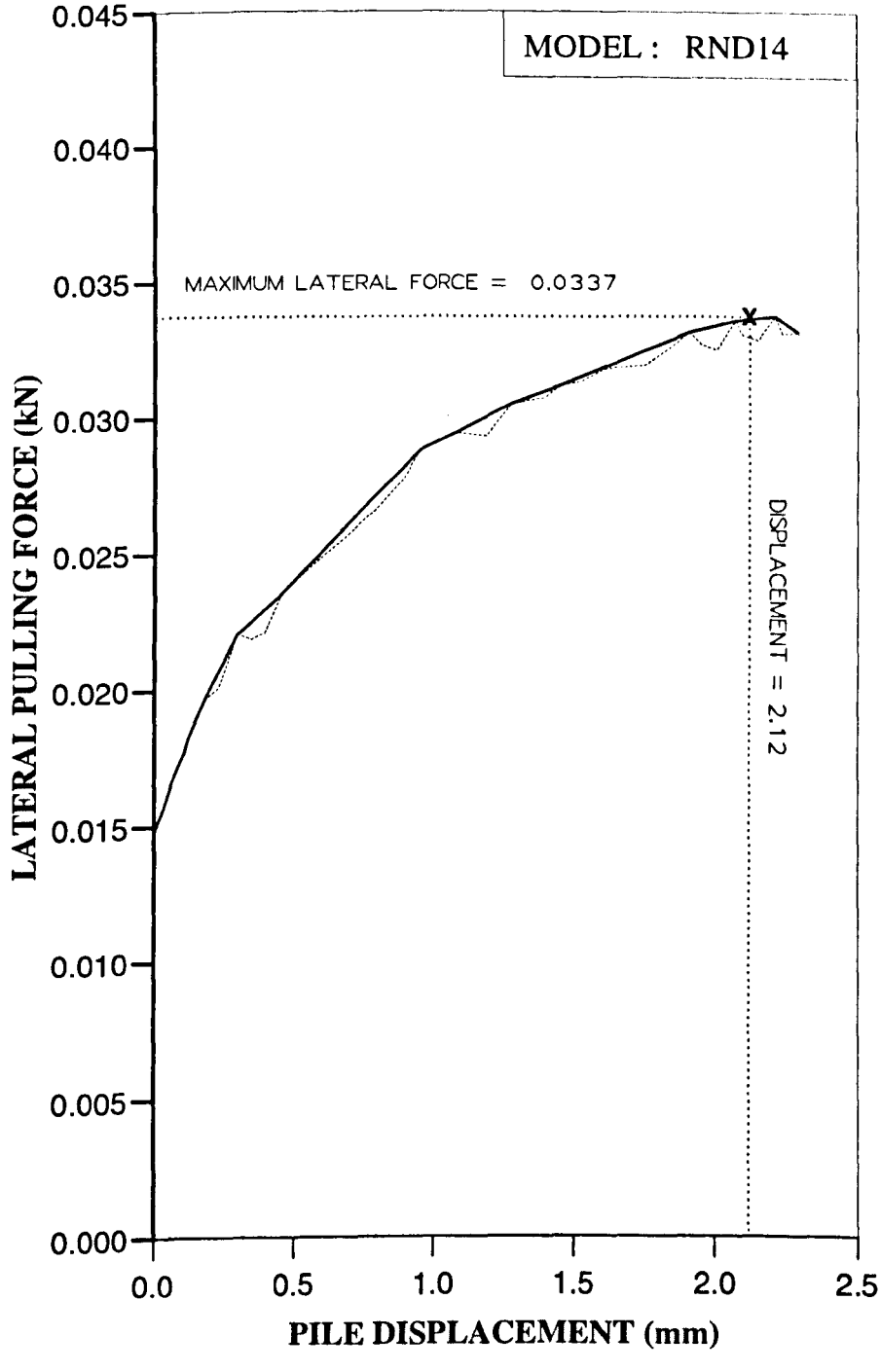

Figure AL18 Variation of lateral force with displacement at ground level for Series 2 test.

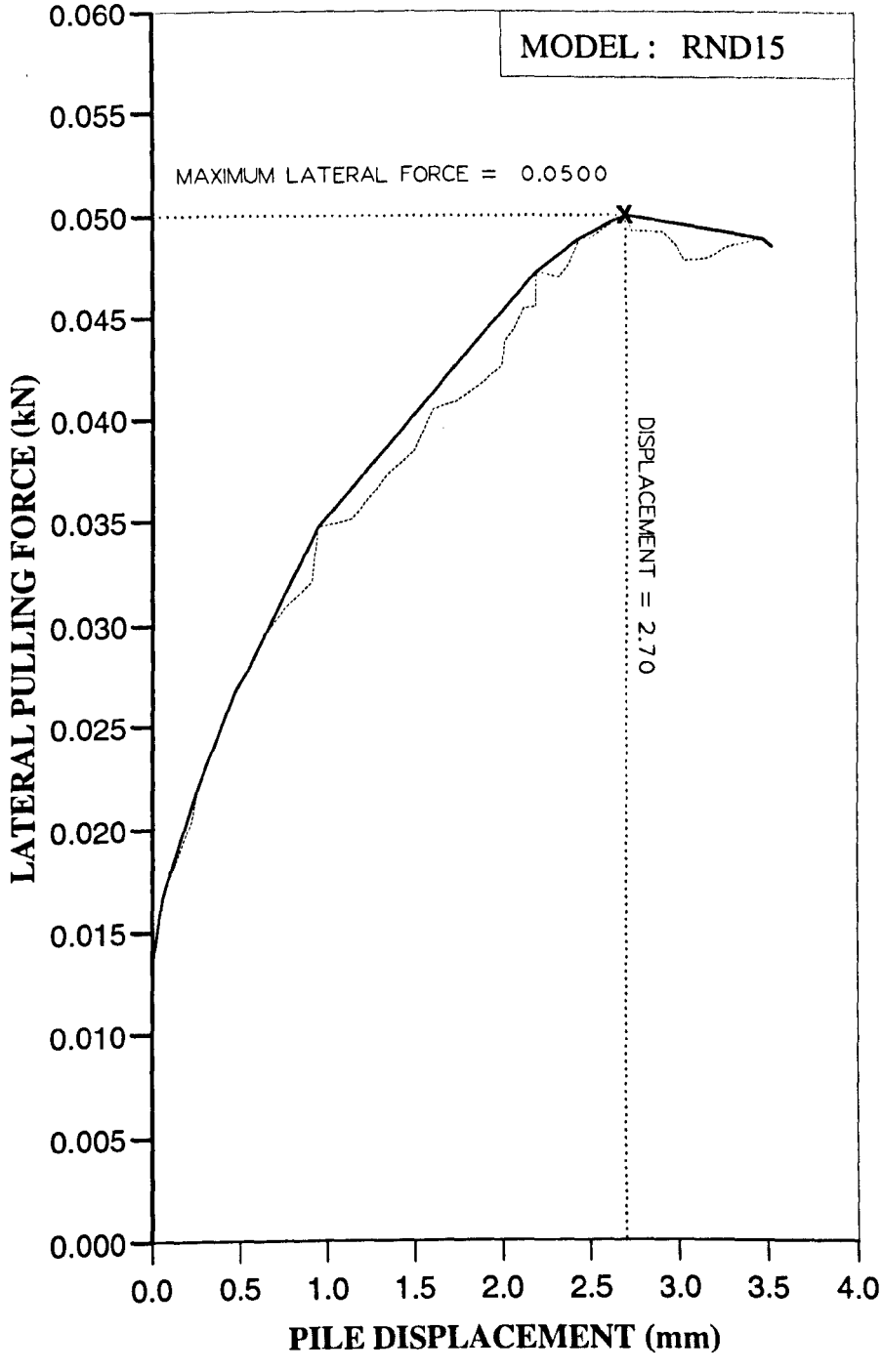

Figure AL19 Variation of lateral force with displacement at ground level for Series 2 test.

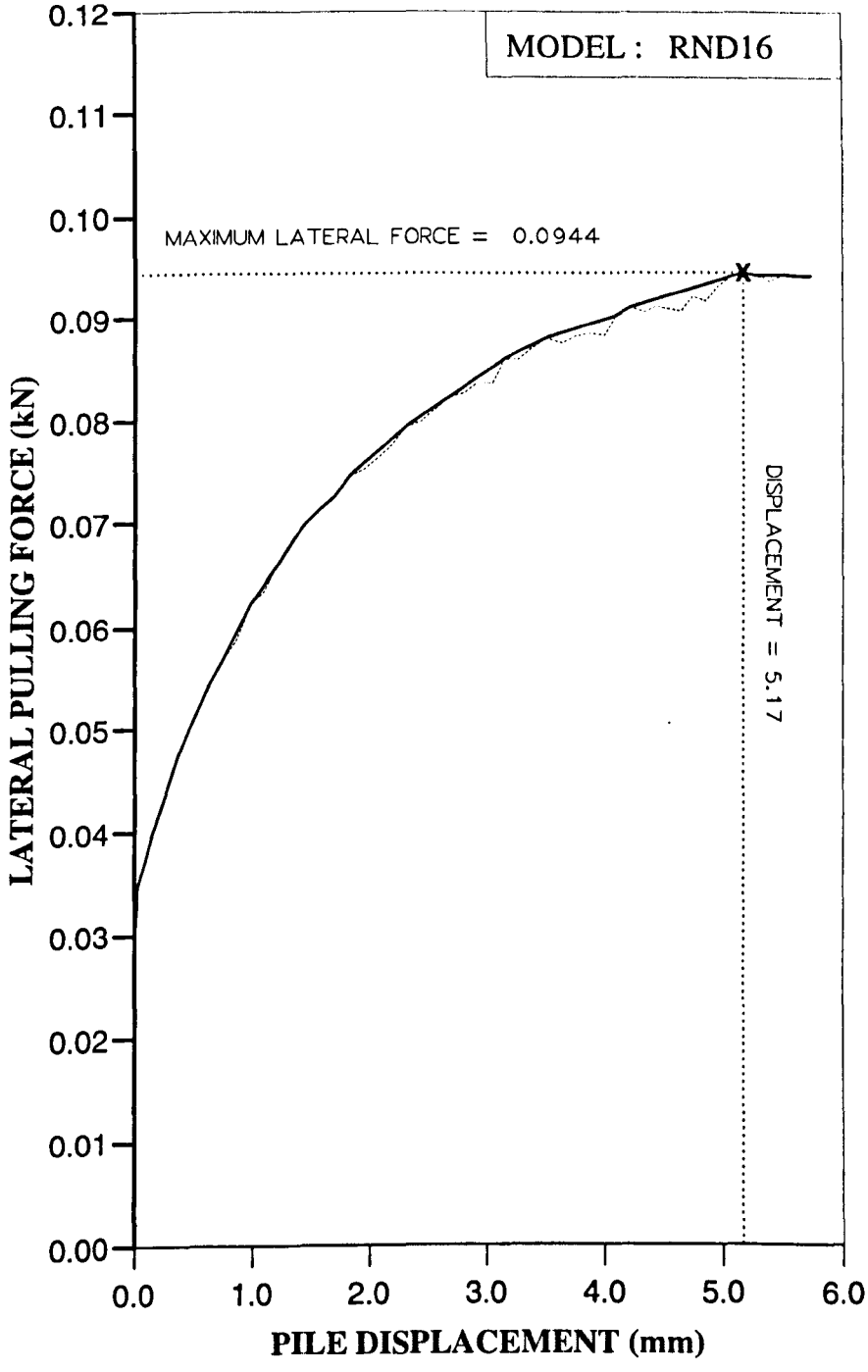

Figure AL20 Variation of lateral force with displacement at ground level for Series 2 test.

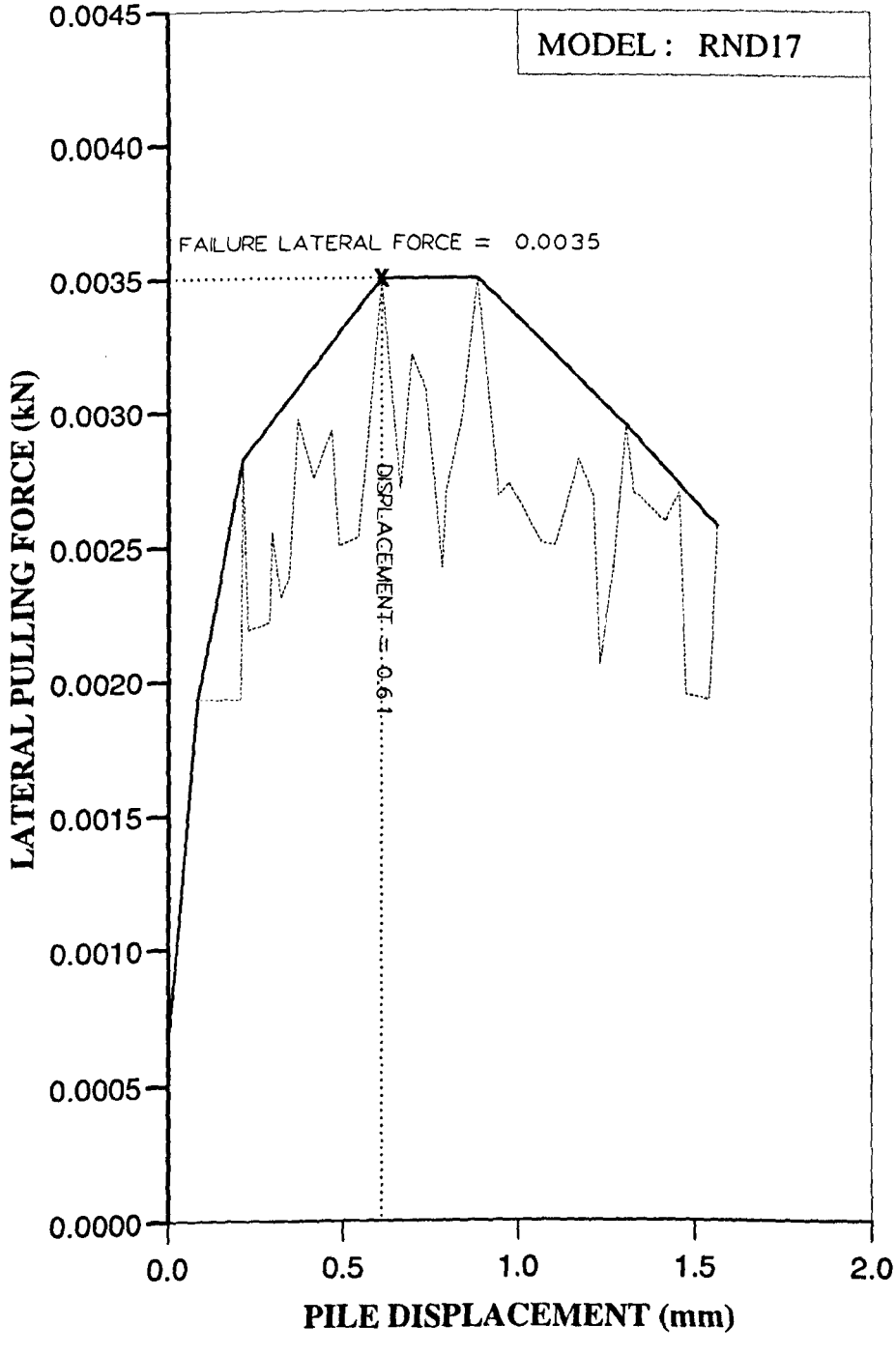

Figure AL21 Variation of lateral force with displacement at ground level for Series 1 test.

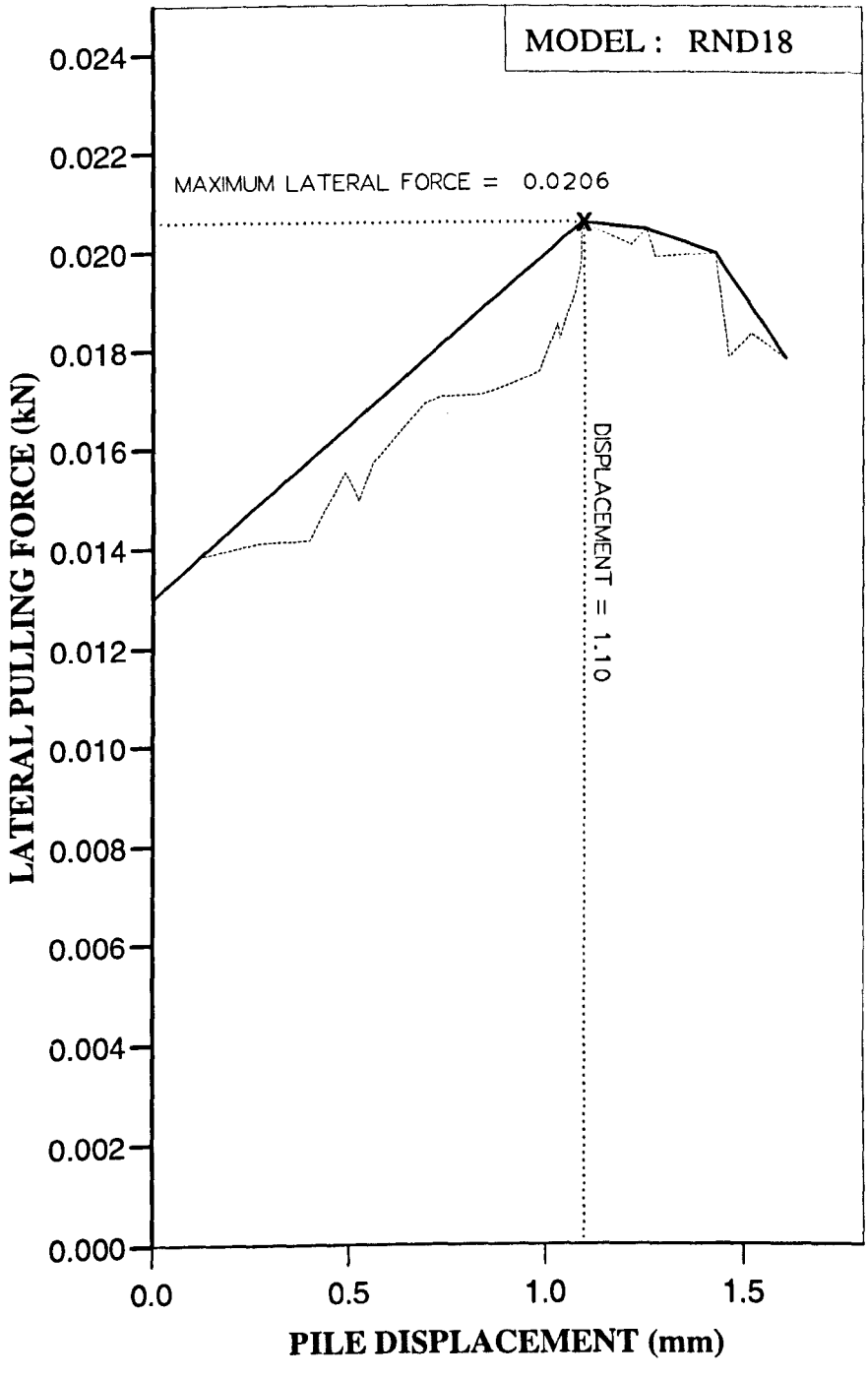

Figure AL22 Variation of lateral force with displacement at ground level for Series 1 test.

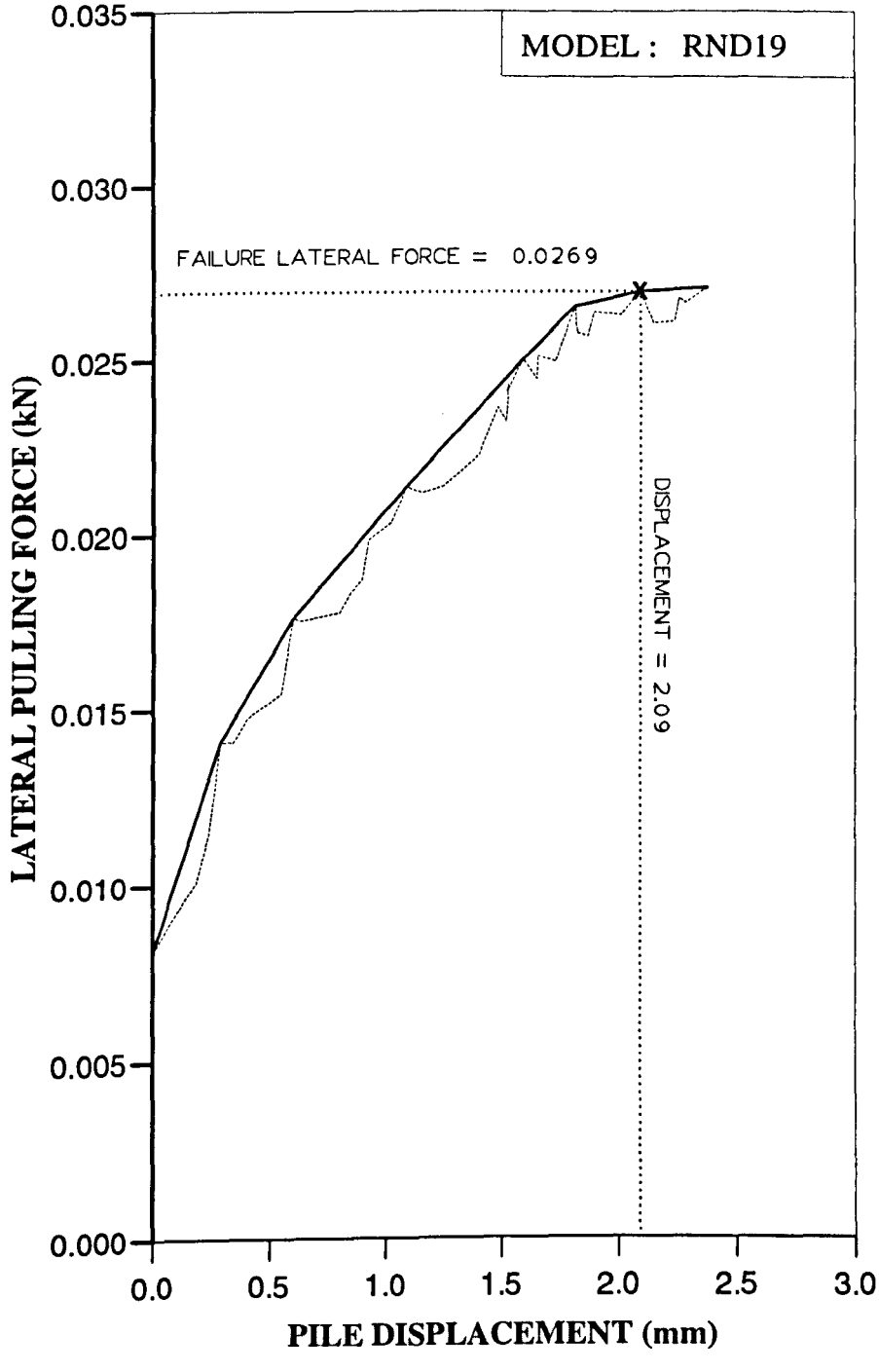

Figure AL23 Variation of lateral force with displacement at ground level for Series 1 test.

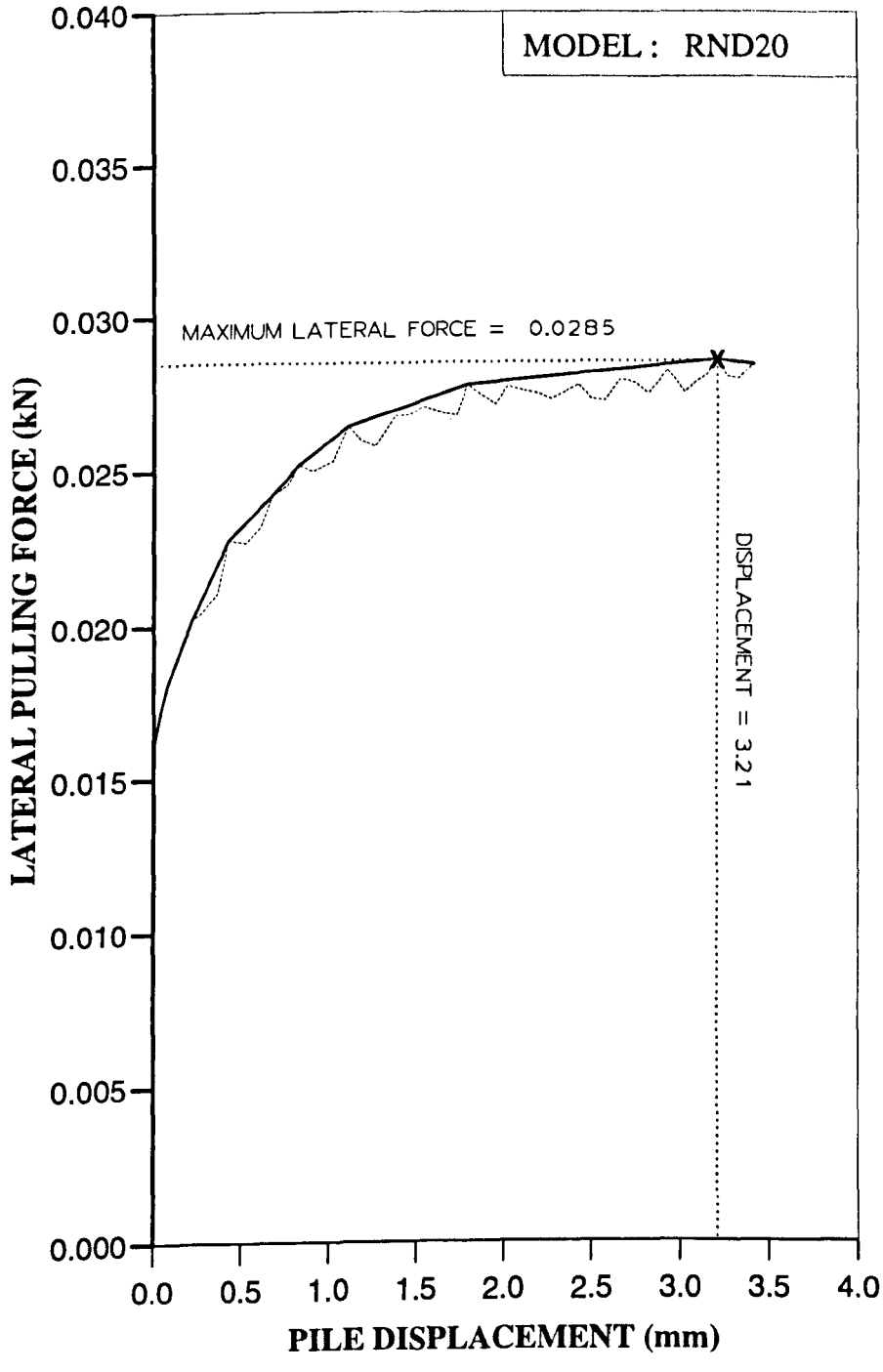

Figure AL24 Variation of lateral force with displacement at ground level for Series 1 test.

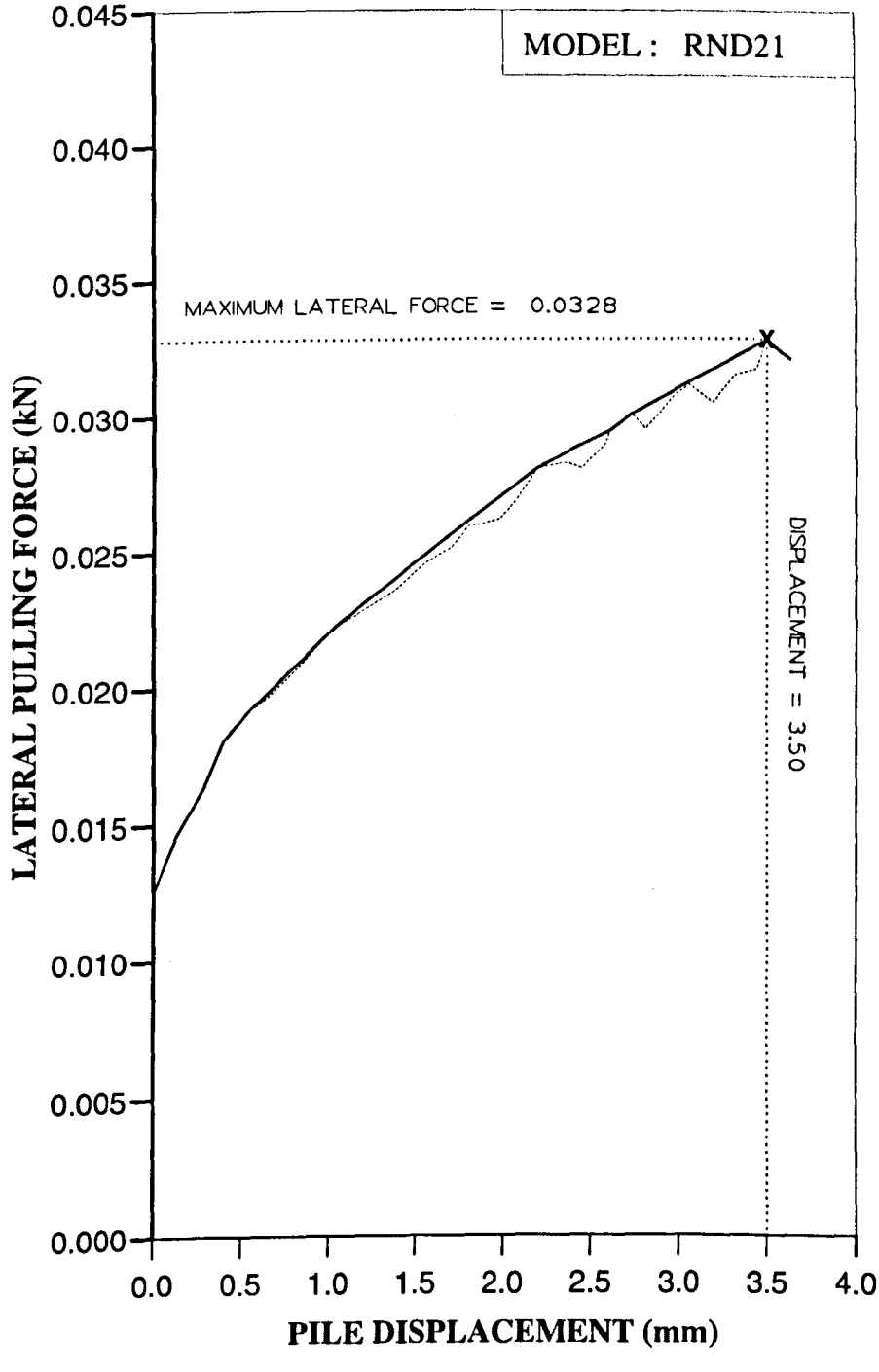

Figure AL25 Variation of lateral force with displacement at ground level for Series 2 test.

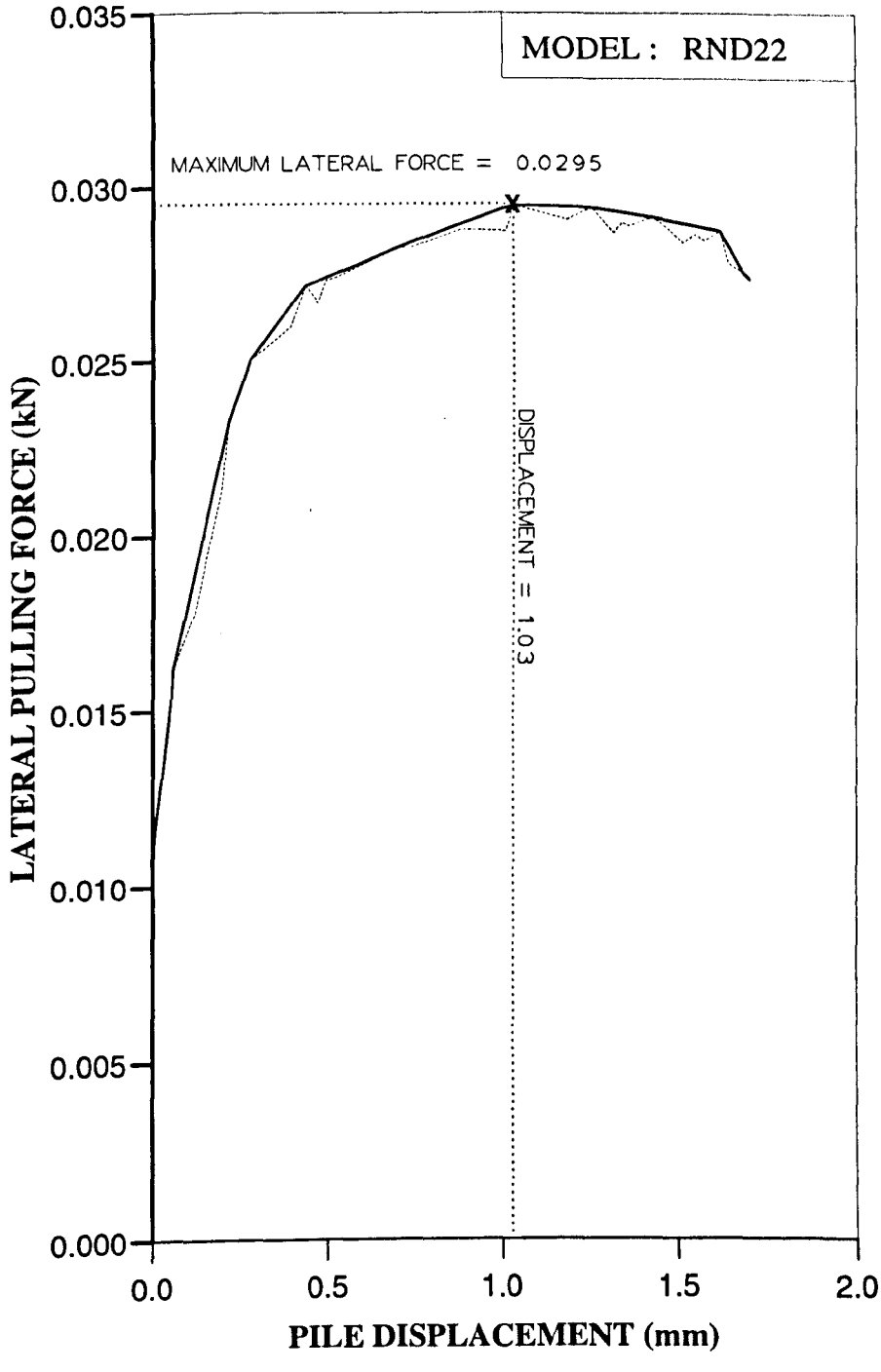

Figure AL26 Variation of lateral force with displacement at ground level for Series 2 test.

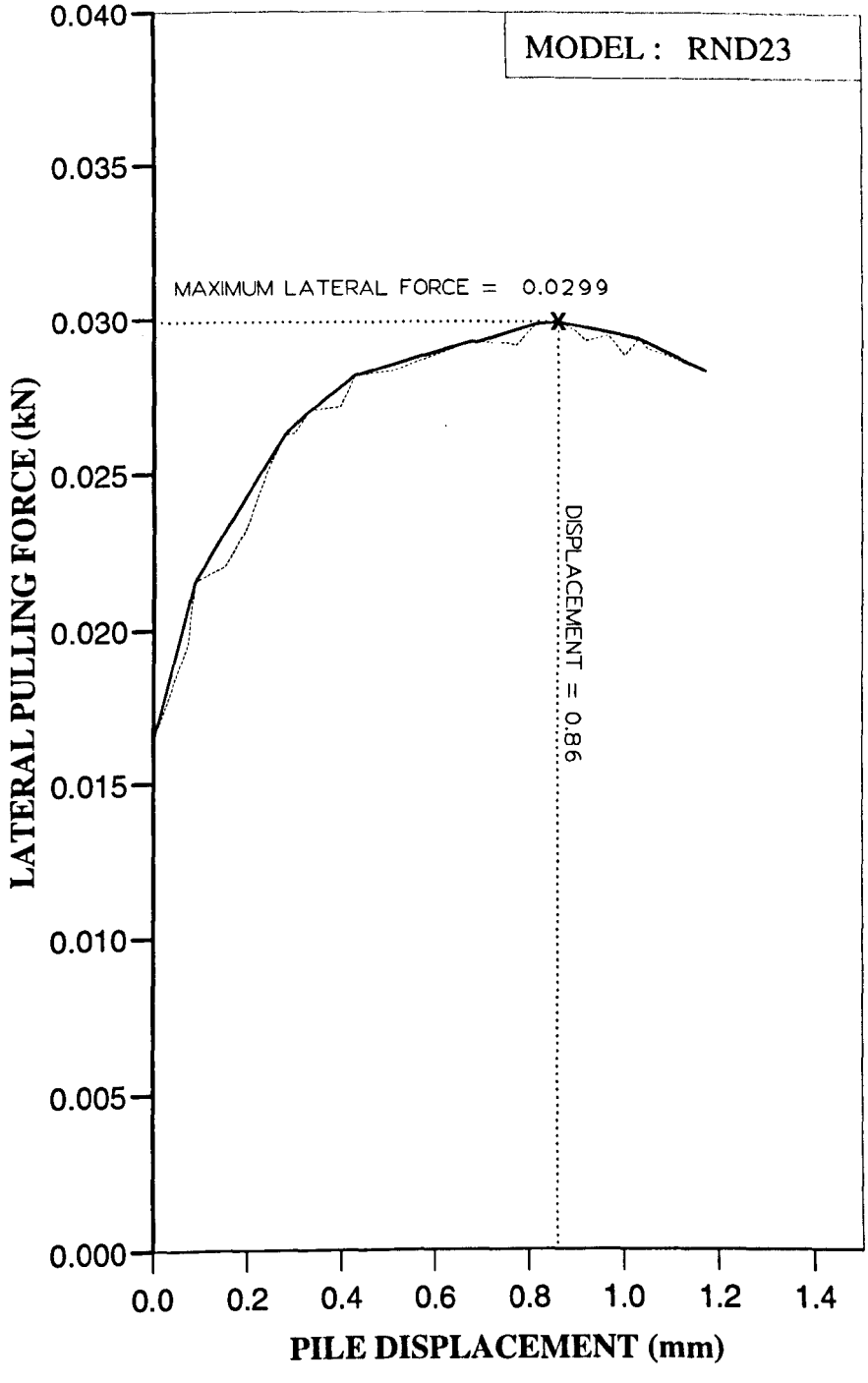

Figure AL27 Variation of lateral force with displacement at ground level for Series 2 test.

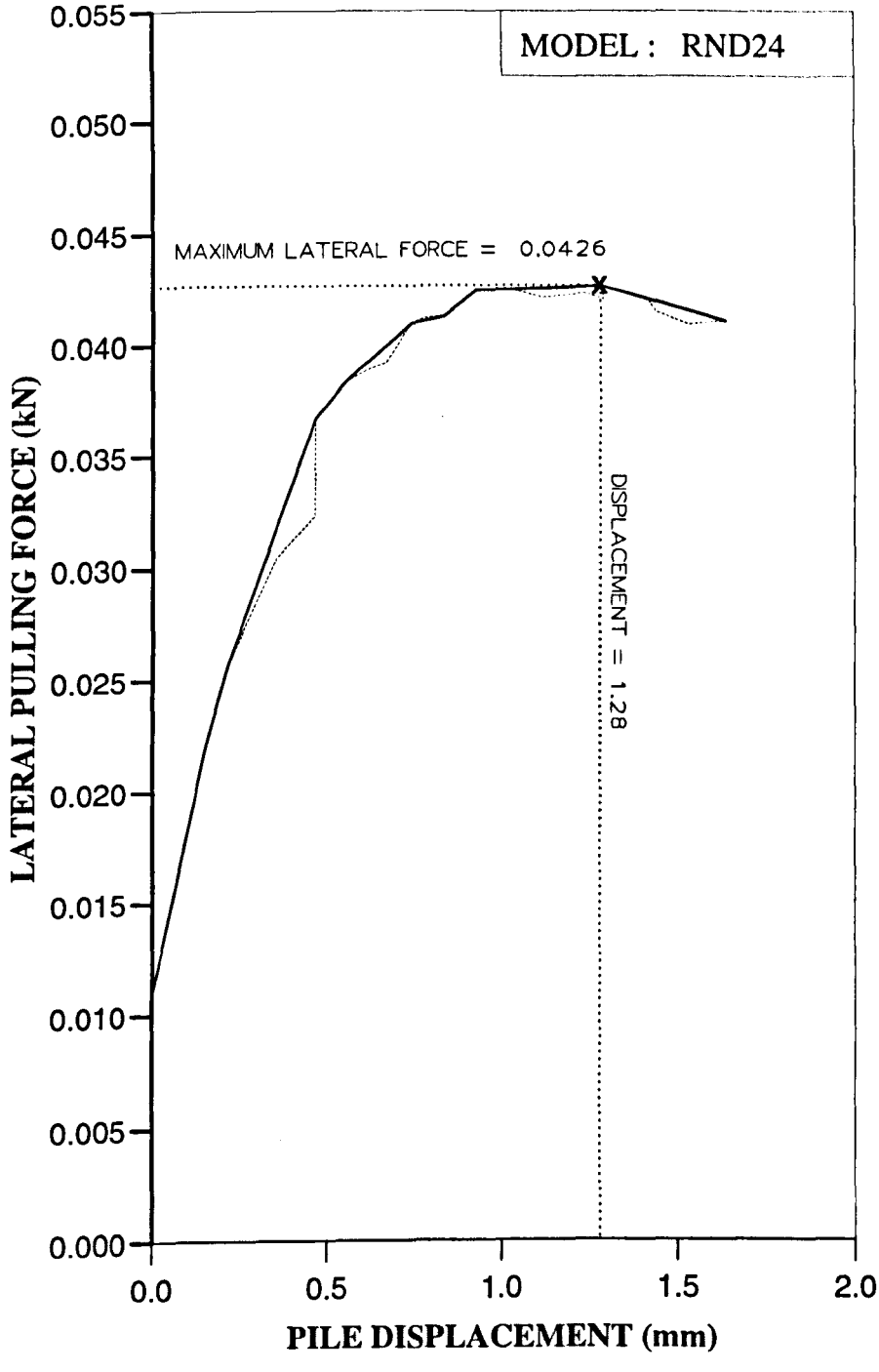

Figure AL28 Variation of lateral force with displacement at ground level for Series 2 test.

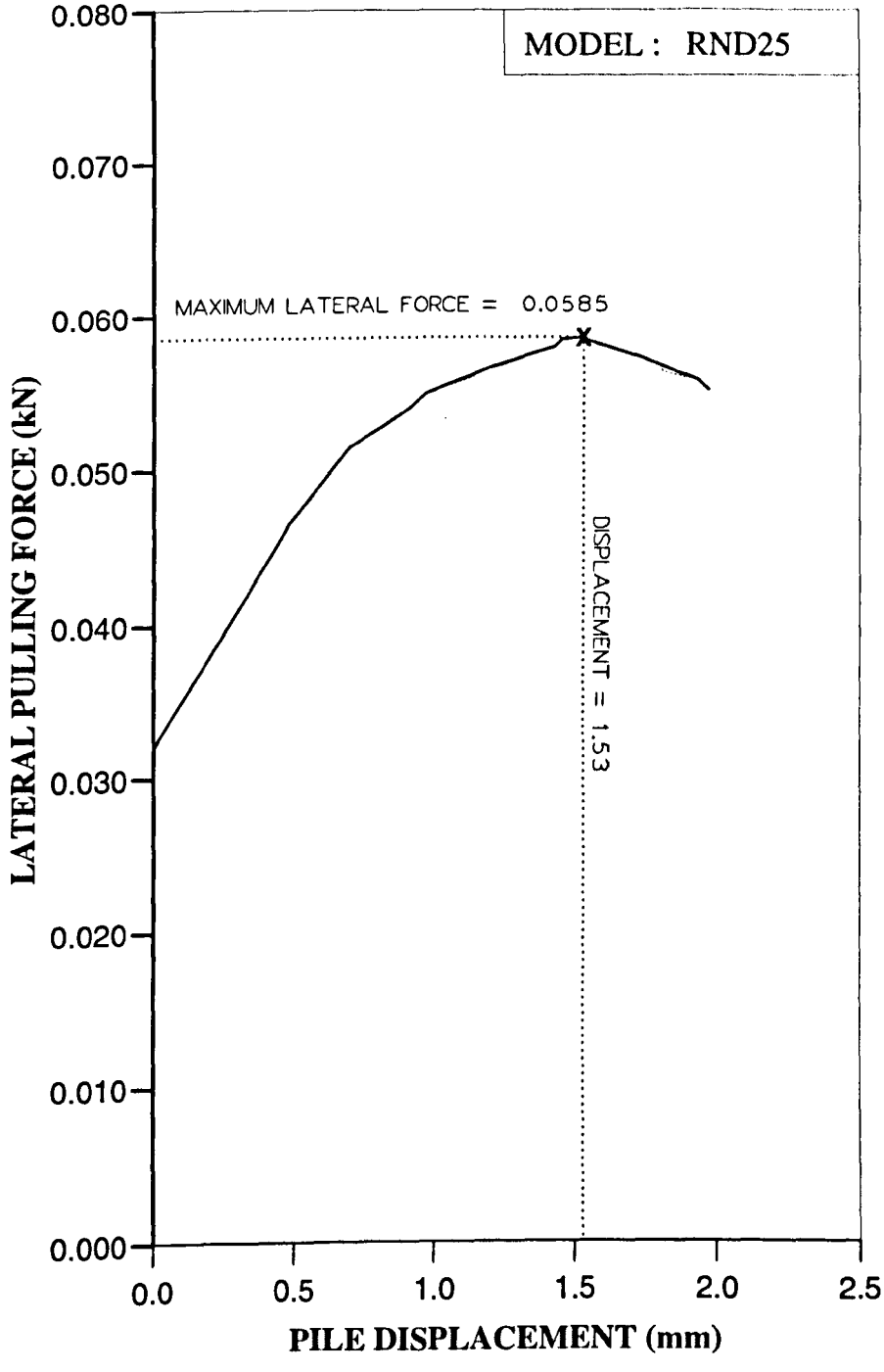

Figure AL29 Variation of lateral force with displacement at ground level for Series 2 test.

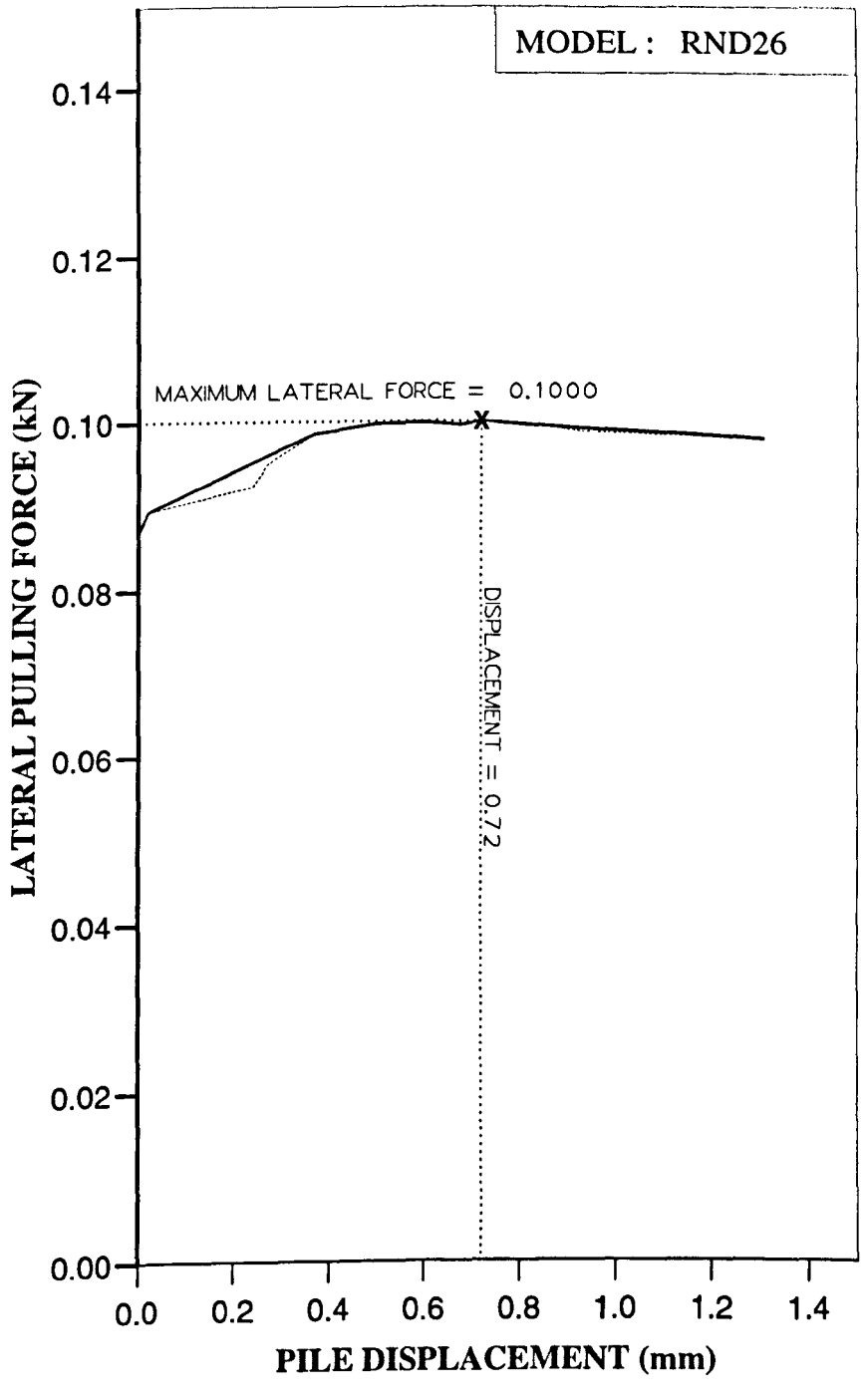

Figure AL30 Variation of lateral force with displacement at ground level for Series 2 test.

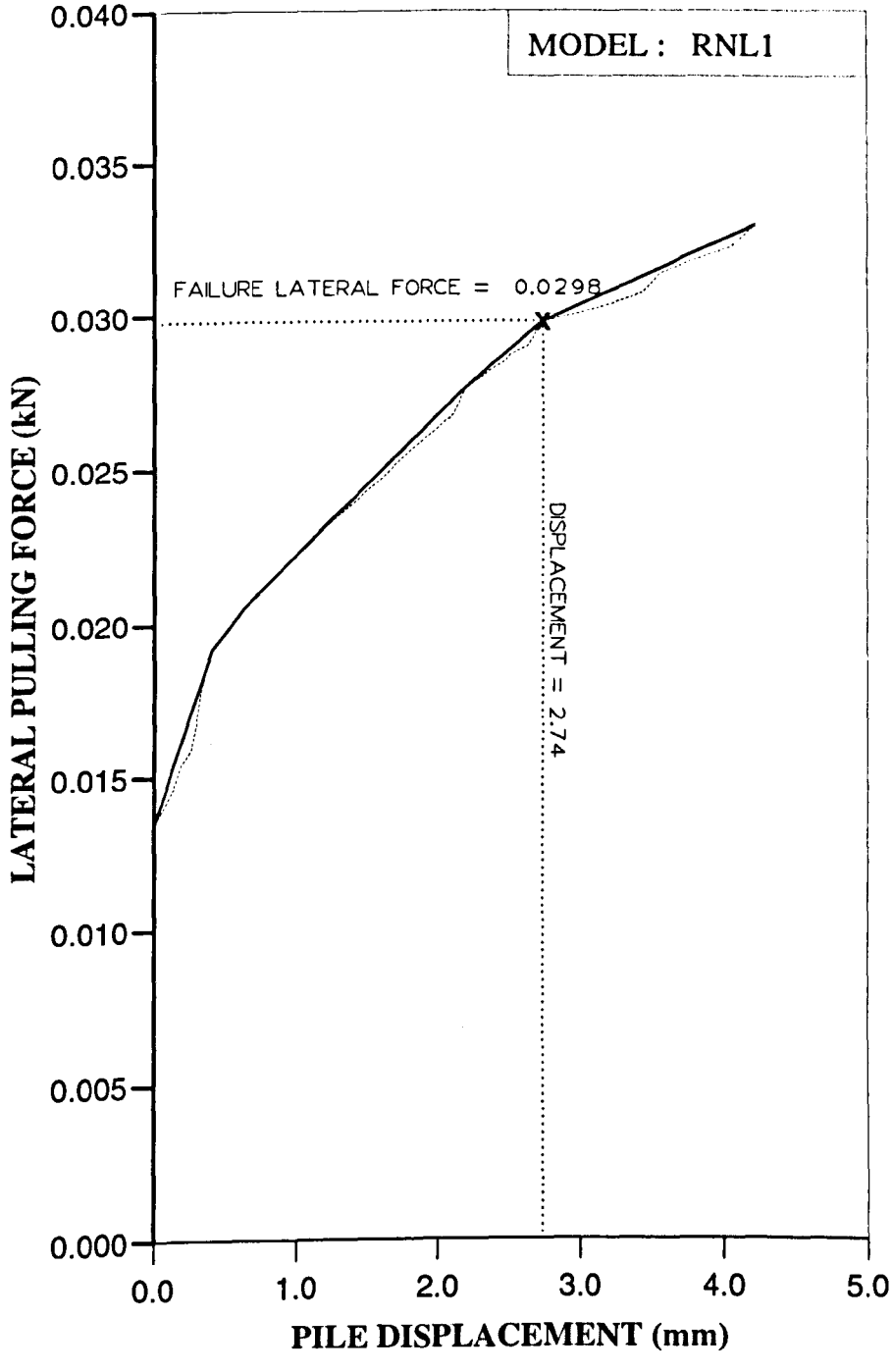

Figure A.31 Variation of lateral force with displacement at ground level for Series 2 test.

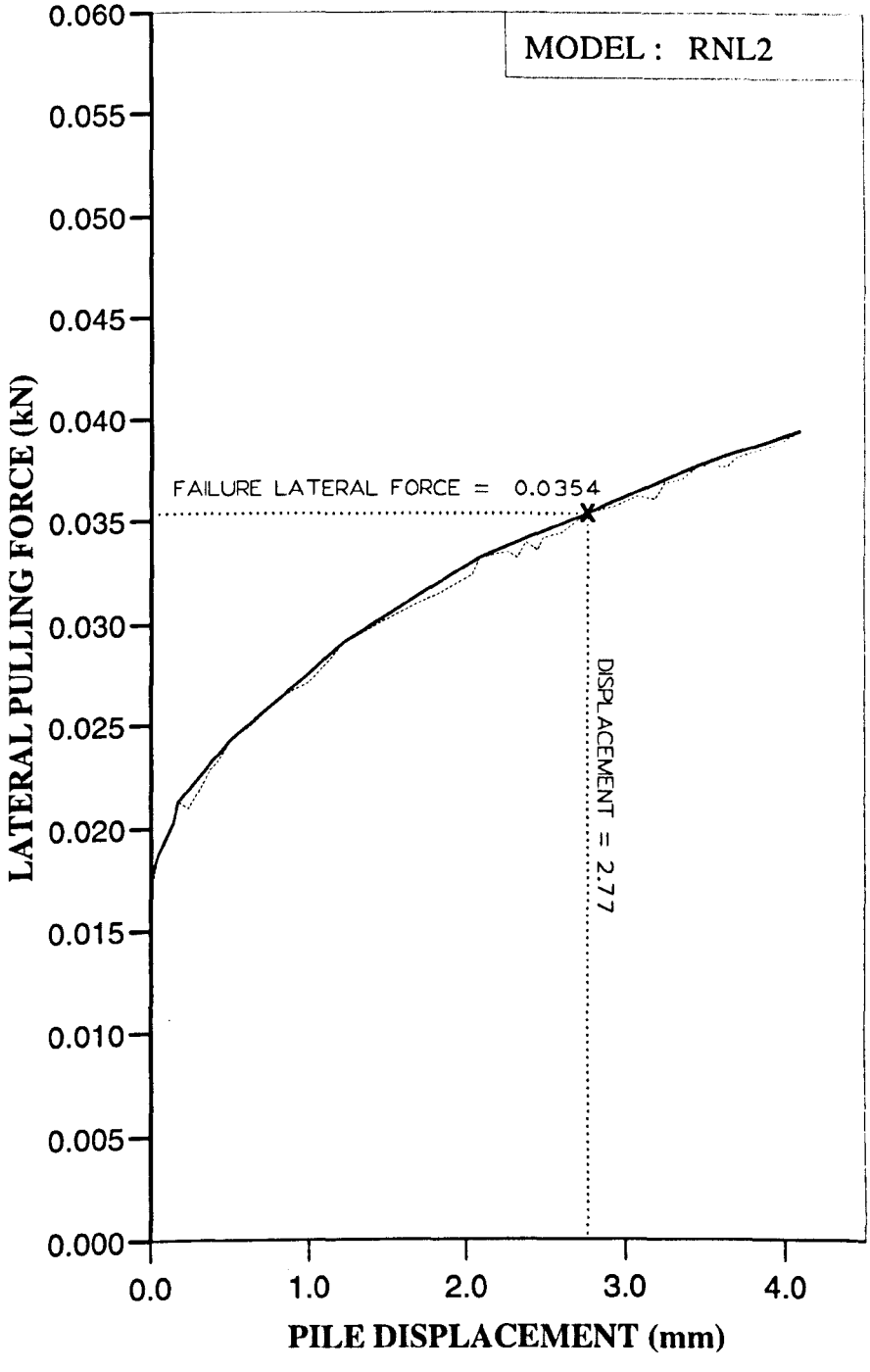

Figure AL32 Variation of lateral force with displacement at ground level for Series 2 test.

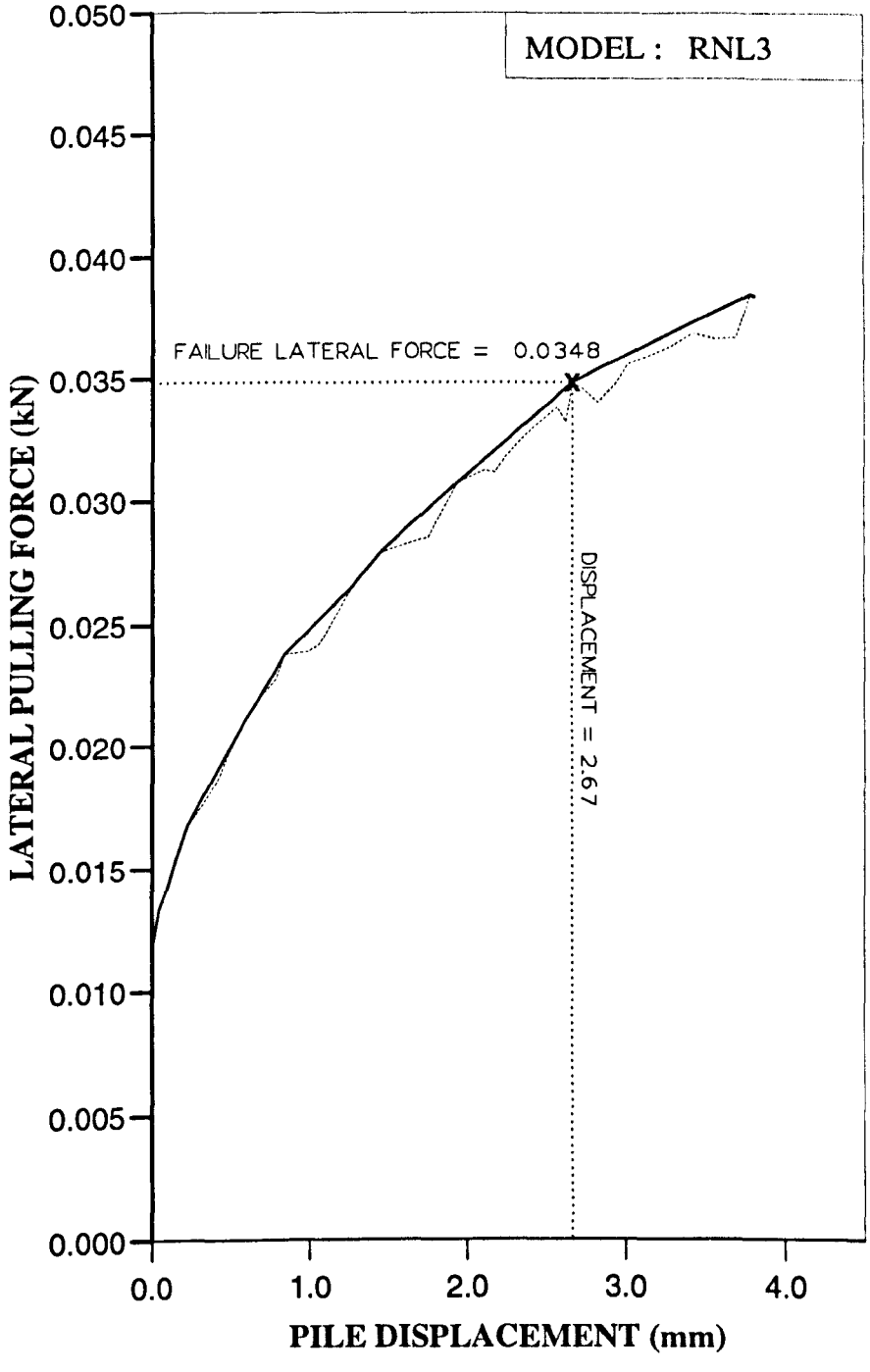

Figure AL33 Variation of lateral force with displacement at ground level for Series 2 test.

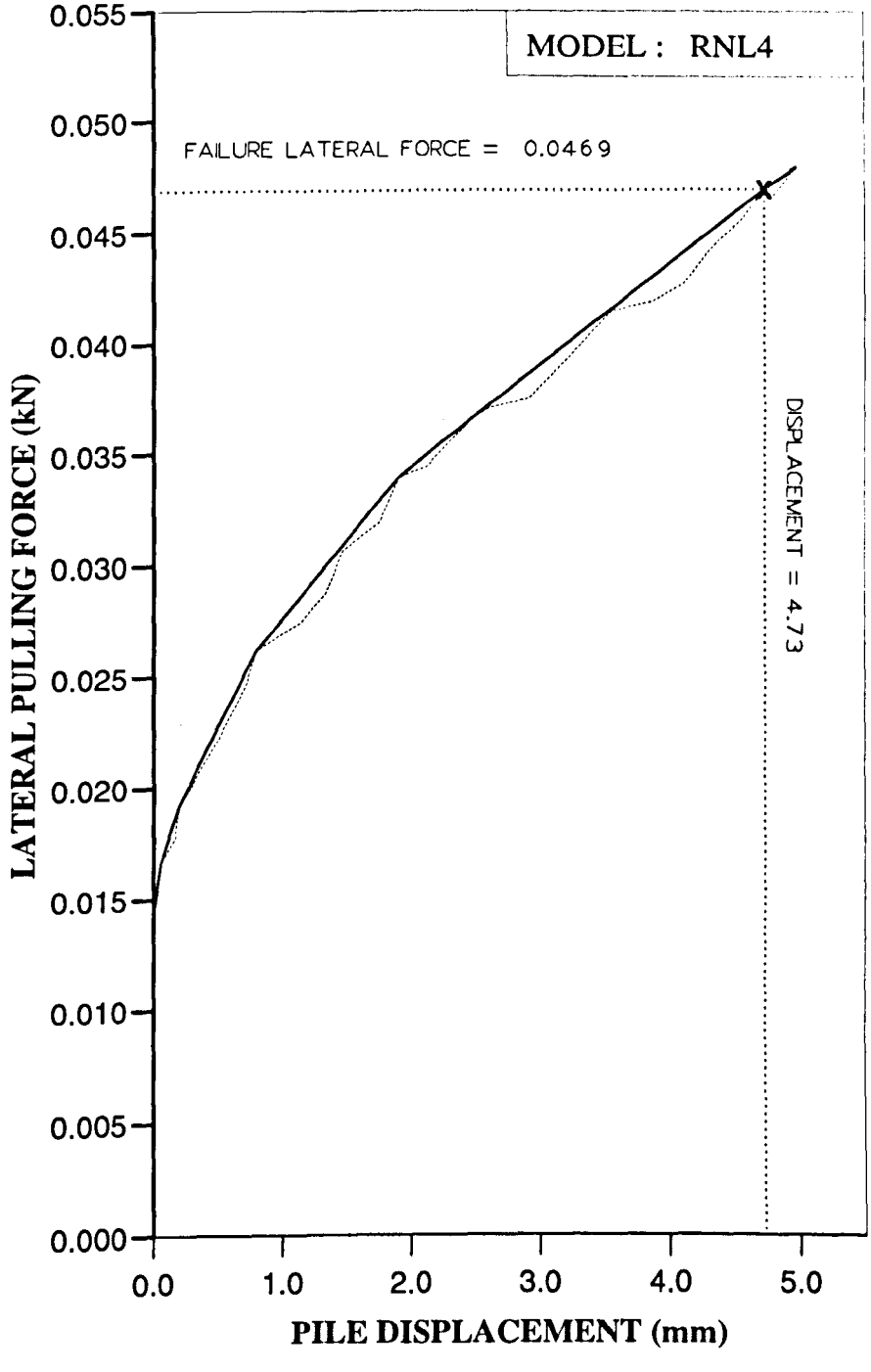

Figure AL34 Variation of lateral force with displacement at ground level for Series 1 test.

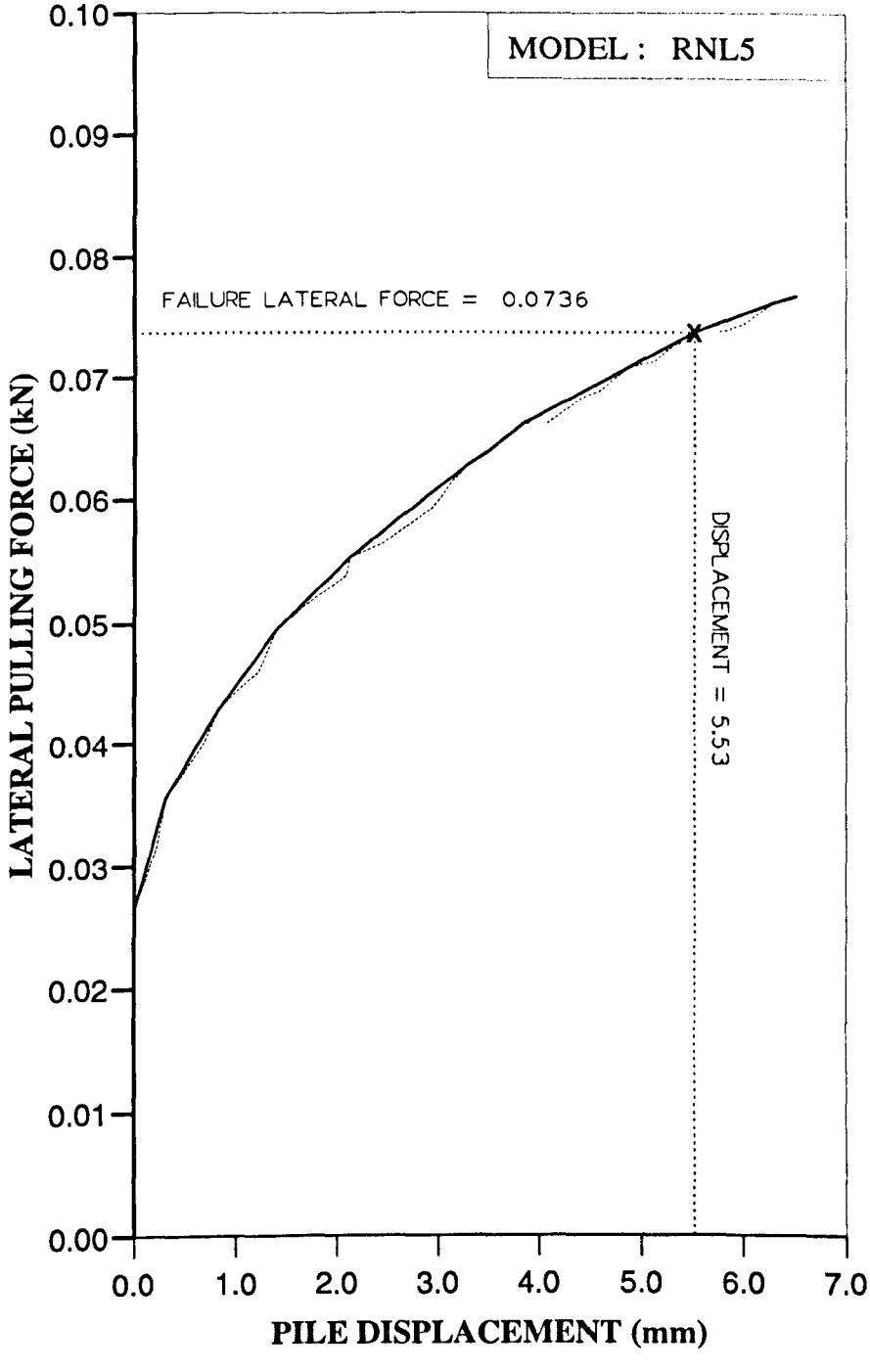

Figure AL35 Variation of lateral force with displacement at ground level for Series 1 test.

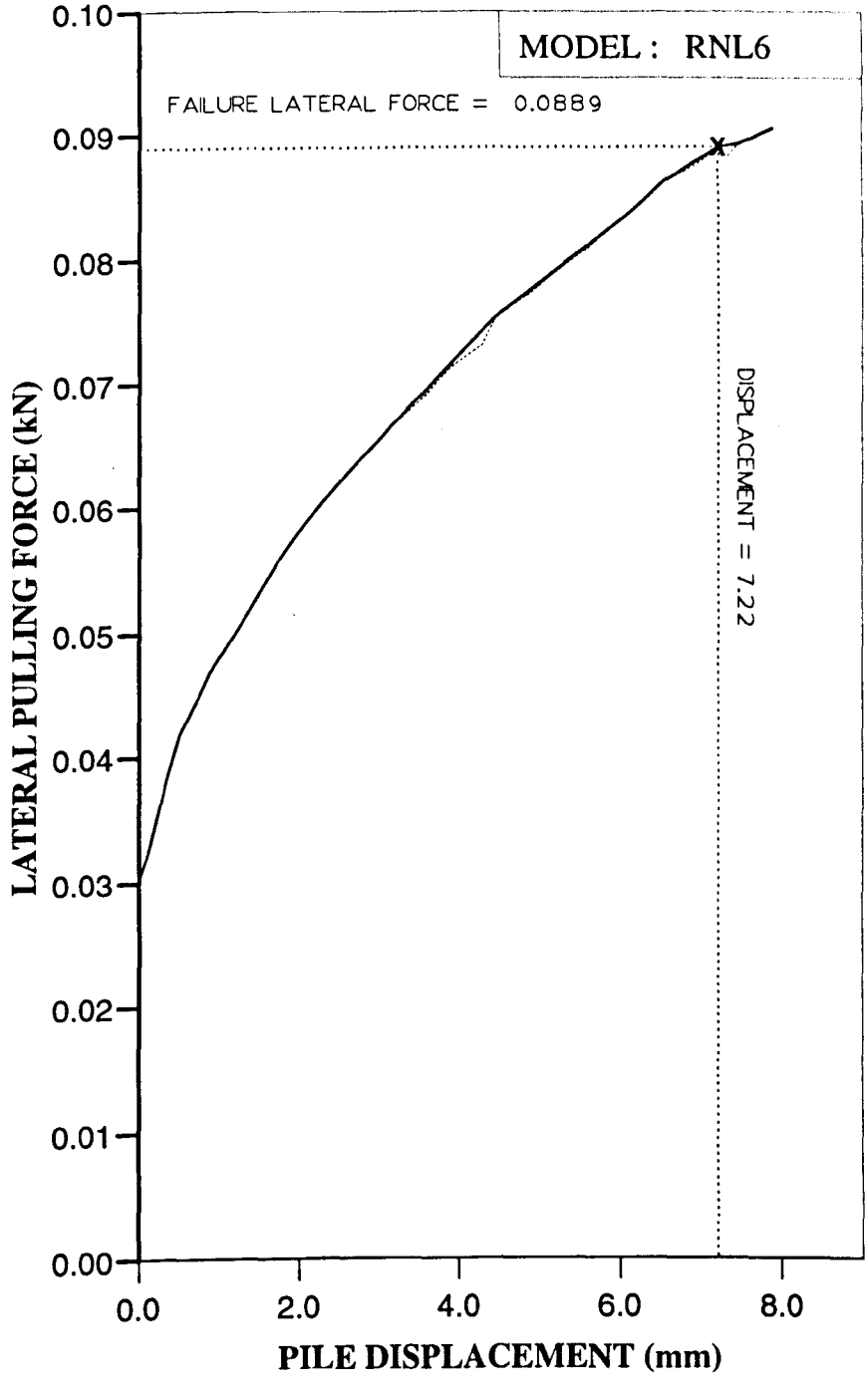

Figure AL36 Variation of lateral force with displacement at ground level for Series 1 test.

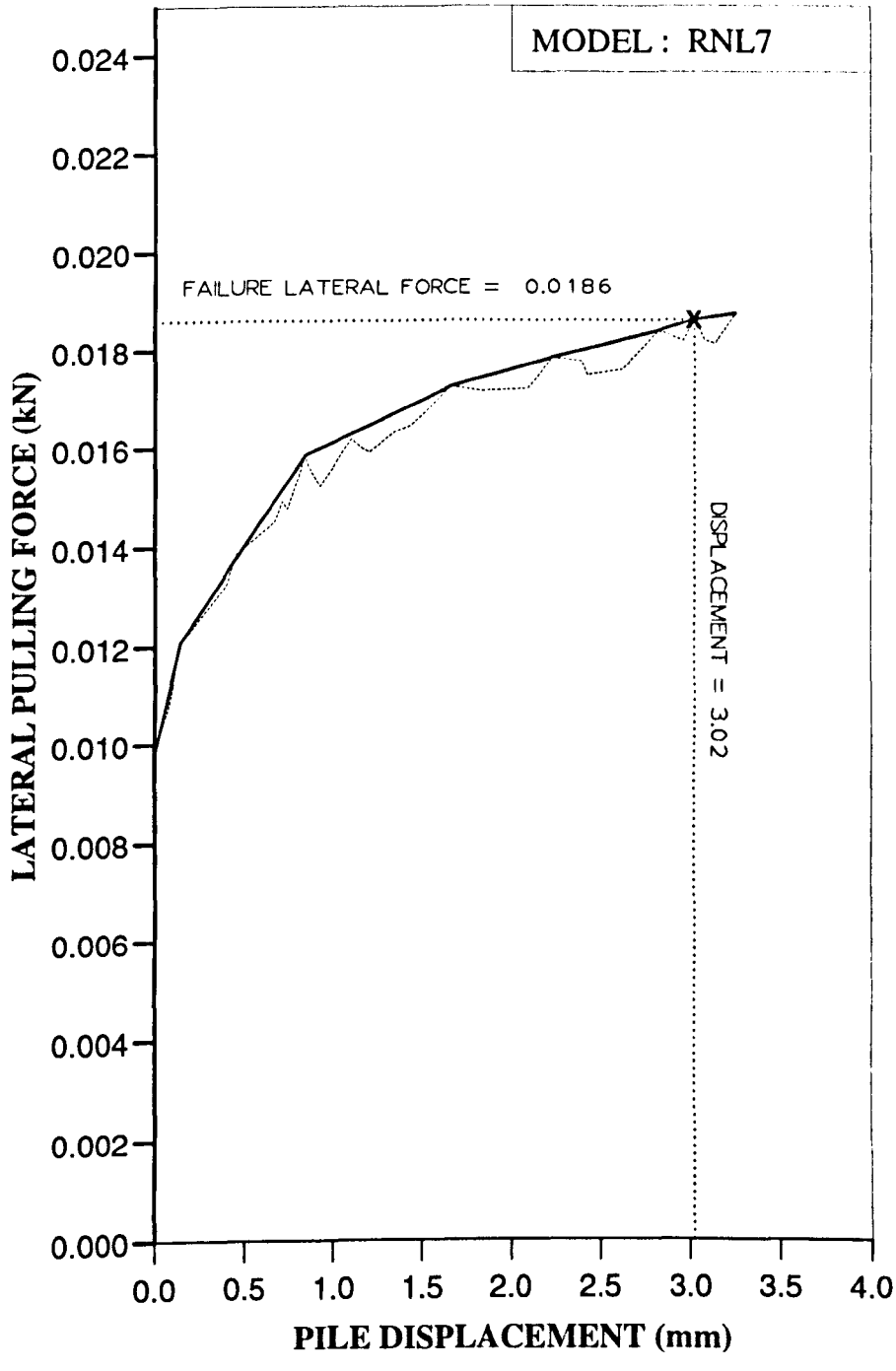

Figure AL37 Variation of lateral force with displacement at ground level for Series 1 test.

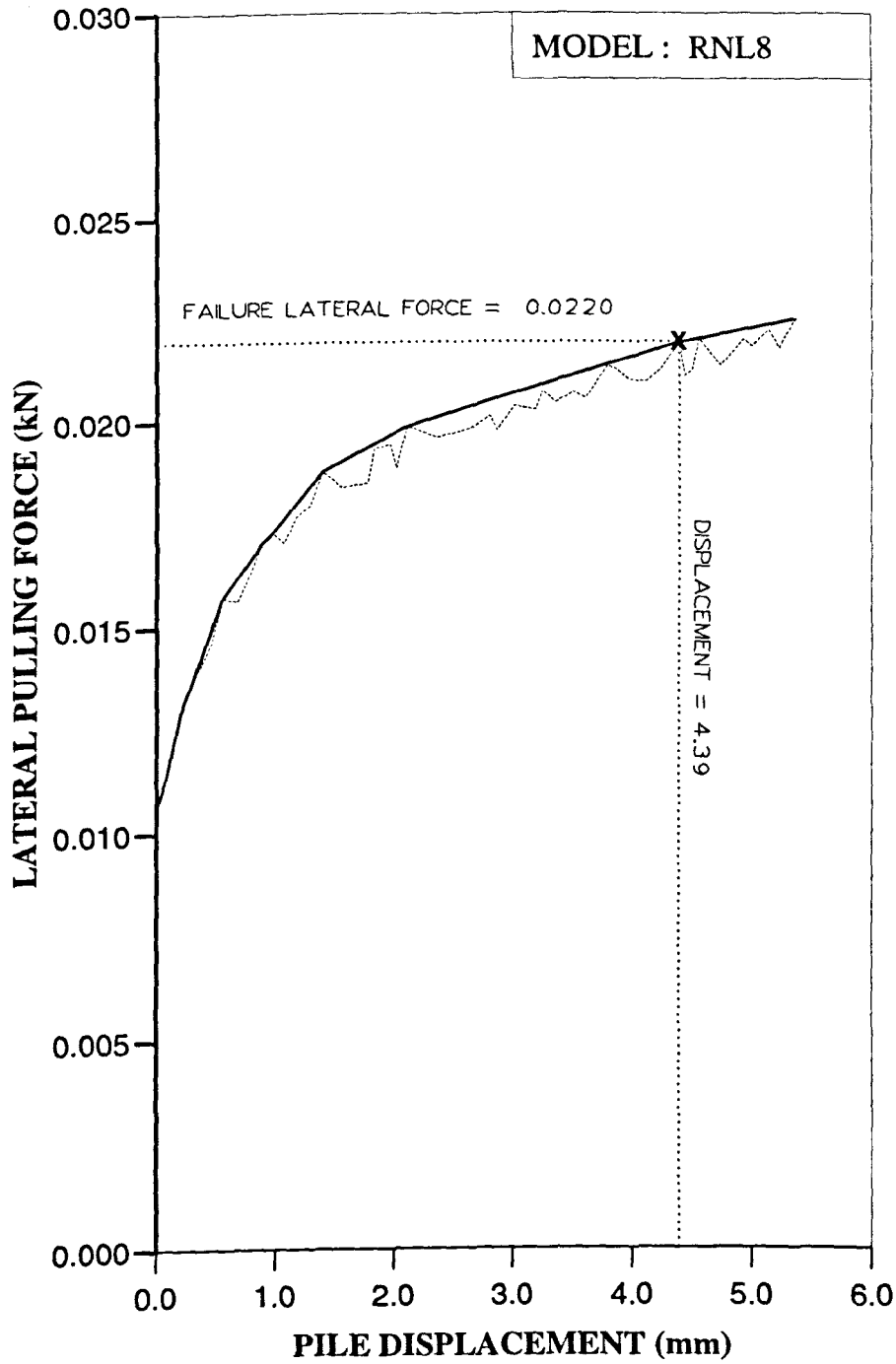

Figure AL38 Variation of lateral force with displacement at ground level for Series 2 test.

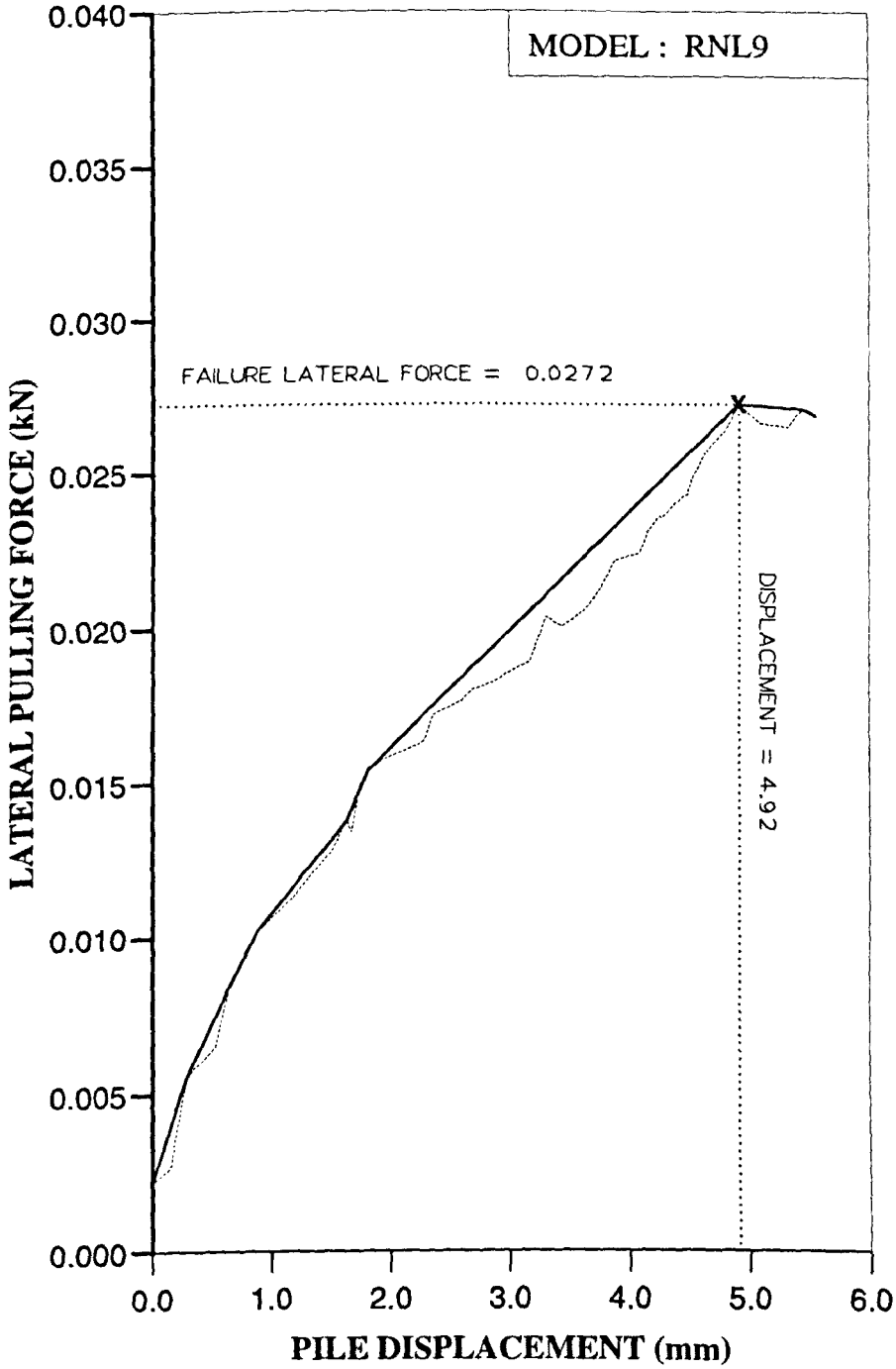

Figure AL39 Variation of lateral force with displacement at ground level for Series 2 test.

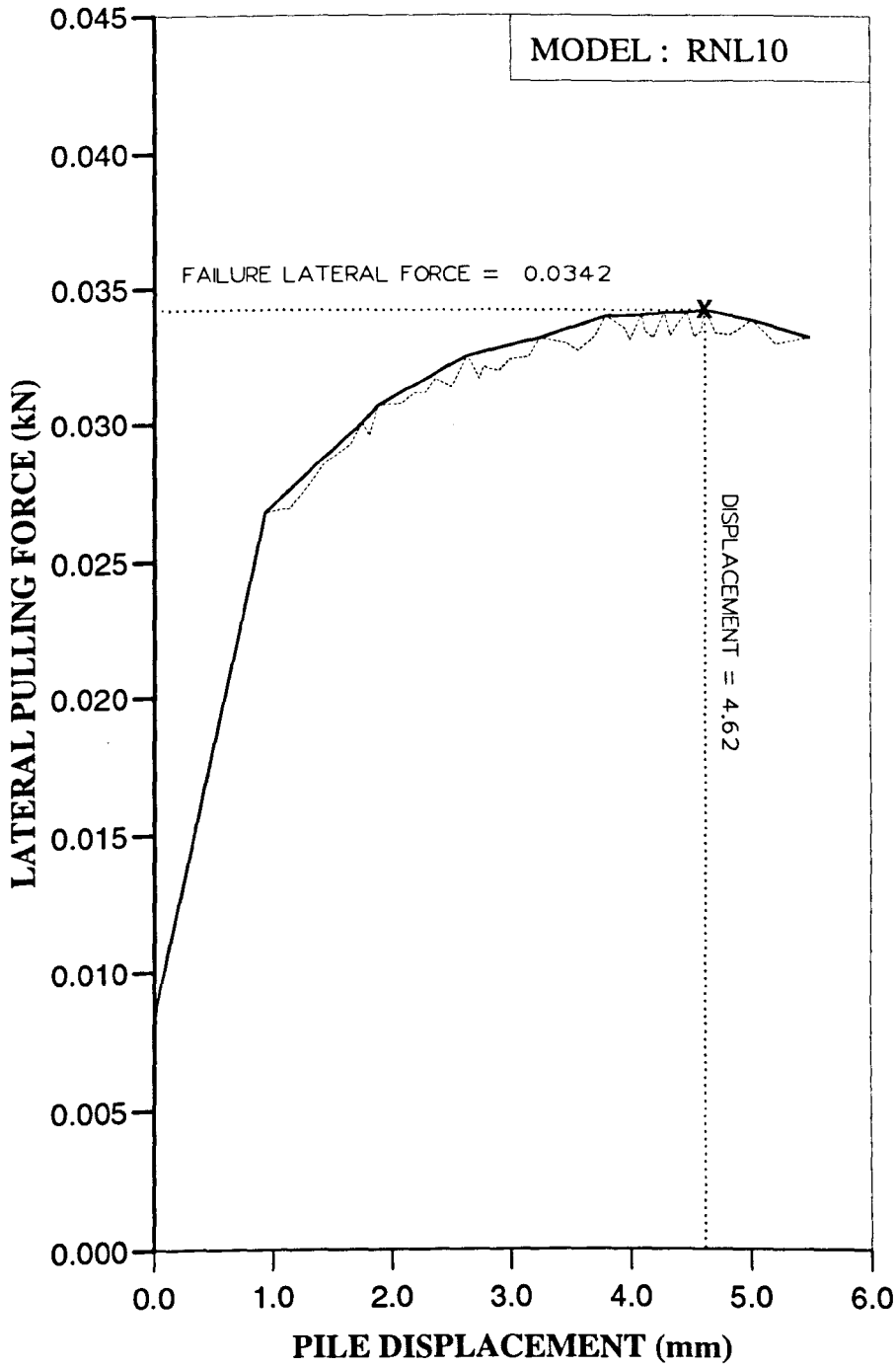

Figure AL40 Variation of lateral force with displacement at ground level for Series 2 test.

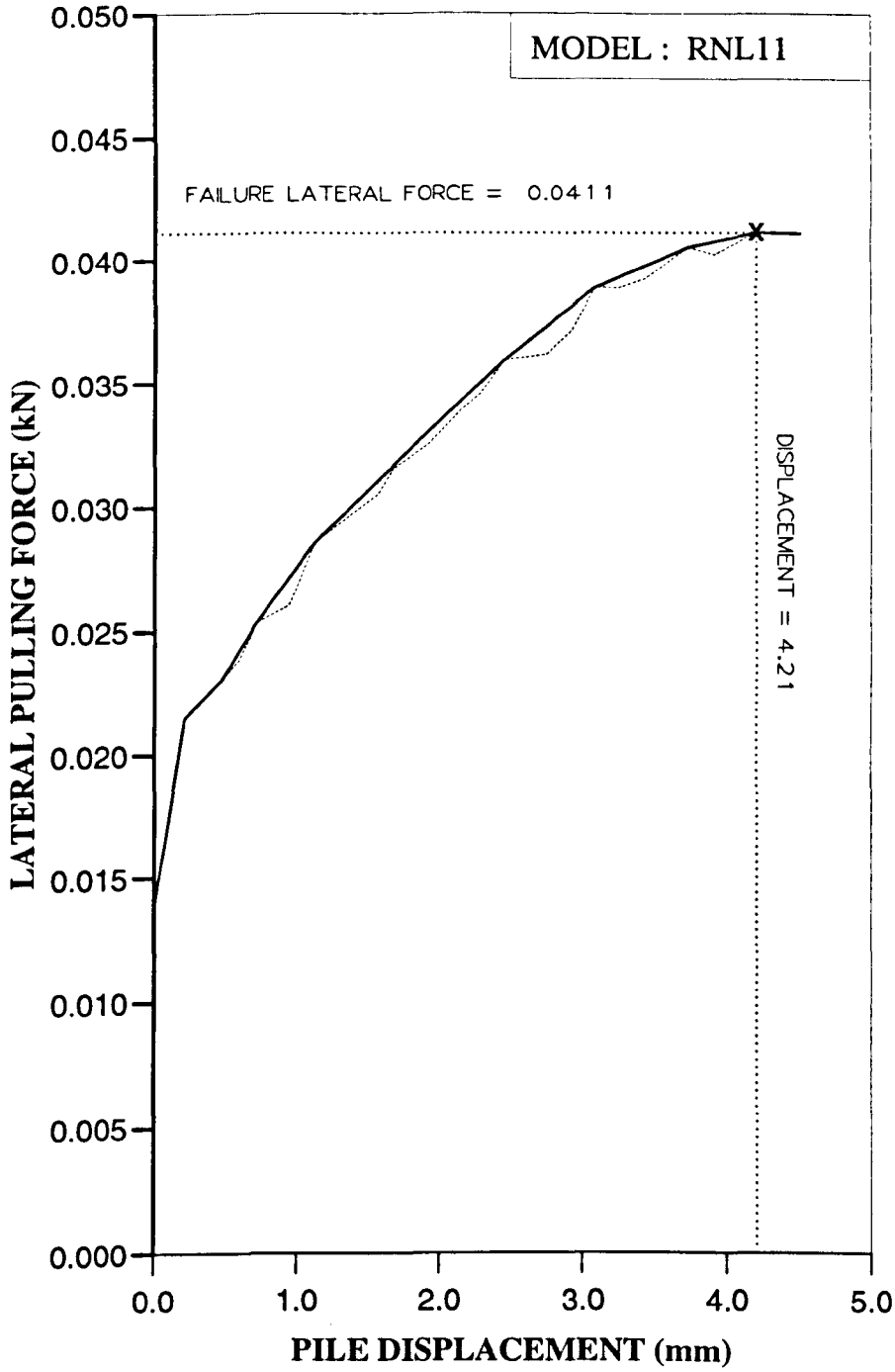

Figure AL41 Variation of lateral force with displacement at ground level for Series 2 test.

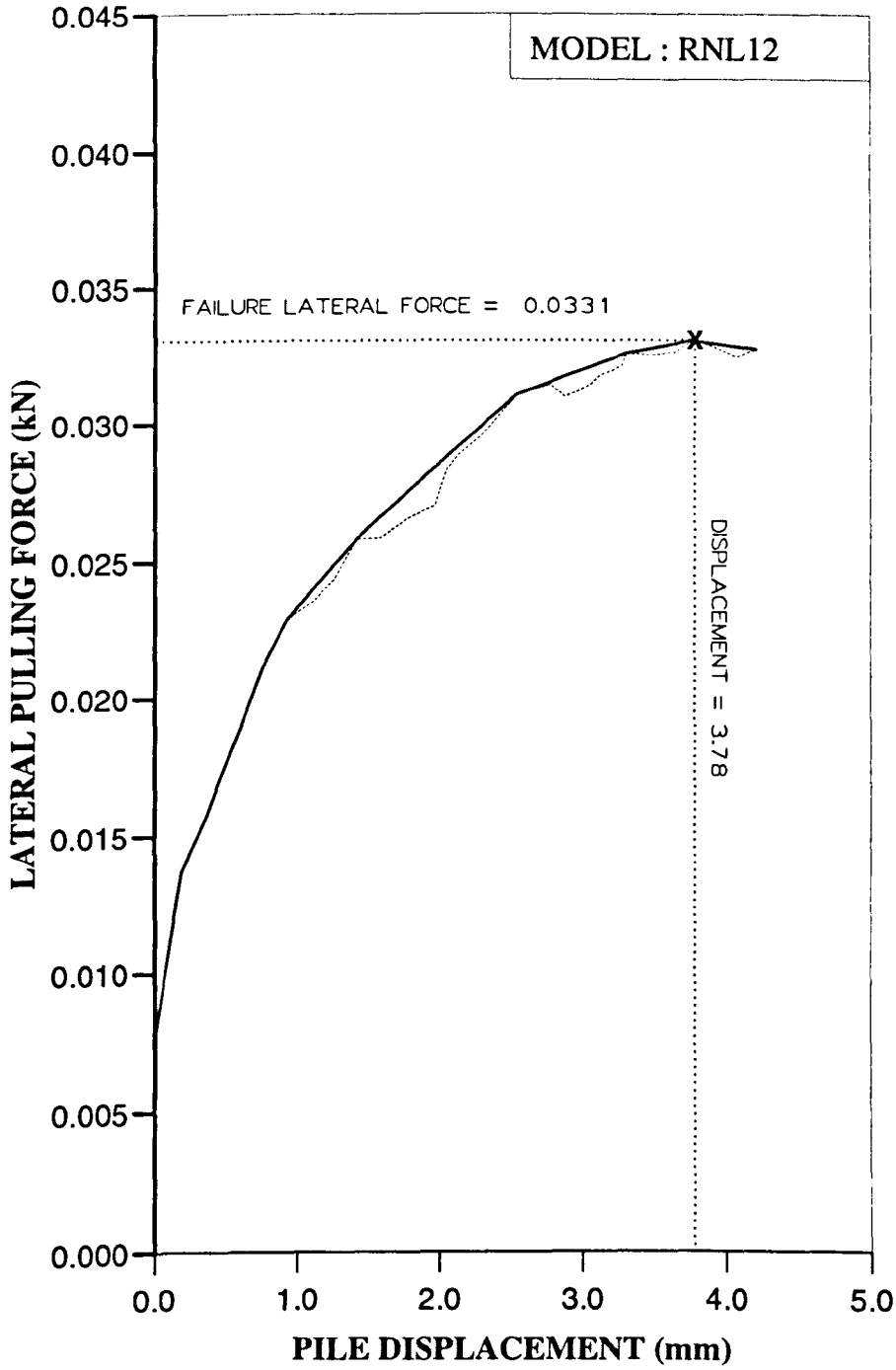

Figure AL42 Variation of lateral force with displacement at ground level for Series 2 test.

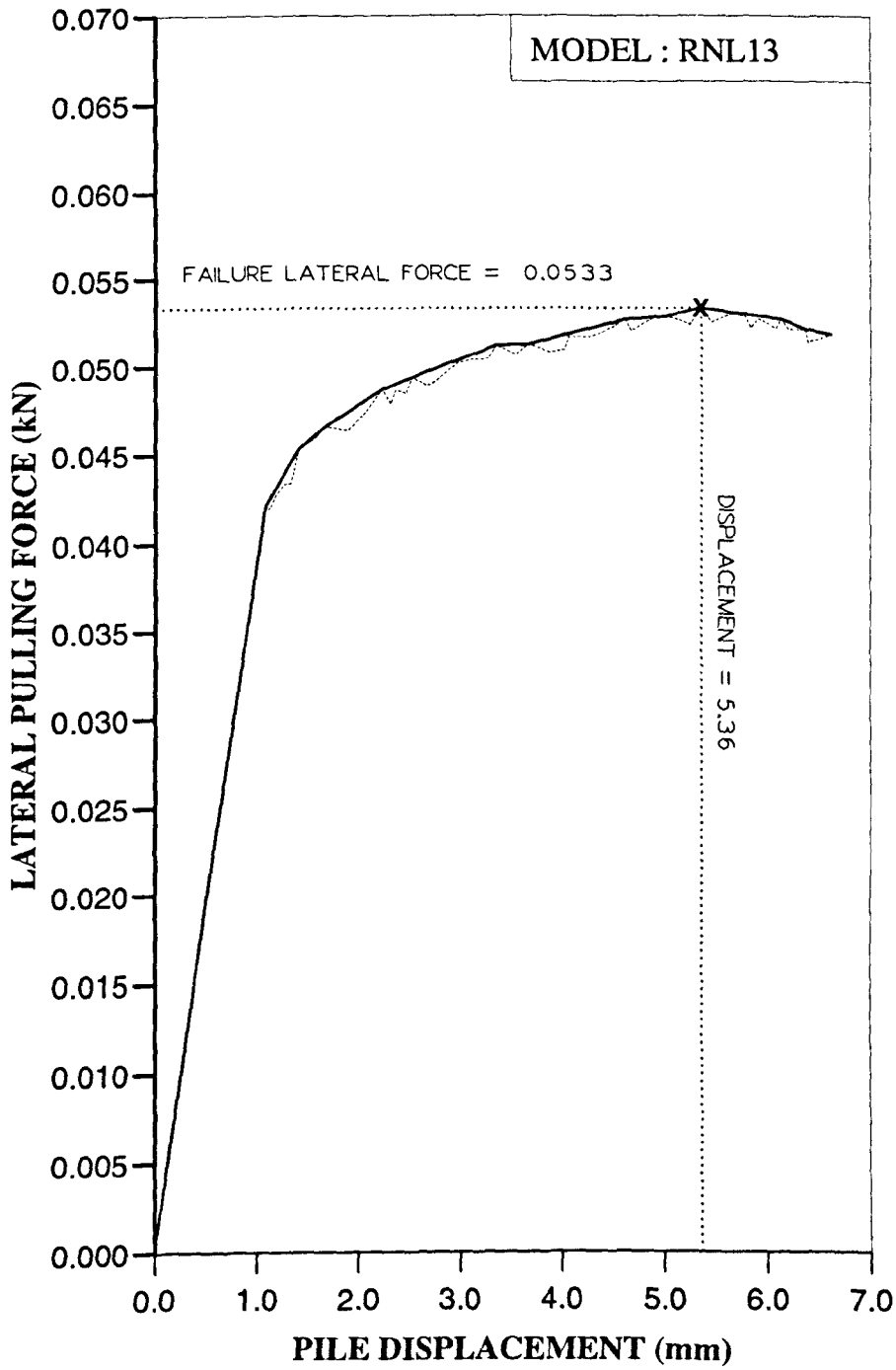

Figure AL43 Variation of lateral force with displacement at ground level for Series 2 test.

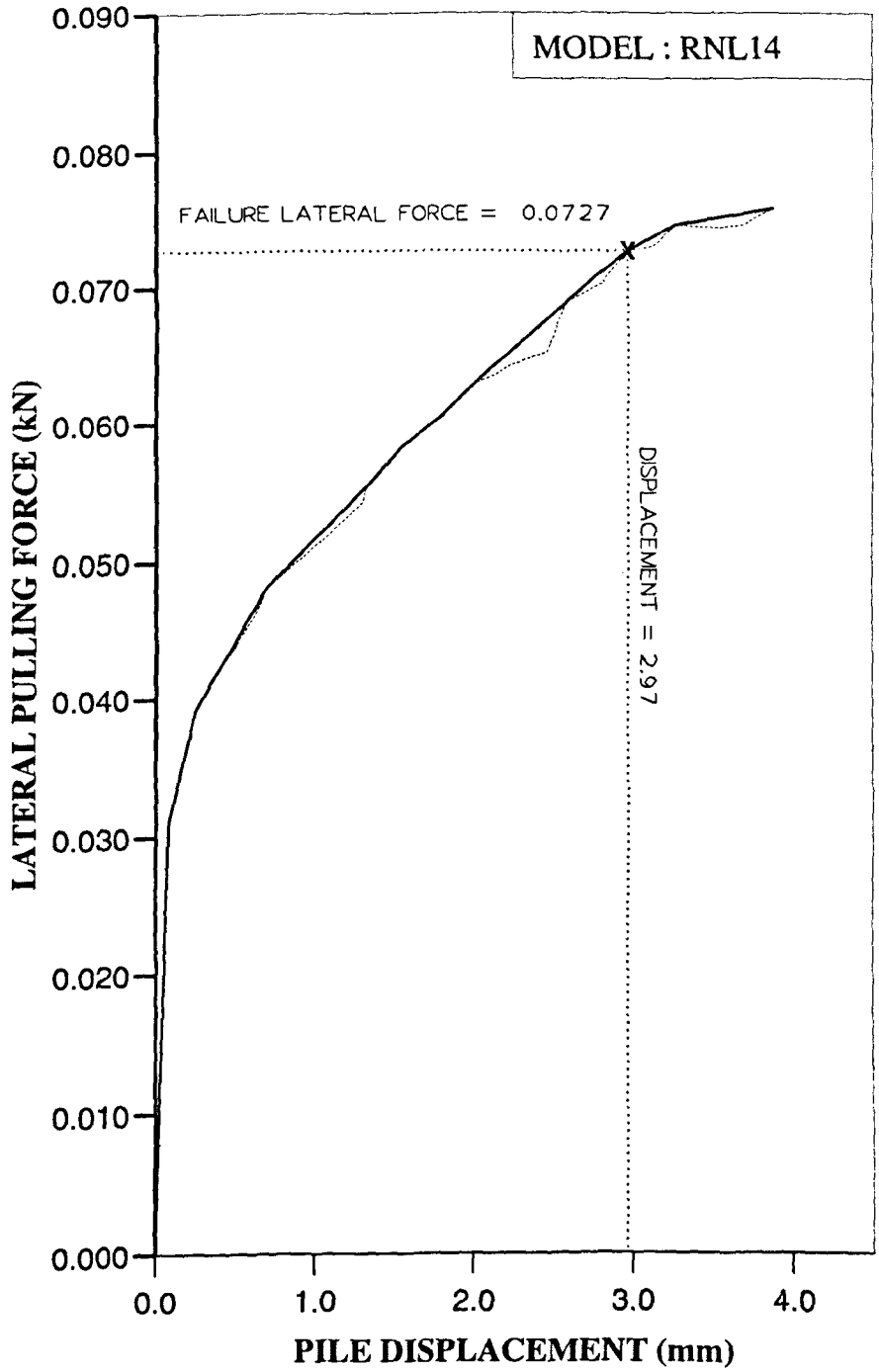

Figure AL44 Variation of lateral force with displacement at ground level for Series 2 test.

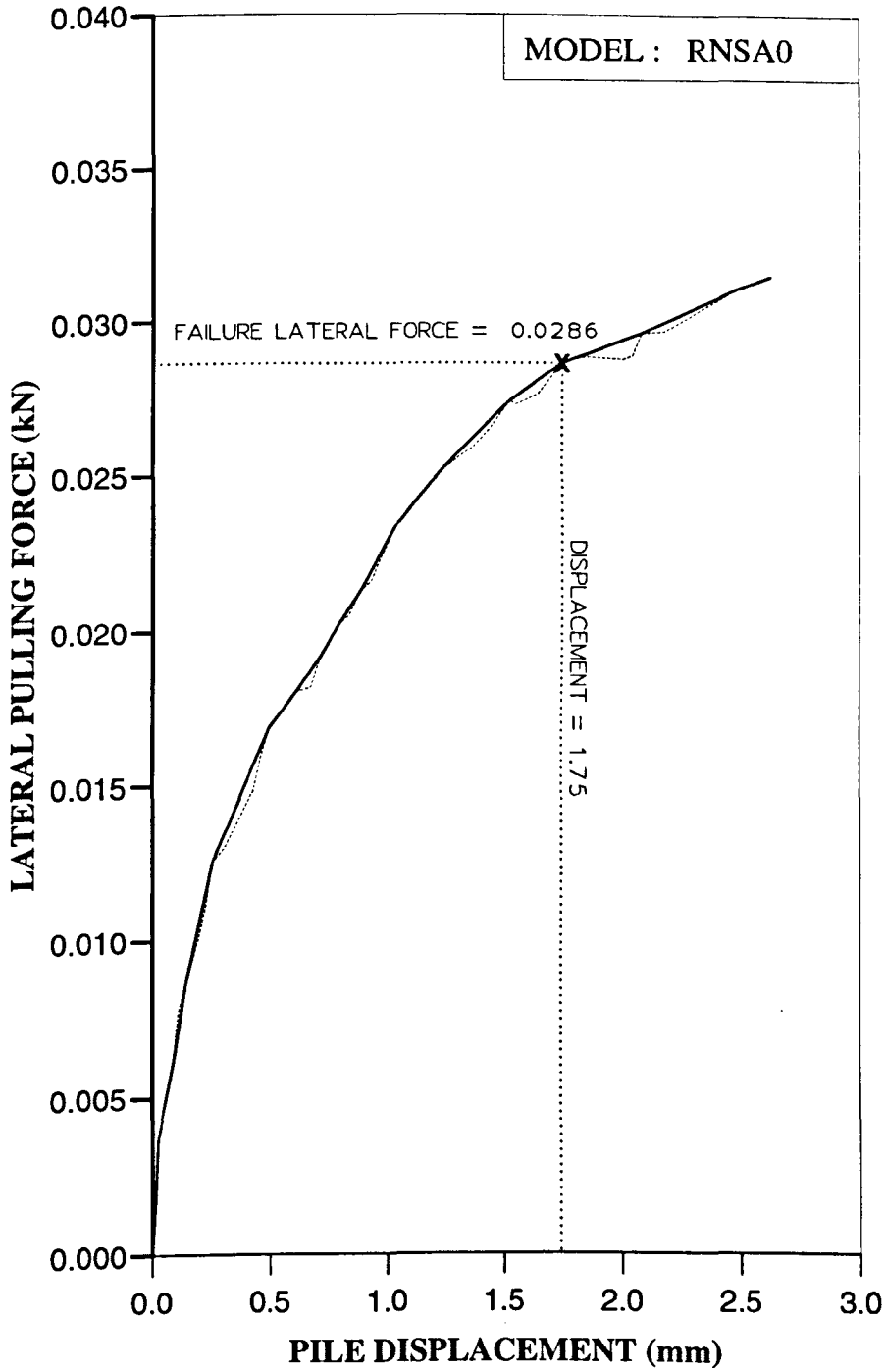

Figure AL45 Variation of lateral force with displacement at ground level for Series 3 test.

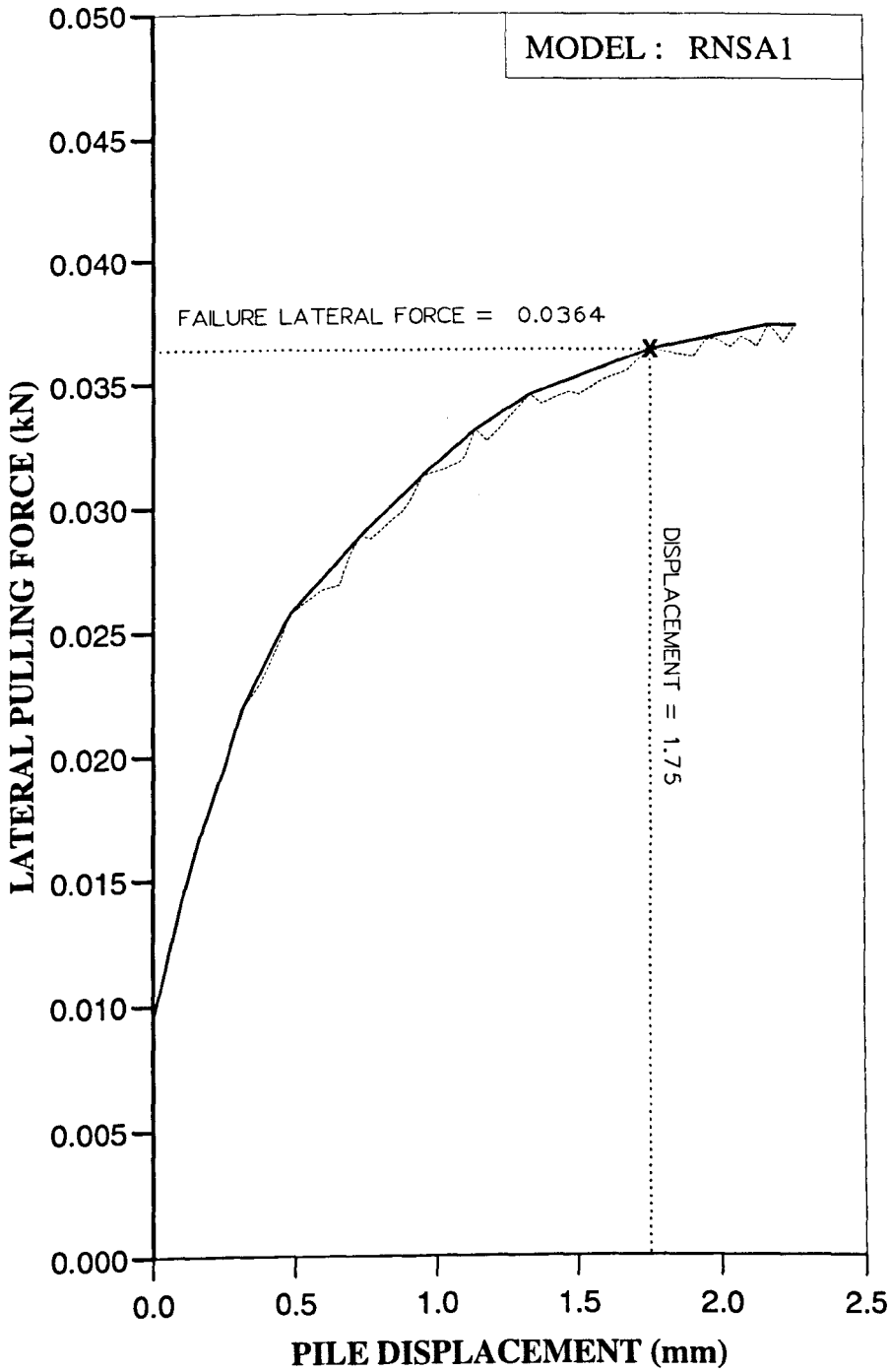

Figure AL46 Variation of lateral force with displacement at ground level for Series 3 test.

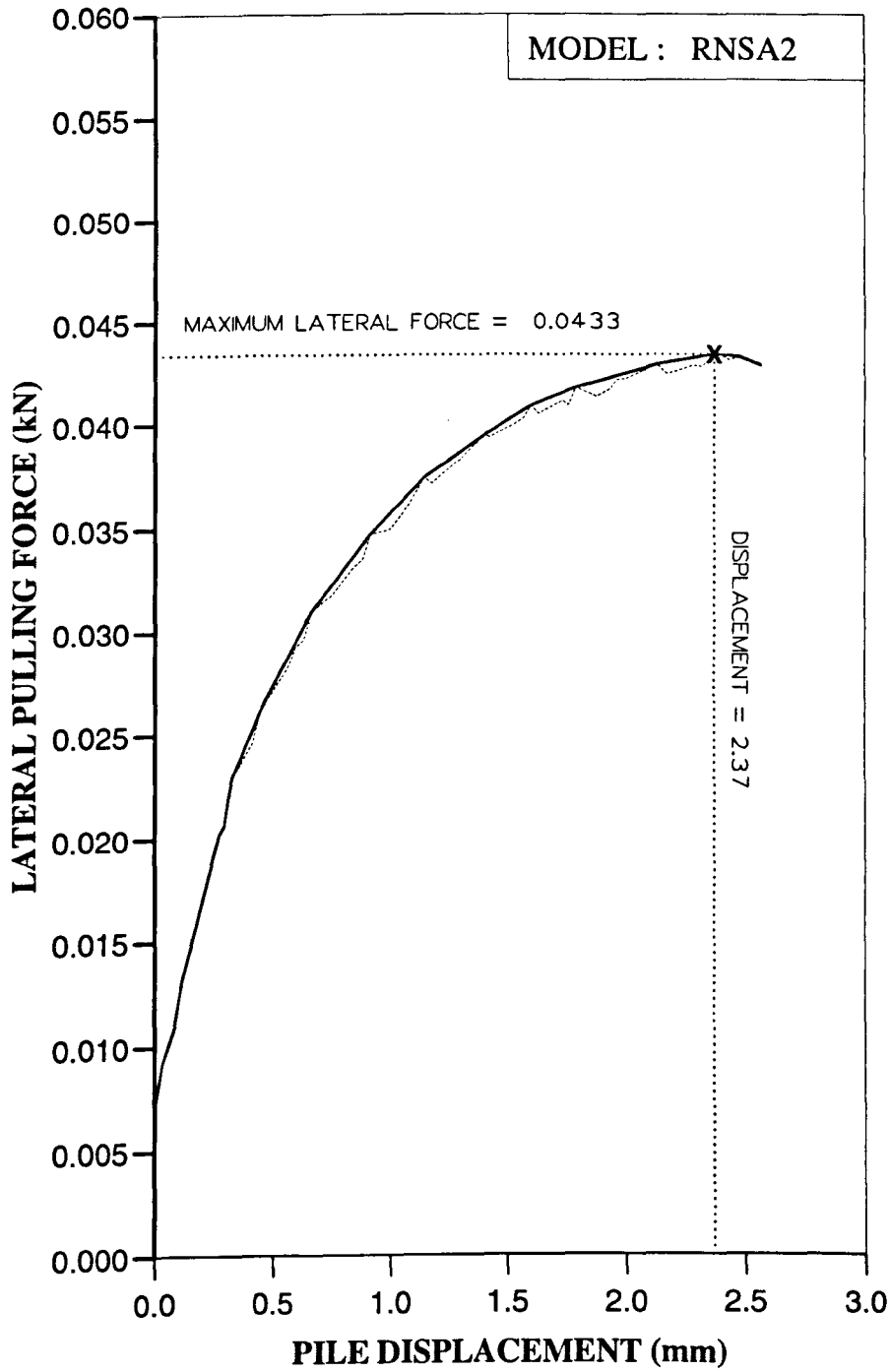

Figure AL47 Variation of lateral force with displacement at ground level for Series 3 test.

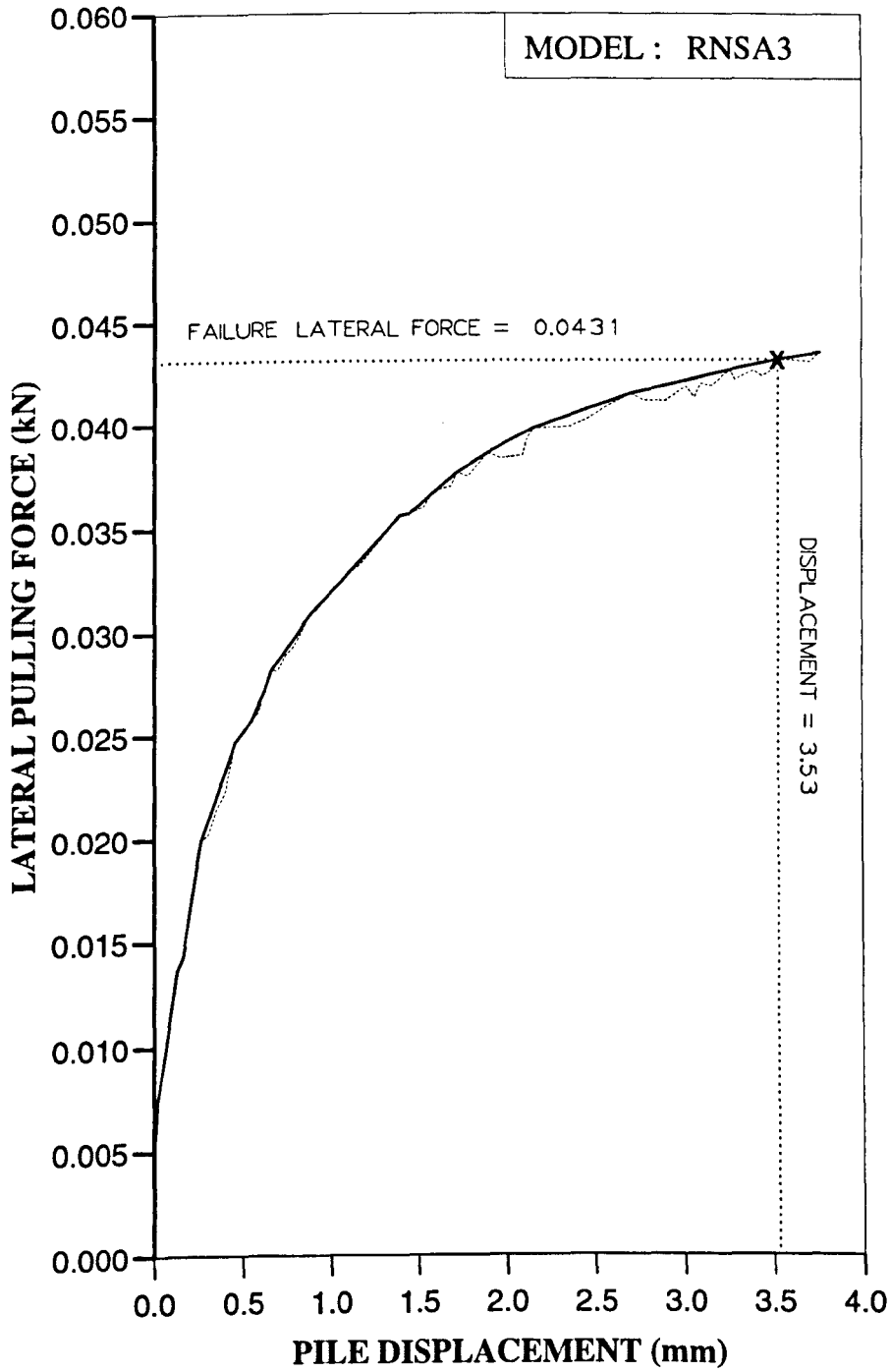

Figure AL48 Variation of lateral force with displacement at ground level for Series 3 test.

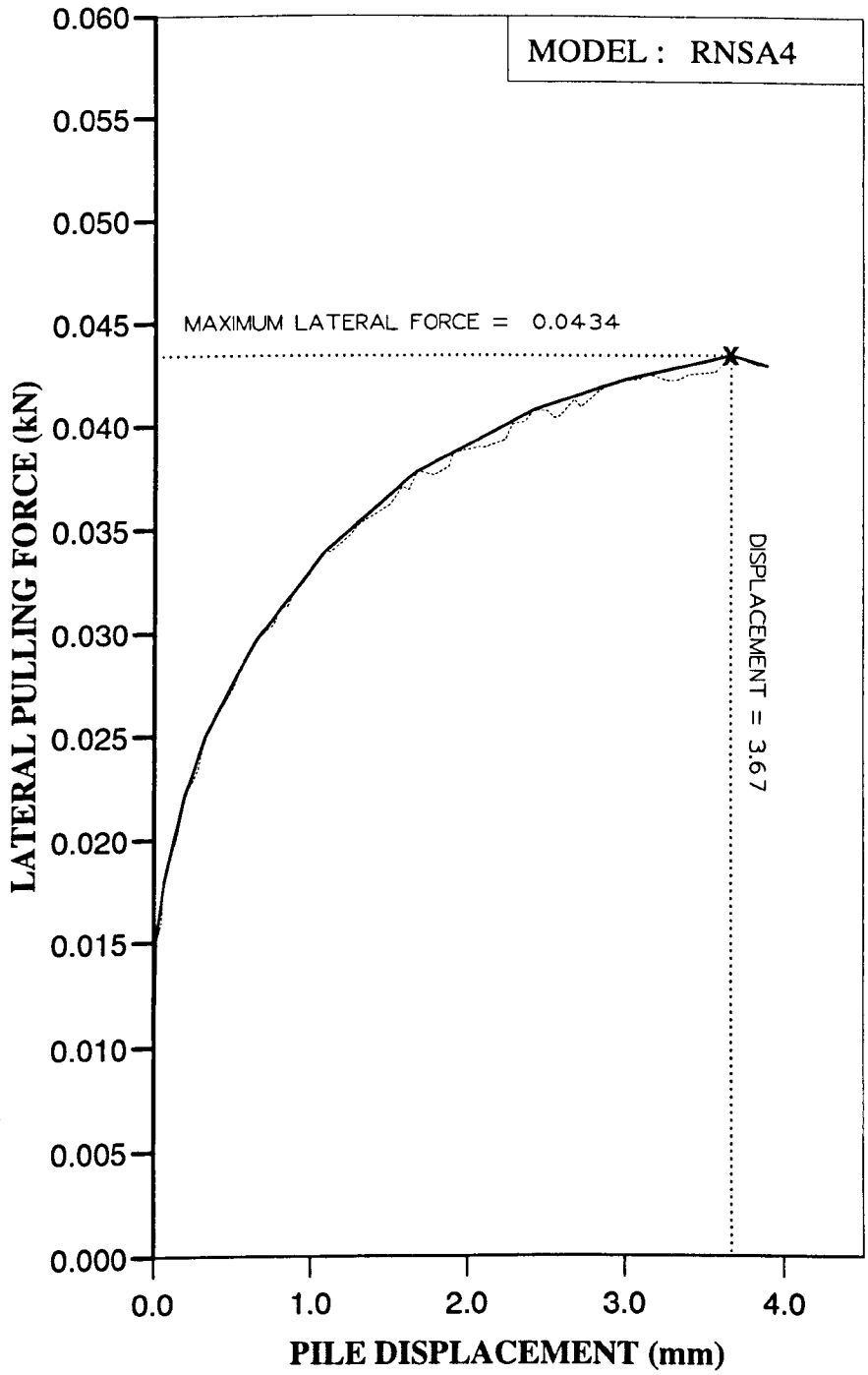

Figure AL49 Variation of lateral force with displacement at ground level for Series 3 test.

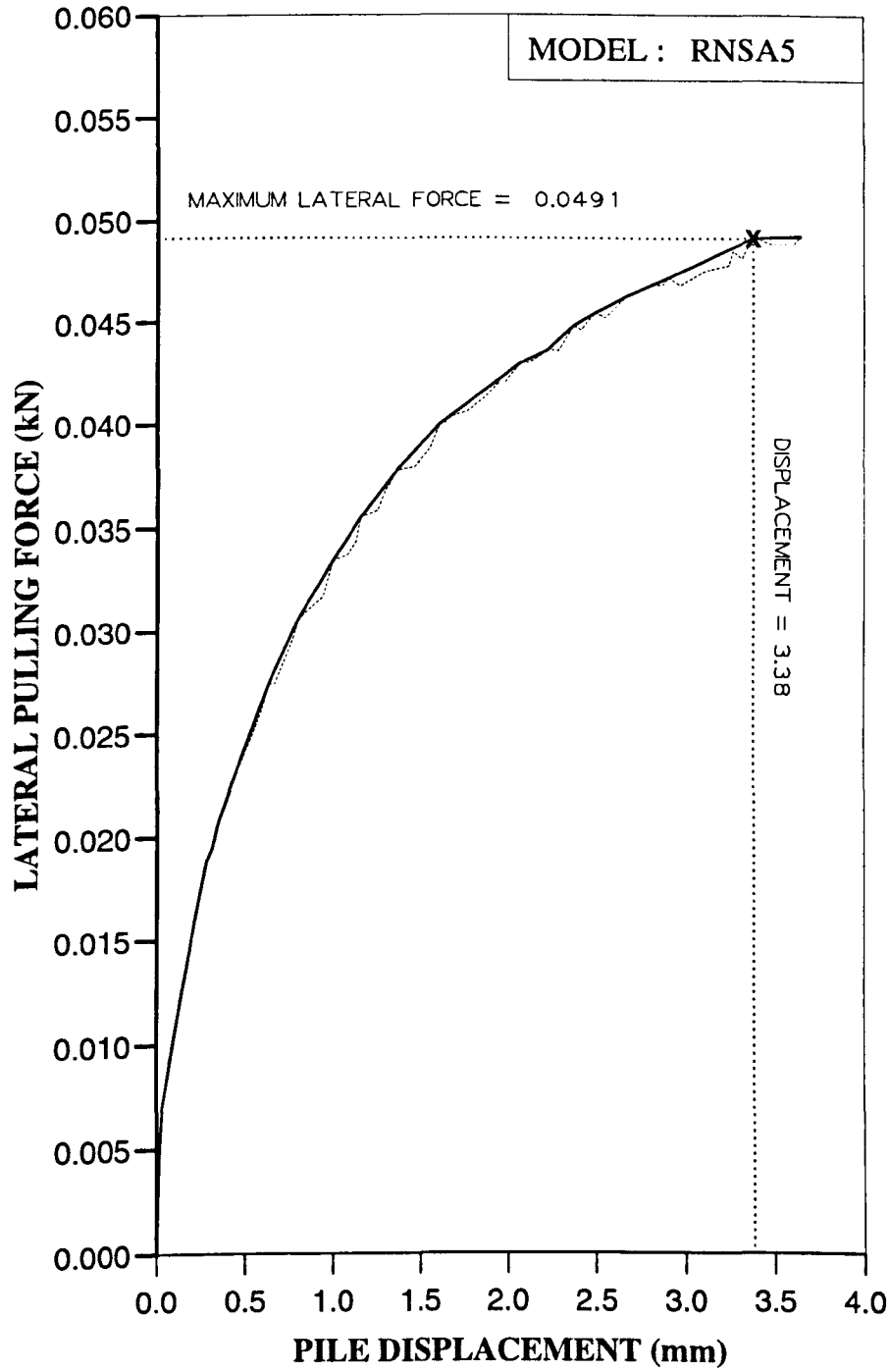

Figure AL50 Variation of lateral force with displacement at ground level for Series 3 test.

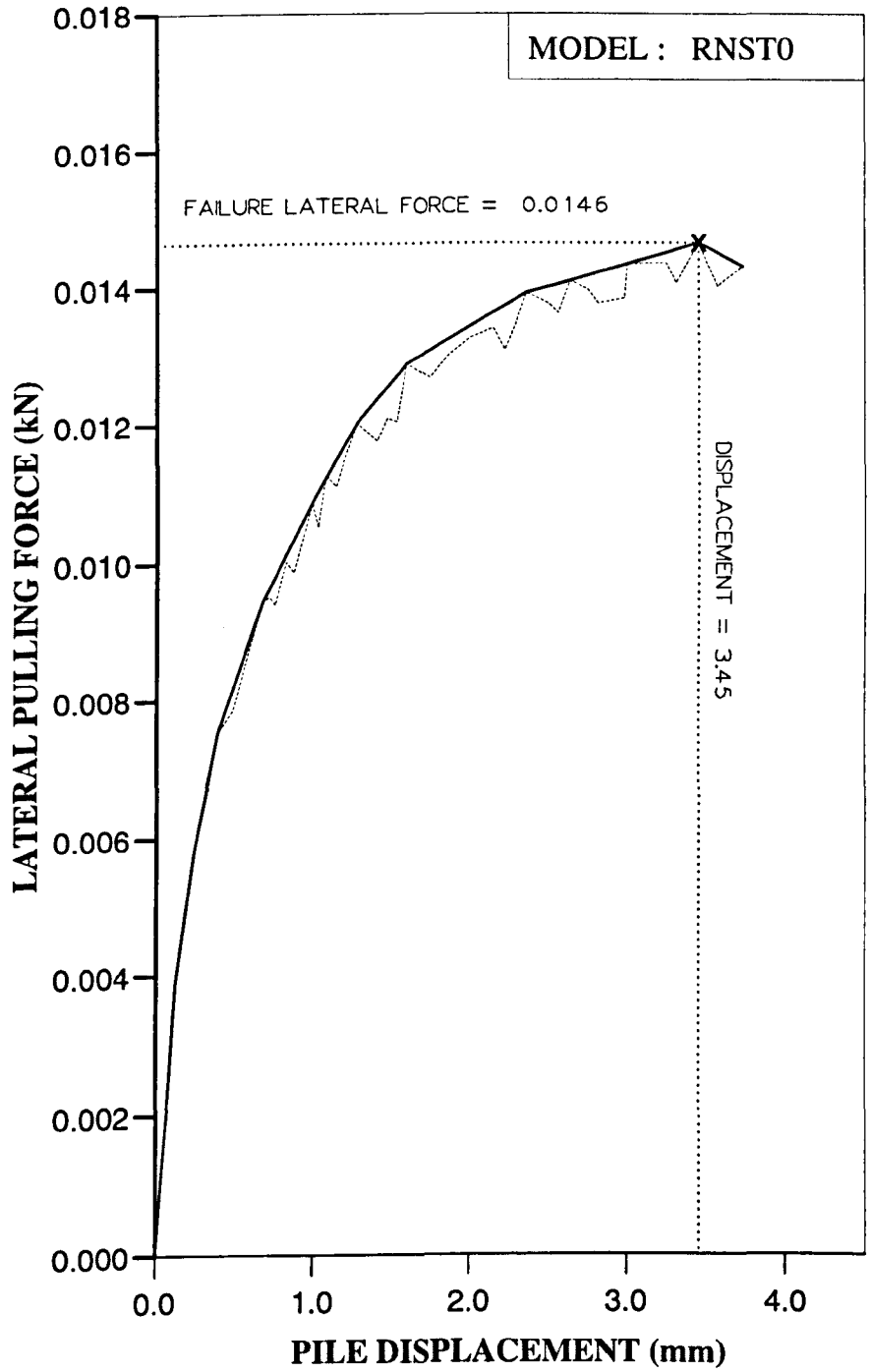

Figure AL51 Variation of lateral force with displacement at ground level for Series 3 test.

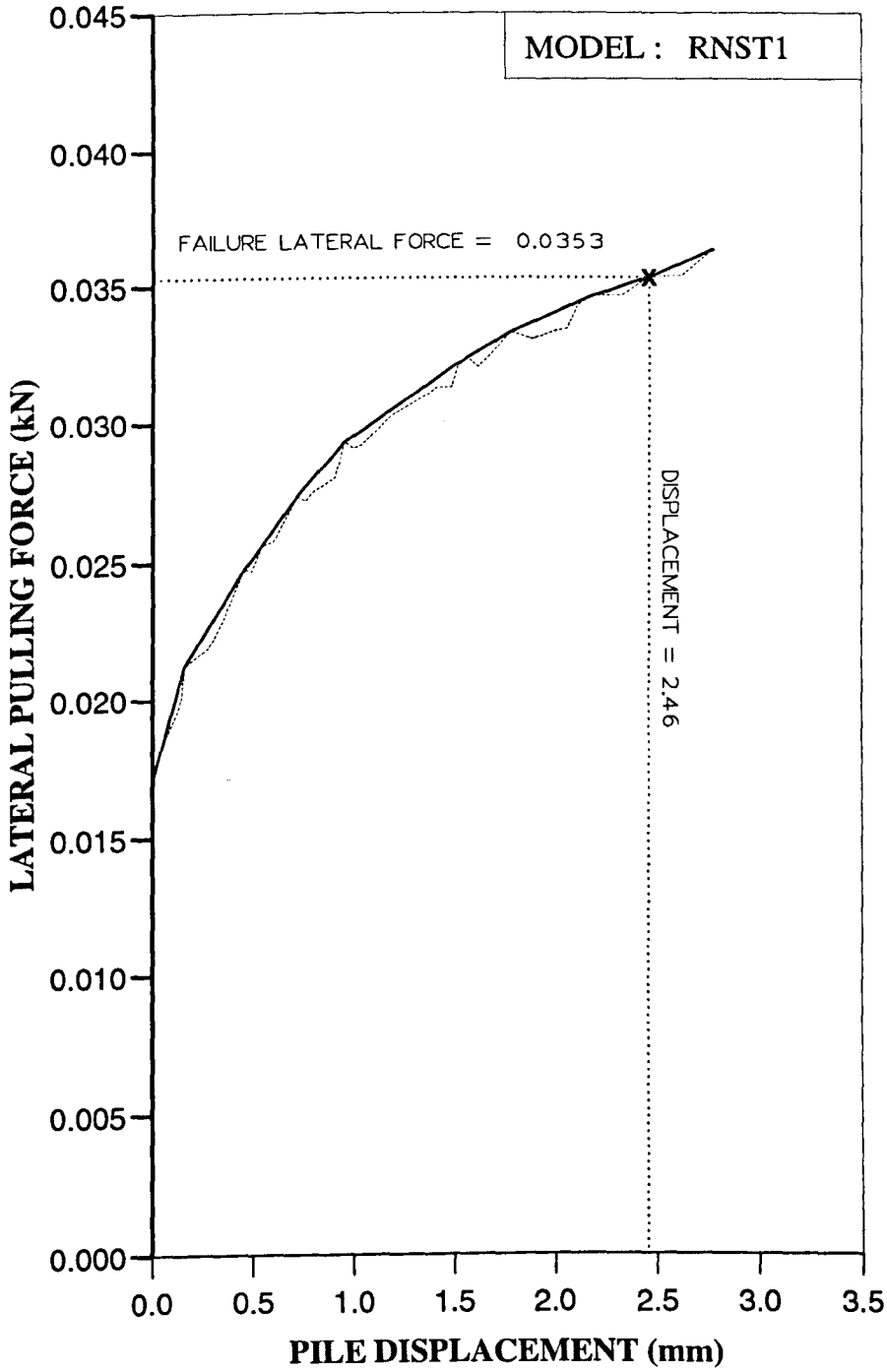

Figure AL52 Variation of lateral force with displacement at ground level for Series 3 test.

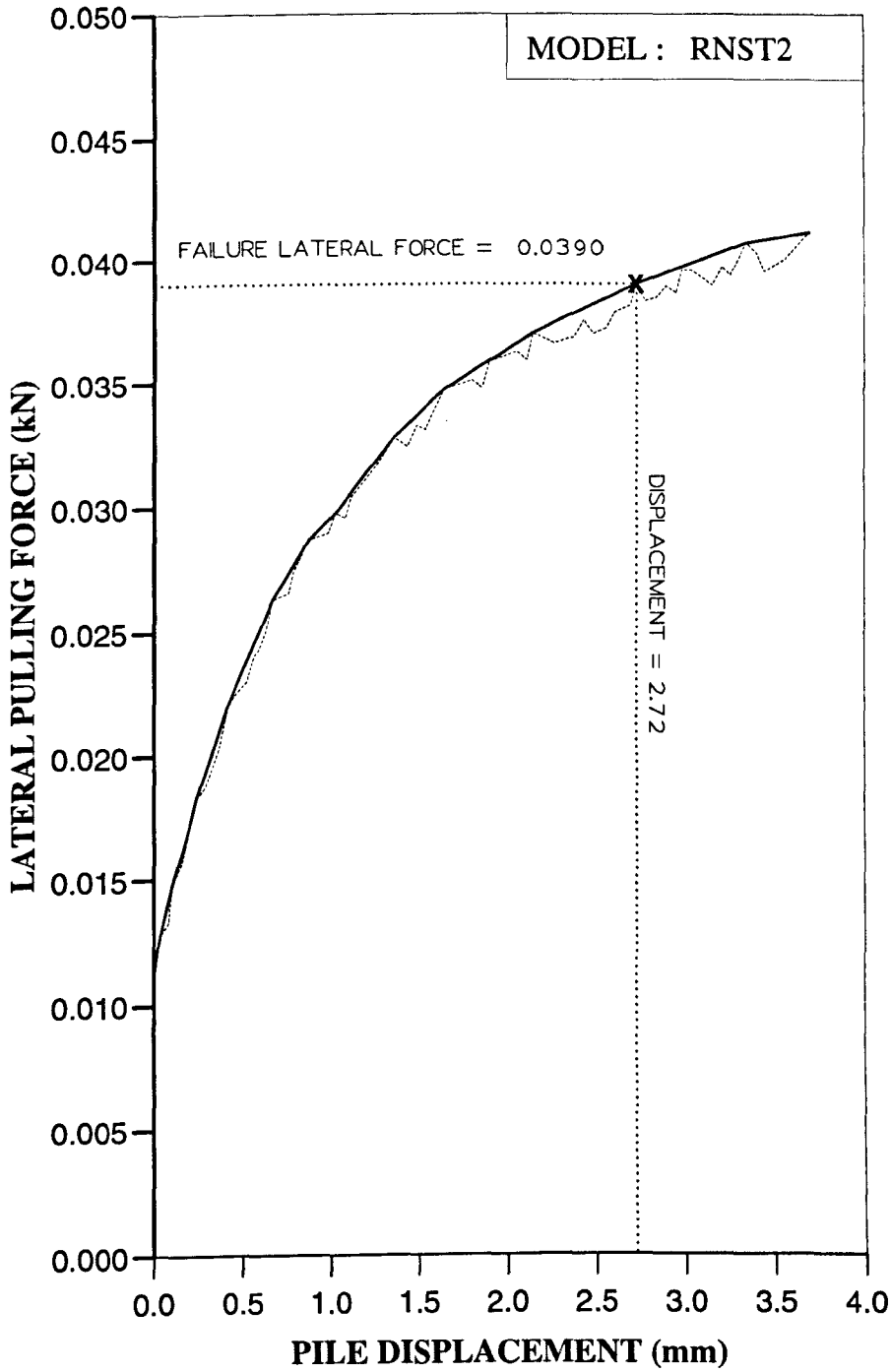

Figure AL53 Variation of lateral force with displacement at ground level for Series 3 test.

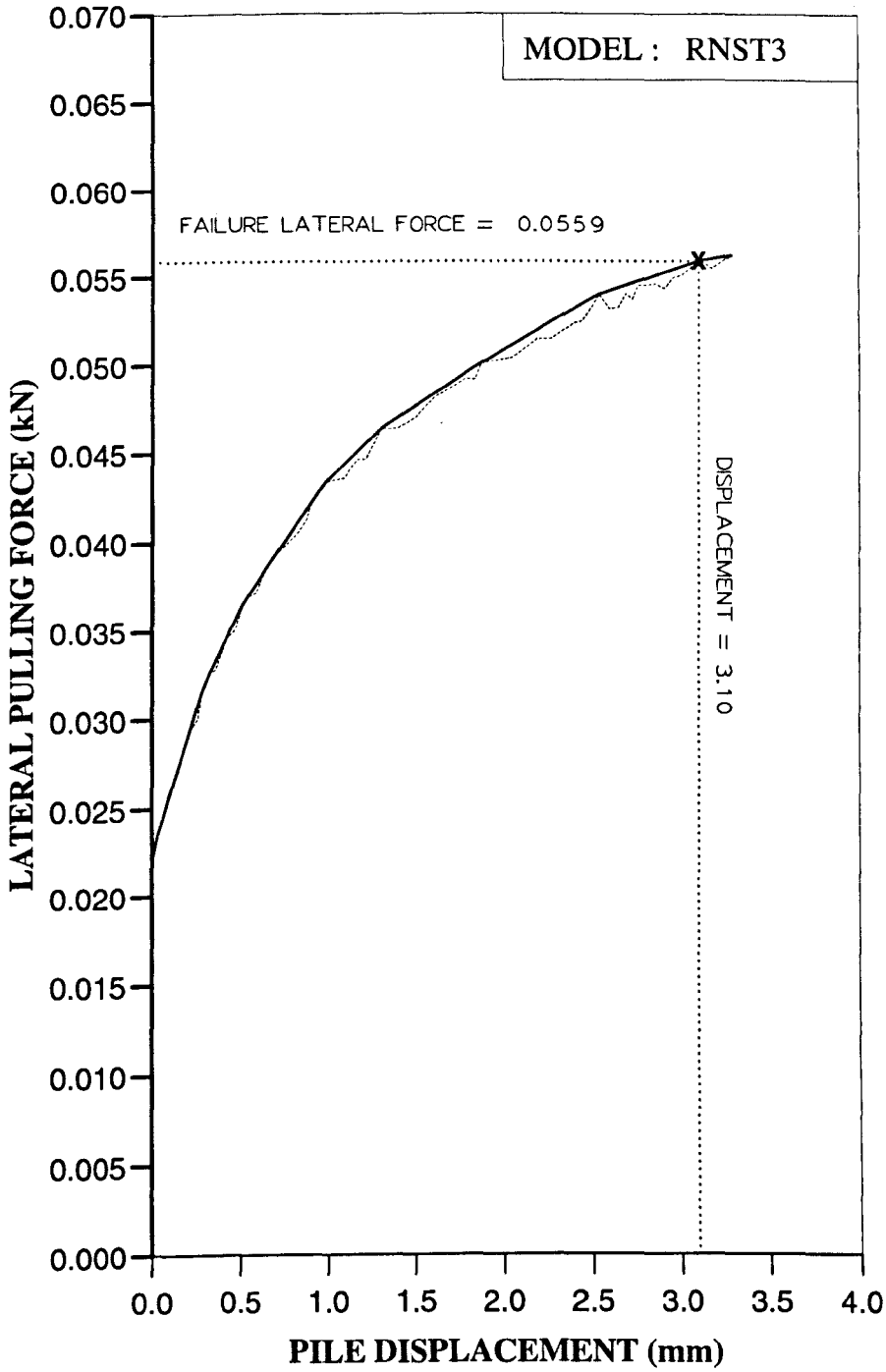

Figure AL54 Variation of lateral force with displacement at ground level for Series 3 test.

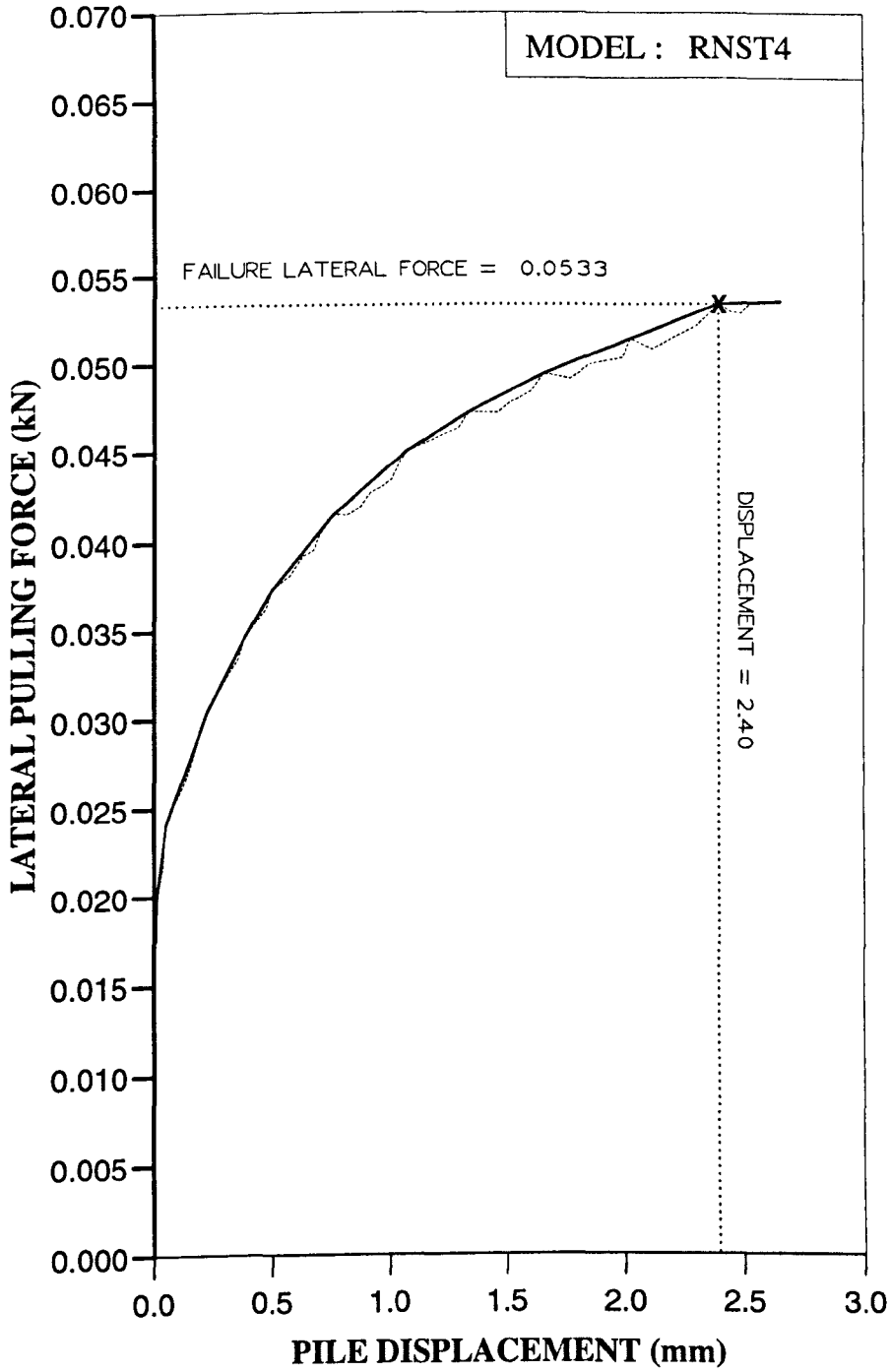

Figure AL55 Variation of lateral force with displacement at ground level for Series 3 test.

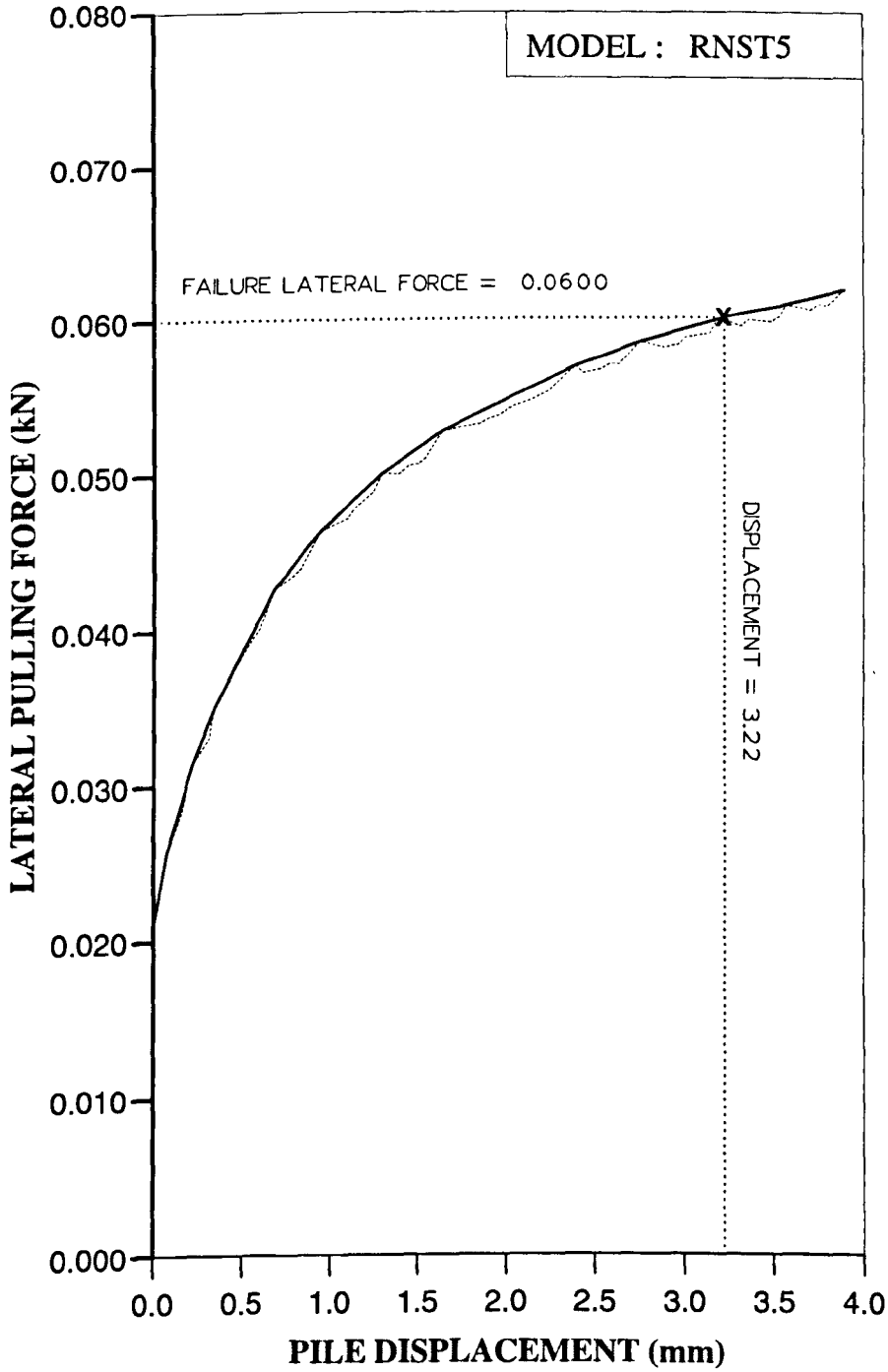

Figure AL56 Variation of lateral force with displacement at ground level for Series 3 test.

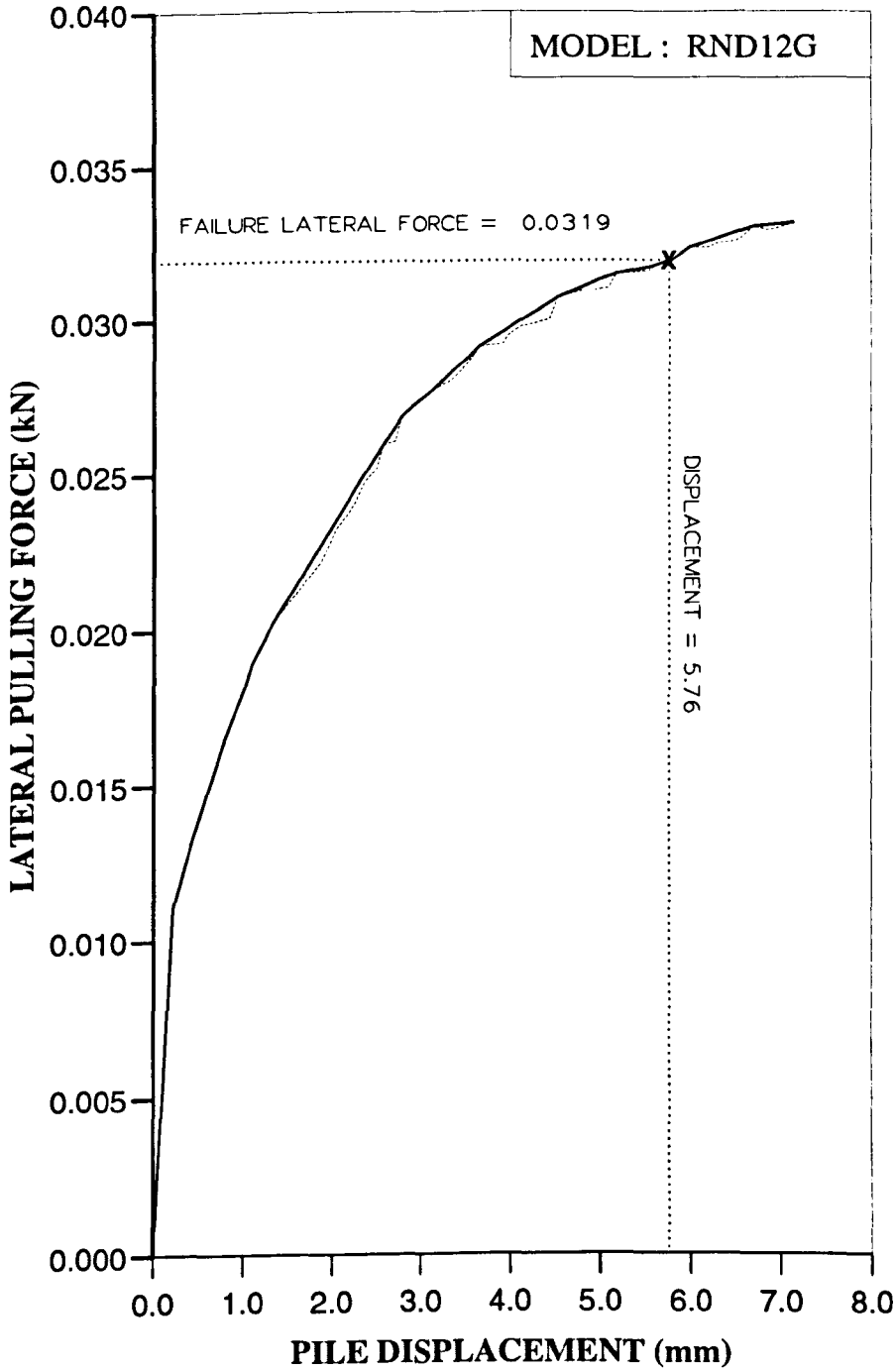

Figure AL57 Variation of lateral force with displacement at ground level for Series 4 test.

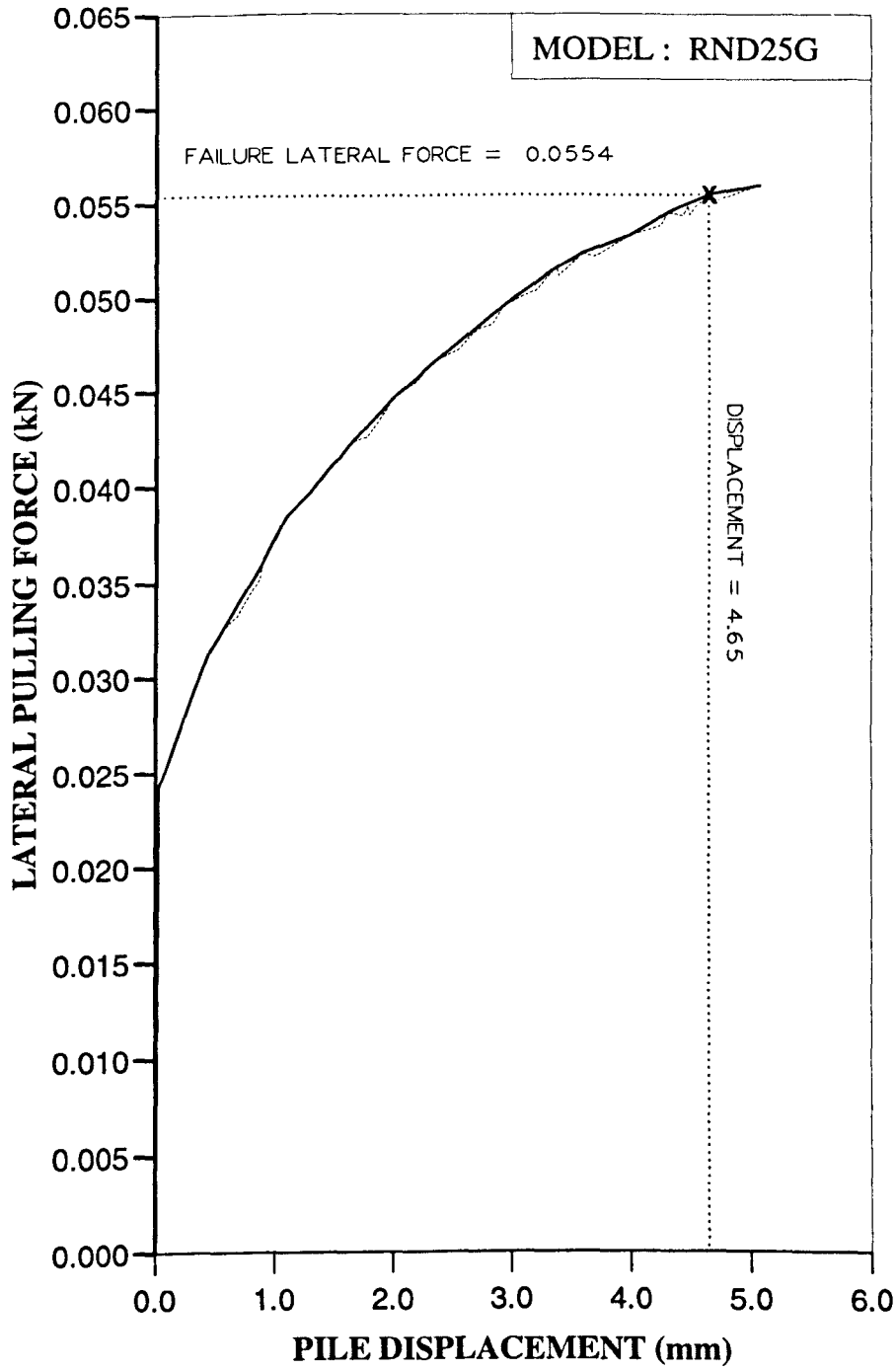

Figure AL58 Variation of lateral force with displacement at ground level for Series 4 test.

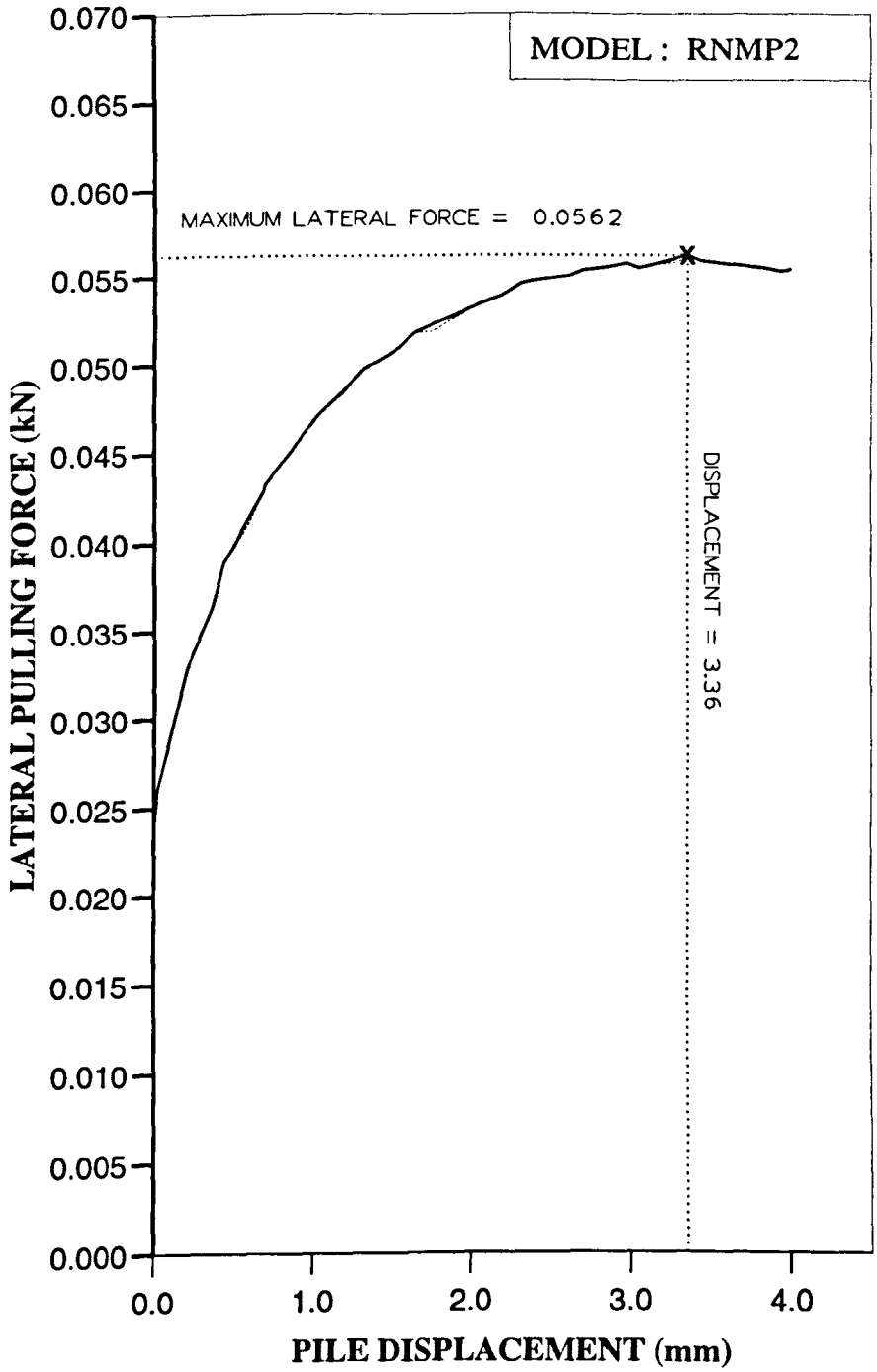

Figure AL59 Variation of lateral force with displacement at ground level for Series 4 test.

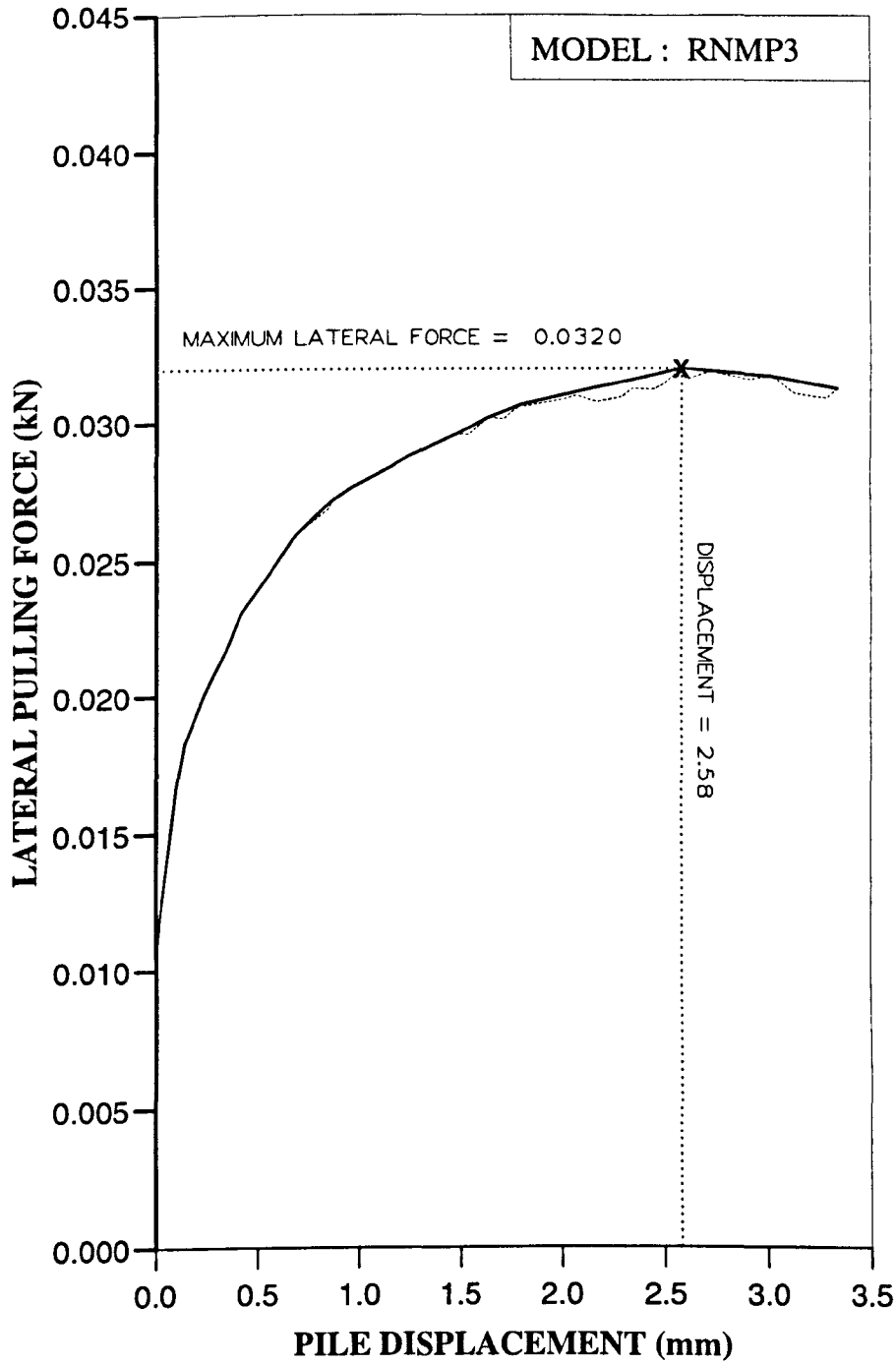

Figure AL60 Variation of lateral force with displacement at ground level for Series 4 test.

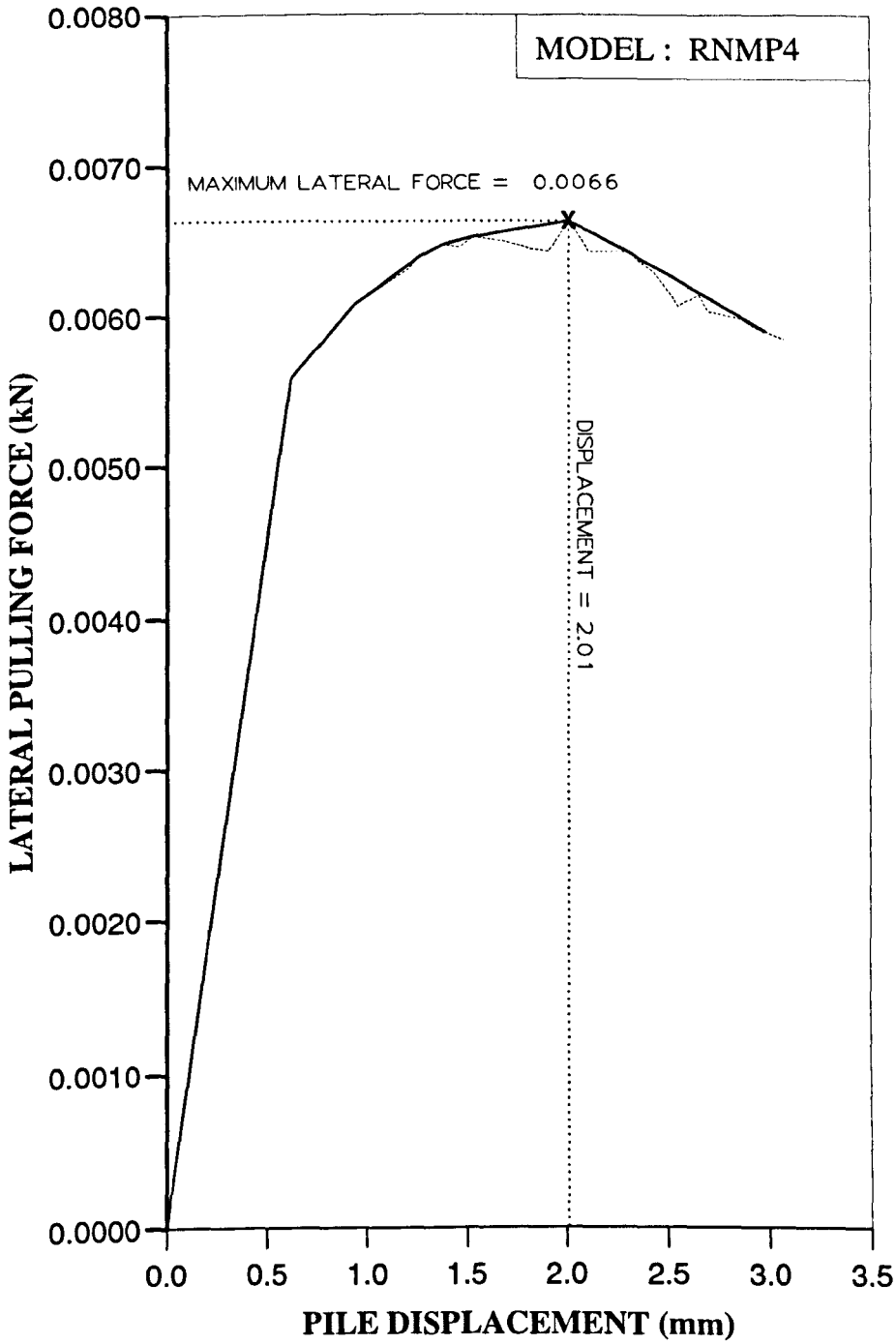

Figure AL61 Variation of lateral force with displacement at ground level for Series 4 test.

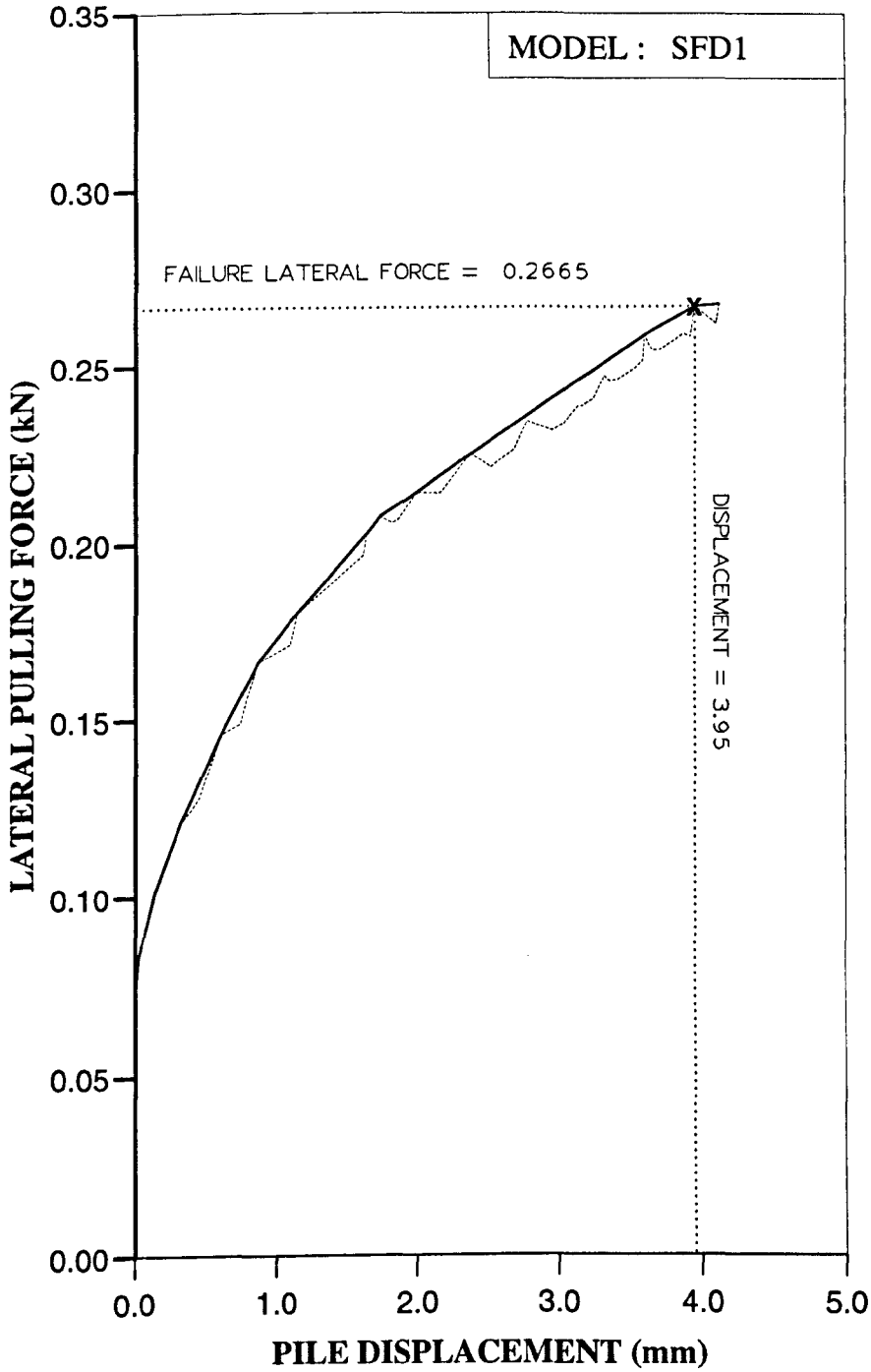

Figure AL62 Variation of lateral force with displacement at ground level for Series 5 test.

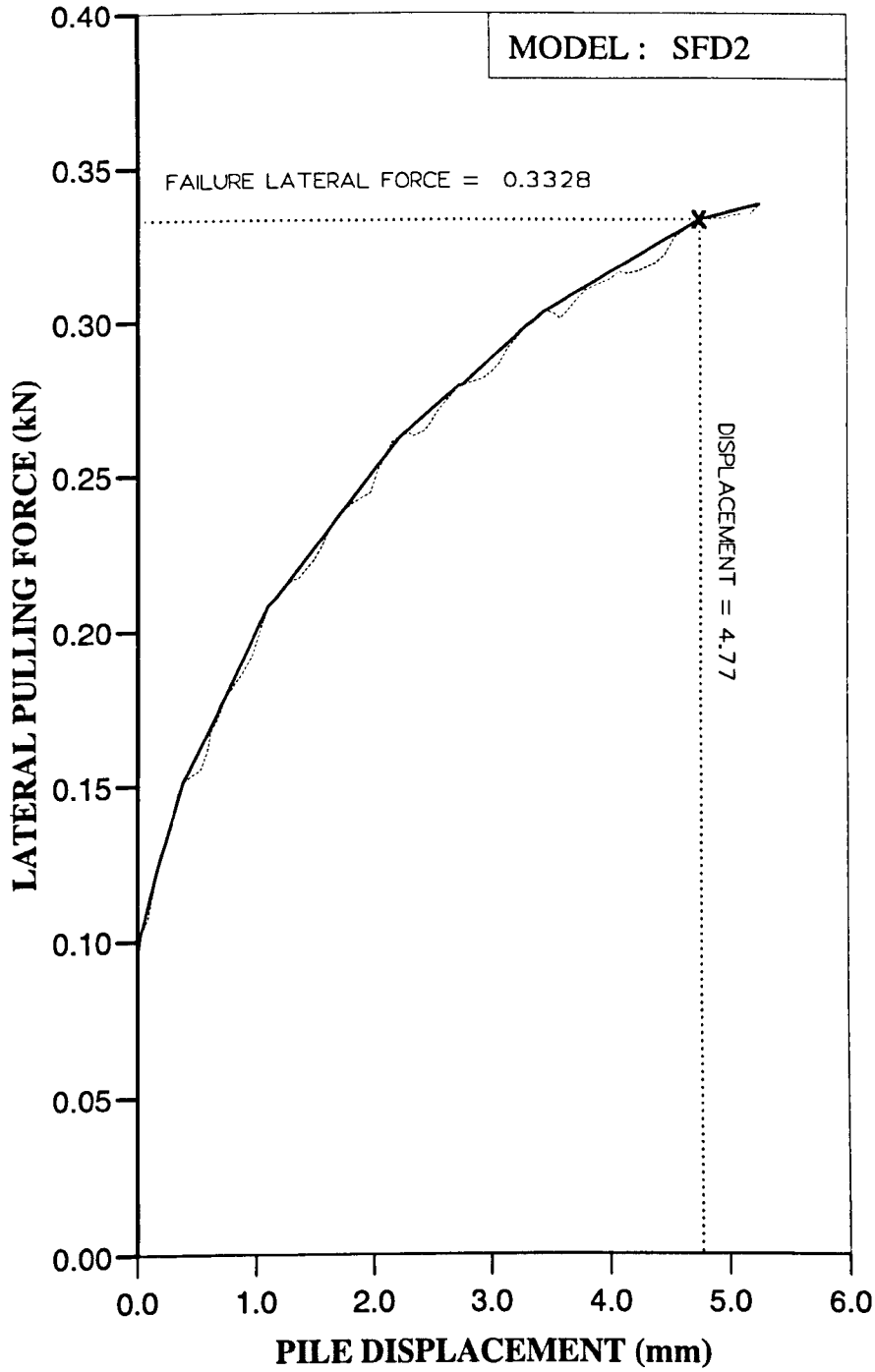

Figure AL63 Variation of lateral force with displacement at ground level for Series 5 test.

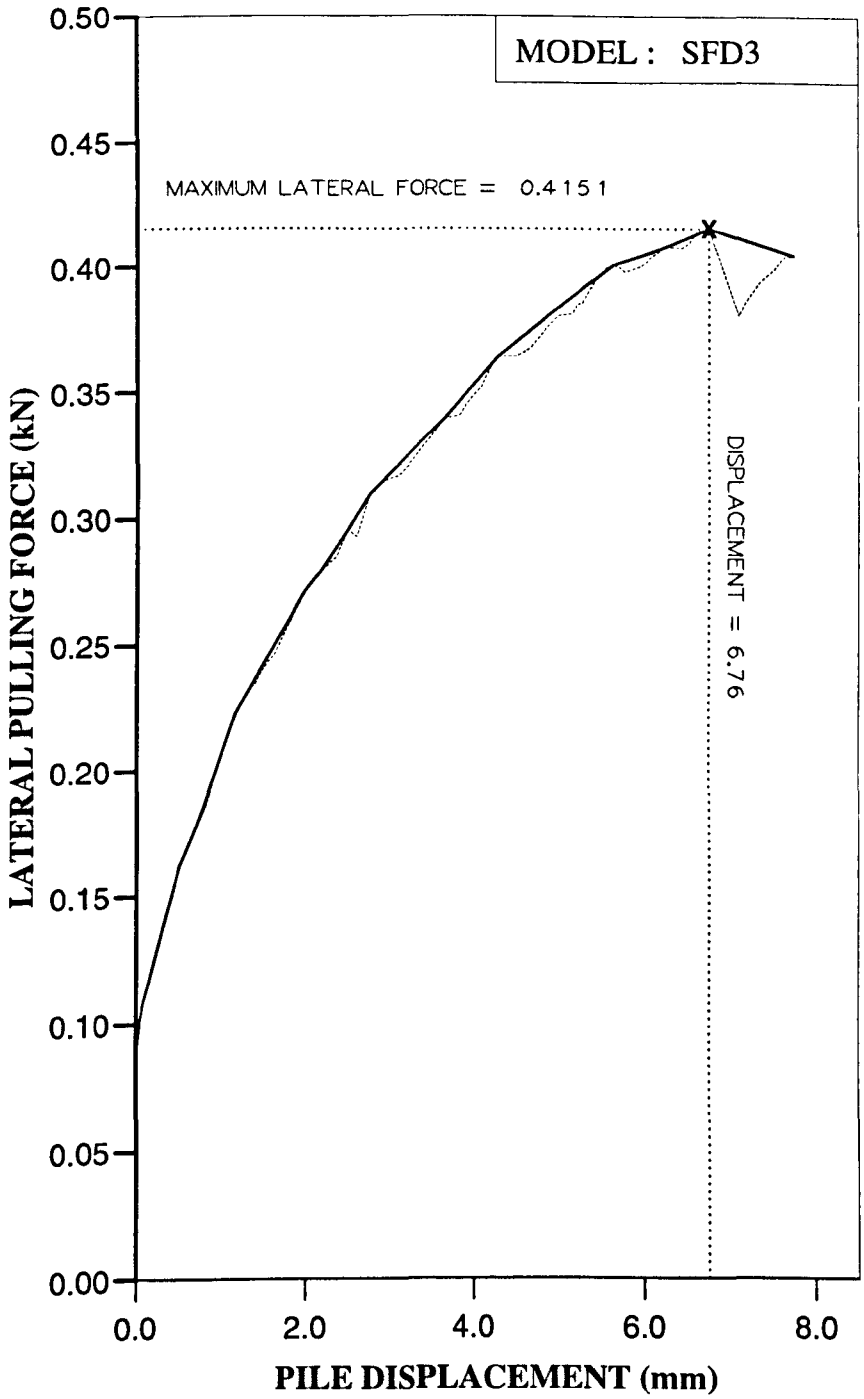

Figure AL64 Variation of lateral force with displacement at ground level for Series 5 test.

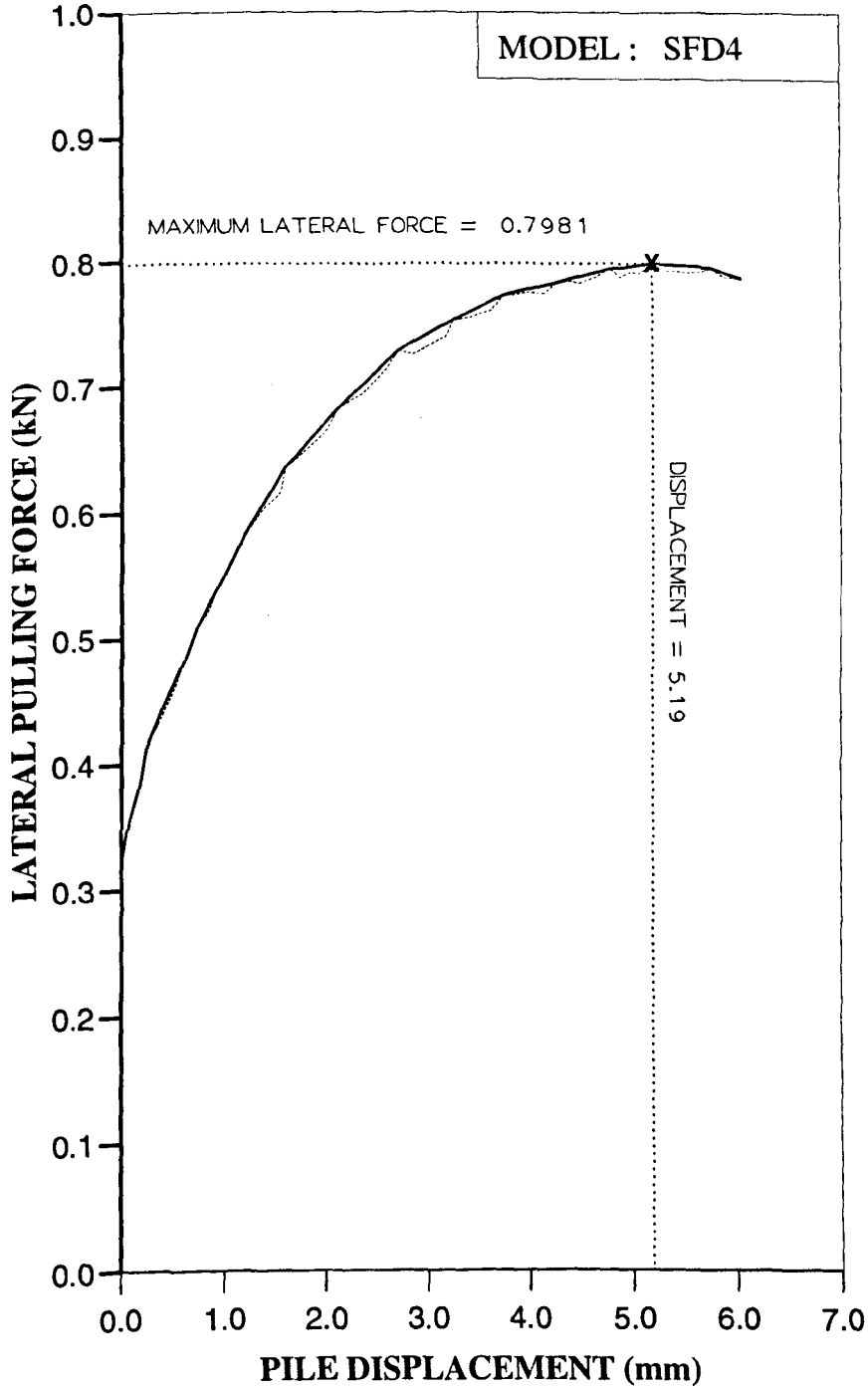

Figure AL65 Variation of lateral force with displacement at ground level for Series 5 test.

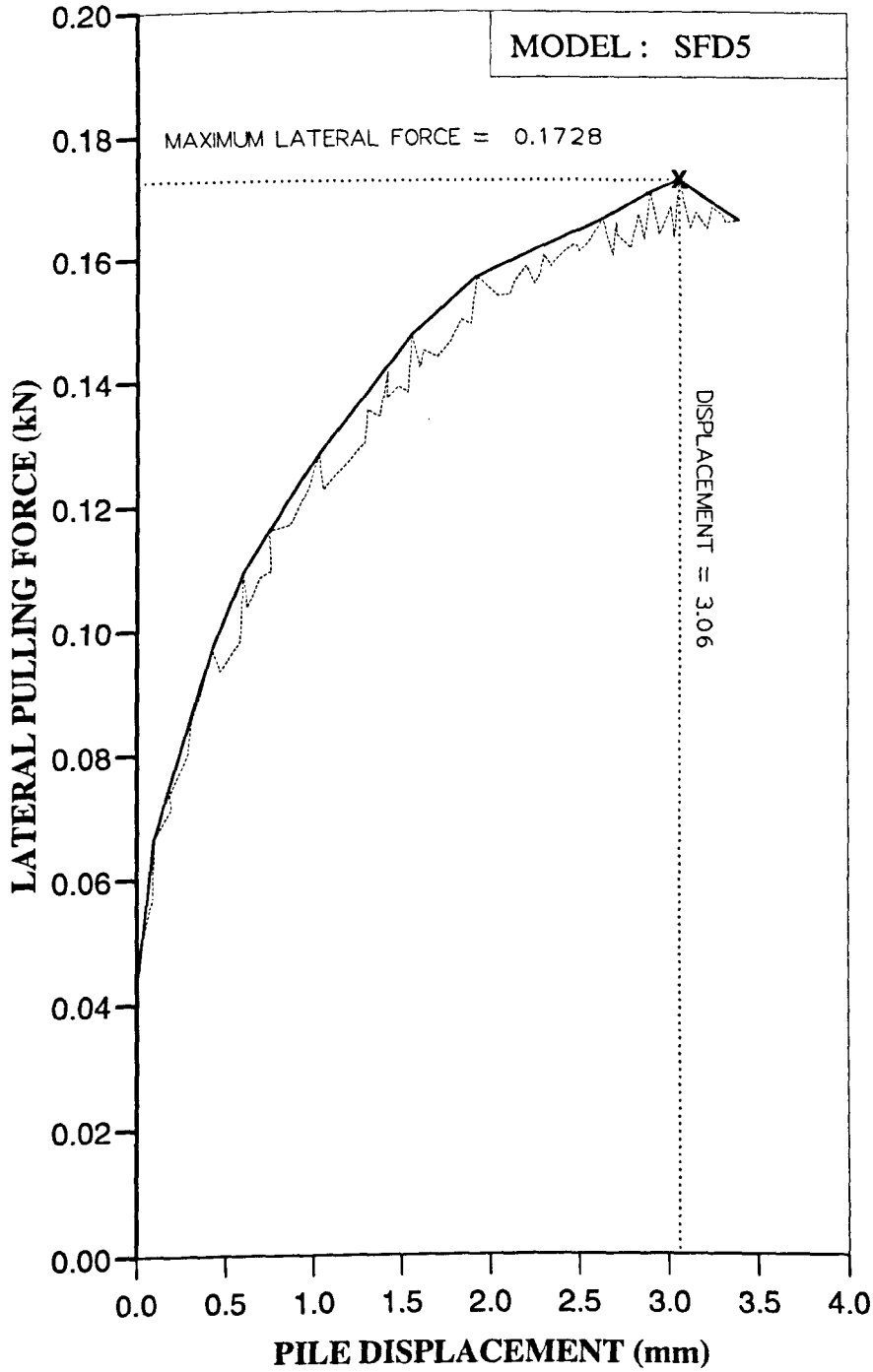

Figure AL66 Variation of lateral force with displacement at ground level for Series 5 test.

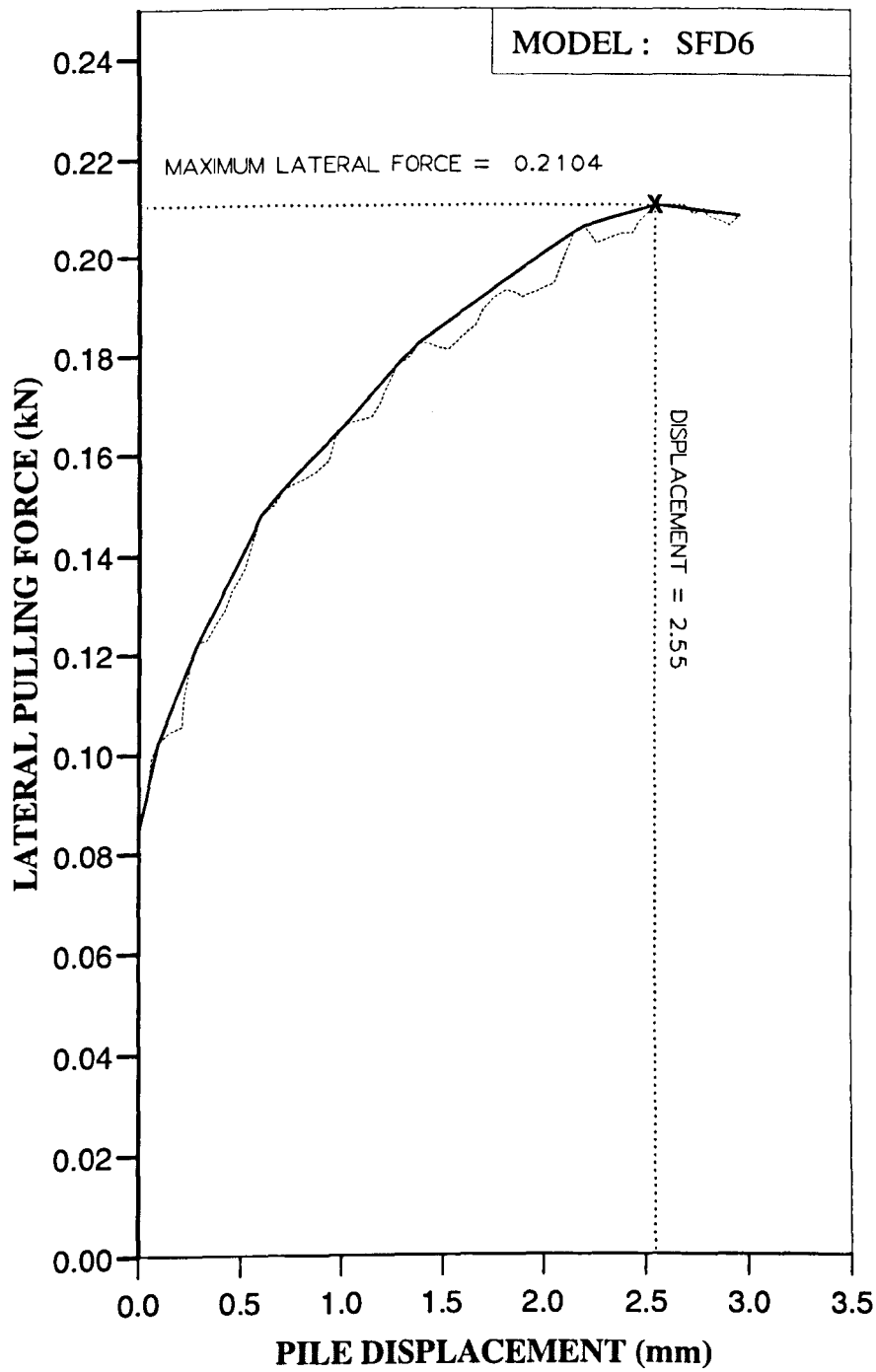

Figure AL67 Variation of lateral force with displacement at ground level for Series 5 test.

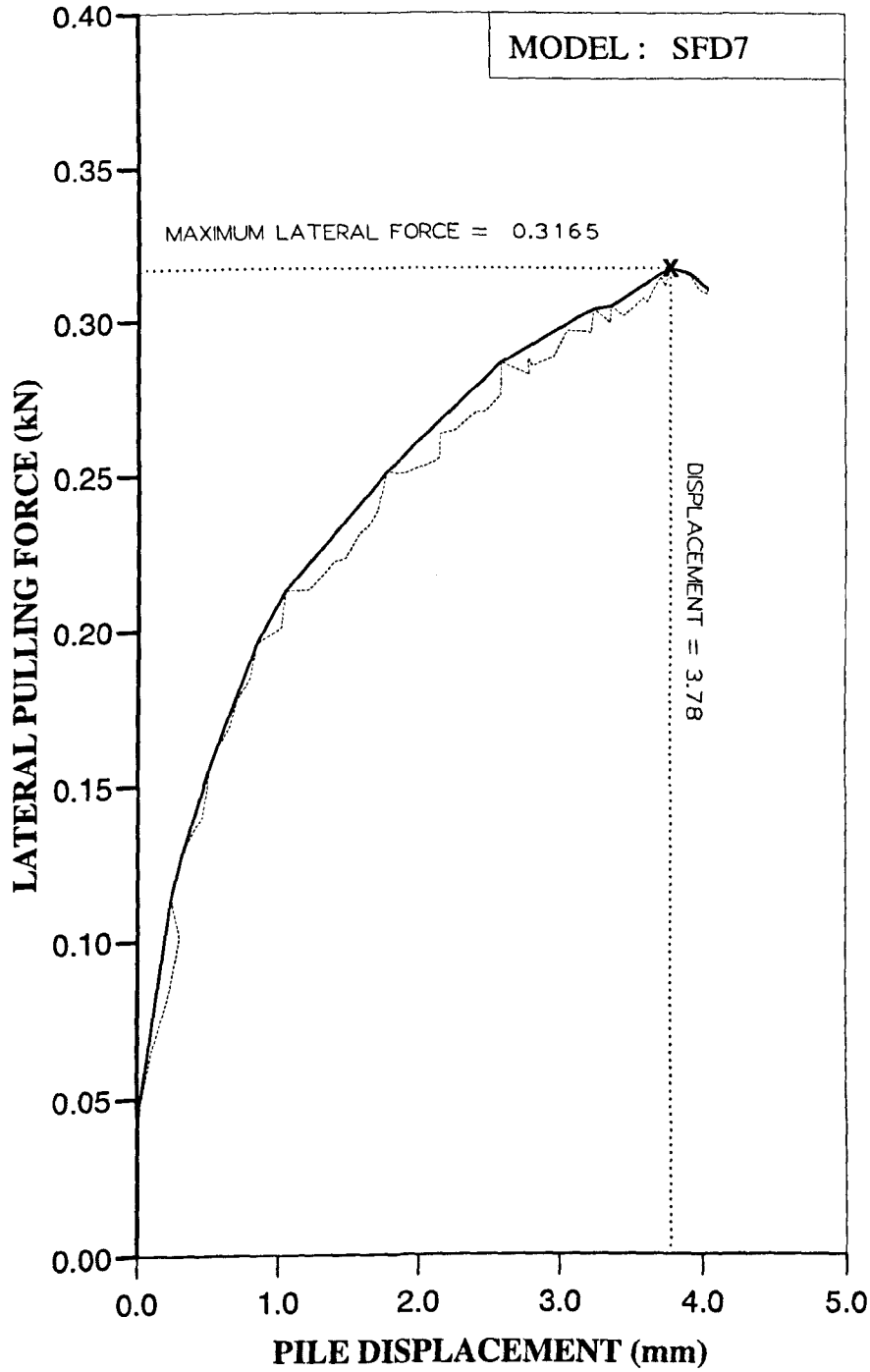

Figure AL68 Variation of lateral force with displacement at ground level for Series 5 test.

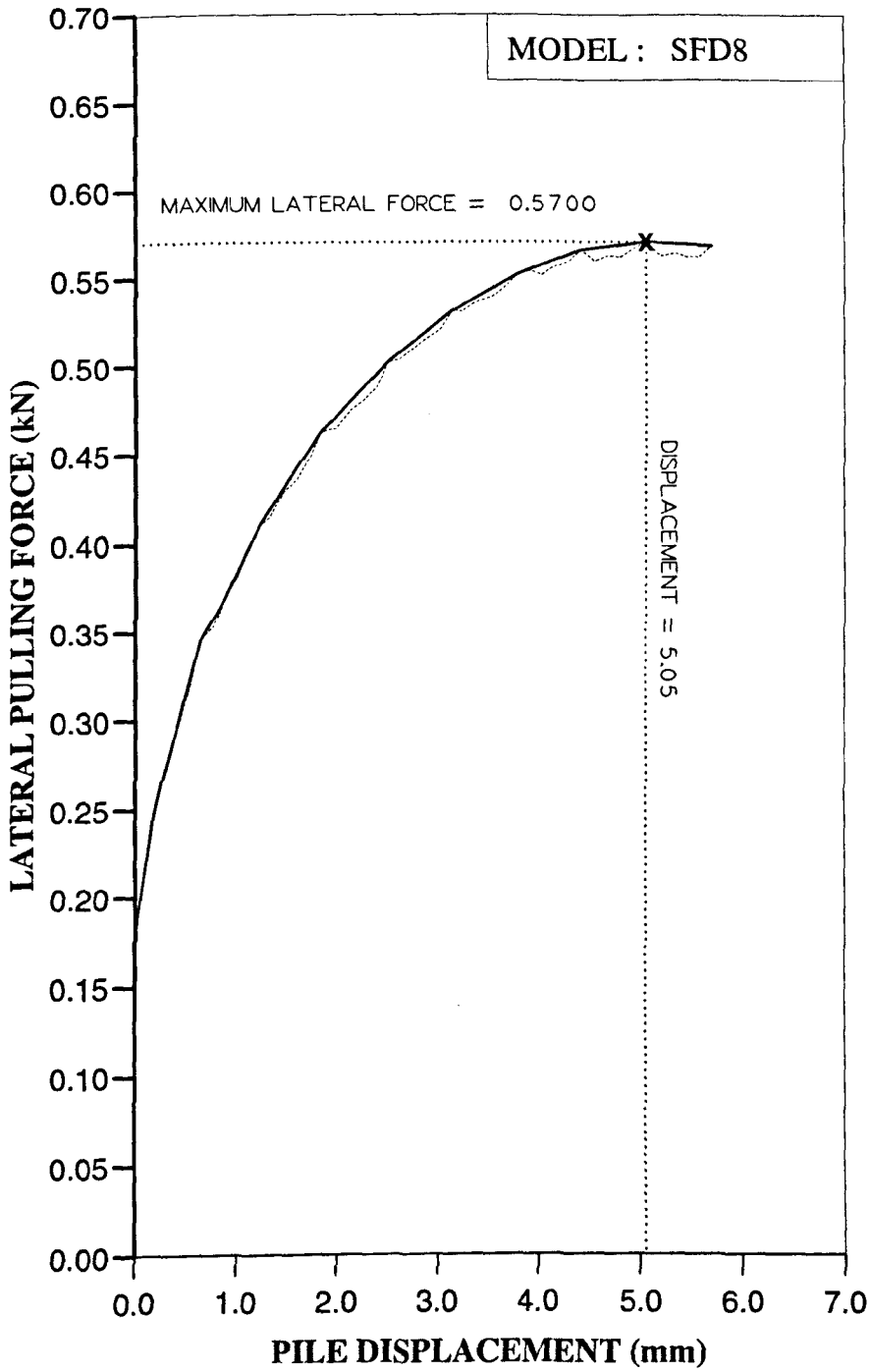

Figure AL69 Variation of lateral force with displacement at ground level for Series 5 test.

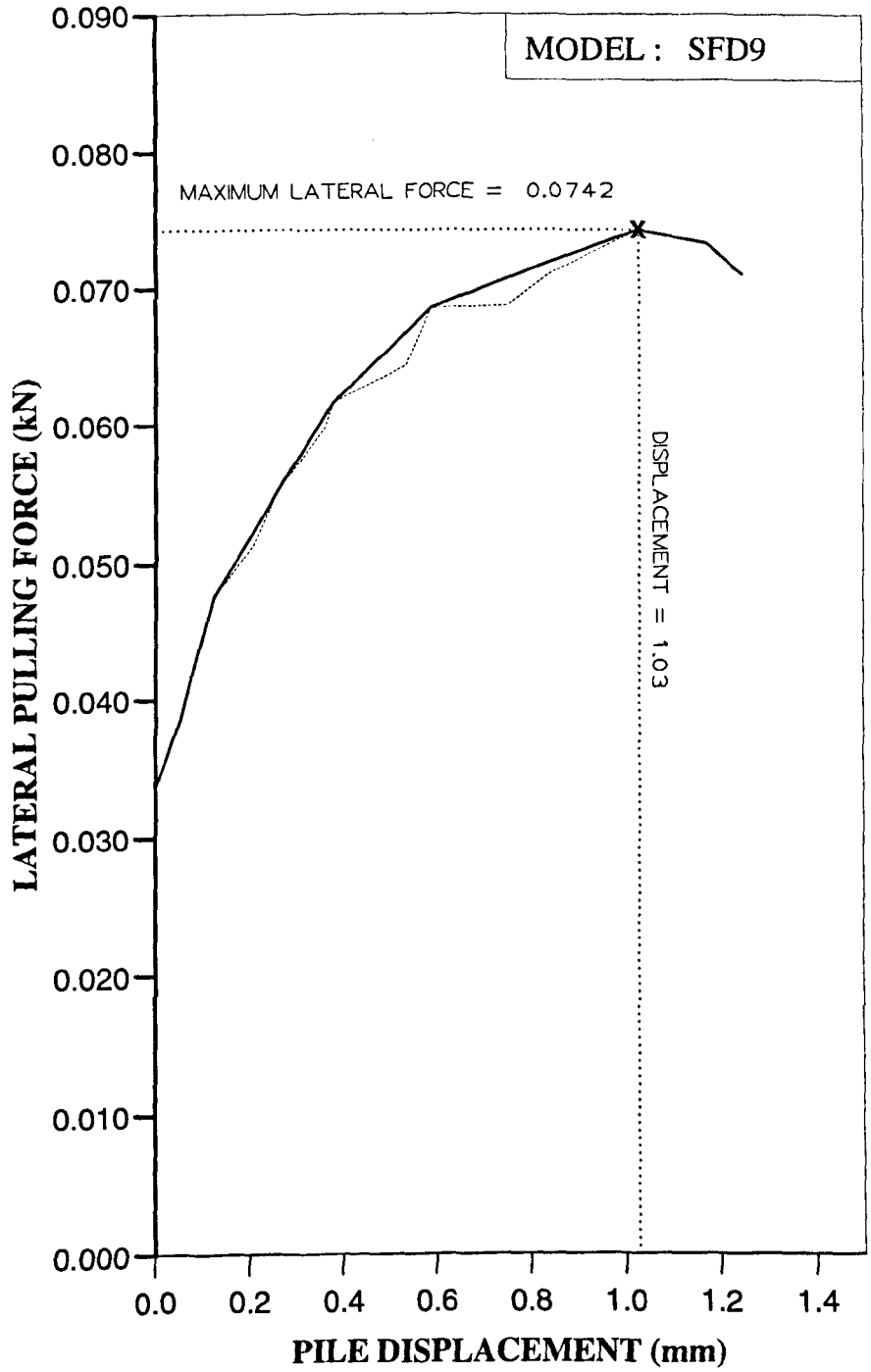

Figure AL70 Variation of lateral force with displacement at ground level for Series 5 test.

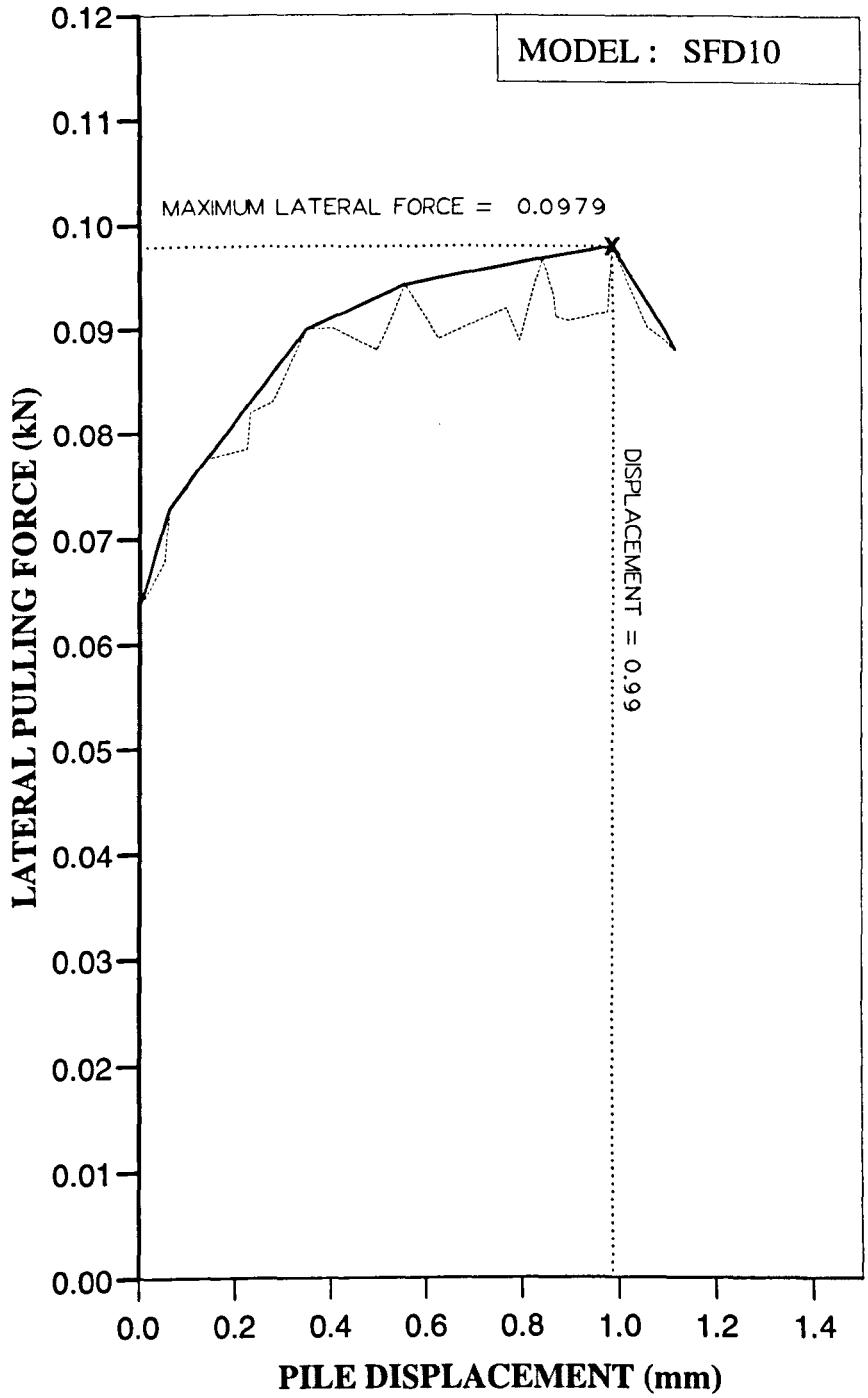

Figure AL71 Variation of lateral force with displacement at ground level for Series 5 test.

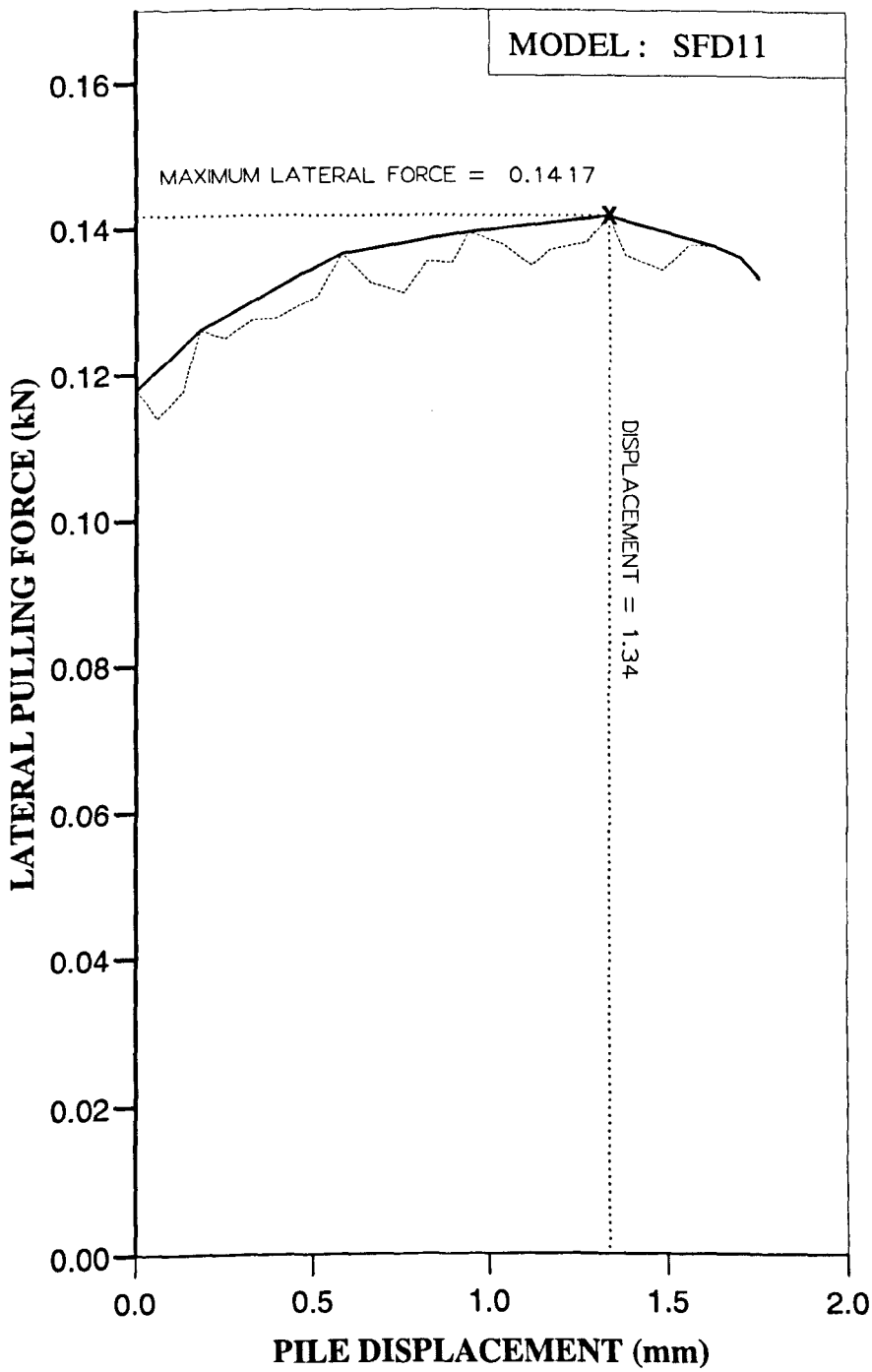

Figure AL72 Variation of lateral force with displacement at ground level for Series 5 test.

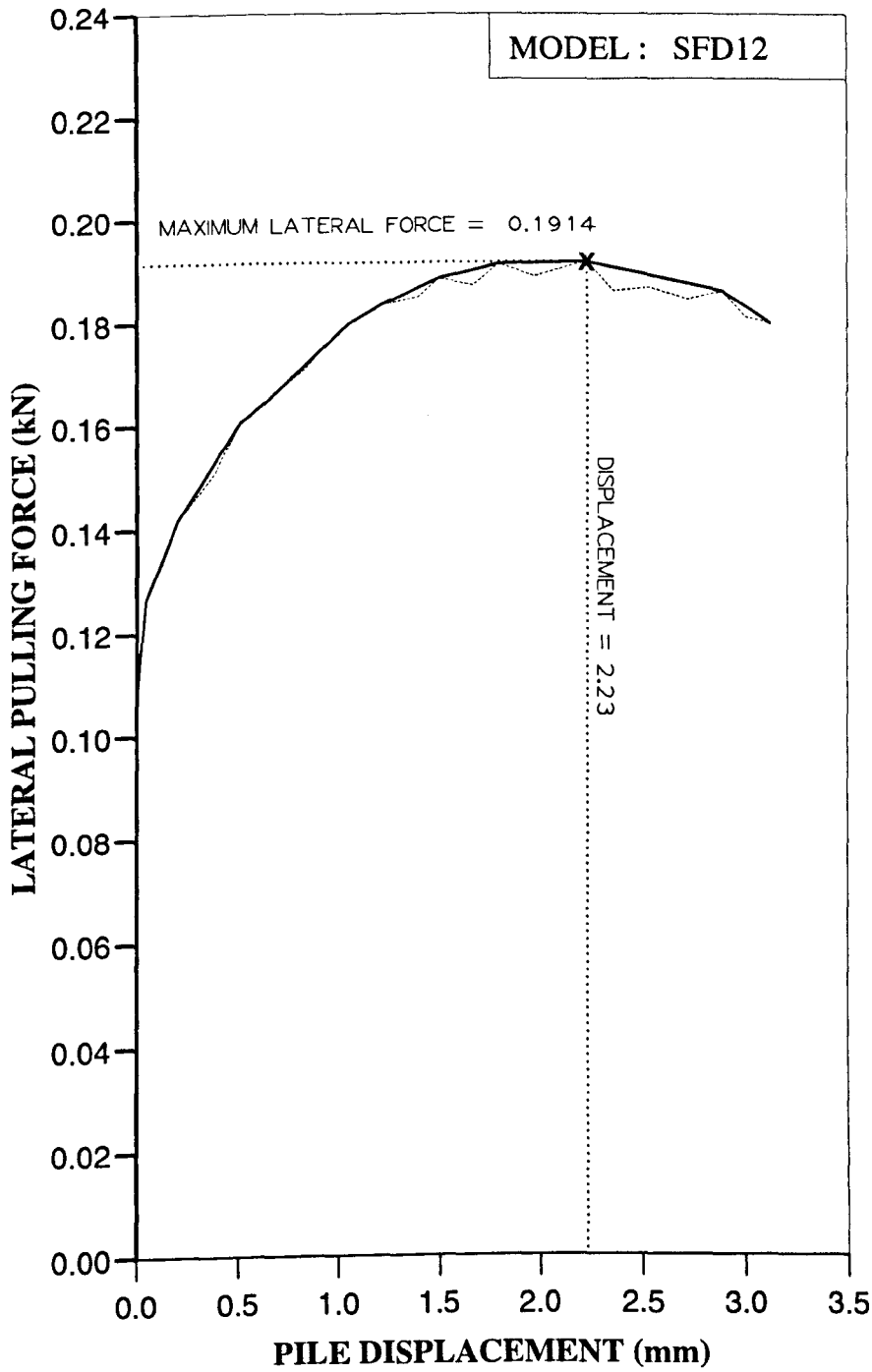

Figure AL73 Variation of lateral force with displacement at ground level for Series 5 test.

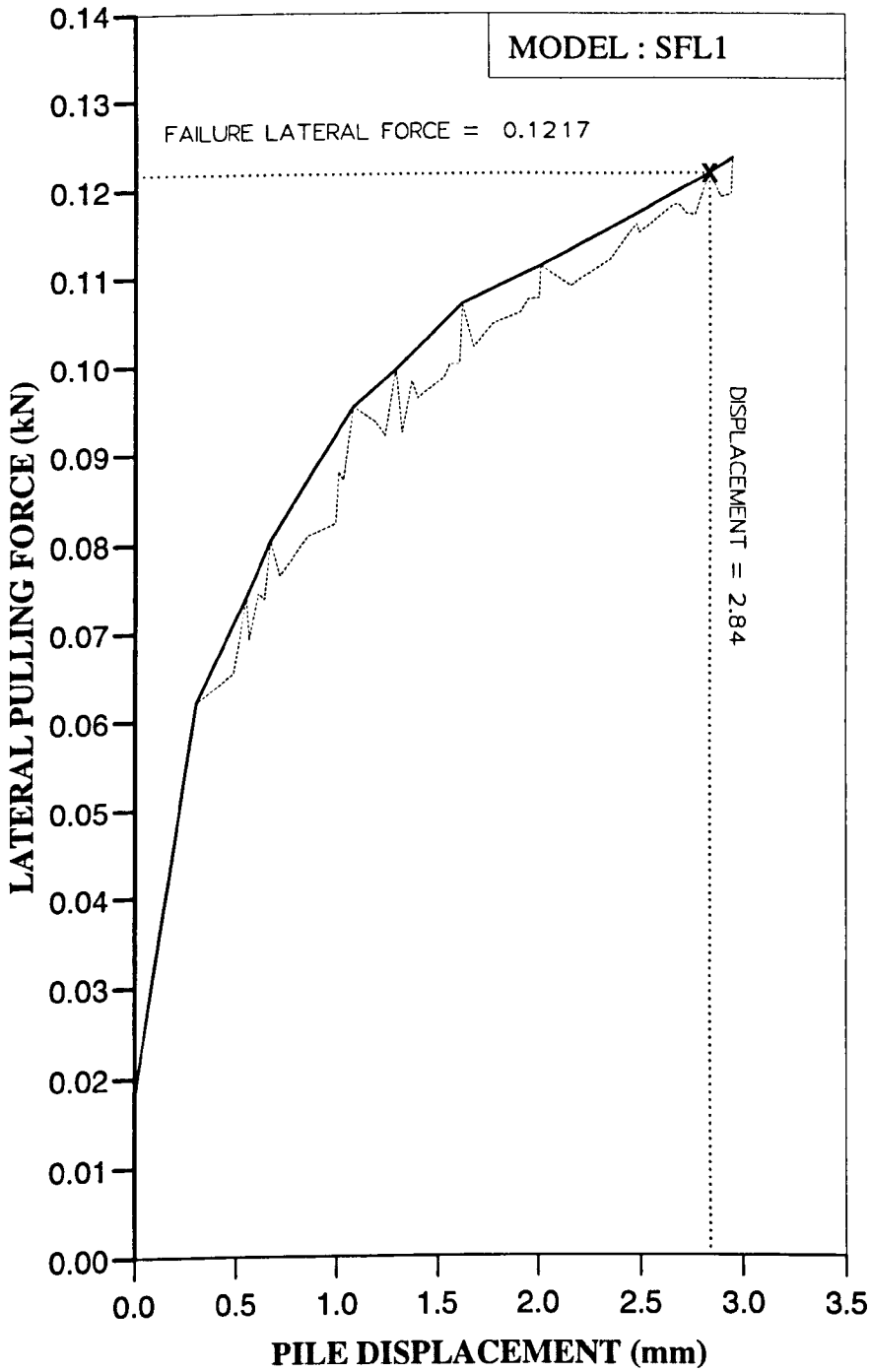

Figure AL74 Variation of lateral force with displacement at ground level for Series 5 test.

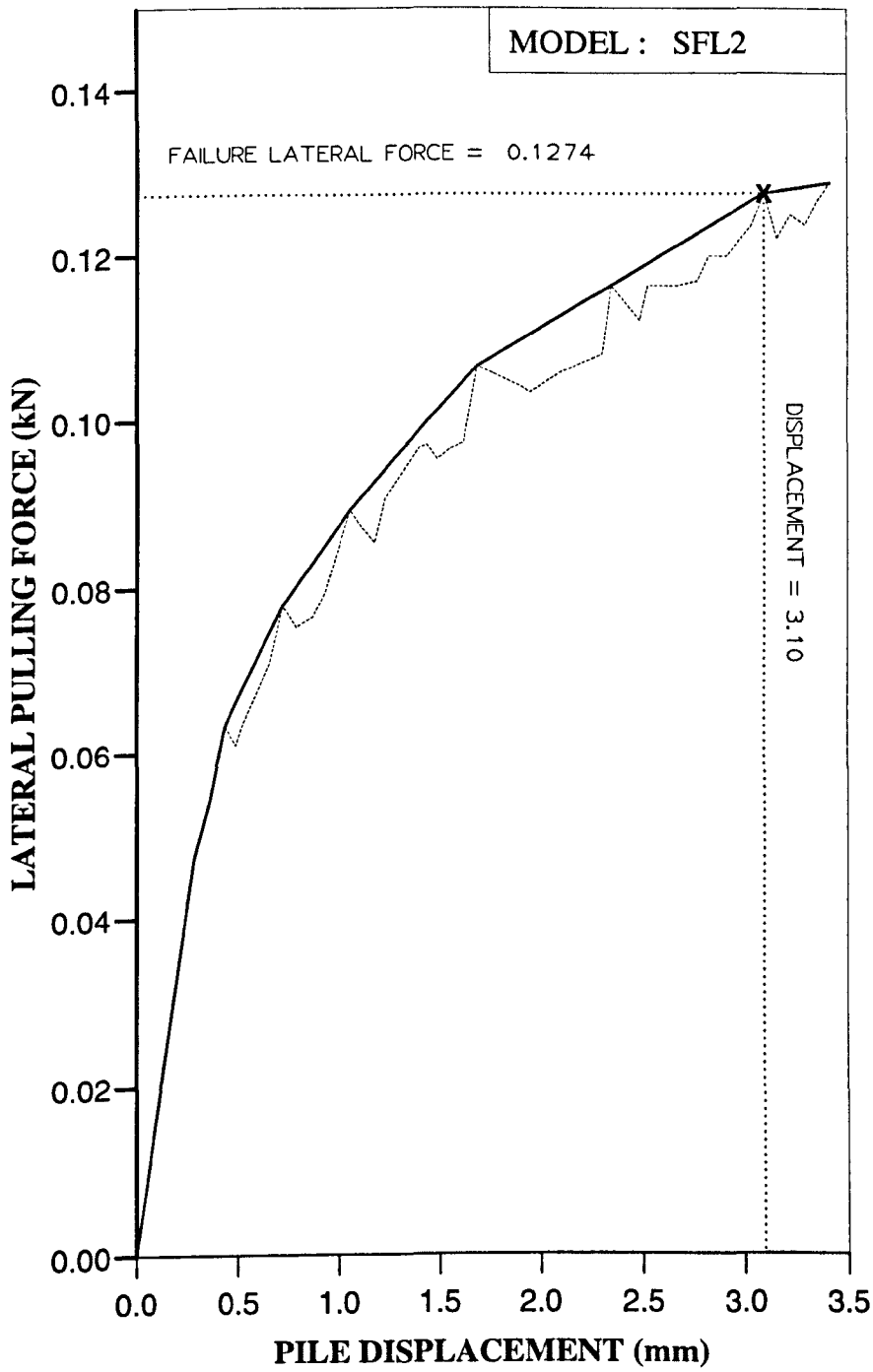

Figure AL75 Variation of lateral force with displacement at ground level for Series 5 test.

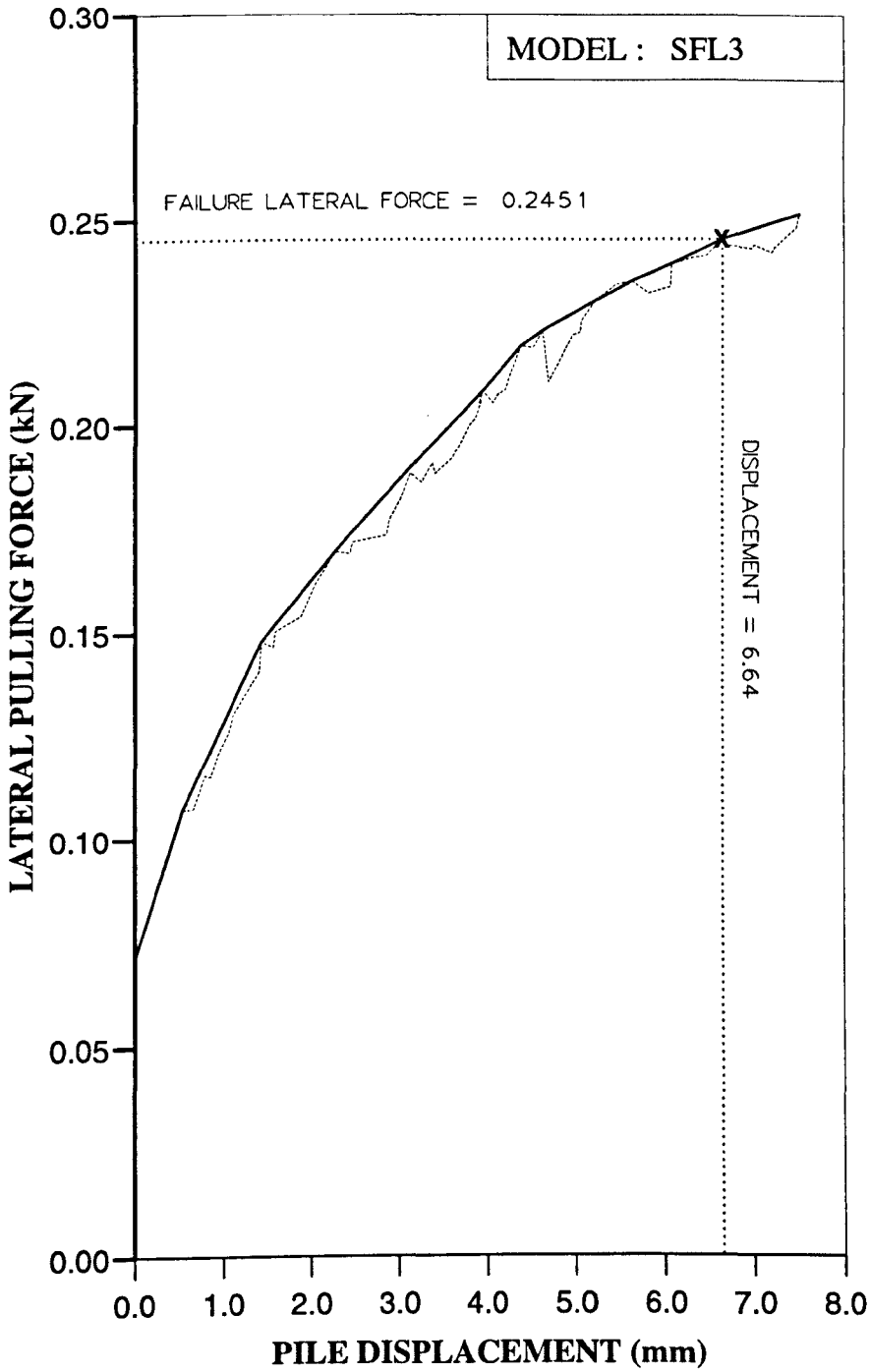

Figure AL76 Variation of lateral force with displacement at ground level for Series 5 test.

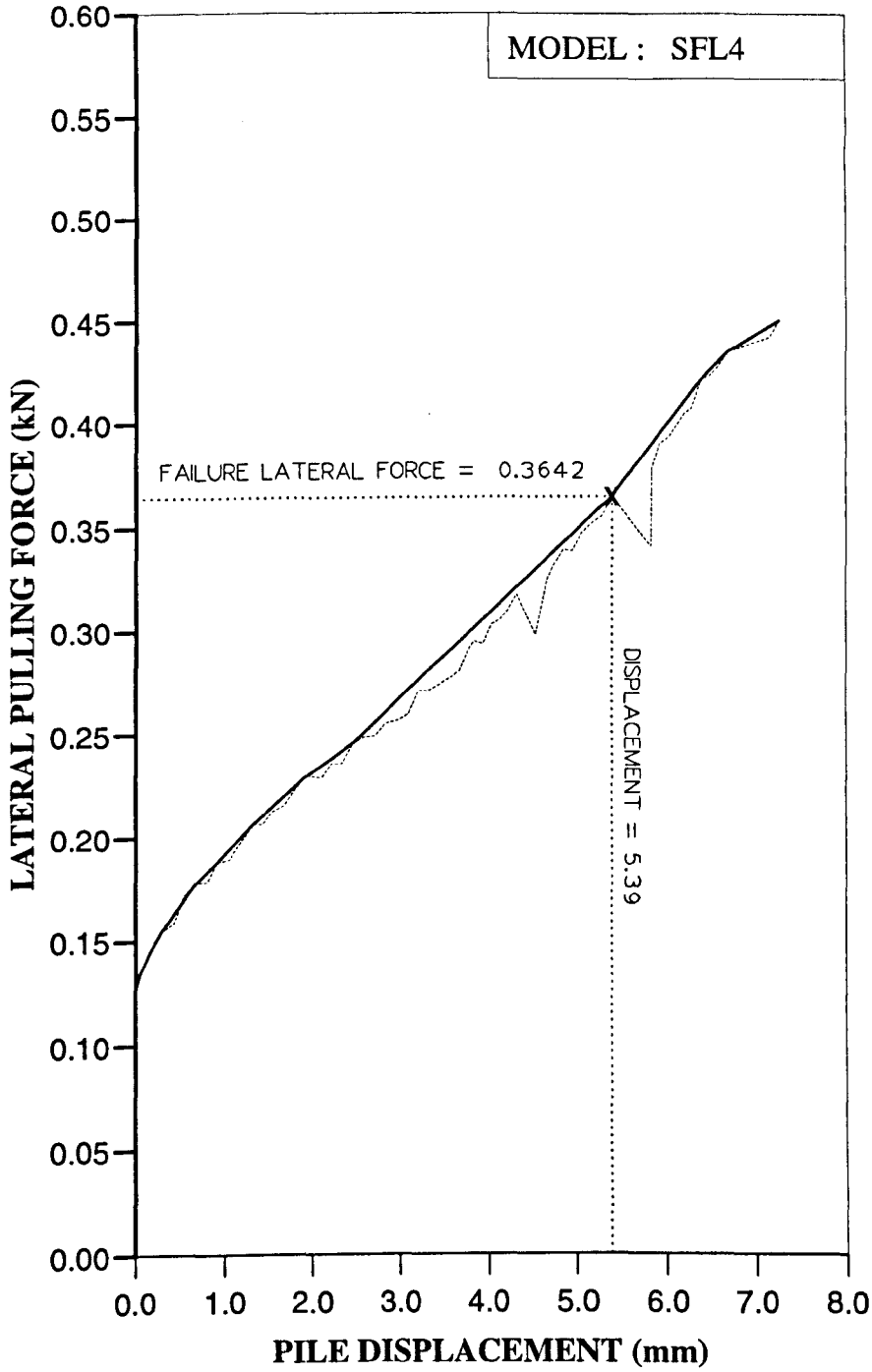

Figure AL77 Variation of lateral force with displacement at ground level for Series 5 test.

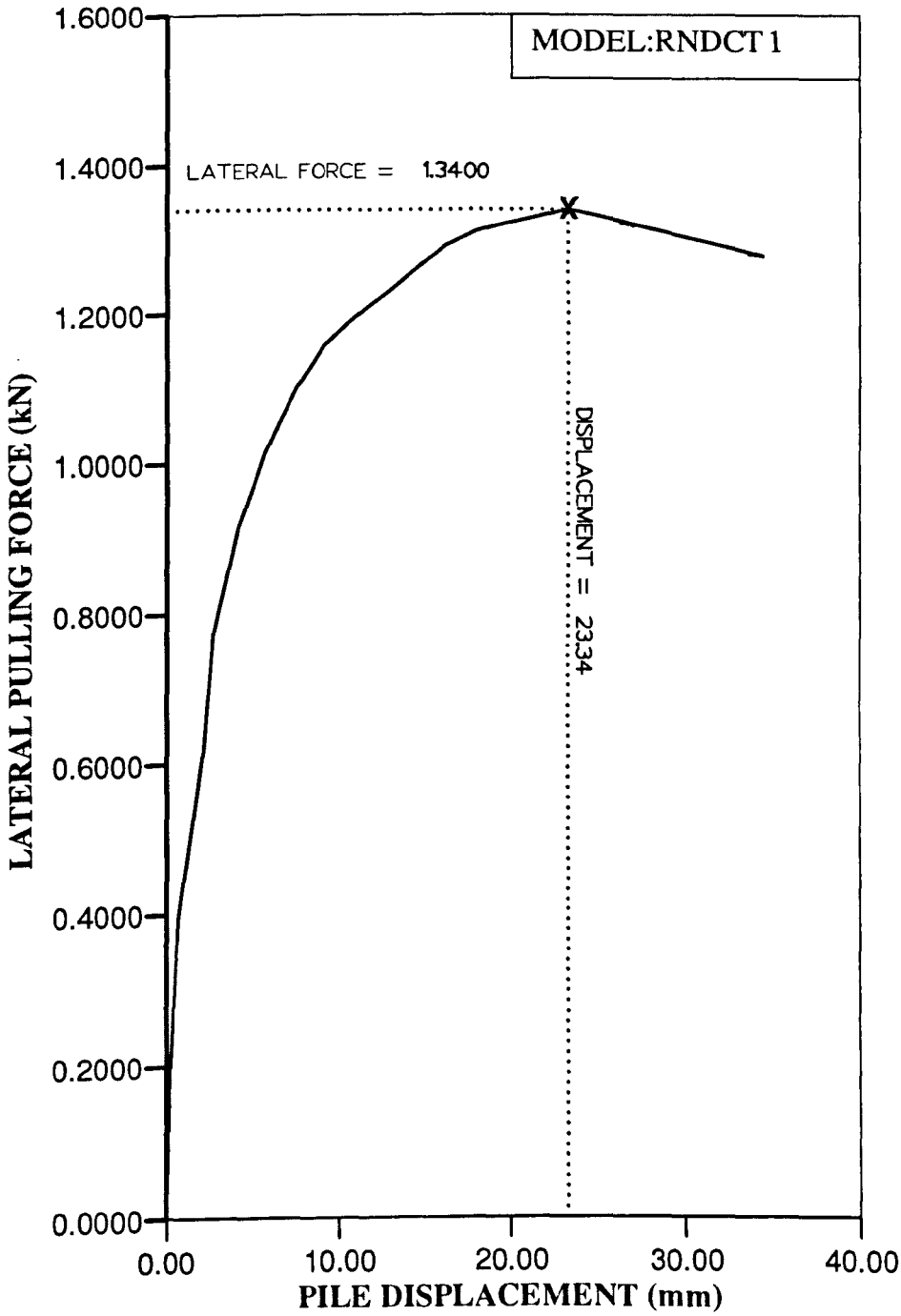

Figure AL78 Variation of lateral force with displacement at ground level for Series 1 test.

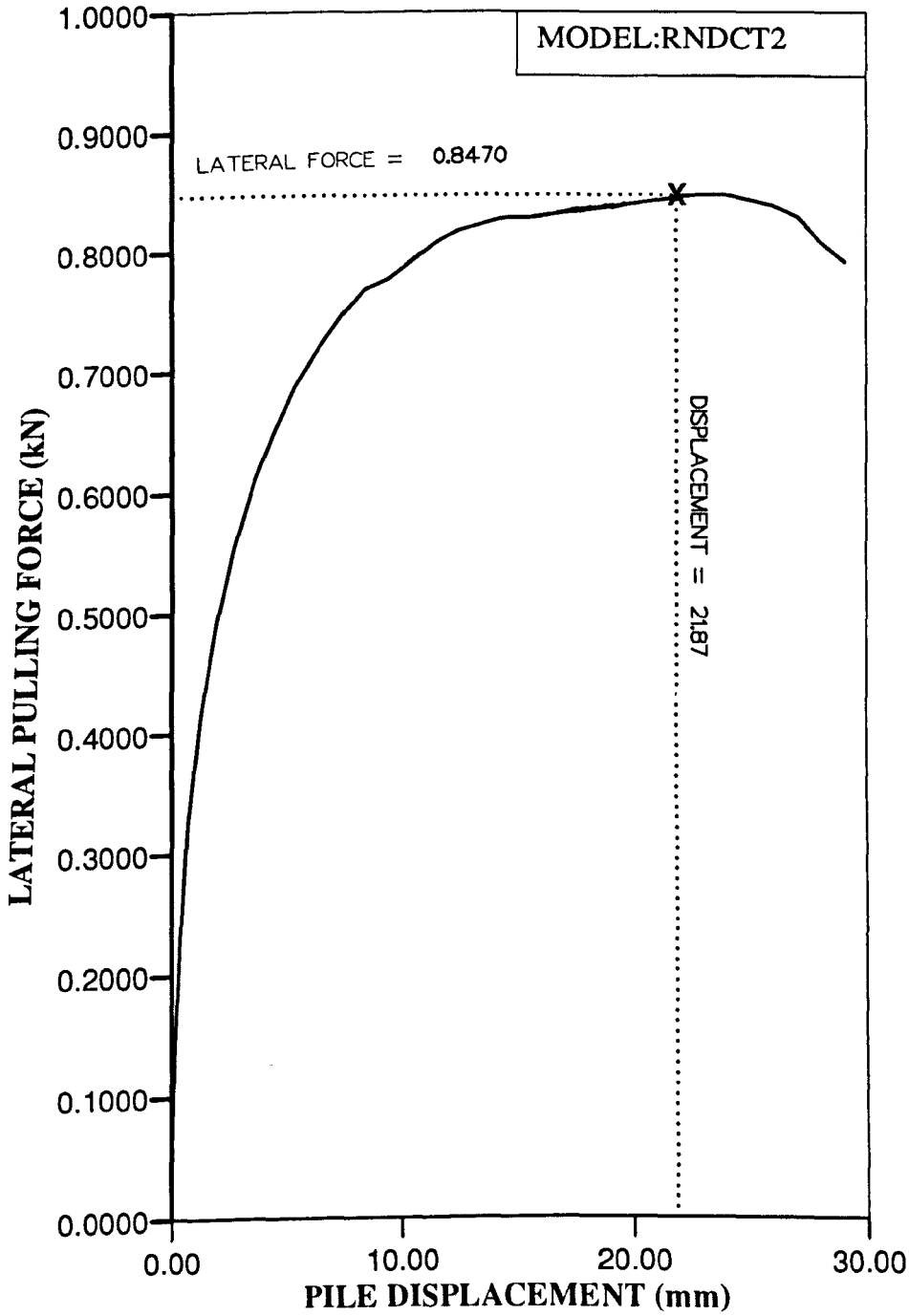

Figure AL79 Variation of lateral force with displacement at ground level for Series 1 test.

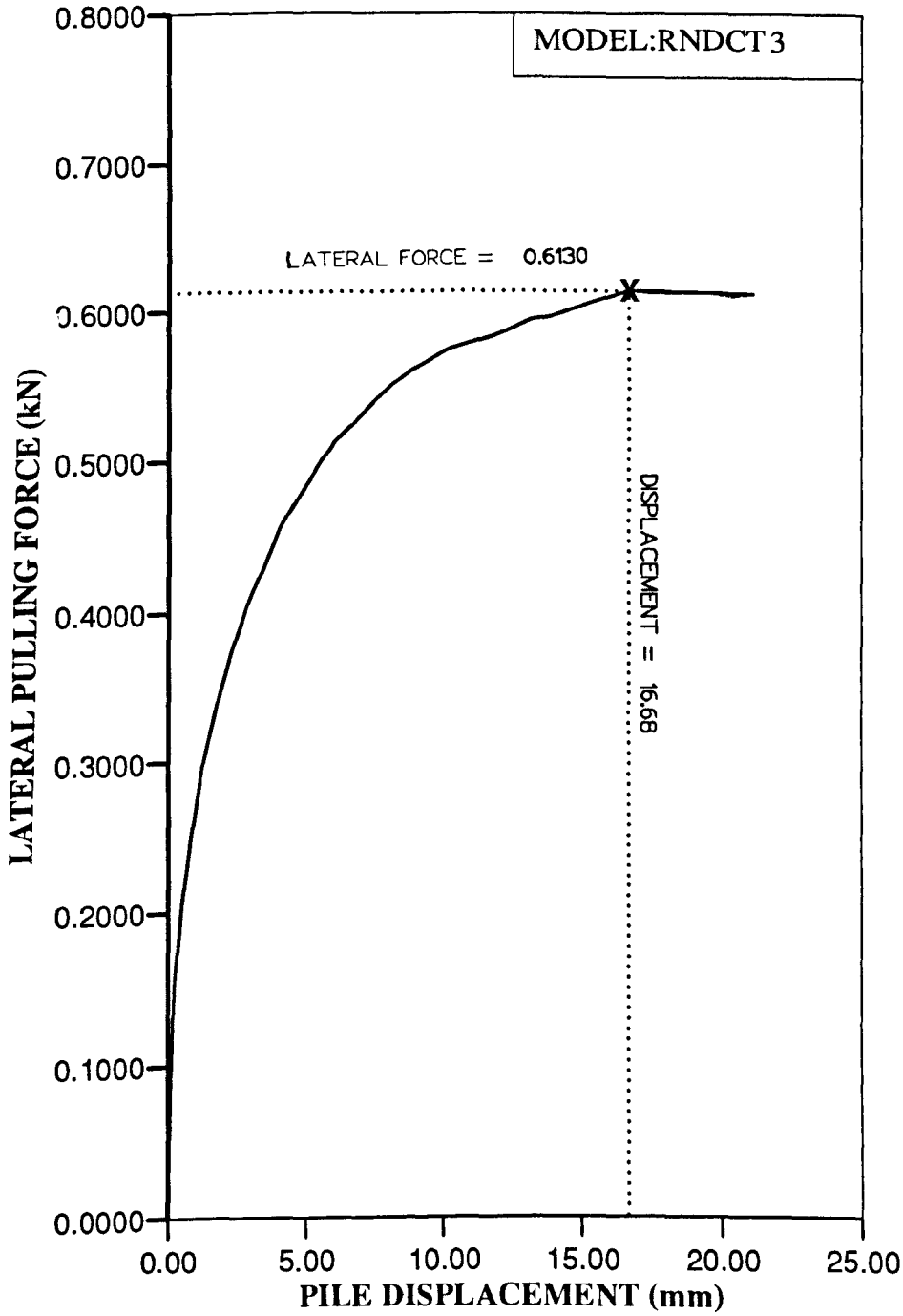

Figure AL80 Variation of lateral force with displacement at ground level for Series 1 test.

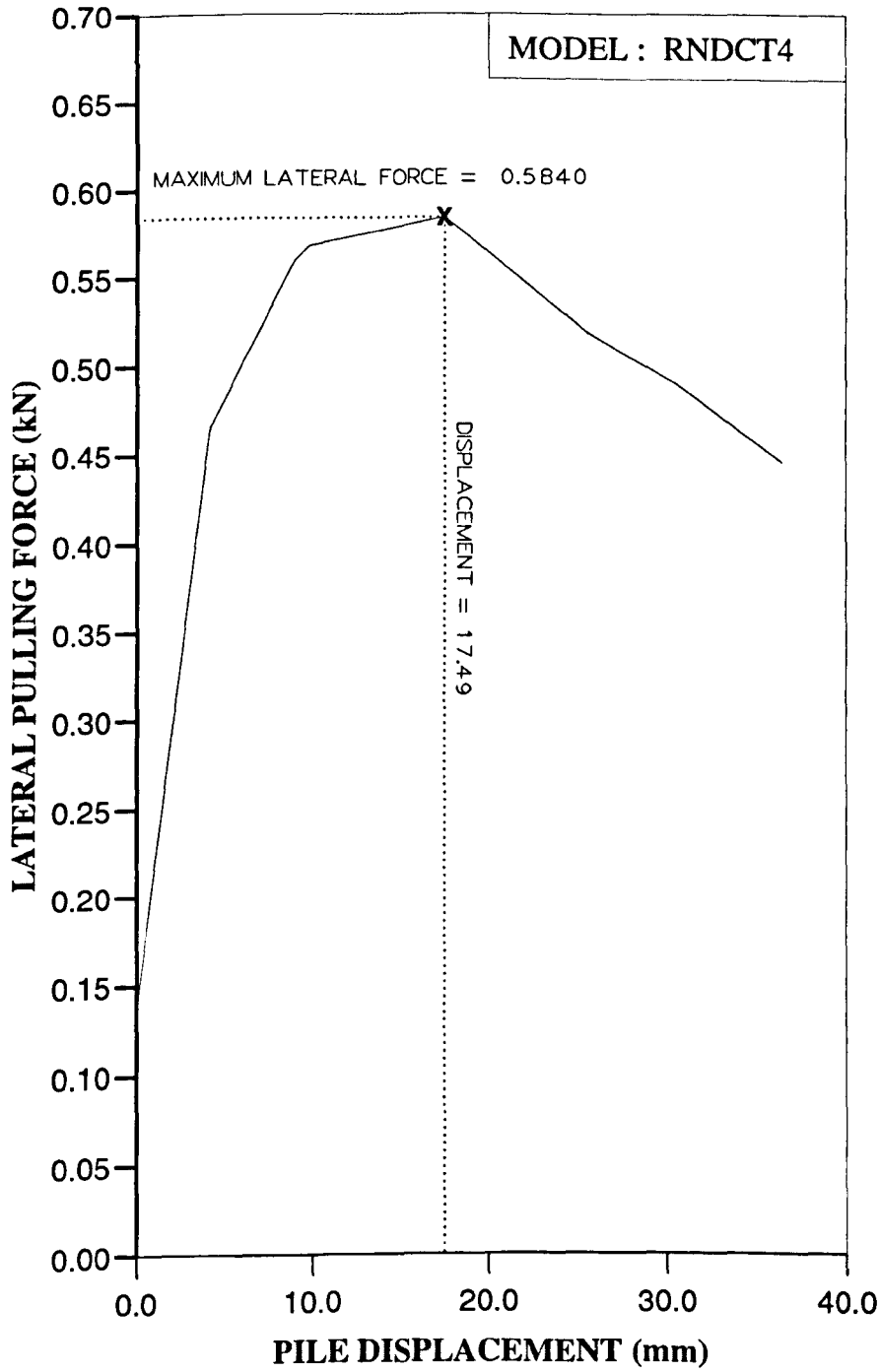

Figure AL81 Variation of lateral force with displacement at ground level for Series 1 test.

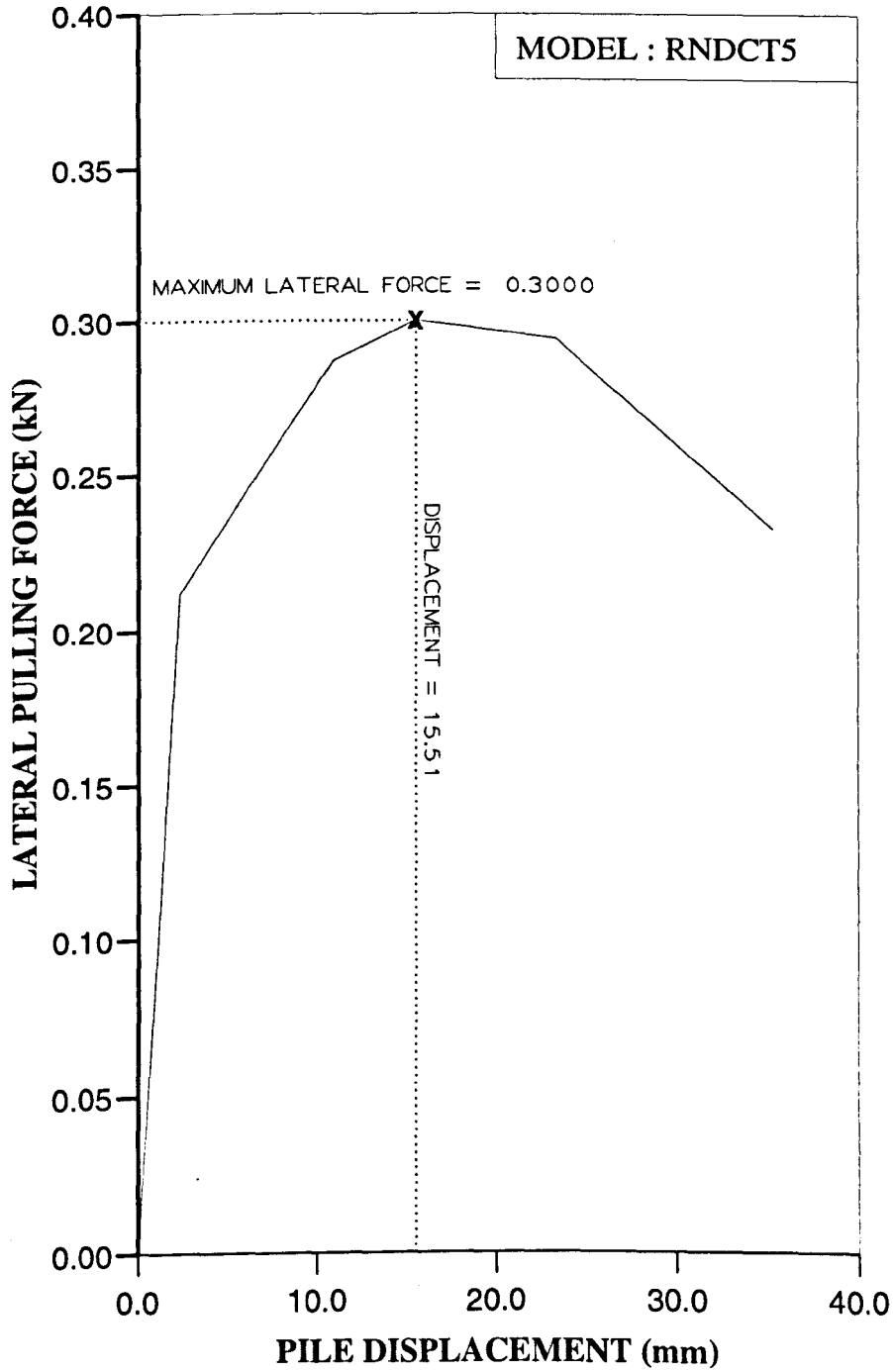

Figure AL82 Variation of lateral force with displacement at ground level for Series 1 test.

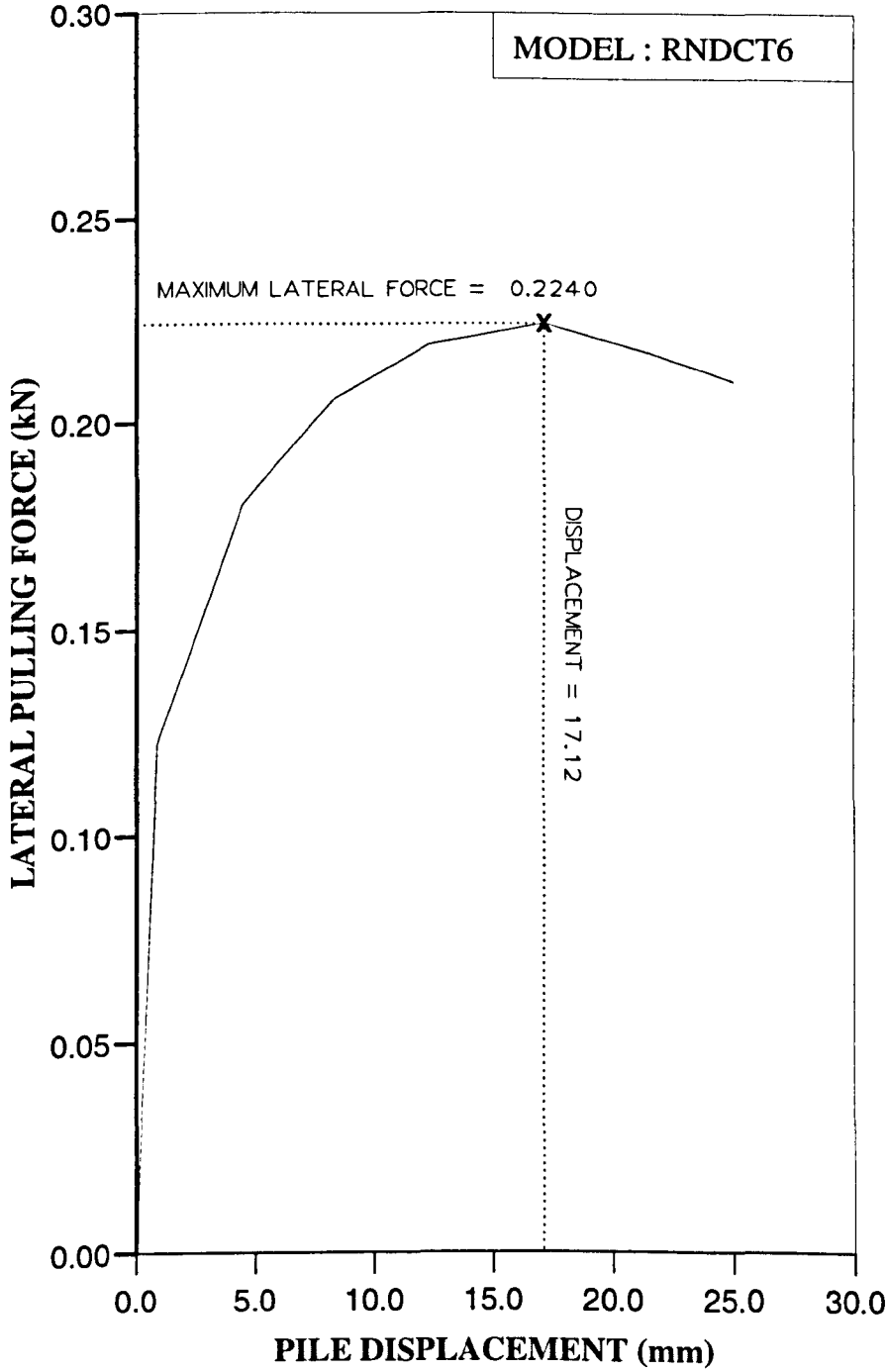

Figure AL83 Variation of lateral force with displacement at ground level for Series 1 test.

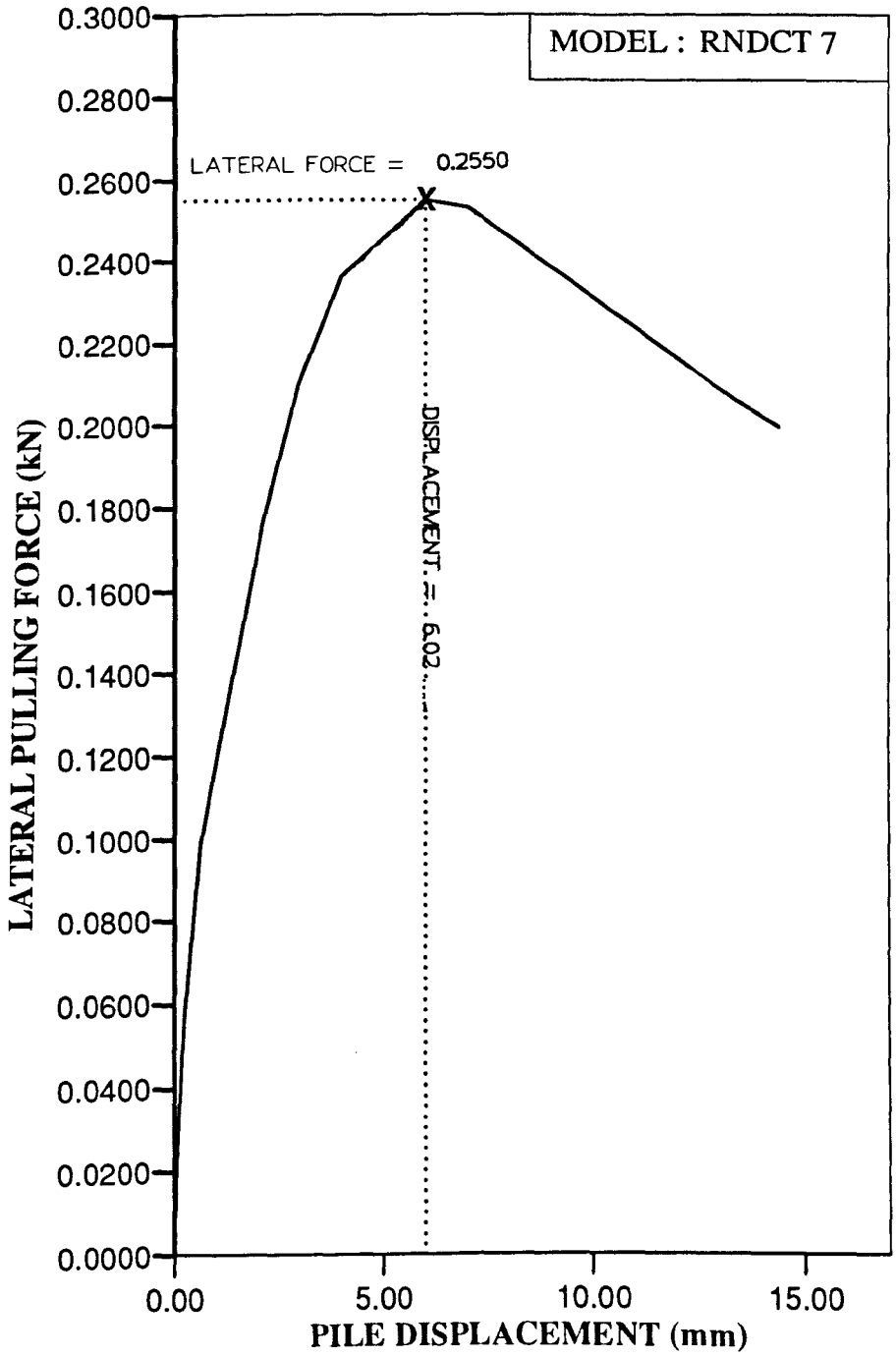

Figure AL84 Variation of lateral force with displacement at ground level for Series 1 test.

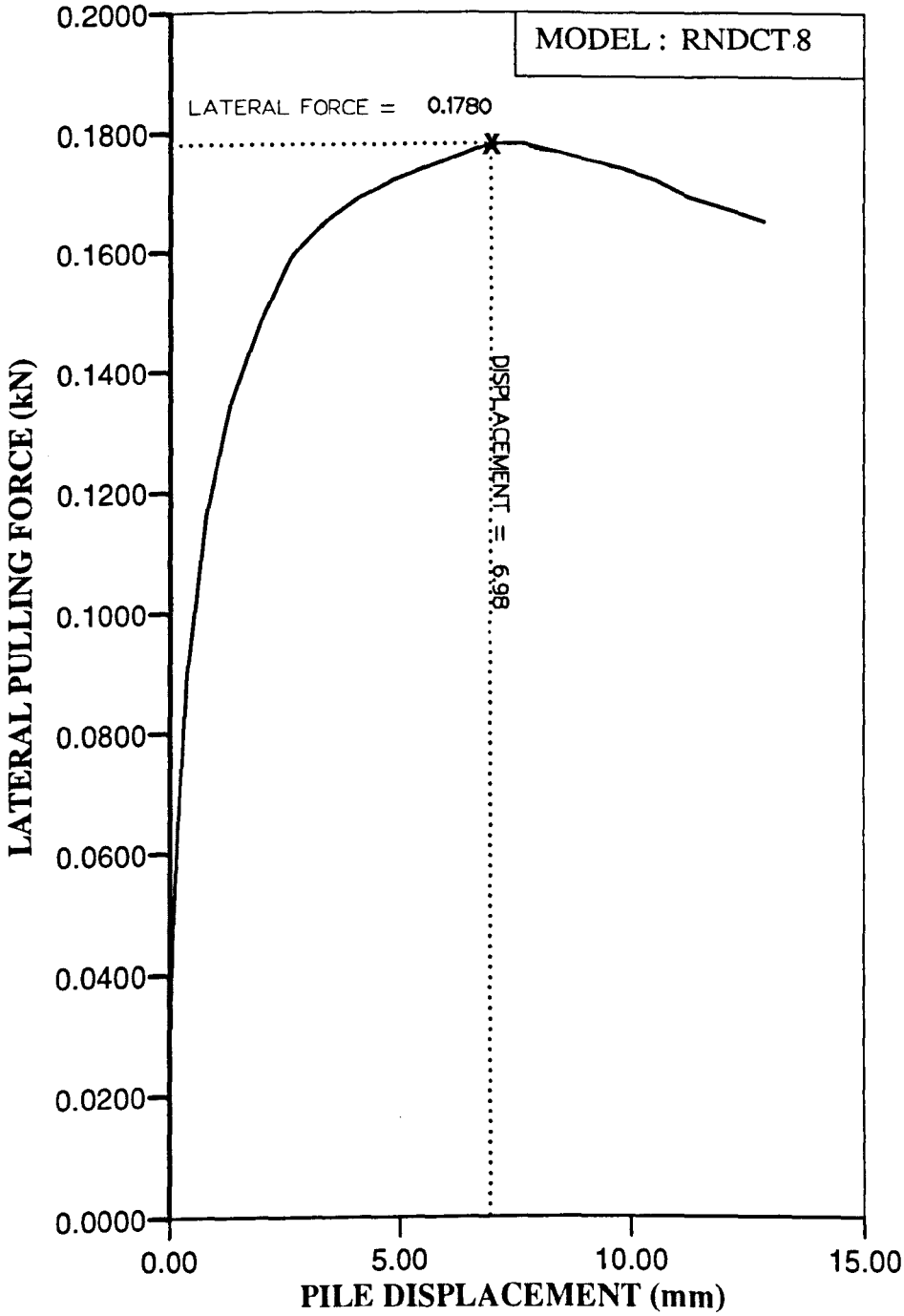

Figure AL85 Variation of lateral force with displacement at ground level for Series 1 test.

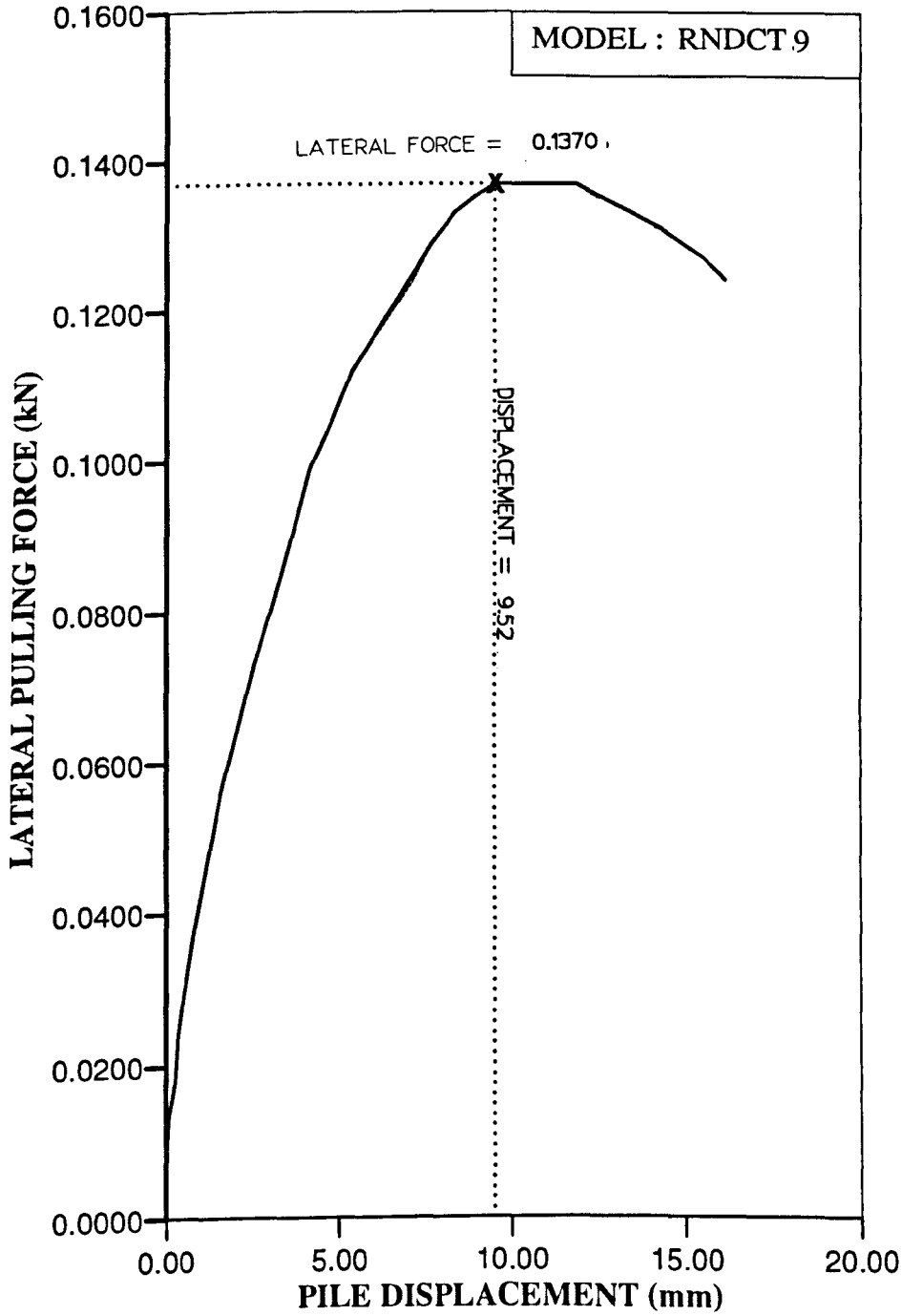

Figure AL86 Variation of lateral force with displacement at ground level for Series 1 test.

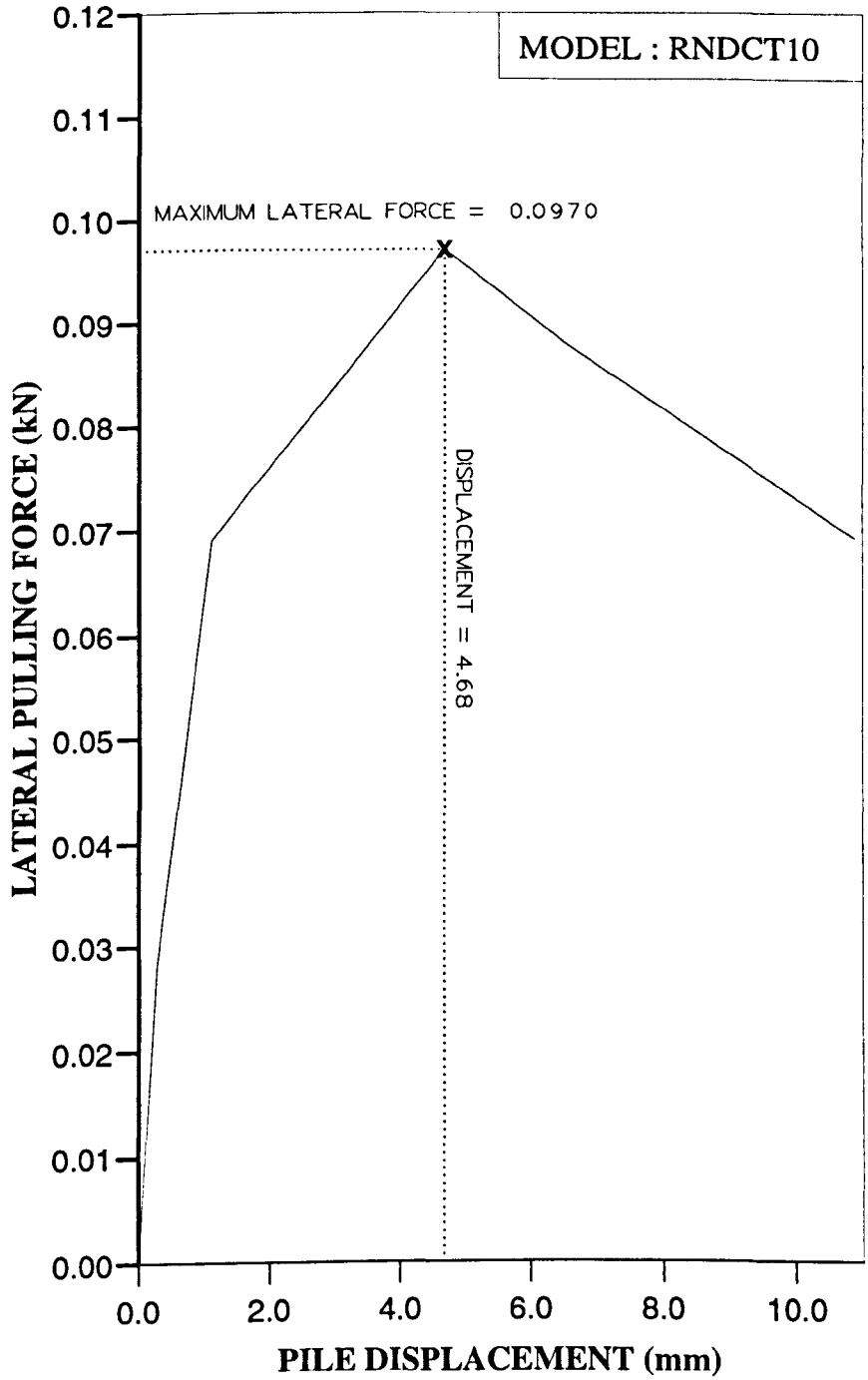

Figure AL87 Variation of lateral force with displacement at ground level for Series 1 test.

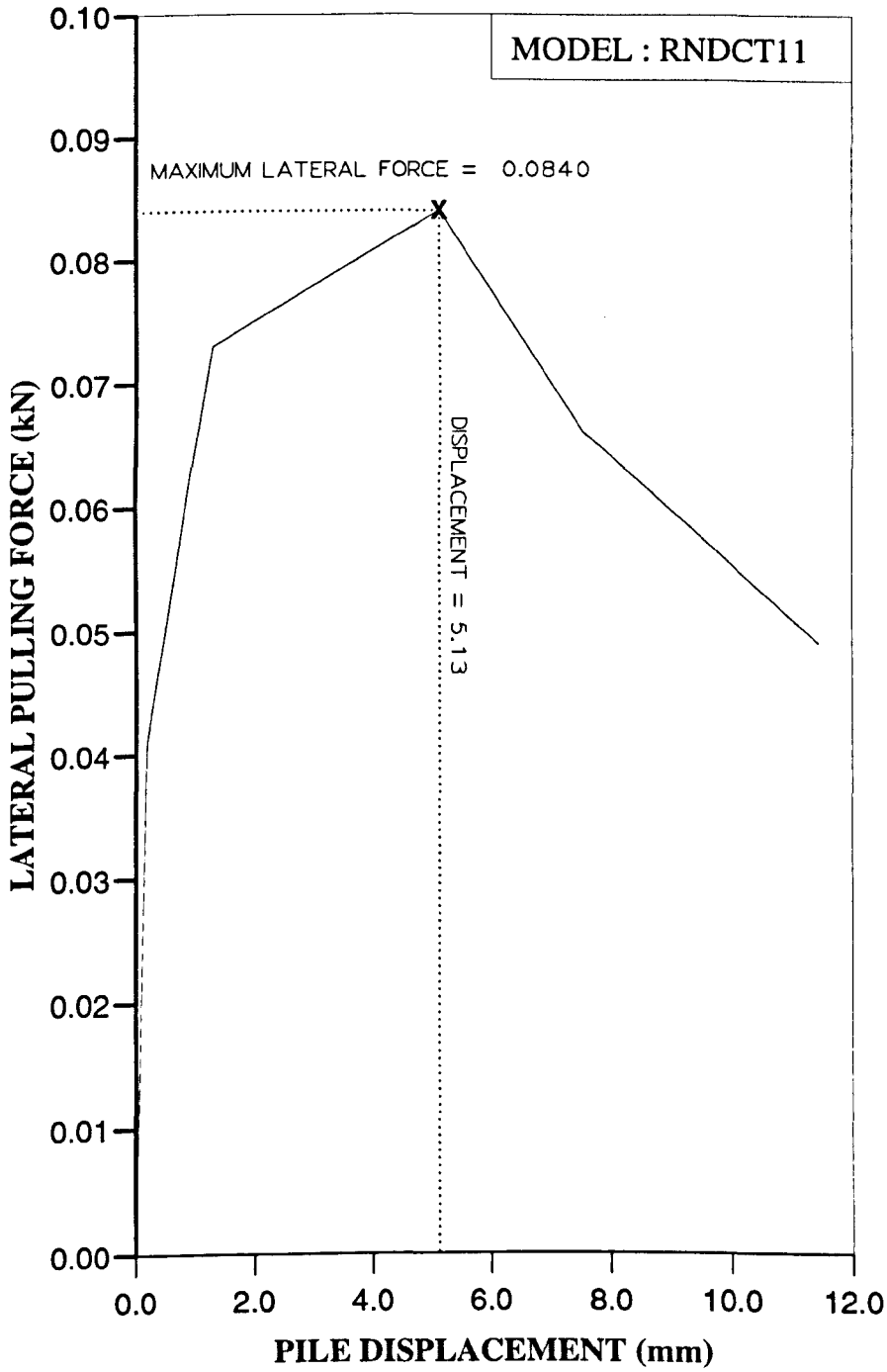

Figure AL88 Variation of lateral force with displacement at ground level for Series 1 test.

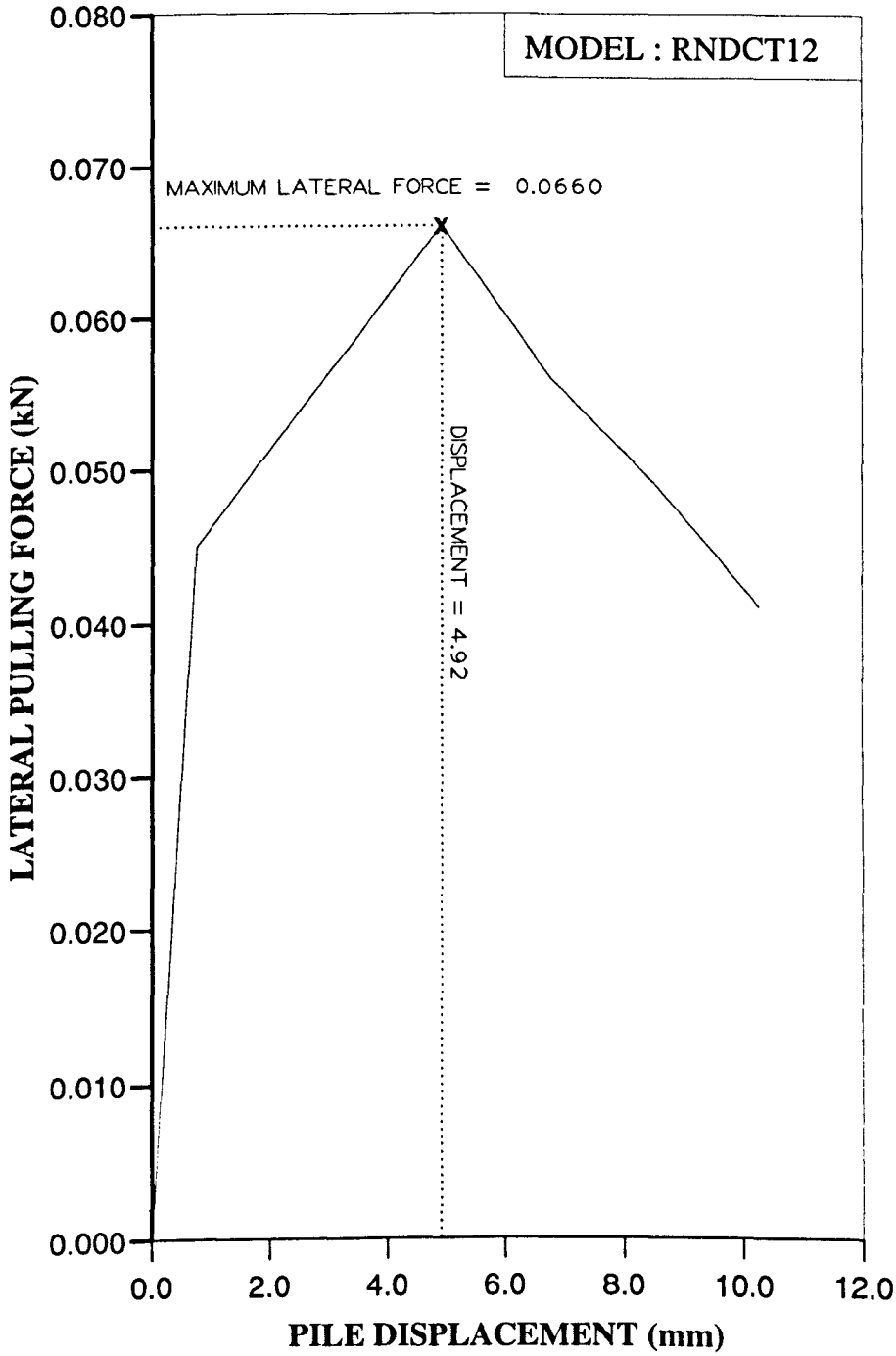

Figure AL89 Variation of lateral force with displacement at ground level for Series 1 test.

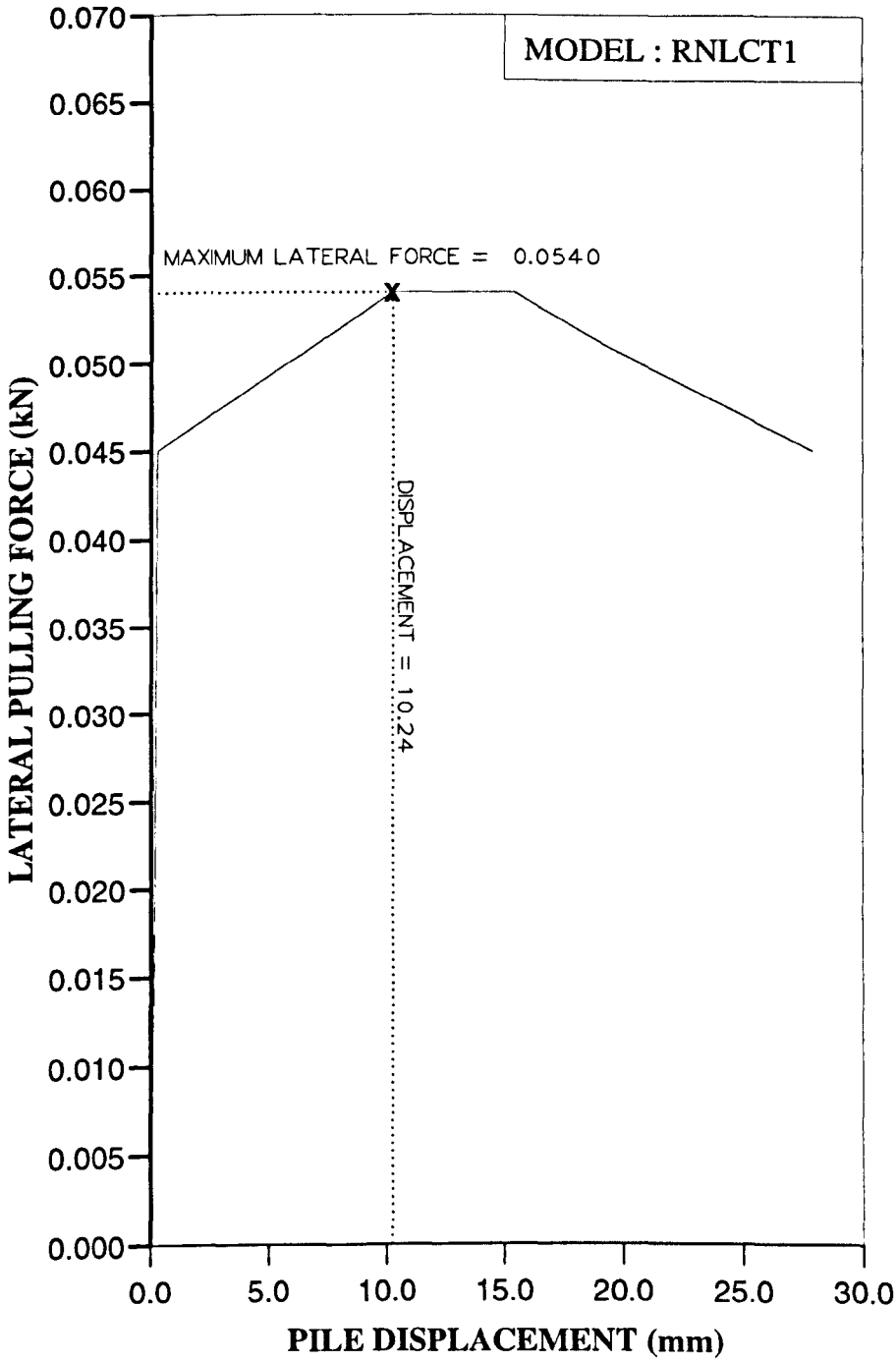

Figure AL90 Variation of lateral force with displacement at ground level for Series 1 test.

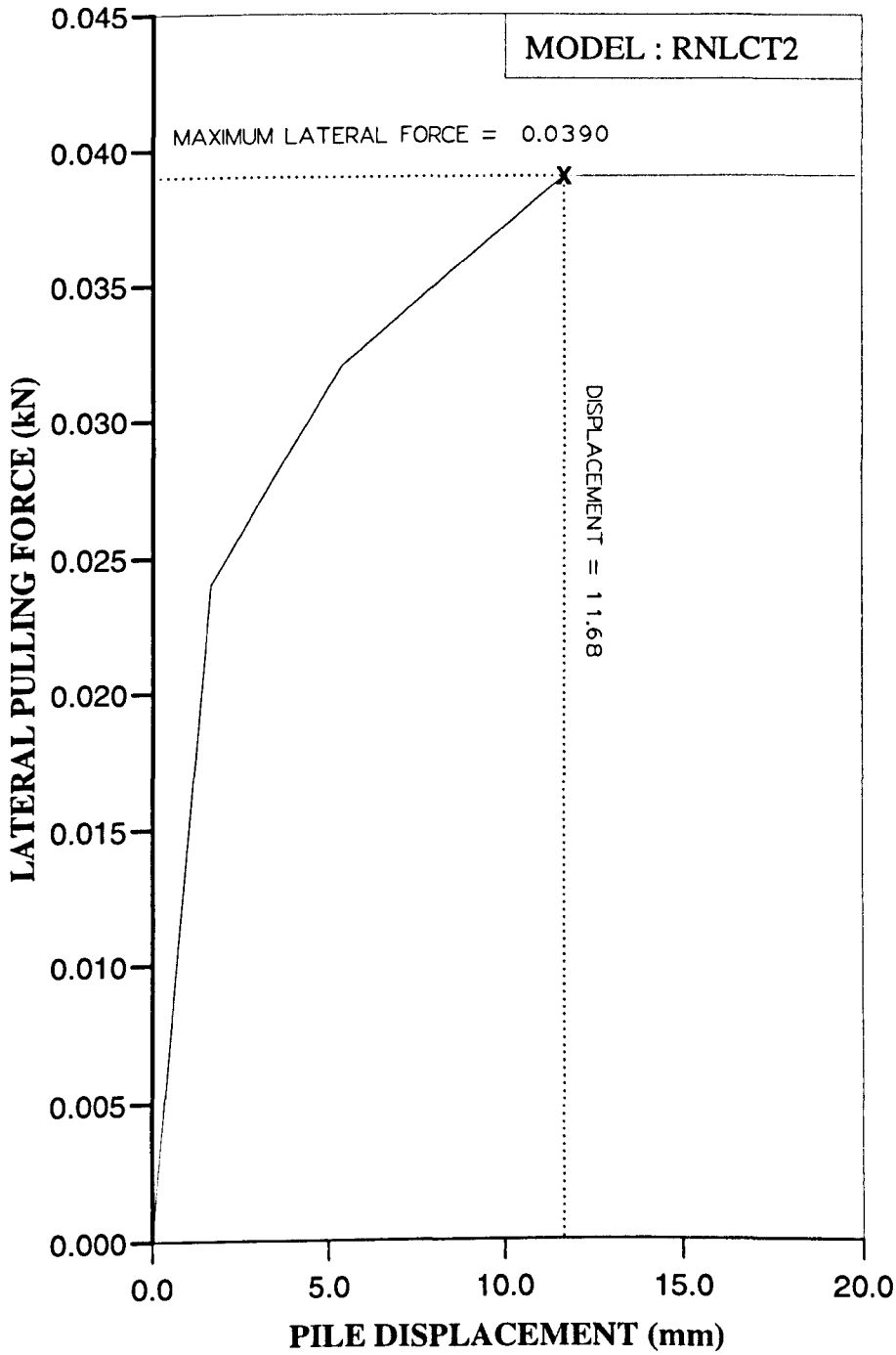

Figure AL91 Variation of lateral force with displacement at ground level for Series 1 test.

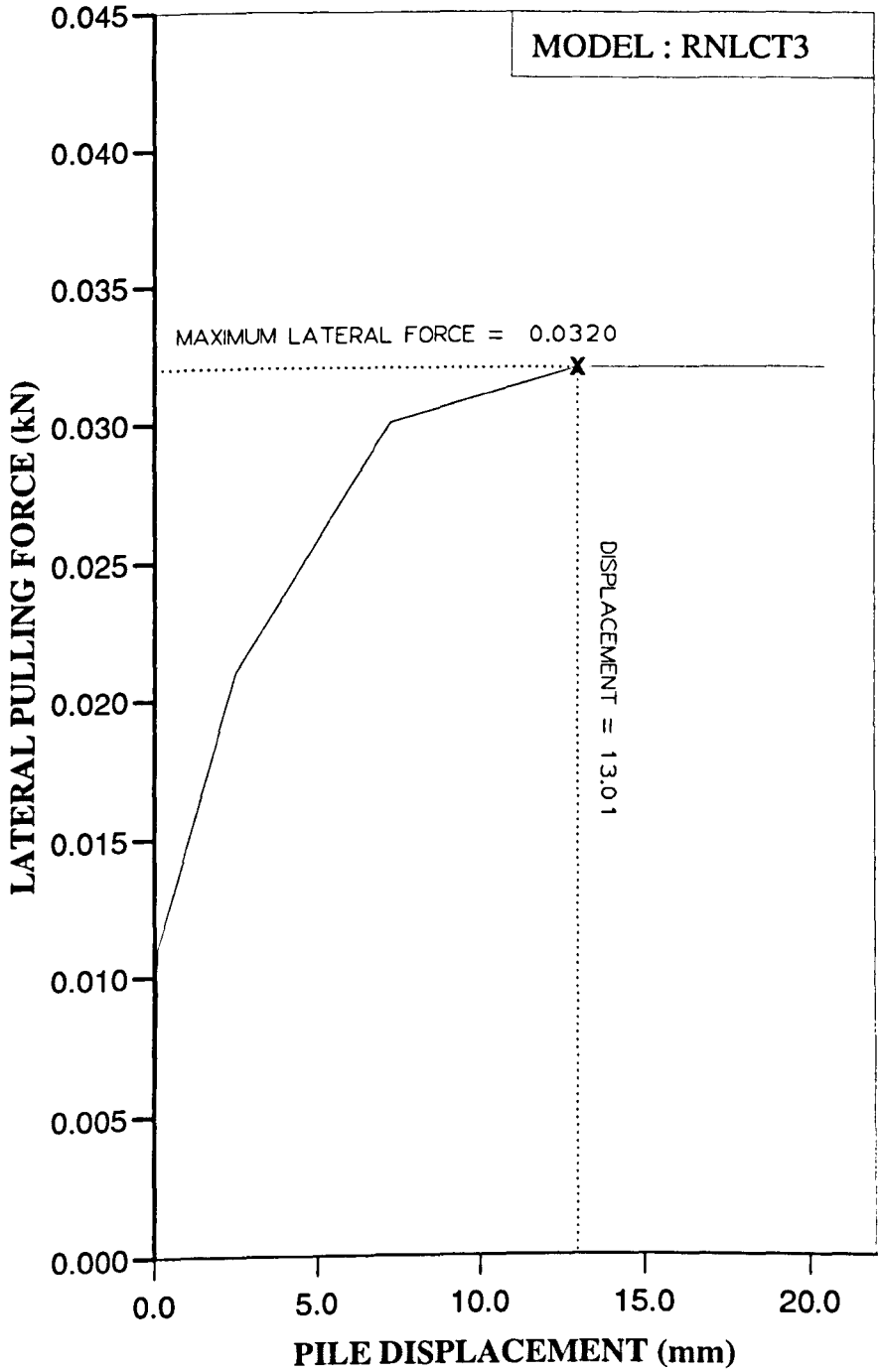

Figure AL92 Variation of lateral force with displacement at ground level for Series 1 test.

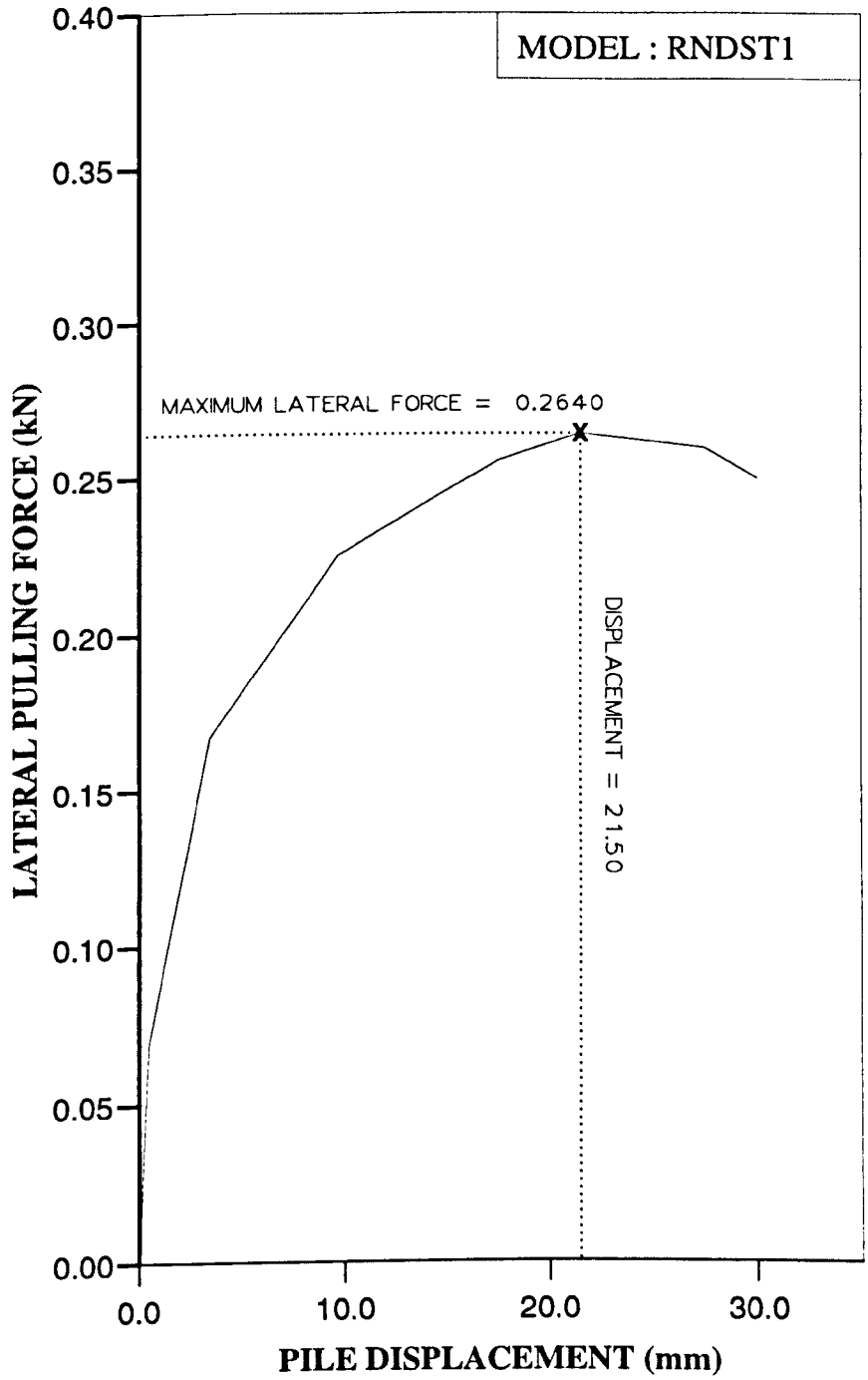

Figure AL93 Variation of lateral force with displacement at ground level for Series 2 test.

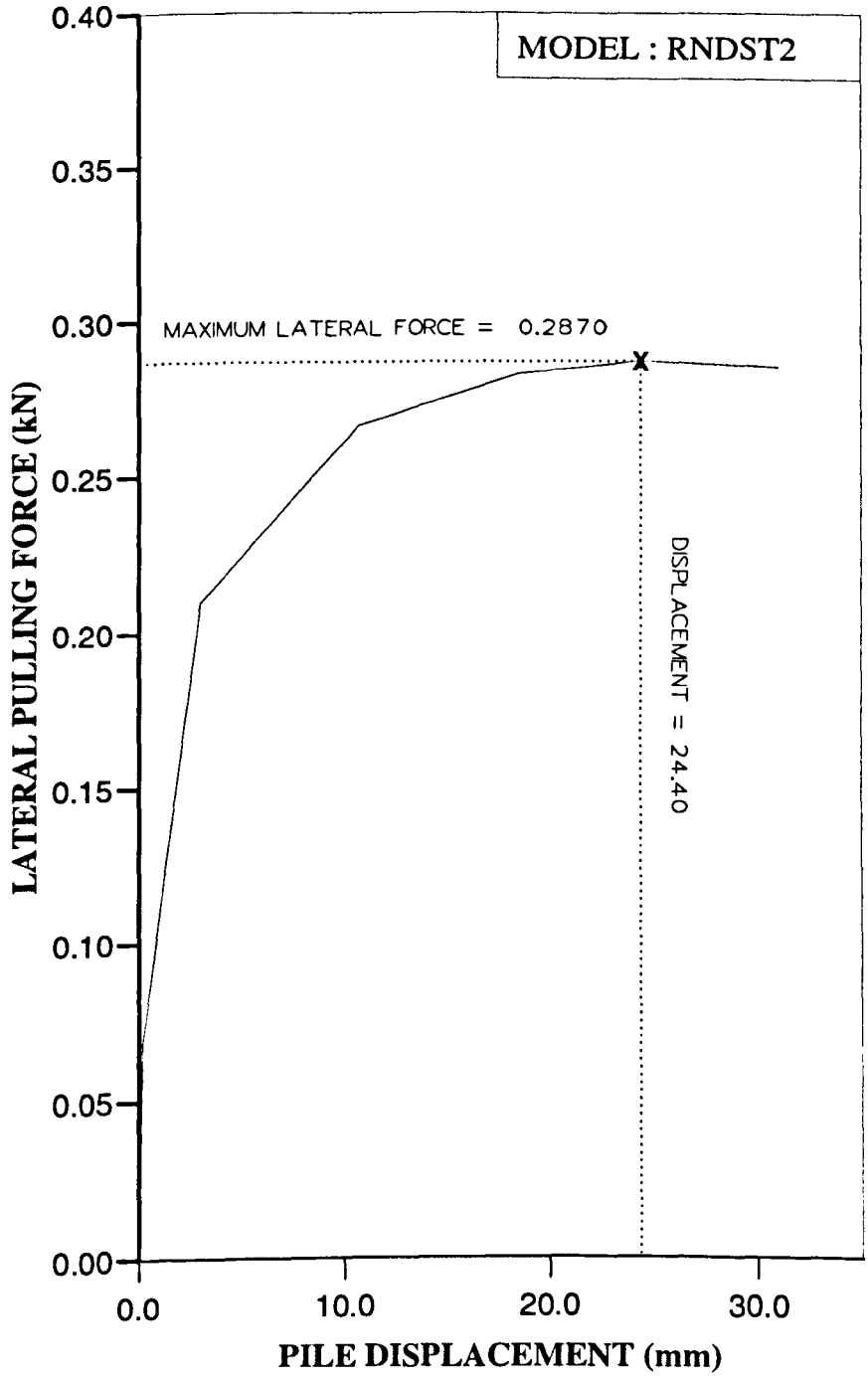

Figure AL94 Variation of lateral force with displacement at ground level for Series 2 test.

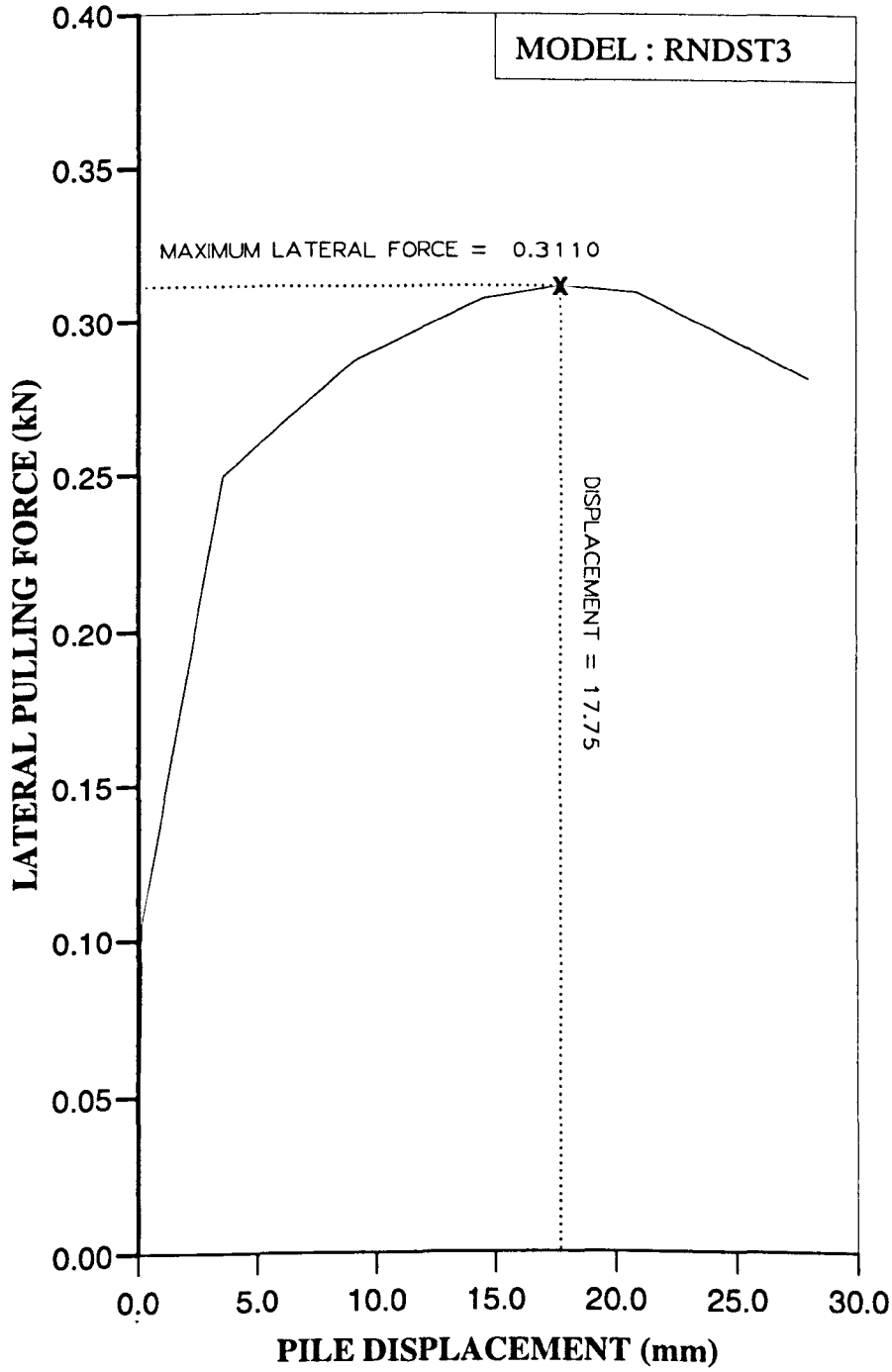

Figure AL95 Variation of lateral force with displacement at ground level for Series 2 test.

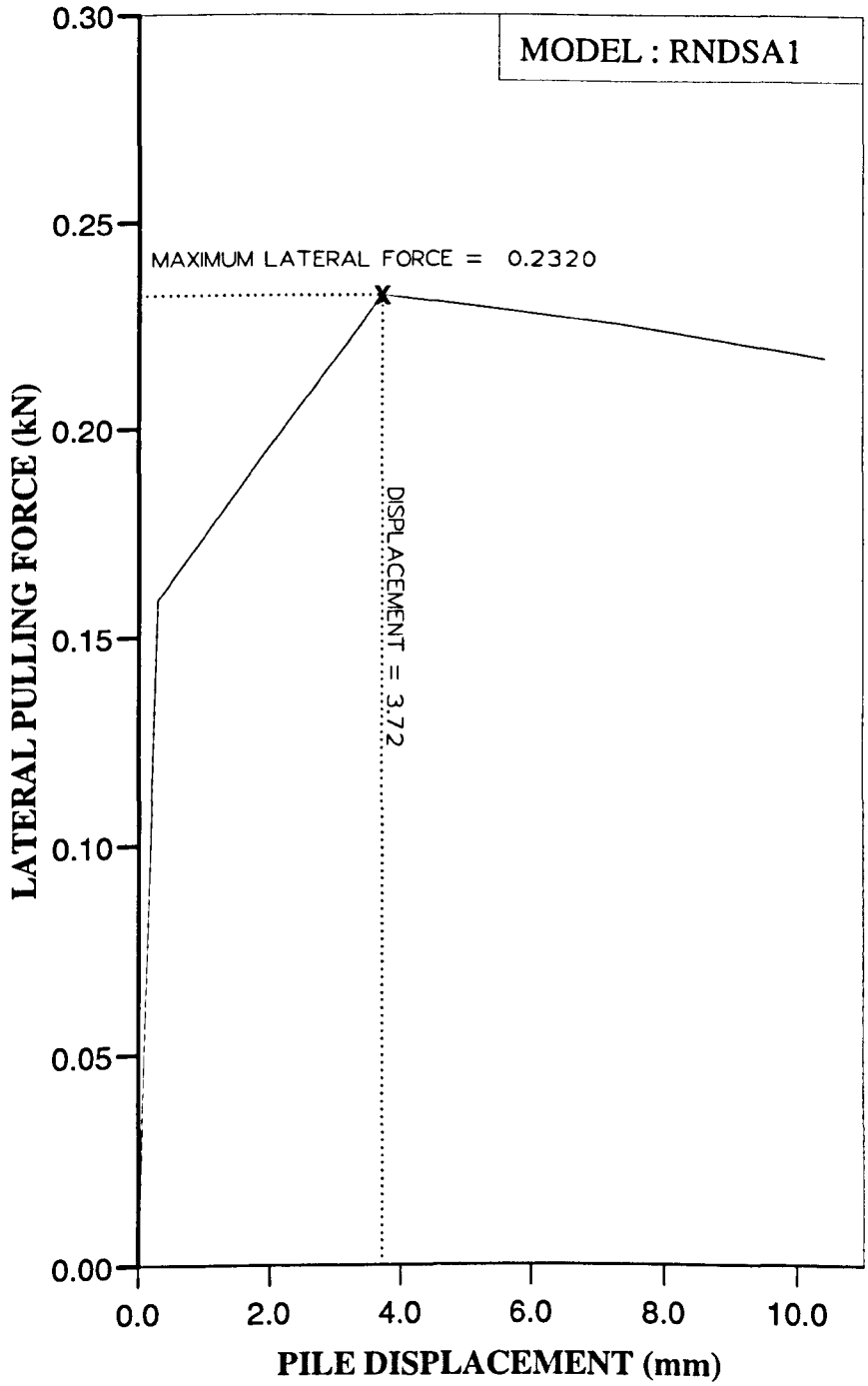

Figure AL96 Variation of lateral force with displacement at ground level for Series 2 test.

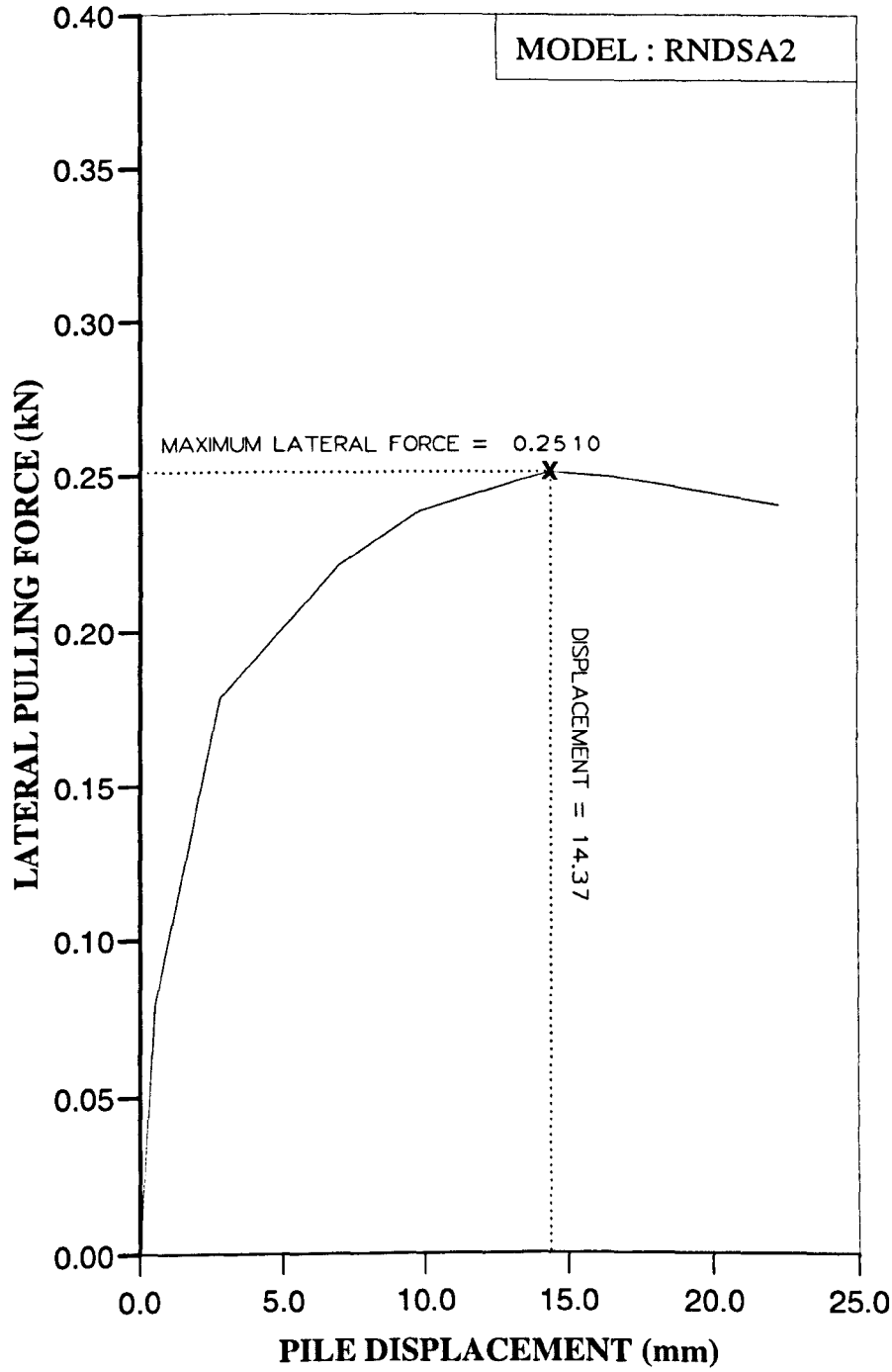

Figure AL97 Variation of lateral force with displacement at ground level for Series 2 test.

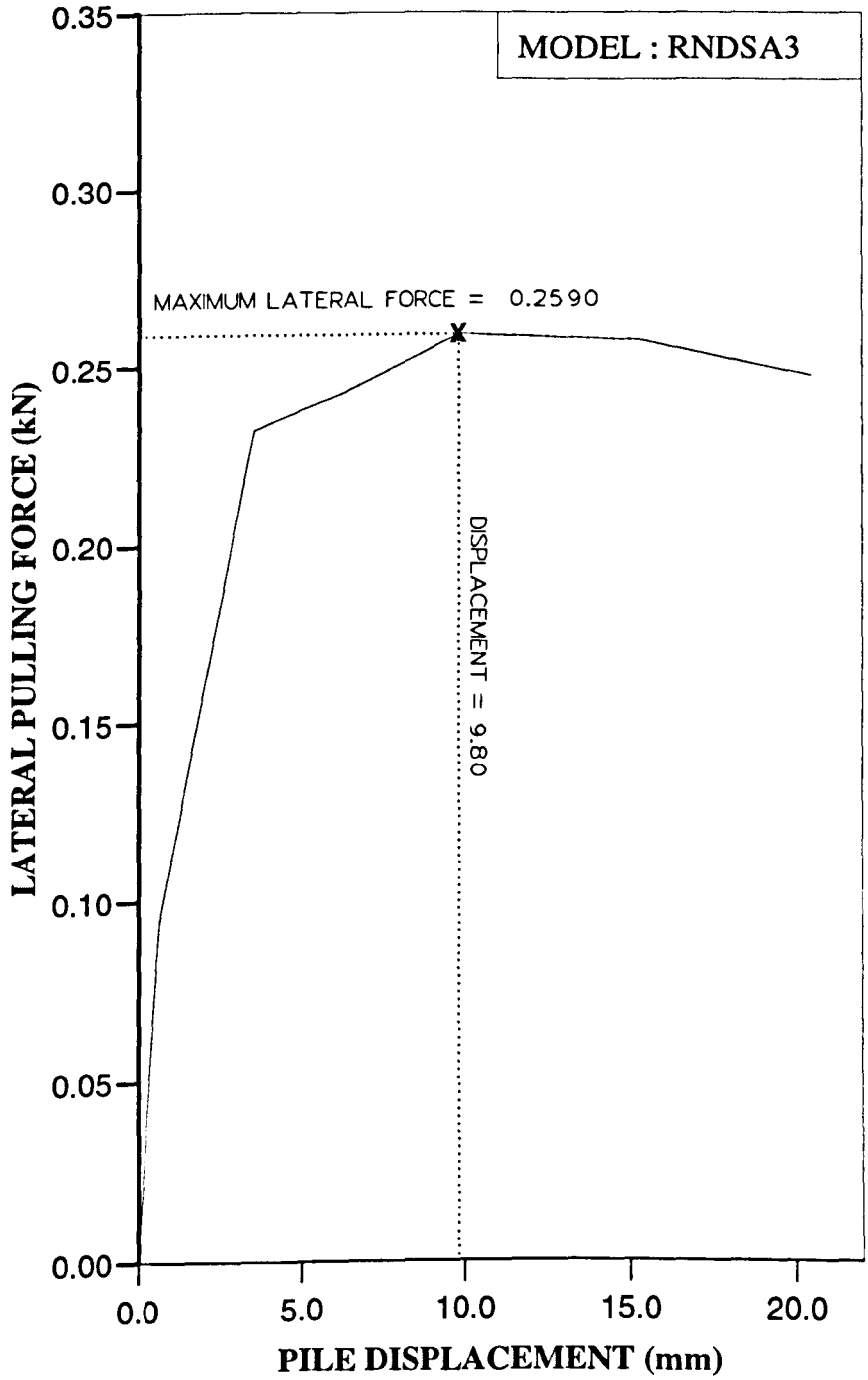

Figure AL98 Variation of lateral force with displacement at ground level for Series 2 test.

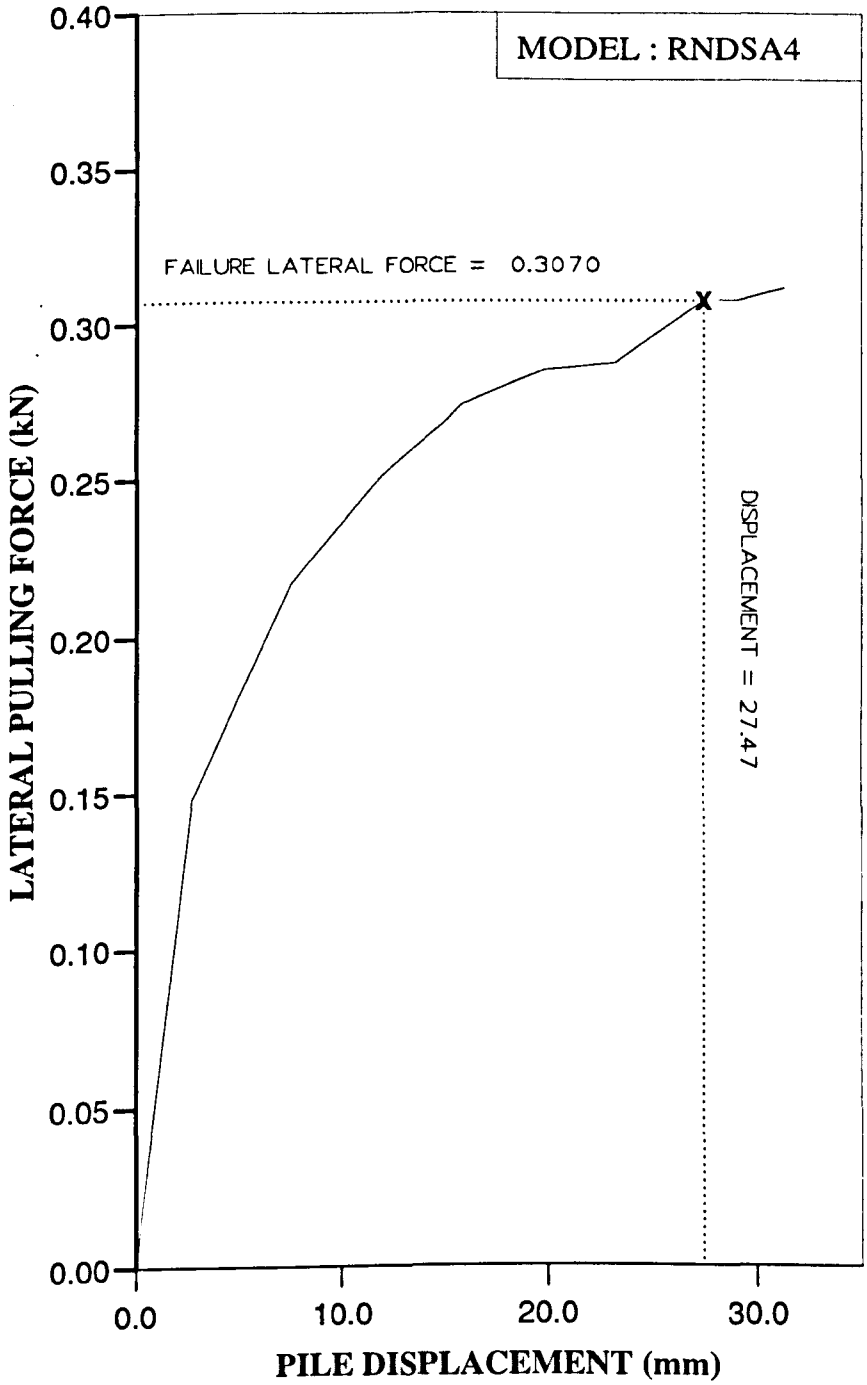

Figure AL99 Variation of lateral force with displacement at ground level for Series 2 test.

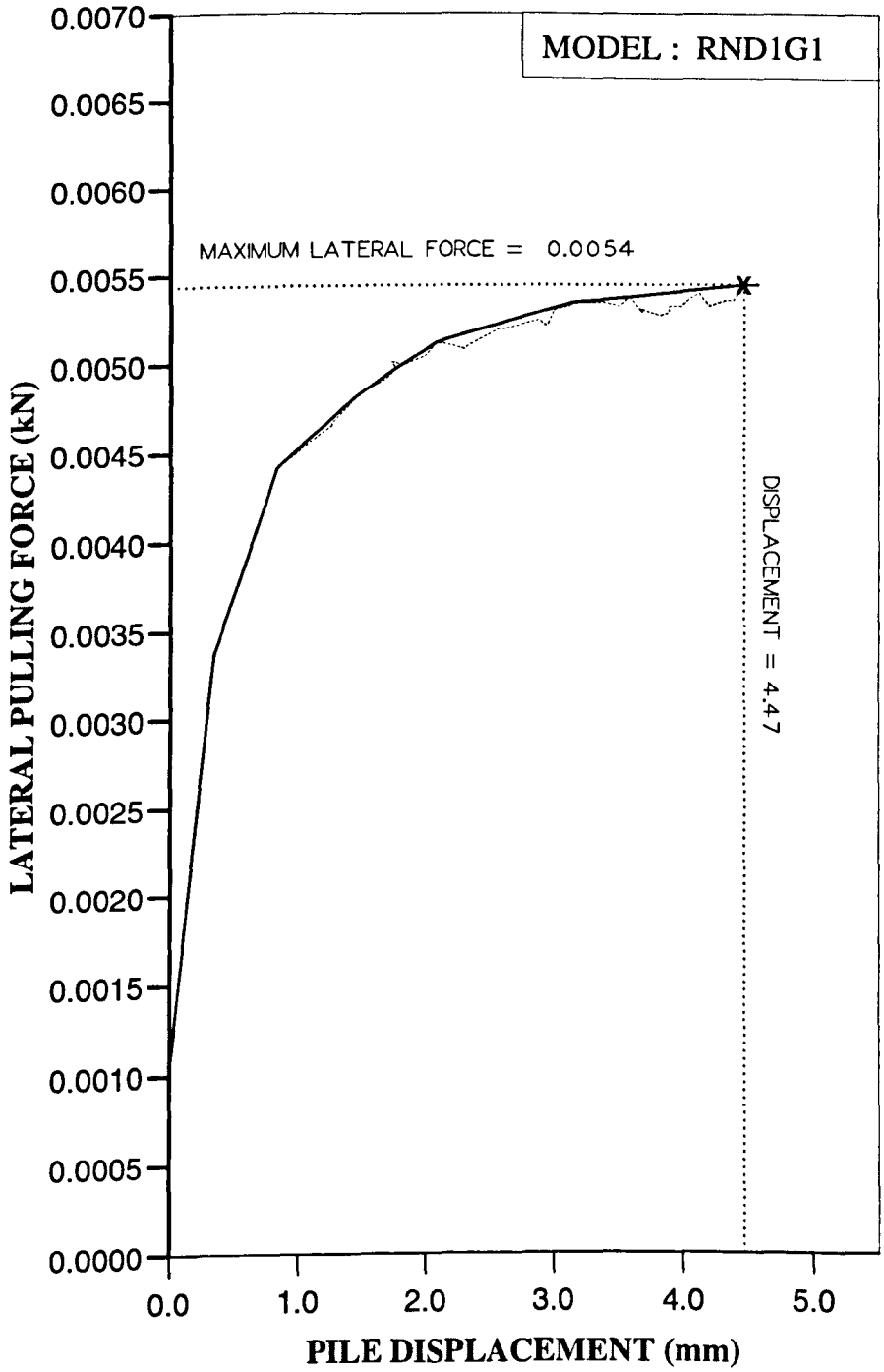

Figure AL100 Variation of lateral force with displacement at ground level for Series 3 test.

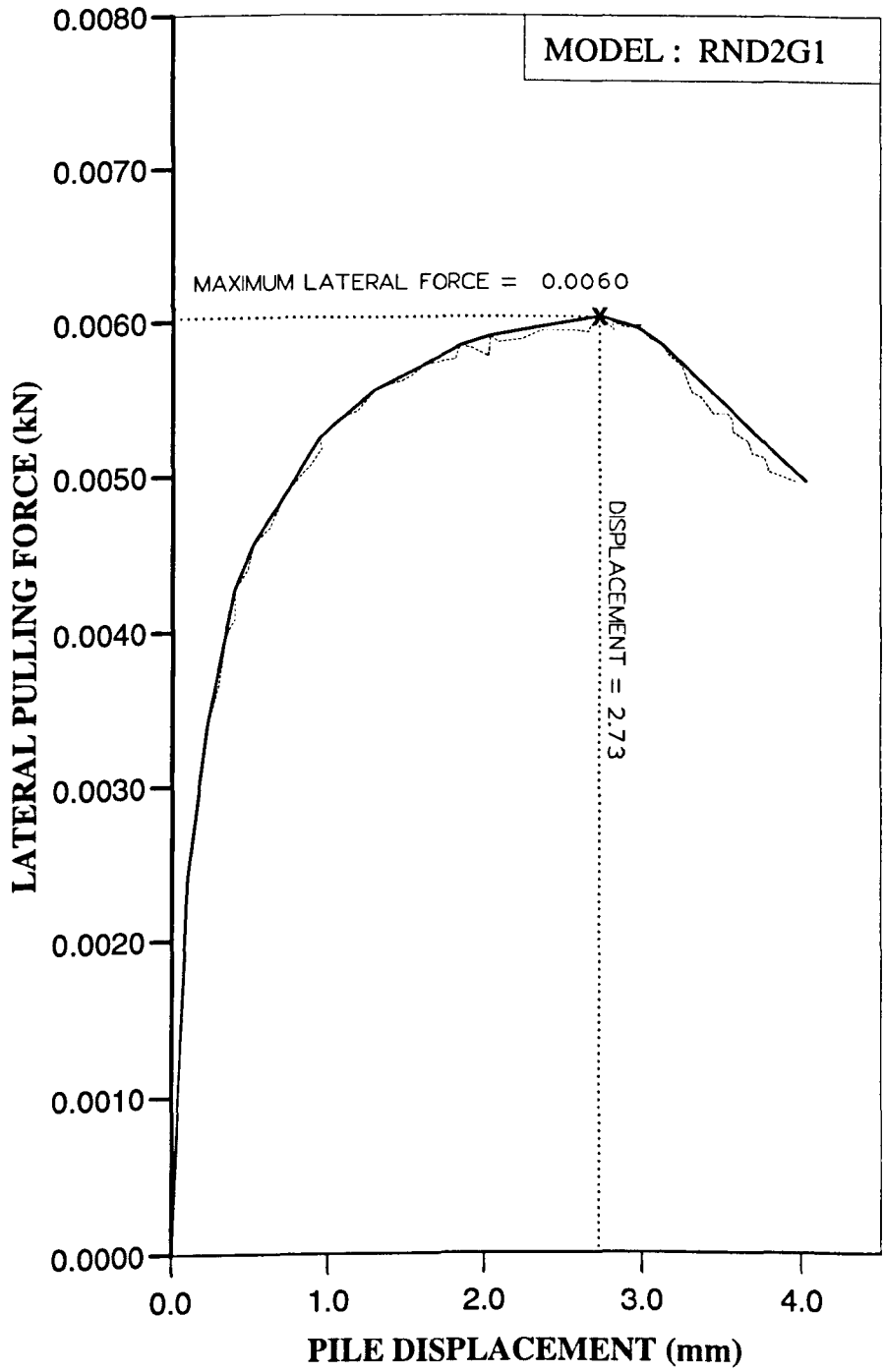

Figure AL101 Variation of lateral force with displacement at ground level for Series 3 test.

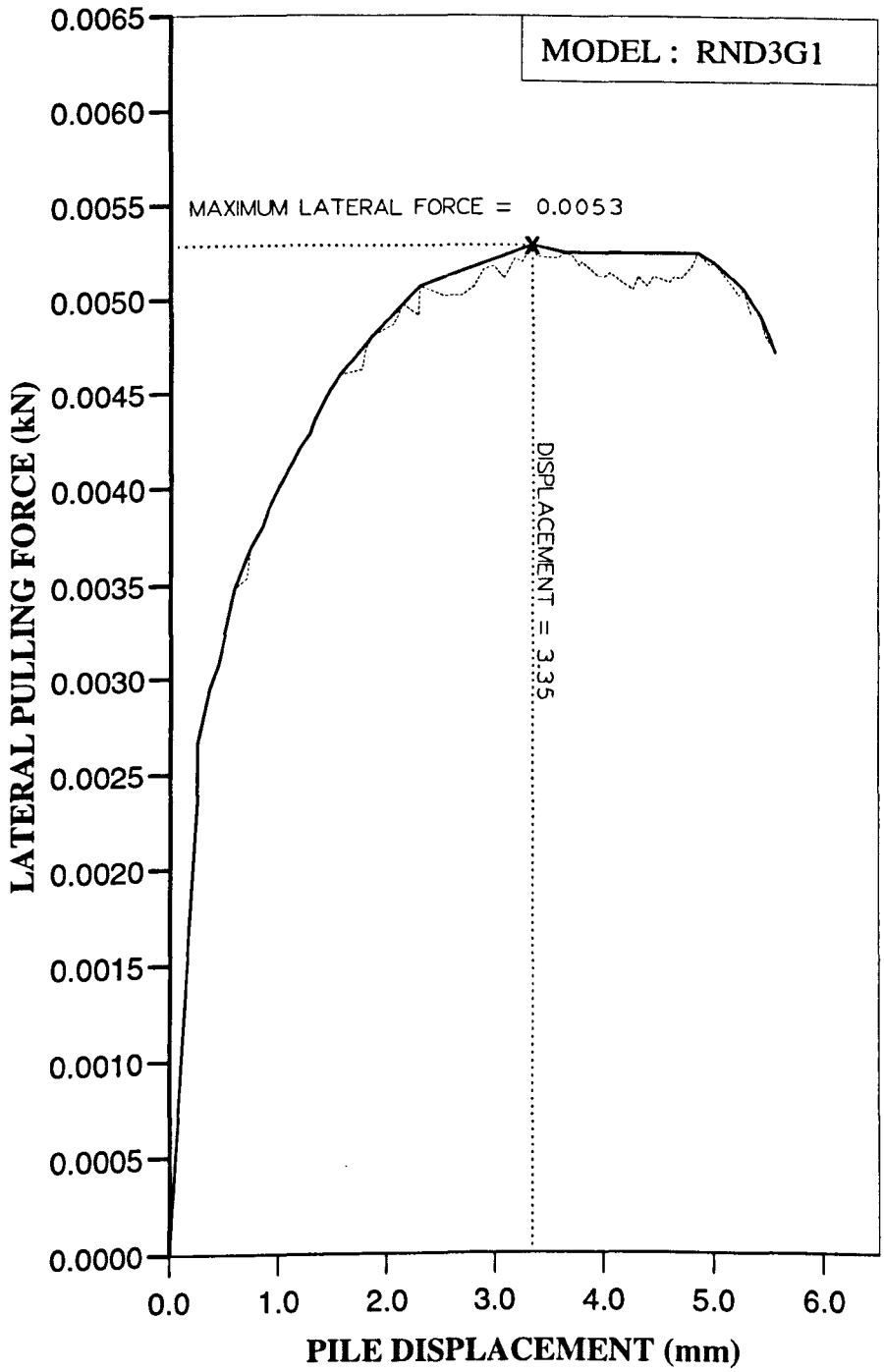

Figure AL102 Variation of lateral force with displacement at ground level for Series 3 test.

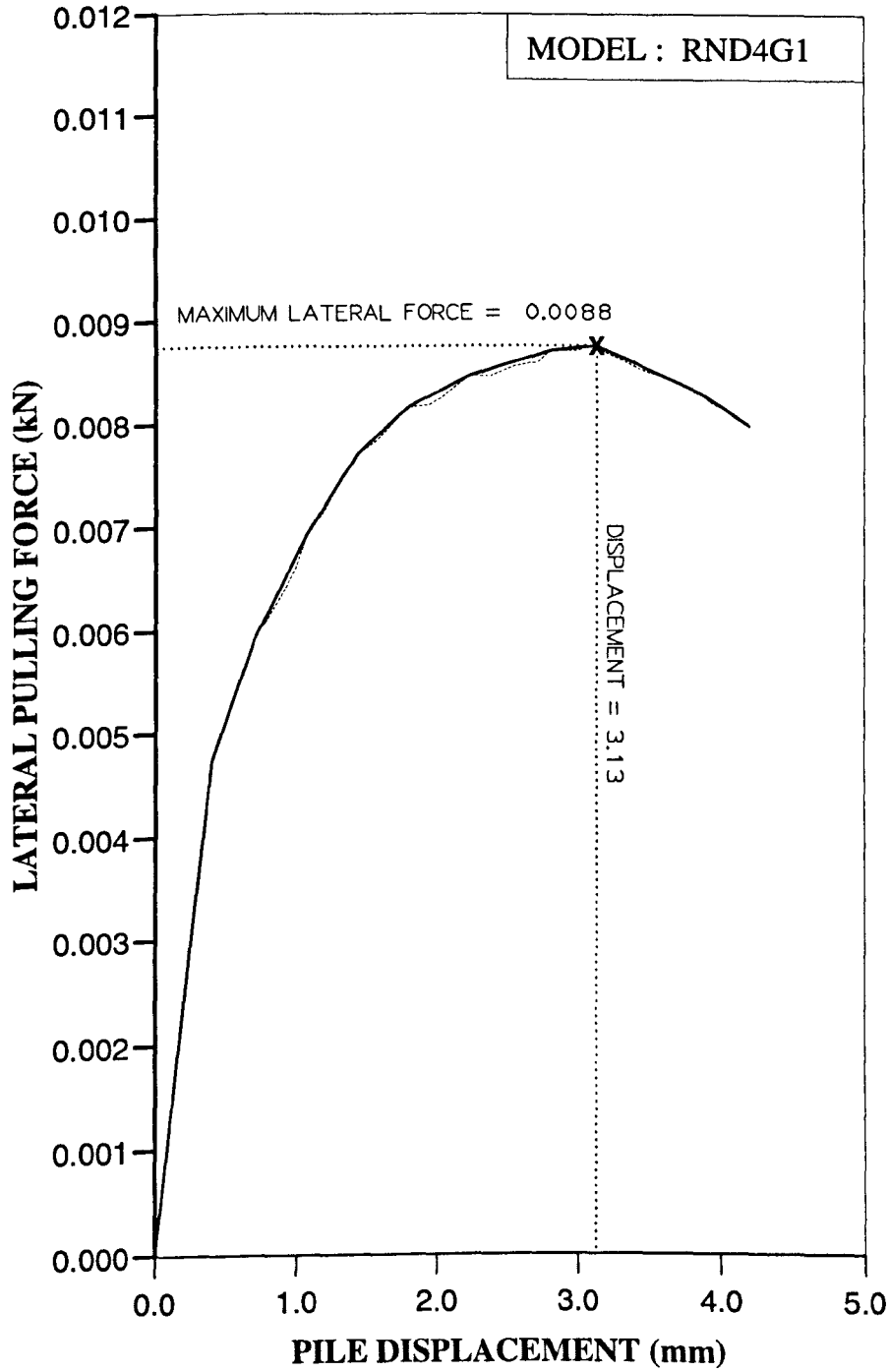

Figure AL103 Variation of lateral force with displacement at ground level for Series 3 test.

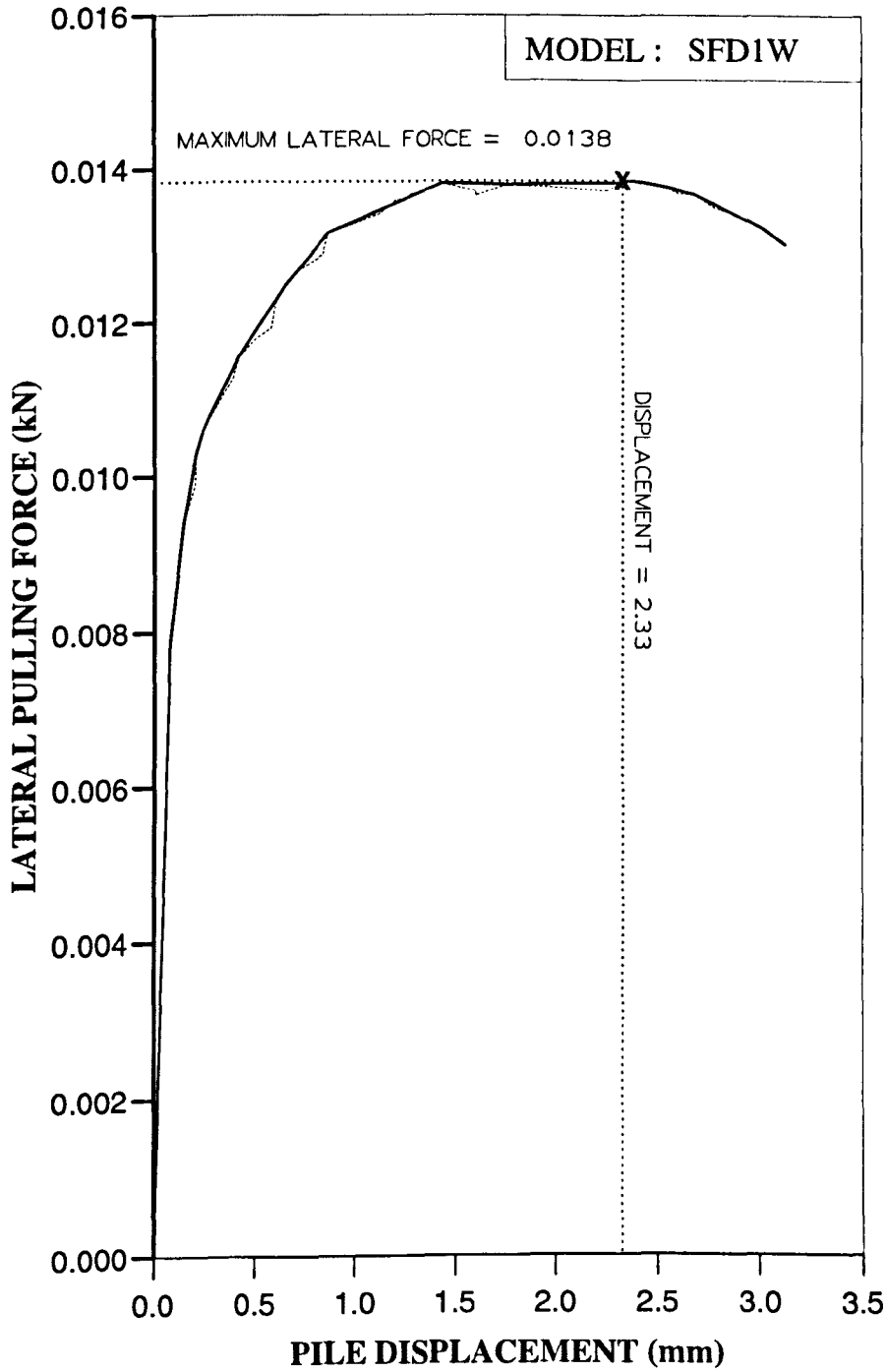

Figure AL104 Variation of lateral force with displacement at ground level for Series 4 test.

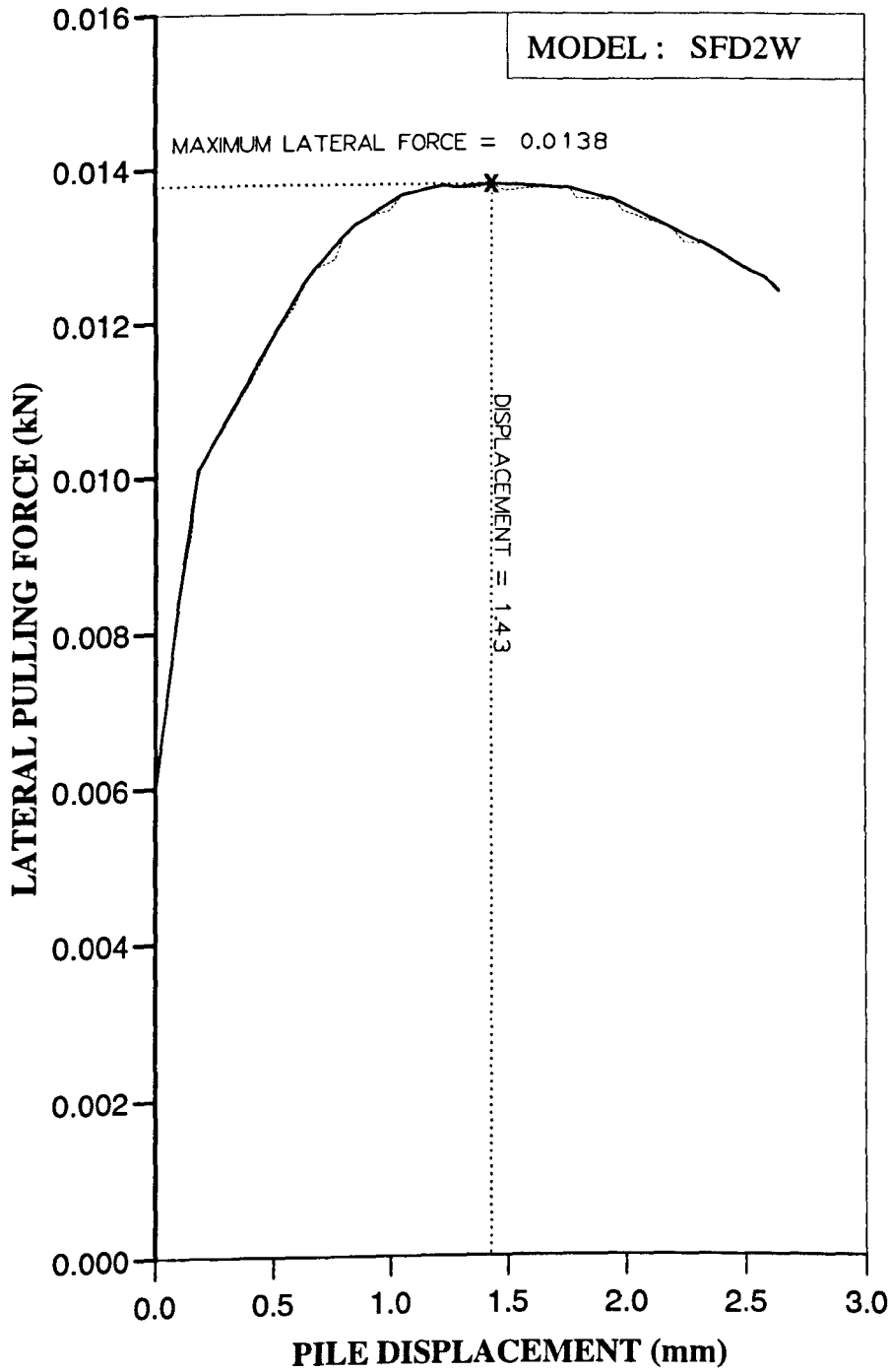

Figure AL105 Variation of lateral force with displacement at ground level for Series 4 test.

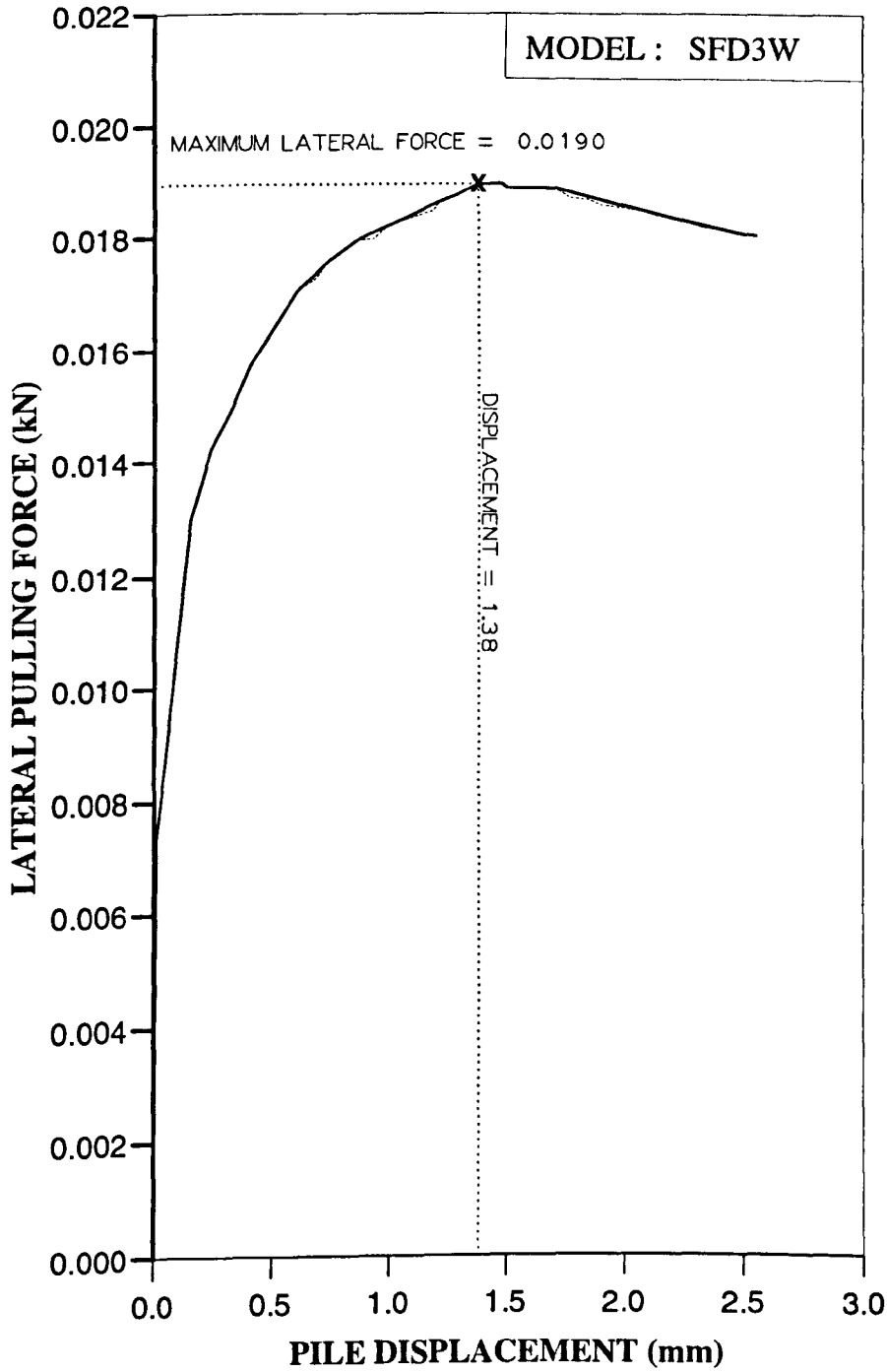

Figure AL106 Variation of lateral force with displacement at ground level for Series 4 test.

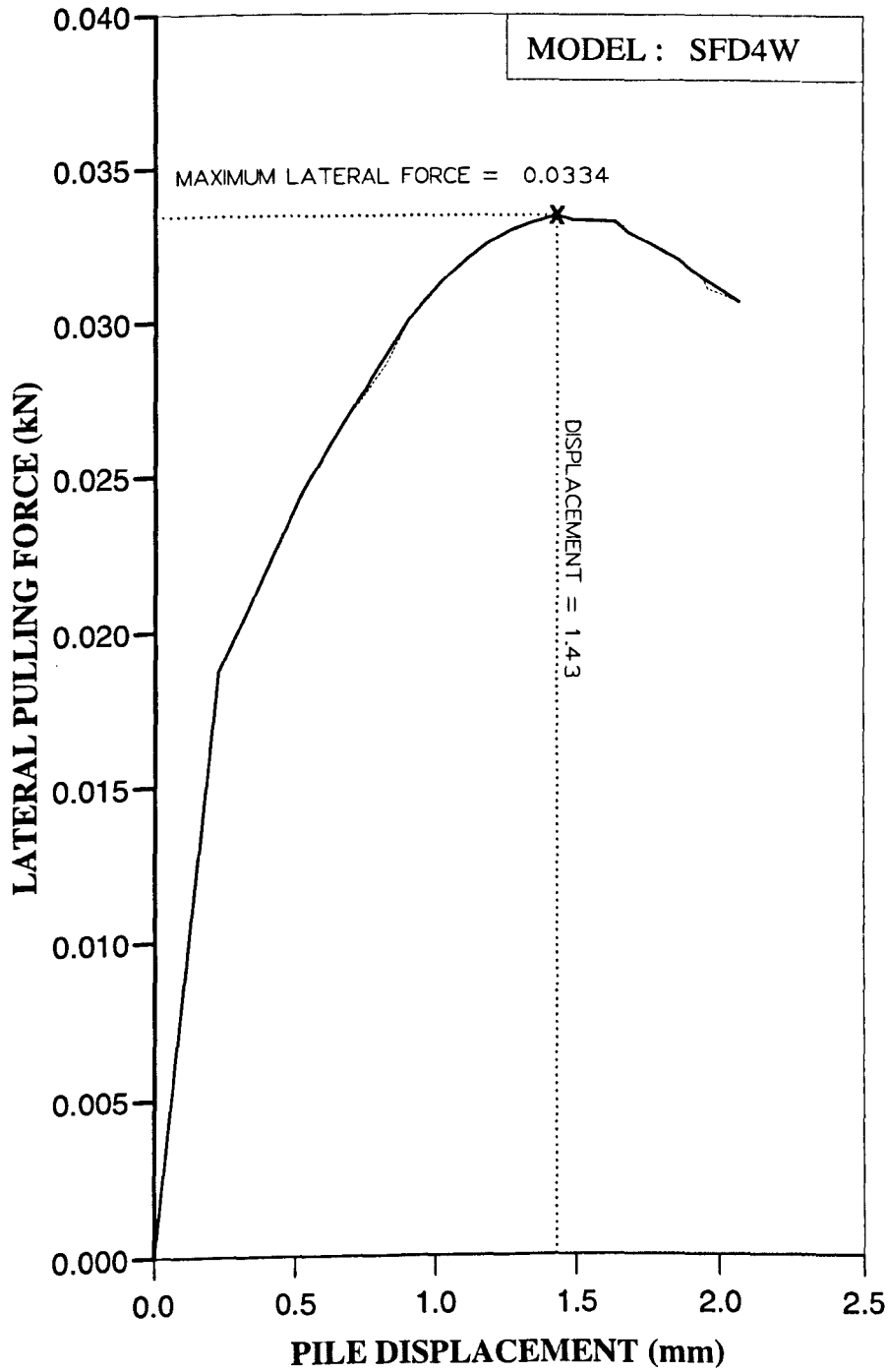

Figure AL107 Variation of lateral force with displacement at ground level for Series 4 test.

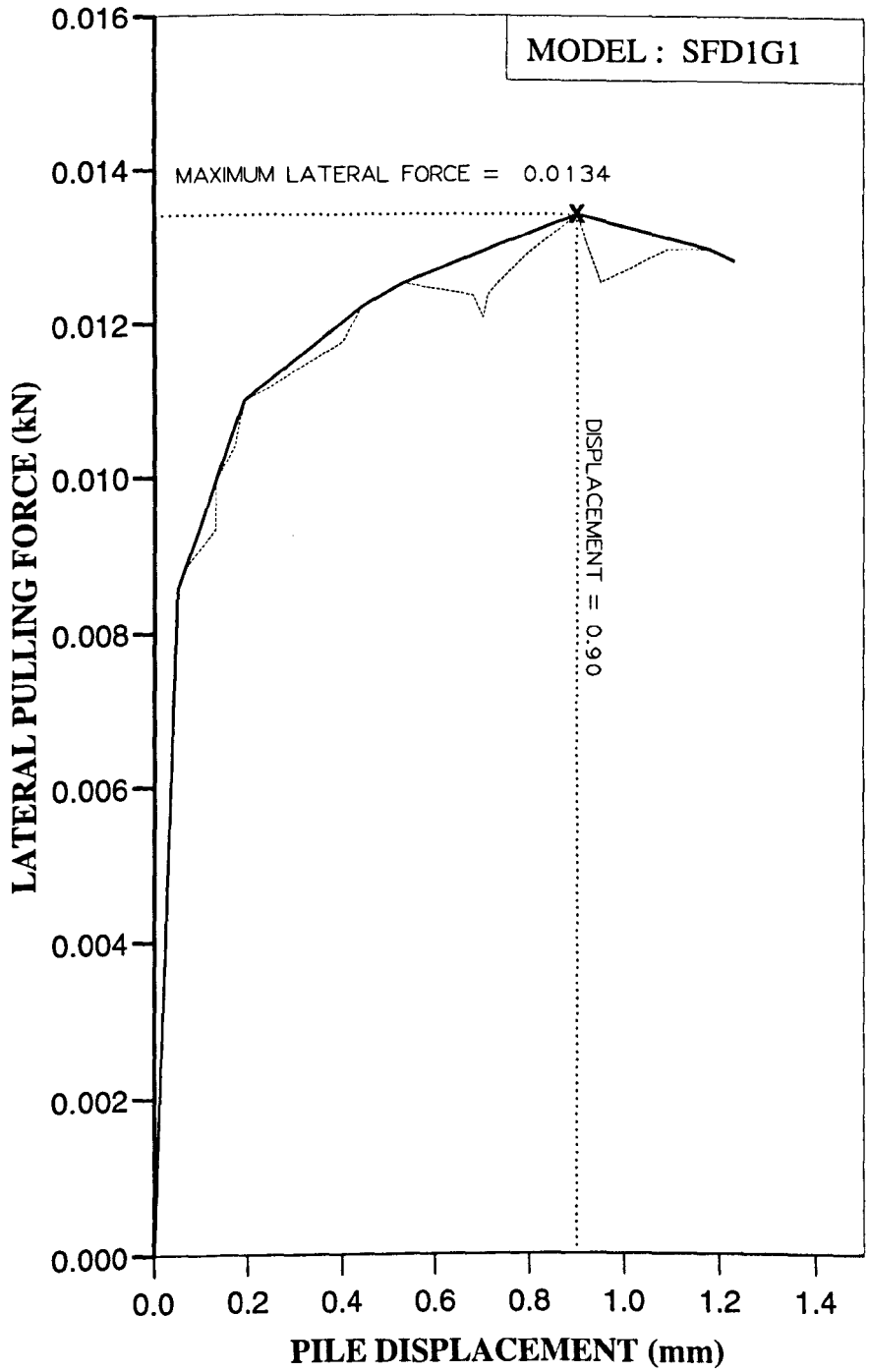

Figure AL108 Variation of lateral force with displacement at ground level for Series 4 test.

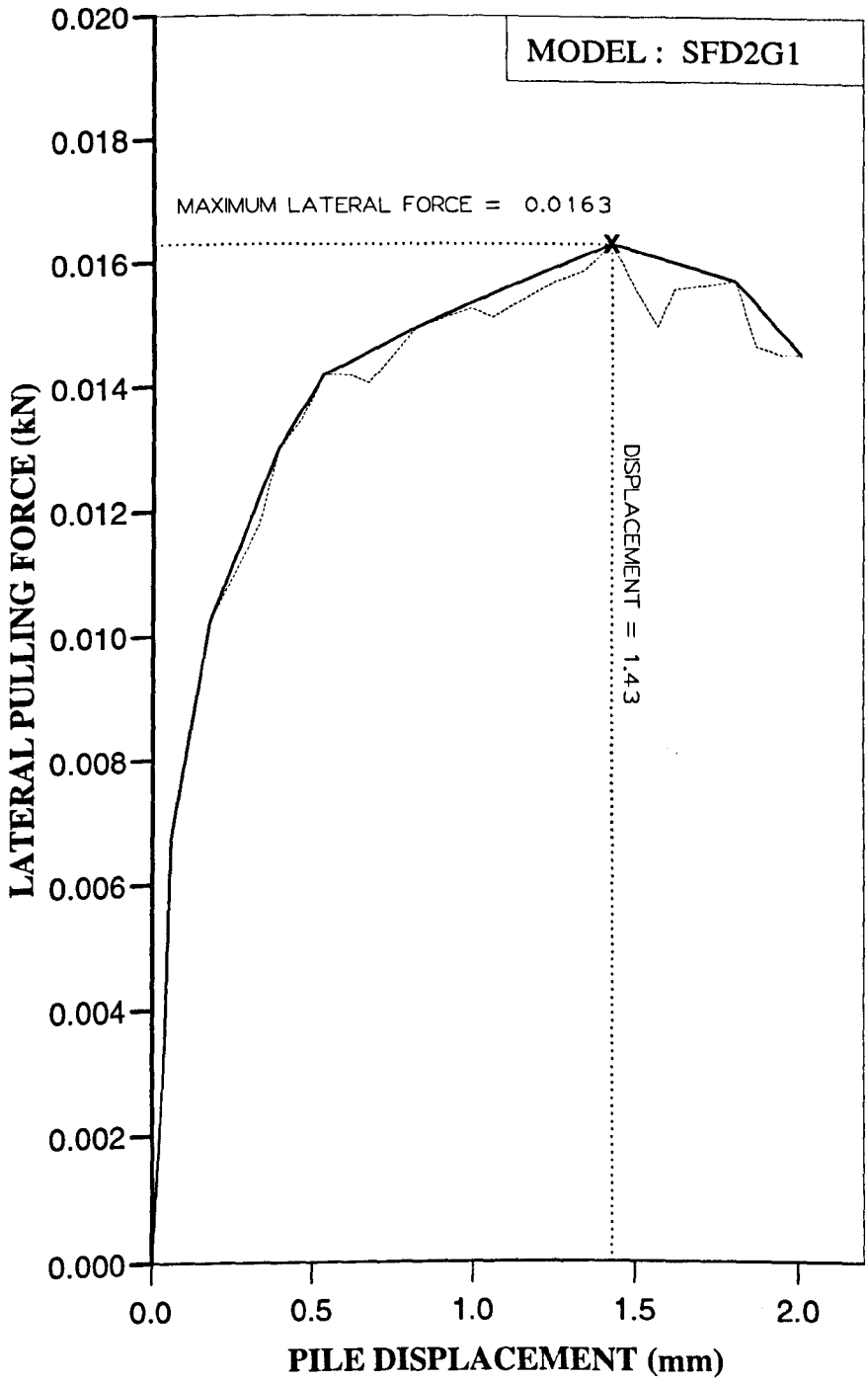

Figure AL109 Variation of lateral force with displacement at ground level for Series 4 test.

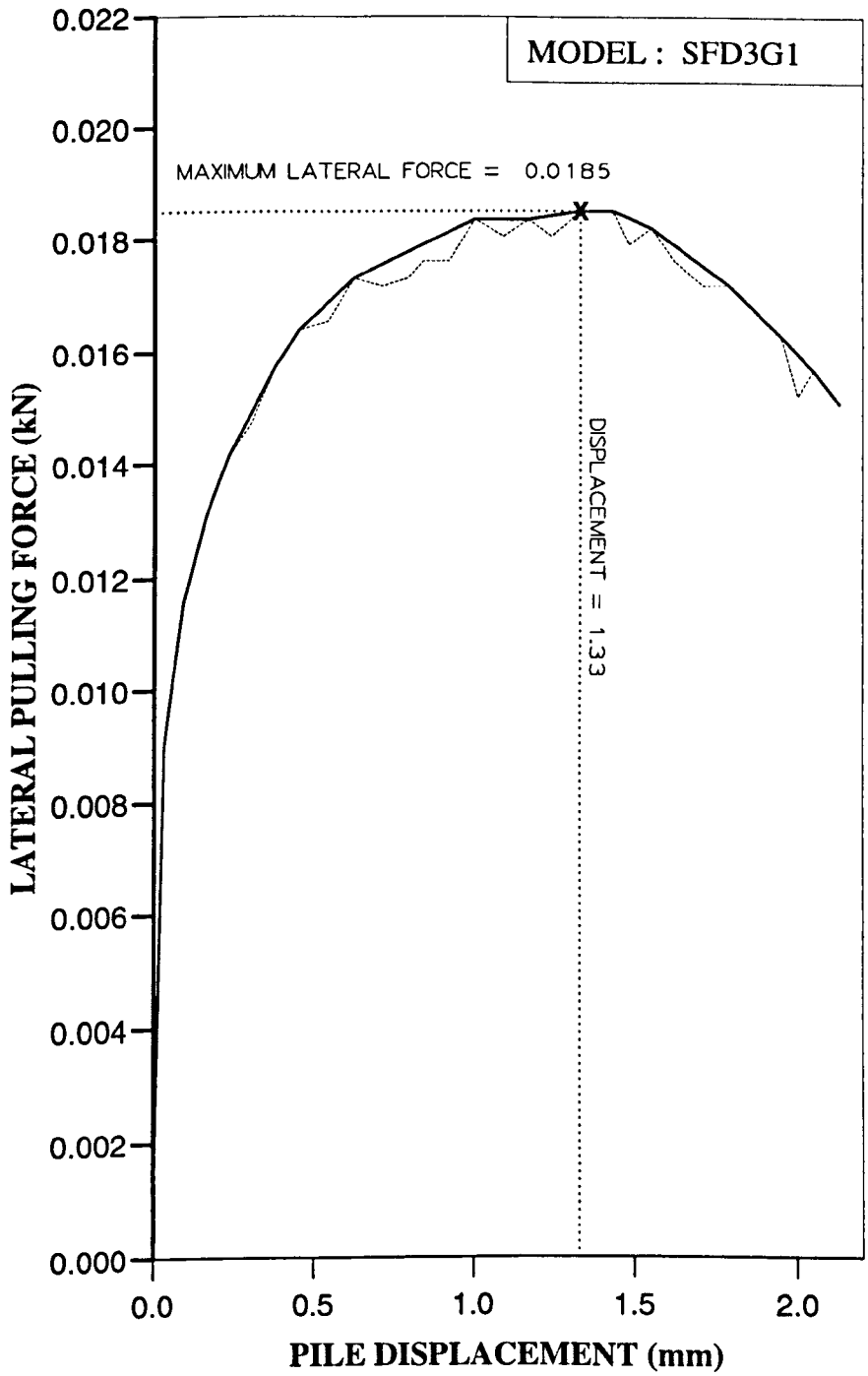

Figure AL110 Variation of lateral force with displacement at ground level for Series 4 test.

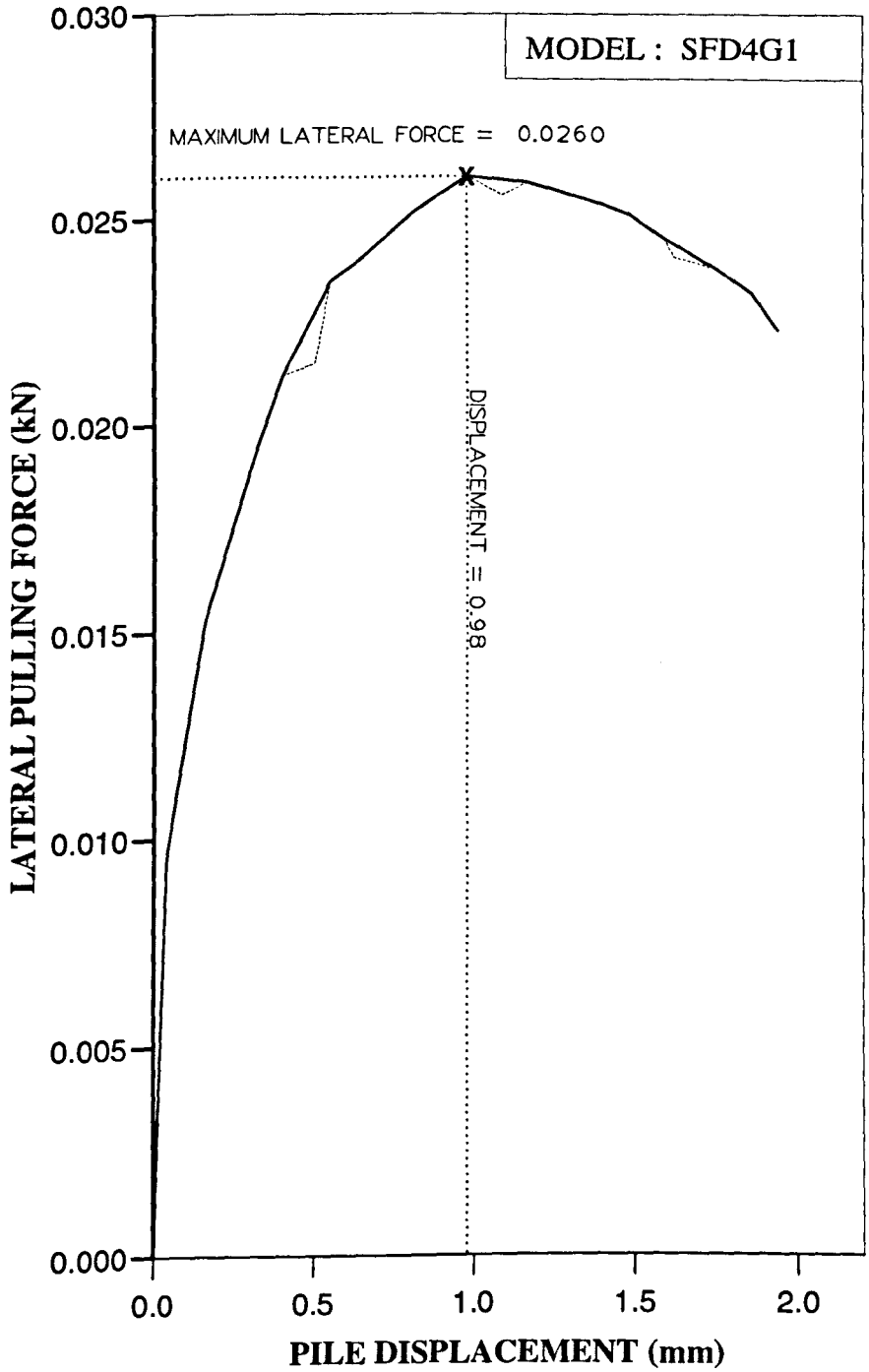

Figure AL111 Variation of lateral force with displacement at ground level for Series 4 test.

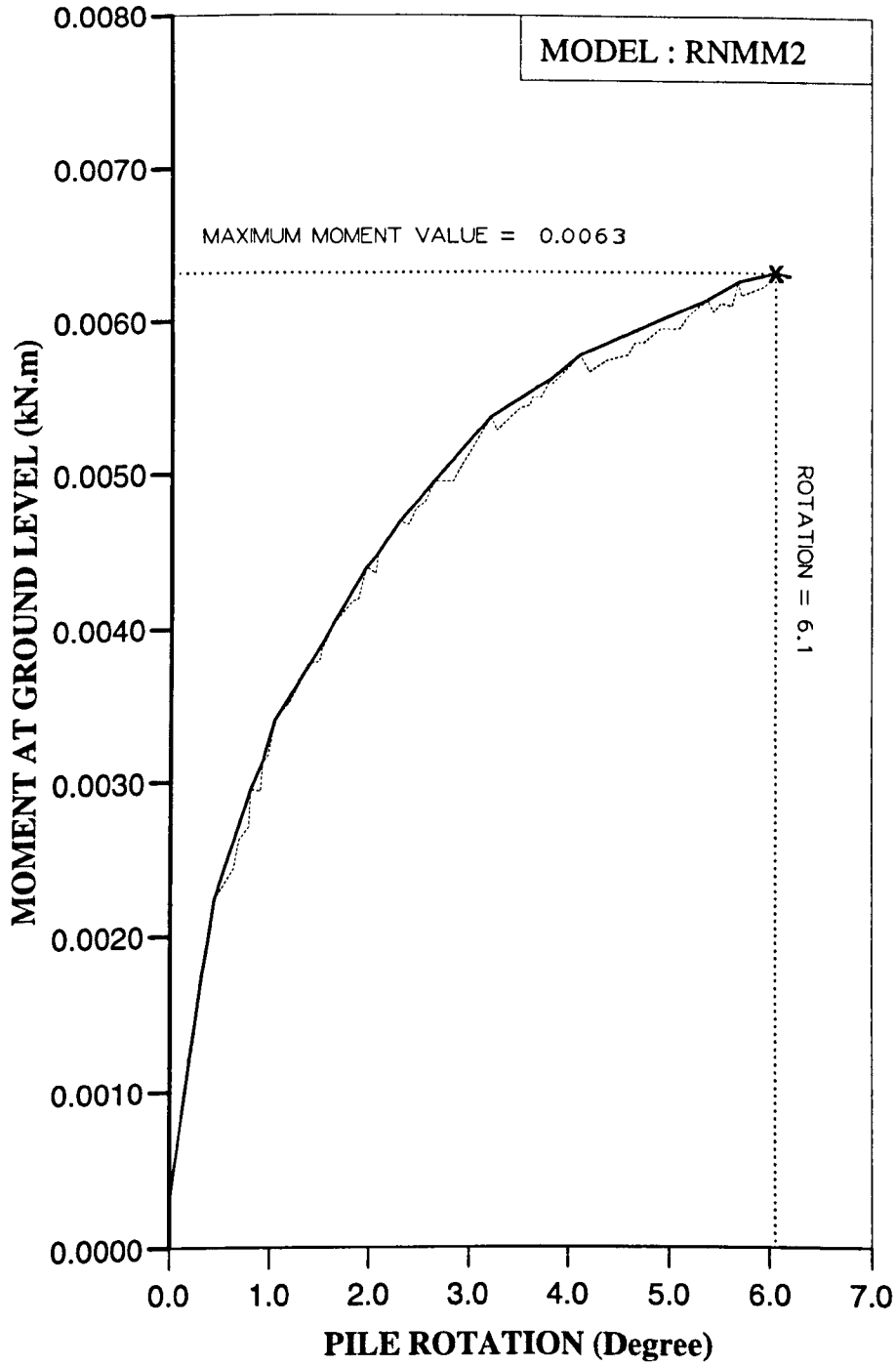

Figure AM1 Variation of moment at ground level with pile rotation for Series 1 test.

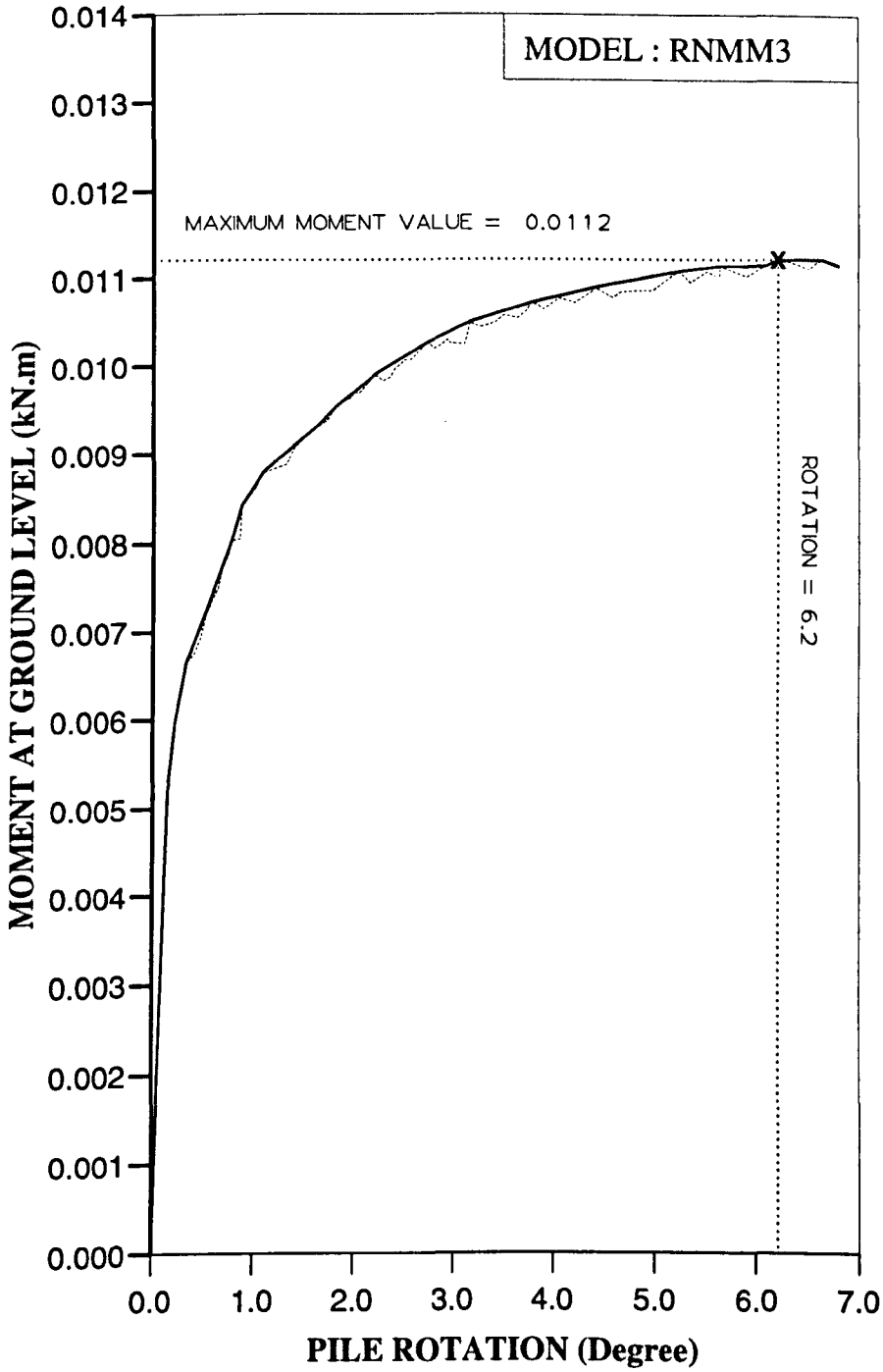

Figure AM2 Variation of moment at ground level with pile rotation for Series 1 test.

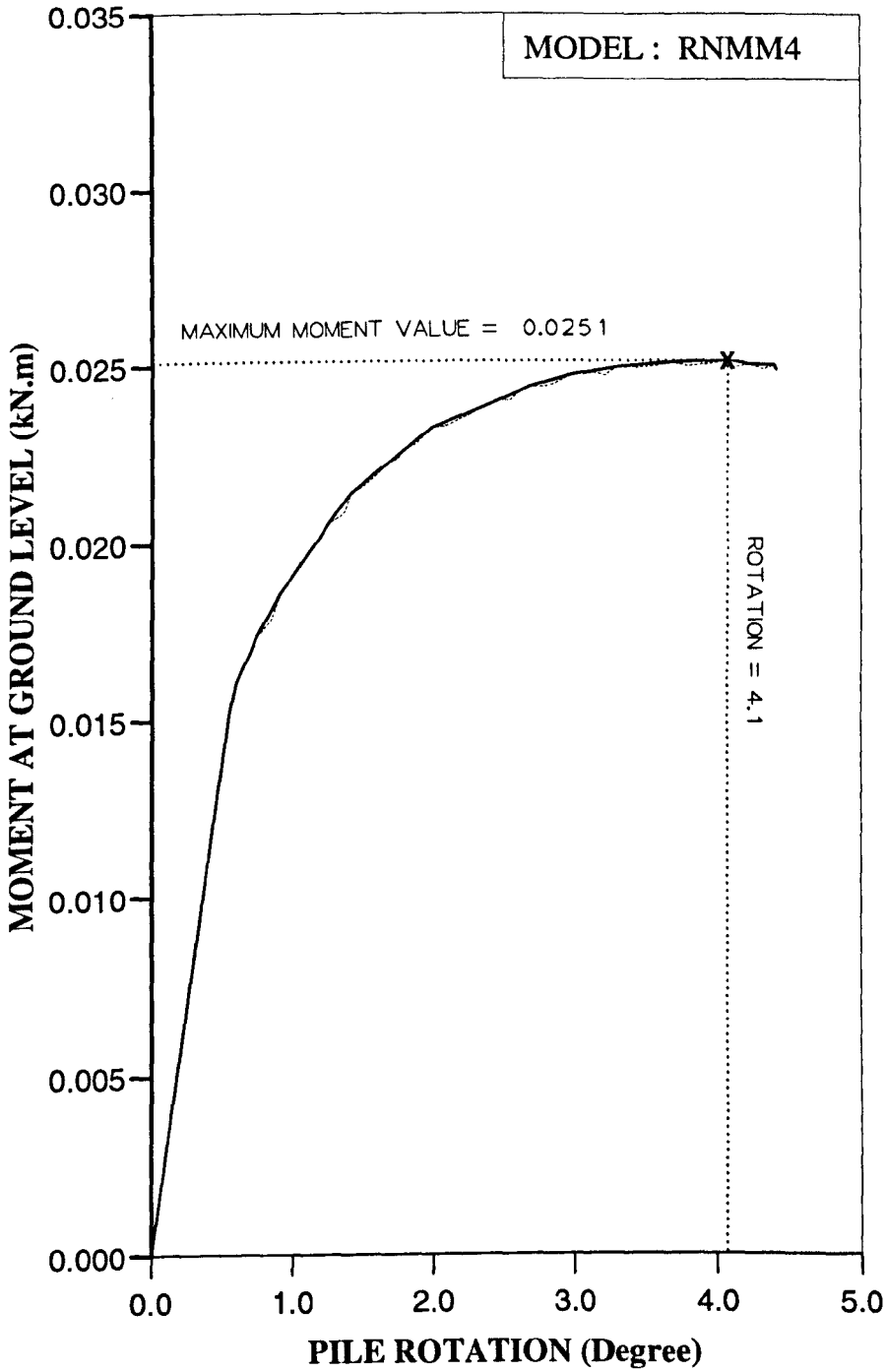

Figure AM3 Variation of moment at ground level with pile rotation for Series 1 test.

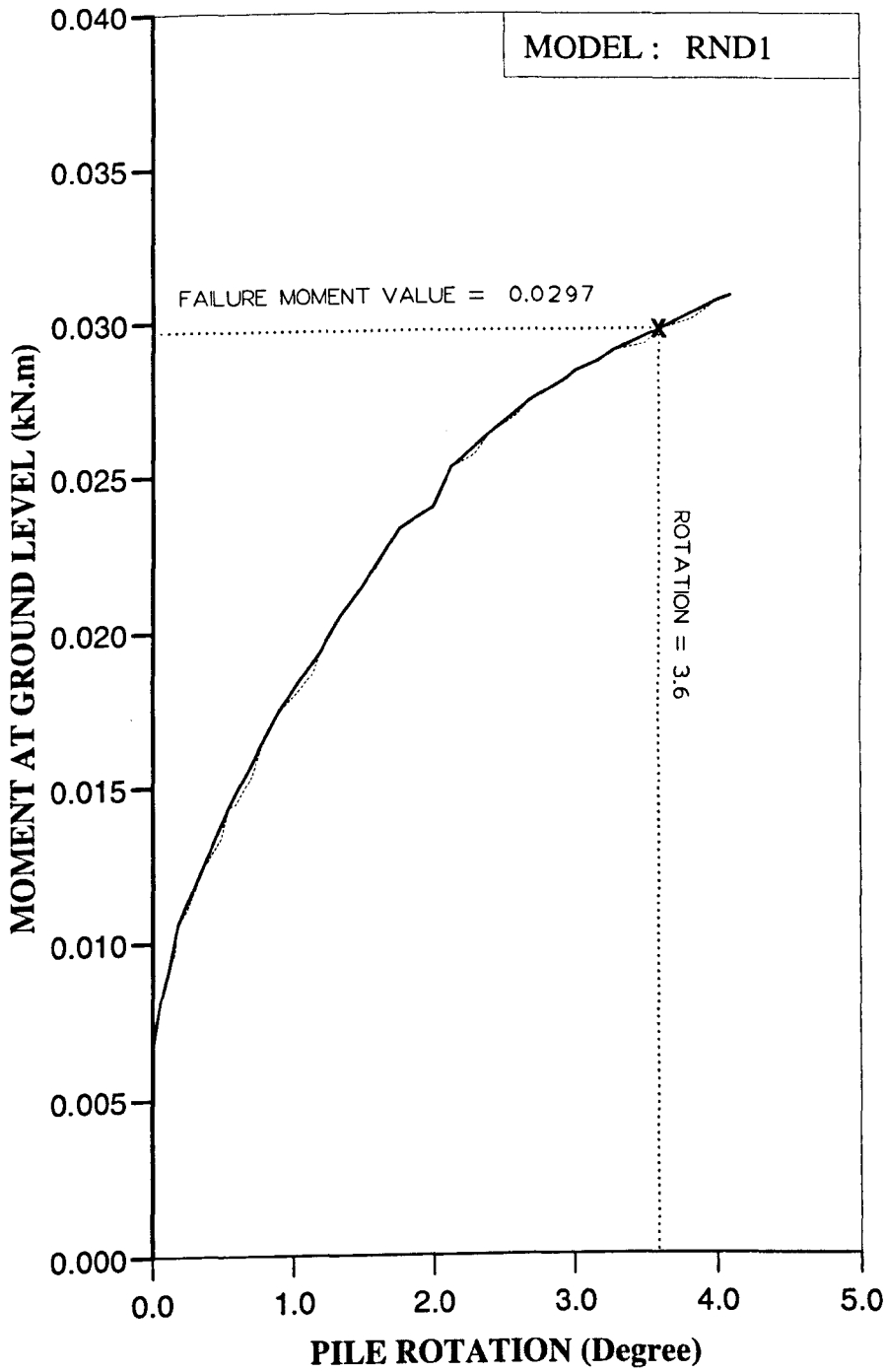

Figure AM5 Variation of moment at ground level with pile rotation for Series 2 test.

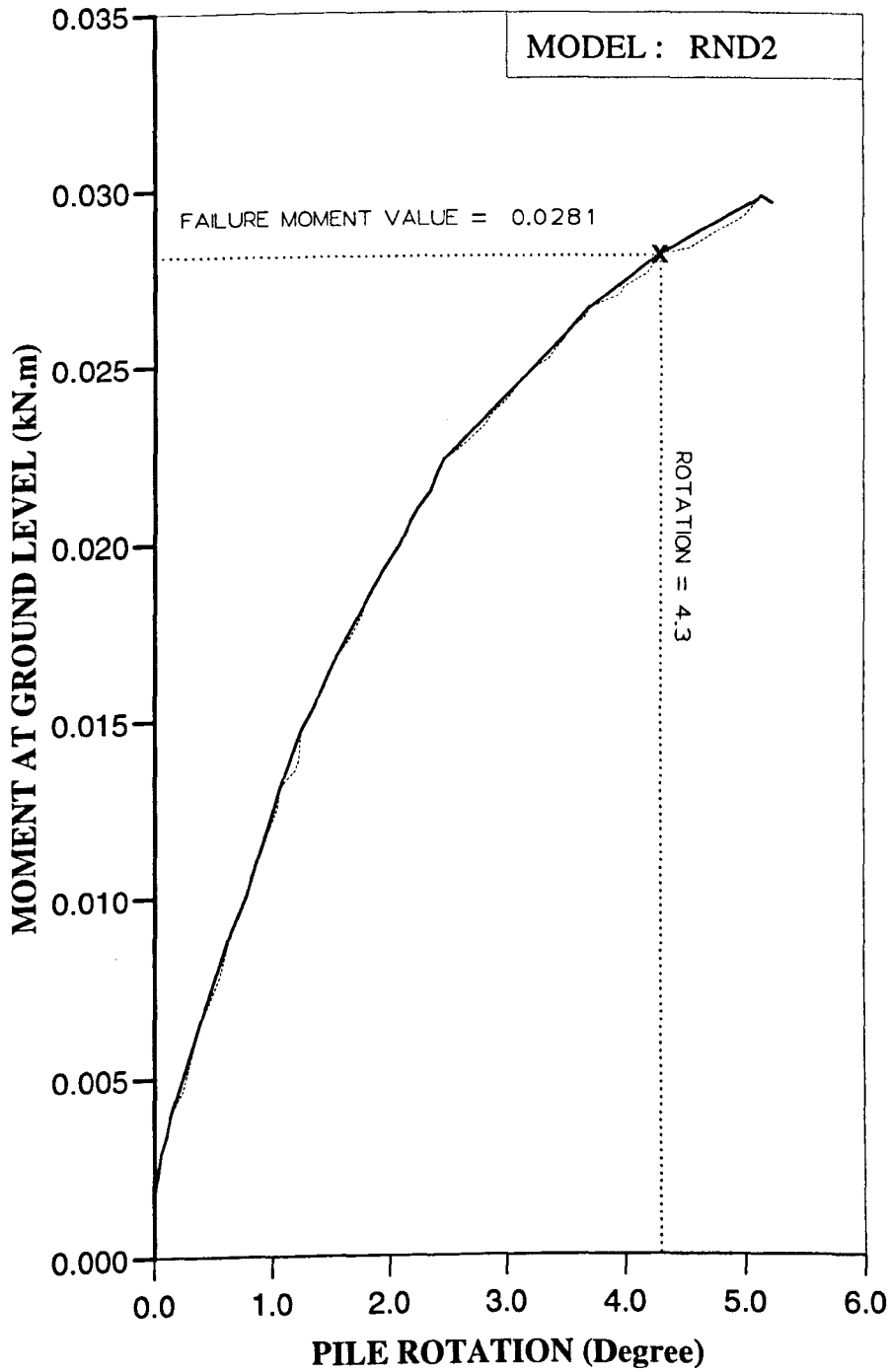

Figure AM6 Variation of moment at ground level with pile rotation for Series 2 test.

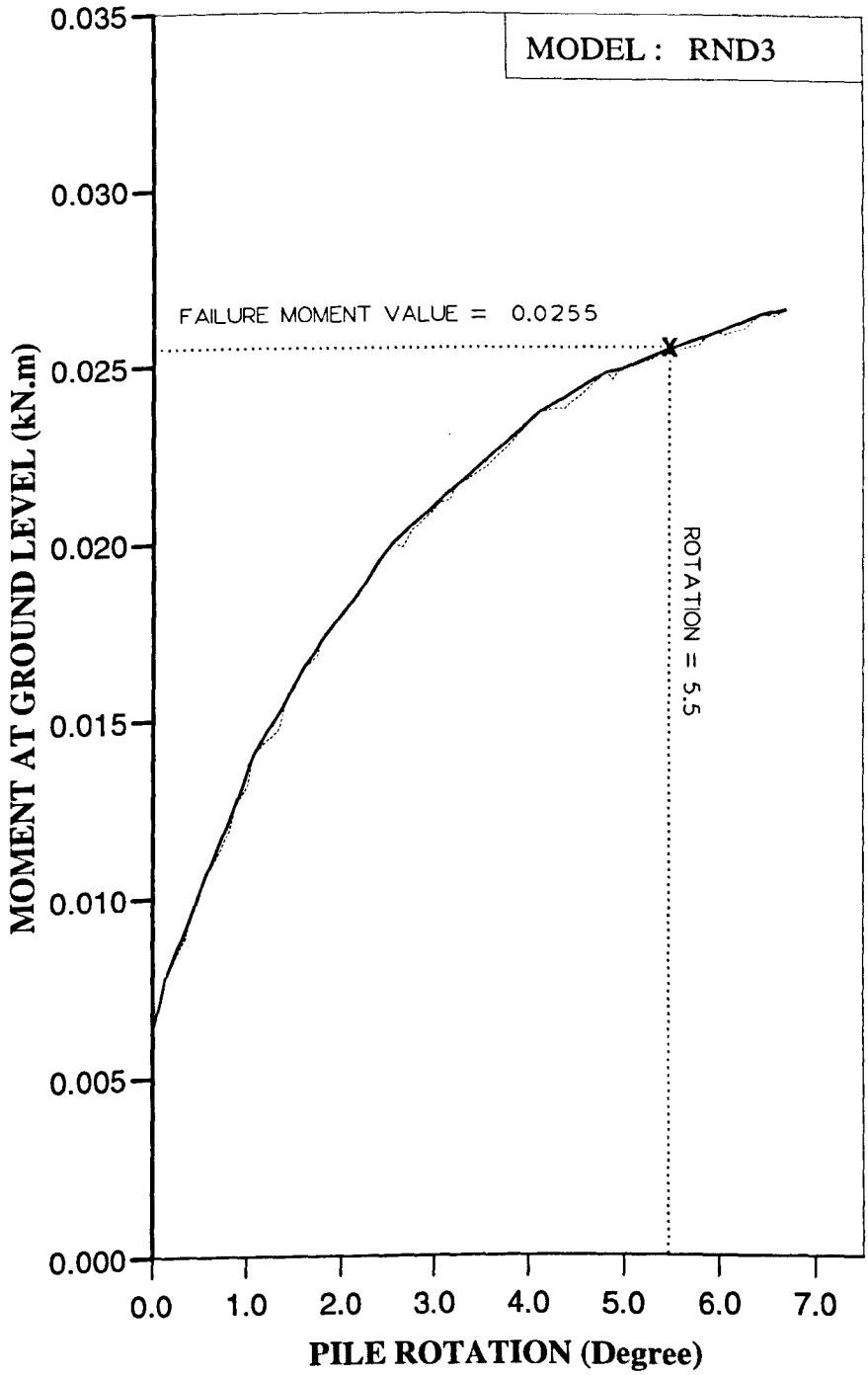

Figure AM7 Variation of moment at ground level with pile rotation for Series 2 test.

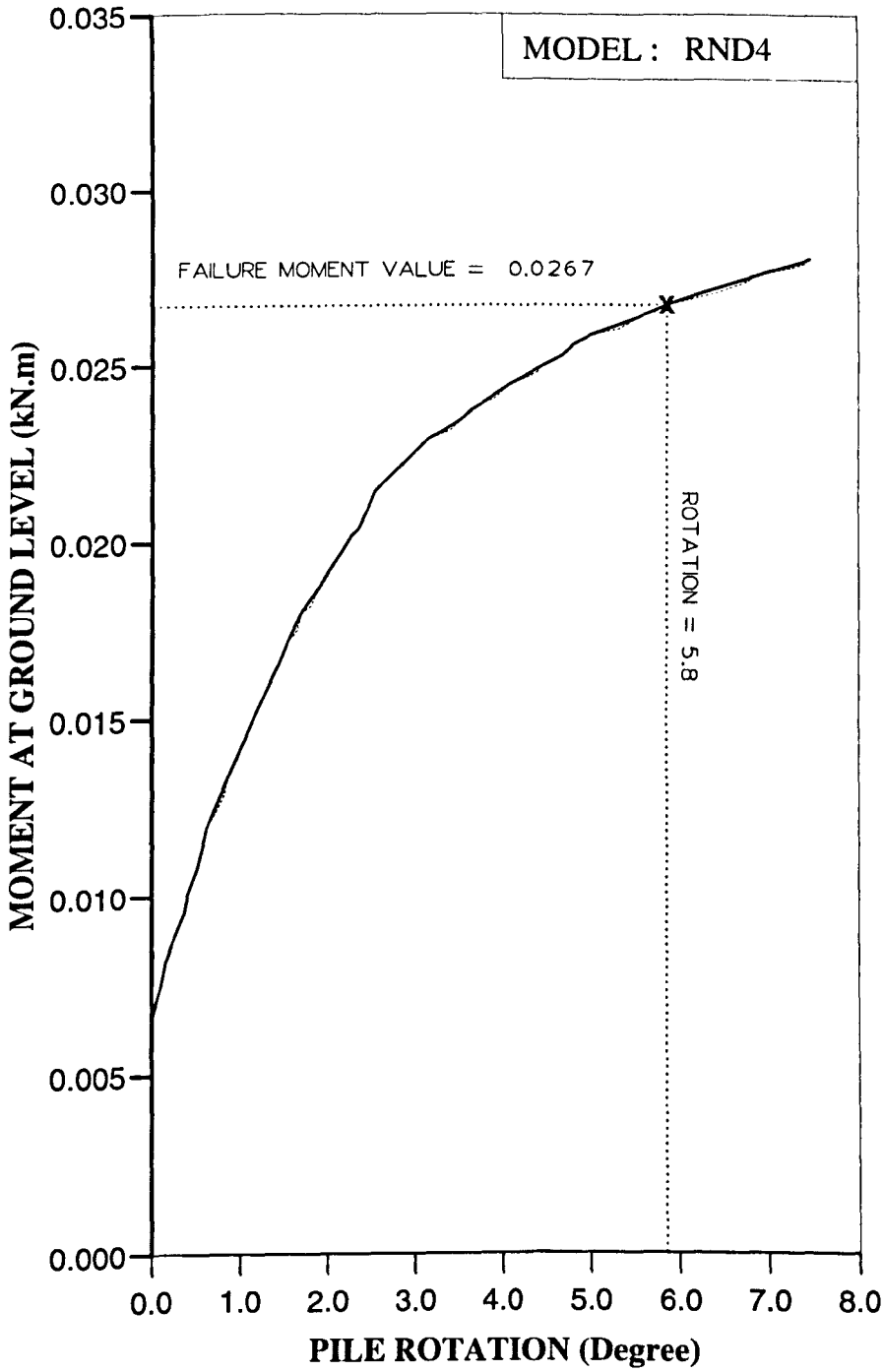

Figure AM8 Variation of moment at ground level with pile rotation for Series 2 test.

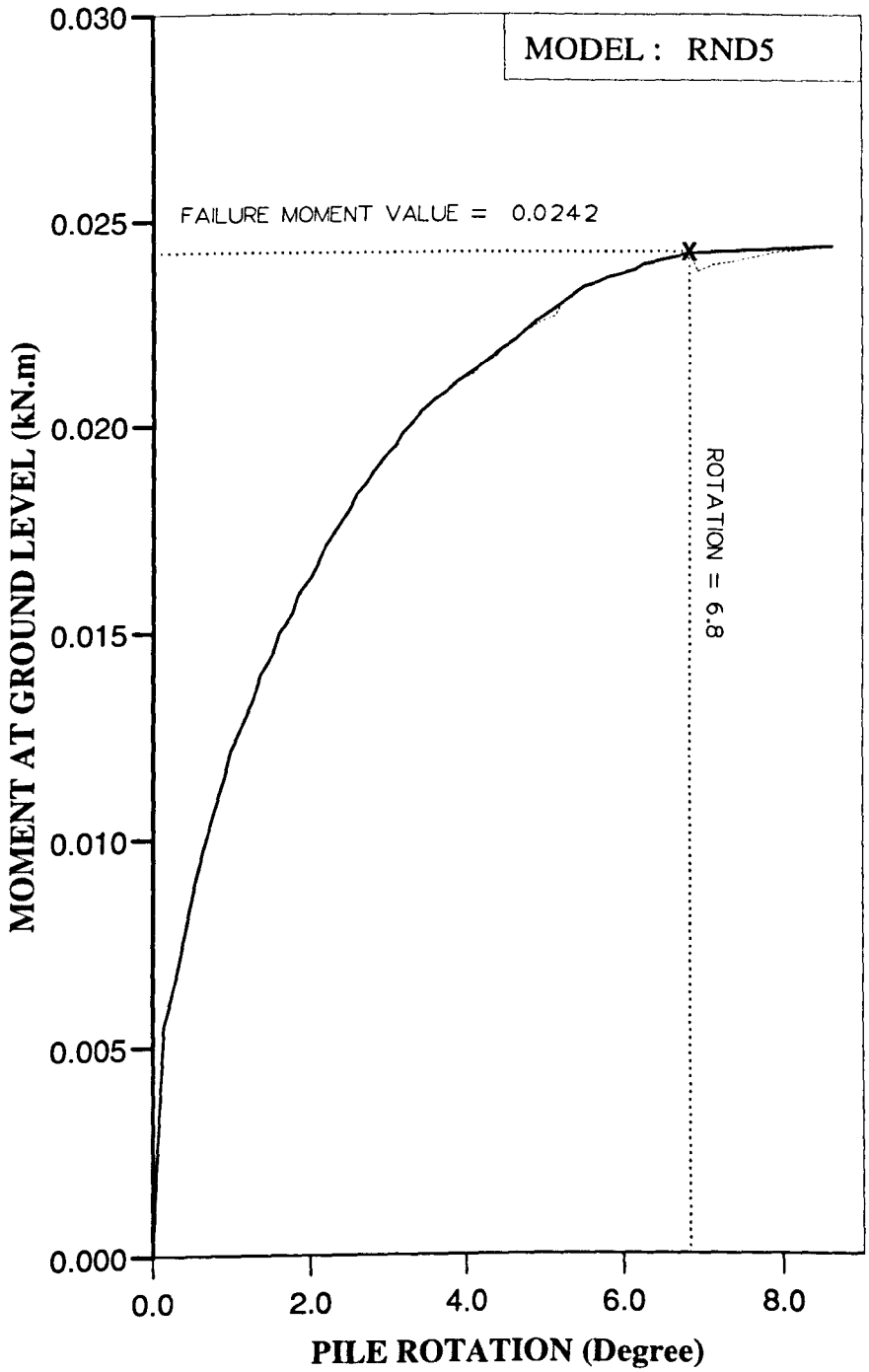

Figure AM9 Variation of moment at ground level with pile rotation for Series 1 test.

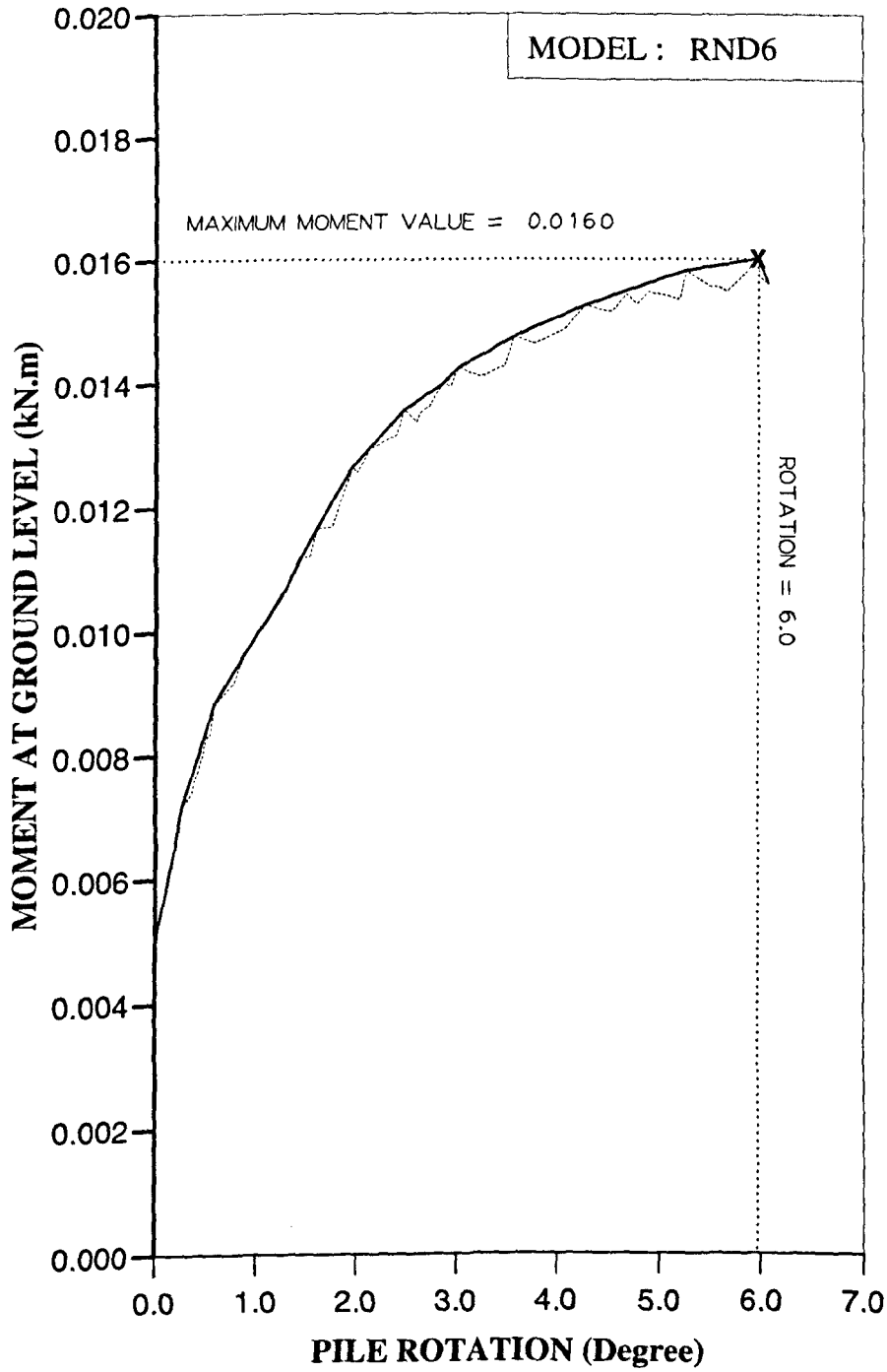

Figure AM10 Variation of moment at ground level with pile rotation for Series 1 test.

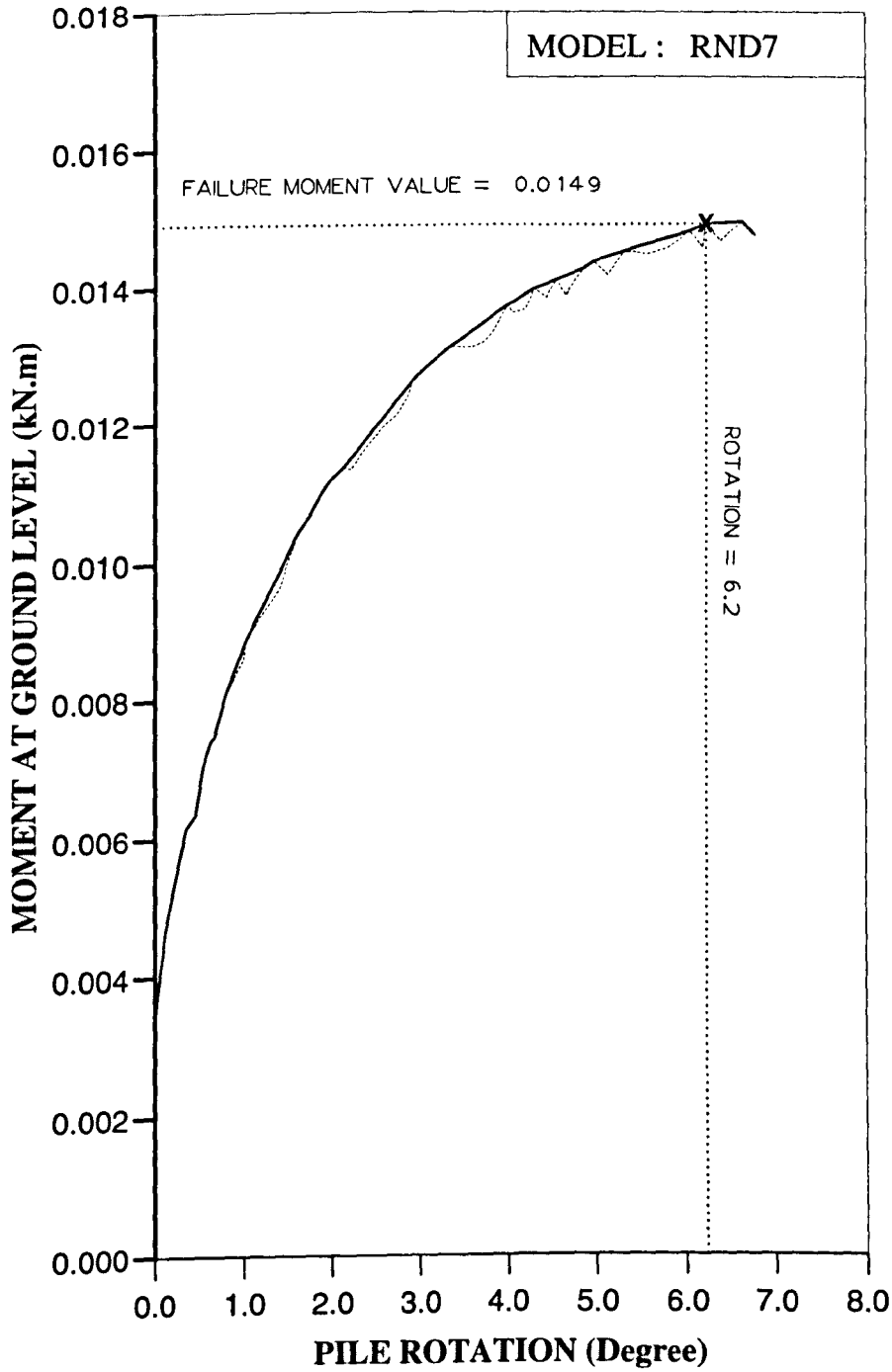

Figure AM11 Variation of moment at ground level with pile rotation for Series 1 test.

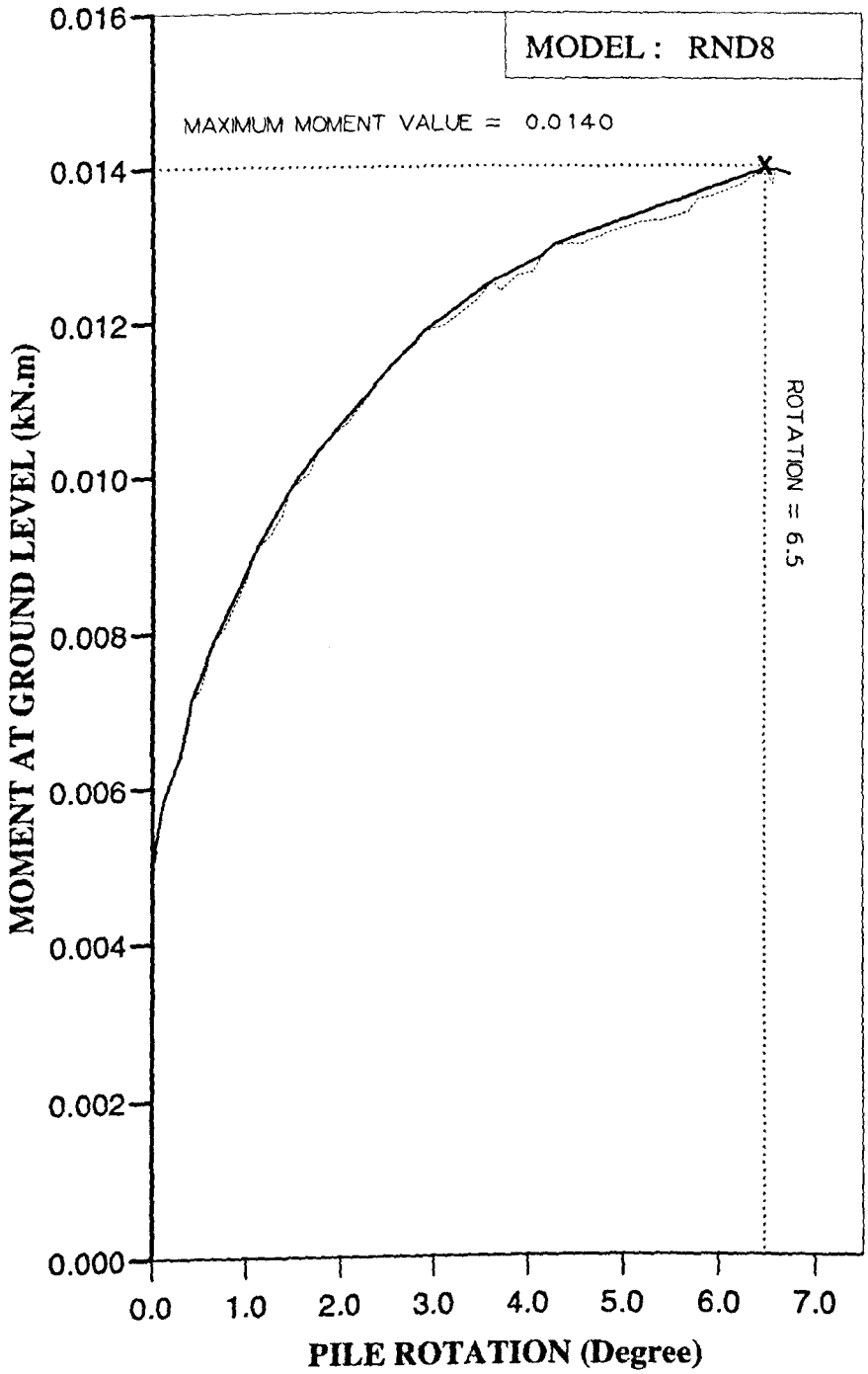

Figure AM12 Variation of moment at ground level with pile rotation for Series 1 test.

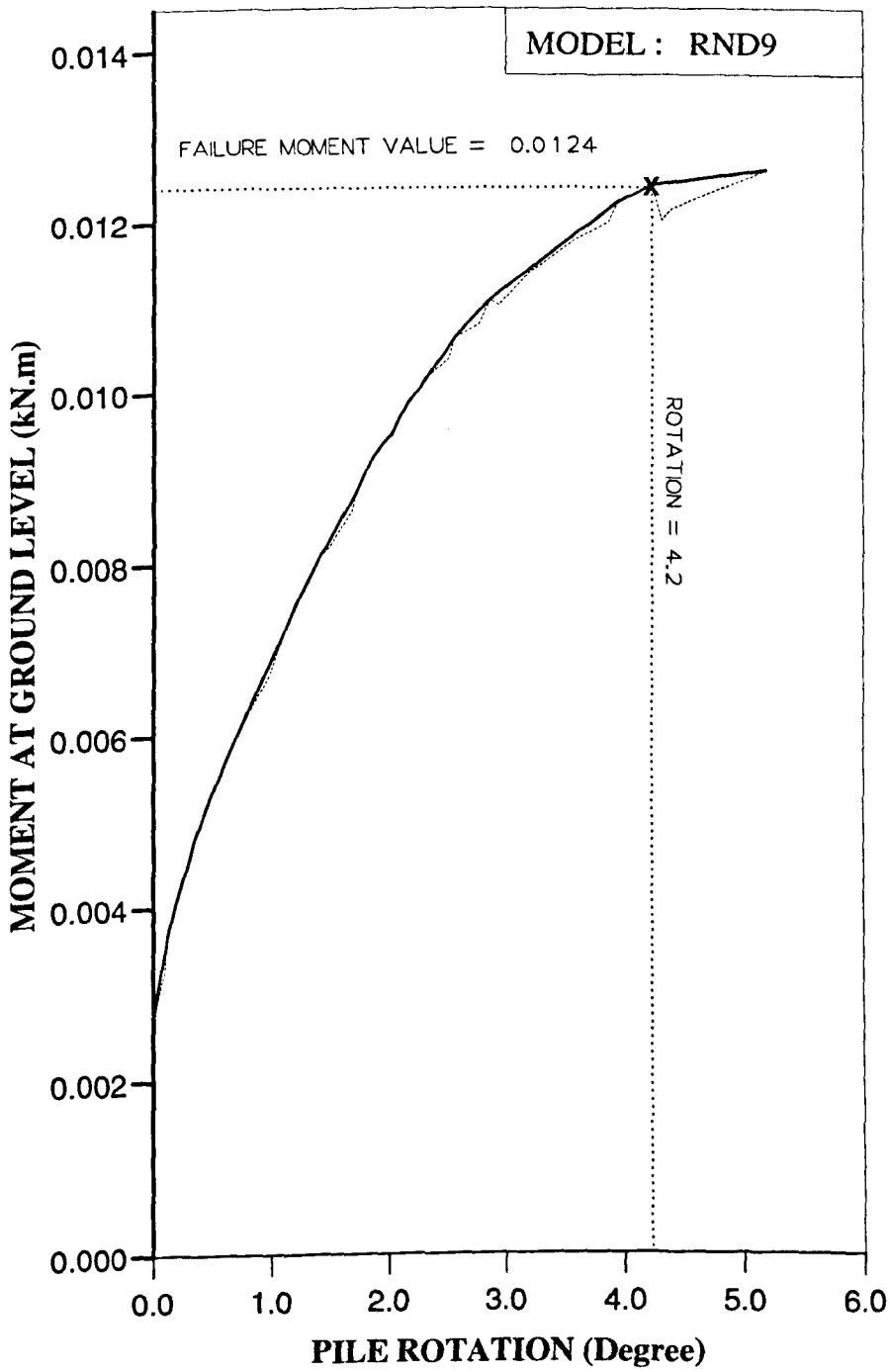

Figure AM13 Variation of moment at ground level with pile rotation for Series 2 test.

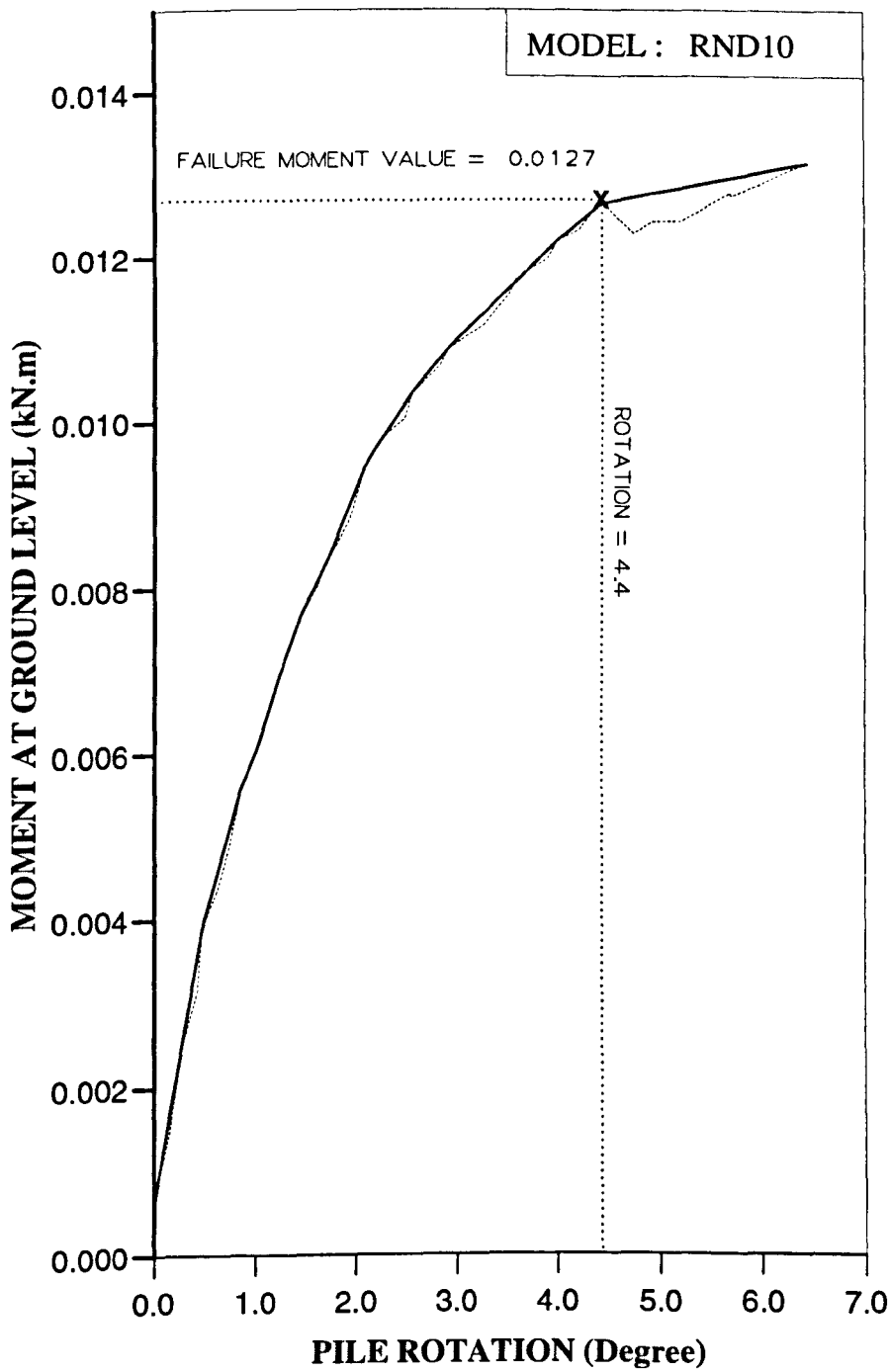

Figure AM14 Variation of moment at ground level with pile rotation for Series 2 test.

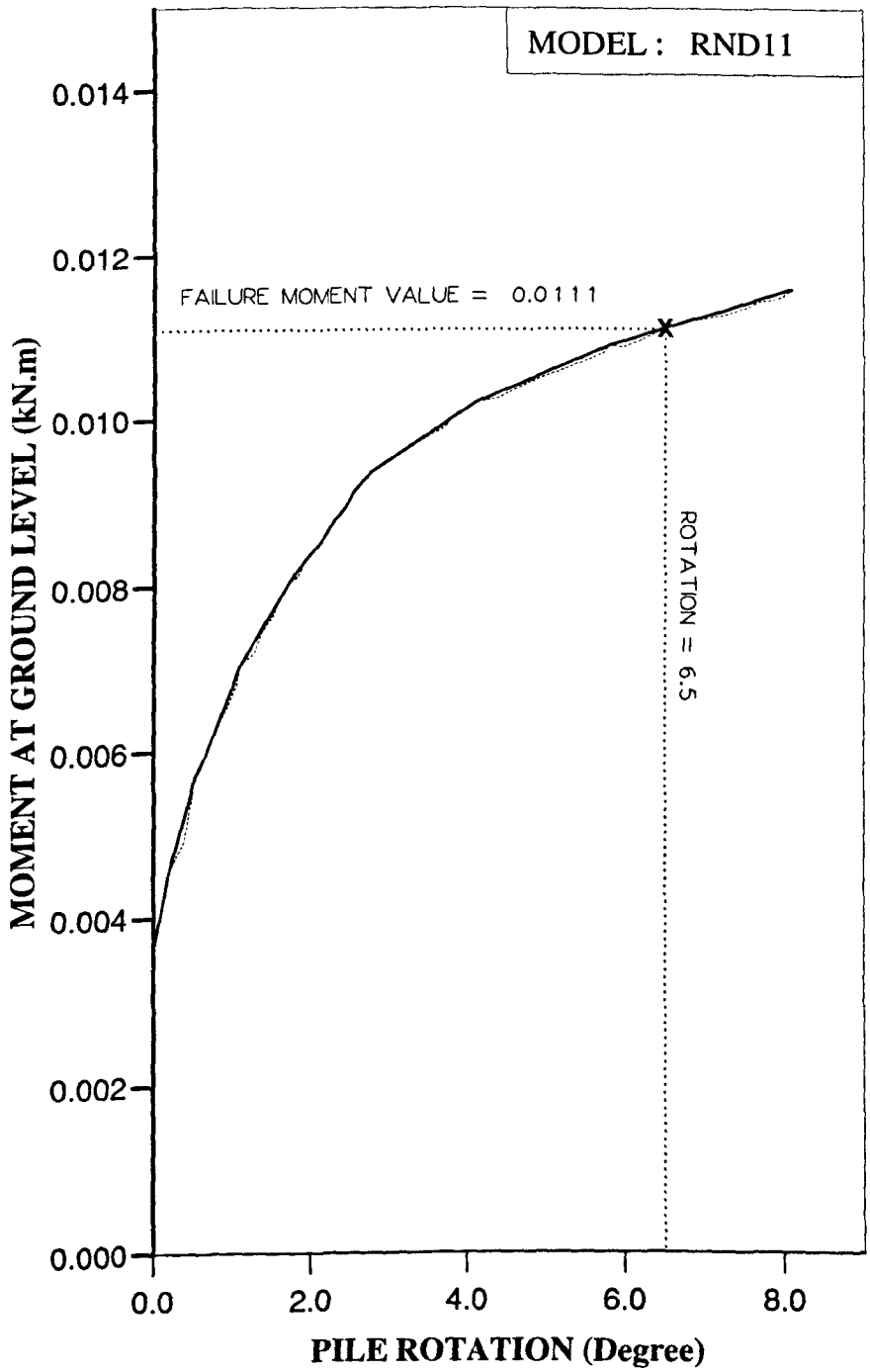

Figure AM15 Variation of moment at ground level with pilerotation for Series 2 test.

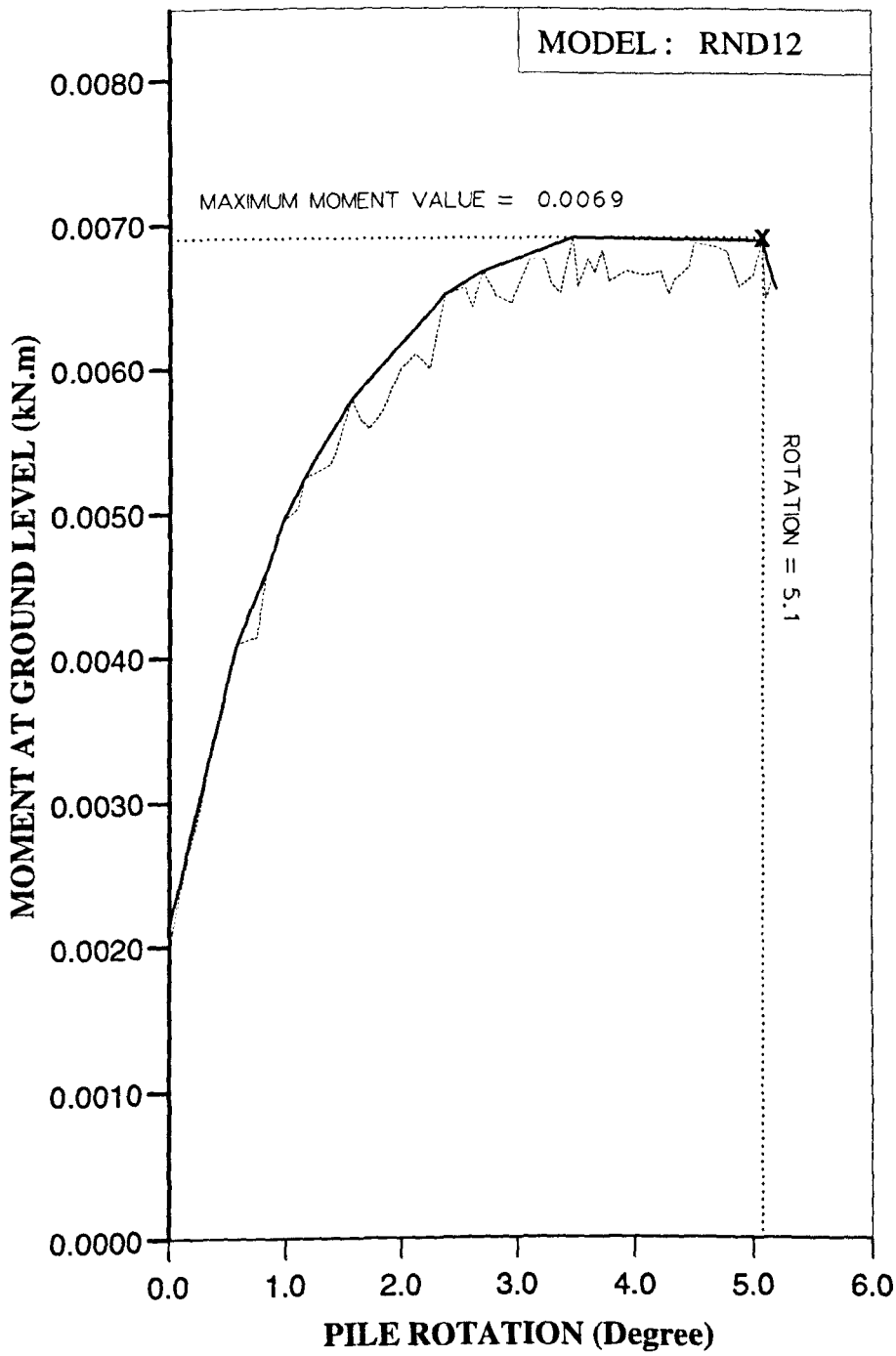

Figure AM16 Variation of moment at ground level with pile rotation for Series 2 test.

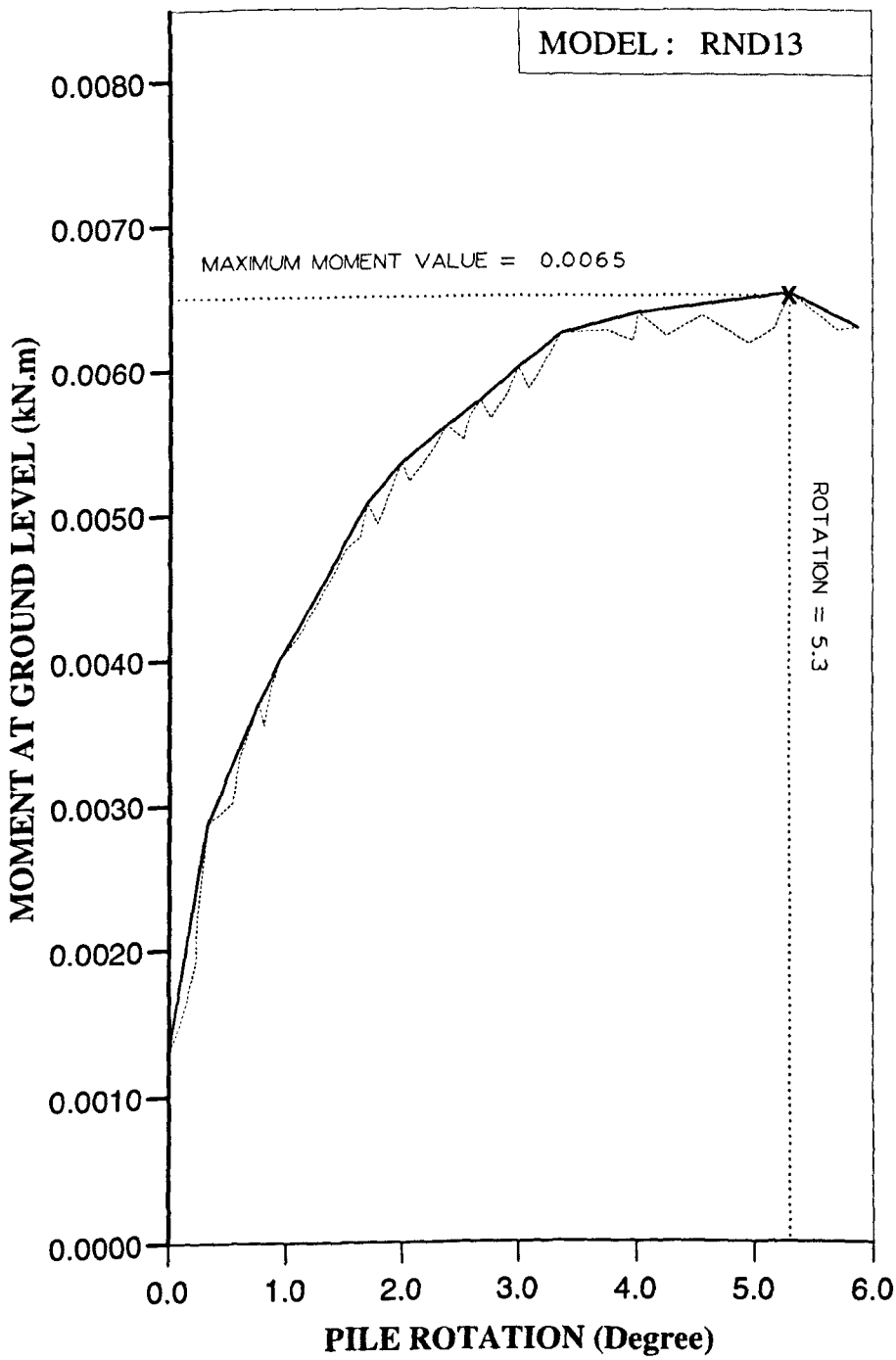

Figure AM17 Variation of moment at ground level with pilerotation for Series 2 test.

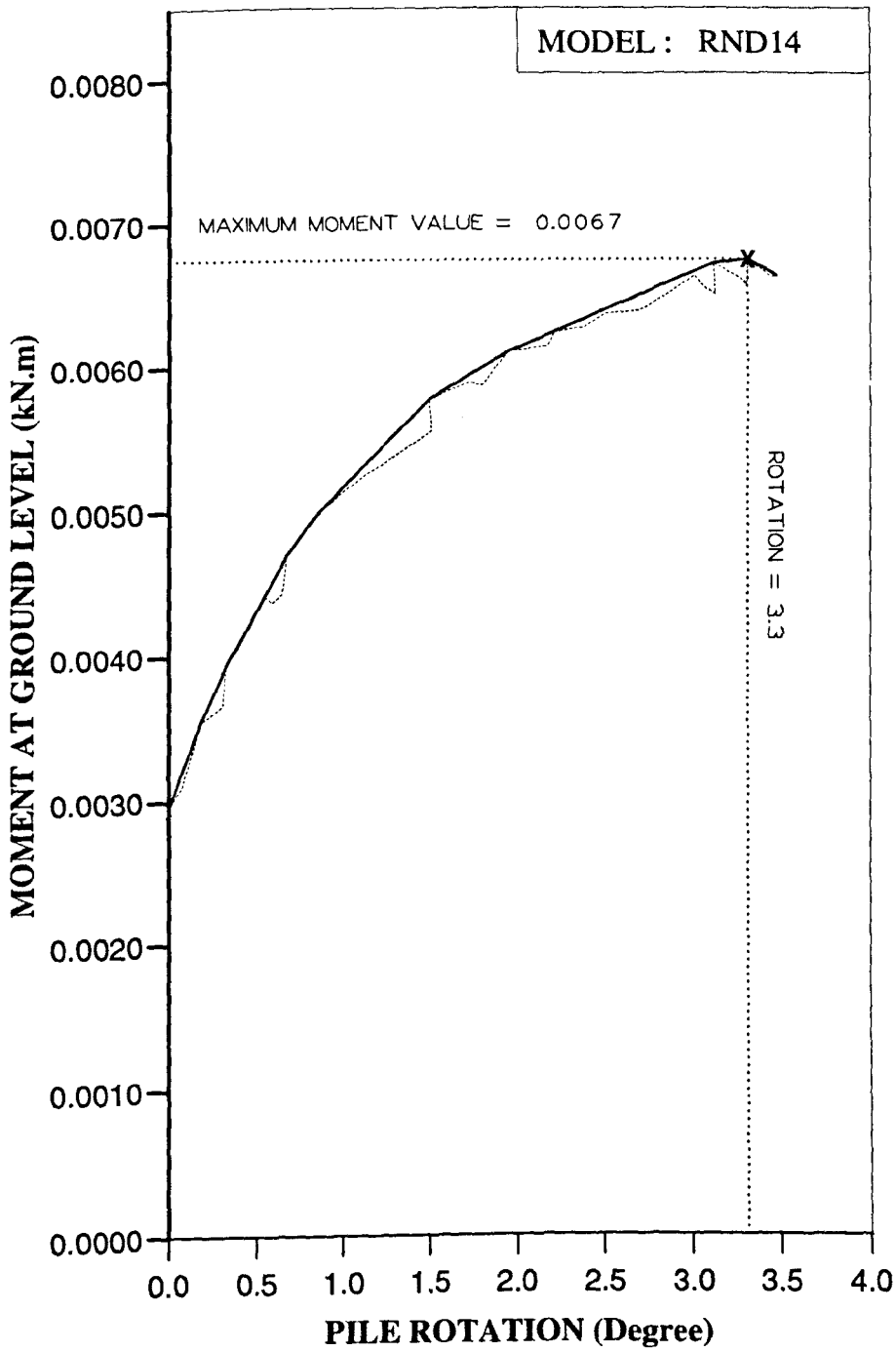

Figure AM18 Variation of moment at ground level with pile rotation for Series 2 test.

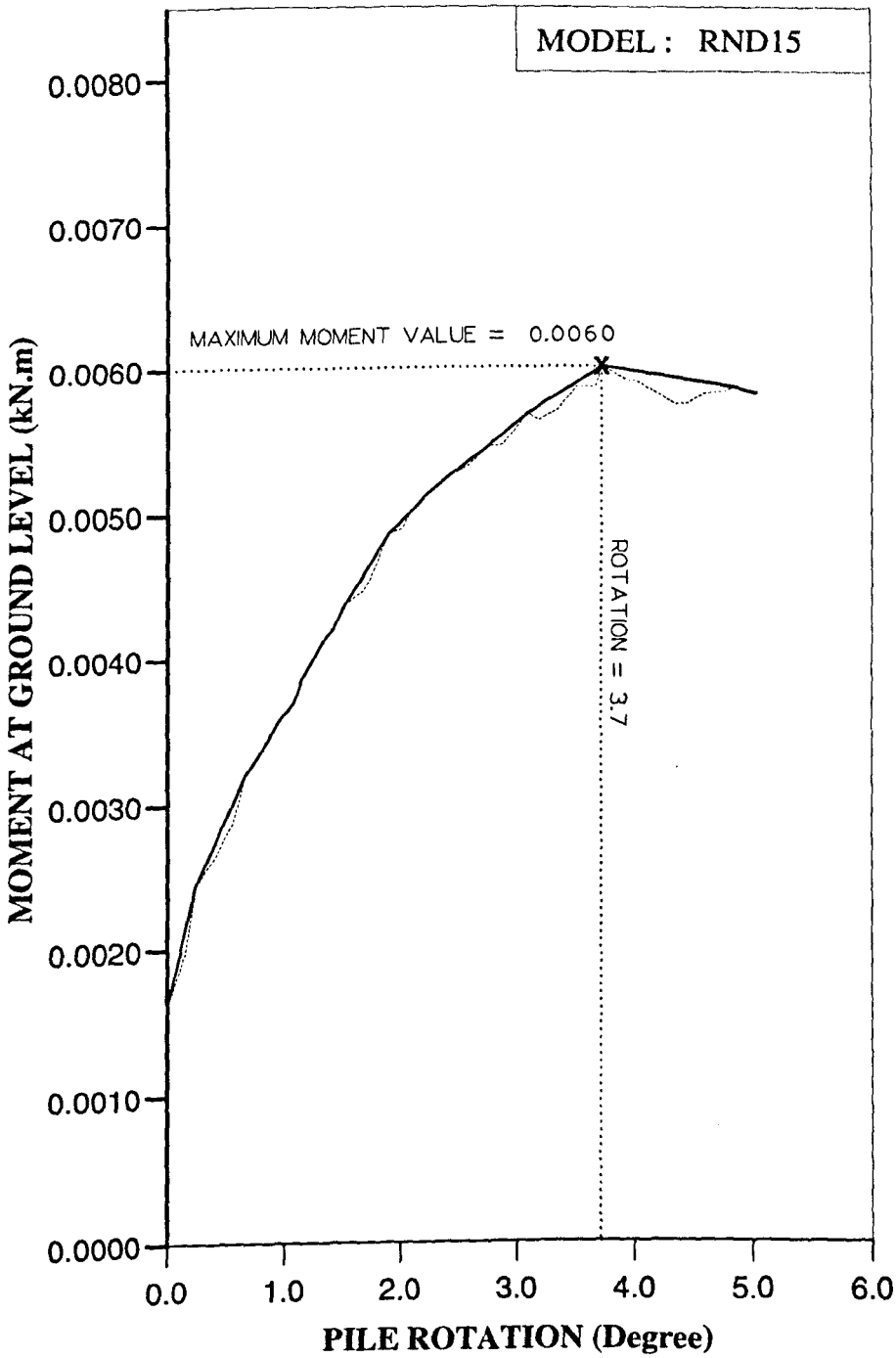

Figure AM19 Variation of moment at ground level with pile rotation for Series 2 test.

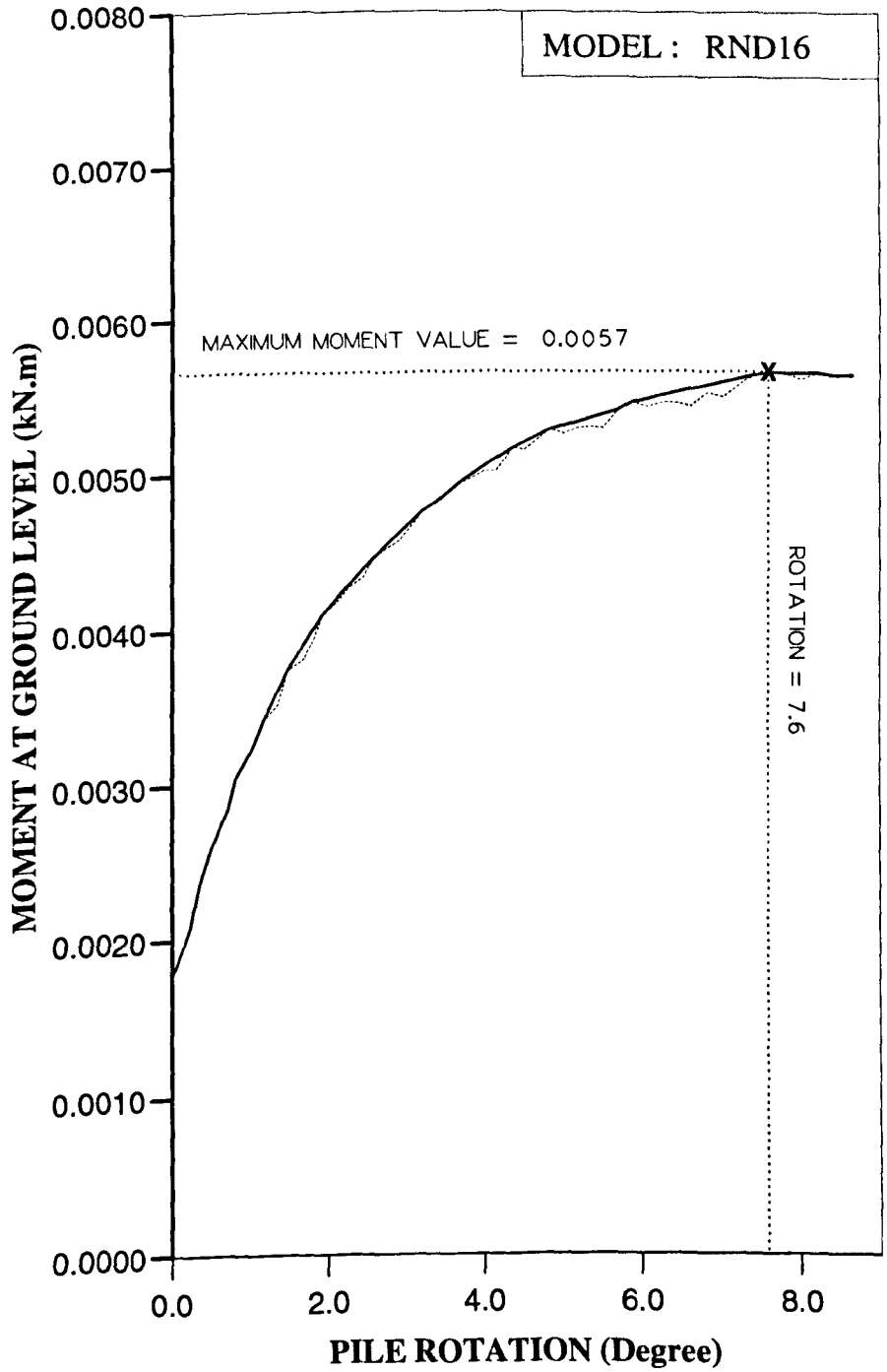

Figure AM20 Variation of moment at ground level with pile rotation for Series 2 test.

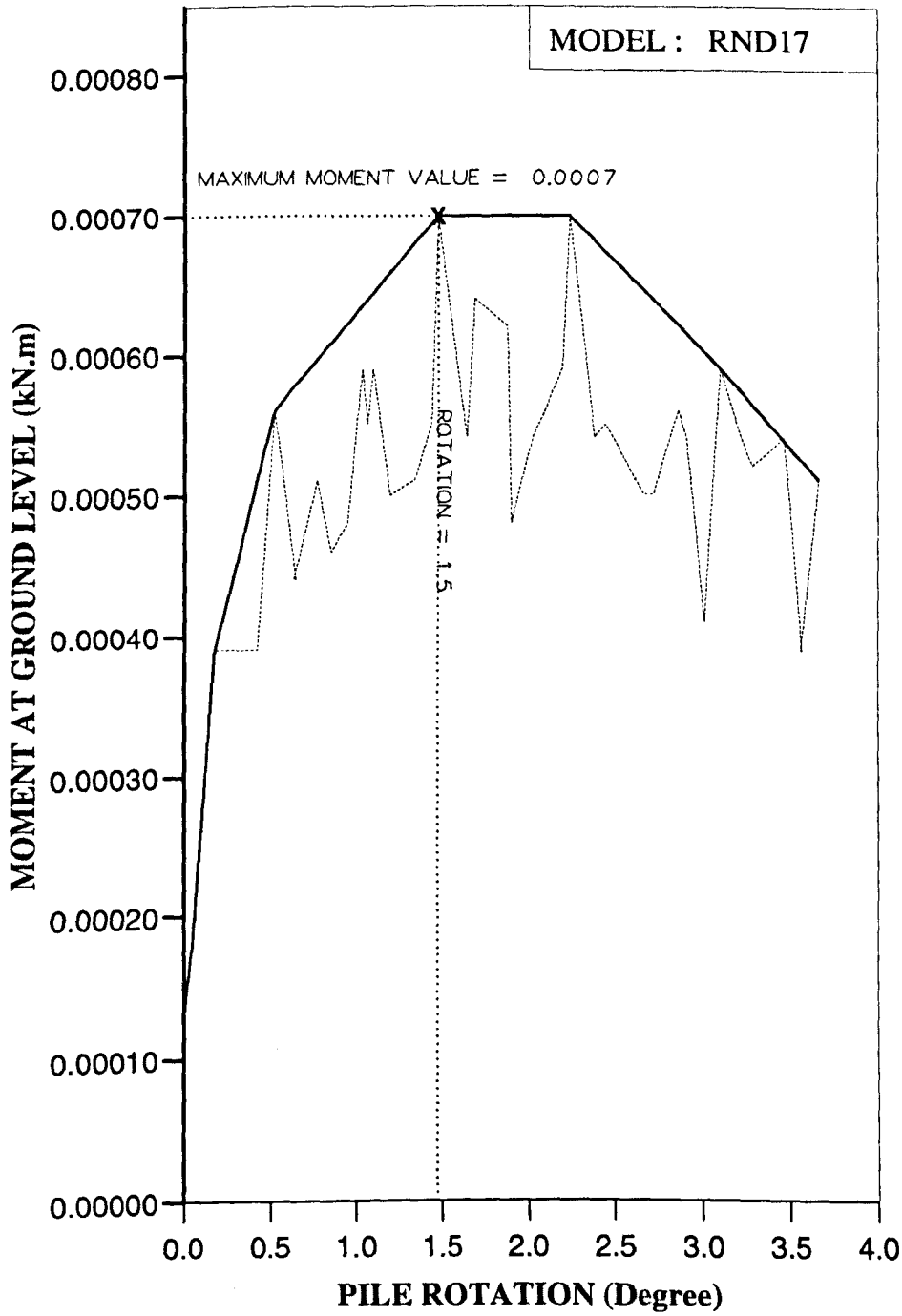

Figure AM21 Variation of moment at ground level with pile rotation for Series 1 test.

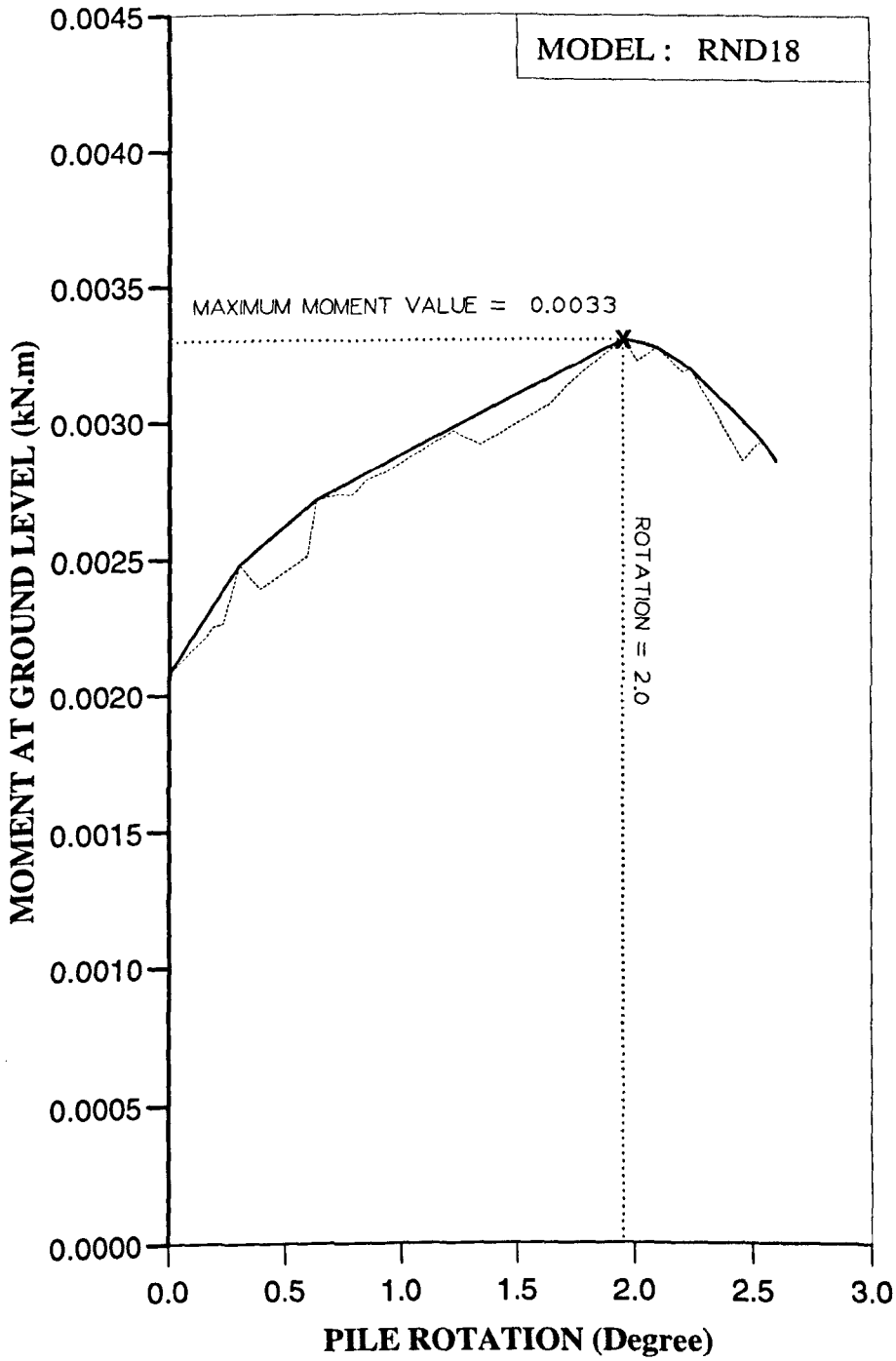

Figure AM22 Variation of moment at ground level with pile rotation for Series 1 test.

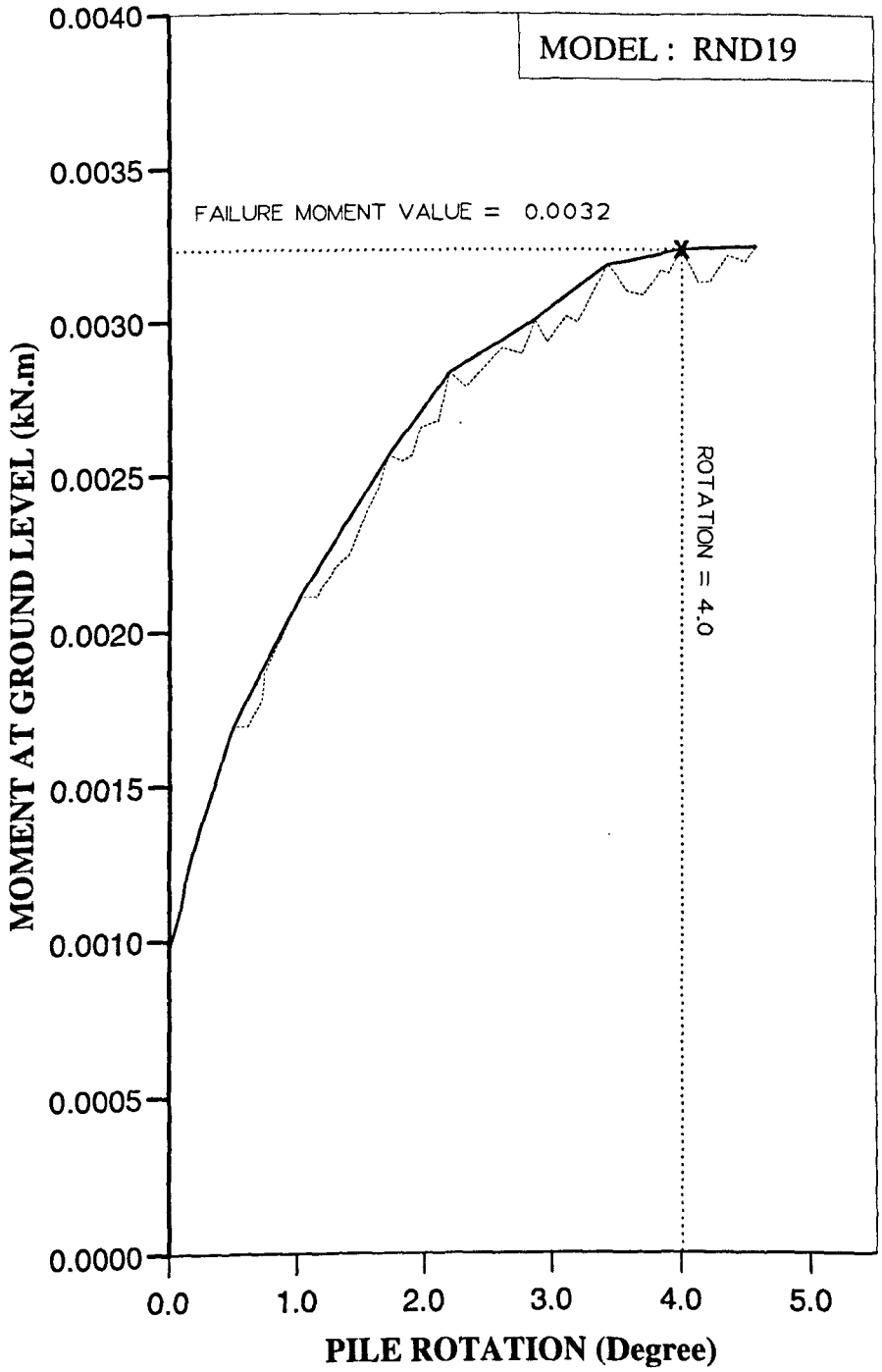

Figure AM23 Variation of moment at ground level with pile rotation for Series 1 test.

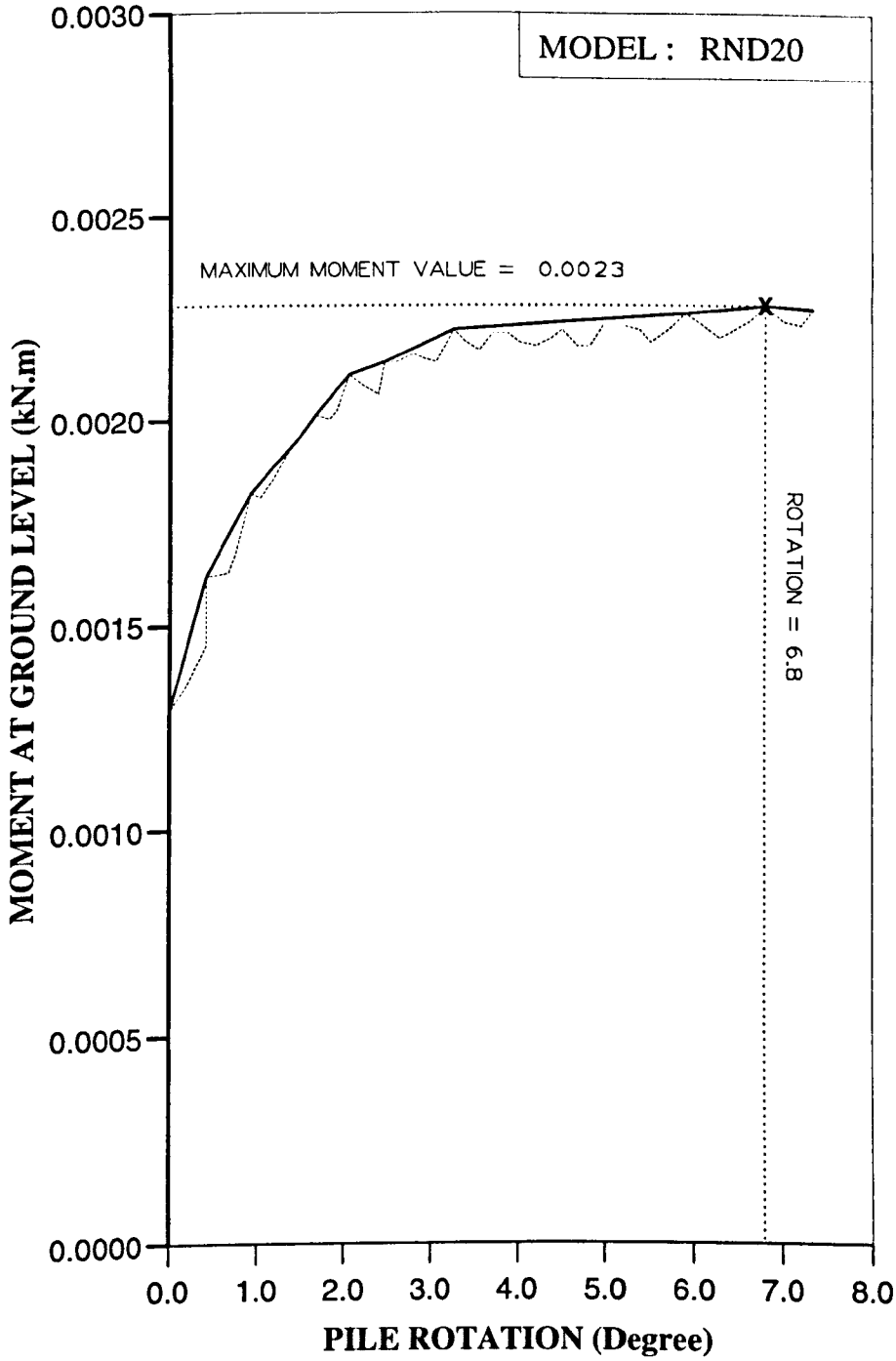

Figure AM24 Variation of moment at ground level with pile rotation for Series 1 test.

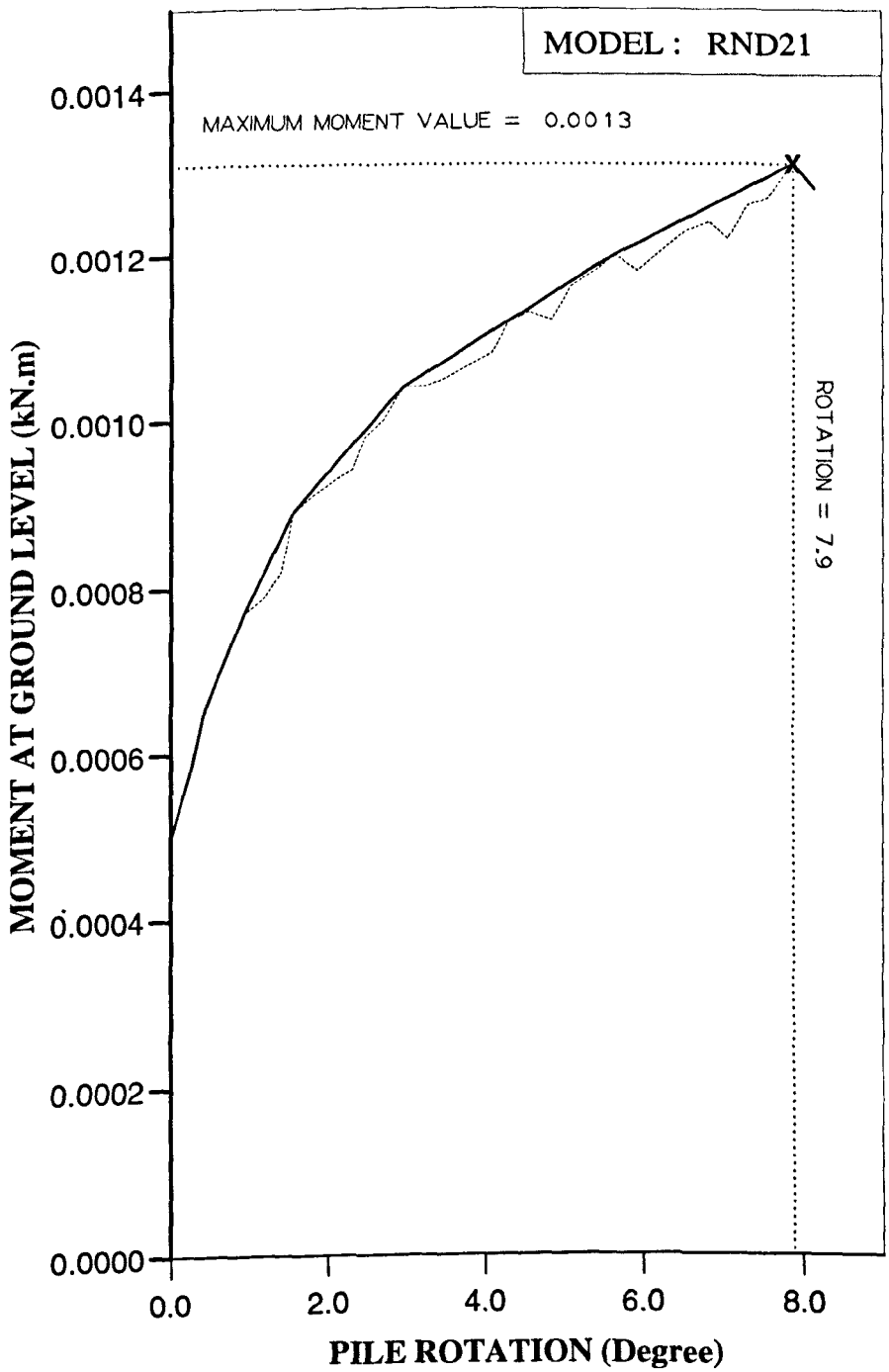

Figure AM25 Variation of moment at ground level with pile rotation for Series 2 test.

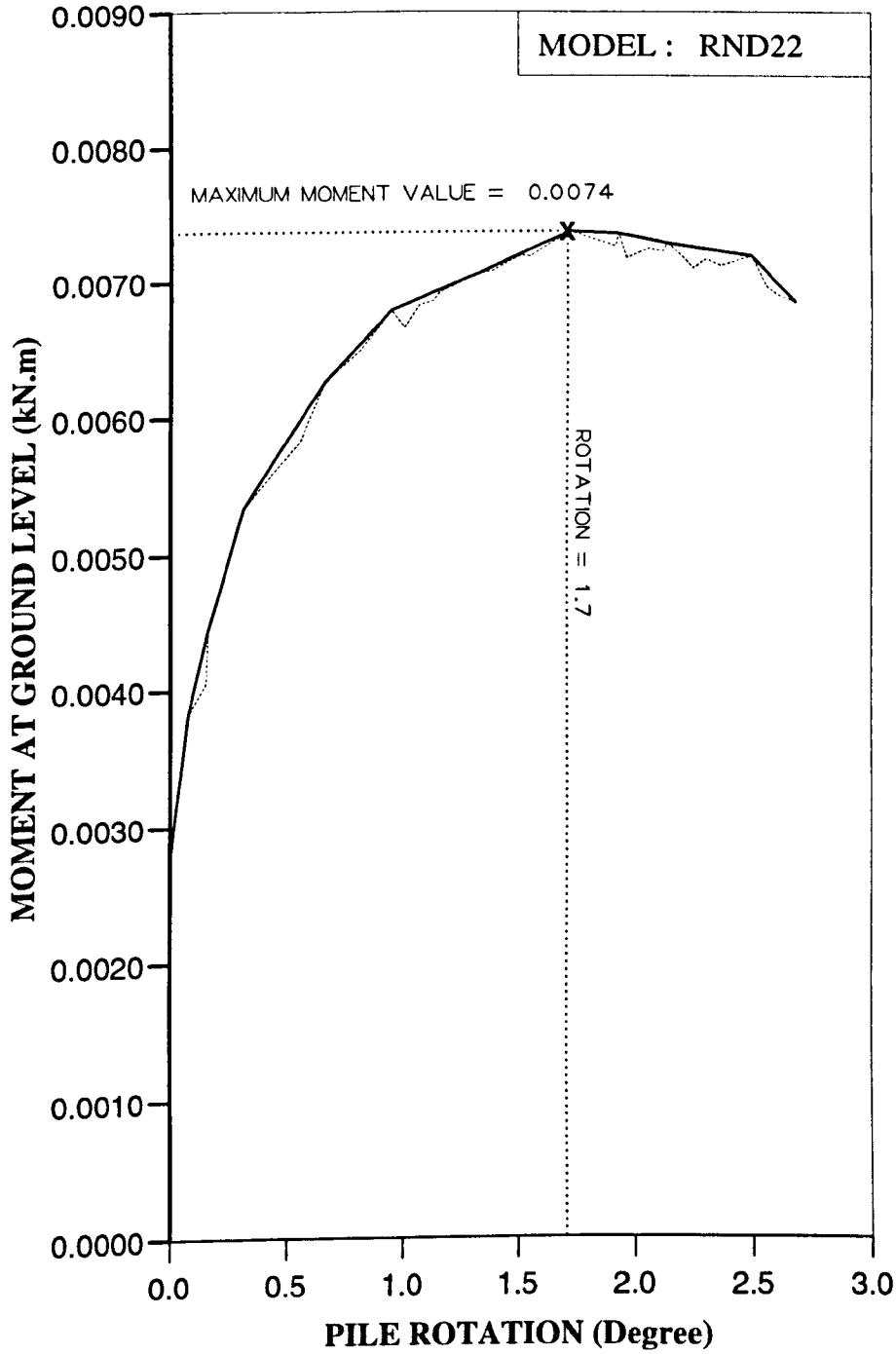

Figure AM26 Variation of moment at ground level with pile rotation for Series 2 test.

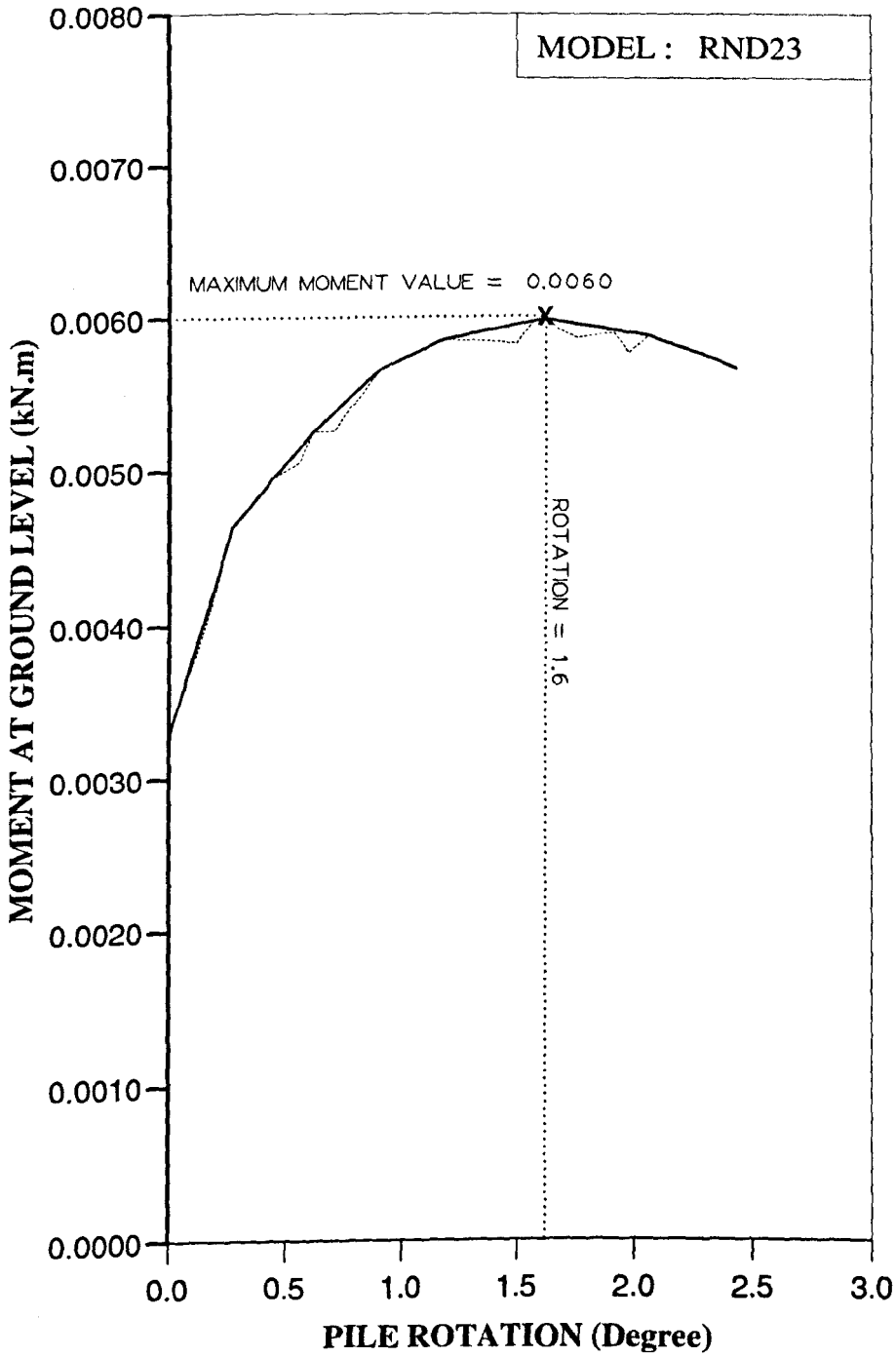

Figure AM27 Variation of moment at ground level with pile rotation for Series 2 test.

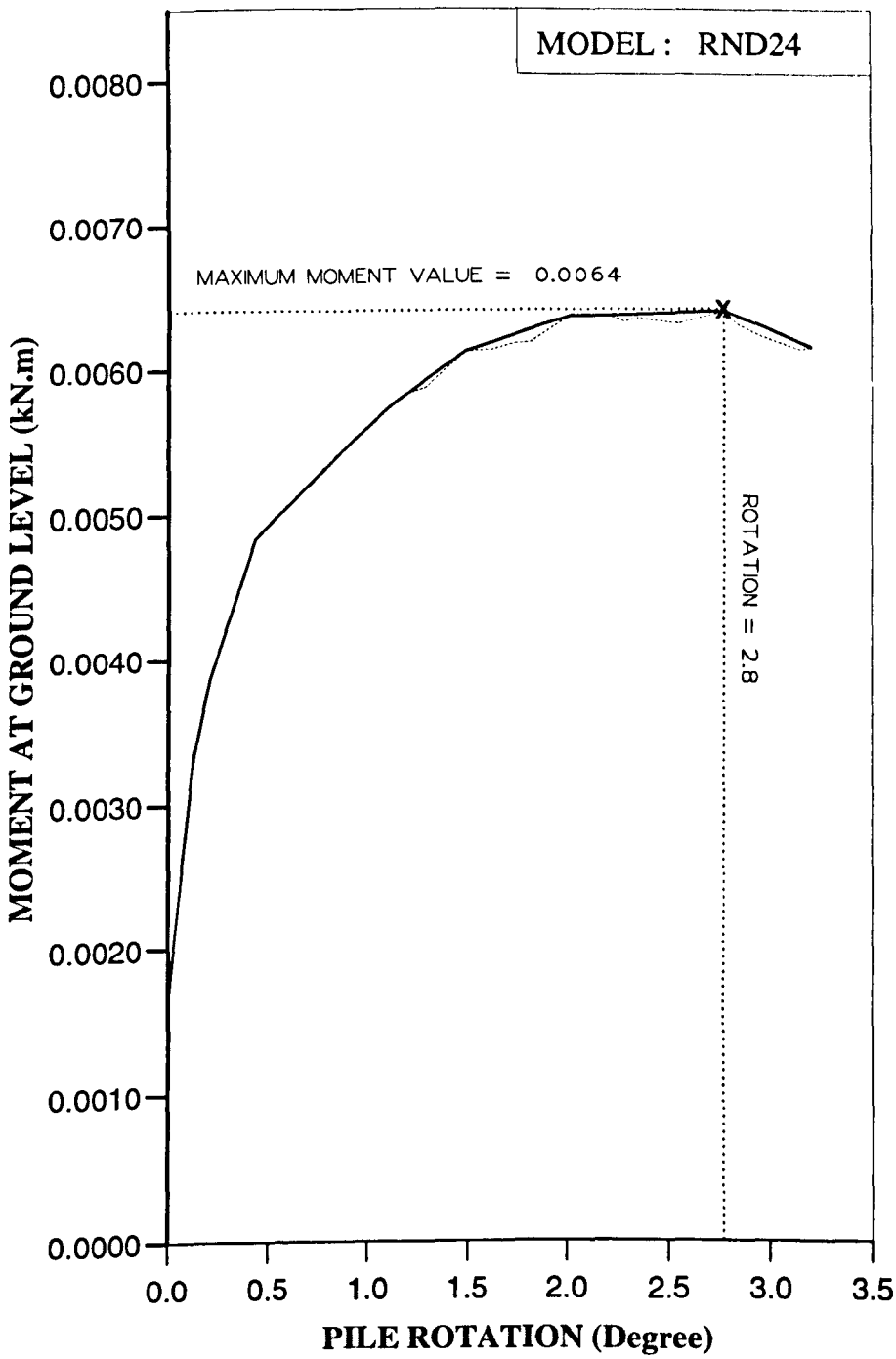

Figure AM28 Variation of moment at ground level with pile rotation for Series 2 test.

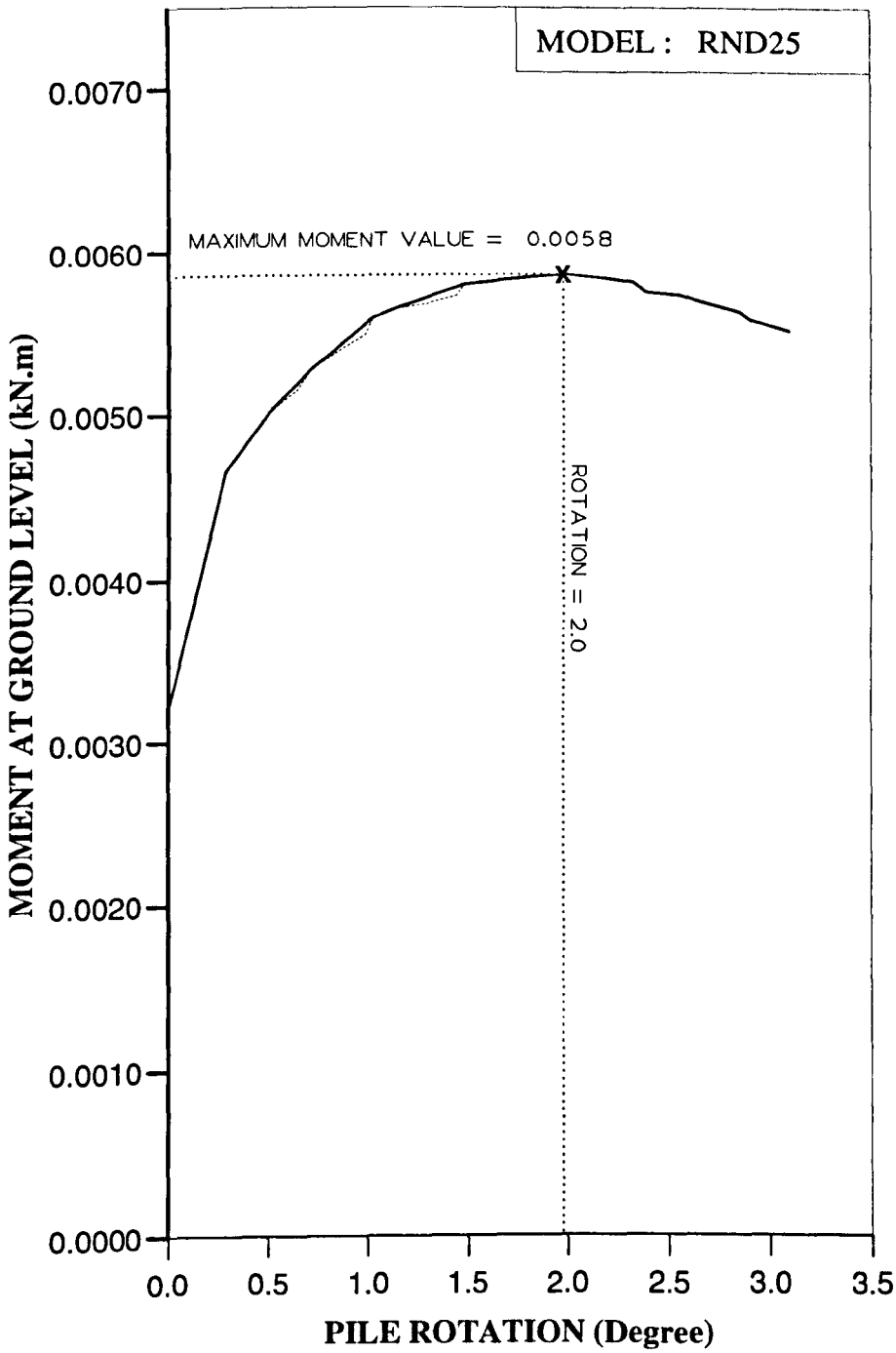

Figure AM29 Variation of moment at ground level with pile rotation for Series 2 test.

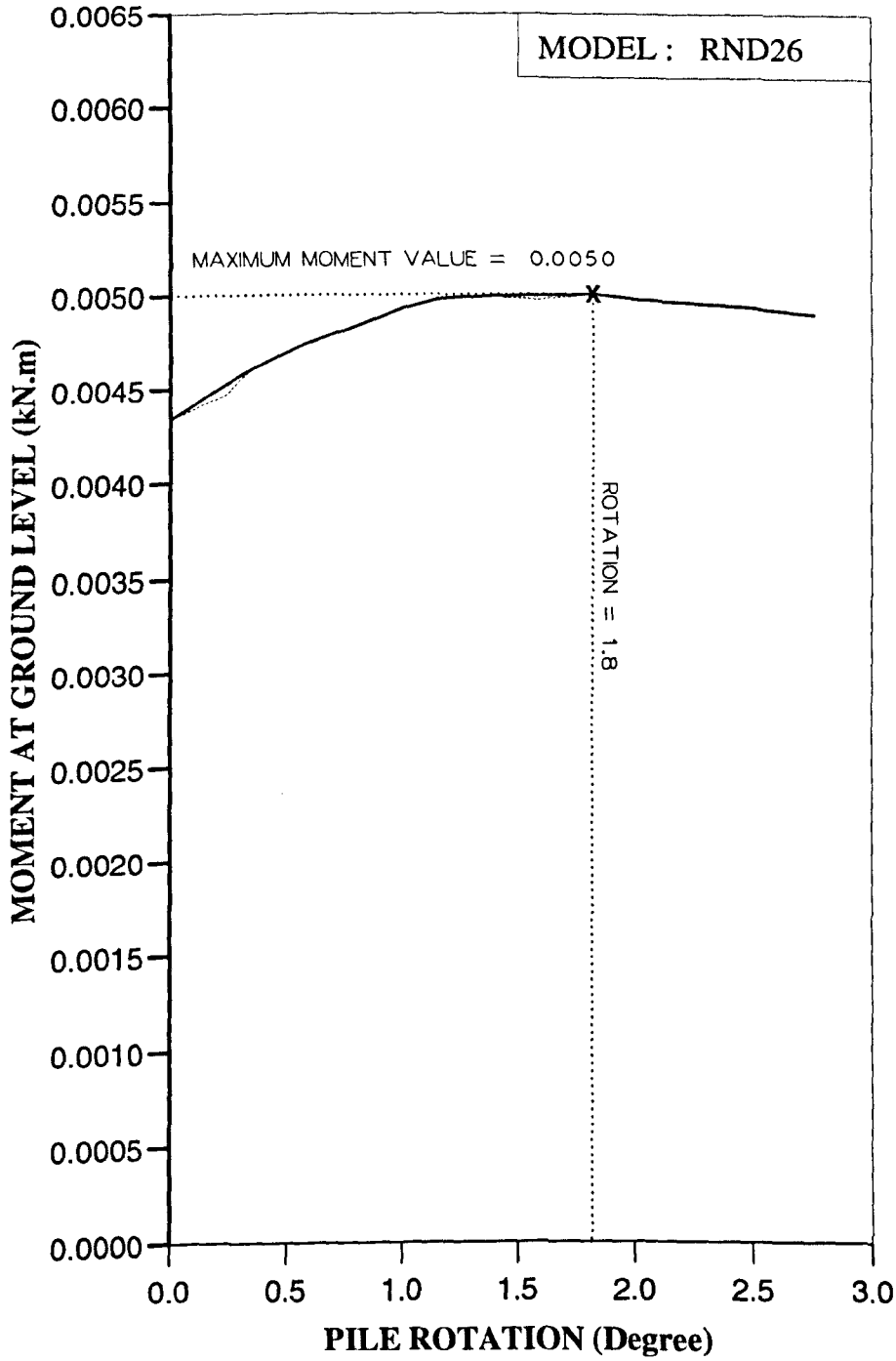

Figure AM30 Variation of moment at ground level with pile rotation for Series 2 test.

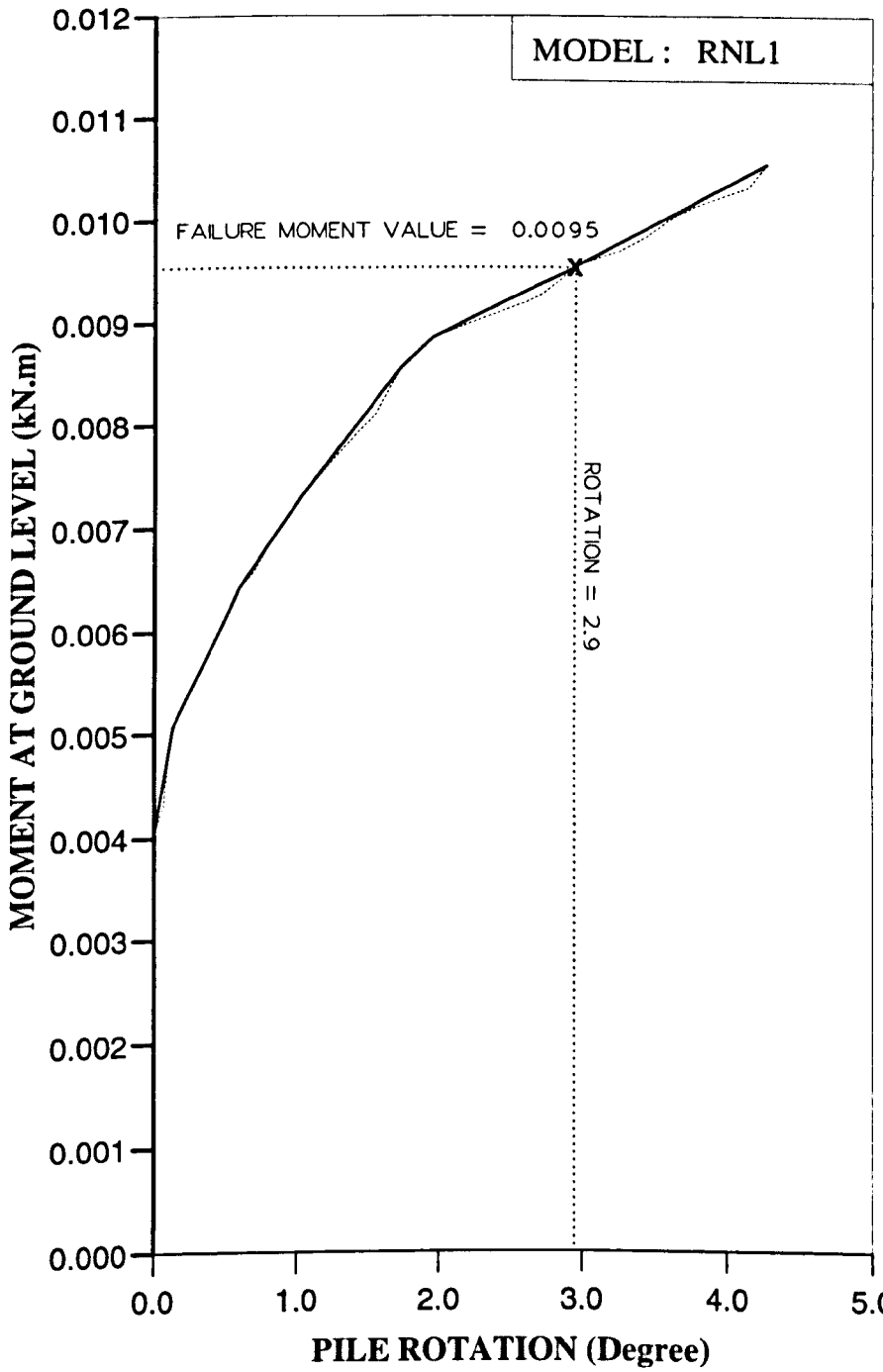

Figure AM31 Variation of moment at ground level with pile rotation for Series 2 test.

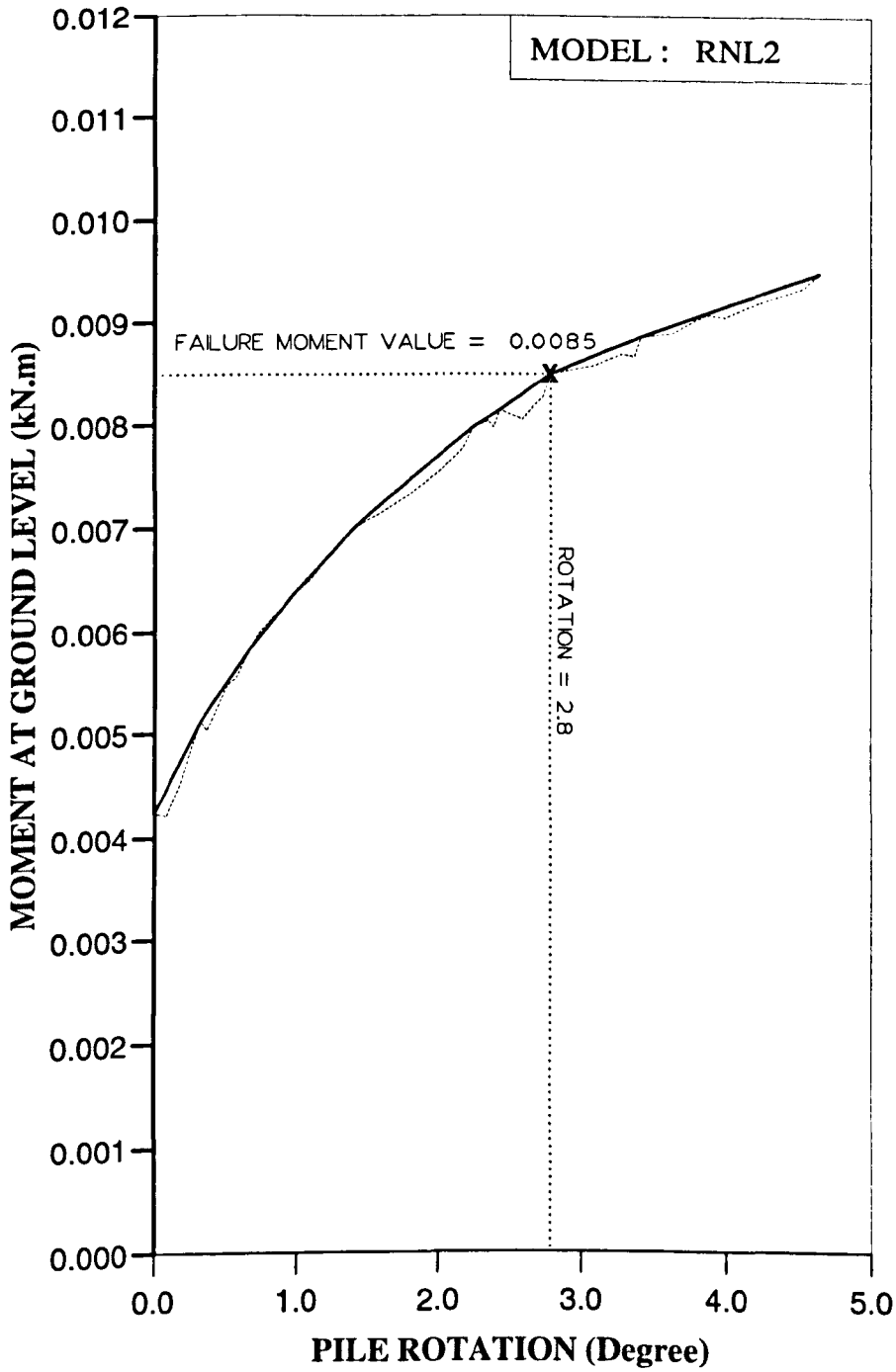

Figure AM32 Variation of moment at ground level with pile rotation for Series 2 test.

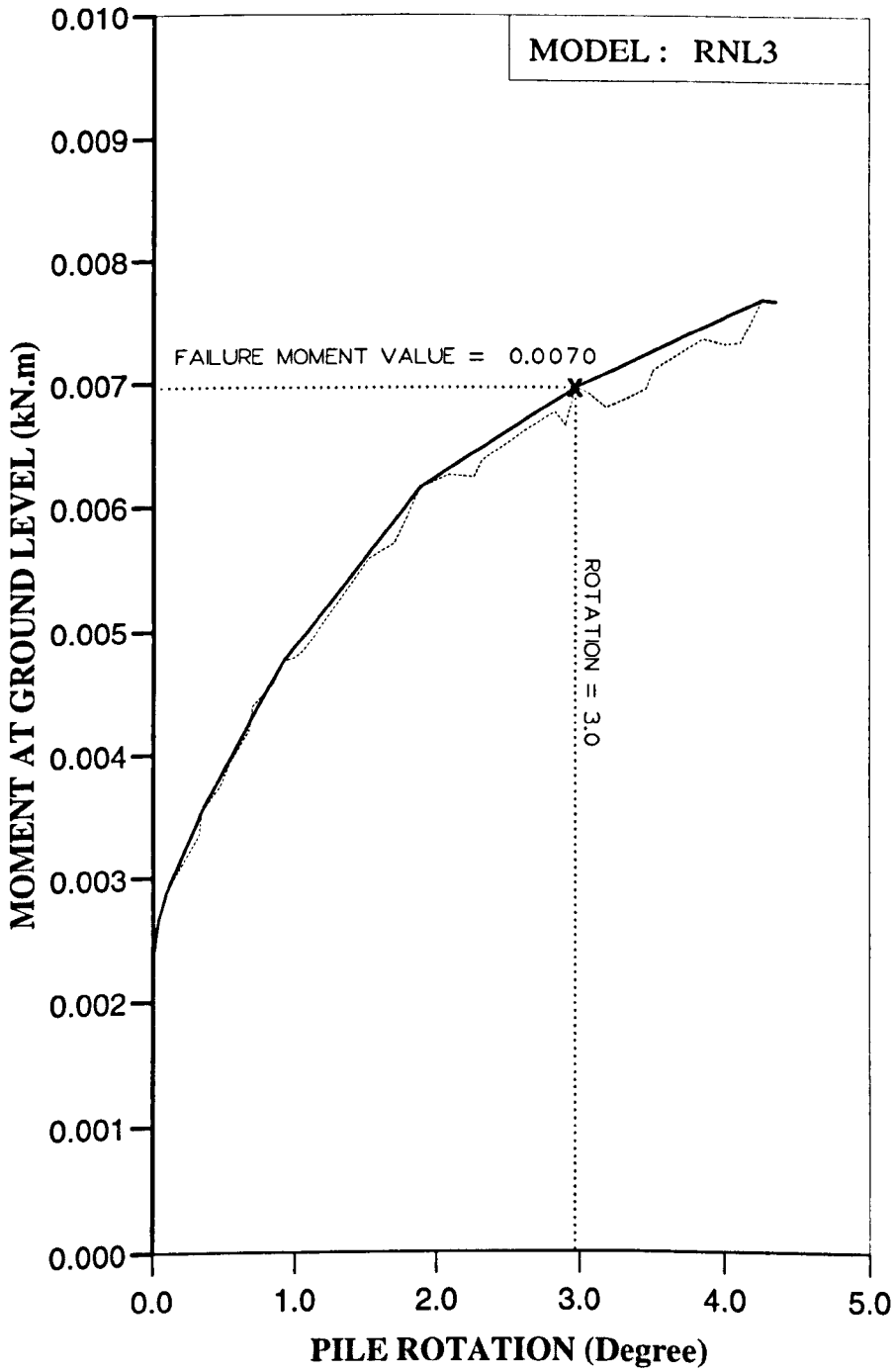

Figure AM33 Variation of moment at ground level with pile rotation for Series 2 test.

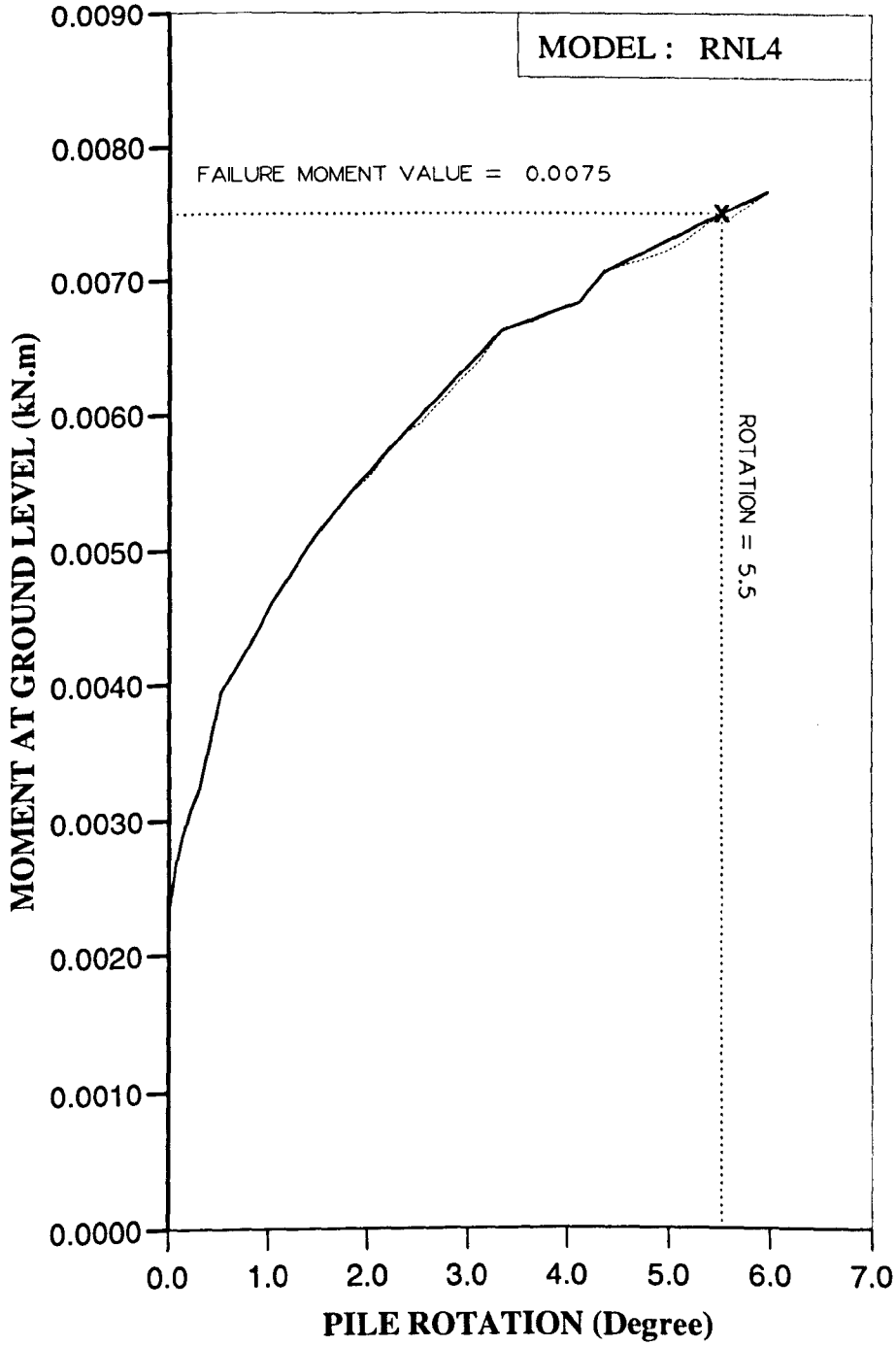

Figure AM34 Variation of moment at ground level with pile rotation for Series 1 test.

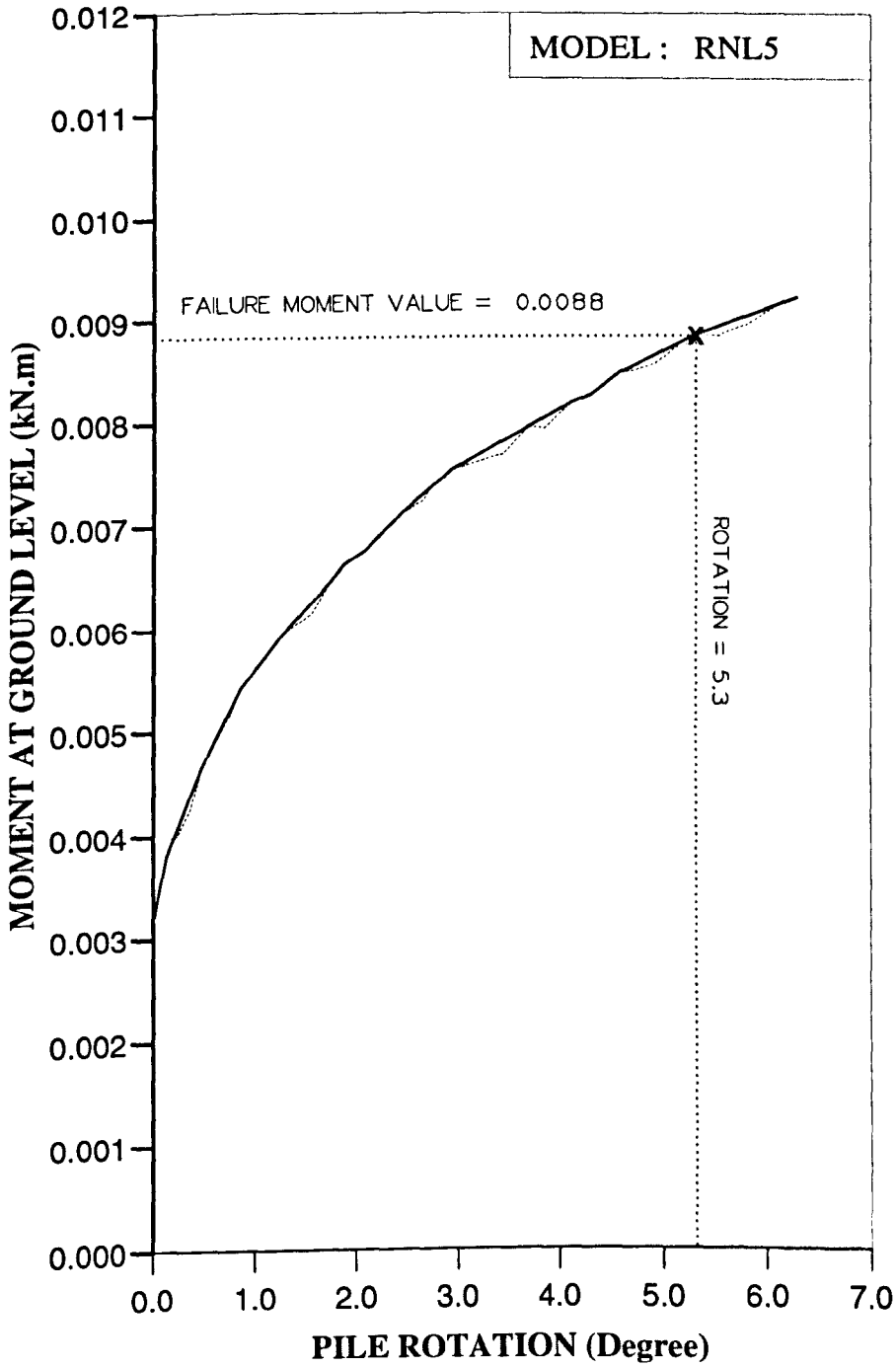

Figure AM35 Variation of moment at ground level with pile rotation for Series 1 test.

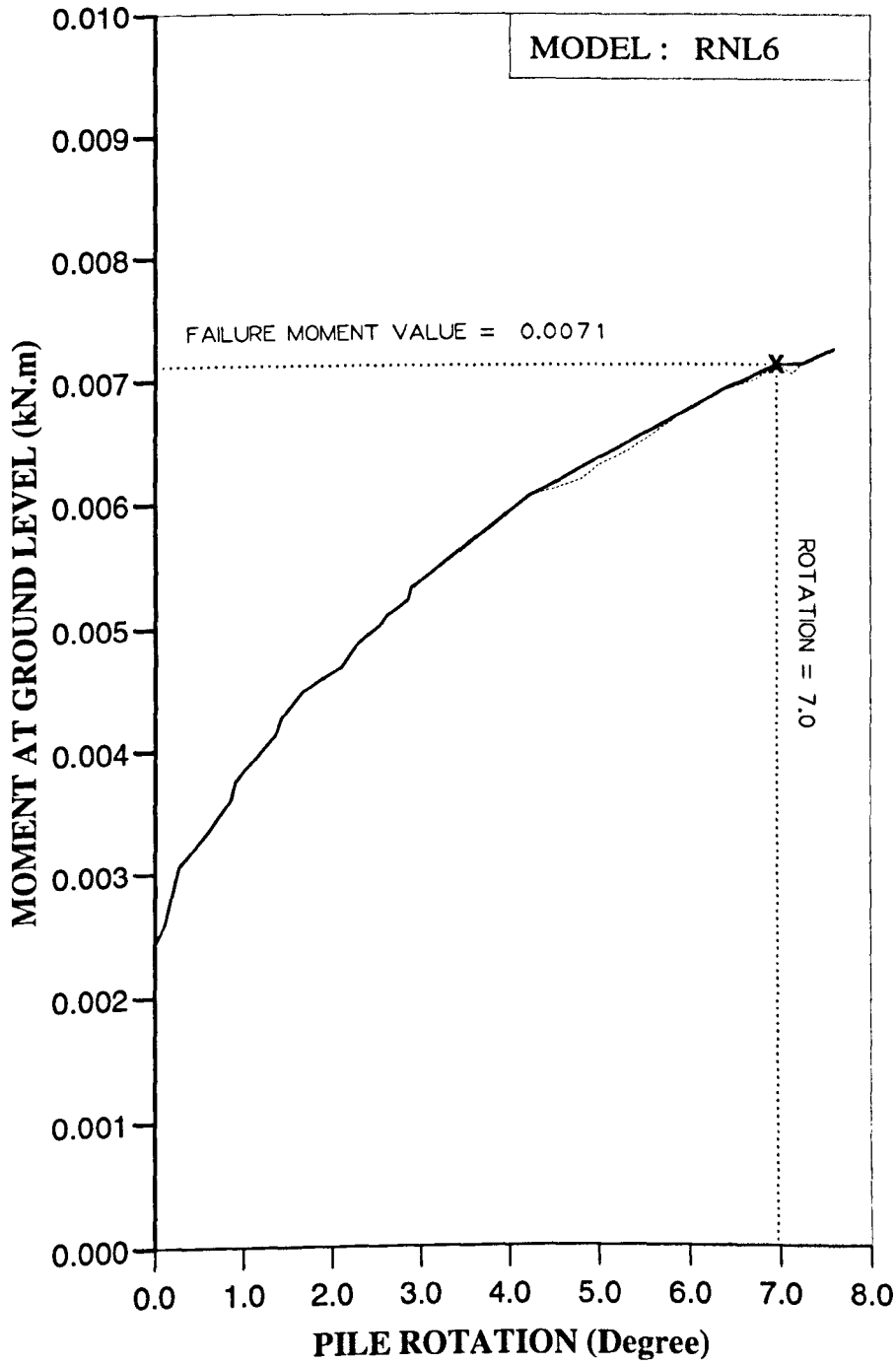

Figure AM36 Variation of moment at ground level with pile rotation for Series 1 test.

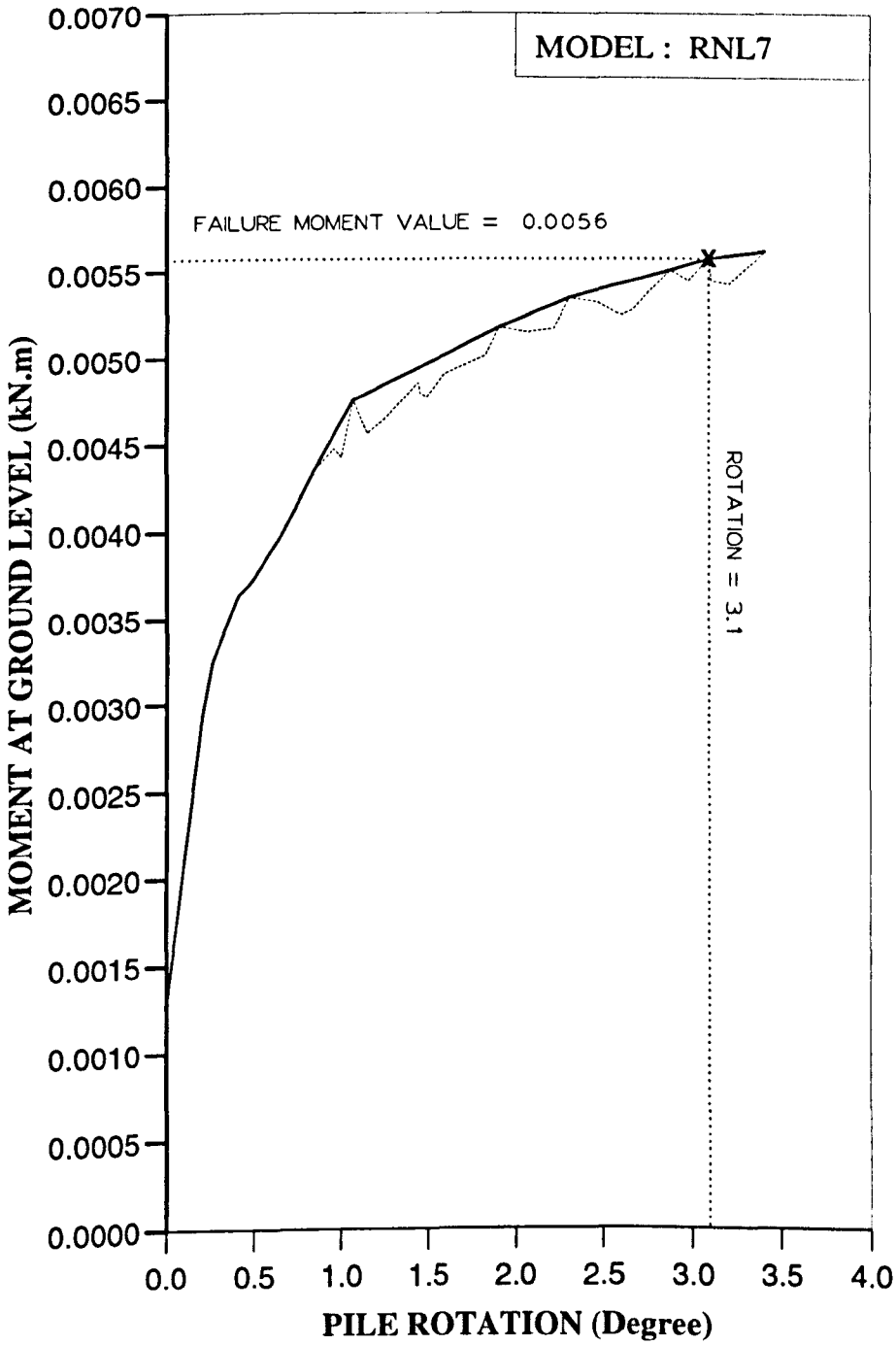

Figure AM37 Variation of moment at ground level with pile rotation for Series 1 test.

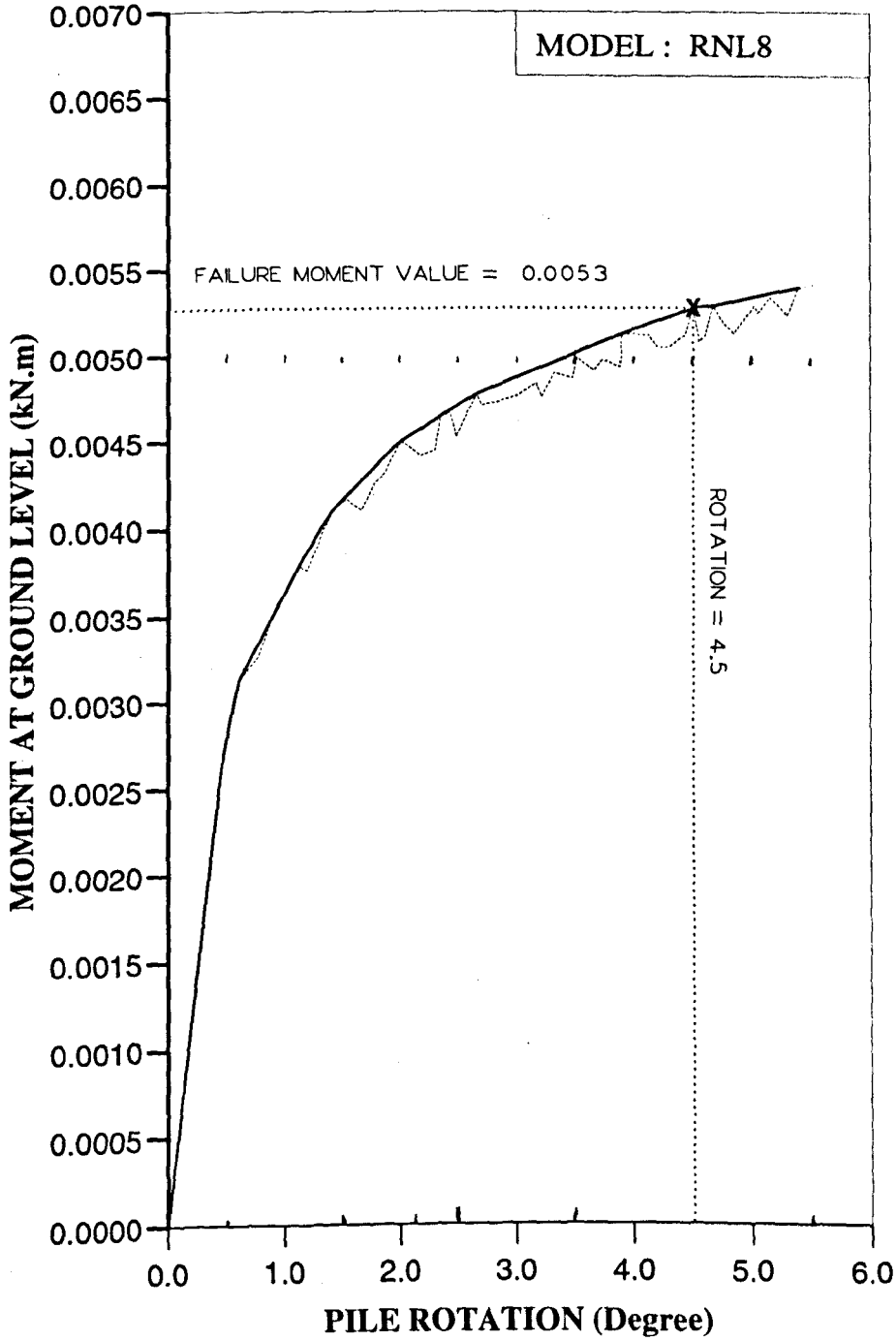

Figure AM38 Variation of moment at ground level with pile rotation for Series 2 test.

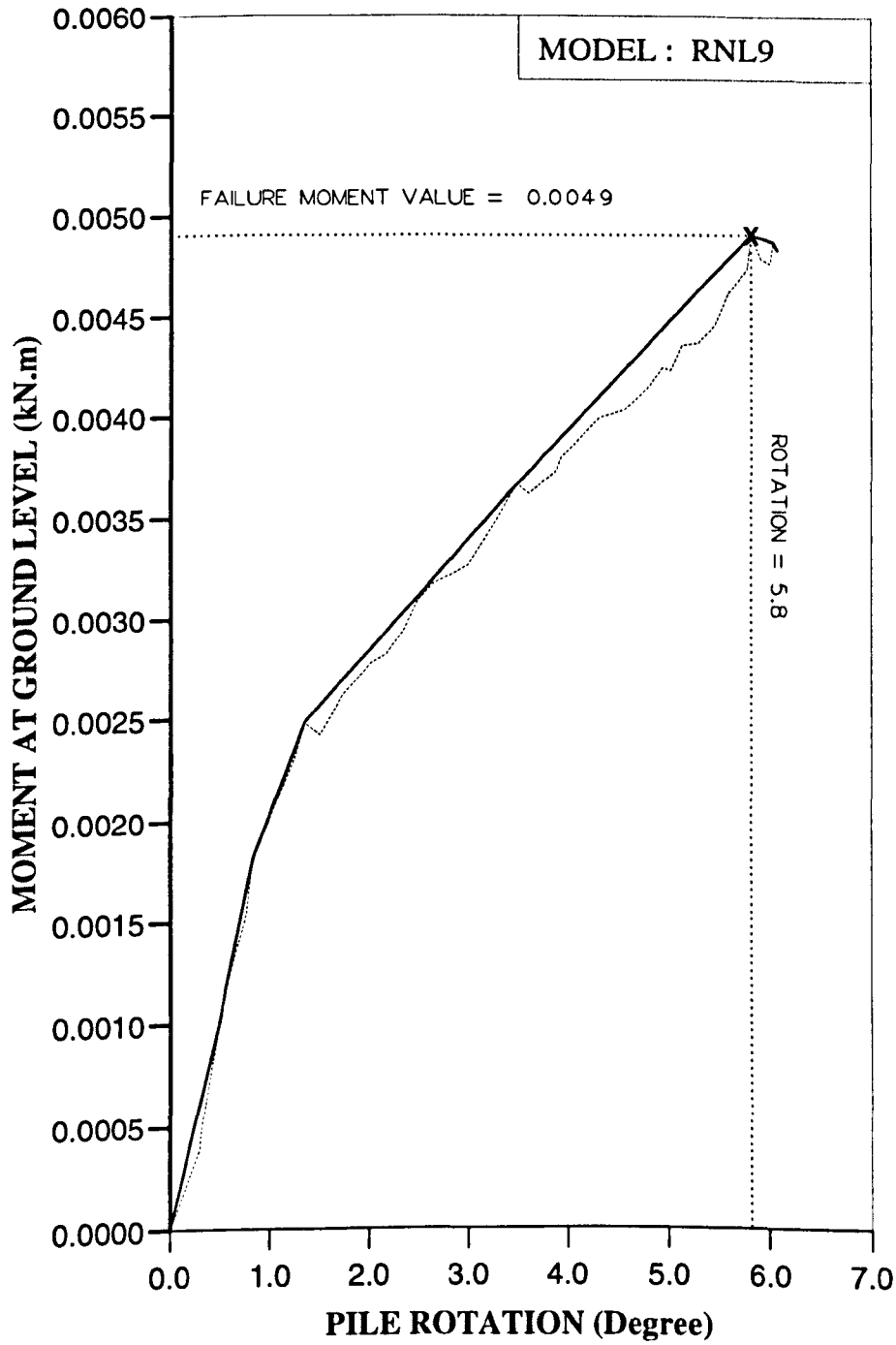

Figure AM39 Variation of moment at ground level with pile rotation for Series 2 test.

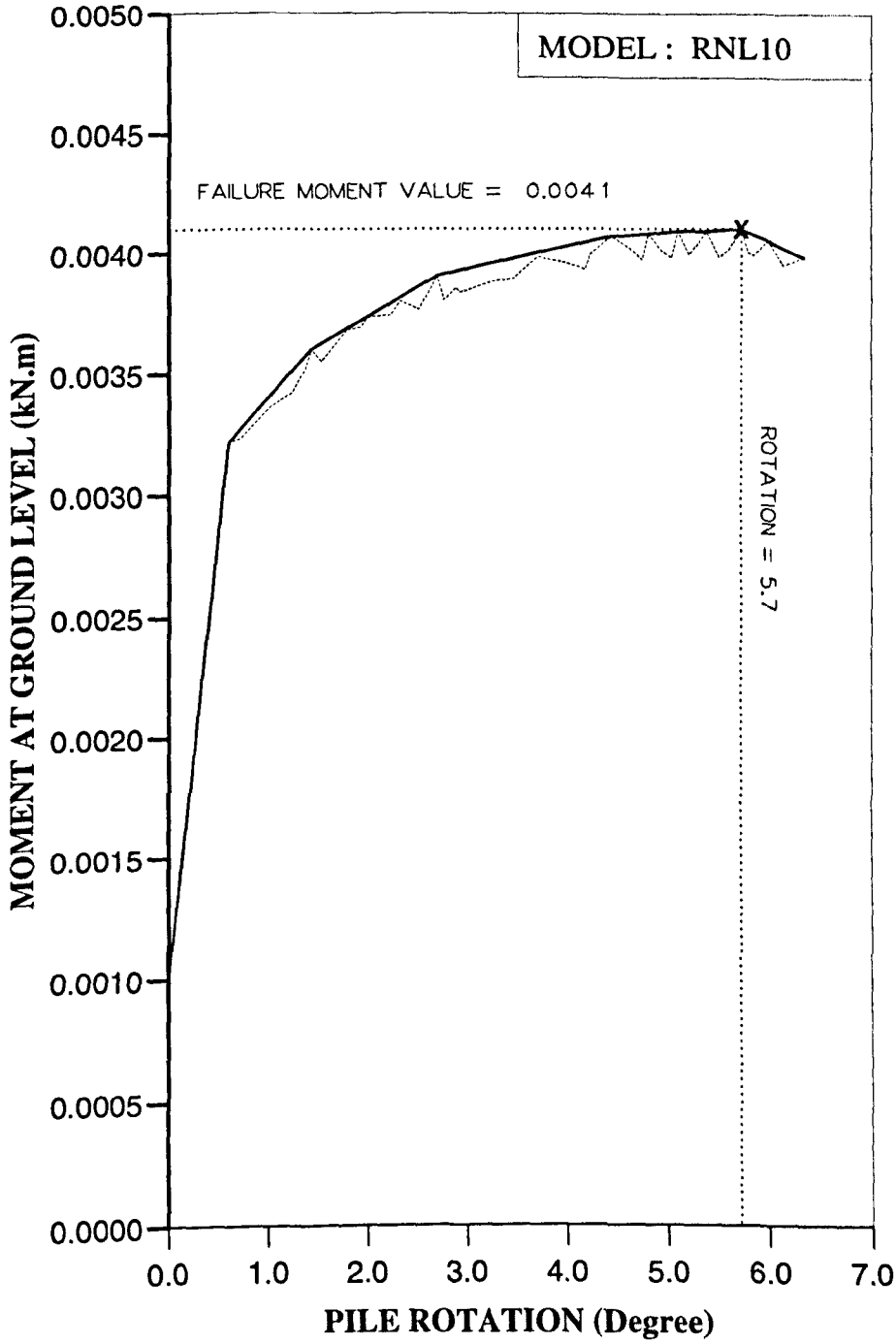

Figure AM40 Variation of moment at ground level with pile rotation for Series 2 test.

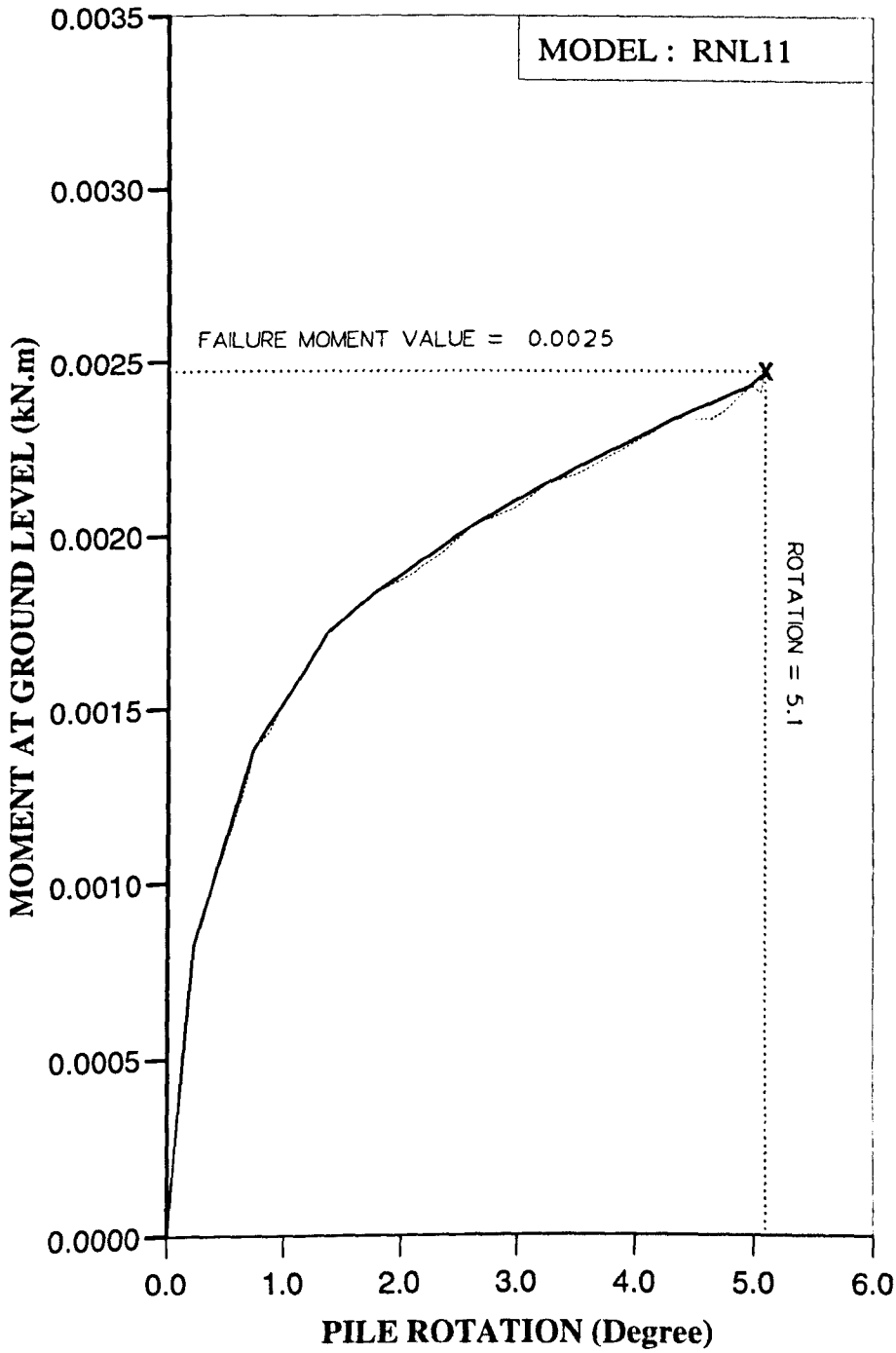

Figure AM41 Variation of moment at ground level with pile rotation for Series 2 test.

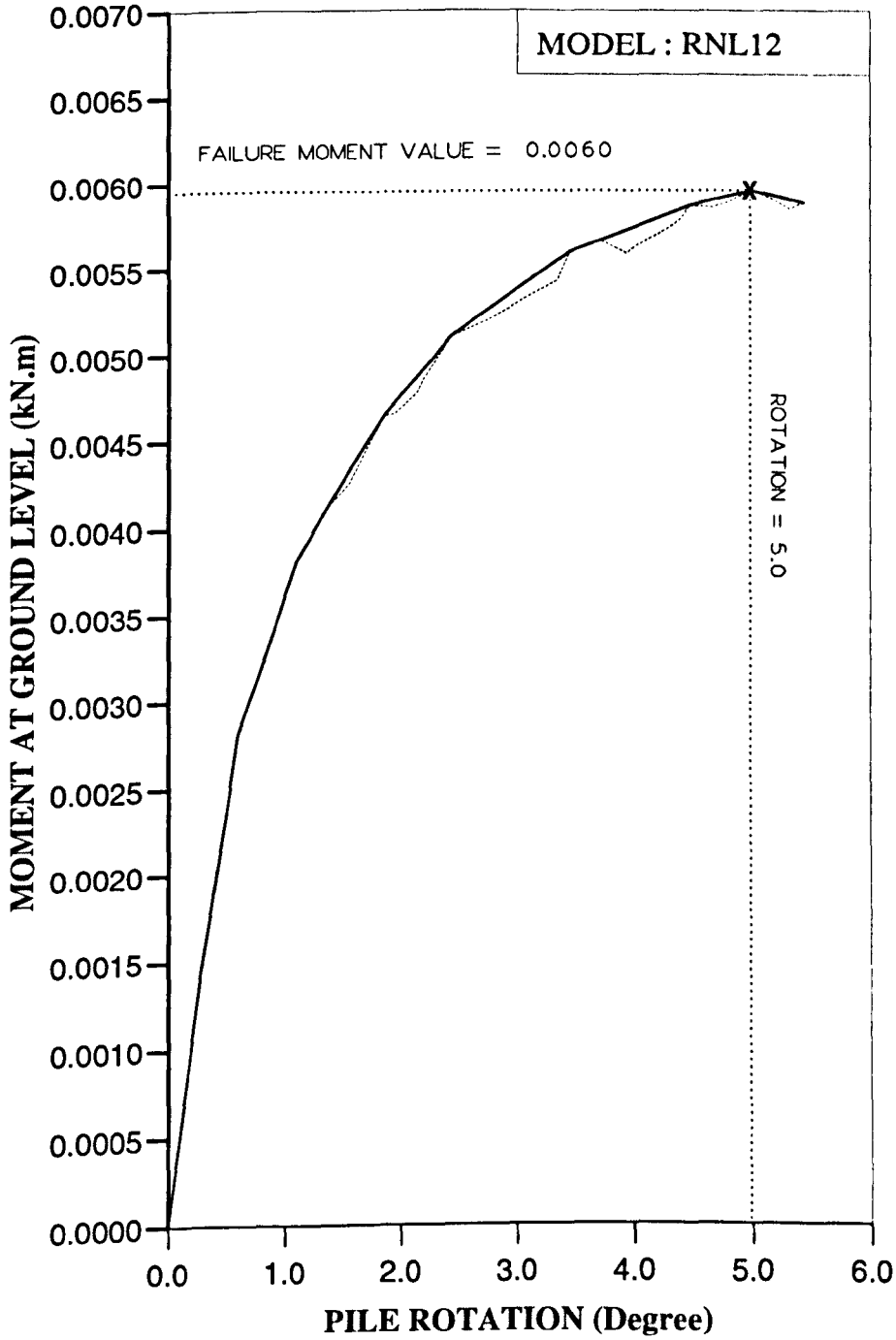

Figure AM42 Variation of moment at ground level with pile rotation for Series 2 test.

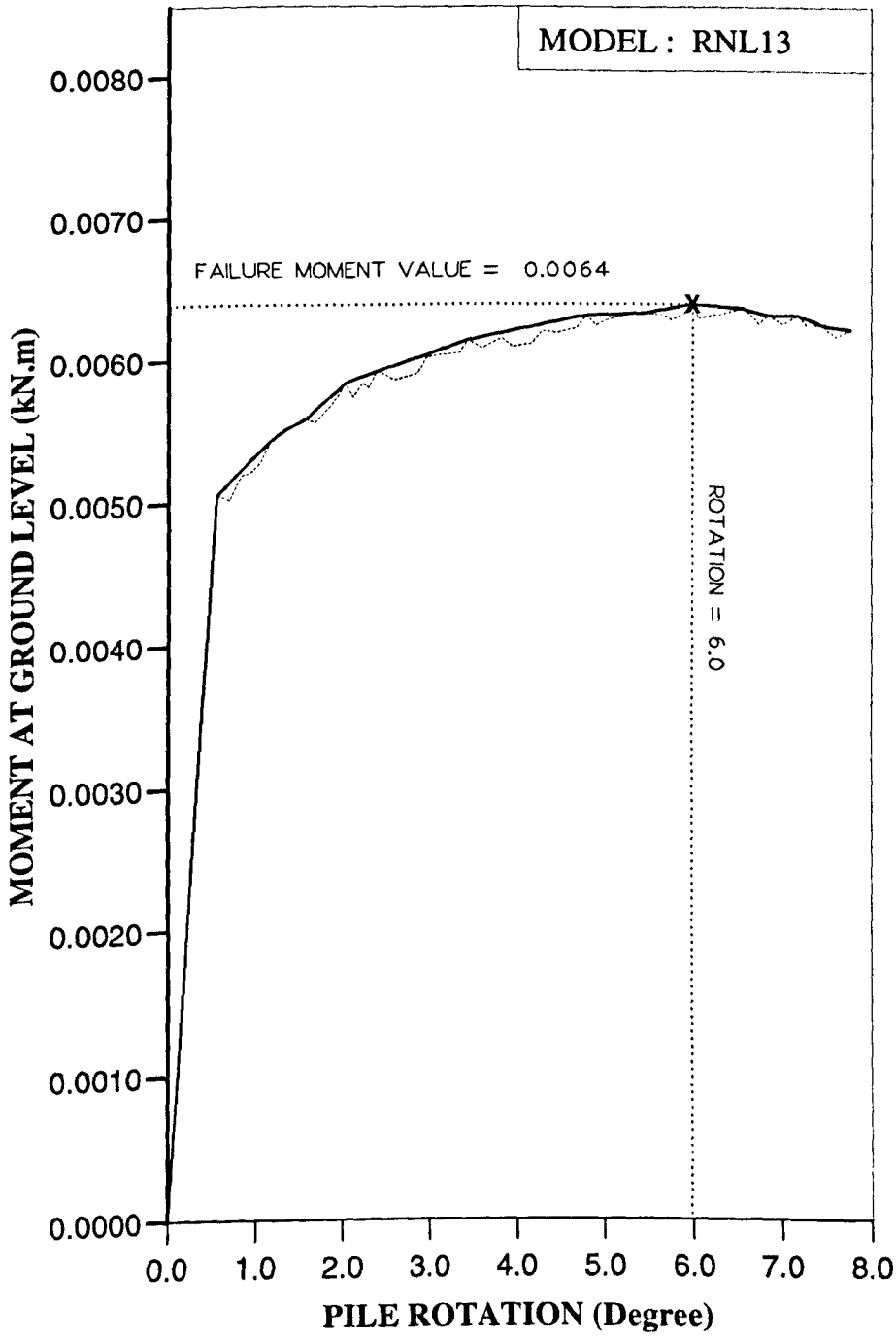

Figure AM43 Variation of moment at ground level with pile rotation for Series 2 test.

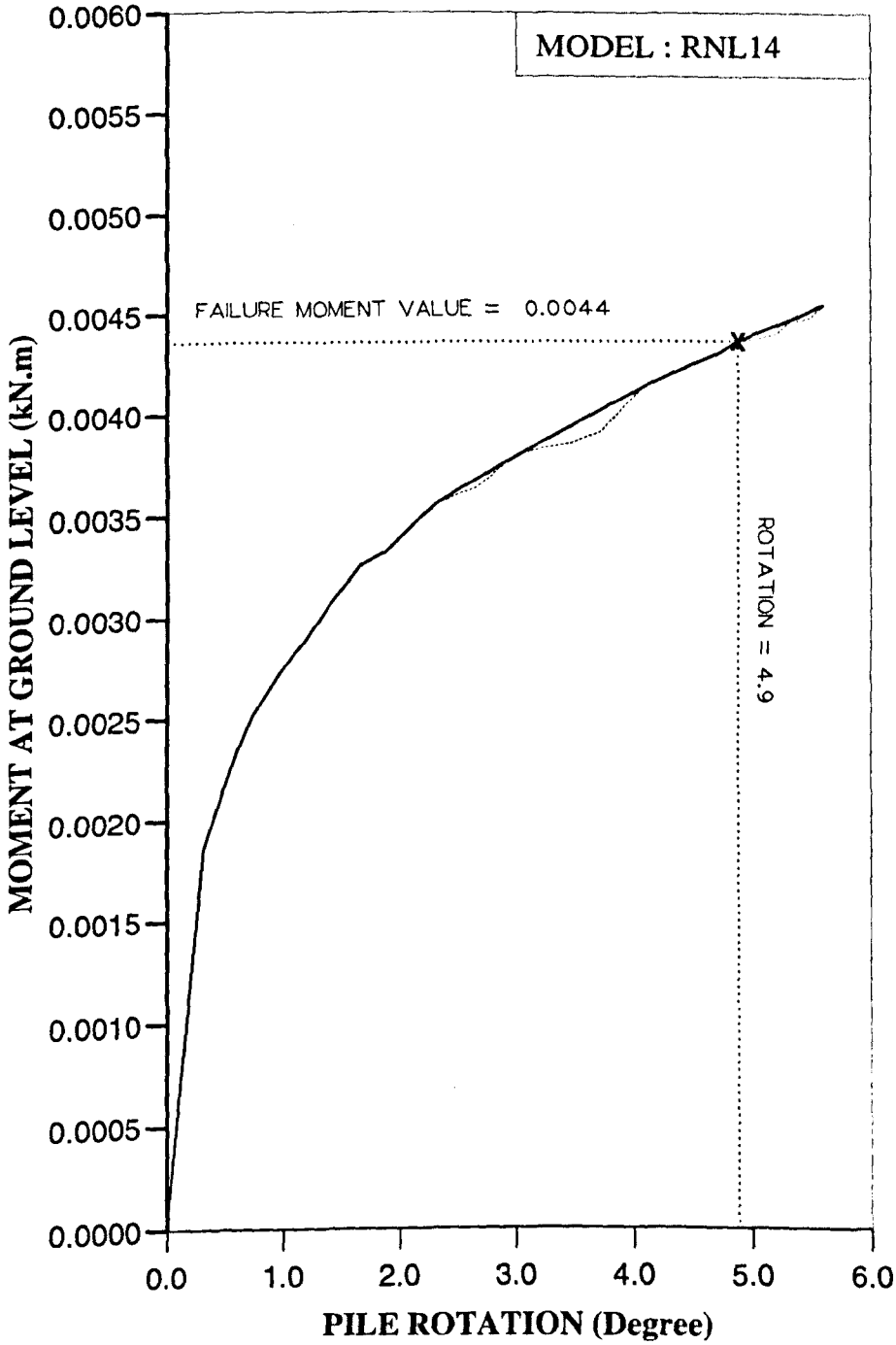

Figure AM44 Variation of moment at ground level with pile rotation for Series 2 test.

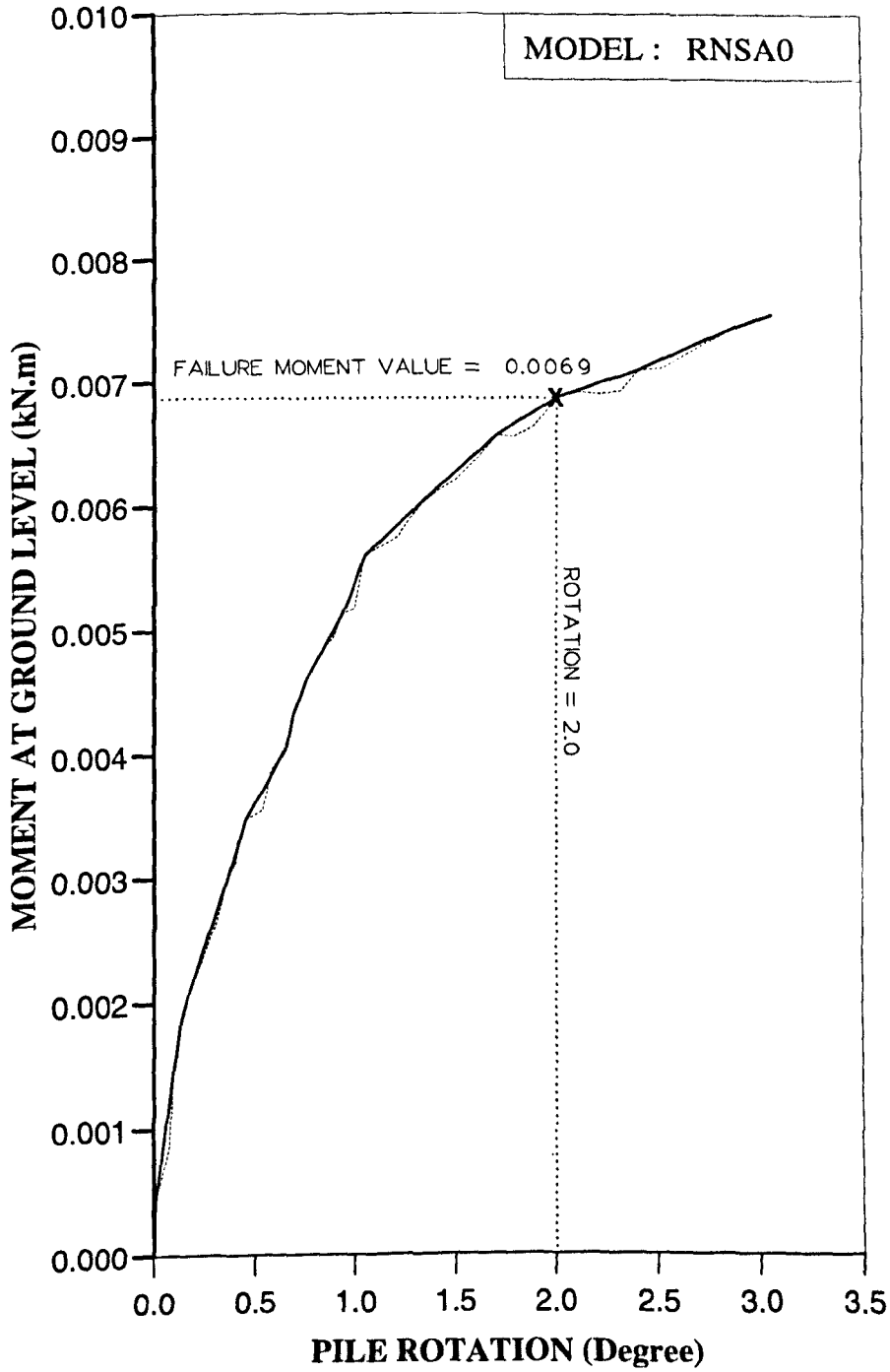

Figure AM45 Variation of moment at ground level with pile rotation for Series 3 test.

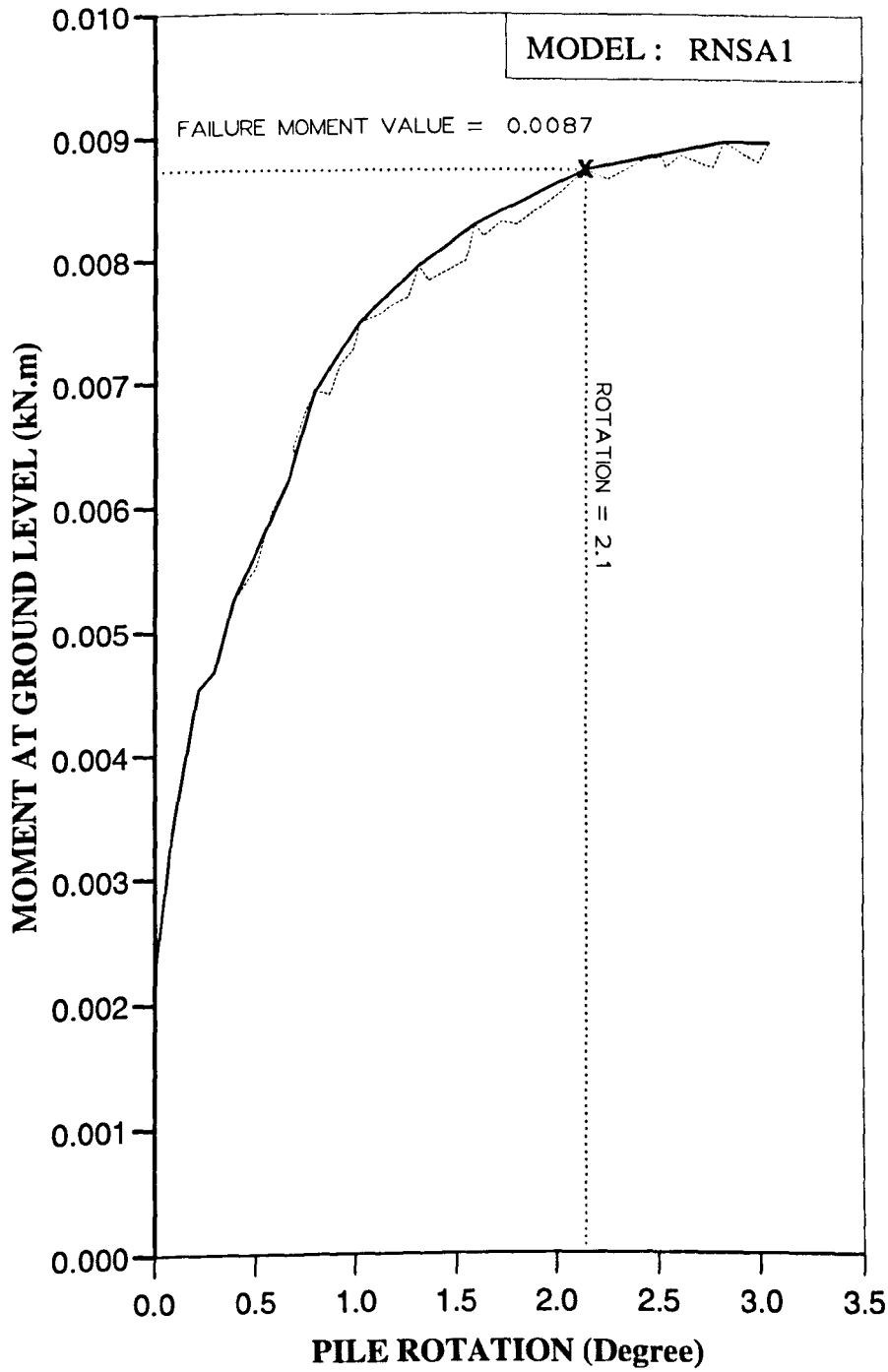

Figure AM46 Variation of moment at ground level with pile rotation for Series 3 test.

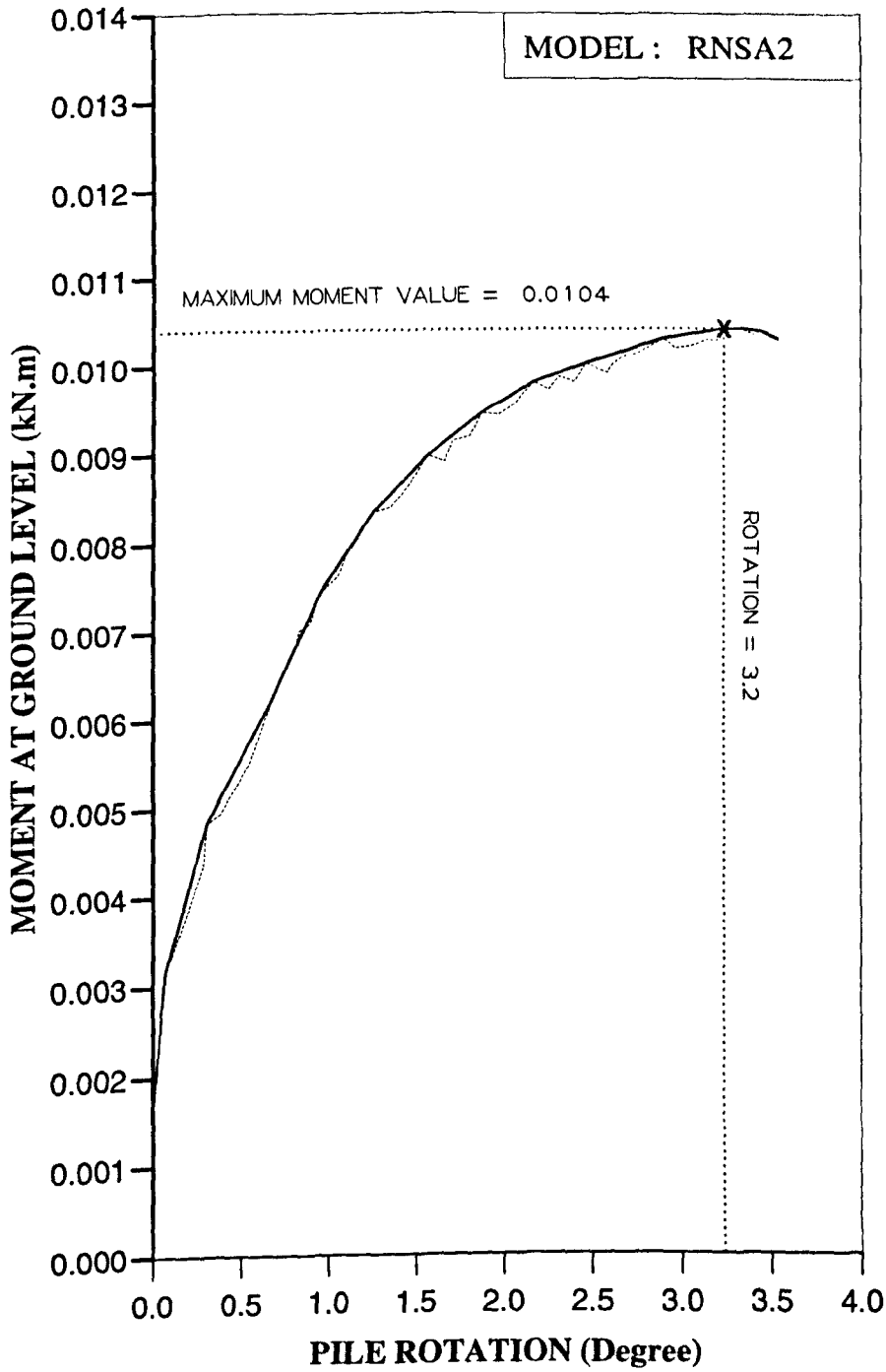

Figure AM47 Variation of moment at ground level with pile rotation for Series 3 test.

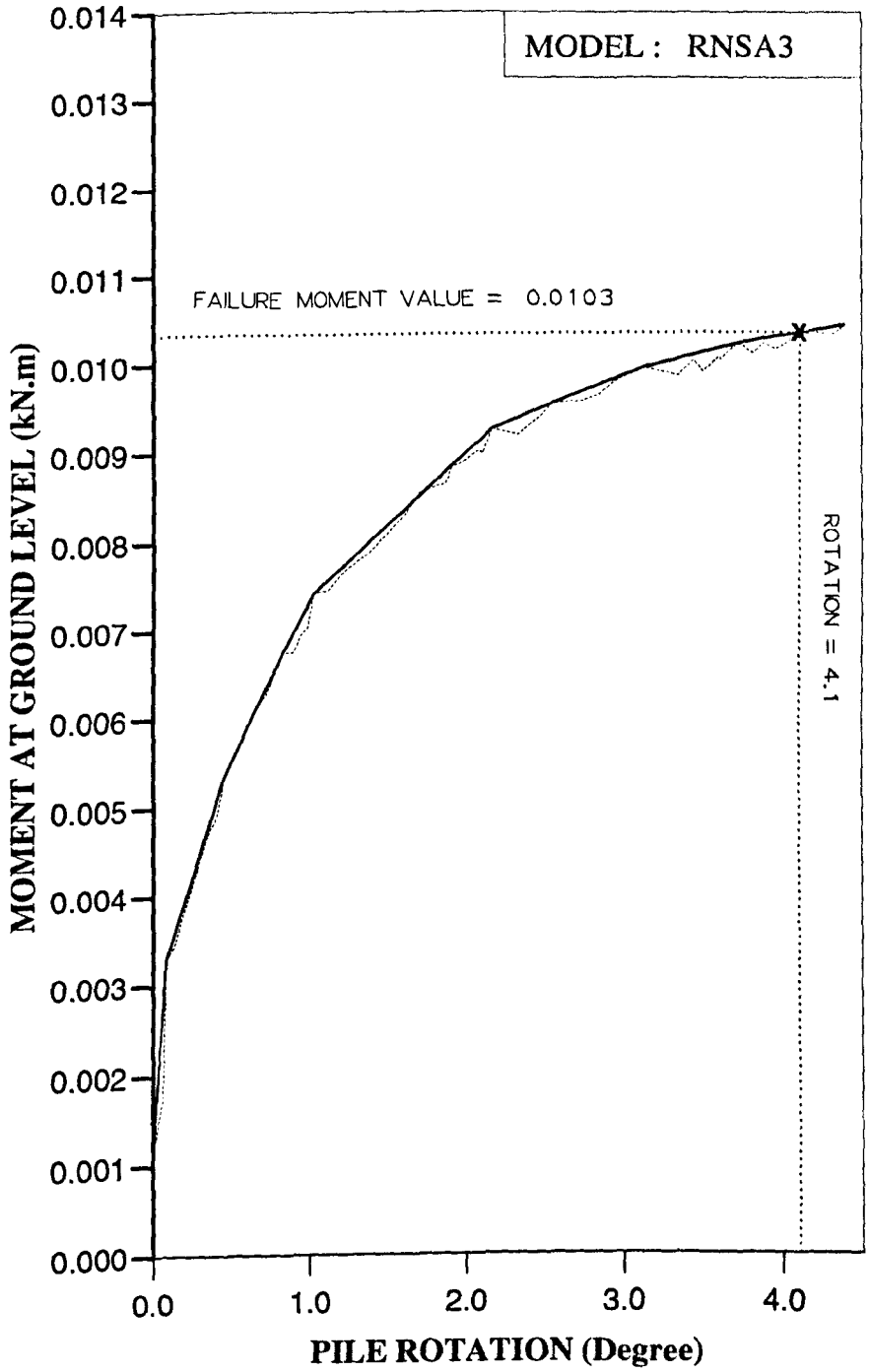

Figure AM48 Variation of moment at ground level with pile rotation for Series 3 test.

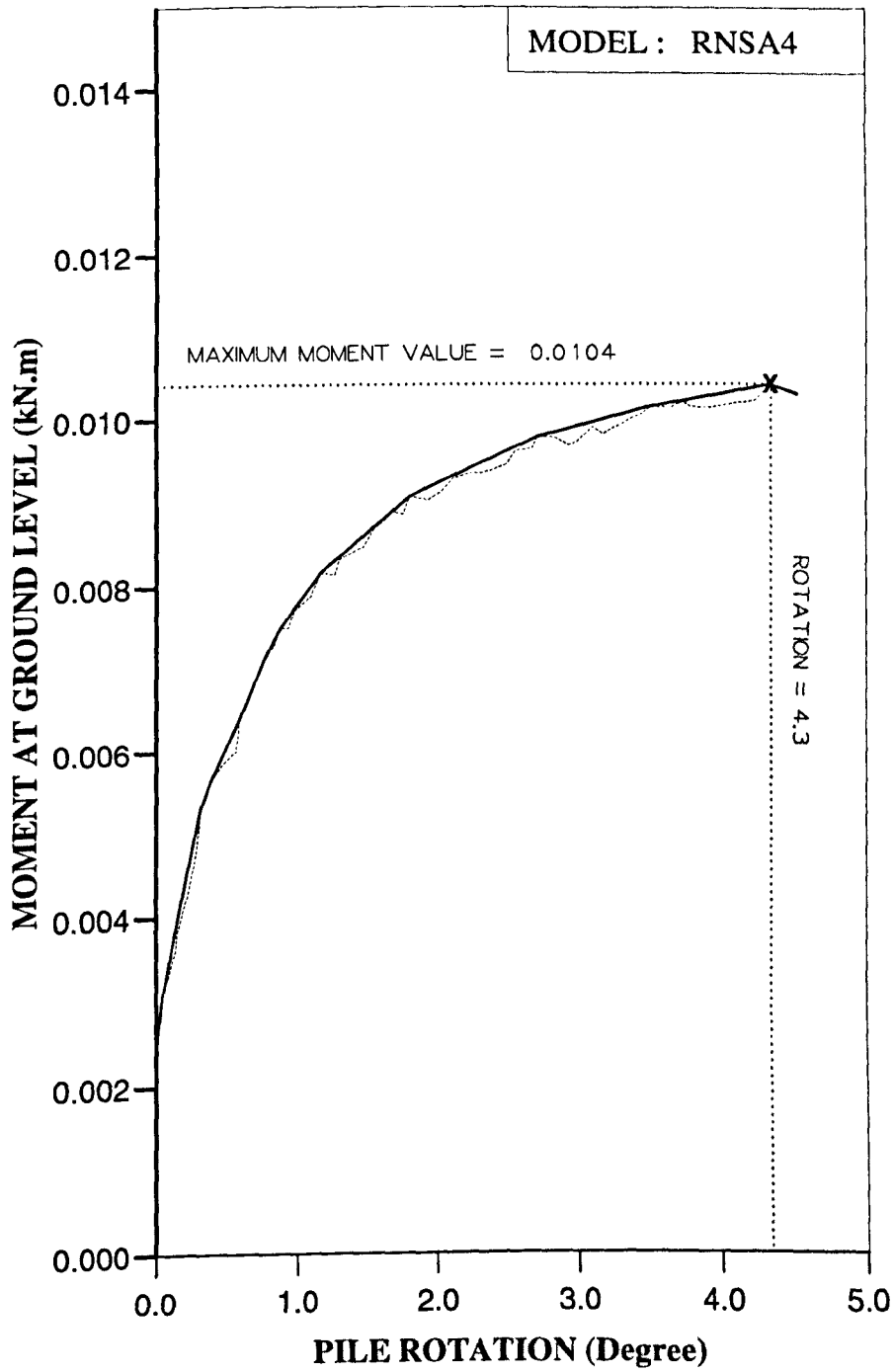

Figure AM49 Variation of moment at ground level with pile rotation for Series 3 test.

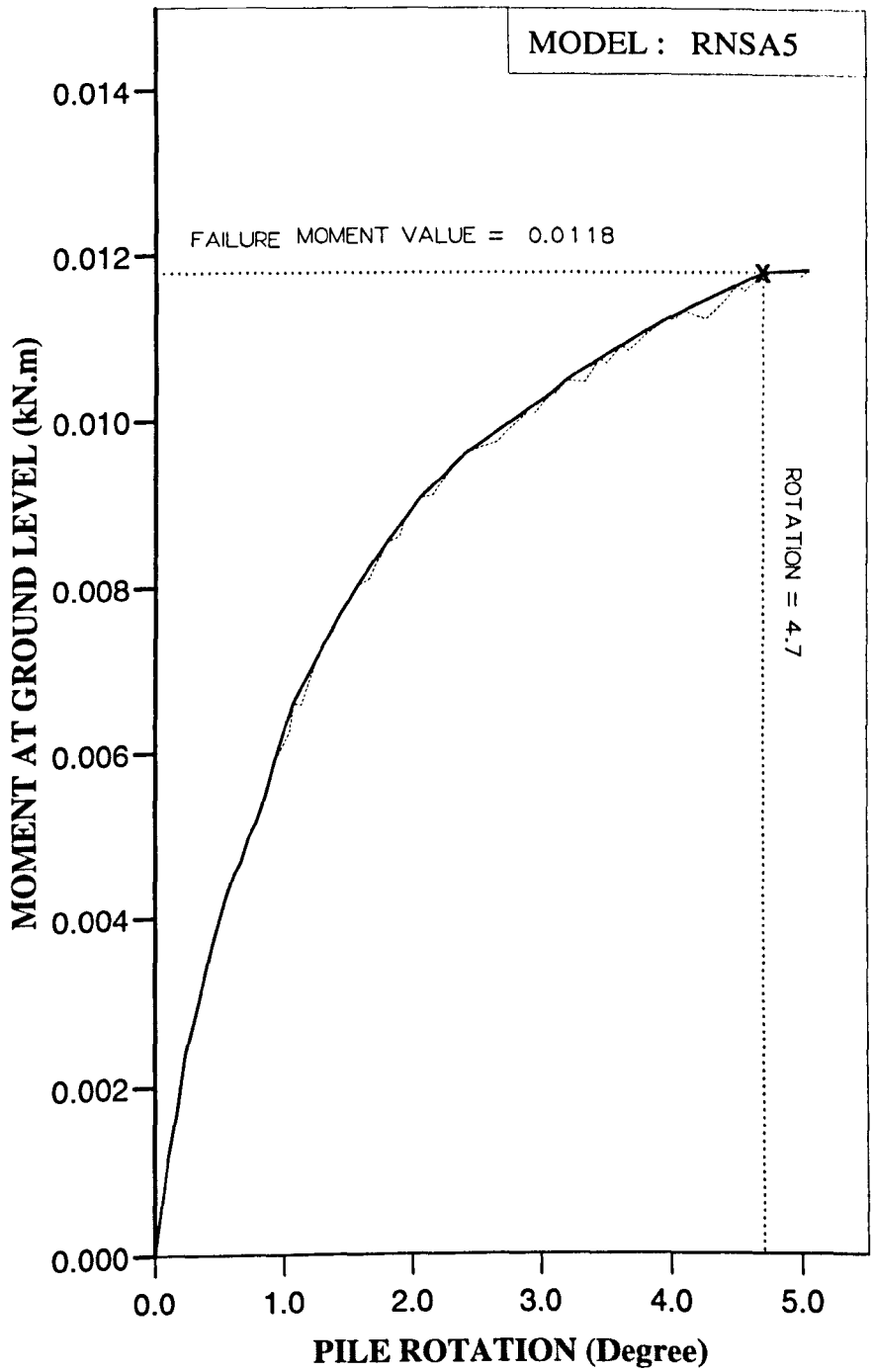

Figure AM50 Variation of moment at ground level with pile rotation for Series 3 test.

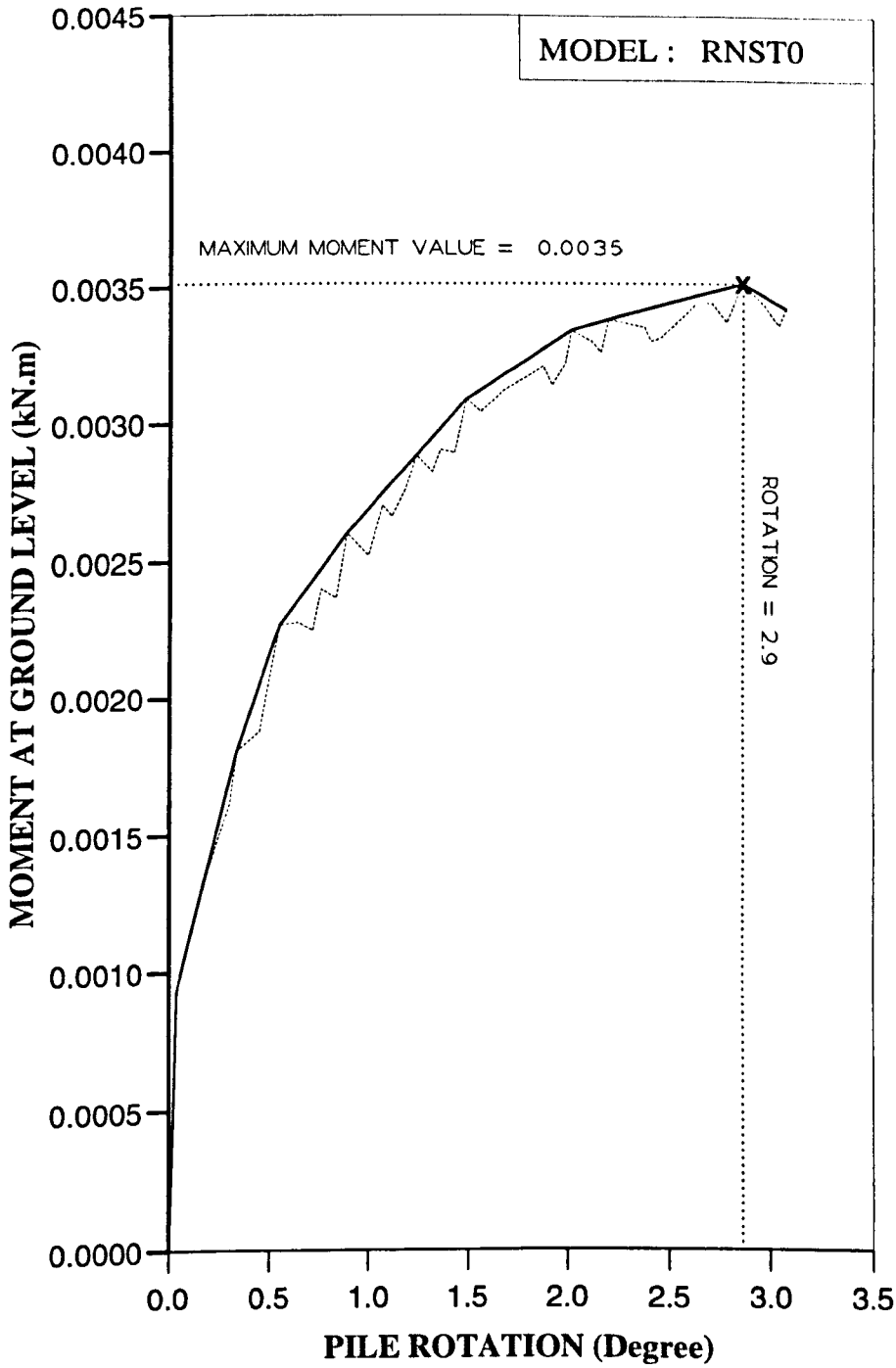

Figure AM51 Variation of moment at ground level with pile rotation for Series 3 test.

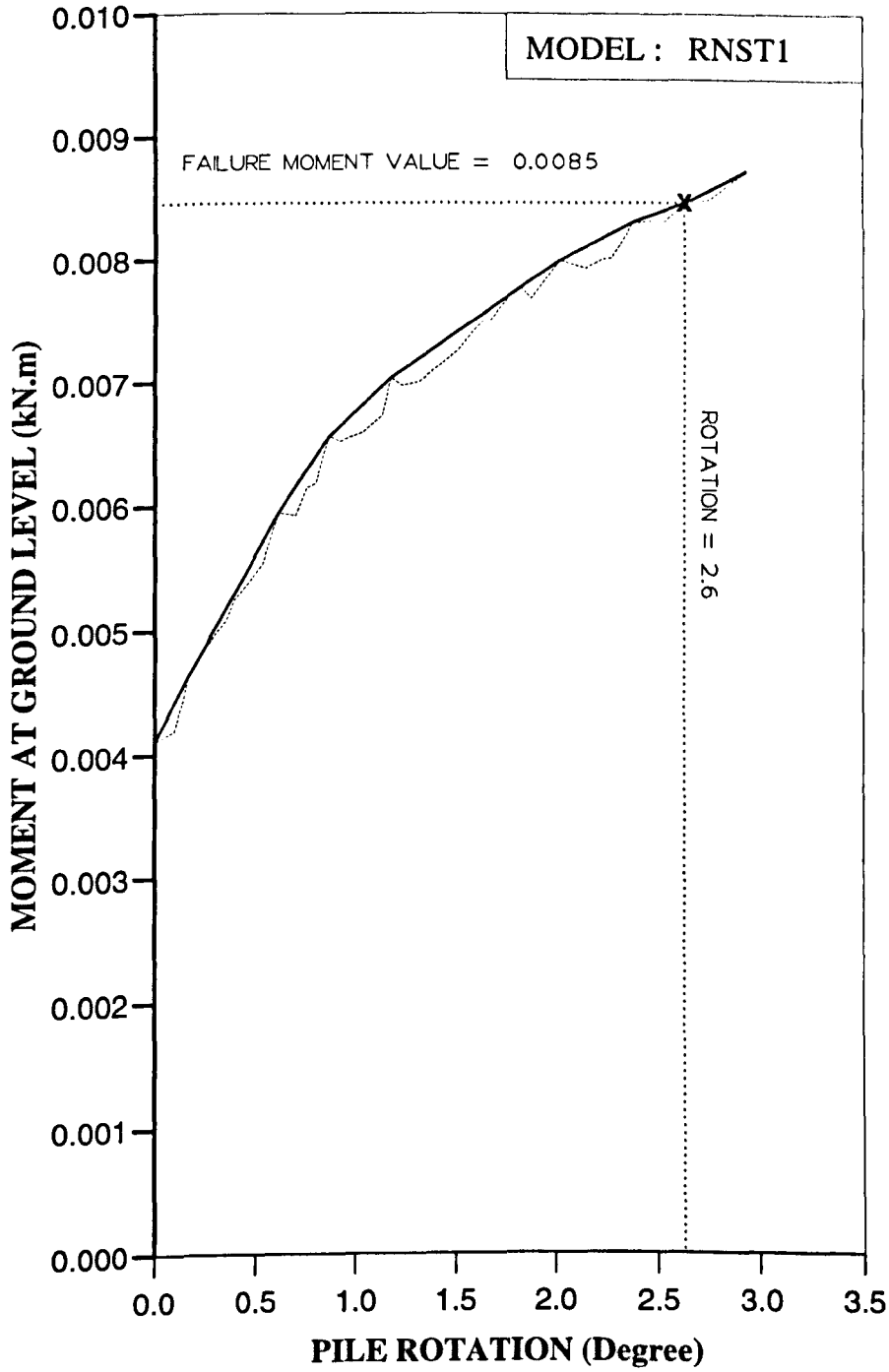

Figure AM52 Variation of moment at ground level with pile rotation for Series 3 test.

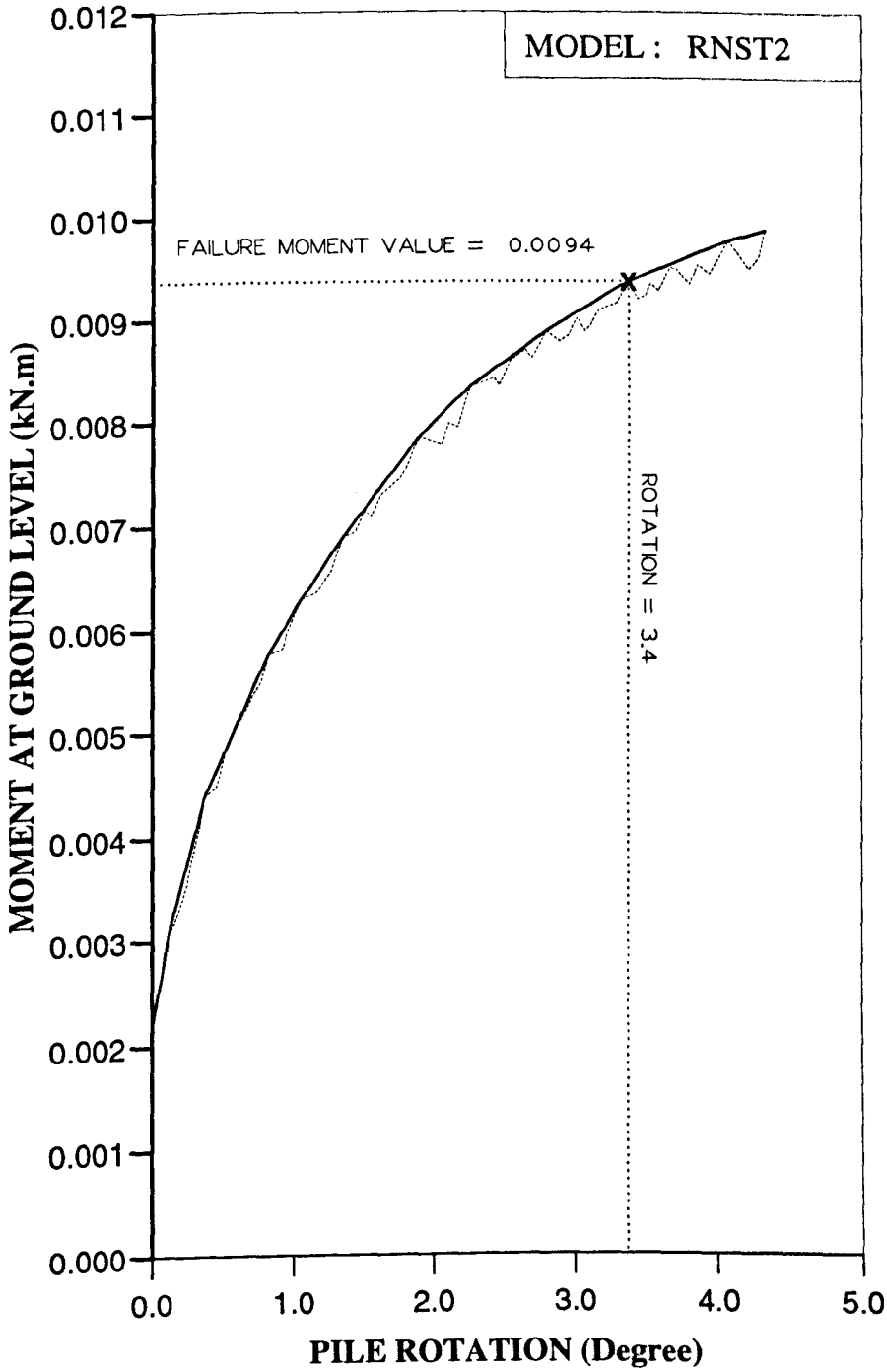

Figure AM53 Variation of moment at ground level with pile rotation for Series 3 test.

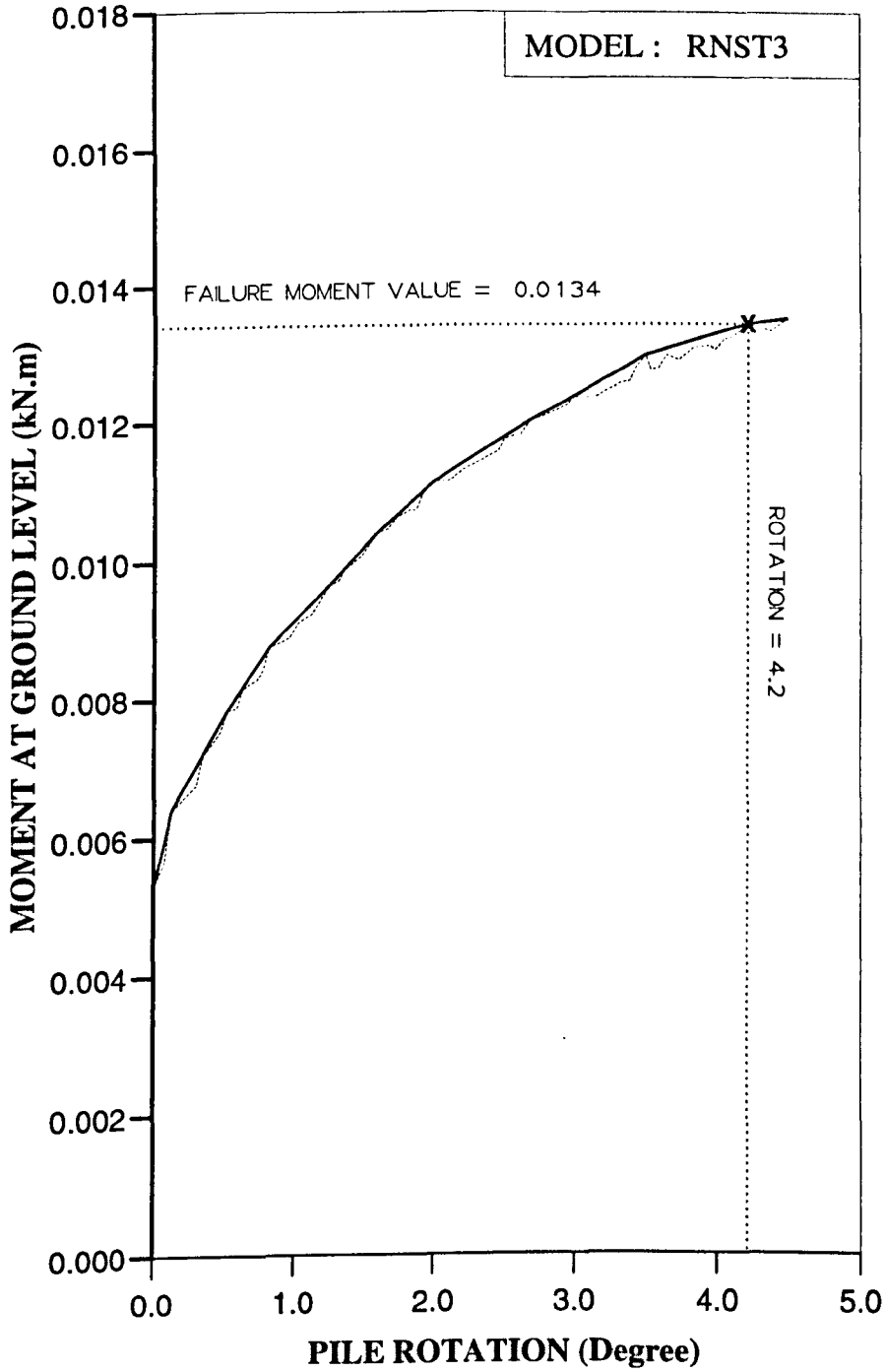

Figure AM54 Variation of moment at ground level with pile rotation for Series 3 test.

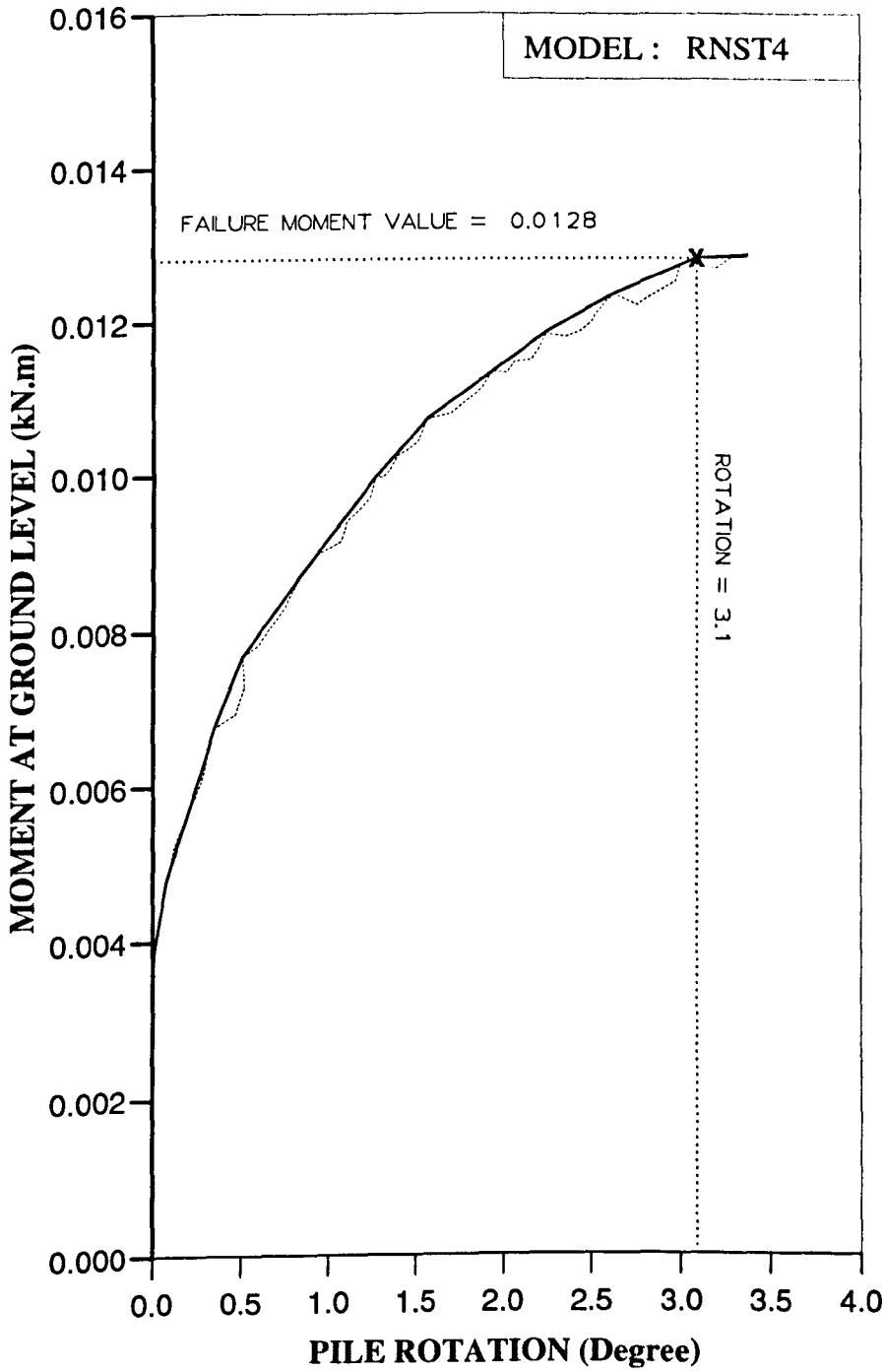

Figure AM55 Variation of moment at ground level with pile rotation for Series 3 test.

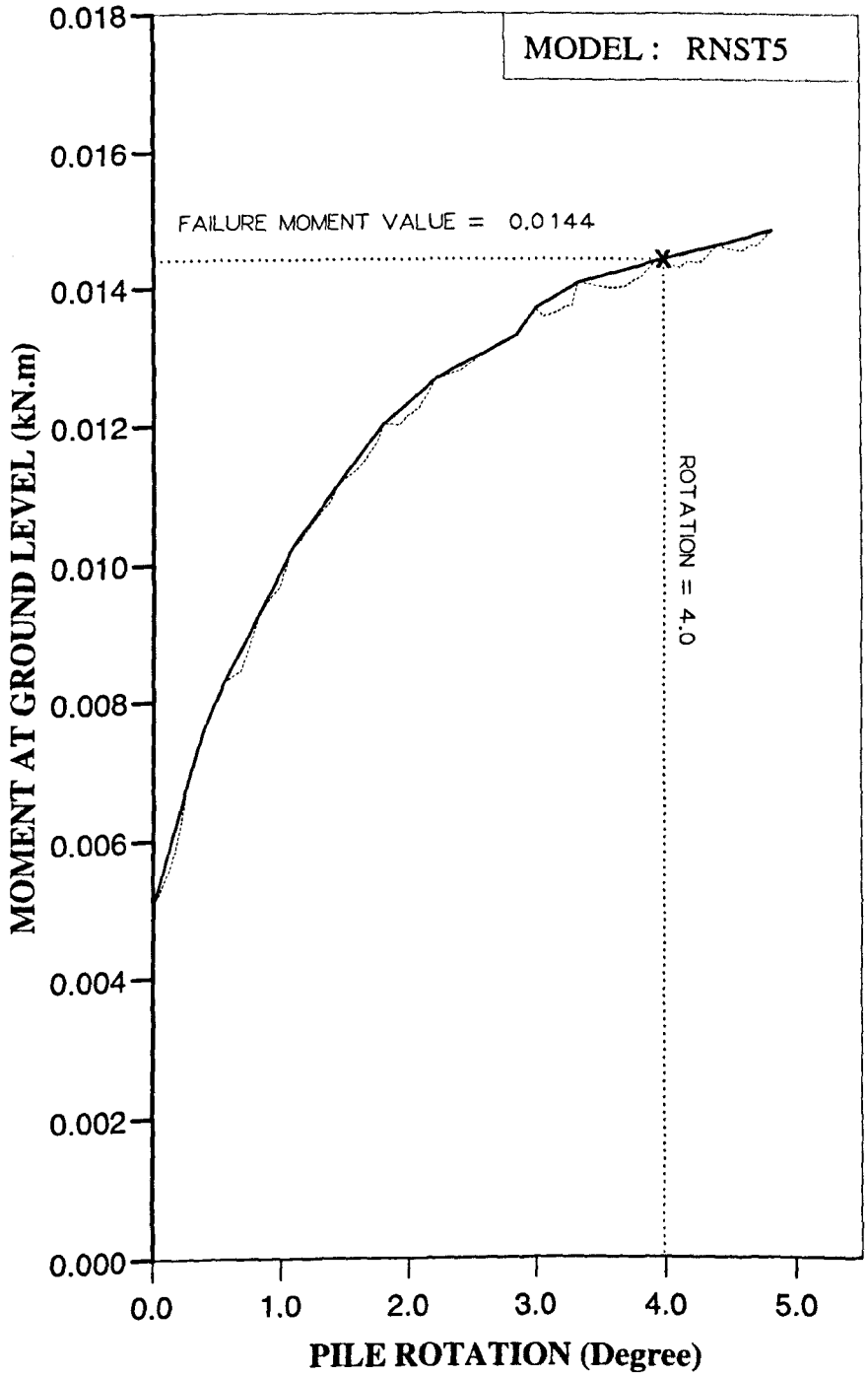

Figure AM56 Variation of moment at ground level with pile rotation for Series 3 test.

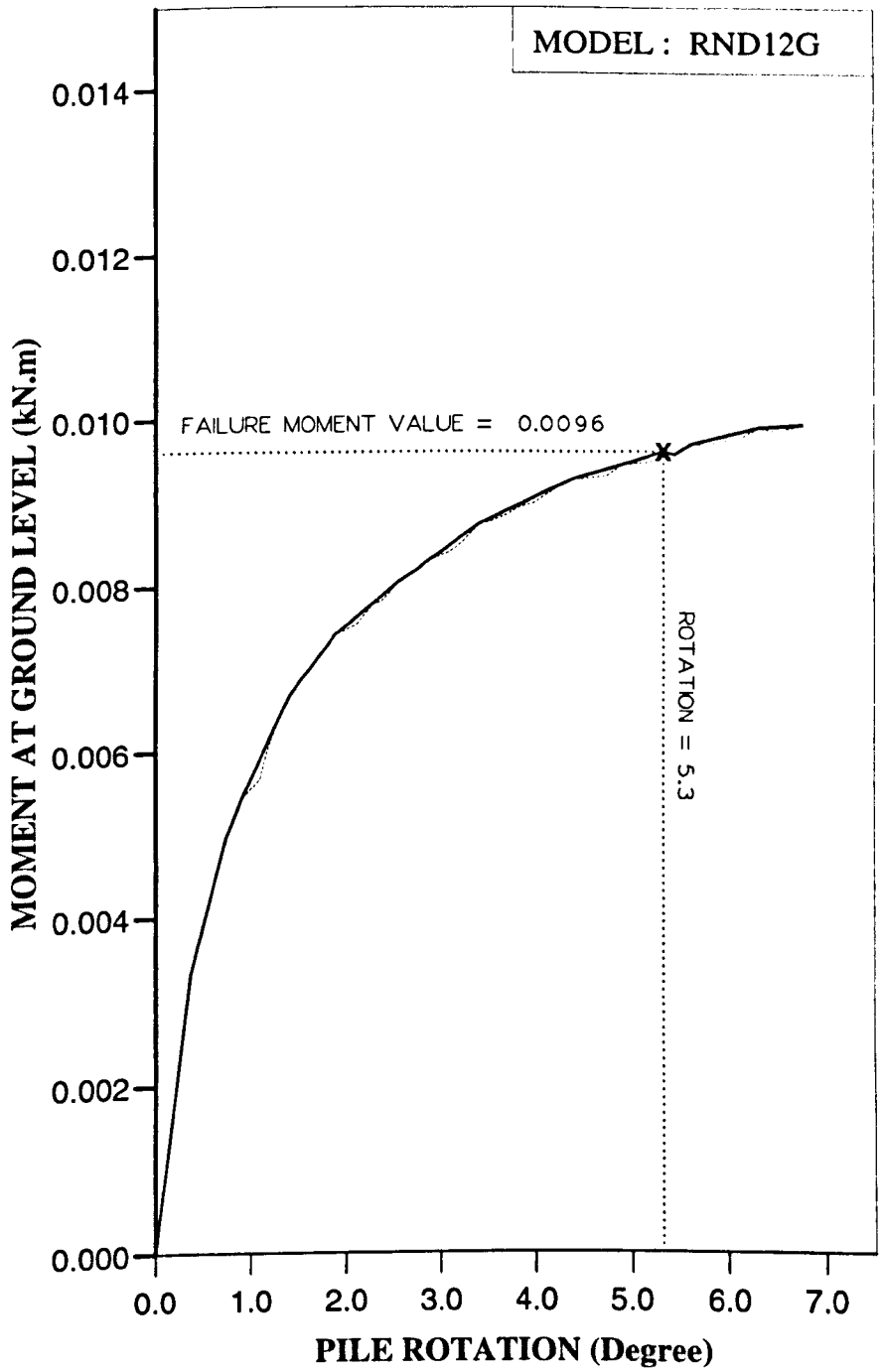

Figure AM57 Variation of moment at ground level with pile rotation for Series 4 test.

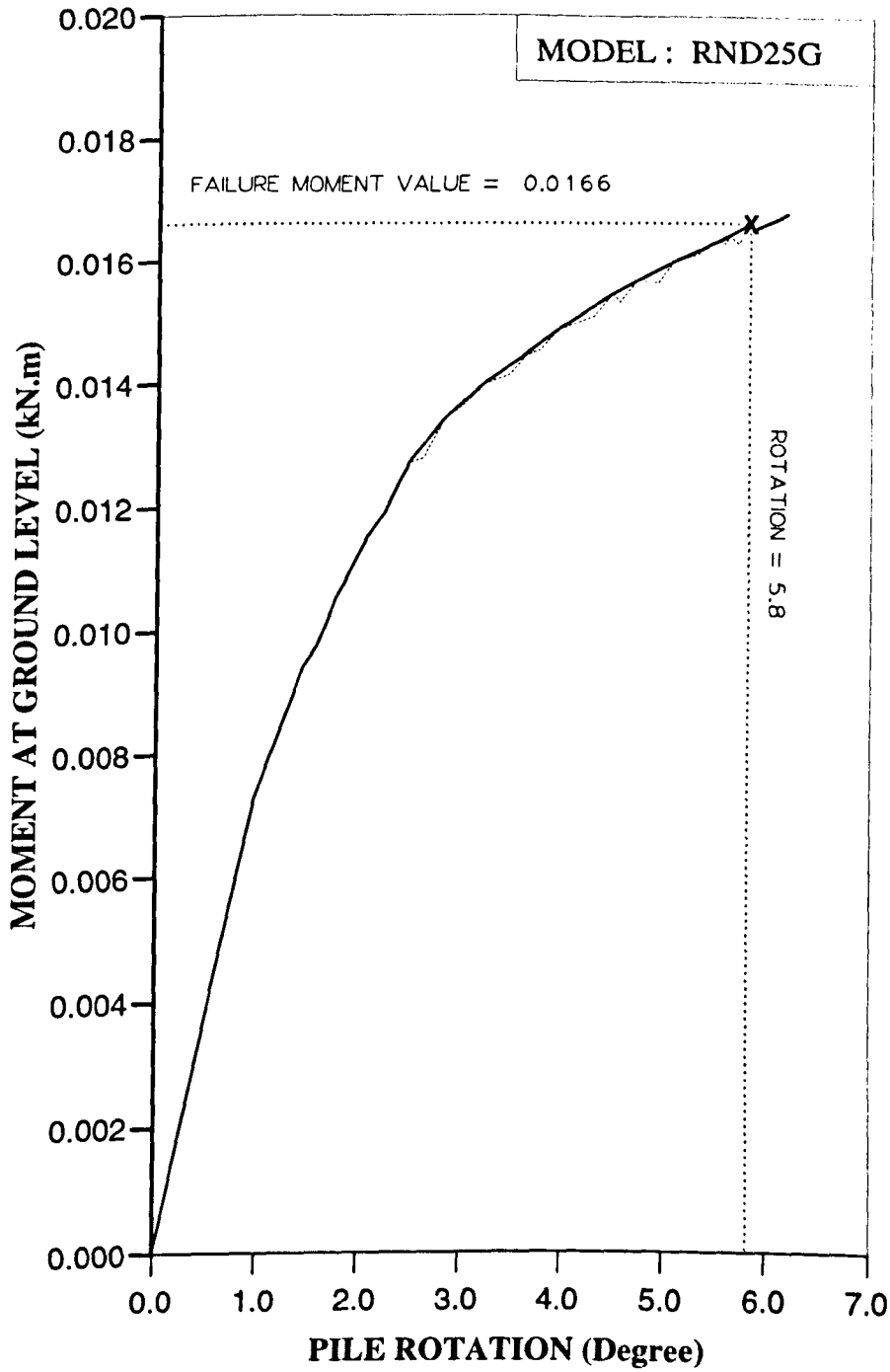

Figure AM58 Variation of moment at ground level with pile rotation for Series 4 test.

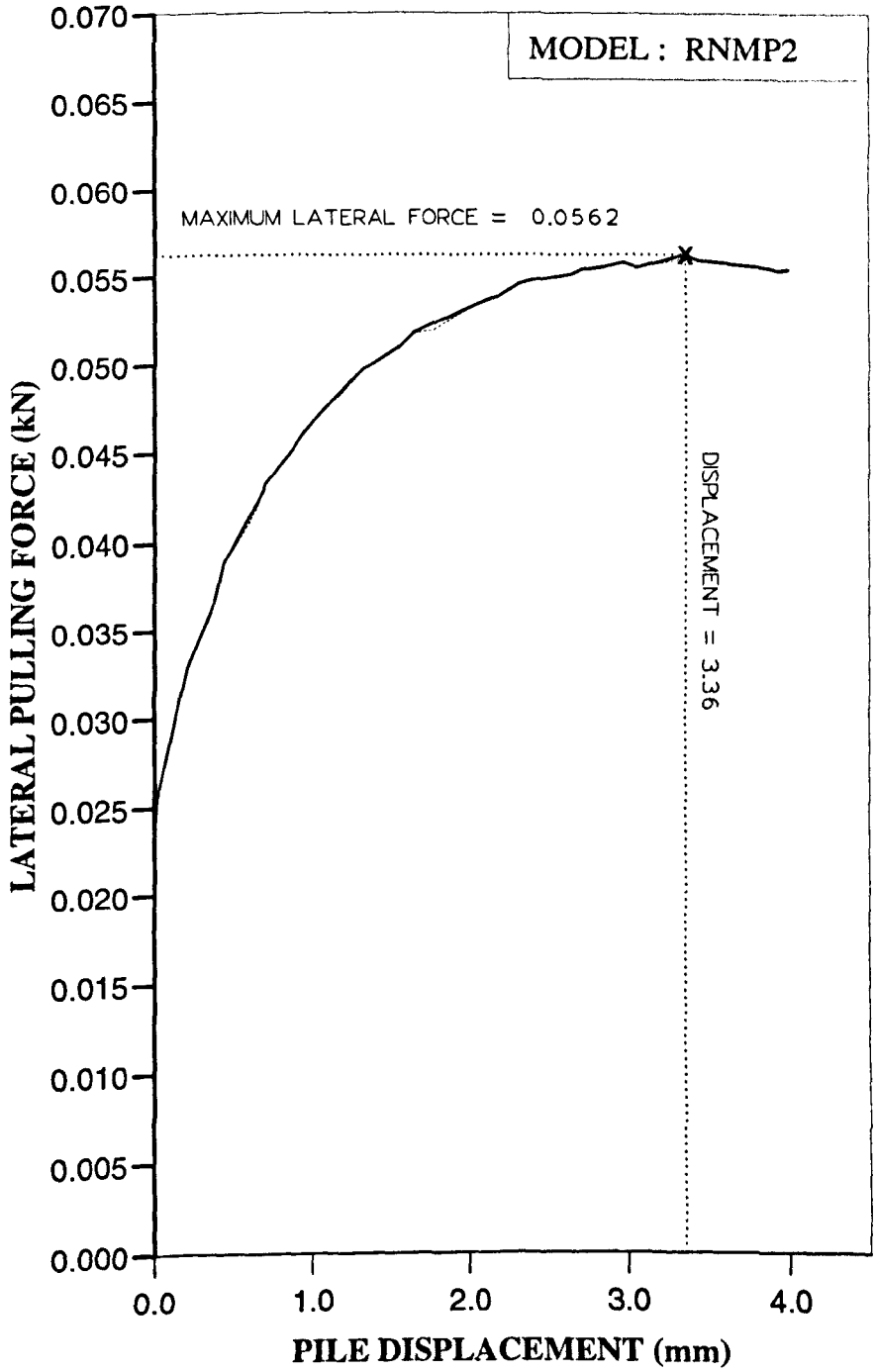

Figure AL59 Variation of lateral force with displacement at ground level for Series 4 test.

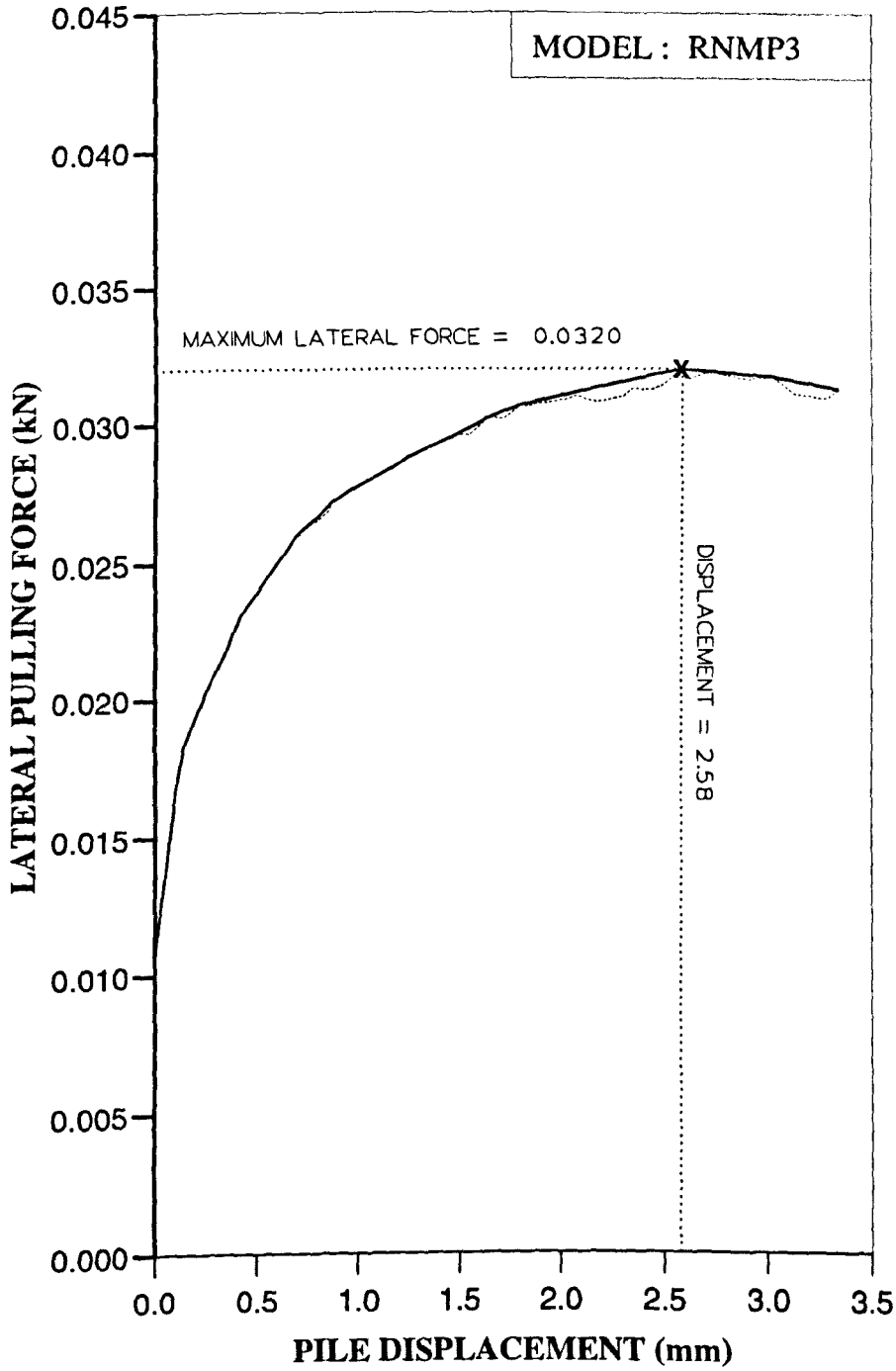

Figure AL60 Variation of lateral force with displacement at ground level for Series 4 test.

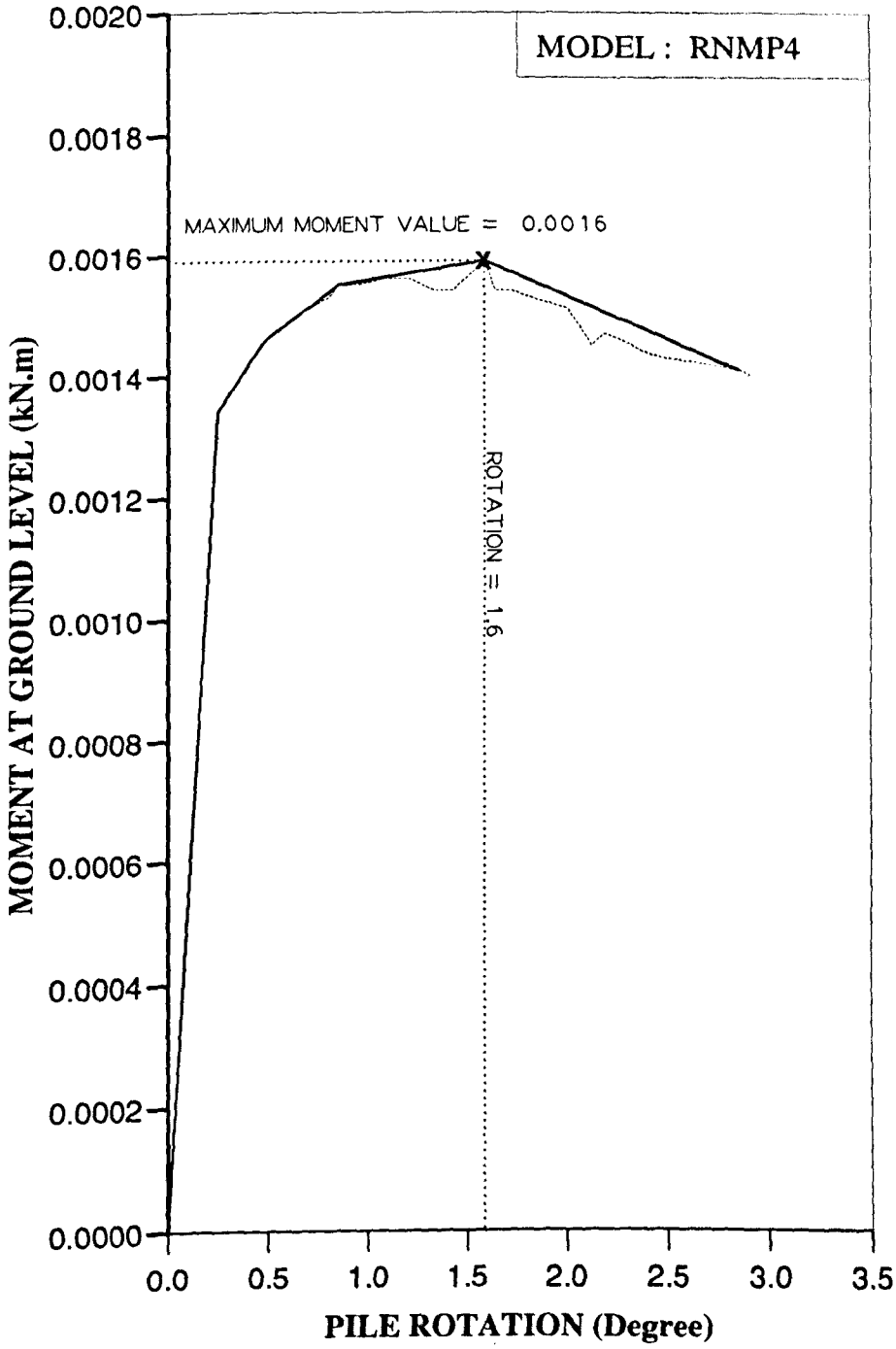

Figure AM61 Variation of moment at ground level with pile rotation for Series 4 test.

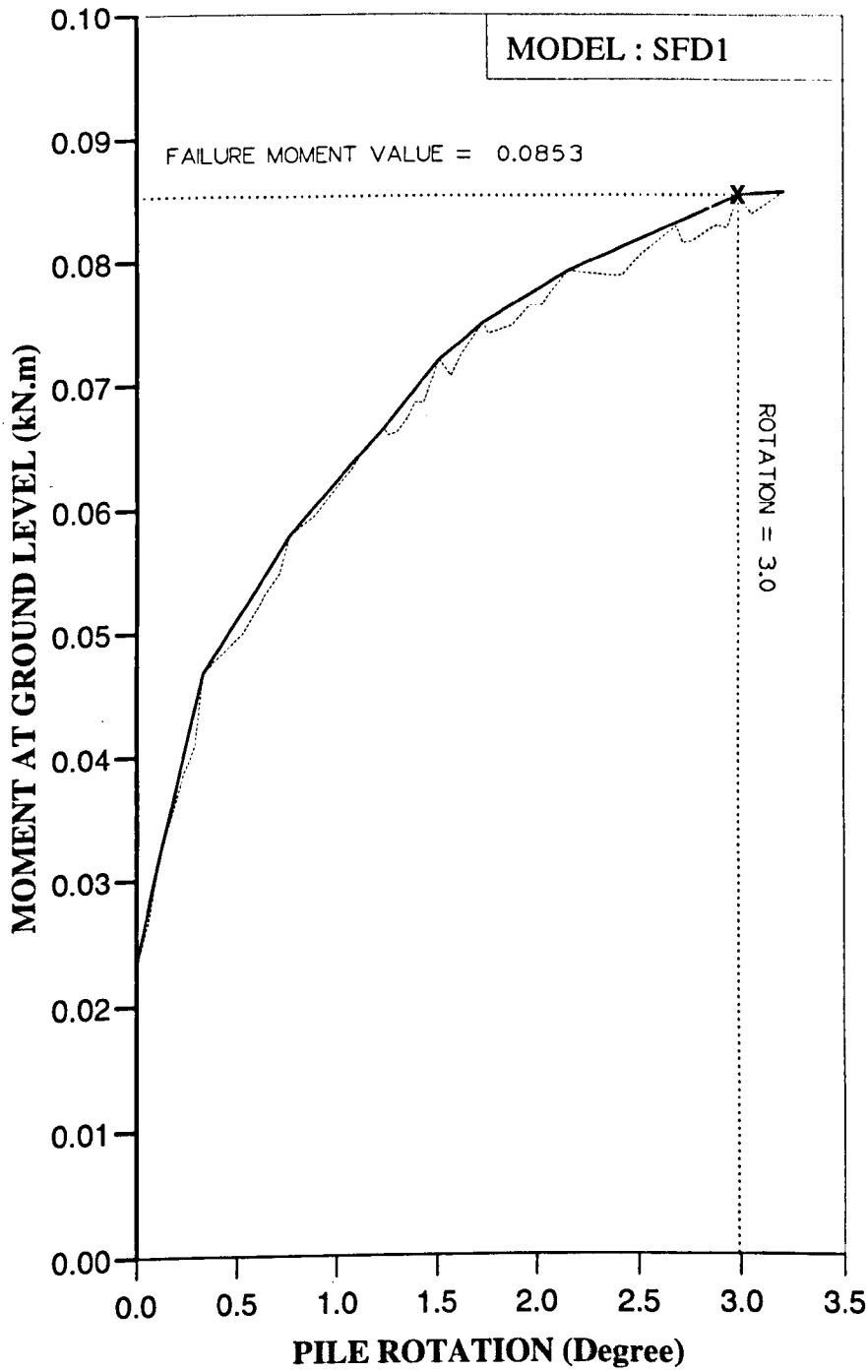

Figure AM62 Variation of moment at ground level with pile rotation for Series 5 test.

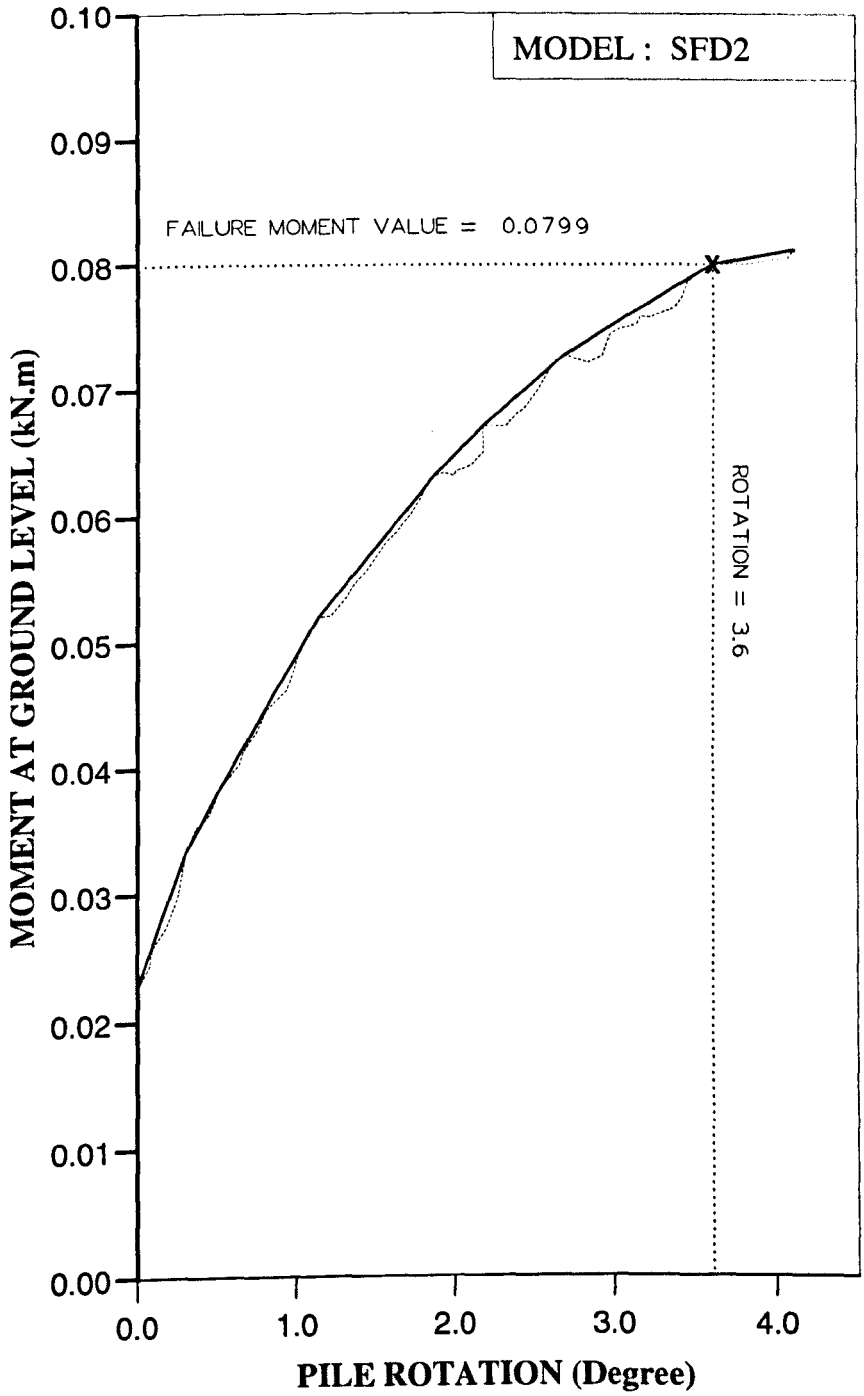

Figure AM63 Variation of moment at ground level with pile rotation for Series 5 test.

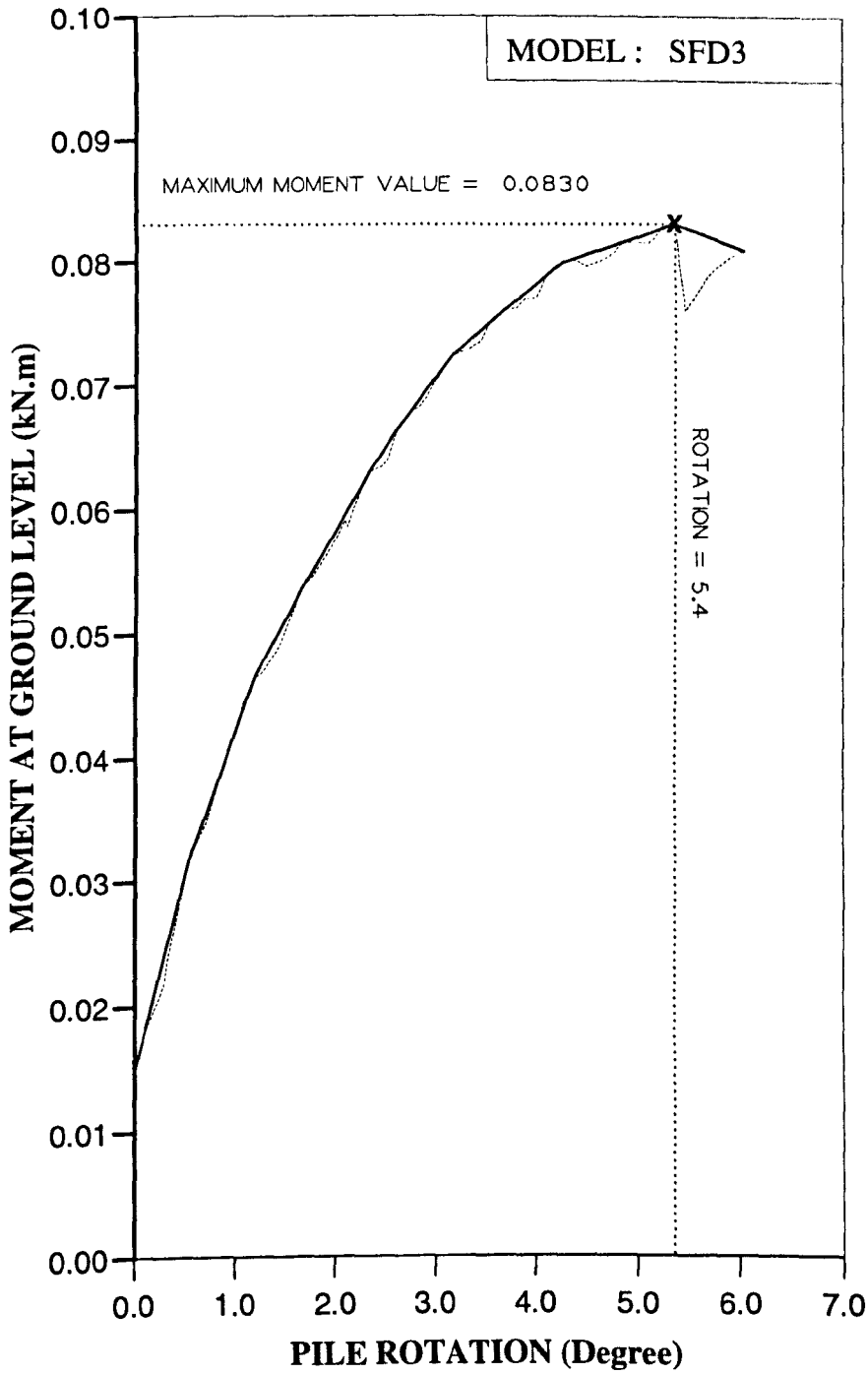

Figure AM64 Variation of moment at ground level with pile rotation for Series 5 test.

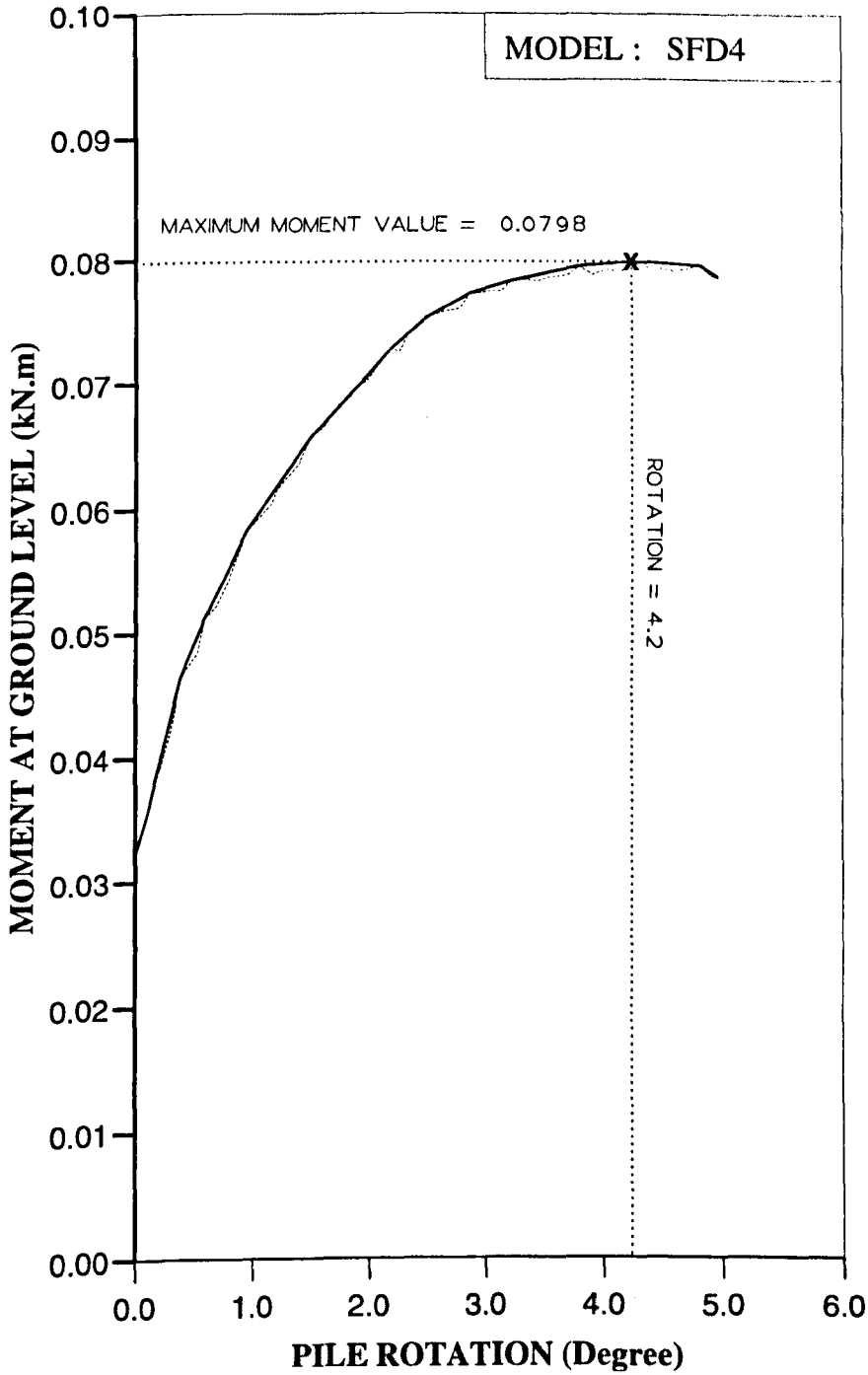

Figure AM65 Variation of moment at ground level with pile rotation for Series 5 test.

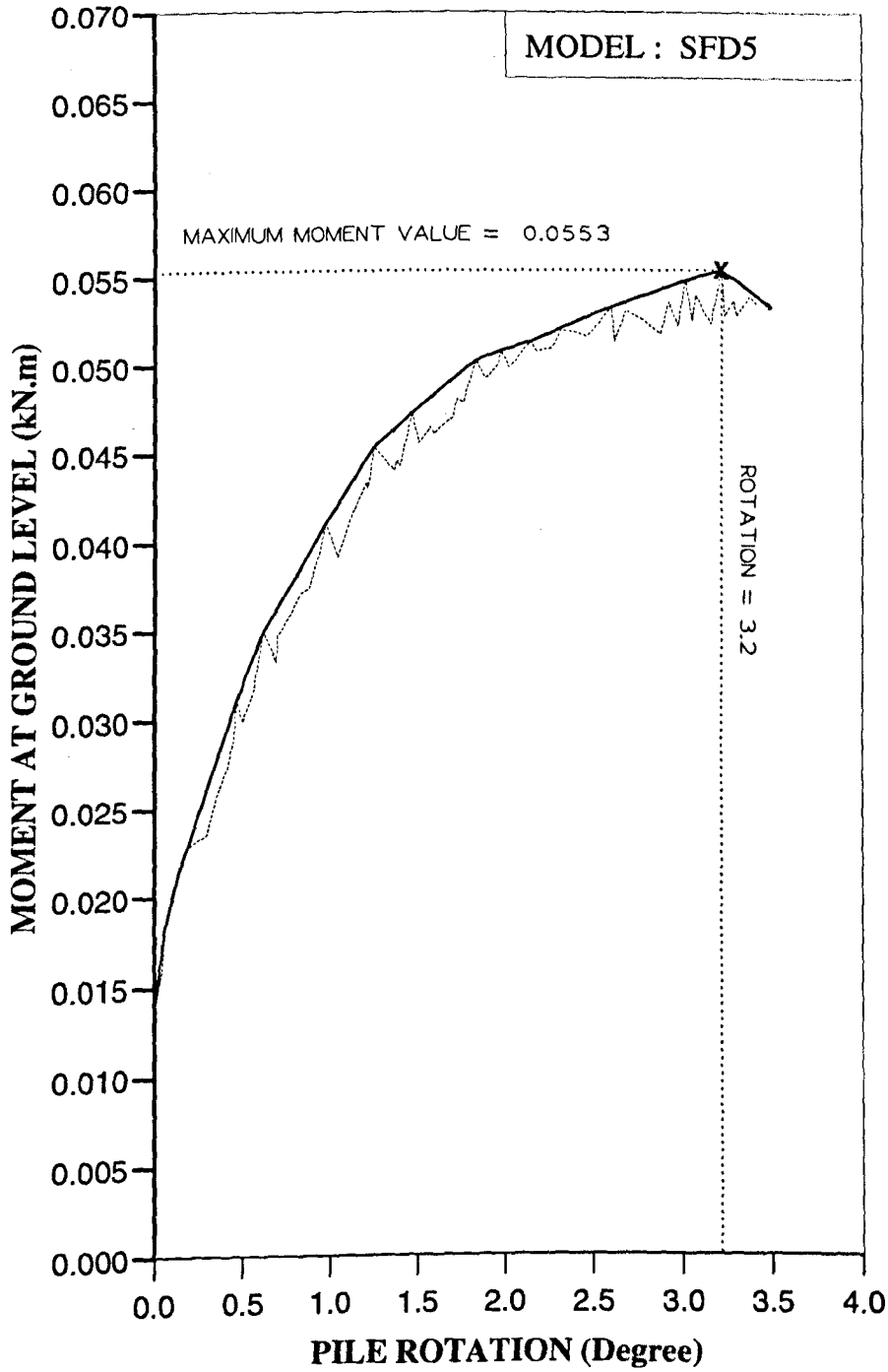

Figure AM66 Variation of moment at ground level with pile rotation for Series 5 test.

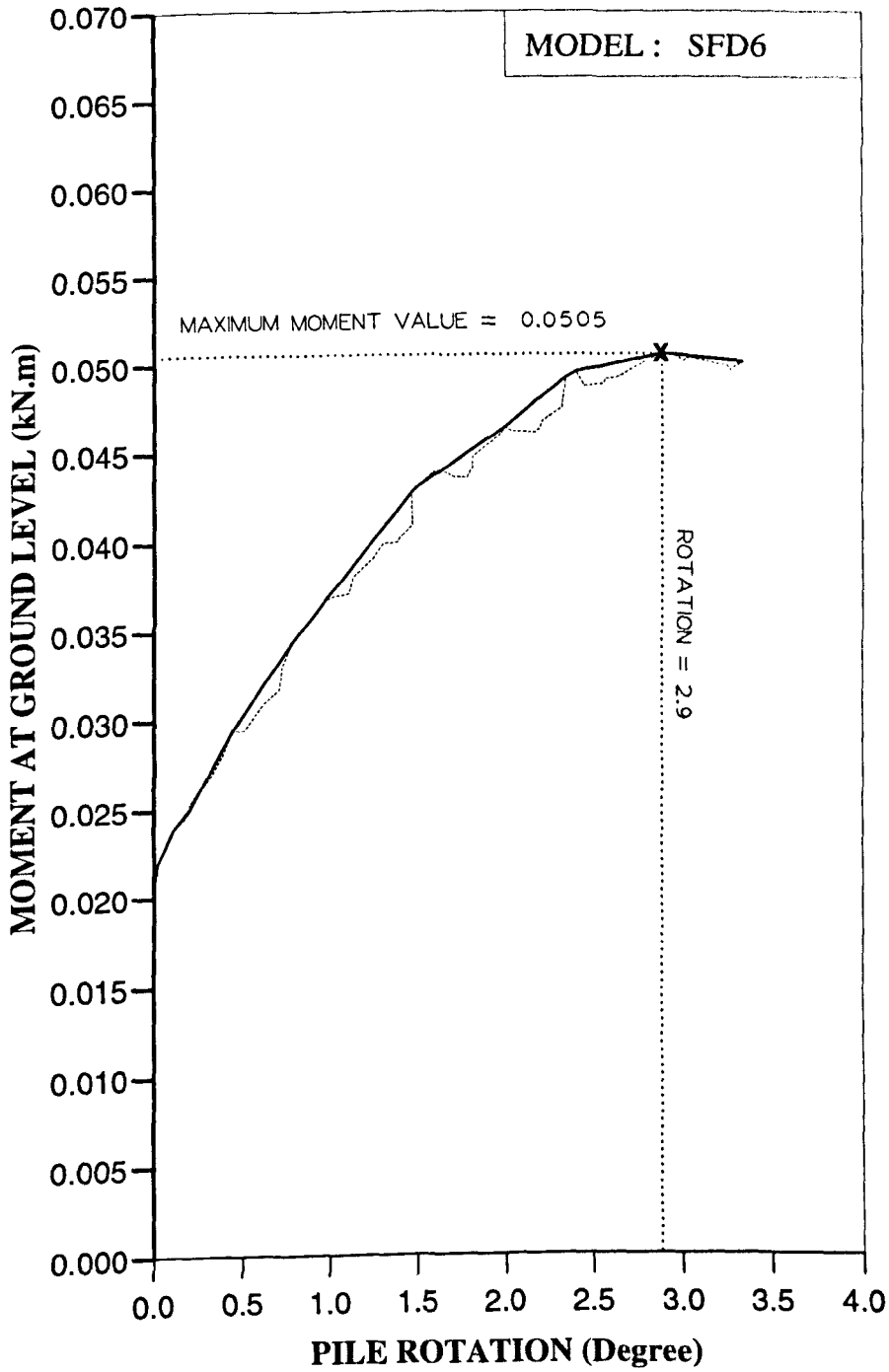

Figure AM67 Variation of moment at ground level with pile rotation for Series 5 test.

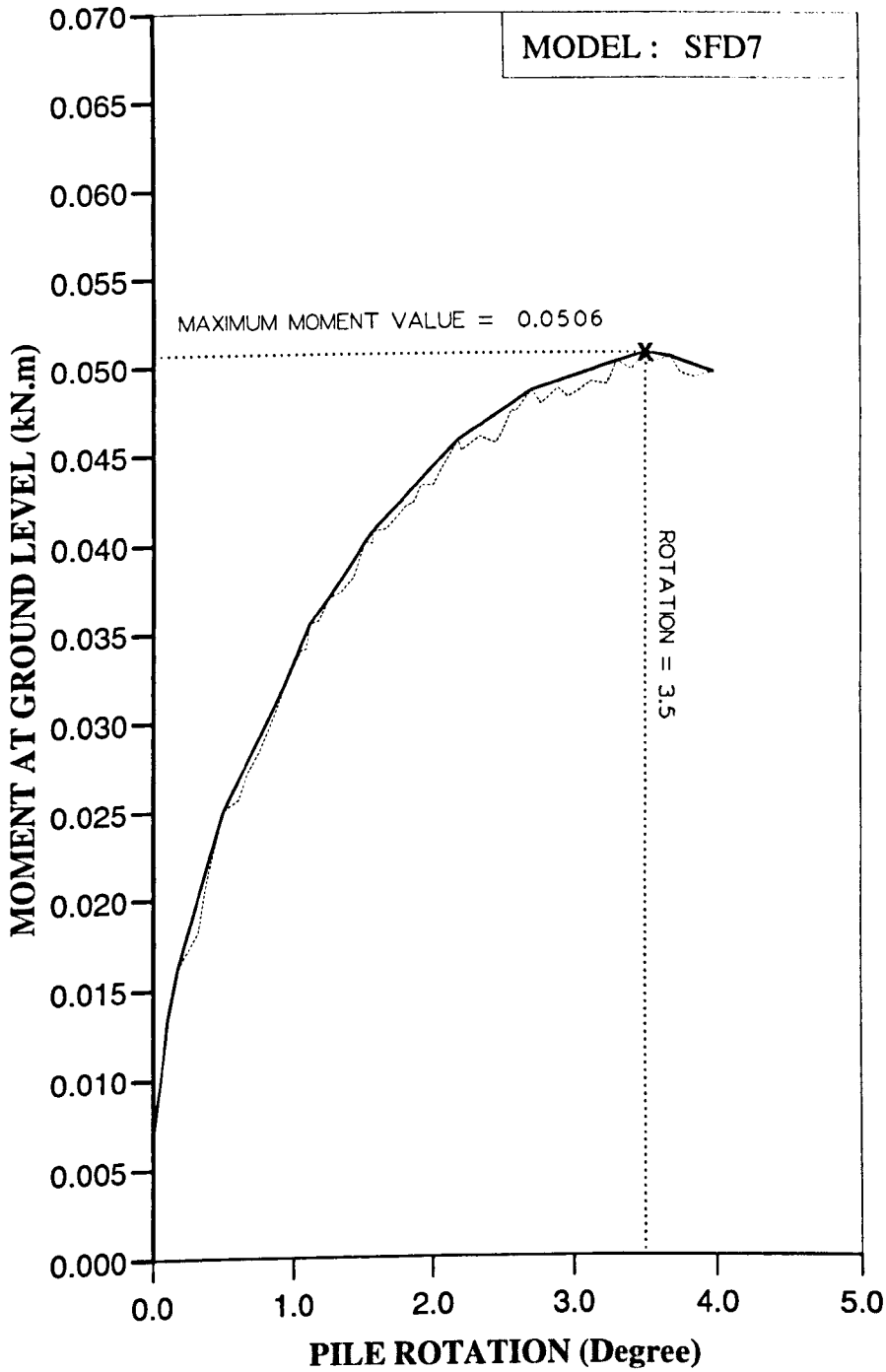

Figure AM68 Variation of moment at ground level with pile rotation for Series 5 test.

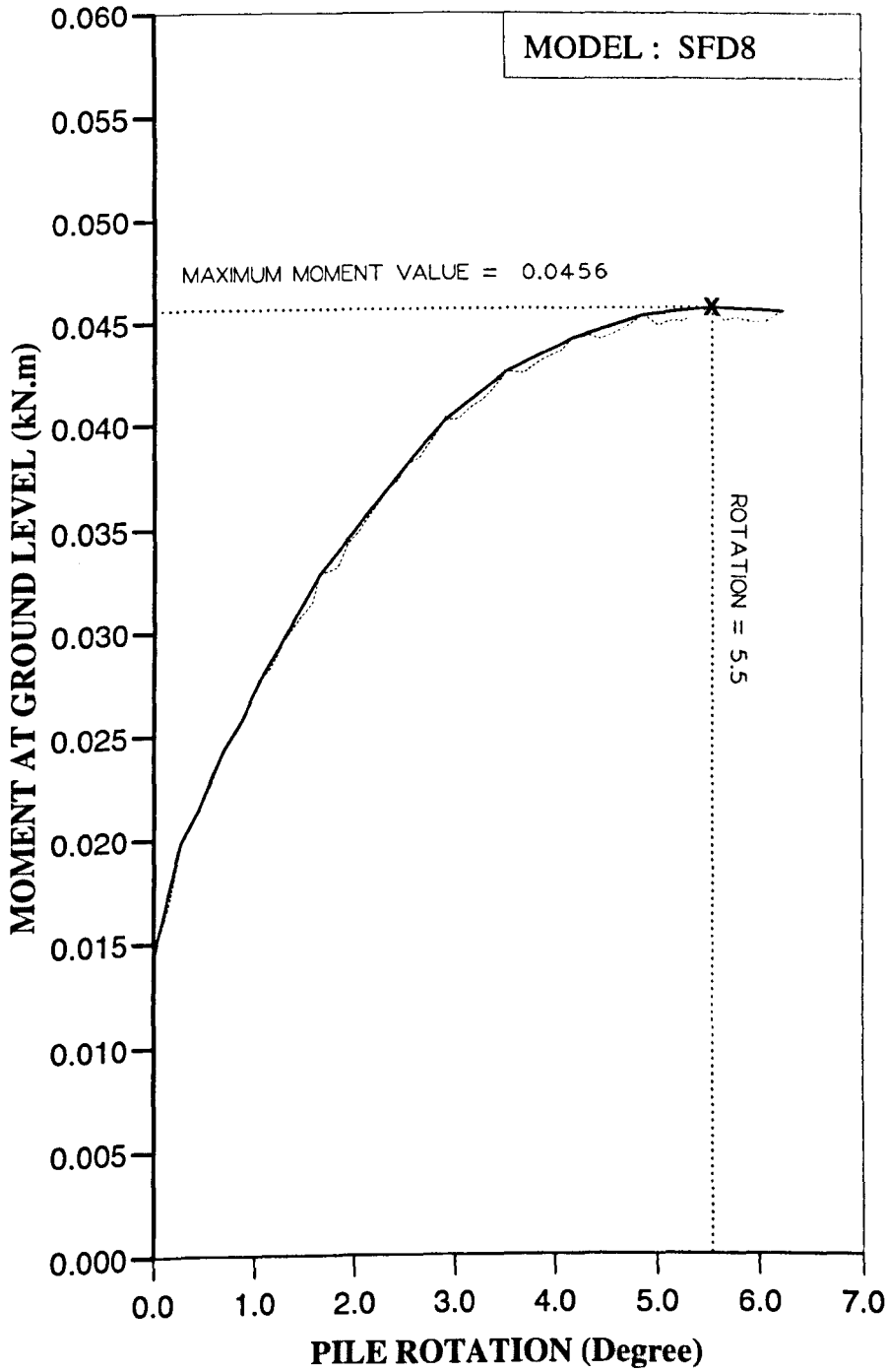

Figure AM69 Variation of moment at ground level with pile rotation for Series 5 test.

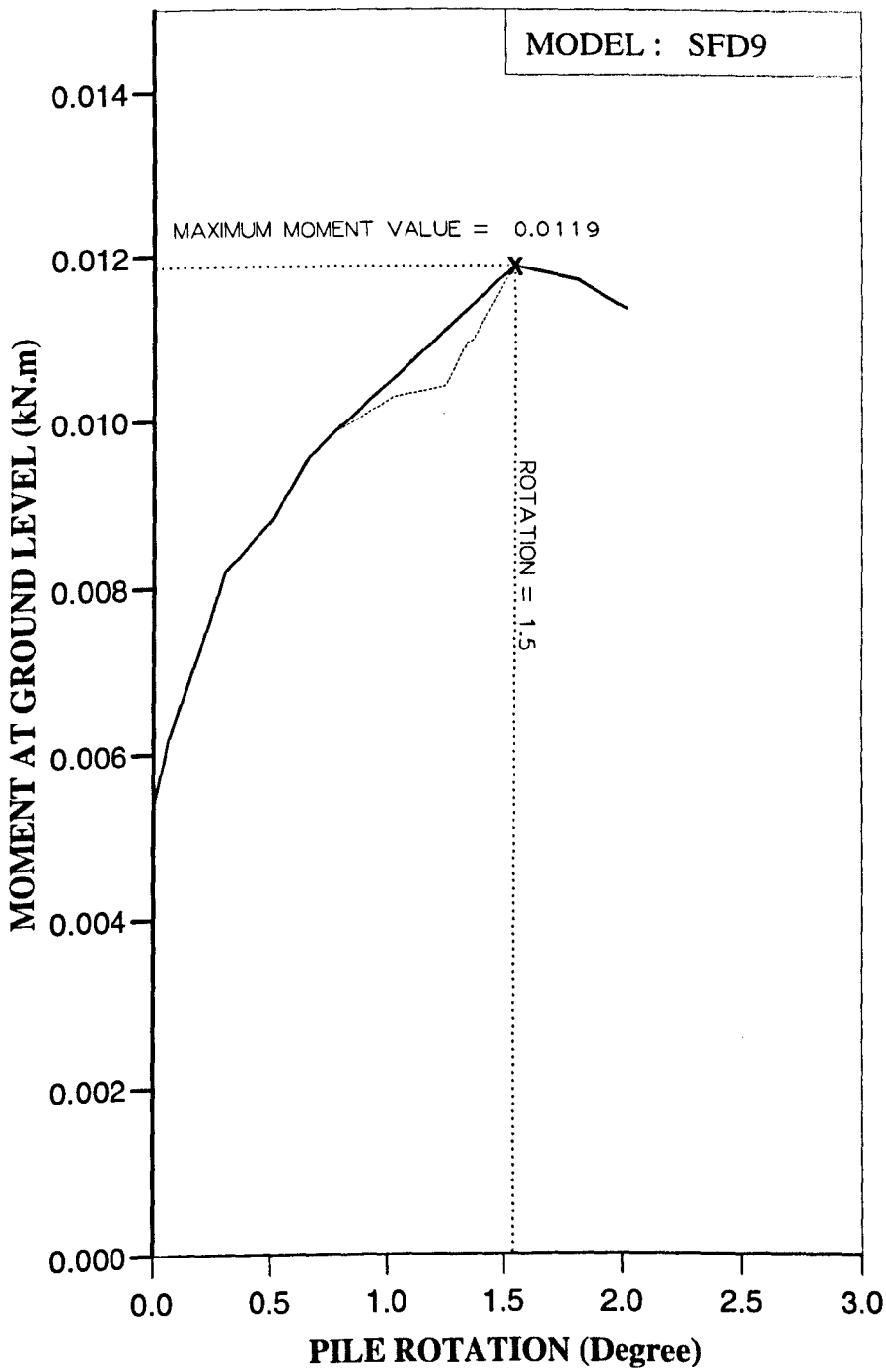

Figure AM70 Variation of moment at ground level with pile rotation for Series 5 test.

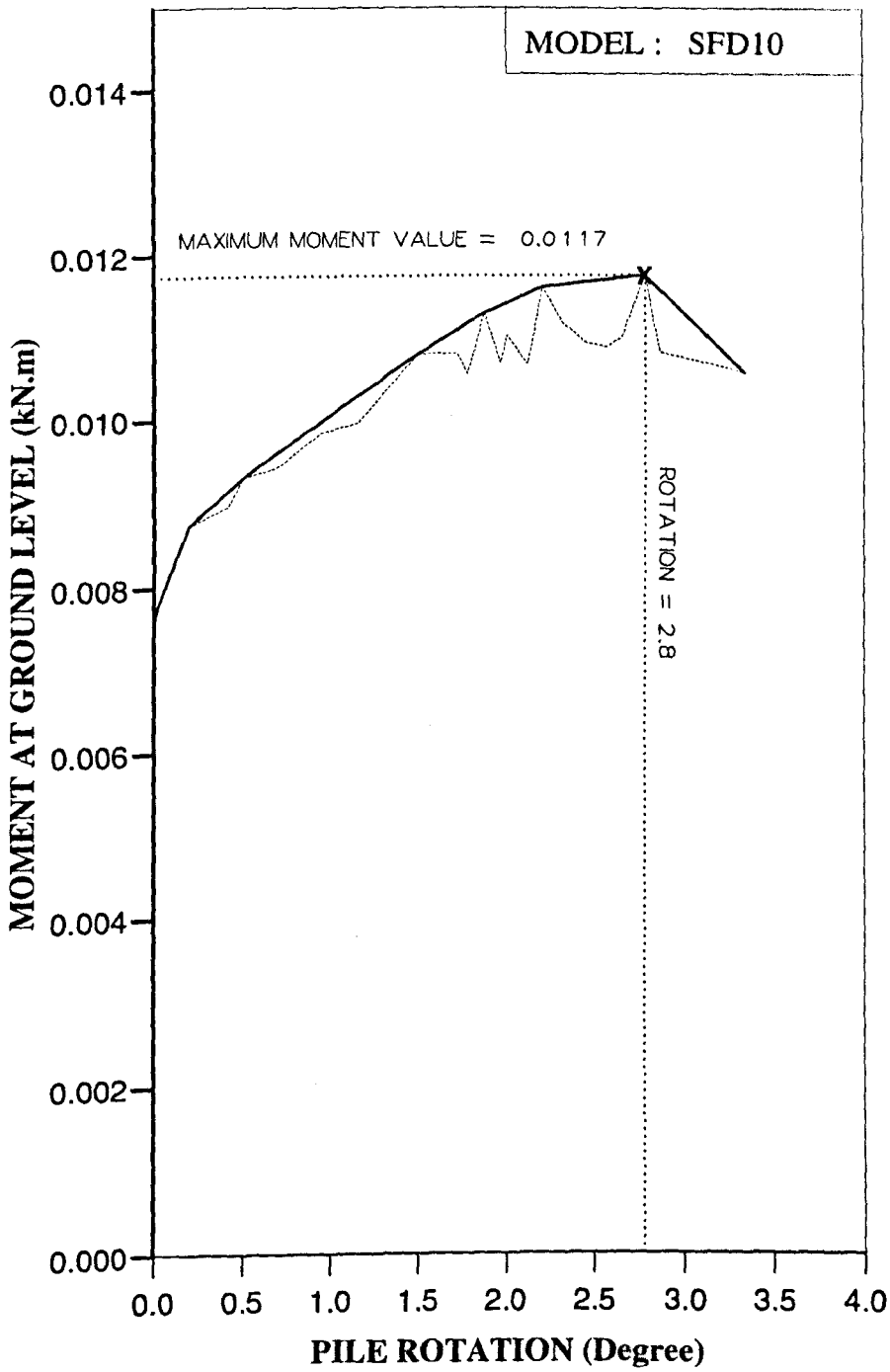

Figure AM71 Variation of moment at ground level with pile rotation for Series 5 test.

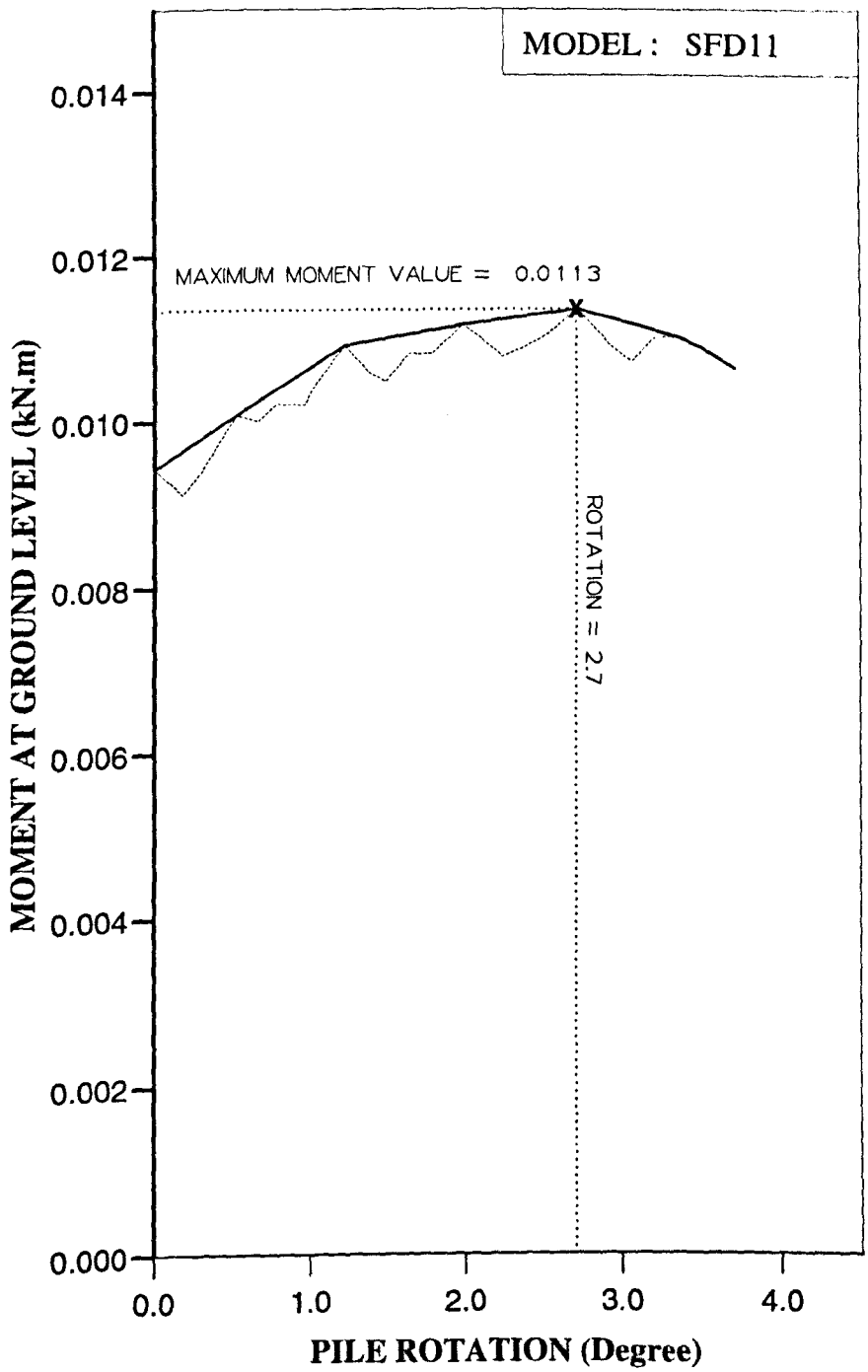

Figure AM72 Variation of moment at ground level with pile rotation for Series 5 test.

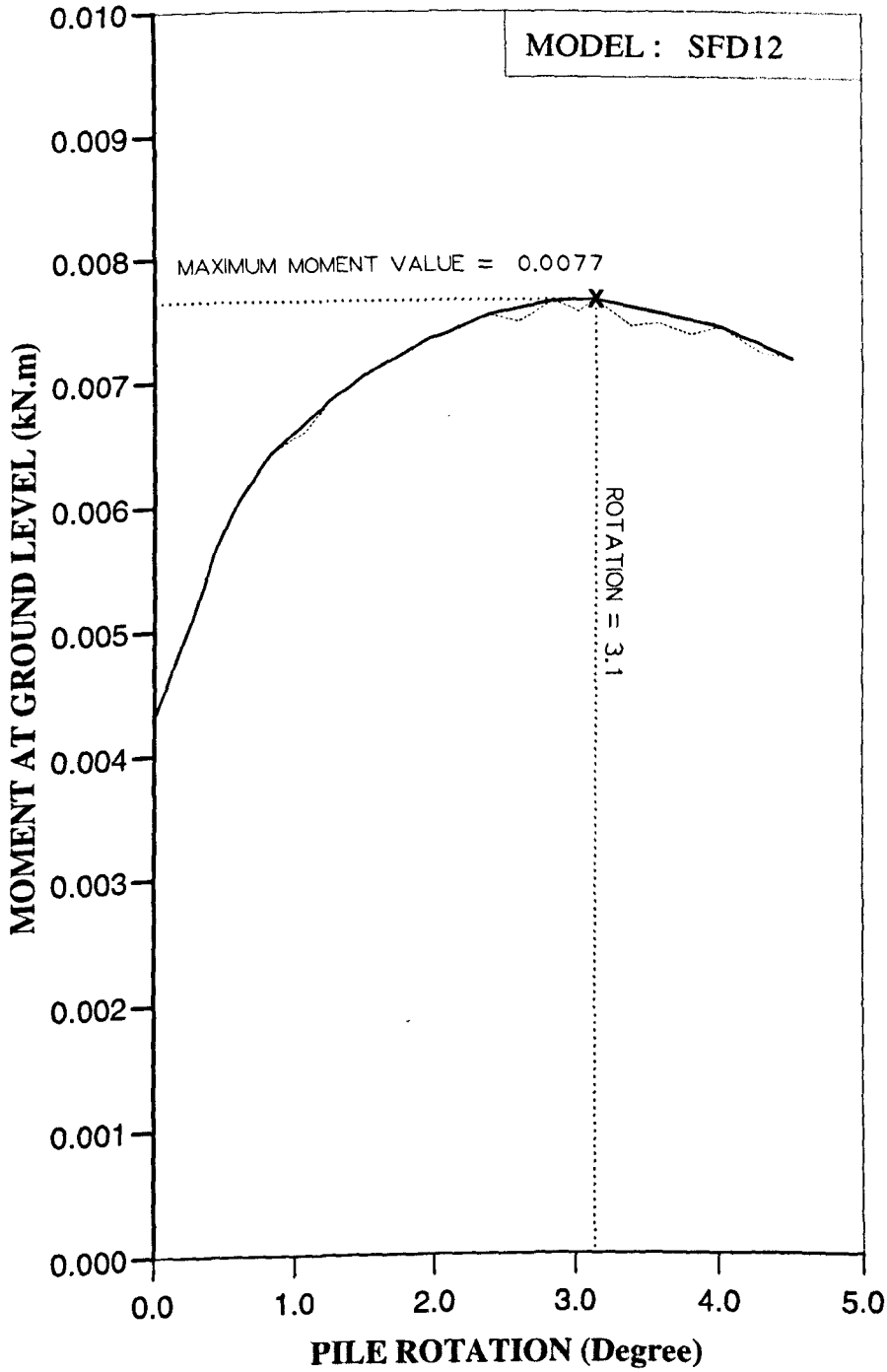

Figure AM73 Variation of moment at ground level with pile rotation for Series 5 test.

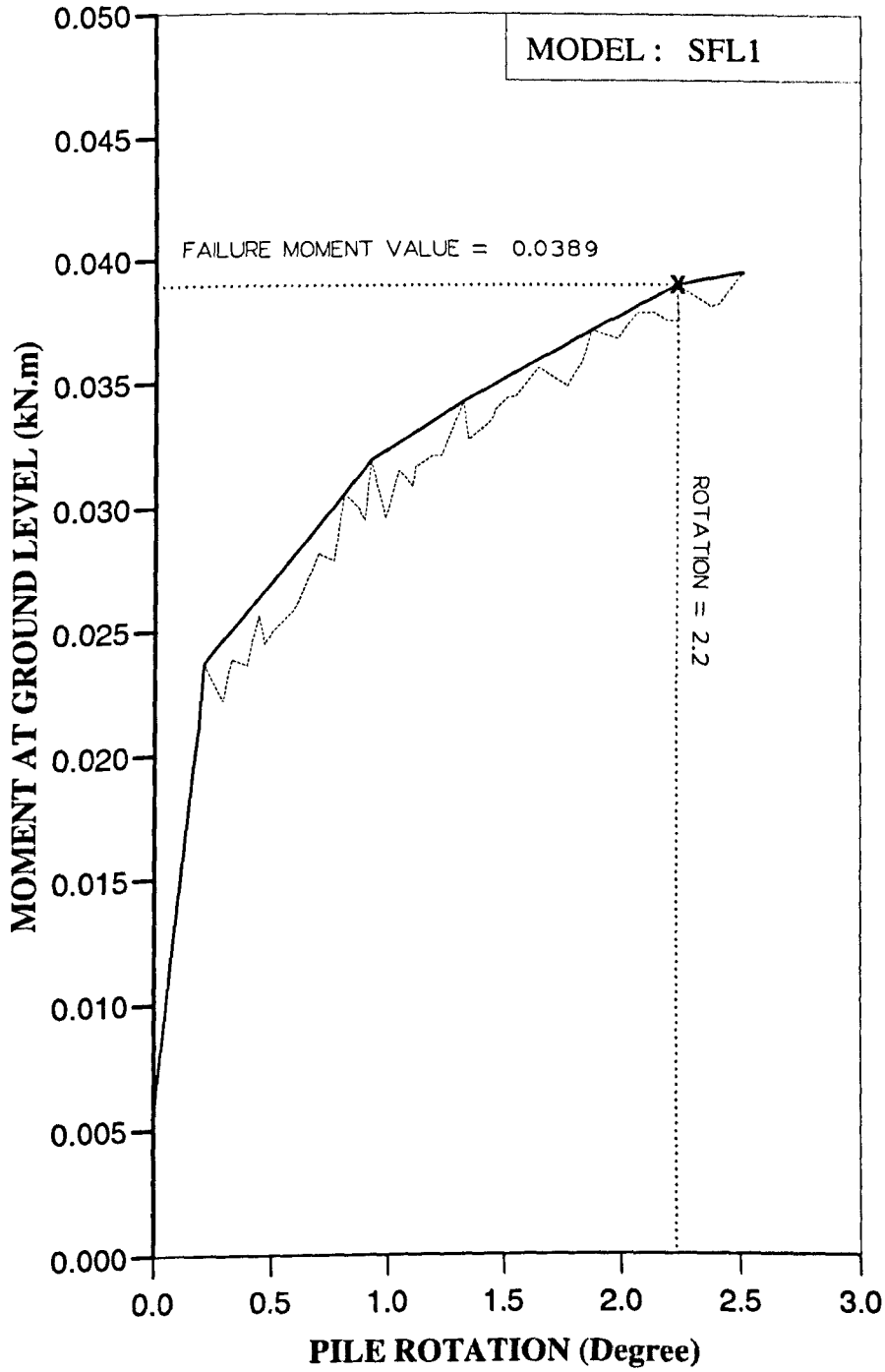

Figure AM74 Variation of moment at ground level with pile rotation for Series 5 test.

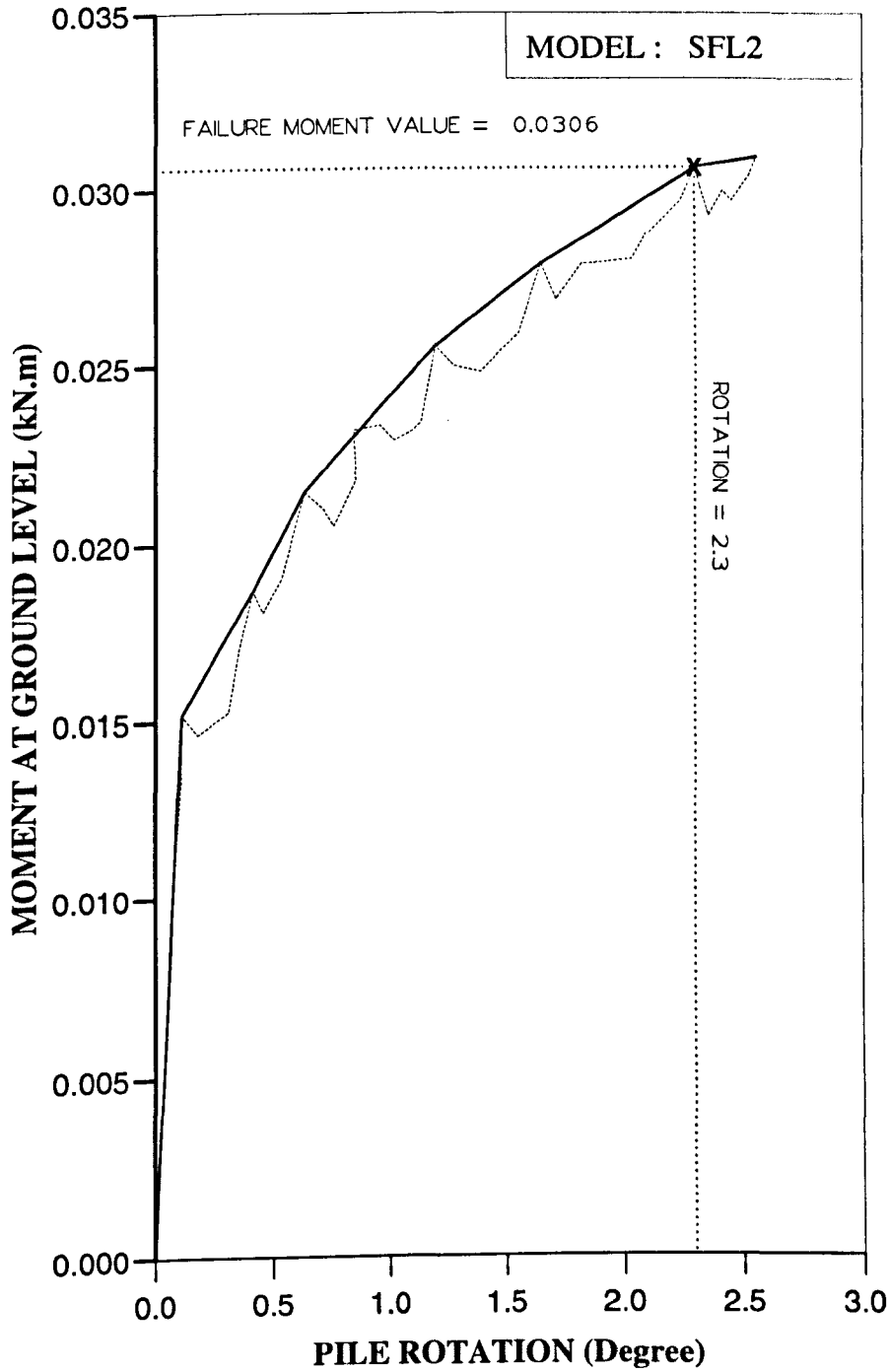

Figure AM75 Variation of moment at ground level with pile rotation for Series 5 test.

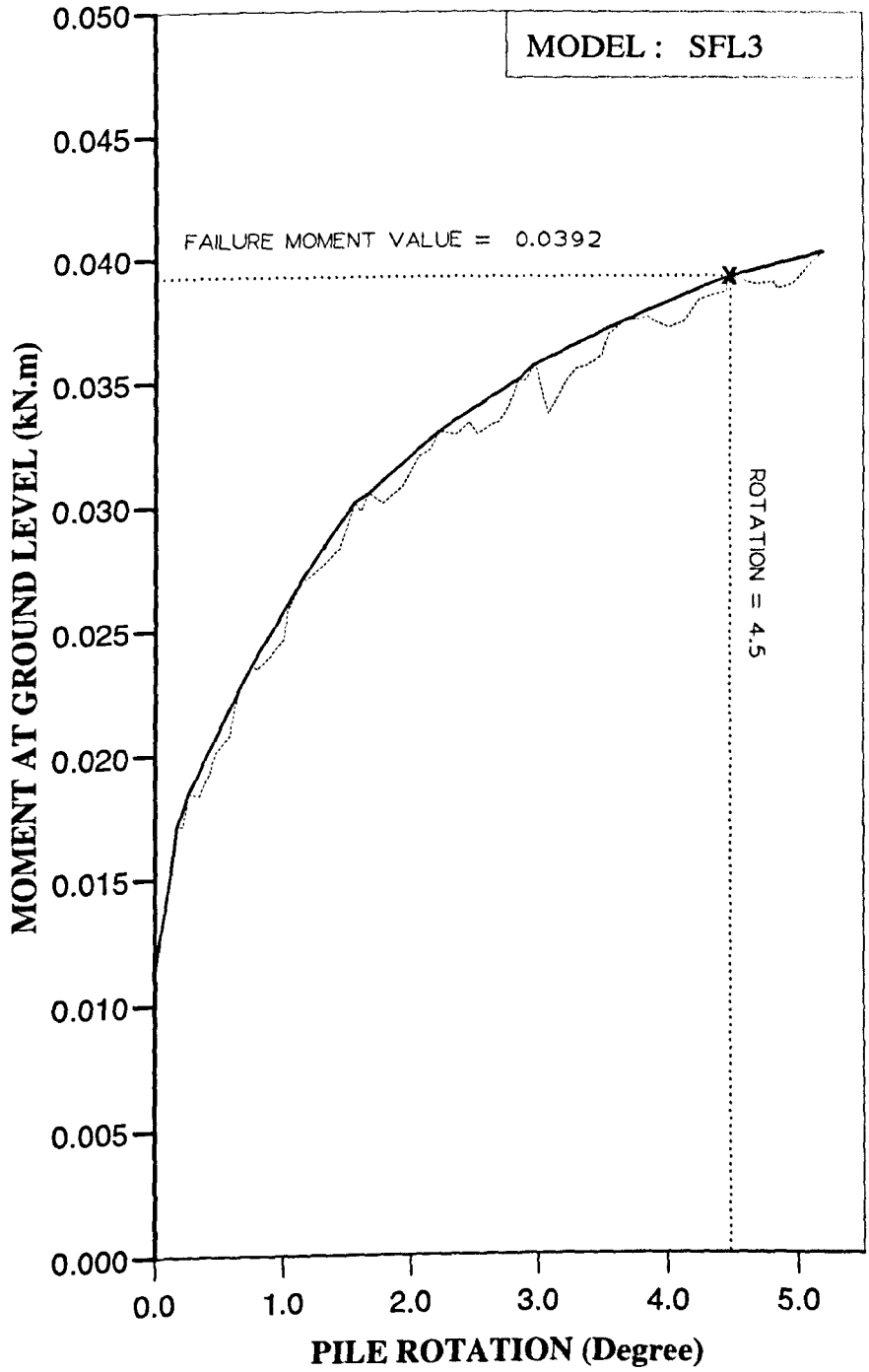

Figure AM76 Variation of moment at ground level with pile rotation for Series 5 test.

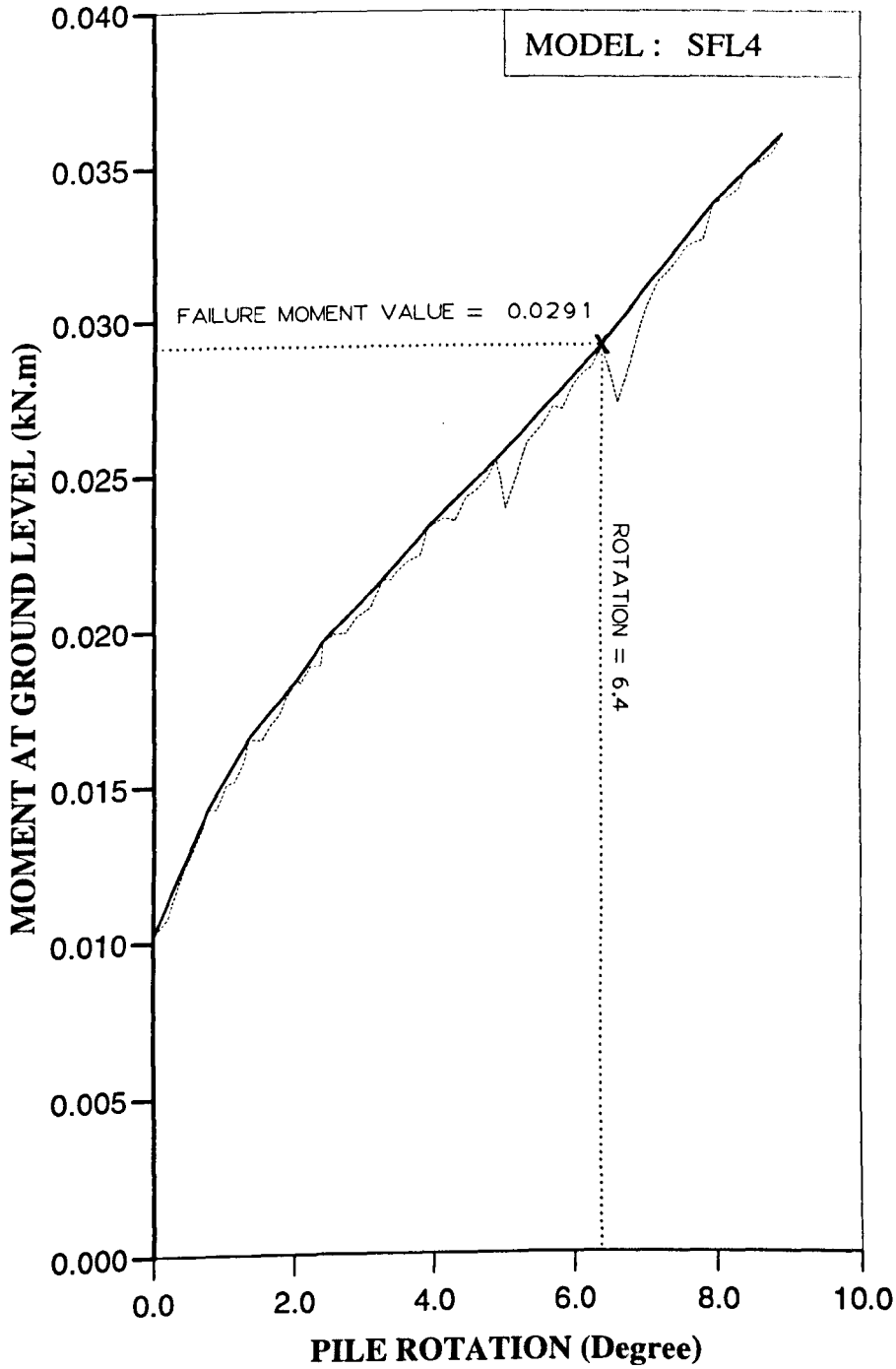

Figure AM77 Variation of moment at ground level with pile rotation for Series 5 test.

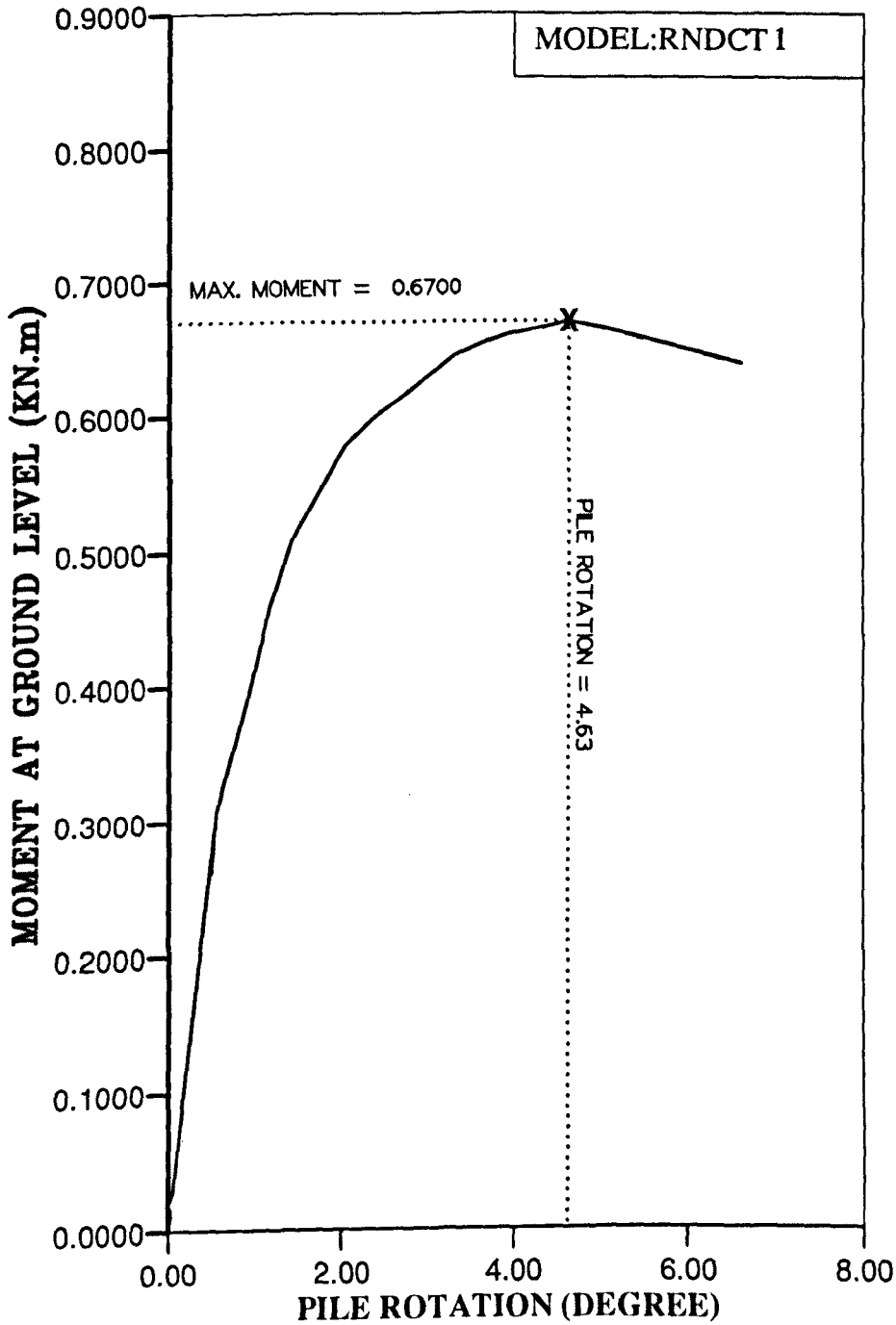

Figure AM78 Variation of moment at ground level with pile rotation for Series 1 test.

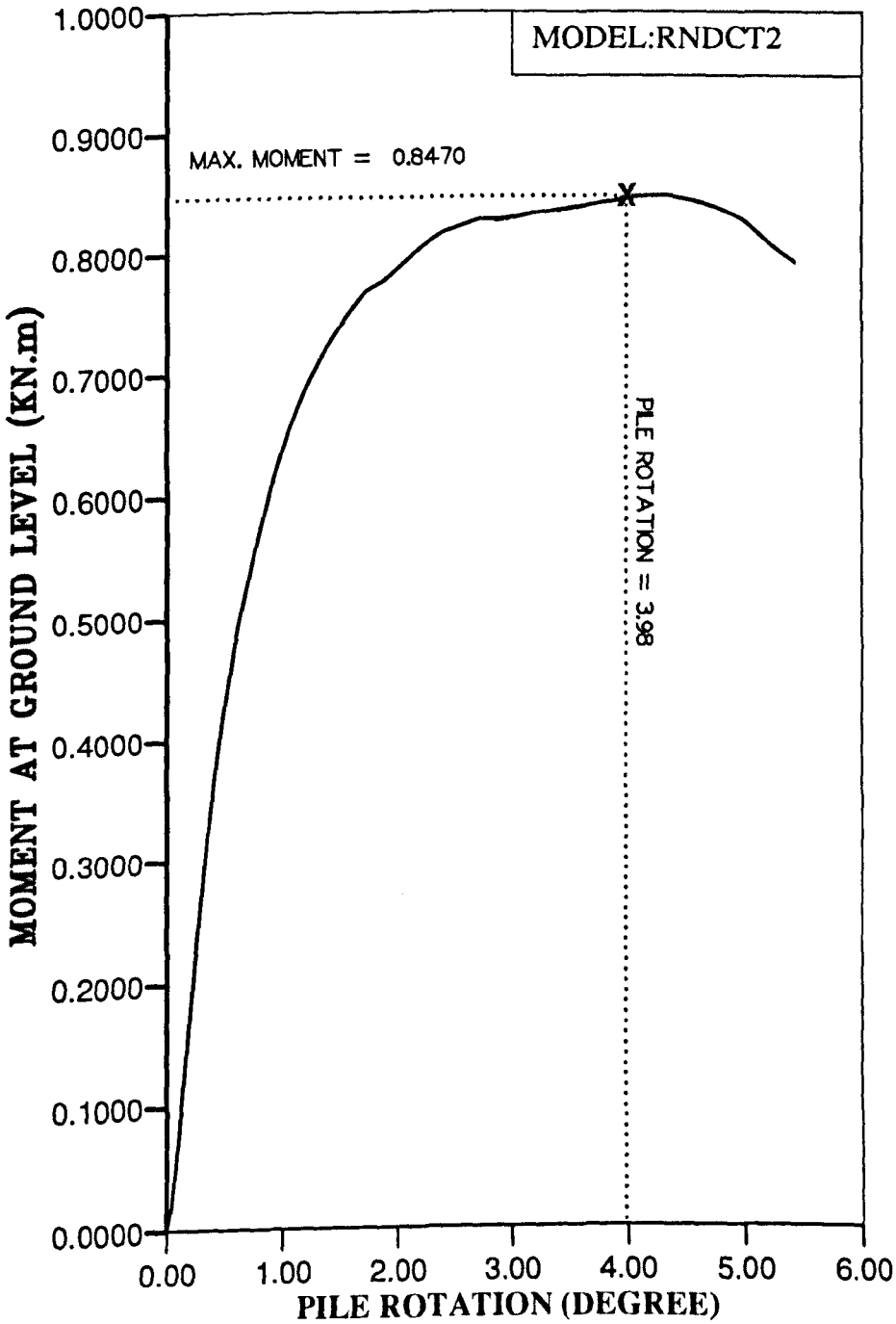

Figure AM79 Variation of moment at ground level with pile rotation for Series 1 test.

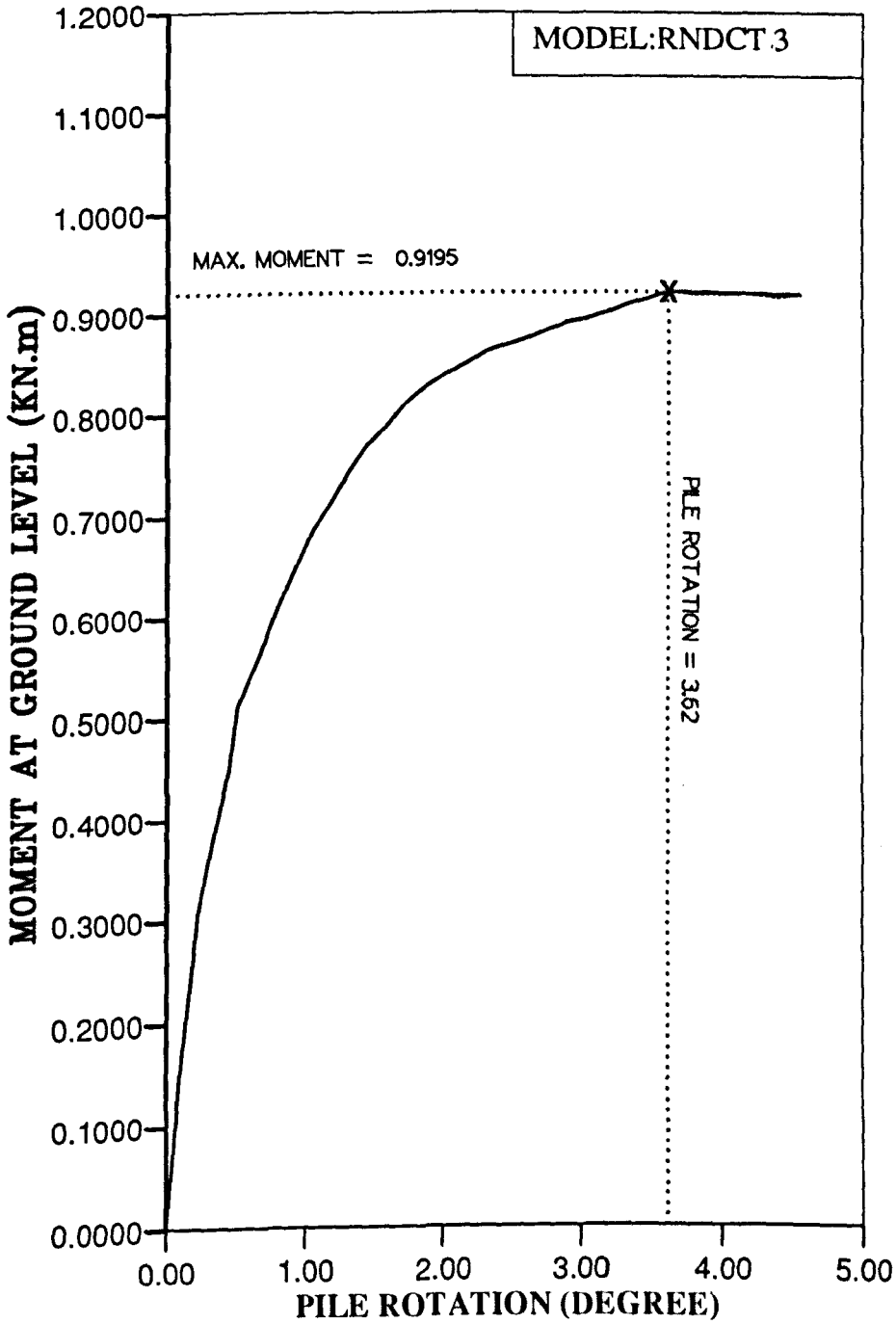

Figure AM80 Variation of moment at ground level with pile rotation for Series 1 test.

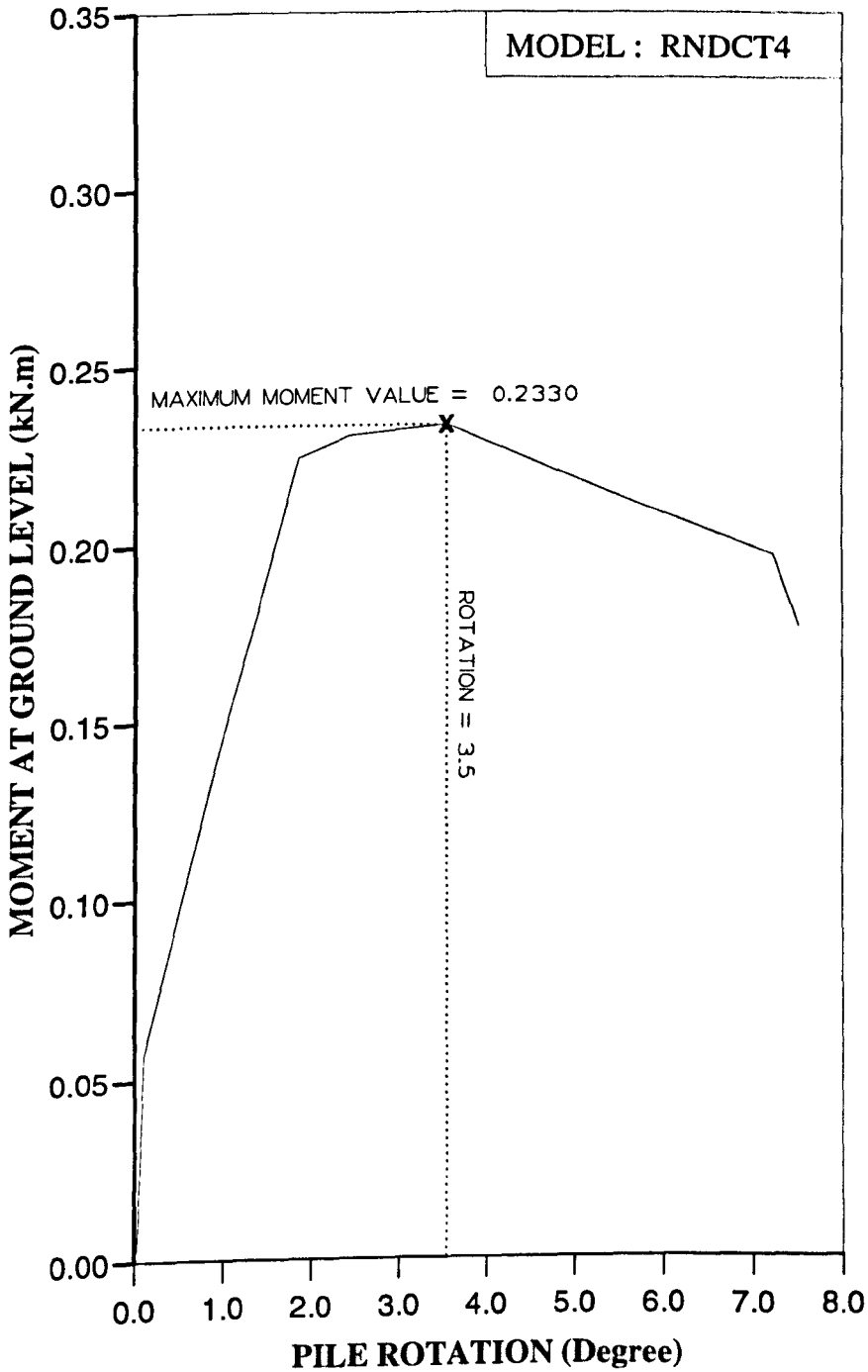

Figure AM81 Variation of moment at ground level with pile rotation for Series 1 test.

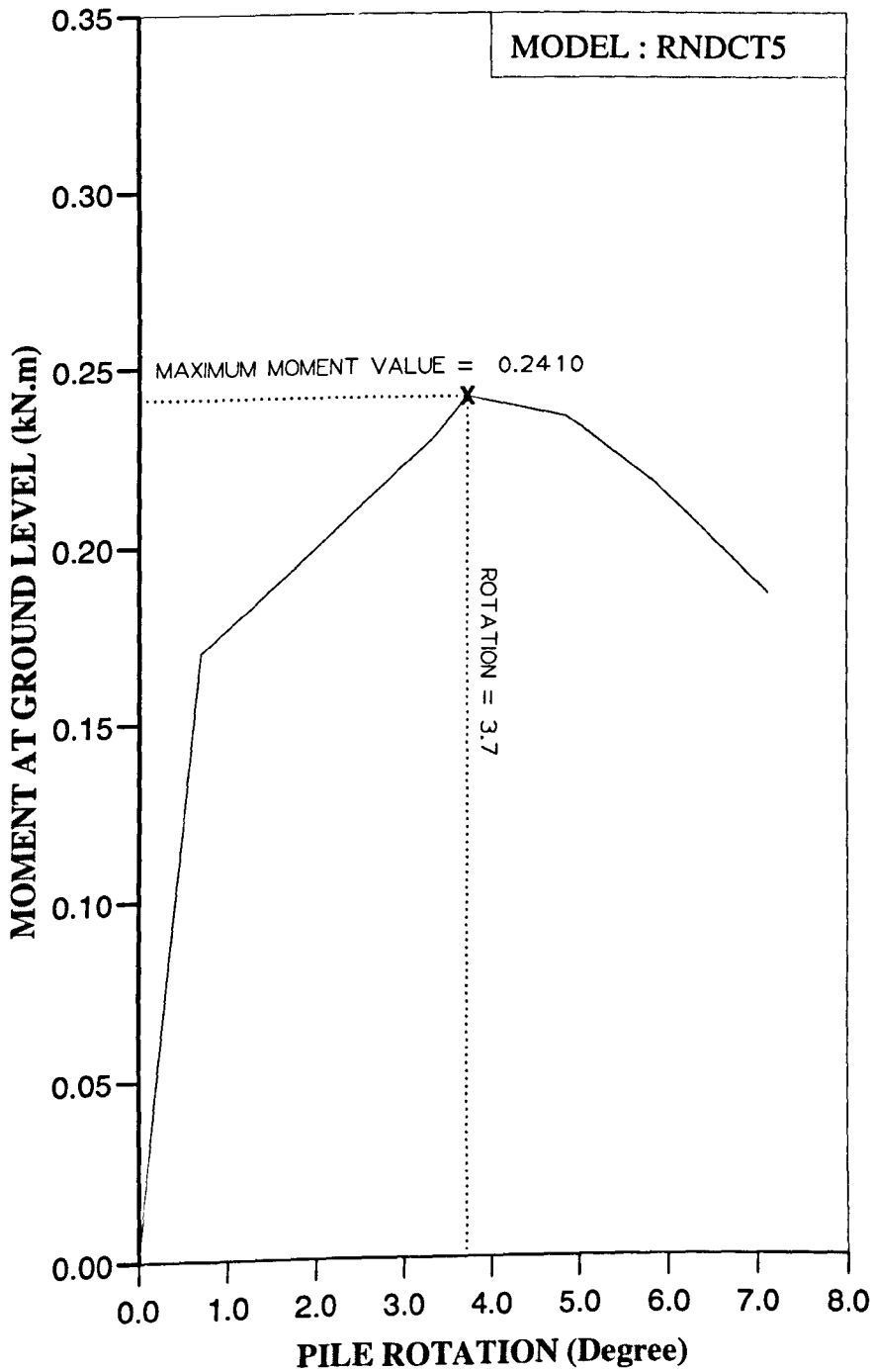

Figure AM82 Variation of moment at ground level with pile rotation for Series 1 test.

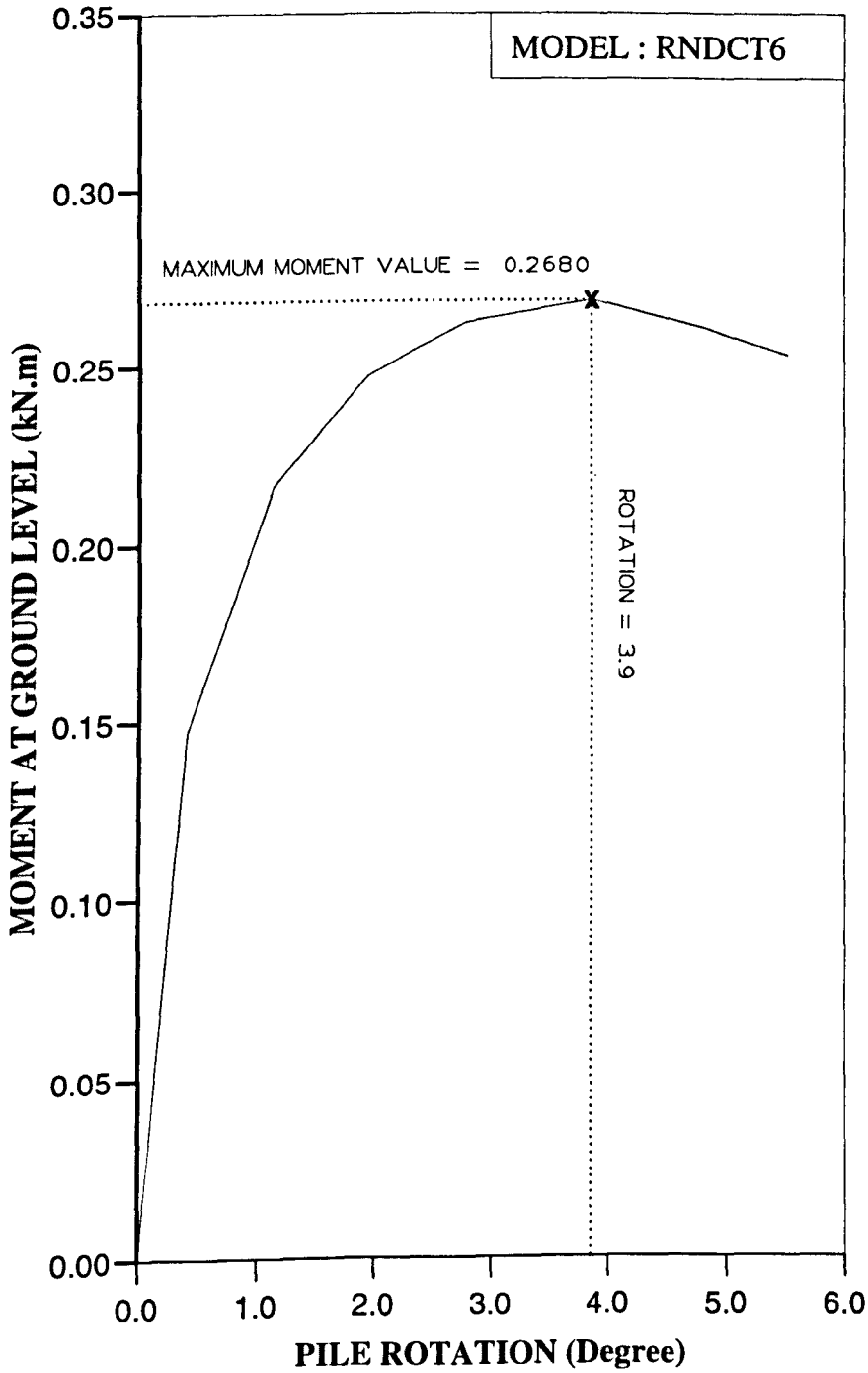

Figure AM83 Variation of moment at ground level with pile rotation for Series 1 test.

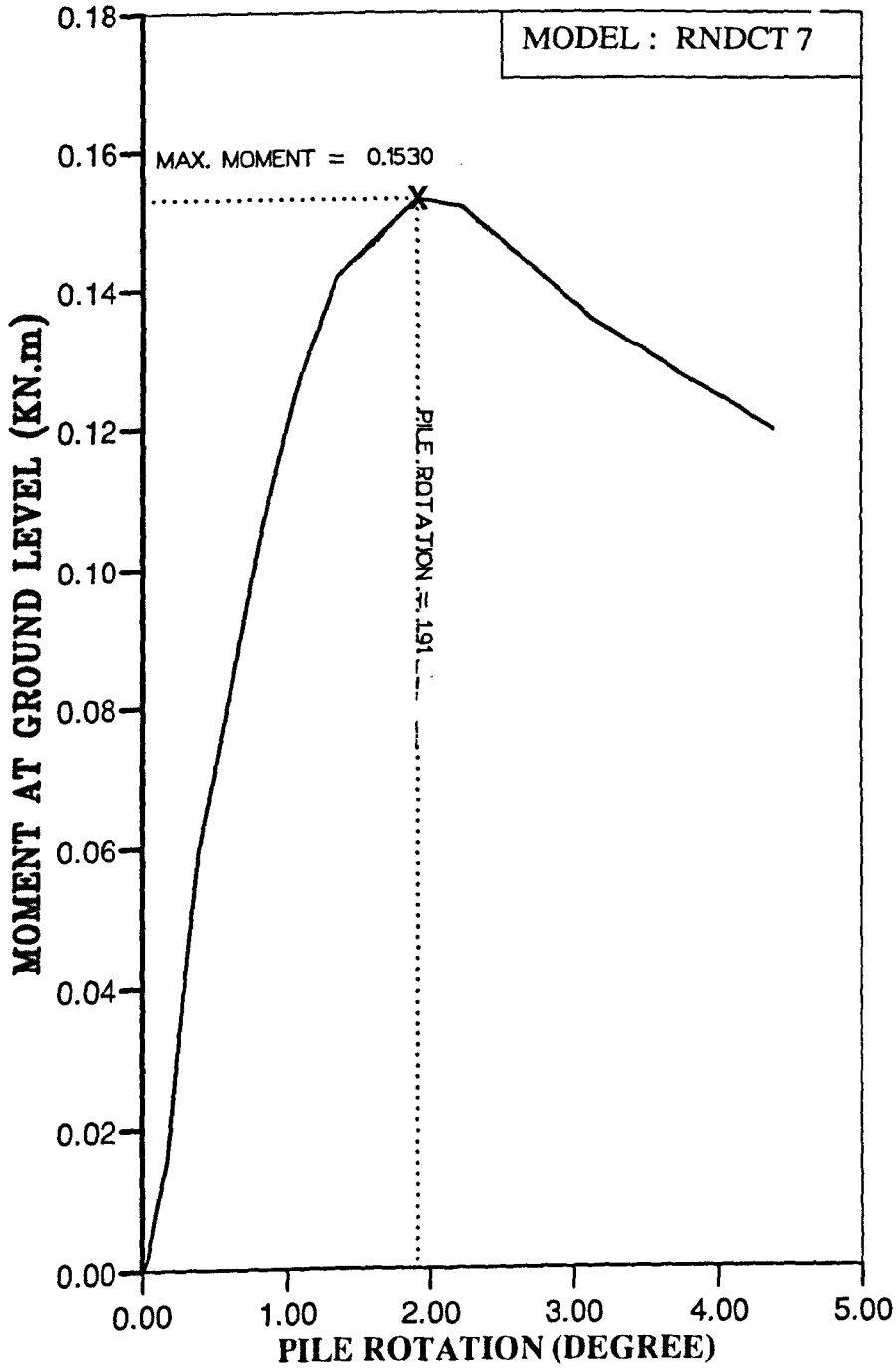

Figure AM84 Variation of moment at ground level with pile rotation for Series 1 test.

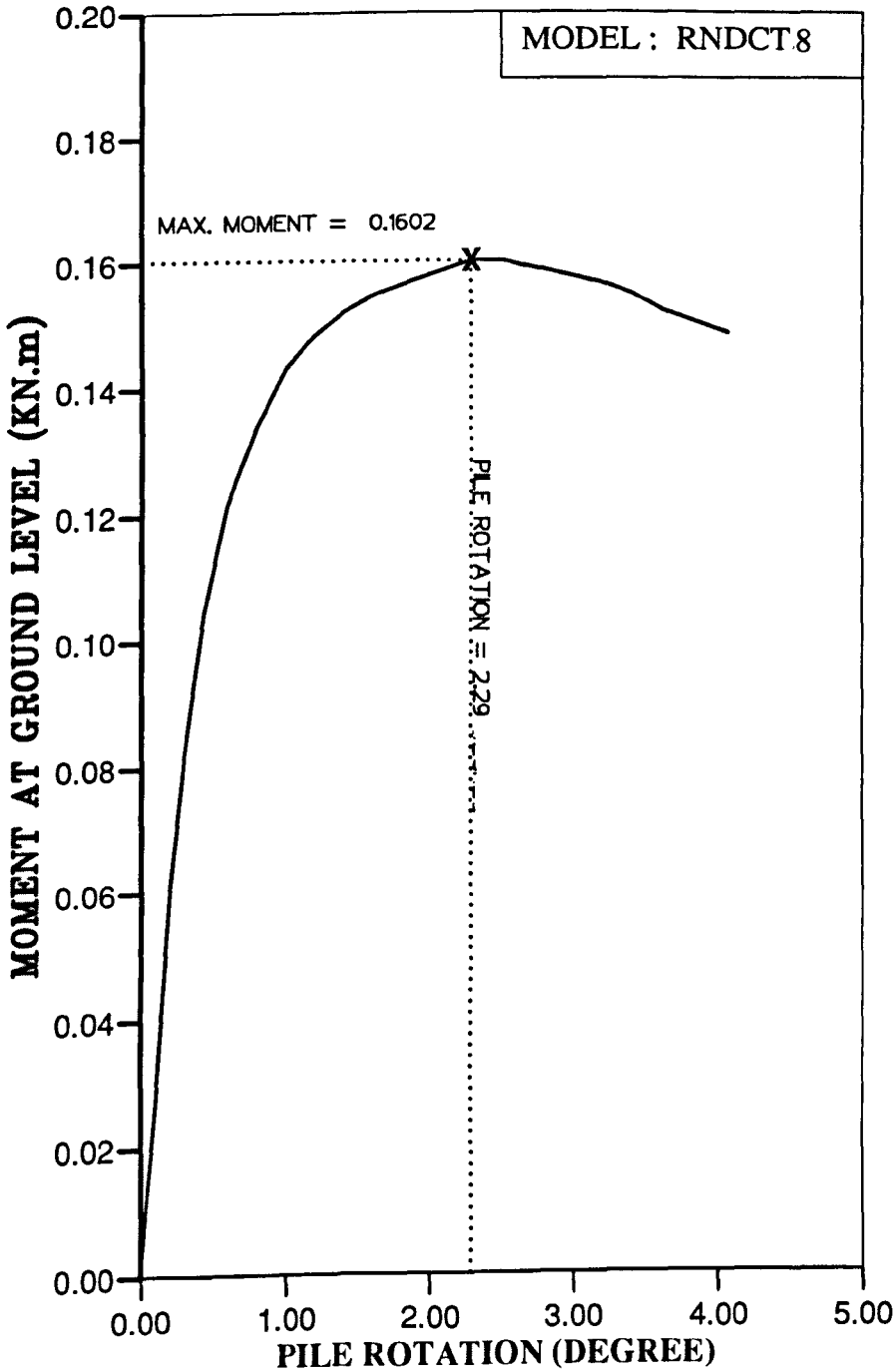

Figure AM85 Variation of moment at ground level with pile rotation for Series 1 test.

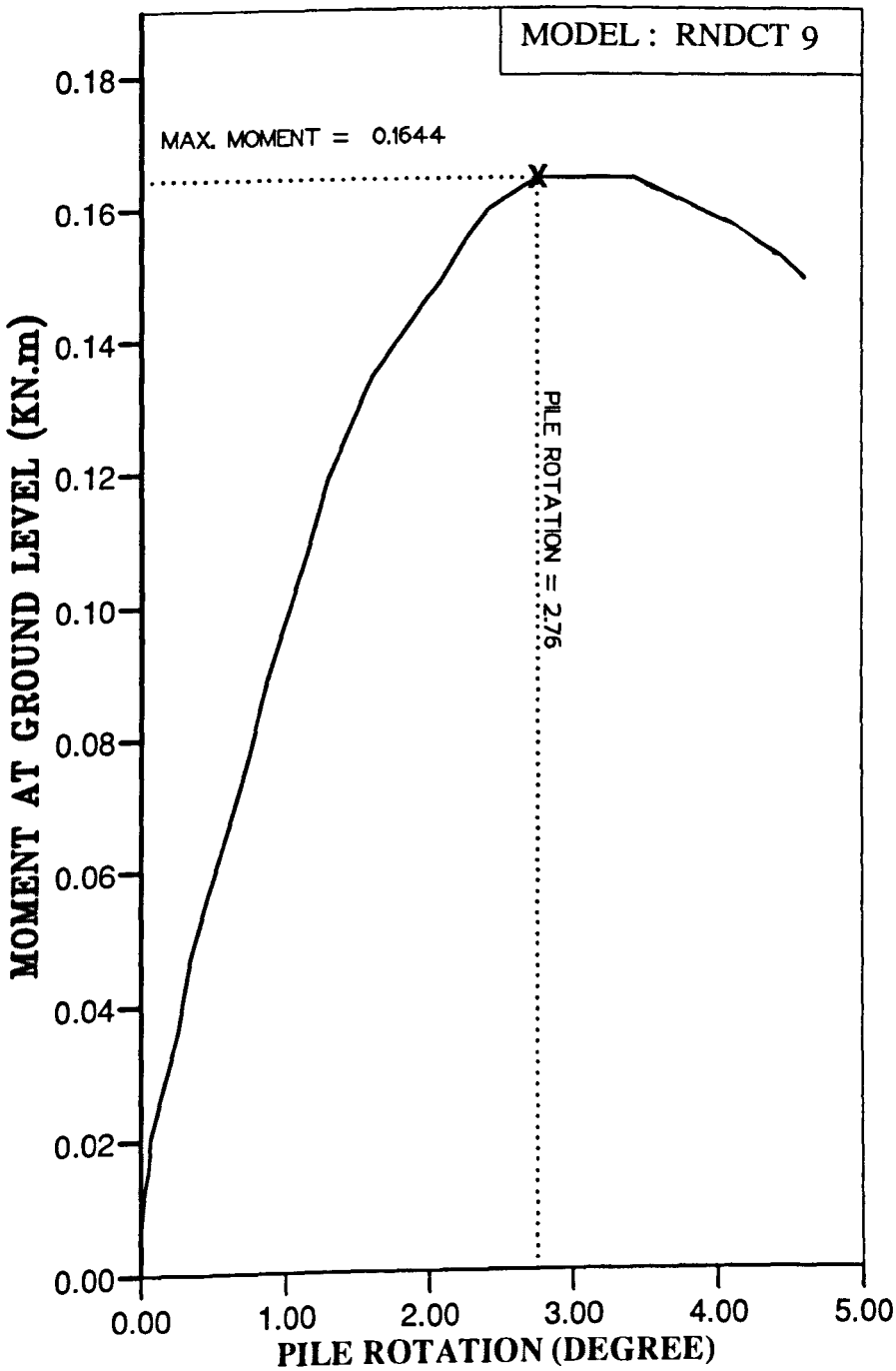

Figure AM86 Variation of moment at ground level with pile rotation for Series 1 test.

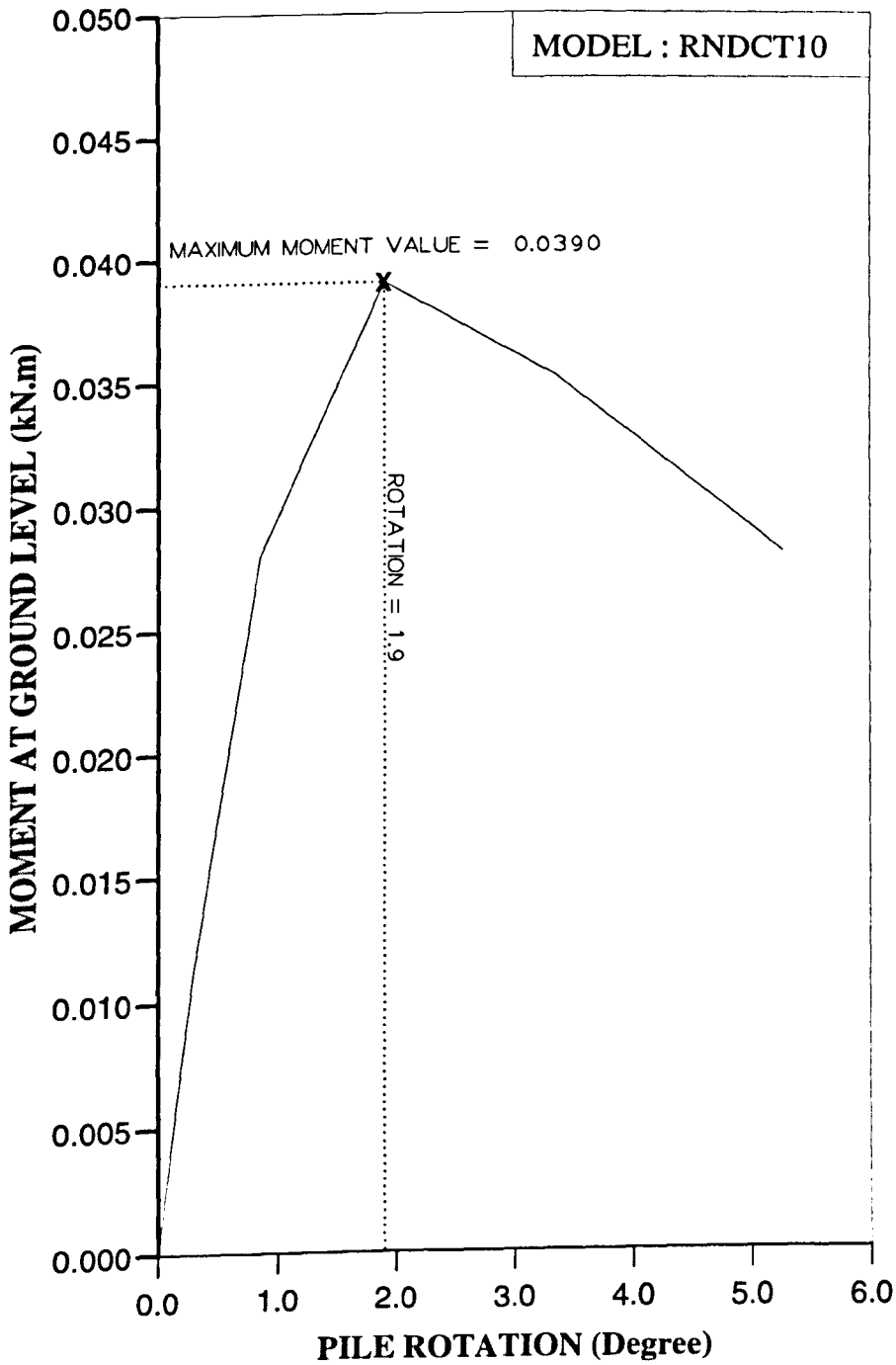

Figure AM87 Variation of moment at ground level with pile rotation for Series 1 test.

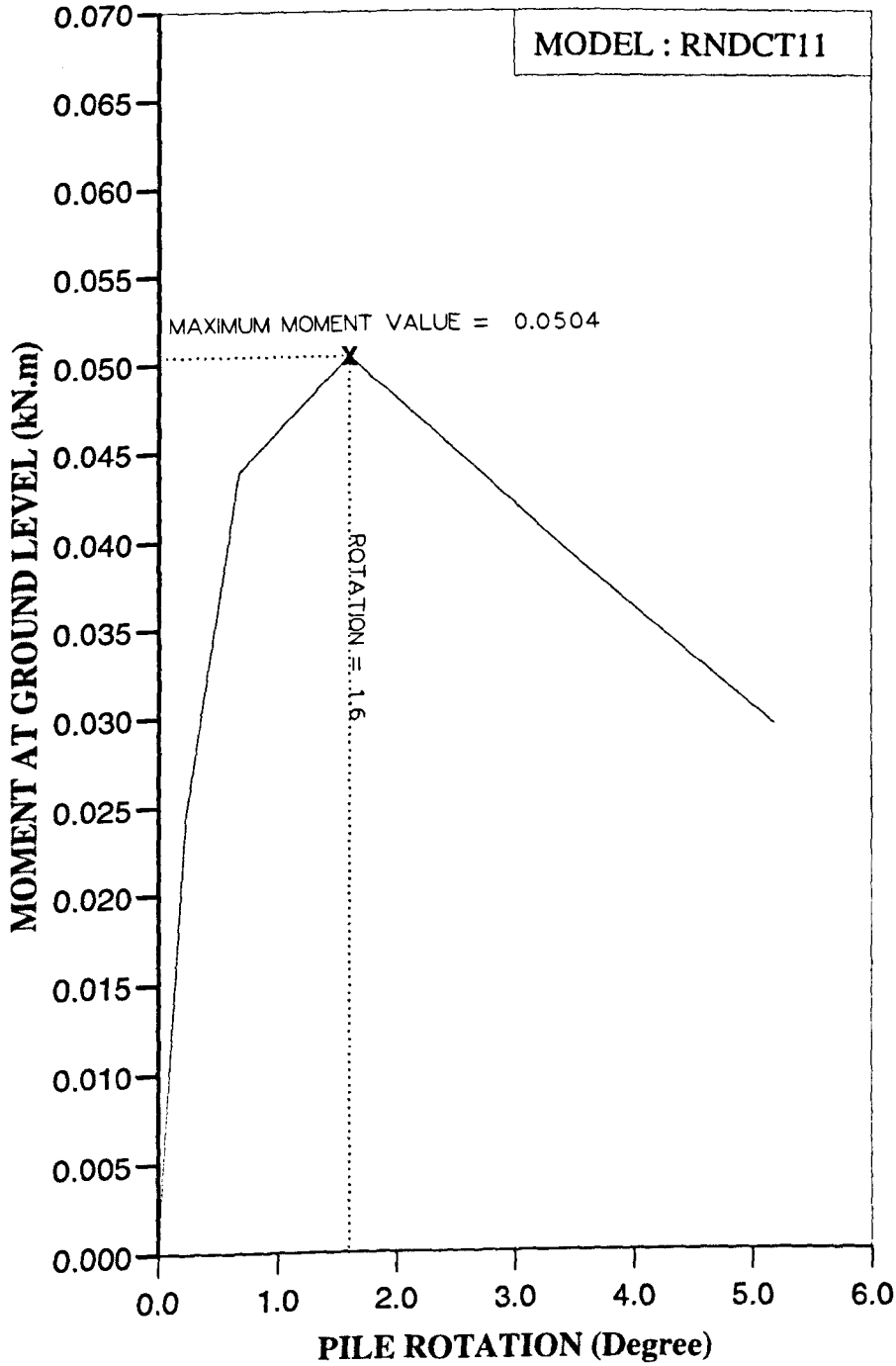

Figure AM88 Variation of moment at ground level with pile rotation for Series 1 test.

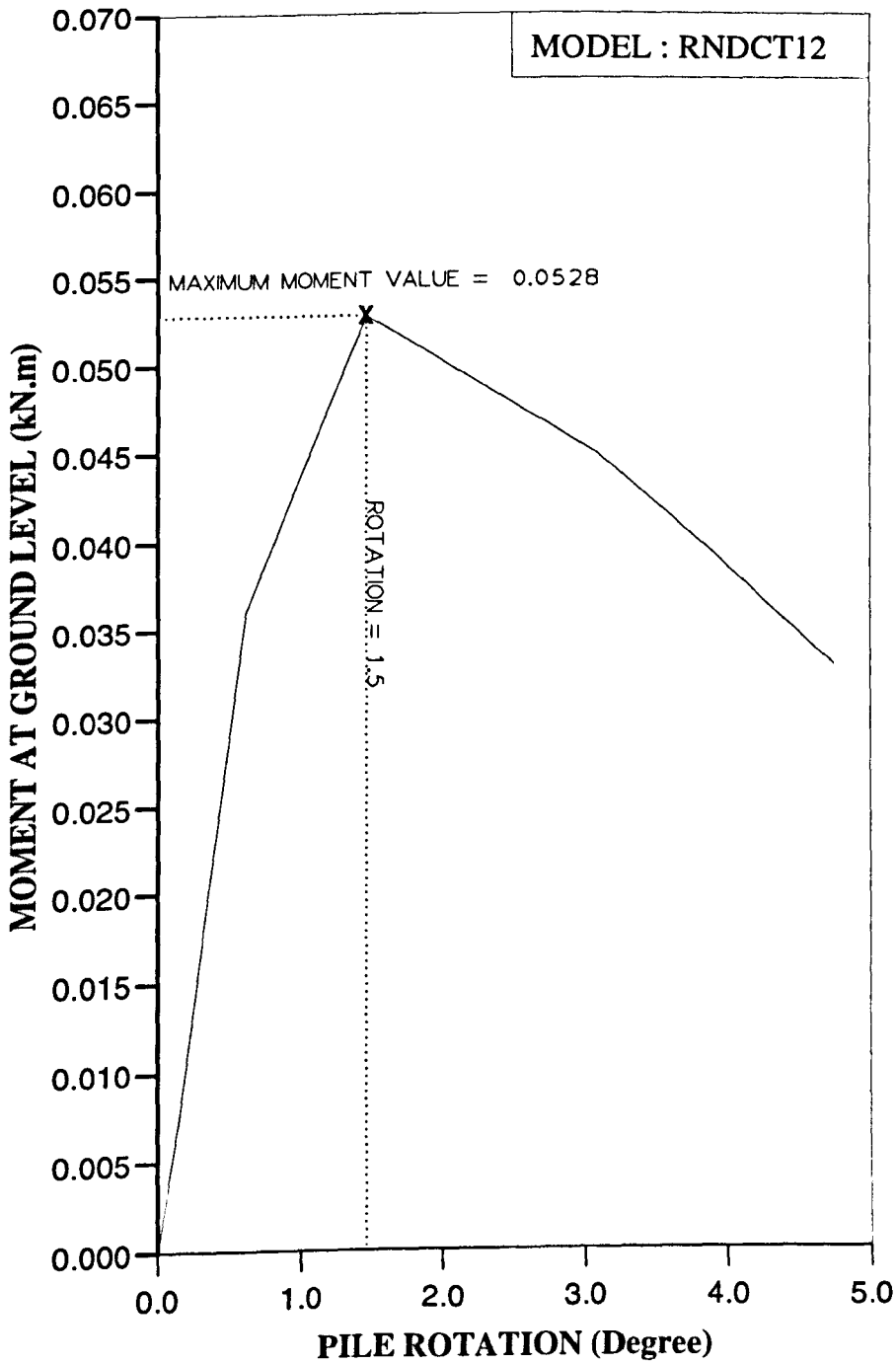

Figure AM89 Variation of moment at ground level with pile rotation for Series 1 test.

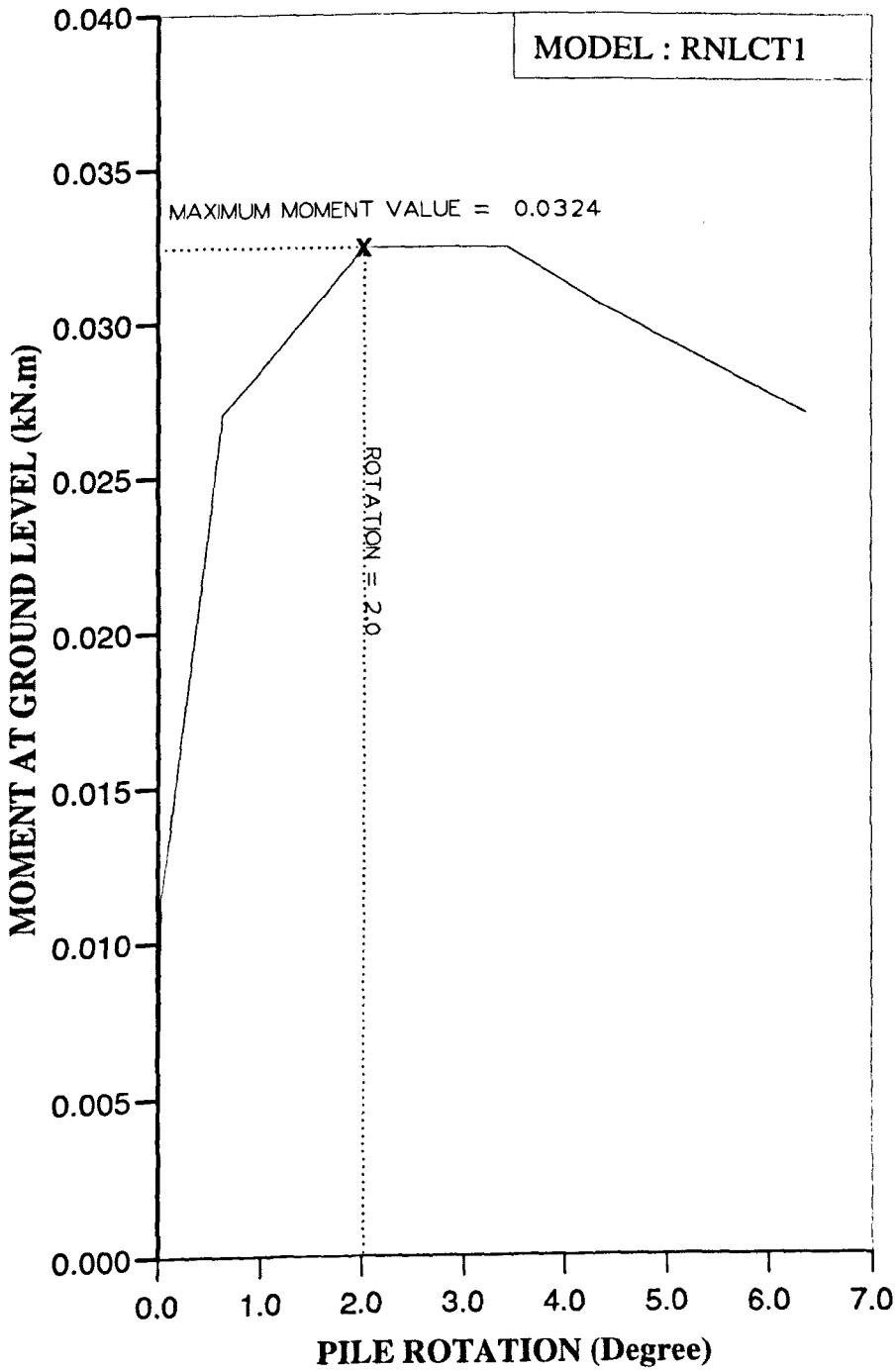

Figure AM90 Variation of moment at ground level with pile rotation for Series 1 test.

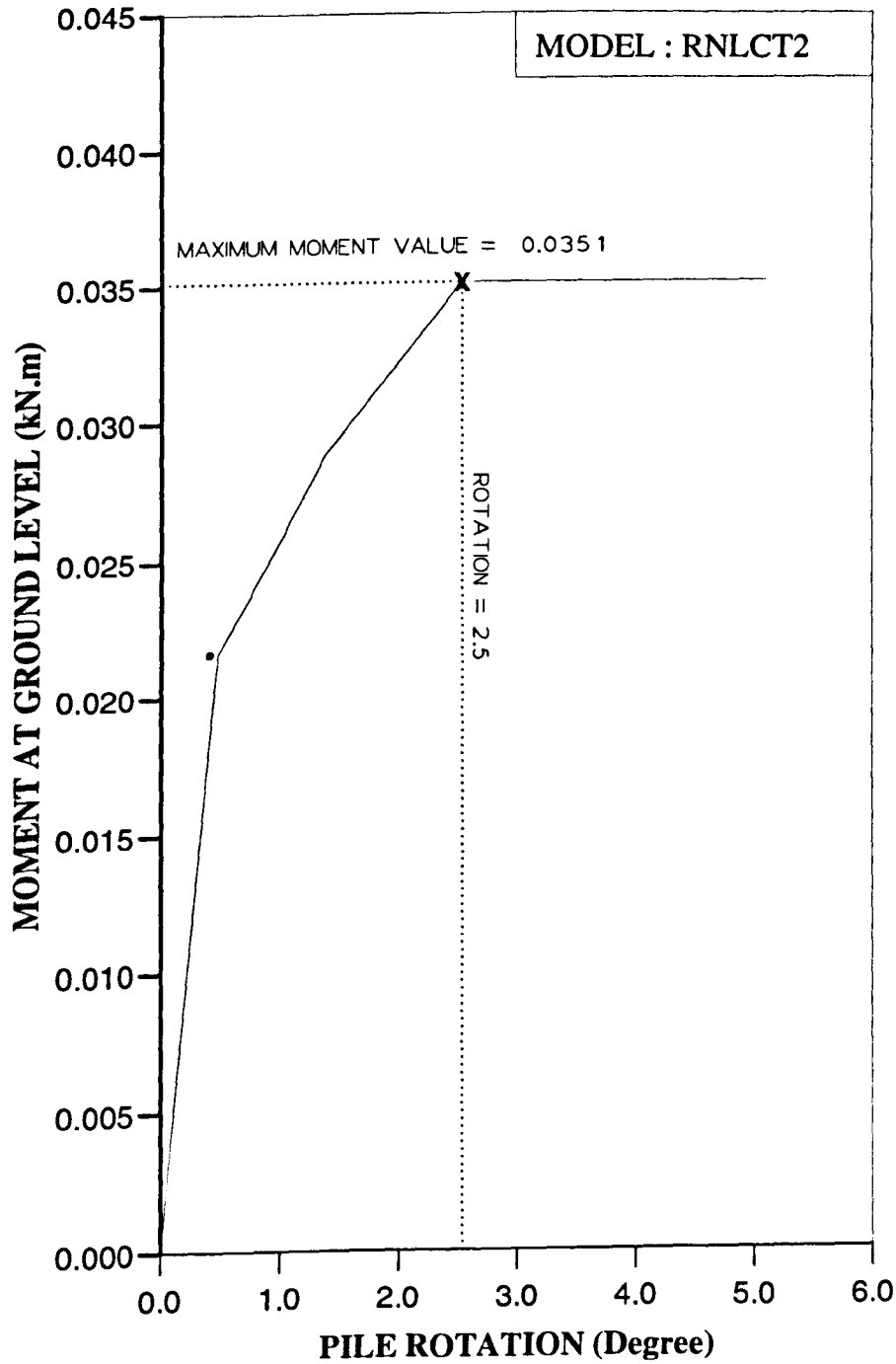

Figure AM91 Variation of moment at ground level with pile rotation for Series 1 test.

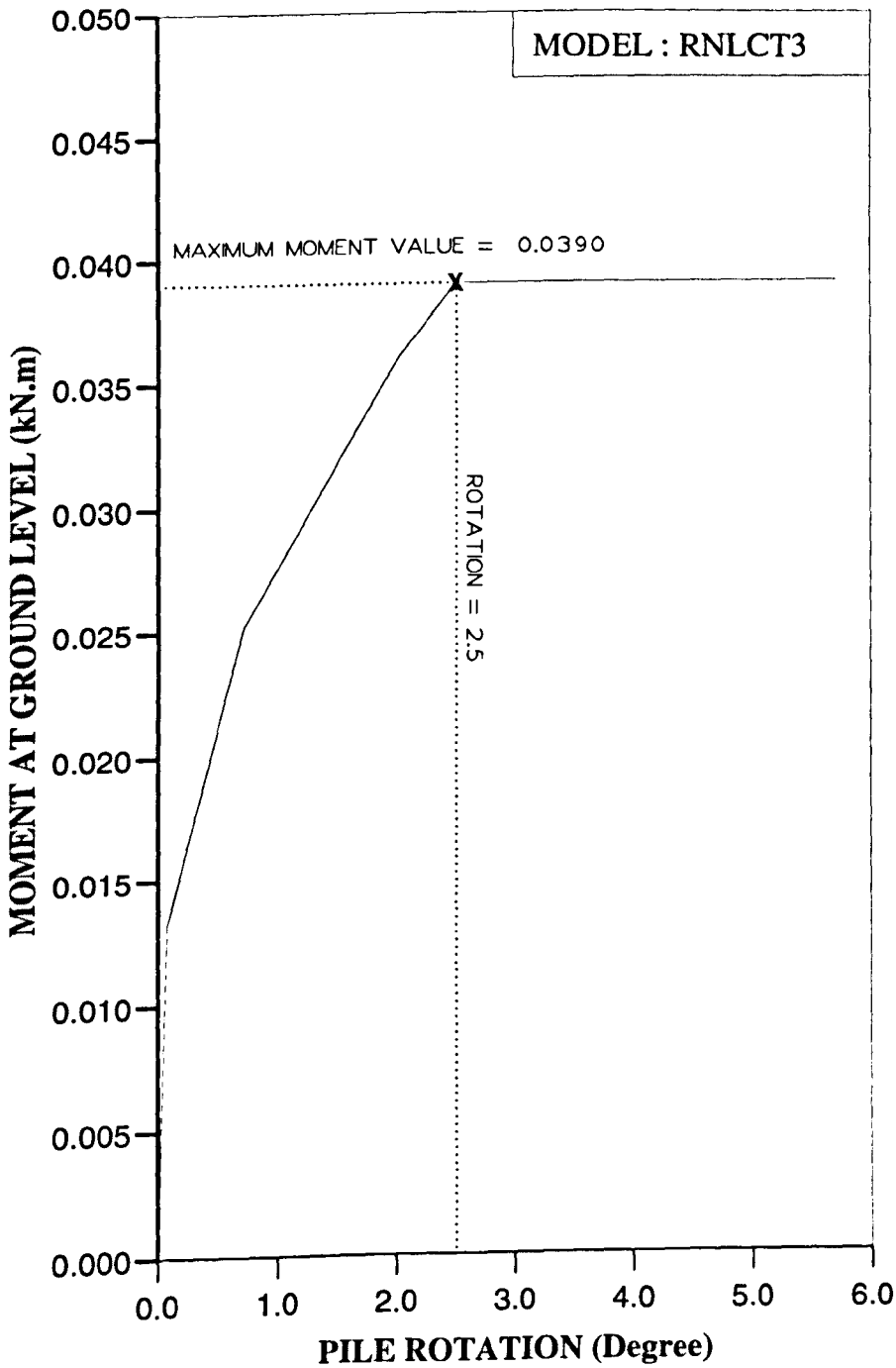

Figure AM92 Variation of moment at ground level with pile rotation for Series 1 test.

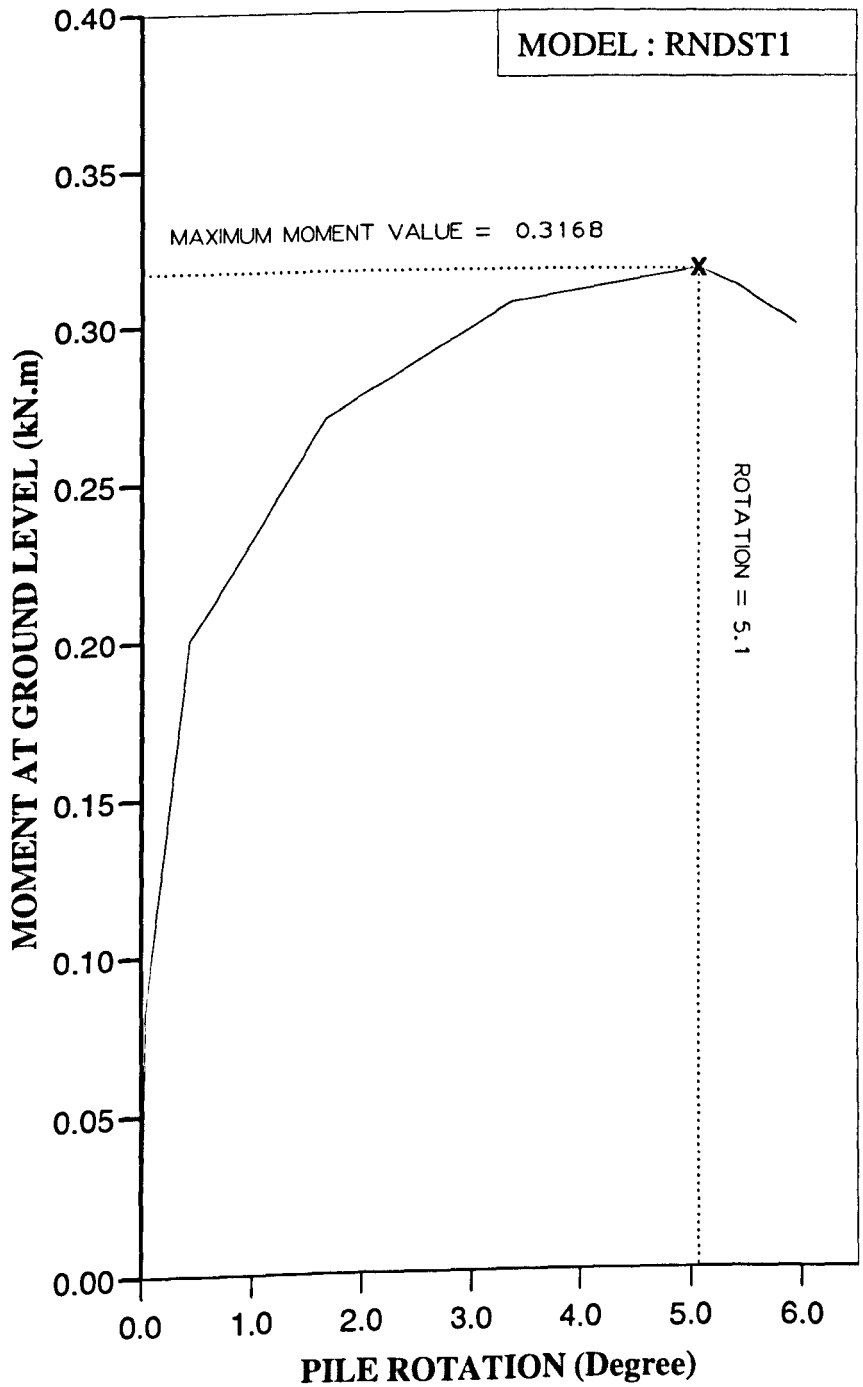

Figure AM93 Variation of moment at ground level with pile rotation for Series 2 test.

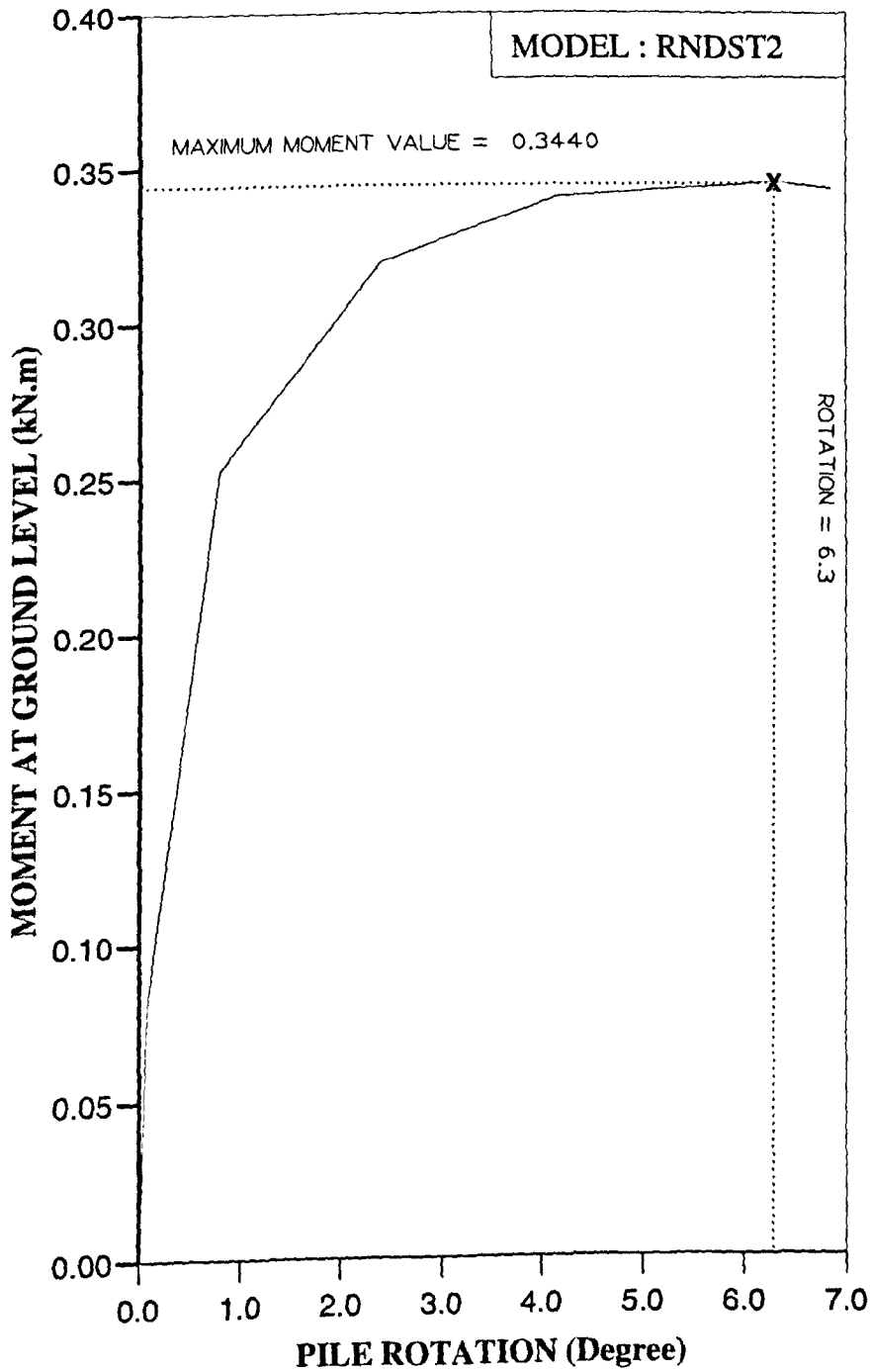

Figure AM94 Variation of moment at ground level with pile rotation for Series 2 test.

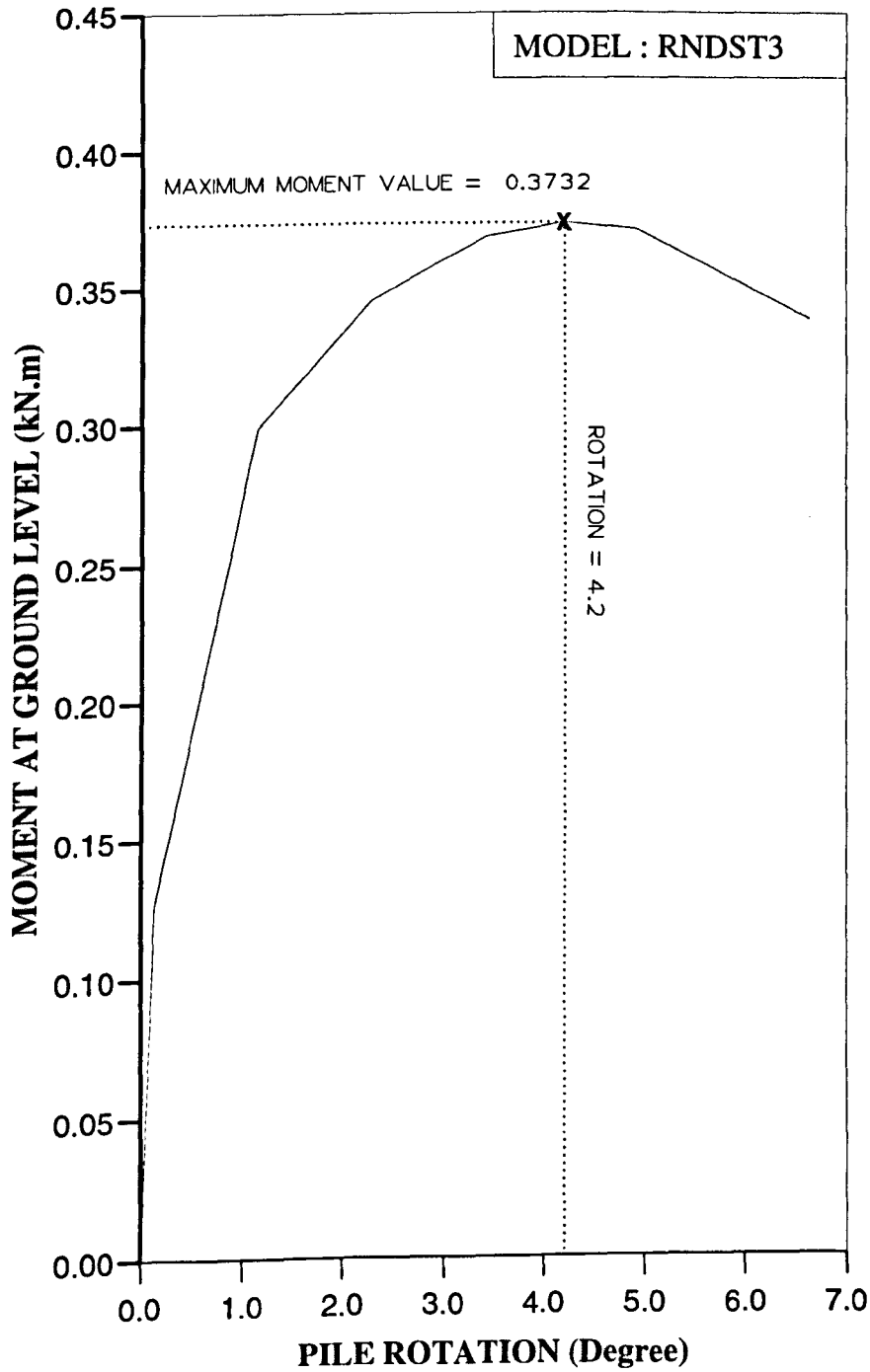

Figure AM95 Variation of moment at ground level with pile rotation for Series 2 test.

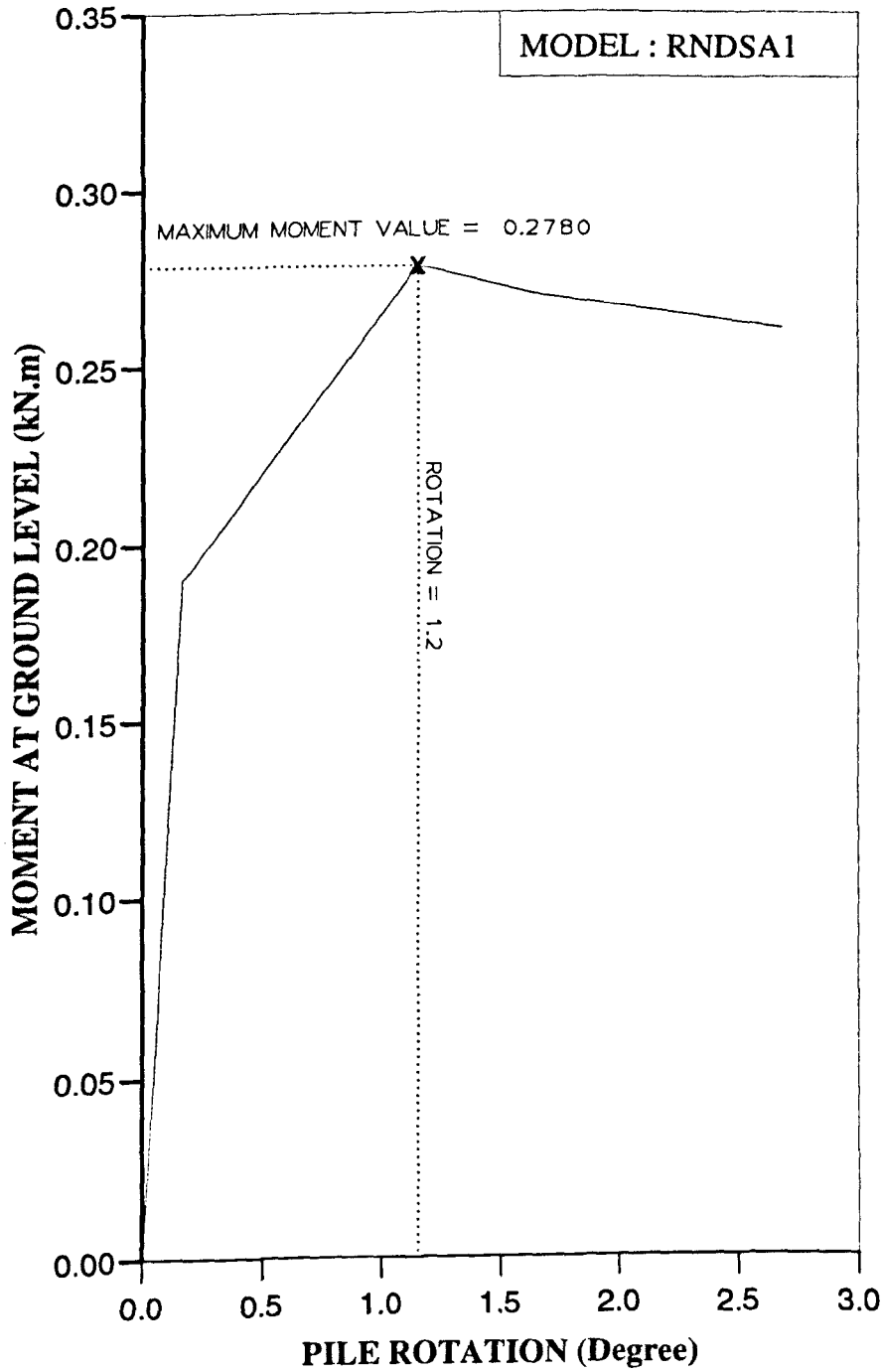

Figure AM96 Variation of moment at ground level with pile rotation for Series 2 test.

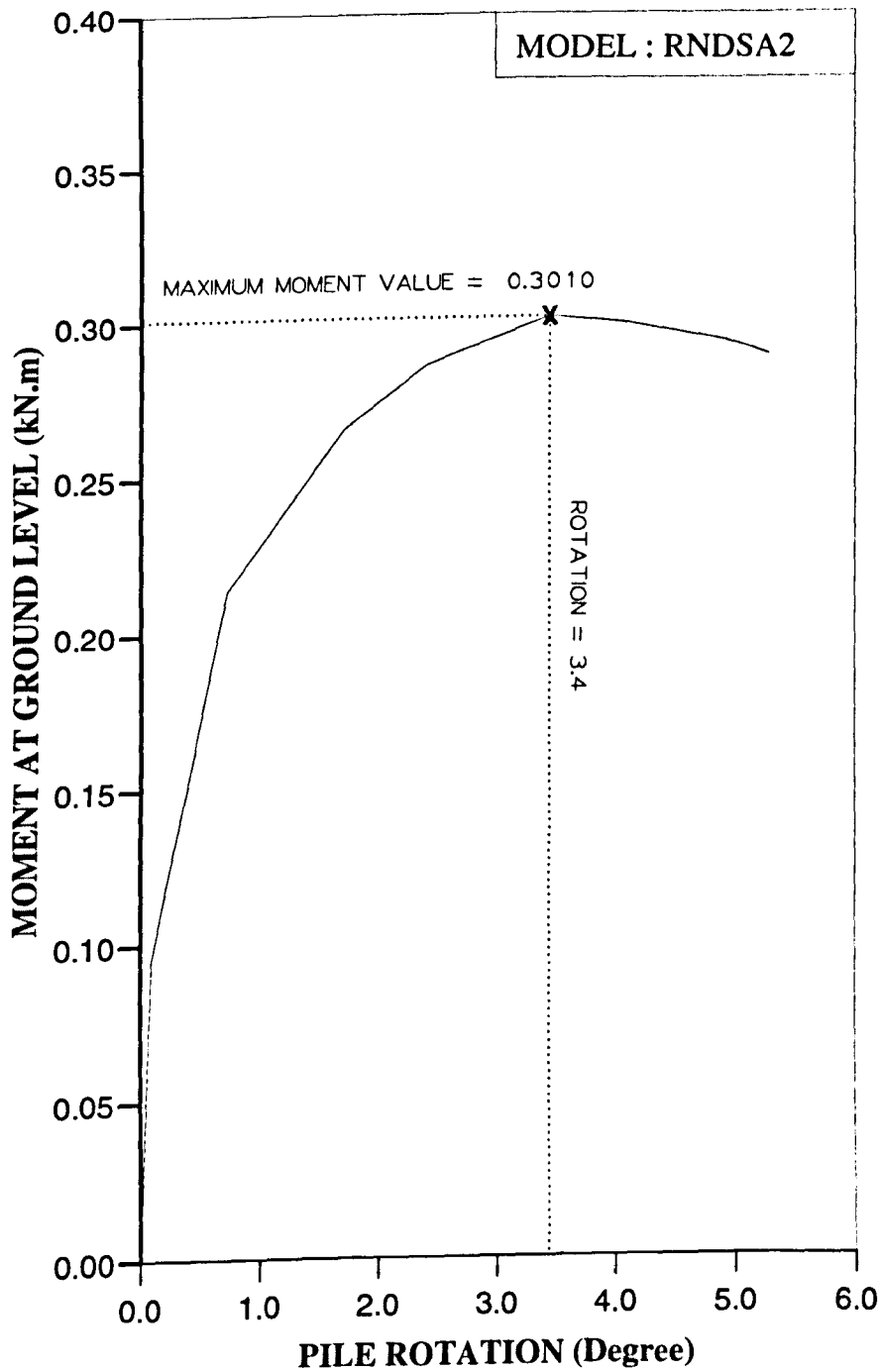

Figure AM97 Variation of moment at ground level with pile rotation for Series 2 test.

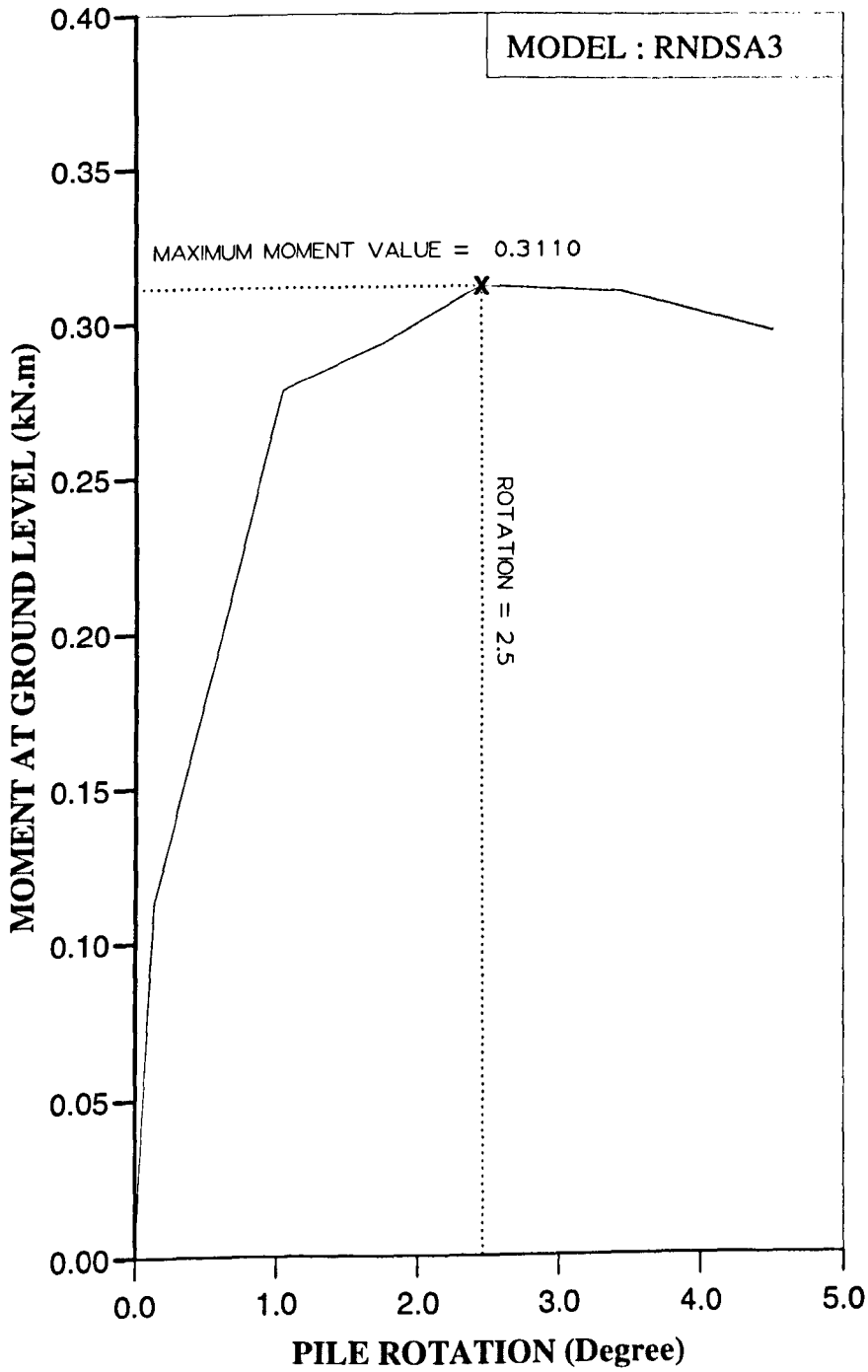

Figure AM98 Variation of moment at ground level with pile rotation for Series 2 test.

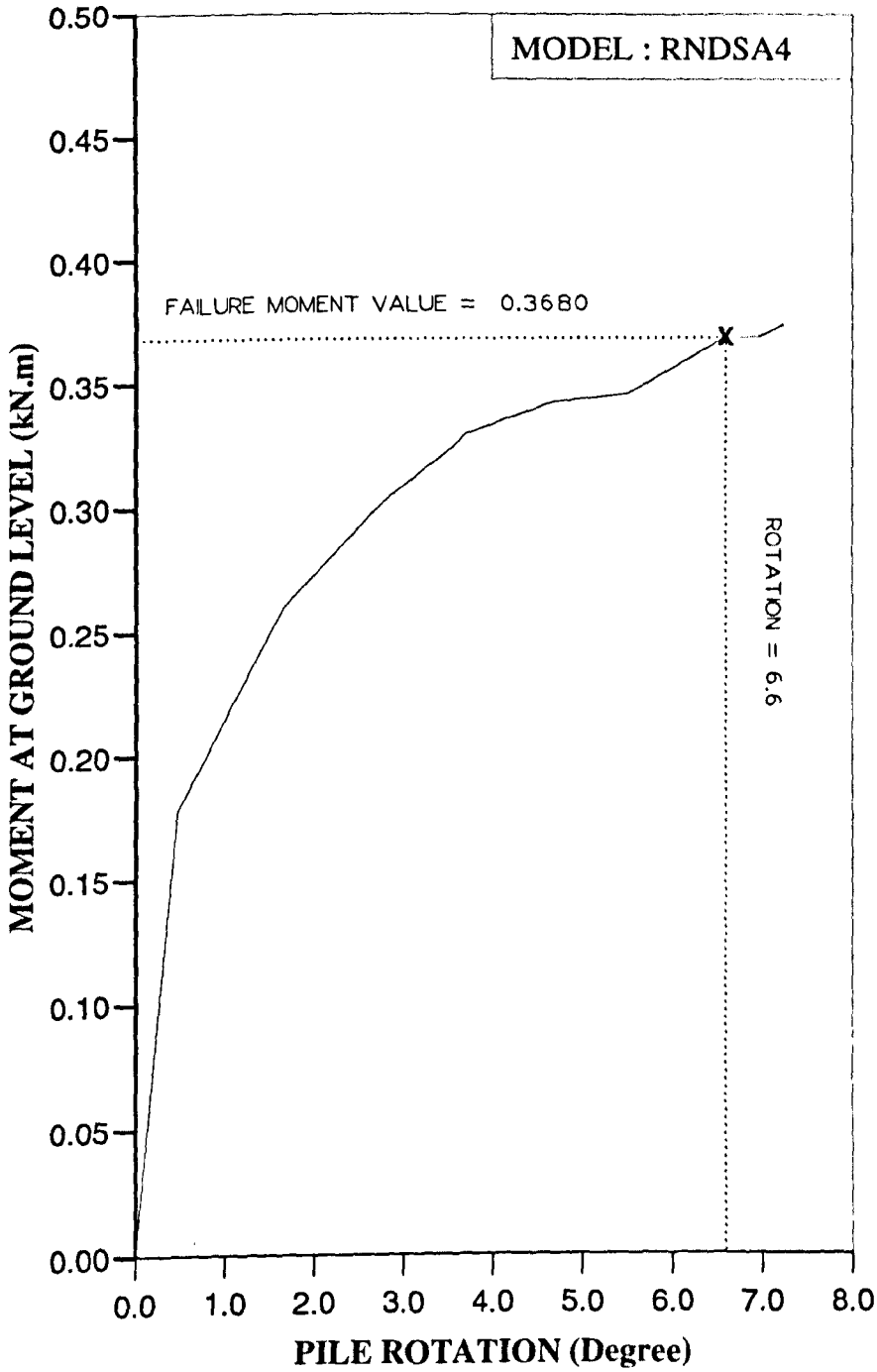

Figure AM99 Variation of moment at ground level with pile rotation for Series 2 test.

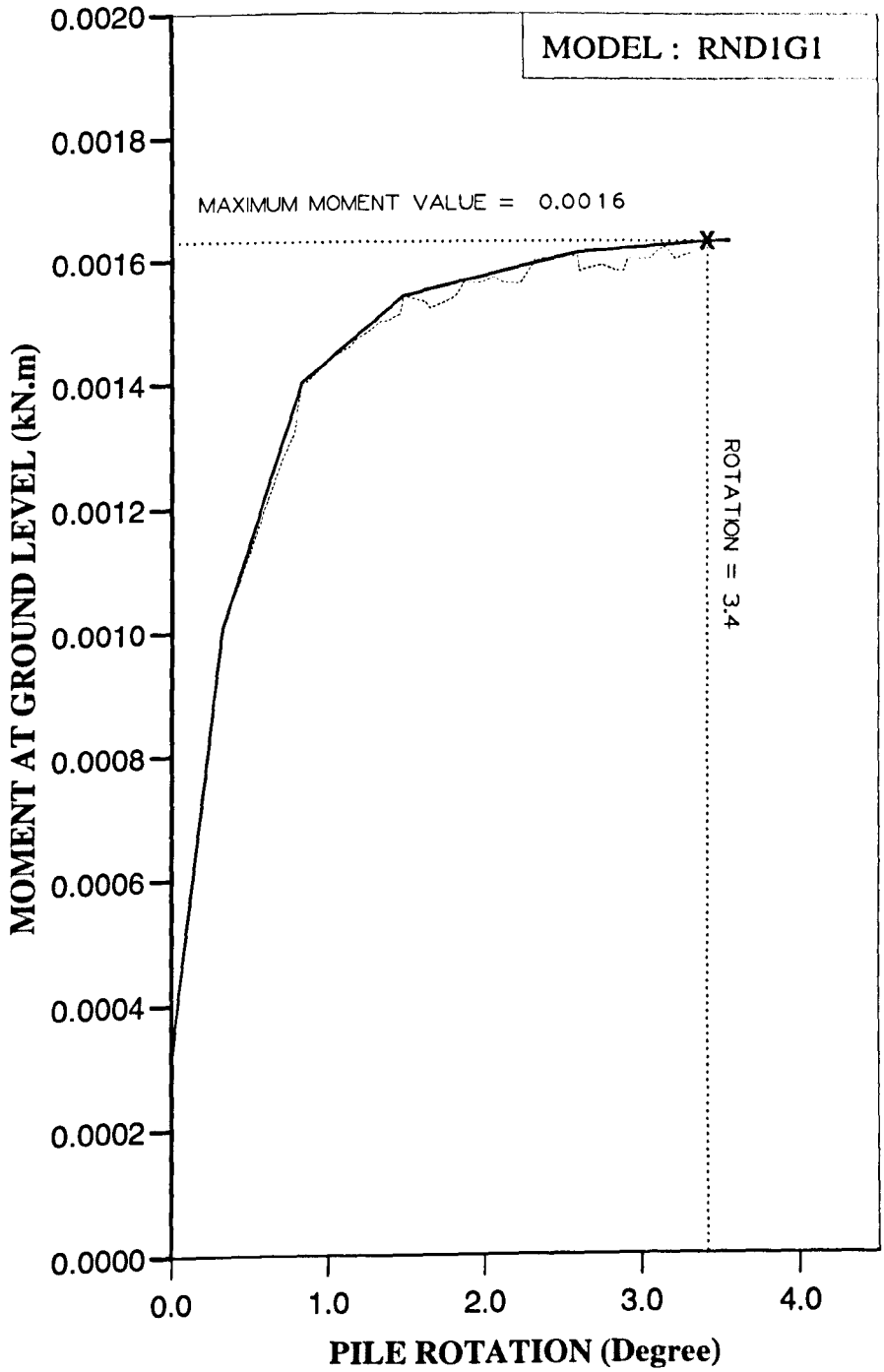

Figure AM100 Variation of moment at ground level with pile rotation for Series 3 test.

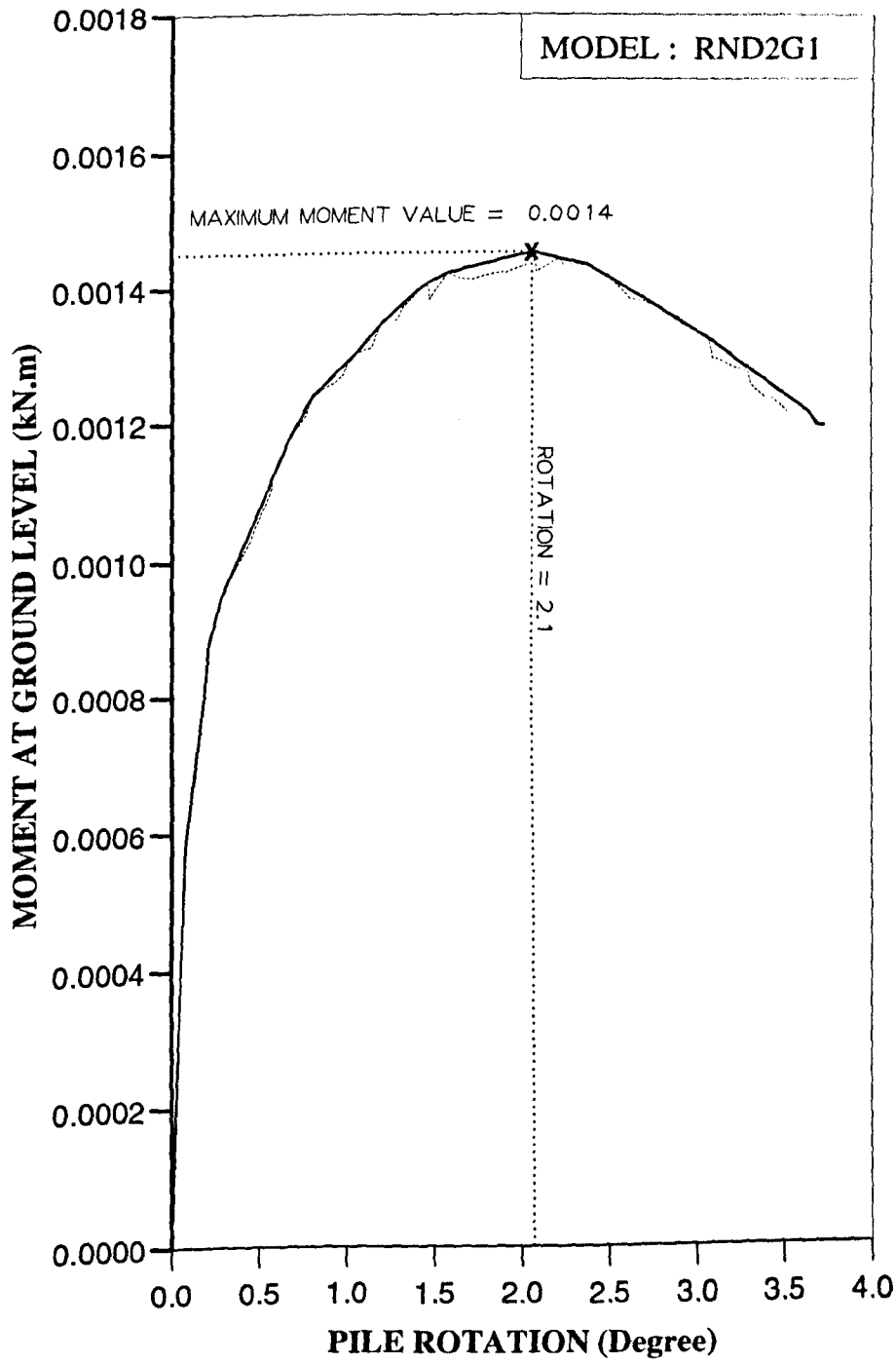

Figure AM101 Variation of moment at ground level with pile rotation for Series 3 test.

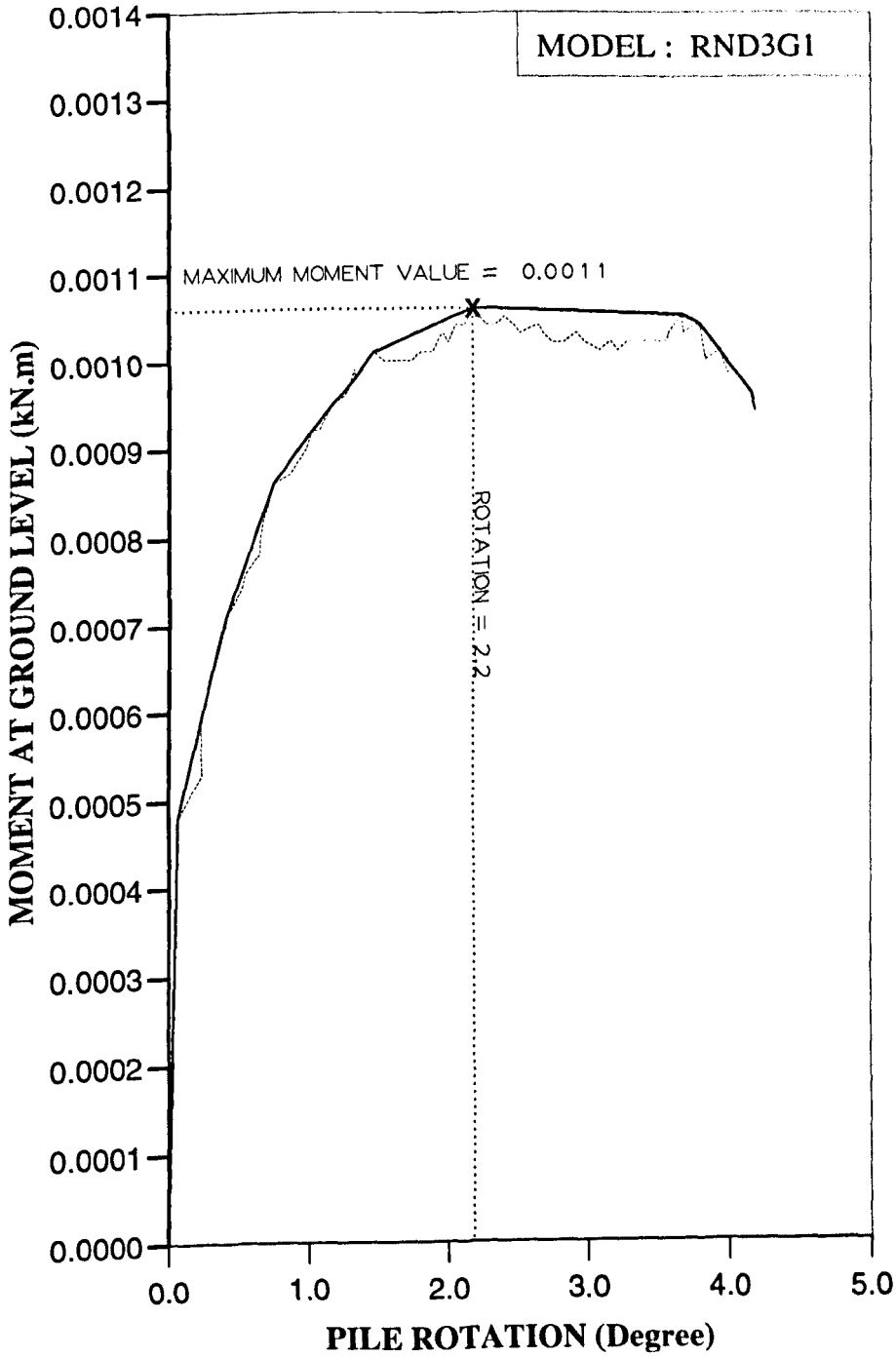

Figure AM1C2 Variation of moment at ground level with pile rotation for Series 3 test.

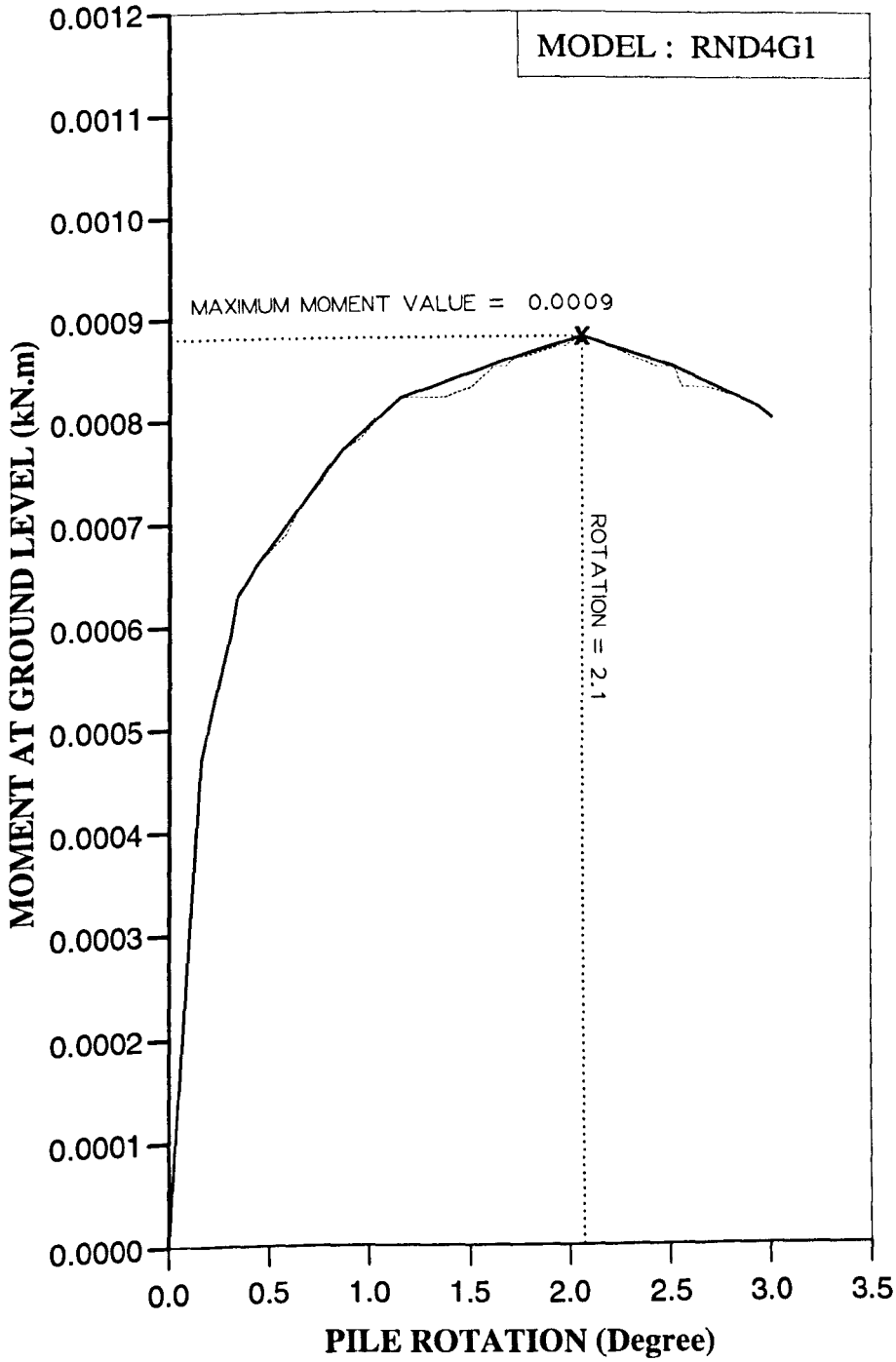

Figure AM103 Variation of moment at ground level with pile rotation for Series 3 test.

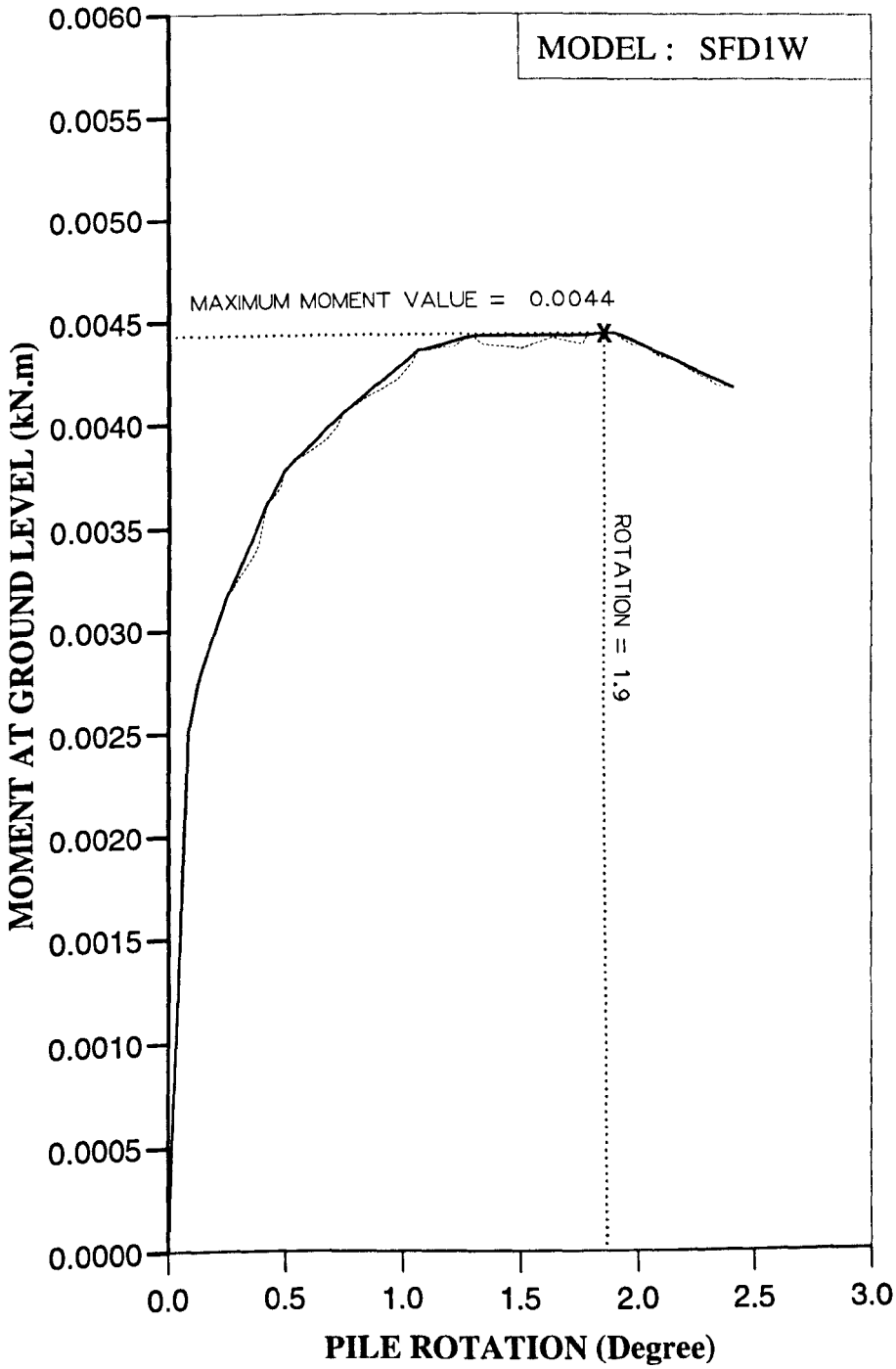

Figure AM104 Variation of moment at ground level with pile rotation for Series 4 test.

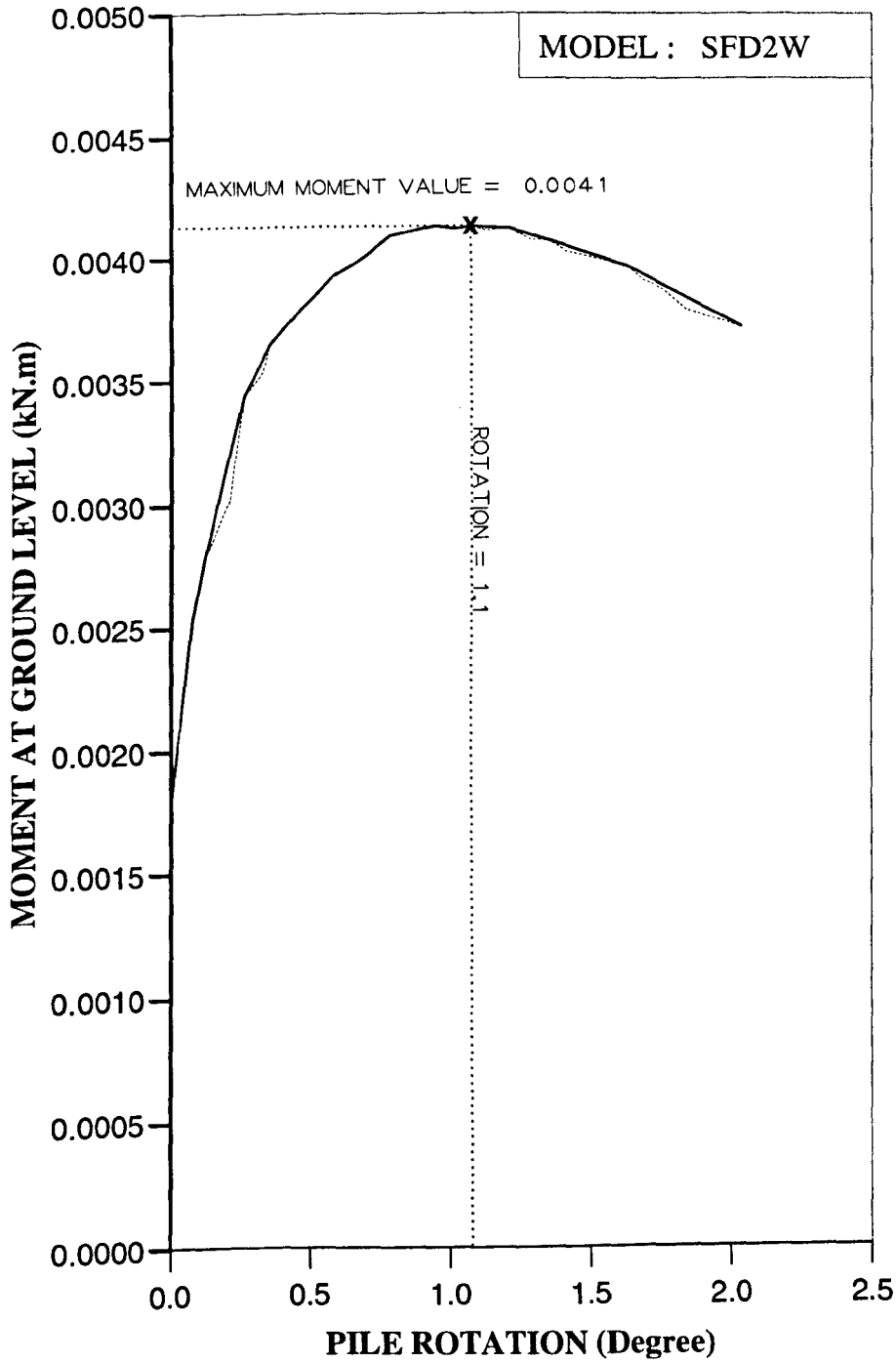

Figure AM105 Variation of moment at ground level with pile rotation for Series 4 test.

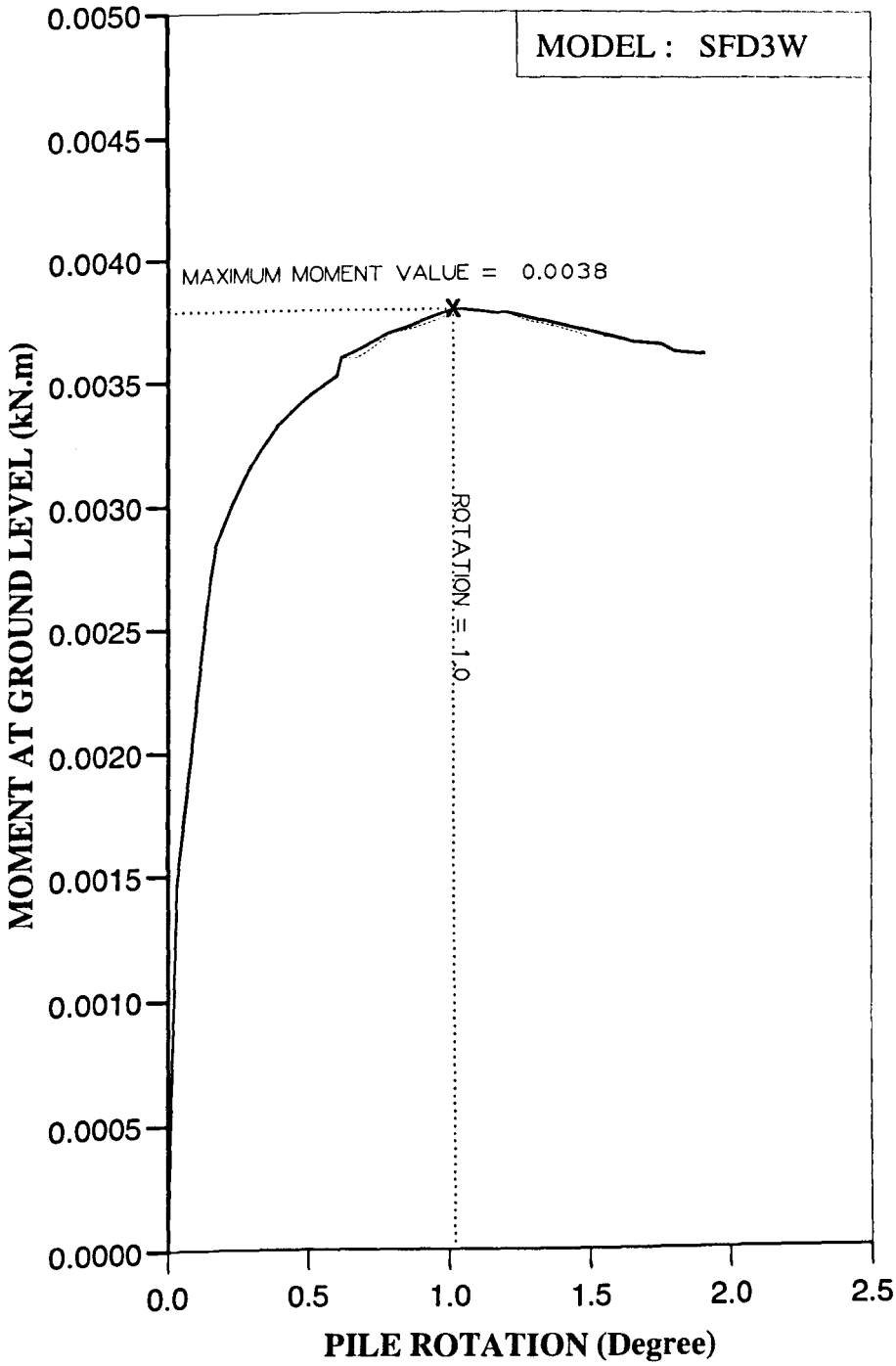

Figure AM106 Variation of moment at ground level with pile rotation for Series 4 test.

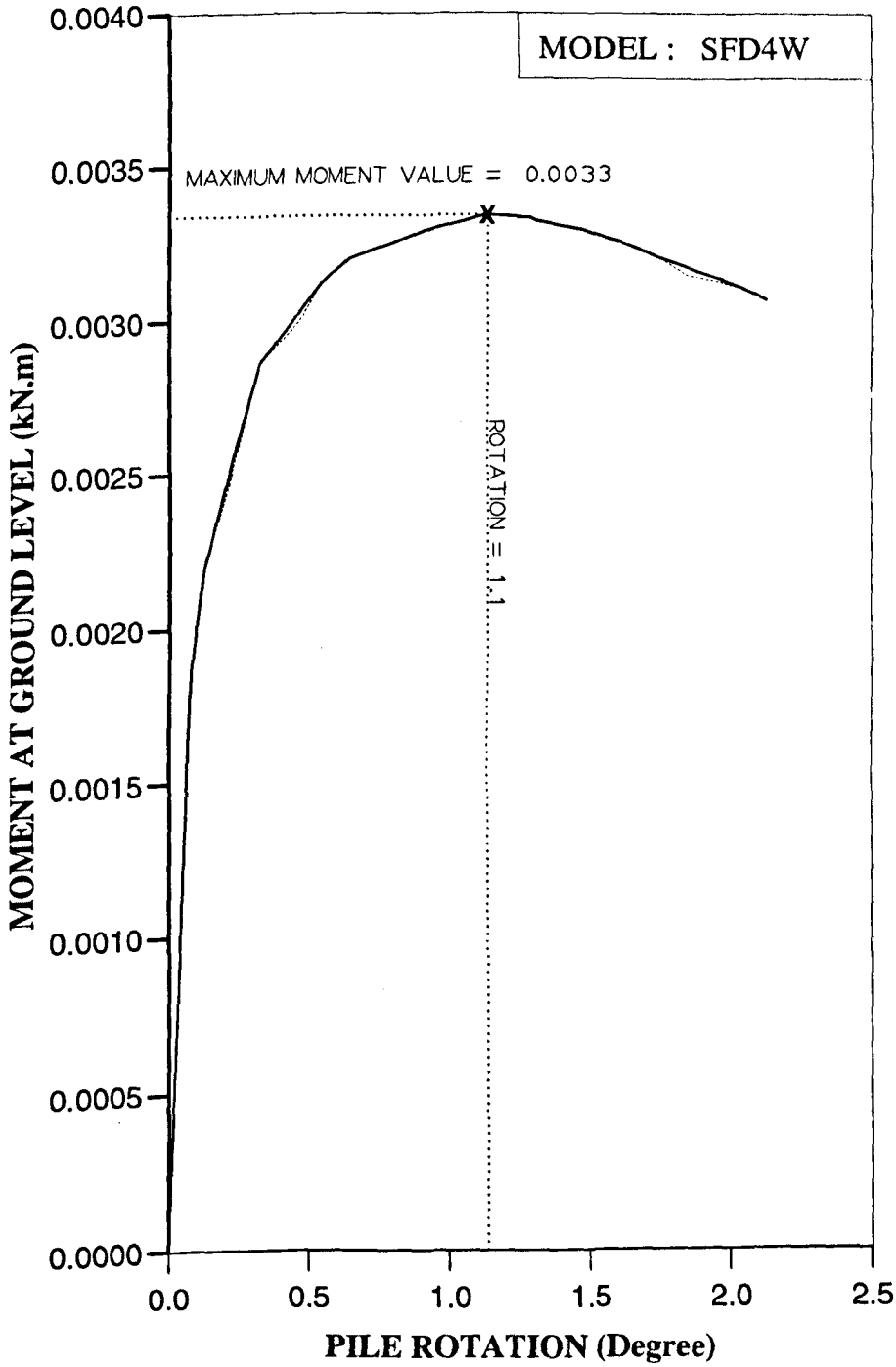

Figure AM107 Variation of moment at ground level with pile rotation for Series 4 test.

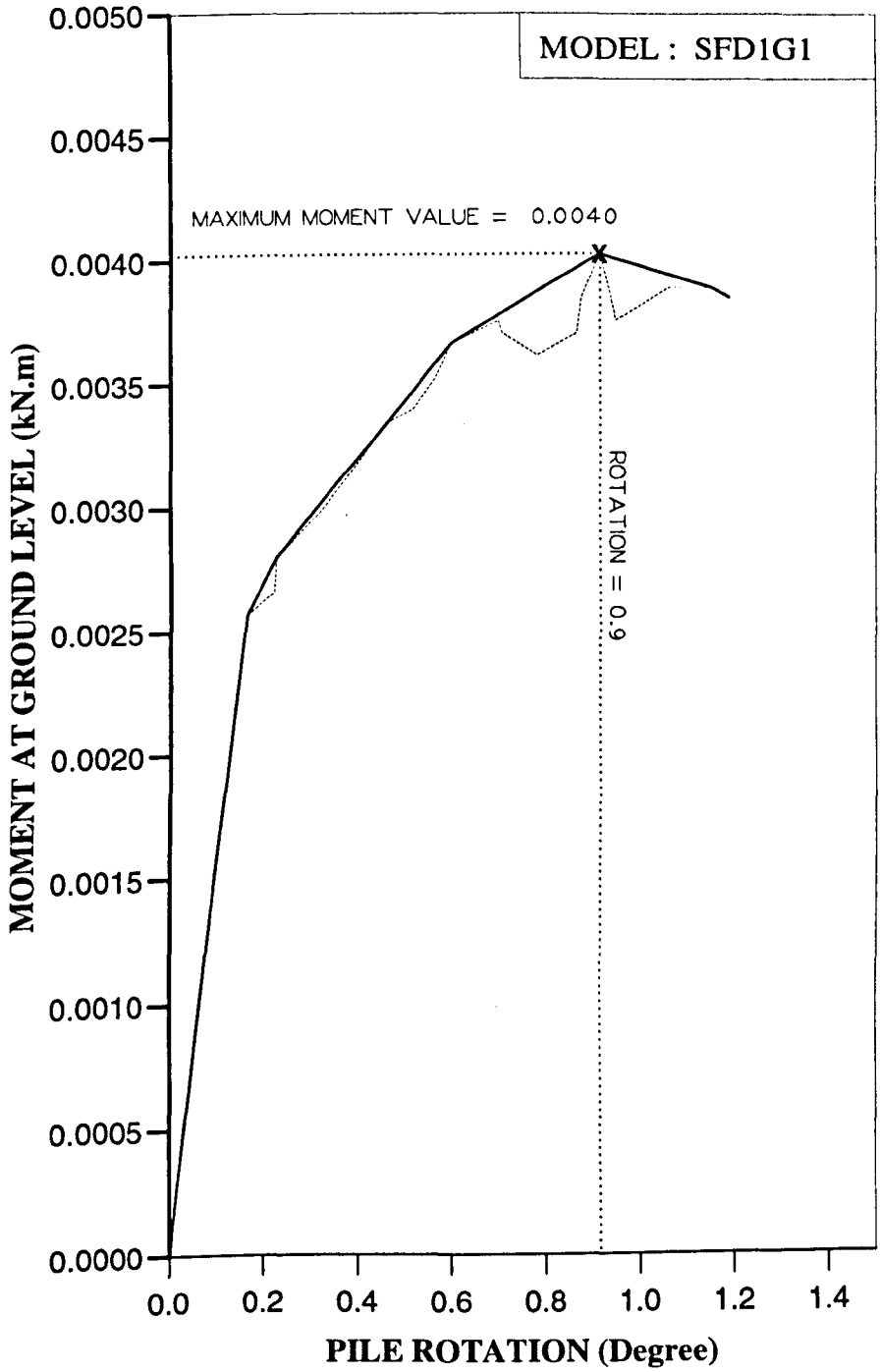

Figure AM108 Variation of moment at ground level with pile rotation for Series 4 test.

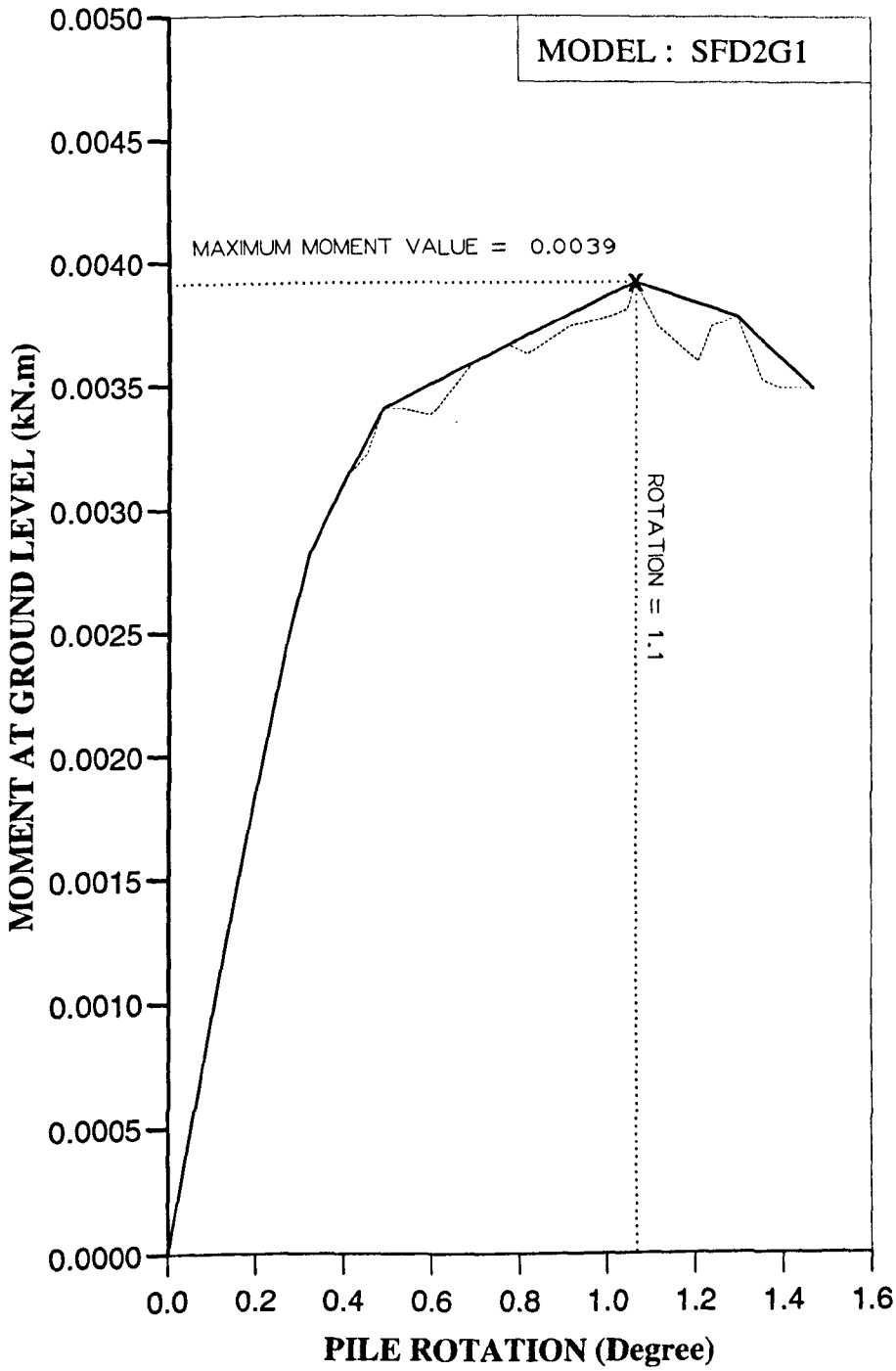

Figure AM109 Variation of moment at ground level with pile rotation for Series 4 test.

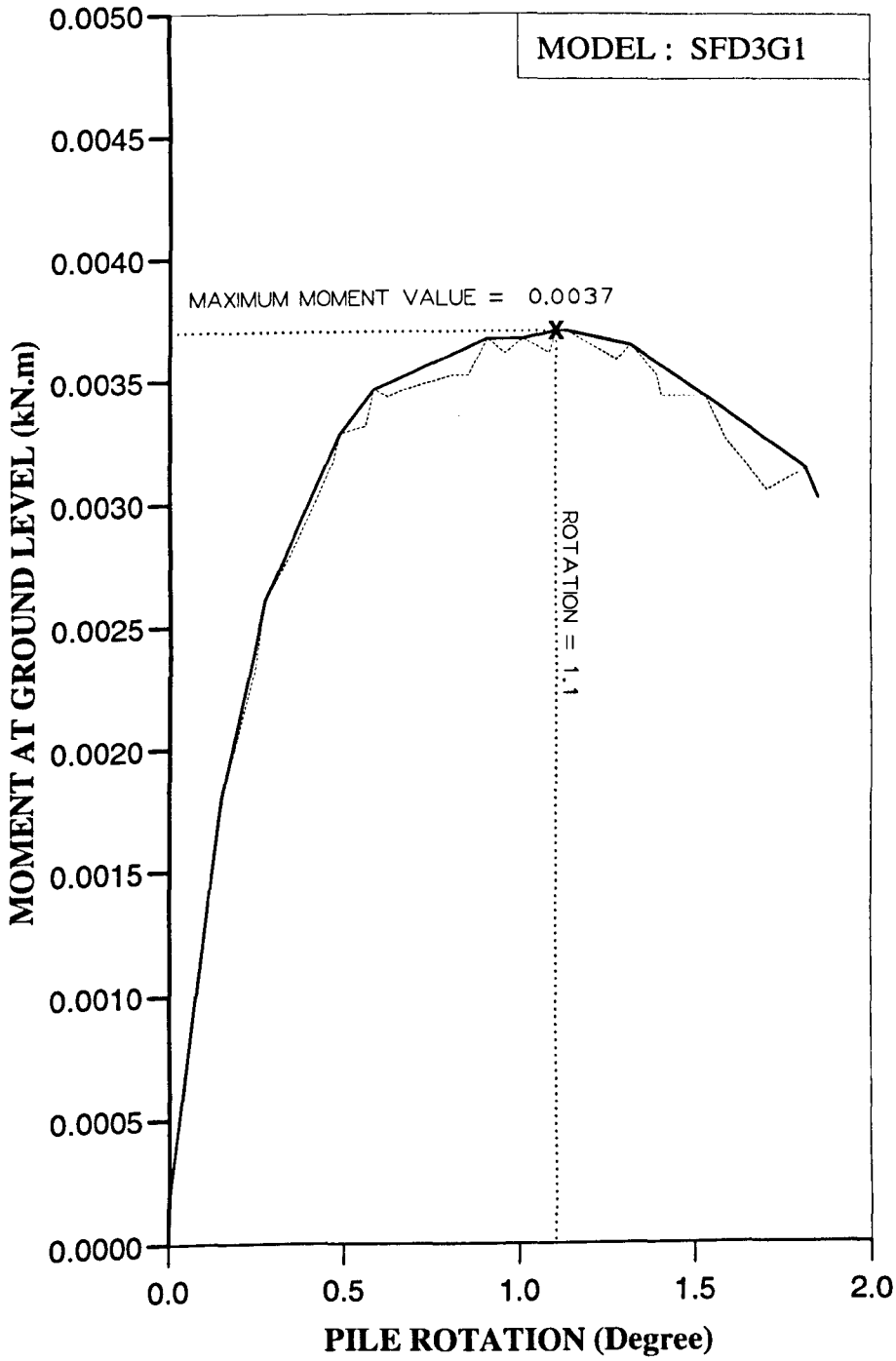

Figure AM110 Variation of moment at ground level with pile rotation for Series 4 test.

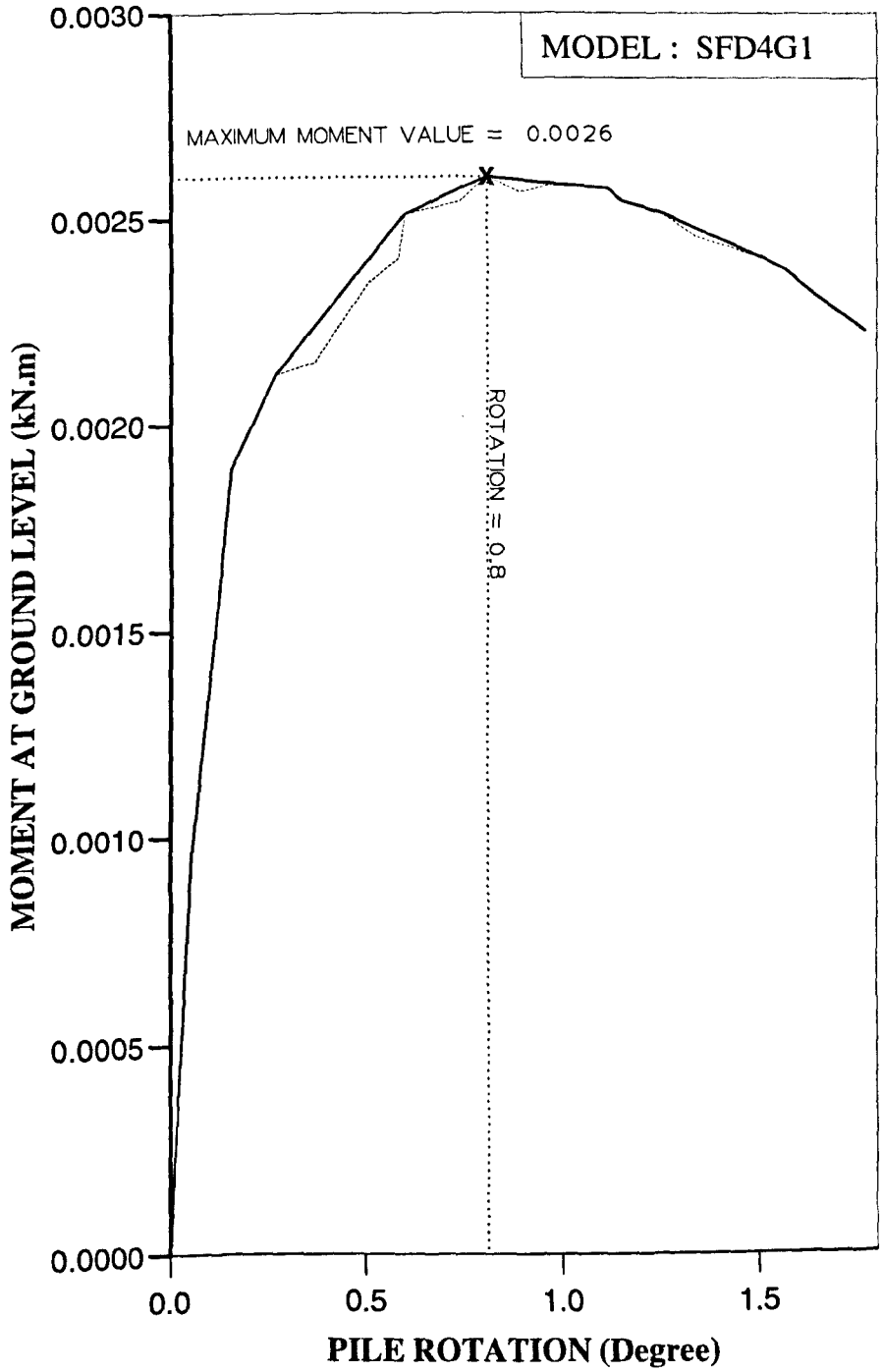

Figure AM111 Variation of moment at ground level with pile rotation for Series 4 test.

APPENDIX B

APPENDIX B

A) METHOD OF CALCULATING SAND PARAMETERS FOR CENTRIFUGAL AND CONVENTIONAL TEST

1) CENTRIFUGAL TEST

a) DENSE PACKING

TEST 1:	Mass of bucket	=	0.6 kg
	Mass of bucket + Sand	=	36.49 kg
	Mass of Sand	=	35.89 kg
	Volume of Sand	=	0.0214 m^3
	Unit weight of Sand	=	1673.9 kg/m^3
Test 2:	Mass of bucket	=	0.6 kg
	Mass of bucket + Sand	=	36.42 kg
	Mass of Sand	=	35.82 kg
	Volume of Sand	=	0.0214 m^3
	Unit weight of Sand	=	1673.8 kg/m^3

Therefore average unit weight = 1673.85 kg/m^3

Average Unit Weight of dense packing = 16.4 kN/m^3

b) LOOSE PACKING

Mass of bucket + Sand	=	32.03 kg
Mass of Sand	=	31.43 kg
Volume of Sand	=	0.0214 m^3
Unit weight of Sand	=	1468.69 kg/m^3
Therefore Unit Weight of loose packing	=	14.4 kN/m^3

2) CONVENTIONAL TEST

a) DENSE PACKING

Mass of Proctor mould	=	4.10 kg
Mass of Proctor mould + Sand	=	5.630 kg
Mass of Sand	=	1.53 kg
Volume of Sand	=	0.0009149 m^3
Unit weight of Sand	=	1672.31 kg/m^3
Unit Weight of dense packing	=	16.4 kN/m^3

b) LOOSE PACKING

Mass of Proctor mould and sand	=	5.445 kg
Mass of sand	=	1.345 kg
Volume of sand	=	0.0009149 m^3
Unit weight of sand	=	1470.11 kg/m^3
Unit Weight of loose packing	=	14.4 kN/m^3

B) METHOD OF CALCULATING DENSITY INDEX AND VOID RATIO OF THE SAND

Specific Gravity (G_s)	= 2.69
Max. Porosity (n_{max})	= 49.5 %
Min. Porosity (n_{min})	= 34 %
Unit weight of water(γ_w)	= 9.81 kN/m^3
Unit weight of Sand (γ_d)	= 16.4 kN/m^3 (Dense Packing)
Unit weight of Sand (γ_l)	= 14.4 kN/m^3 (Loose Packing)

$$Density Index (I_d) = \frac{e_{max} - e}{e_{max} - e_{min}} \quad (1)$$

$$e_{max} = n_{max}(1 + e_{max}) \quad (2)$$

$$e_{max} = \frac{n_{max}}{1 - n_{max}} \quad (2a)$$

$$e_{max} = \frac{0.495}{1 - 0.495}$$

$$e_{max} = 0.98\%$$

Similarly

$$e_{min} = \frac{0.34}{1 - 0.34}$$

$$e_{min} = 0.52\%$$

Void ratio for the test sand is :-

$$\gamma_s = \frac{(G_s + S_r e)\gamma_s}{(1 + e)} \quad (3)$$

Since Sr = 0 then

$$\gamma_s = \frac{G_s \gamma_w}{1 + e} \quad (3a)$$

therefore

$$e_{dense} = \frac{2.65(9.81)}{16.4} - 1$$

$$e_{dense} = 0.59$$

Similarly

$$e_{loose} = \frac{2.65(9.81)}{14.4} - 1$$

$$e_{loose} = 0.81$$

So

$$I_{dmax} = \frac{0.98 - 0.59}{0.98 - 0.52}$$

$$= 0.848$$

$$= 84.8\ \%$$

and

$$I_{dmin} = \frac{0.98 - 0.81}{0.98 - 0.52}$$

$$= 0.370$$

$$= 37\ \%$$

APPENDIX C

APPENDIX C

LOAD CELL AND LINEAR POTENTIOMETERS CALIBRATION

i) Load cell calibrations for the Centrifugal Test

Two load cells, with different load capacities were used in the tests. A 250lb capacity load cell was used to obtain readings from a single pile while a 2000lb capacity load cell was used for a continuous pile. Calibration was done against a proving ring. The calibration factor of the proving ring was 1 div. = 5.854N

Two sets of readings were taken, one during loading and one during unloading of the load cell. Load cell readings were recorded for every 20 division of the proving ring. The load cell was connected to the data logger readings of the load cell output were then recorded on computer linked to the data logger. The proving ring readings were then plotted against the load cell readings to obtain the calibration value of the load cell. The correlation of the readings were shown in Fig.C1

ii) Calibration of linear potentiometers for Centrifugal Tests

Three linear potentiometers were used in this work to determine the rotation of the pile. Each linear potentiometer was calibrated independently where the movement of the pointer was controlled by a micrometer screw gauge. The devices were connected

Division of Proving Ring	Load (kN)	Reading 1 (mV)	Reading 2 (mV)	Average Reading (mV)
0.00	0.00	0.434	0.242	0.338
20	0.117	6.609	6.463	6.536
40	0.234	12.915	12.837	12.876
60	0.351	19.422	19.295	19.356
80	0.468	25.658	25.725	25.692
100	0.585	32.056	32.037	32.047
120	0.702	38.955	38.902	38.929
140	0.820	45.434	45.385	45.410
160	0.937	52	51.927	51.964
180	1.054	58.153	58.320	58.237
200	1.171	64.534	64.534	64.534

Table C1 : Calibration reading of a 250 lb load cell used in a single pile test

to the data logger at channels 21,23 and 25 for the top, middle and bottom linear potentiometers respectively. A movement at every 0.1 inches was compared with the output from each linear potentiometer. The first 10 readings of each linear potentiometer were recorded during the increasing movement of the micrometer screw gauge while the second set of readings were taken when the micrometer was unscrewed back to the normal position. The movement of the micrometer screw gauge was then plotted against the average linear potentiometer to obtain the calibration reading. Graphs of the linear potentiometer calibrations are shown in Fig.C2(a), C2(b) and C2(c).

Division of Proving Ring	Load (kN)	Reading 1 (mV)	Reading 2 (mV)	Average Reading (mV)
0.00	0.00	0.324	0.331	0.327
20	0.117	1.099	1.087	1.093
40	0.234	1.858	1.859	1.859
60	0.351	2.617	2.627	2.622
80	0.468	3.418	3.425	3.422
100	0.585	4.244	4.217	4.231
120	0.702	5.014	4.980	4.997
140	0.820	5.803	5.756	5.780
160	0.937	6.562	6.521	6.542
180	1.054	7.309	7.309	7.303
200	1.171	8.057	8.057	8.057

Table C2 : Calibration reading of a 2000 lb load cell used in the continuous pile test

Appendix C

Distance travel(ins)	Distance travel(mm)	Top 1 Ω	Top 2 Ω	Average Ω	Middle 1 Ω	Middle 2 Ω	Average Ω	Bottom 1 Ω	Bottom 2 Ω	Average Ω
0.00	0.00	19290	19292	19291	19309	19310	19309.5	19311	19319	19315
0.10	2.54	17640	17636	17638	17680	17679	17679.5	17634	17641	17637.5
0.20	5.08	16005	15992.6	15998.8	16022	16023.6	16022.8	15916	15919	15917.5
0.30	7.62	14285	14317.3	14301.2	14304	14304	14304	14149	14156.1	14152.6
0.40	10.16	12604.5	12611.2	12607.9	12536.1	12538.3	12537.2	12461.2	12470.1	12465.7
0.50	12.70	10849.7	10860.3	10855	10785	10785.7	10785.35	10703.3	10708.3	10705.8
0.60	15.24	9138.2	9140.5	9139.35	9029.3	9029.2	9029.25	8937.4	8941.2	8939.3
0.70	17.78	7360.4	7379.6	7370	7313.7	7312.4	7313.05	7212.7	7214.4	7213.55
0.80	20.32	5596	5590.8	5593.40	5597.5	5595.7	5596.6	5515.7	5515.6	5516.5
0.90	22.86	3830.2	3832.9	3831.55	3867.7	3859.9	3863.80	3836.2	3834	3835.1
1.00	25.40	2074.8	2074.8	2074.8	2132.4	2132.4	2132.4	2161.6	2161.6	2161.6

Table C3 : Calibrations readings of the top, middle and bottom linear plastic conductive potentiometers.

iii) Load cell calibrations for the Conventional Test

In the conventional tests a switch box and a digital display were used instead of the data logger. The digital display was connected to the switch box where each switch is incorporated to a specific channel for the device used.

During the calibration of the load cell a secure point is used to hang the load cell. Hanging loads, including the hanger, were added in 20 lbs weight increment. Each load was compared with the reading on the digital display in milli-volt. The load reading was plotted against the digital display value, as shown in Fig.C3 and the calibration of the load cell obtained.

Load (lbs)	Display Reading(mV)
Hanger	0.70
20	1.13
40	1.54
60	1.95
80	2.36
100	2.77
120	3.18
140	3.60
160	4.02

Table C4 : Load cell calibration in a conventional test

iv) Calibration of Linear Voltage Displacement Transducers(LVDT's) for the Conventional Test

Similar to the calibration of the linear potentiometer used in the centrifuge test, the movement of the LVDT's is controlled by the micrometer screw gauge. An increment of every 0.05 inches was adopted to compare with the output from the LVDT's. The two LVDT's used in the test, were calibrated independently. The devices were also connected to digital display units where the readings were given in milli-volt. Results shown in Fig.C4 were used to obtain the calibrations reading.

Distance Travel (Inches)	Channel 3 (Top Device) (V)	Channel 2 (Bot. device) (V)
0.00	-1.941	-0.754
0.05	-1.831	-0.642
0.10	-1.720	-0.530
0.15	-1.611	-0.418
0.20	-1.502	-0.307
0.25	-1.393	-0.195
0.30	-1.285	-0.083
0.35	-1.176	+0.028
0.40	-1.067	+0.140
0.45	-0.959	+0.252
0.50	-0.850	+0.364
0.55	-0.742	+0.476
0.60	-0.635	+0.589
0.65	-0.526	+0.701
0.70	-0.418	+0.814

0.75	-0.310	+0.928
0.80	-0.202	+1.041
0.85	-0.093	+1.155
0.90	+0.015	+1.268
0.95	+0.124	+1.382
1.00	+0.233	+1.495

Table C5 : Linear Voltage Displacement Transducer calibration

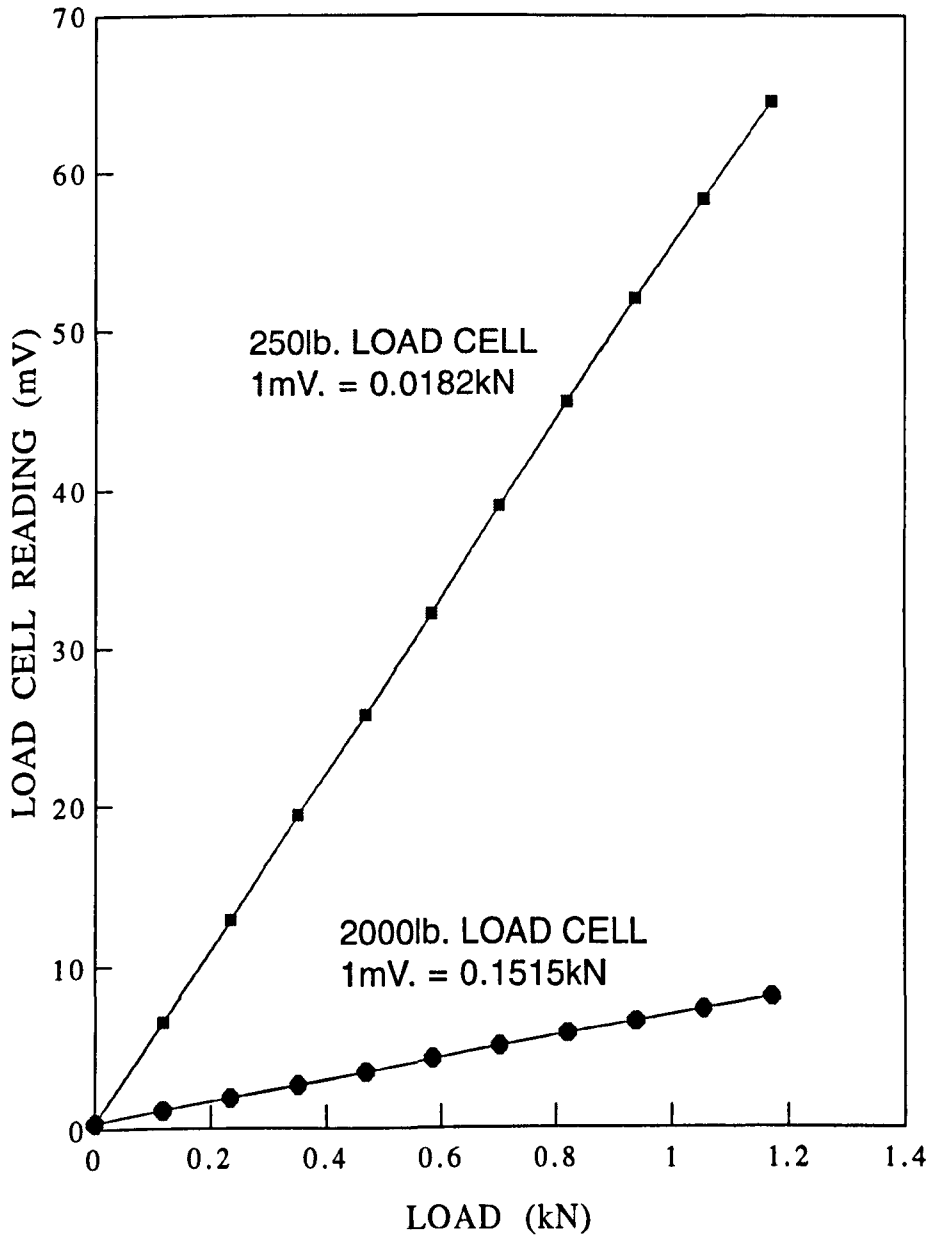

Figure C1 Calibration of load cell for centrifugal test

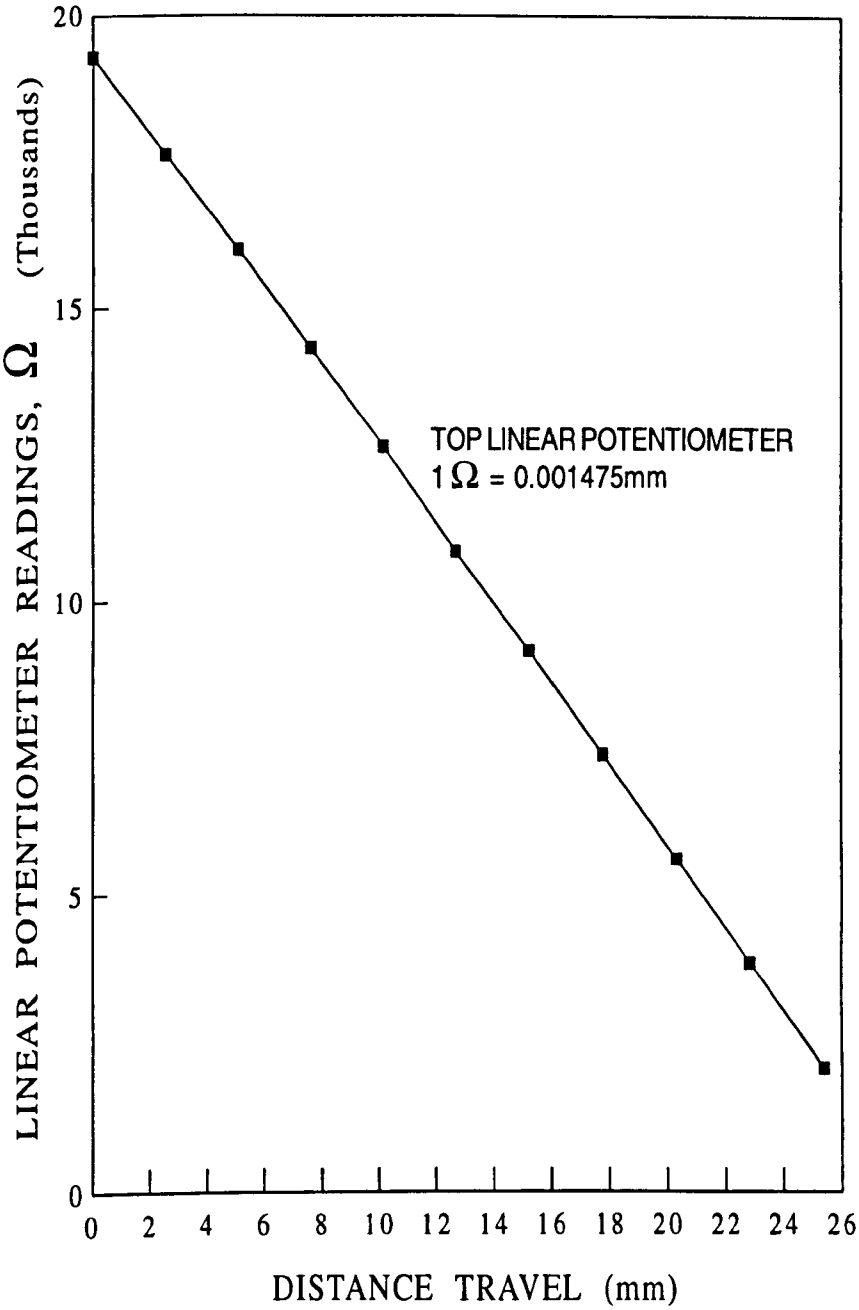

Figure C2(a) Calibration of top linear potentiometer for centrifugal test

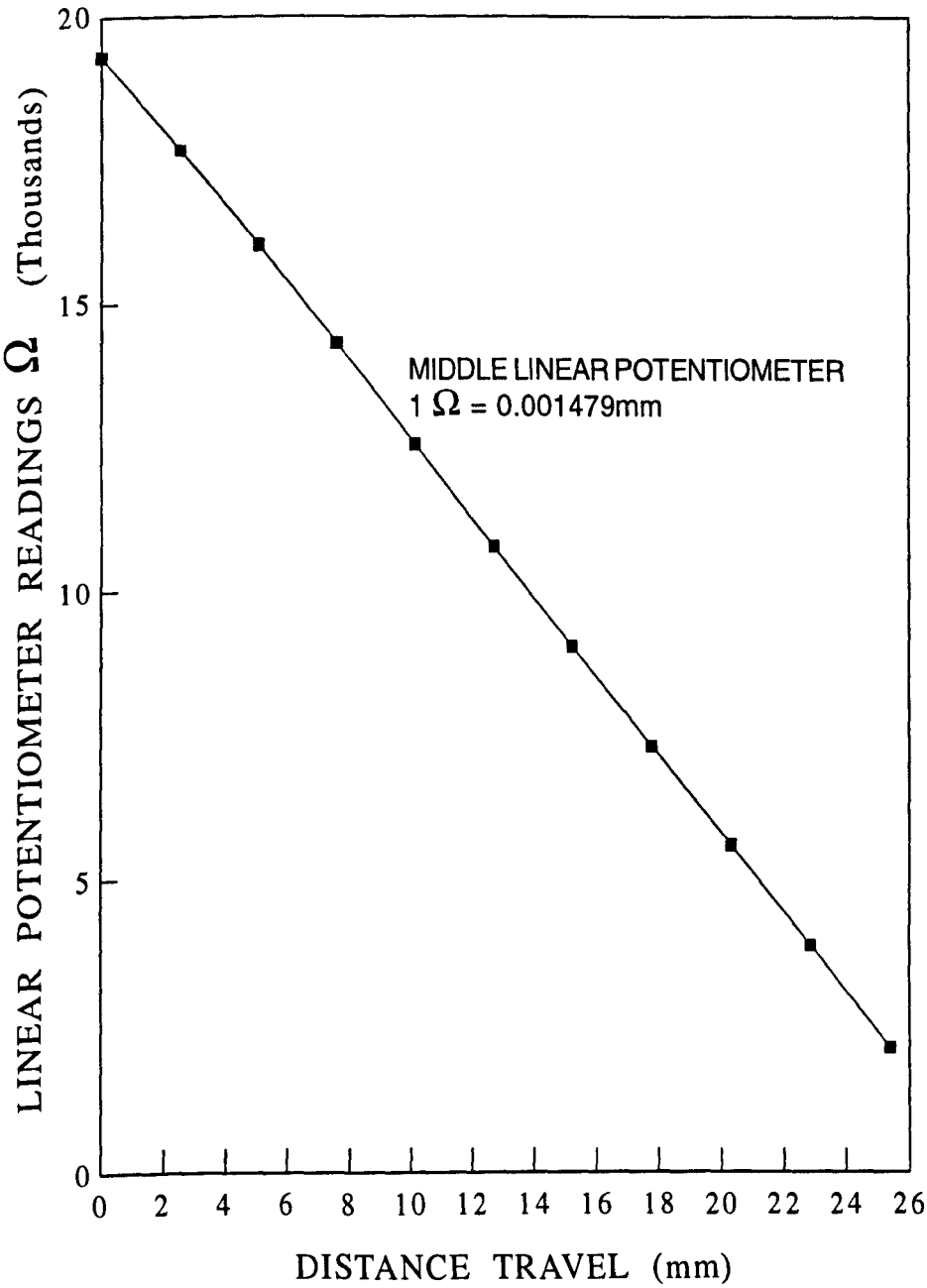

Figure C2(b) Calibration of middle linear potentiometer for centrifugal test

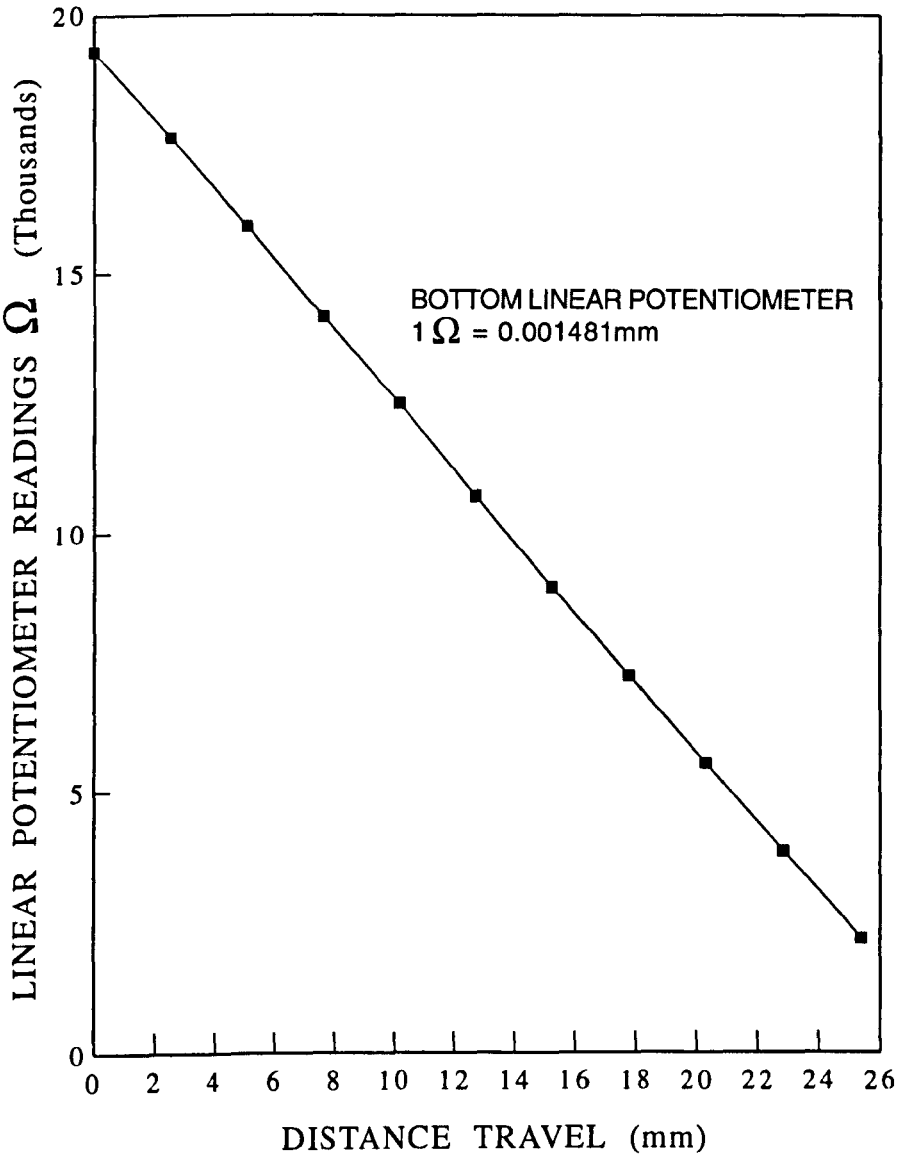

Figure C2(c) Calibration of bottom linear potentiometer for centrifugal test

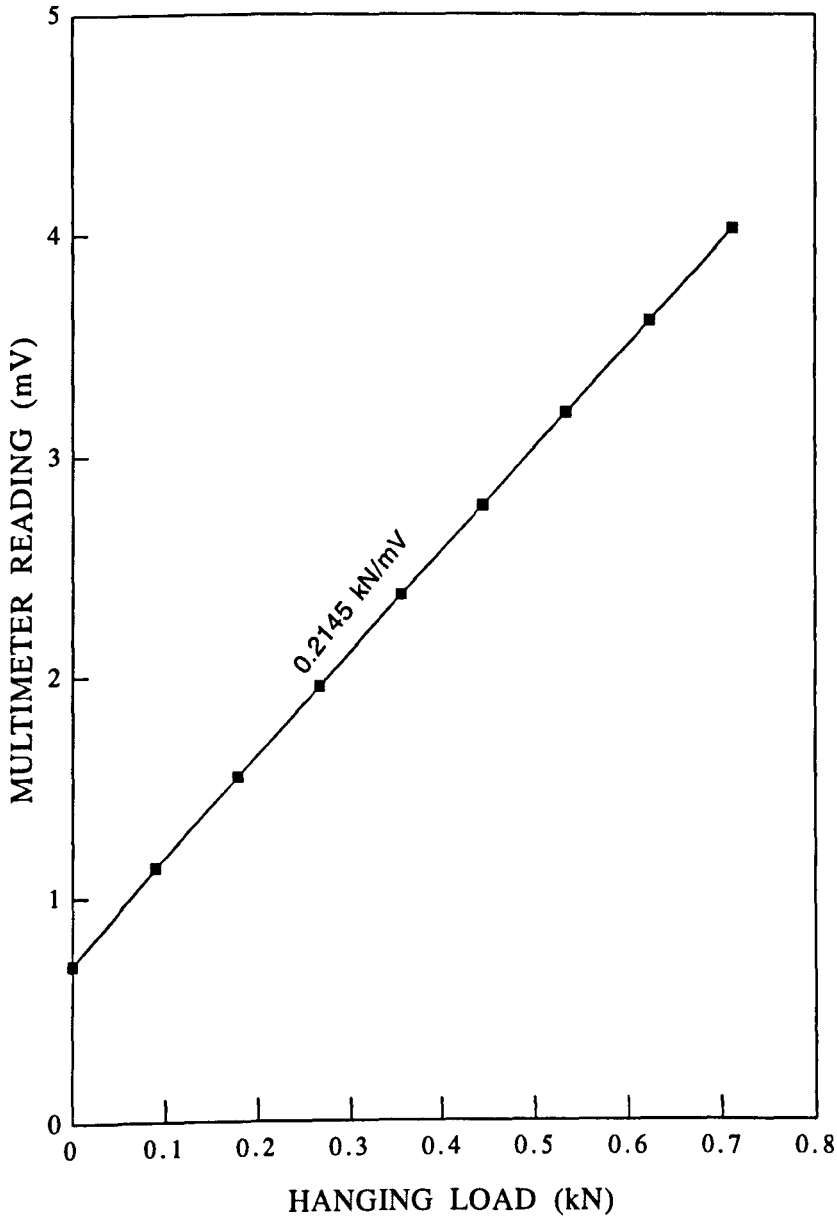

Figure C3 Calibration of SANGAMO load cell for conventional test

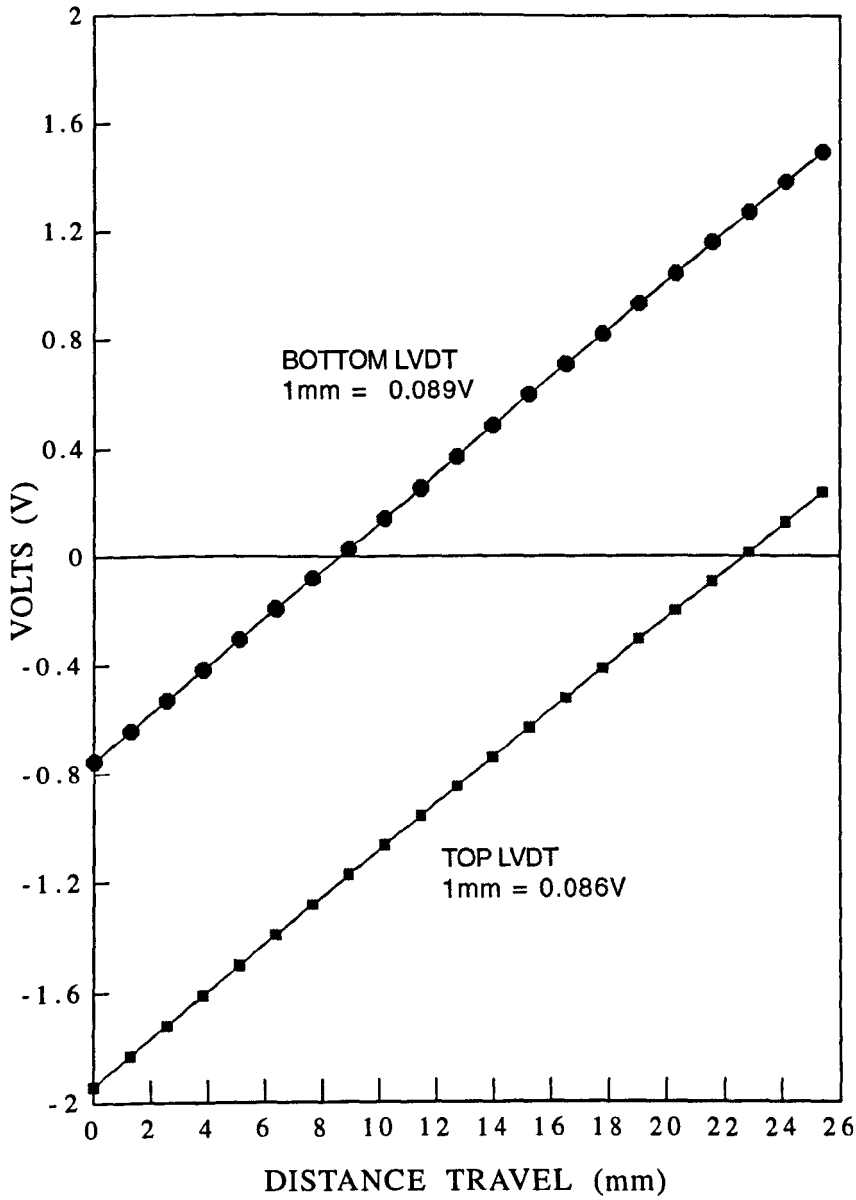

Figure C4 Calibration of LVDT's for conventional test

APPENDIX D

APPENDIX D

D1 : PROGRAMME TO READ THE DATA FROM DATA LOGGER

```
   10REM*************************************************************
   20REM** Ph.D (GEOTECH. ENG. 1991/94 (RAMLI NAZIR)TO INVESTIGATE THE **
   22REM** MOMENT CARRYING CAPACITY OF A CIRCULAR SHORT PILE IN SAND   **
   40REM*************************************************************
   50ON ERROR GOTO1810
   55*ADFS
   60CLOSE#0
   70*INITIALISE
   80MODE128
   90@%=&2030A
  100DIMZ(200,4),x1(200),x2(200),x3(200),x4(200),y(200),sload(200),temp(200):Z
1:length=215:gamma = 0
  110*STYLE CL
  120PROCInitialise
  130IF FF=1 THEN T=1000:GOTO860
  140DA$=TIME$
  150PROCTest_no
  160PO%=OPENOUT(TN$)
  170PRINT#PO%,diameter
  180PRINT#PO%,pileweight
  190PRINT#PO%,DA$
  200PRINT#PO%,LCAL
  210PRINT#PO%,D1CAL
  211PRINT#PO%,D2CAL
  212PRINT#PO%,D3CAL
  213PRINT#PO%,datum
  214PRINT#PO%,spacing
  215PRINT#PO%,position
  220PRINT#PO%,SPEED
  230PRINT#PO%,g
  250PRINT#PO%,condition$
  255:
  260*IEEE
  270T=0:CO=0
  280cmd%=OPENIN("COMMAND")
  290data%=OPENIN("DATA")
  300PRINT#cmd%,"BBC DEVICE NO",0
  310PRINT#cmd%,"CLEAR"
  320Endtime=TIME + 400
  330REPEAT UNTIL TIME>Endtime
  340PRINT#cmd%,"REMOTE ENABLE"
  350PRINT#cmd%,"LOCAL LOCKOUT"
  360PRINT#cmd%,"END OF STRING",CHR$(13)
  370orion%=OPENIN("16")
  380PRINT#cmd%,"UNLISTEN"
  390PRINT#cmd%,"LISTEN",orion%,"EXECUTE"
  400RESTORE700
  405:
  410CLS
  420DA$=TIME$:PRINTTIME$:PRINT:PRINT"TEST NO. "TN$:PRINT
  430PRINT"     LOAD                    DEFLECTION"
  440PRINT"     CELL        TOP          MIDDLE         BOTTOM      ROTATION "
  450PRINT"-------------------------------------------------------------------"
  460VDU28,0,26,79,5
  470READ task$
  480IF task$="END"THEN 510
  490PRINT#data%,task$
  500GOTO470
  510PRINT#cmd%,"UNLISTEN"
  520IF INKEY(-33)THENPROCSend_command
  530IF INKEY(-117)THENSOUND1,-15,53,2:GOTO390
  540IF INKEY(-120)THENSOUND1,-15,53,2:PROCTerminate :GOTO850
  550PRINT#cmd%,"STATUS"
```

```
  560INPUT#cmd%,state%
  570IF (state% AND 32)<>32 THEN GOTO670
  580PROCSerial_poll
  590IF (ASC(orionstatus$)AND 64)<>64 THEN690
  600PROCCollect_data
  610IF LEFT$(oriondata$,1)<>"C"  THEN 520
  620OD$=MID$(oriondata$,6,8)+MID$(oriondata$,26,8)+MID$(oriondata$,46,8)+MID$(
riondata$,66,8)
  630reading$=OD$
  640T=T+1:count=T:I=T:PROCCrunch
  650PRINTload"   "top_deflection"   "middle_deflection"   "bottom_deflection"
"rotation"   "count
  660PROCDump
  670GOTO520
  680:
  690PRINT"Request not from ORION":PROCTerminate
  700DATA "HA"
  710DATA "CH 1 SE 645"
  720DATA "CH 21-25 SE 685"
  730DATA "TA 1 OP ME TR TI DE 0 CO * RE IN IN 15"
  740DATA "TA 1 CH 1,21,23,25 AT F LO EV FO CO MA VA TO GP"
  750DATA "MO OF"
  760DATA "RU"
  770DATA "END"
  780:
  790DEFPROCDump
  800*ADFS
  810PRINT#PO%,reading$
  820*IEEE
  830ENDPROC
  840:
  850*ADFS
  860CLOSE#0:ZO%=OPENIN(TN$)
  870VDU26
  880INPUT#ZO%,diameter:DM$=STR$(diameter)
  890INPUT#ZO%,pileweight:pw$=STR$(pileweight)
  900INPUT#ZO%,DA$
  910INPUT#ZO%,LCAL:L$=STR$(LCAL)
  920INPUT#ZO%,D1CAL:D1$=STR$(D1CAL)
  921INPUT#ZO%,D2CAL:D2$=STR$(D2CAL)
  922INPUT#ZO%,D3CAL:D3$=STR$(D3CAL)
  923INPUT#ZO%,datum
  924INPUT#ZO%,spacing
  925INPUT#ZO%,position
  930INPUT#ZO%,SPEED
  940INPUT#ZO%,g
  960INPUT#ZO%,condition$
  965IF condition$="LOOSE" THEN gamma= 14.2 ELSE gamma =16
  970PROCCheck
  980:
  990VDU2
  995PRINT
 1000PRINT"DATE OF TEST     = ";DA$;
 1010PRINT "        TEST NO.   = ";
 1020*STYLE N
 1030PRINTTN$
 1040*STYLE XN
 1050PRINT STRING$(96,"-")
 1060PRINT
 1080PRINT"                              SAND CONDITION (DENSE/LOOSE) = ";condition$
 1090PRINT"                                   PILE DIAMETER  = ";diameter
 1100PRINT"                                  WEIGHT OF PILE  = ";pileweight
 1110PRINT"                                SPEED OF ROTATION  = ";SPEED
 1120PRINT"                              GRAVITATIONAL FORCE  = ";g
 1122PRINT"            SPACING OF DISPLACENT TRANSDUCERS (mms.) = ";spacing
 1123PRINT"     POSITION OF LOAD CELL (ABOVE SAND LEVEL) (mms.) = ";datum
```

```
 1124PRINT"        BOTTOM DISP. TRANS. FROM DATUM LEVEL ( mms.) = "position
 1130PRINT:PRINT
 1140PRINT"              LOAD CELL CALIBRATION FACTOR ( KN/DIV ) = "L$
 1150PRINT"   TOP DISPLACEMENT TRANSDUCER CAL.  FACTOR (mm/DIV) = "D1$
 1151PRINT"MIDDLE DISPLACEMENT TRANSDUCER CAL.  FACTOR (mm/DIV) = "D2$
 1152PRINT"BOTTOM DISPLACEMENT TRANSDUCER CAL.  FACTOR (mm/DIV) = "D3$
 1160PRINT:PRINT
 1170@%=&2030C
 1180PRINT"                    MODEL TEST RESULTS
    PROTOTYPE TEST RESULTS":PRINT
 1190PRINT"       MODEL       TOP       MIDDLE      BOTTOM                    TO'
AL      TOP          MIDDLE          BOTTOM"
 1200PRINT"       LOAD        DEF.        DEF.        DEF.                  RESIS'
ANCE   DISP.          DISP.           DISP.  "
 1210*UNDERLINE ON
 1220PRINT"        KN.                    mms.
N.                    mms.                          "
 1230*UNDERLINE OFF
 1240Z$="":X=0:Z=0
 1250v=0
 1260FORI=1TOT
 1270INPUT#Z0%,A$:reading$=A$:PROCCrunch:PROCPrototype
 1280PRINTload,top_deflection,middle_deflection,bottom_deflection,rotation,,res
stance,top_displacement,middle_displacement,bottom_displacement"     "STR$(I)
 1290NEXTI
 1300PRINT
 1310CLOSE#Z0%
 1320*PCODE 12
 1330*INITIALISE
 1340VDU3
 1345A$=GET$:IFA$=""THEN1345
 1350PROCGraph
 1360*PCODE 12
 1370PROCPlotmate
 1380END
 1390:
 1400DEFPROCCheck
 1410CLS:PRINT"HERE ARE THE LIST OF CALIBRATIONS:"
 1420PRINT"1. DIAMETER OF PILE                                    = ";DM$
 1430PRINT"2. WEIGHT OF PILE                                      = ";pw$
 1440PRINT"3. LOAD CELL CALIBRATION                               = ";L$
 1450PRINT"4. TOP DISPLACEMENT TRANSDUCER CALIBRATION             = ";D1$
 1451PRINT"5. MIDDLE DISPLACEMENT TRANSDUCER CALIBRATION          = ";D2$
 1452PRINT"6. BOTTOM DISPLACEMENT TRANSDUCER CALIBRATION          = ";D3$
 1453PRINT"7. SPACING OF DISPLACEMENT TRANSDUCERS                 = ";spacing
 1454PRINT"8. POSITION OF LOAD CELL (ABOVE SAND LEVEL) (mms.)     = ";datum
 1455PRINT"9. BOTTOM DISP. TRANS. FROM DATUM LEVEL ( mms.)        = ";position
 1460PRINT"10.SPEED OF ROTATION (r.p.m.)                          = ";SPEED
 1470PRINT"11.GRAVITY FIELD                                       = ";g
 1490PRINT"12.SAND CONDITION (DENSE/LOOSE)                        = ";condition$
 1500PRINT:PRINT:PRINT"ARE THESE O.K ?";:INPUT A$
 1510IFA$="Y"THENGOTO1630
 1520INPUT "ENTER THE LINE NO. TO BE ALTERED";N
 1530IFN>12 OR N<0 THEN 1520
 1540ON N GOTO 1550,1560,1570,1580,1581,1582,1583,1584,1585,1590,1600,1610
 1550INPUT"DIAMETER OF PILE = ";diameter:DM$=STR$(diameter):GOTO1410
 1560INPUT"WEIGHT OF PILE + TIE BAR = ";pileweight:pw$=STR$(pileweight):GOTO14
 1570INPUT "LOAD CELL CALIBRATION = ";LCAL:L$=STR$(LCAL):GOTO1410
 1580INPUT"TOP DISPLACEMENT TRANSDUCER CALIBRATION = ";D1CAL:D1$=STR$(D1CAL):G
O1410
 1581INPUT"MIDDLE DISPLACEMENT TRANSDUCER CALIBRATION = ";D2CAL:D2$=STR$(D2CAL
GOTO1410
 1582INPUT"BOTTOM DISPLACEMENT TRANSDUCER CALIBRATION = ";D3CAL:D3$=STR$(D3CAL
GOTO1410
 1583INPUT" SPACING OF DISPLACEMENT TRANSDUCERS                   = ";spacing:GOTO14
 1584INPUT" POSITION OF LOAD CELL (ABOVE SAND LEVEL) (mms.) = ";datum:GOTO1410
```

```
1585INPUT" BOTTOM DISP. TRANS. FROM DATUM LEVEL ( mms.)     = ";position:GOTO14
0
1590INPUT"SPEED OF ROTATION (r.p.m.)          = ";SPEED:GOTO1410
1600INPUT"GRAVITY FIELD                       = ";g:GOTO1410
1610INPUT"SAND CONDITION (DENSE/LOOSE)        = ";condition$
1622IF condition$="LOOSE" THEN gamma= 14.2 ELSE gamma =16
1623GOTO1410
1630CLS:ENDPROC
1640:
1650DEFPROCInitialise
1660CLS:PRINT"Do you wish to read an existing test file (Y/N)";:INPUT A$
1670IFA$="Y"THENFF=1:GOTO1680 ELSE FF=0:GOTO1700
1680*CAT
1690PRINT"INPUT TEST NO.";:INPUT TN$
1700ENDPROC
1710:
1720DEFPROCCrunch
1730Q=1
1740FORY=1TO4:Z(I,Y)=VAL(MID$(reading$,Q,8))
1750Q=Q+8
1760NEXTY
1770load=(Z(I,1)-Z(1,1))*VAL(L$):moment=load*datum/1000:y(I)=moment
1780top_deflection=(Z(I,2)-Z(1,2))*VAL(D1$)*-1:x1(I)=top_deflection
1781middle_deflection=(Z(I,3)-Z(1,3))*VAL(D2$)*-1:x2(I)=middle_deflection
1782bottom_deflection=(Z(I,4)-Z(1,4))*VAL(D3$)*-1:x3(I)=bottom_deflection
1783difference=top_deflection-bottom_deflection
1784rotation=DEG(ATN(difference/spacing/2)):x4(I)=rotation
1790ENDPROC
1800:
1810IF ERR =6 THEN count=I-1:GOTO1300
1820PRINT"ERROR NO. =";ERR;" AT LINE NO. ";ERL
1830VDU3:END
1840:
1970DEF PROCSerial_poll
1980PRINT#cmd%,"SERIAL POLL",orion%,1
1990INPUT#cmd%,orionstatus$
2000ENDPROC
2010:
2020DEF PROCCollect_data
2030PRINT#cmd%,"TALK",orion%
2040INPUT#data%,oriondata$
2050PRINT#cmd%,"UNTALK"
2060length=LEN(oriondata$)
2070oriondata$=LEFT$(oriondata$,length-1)
2080ENDPROC
2090:
2100DEF PROCSend_command
2110SOUND1,-15,53,2
2120INPUT LINE "Enter Command : "command$
2130IF command$=""THEN910
2140PRINT#cmd%,"LISTEN",orion%,"EXECUTE"
2150PRINT#data%,command$
2160PRINT#cmd%,"UNLISTEN"
2170ENDPROC
2180:
2190DEF PROCTerminate
2200PRINT"Prog terminated"
2210PRINT#cmd%,"LISTEN",orion%,"EXECUTE"
2220PRINT#data%,"HA"
2230PRINT#cmd%,"UNLISTEN"
2240PRINT#cmd%,"REMOTE DISABLE"
2250ENDPROC
2260:
2270DEF PROCTest_no
2280CLS:INPUT "TEST NO = ";TN$
2290INPUT"DIAMETER OF PILE                    = ";diameter:DM$=STR$(diameter)
```

Appendix D

```
 2300INPUT"WEIGHT OF PILE                          = ";pileweight:pw$=STR$(pilewei
ht)
 2310INPUT"LOAD CELL CALIBRATION                   = ";LCAL:L$=STR$(LCAL)
 2320INPUT"TOP DISPLACEMENT TRANSDUCER CALIBRATION = ";D1CAL:D1$=STR$(D1CAL)
 2321INPUT"MIDDLE DISPLACEMENT TRANSDUCER CALIBRATION = ";D2CAL:D2$=STR$(D2CAL
 2322INPUT"BOTTOM DISPLACEMENT TRANSDUCER CALIBRATION = ";D3CAL:D3$=STR$(D3CAL
 2323INPUT"SPACING OF DISPLACENT TRANSDUCERS (mms.) = ";spacing
 2324INPUT"POSITION OF LOAD CELL (ABOVE SAND LEVEL) (mms.) = ";datum
 2325INPUT"BOTTOM DISP. TRANS. FROM DATUM LEVEL ( mms.) = "position
 2330INPUT"SPEED OF ROTATION (r.p.m.)              = ";SPEED
 2340INPUT"GRAVITY FIELD                           = ";g
 2360INPUT"SAND CONDITION (DENSE/LOOSE)           = ";condition$
 2362IF condition$="LOOSE" THEN gamma= 14.2 ELSE gamma =16
 2370PROCCheck
 2380ENDPROC
 2390:
 2400DEF PROCSort
 2410Q=1
 2420FORY=1TO8:Z(I,Y)=VAL(MID$(A$,Q,8)):PRINTZ(I,Y);
 2430Q=Q+8
 2440NEXTY
 2450PRINT
 2460A$=""
 2470ENDPROC
 2480:
 2490DEFPROCPrototype
 2500resistance=load*g*g:top_displacement=top_deflection*g:middle_displacement:
iddle_deflection*g:bottom_displacement=bottom_deflection*g
 2510ENDPROC
 2520:
 2530DEFPROCRaw
 2540INPUT"TEST NO. = ";TN$
 2550ZO%=OPENIN(TN$)
 2560INPUT#ZO%,diameter,pileweight,DA$,LCAL,D1CAL,D2CAL,D3CAL,datum,spacing,pos
tion,SPEED,g,condition$
 2570VDU2
 2580PRINTTN$,DA$:PRINT
 2590FORX=1TO1000
 2600INPUT#ZO%,A$
 2610PRINTSTR$(X),A$
 2620NEXTX
 2630CLOSE#0:*PCODE12:VDU3
 2640ENDPROC
 2650:
 2660DEFPROCGraph
 2670VDU23,1,0;0;0;0;:REM CURSOR OFF
 2680PROCChar
 2690X%=50:Y%=100
 2700CLS
 2710VDU29,150;150;
 2720MOVE0,800:DRAW0,0:DRAW1100,0:DRAW1100,800:DRAW0,800
 2730FORX=0TO1100 STEP50:MOVEX,8:DRAWX,0:NEXT
 2740FORX=0TO800 STEP50:MOVEX,800:DRAWX,792:NEXT
 2750MOVE800,800:DRAW800,700:DRAW1100,700
 2760VDU5:FORX=0 TO 1100 STEP100:MOVEX-20,-30:X$=STR$(INT(10*X/X%+.5)/10)
 2770IFLENX$<2 THENX$=X$+".0"
 2780PRINTX$:NEXT
 2790MOVE850,760:PRINTTN$
 2800FORY=0TO800 STEP 80:MOVE0,Y:DRAW 8,Y:MOVE-80,Y+10:PRINTLEFT$(STR$(INT((10(
*Y/Y%)*10+.5)/10),5):NEXT
 2810FORY=0TO640  STEP 80:MOVE1100,Y:DRAW 1092,Y:NEXT
 2820PRINT TAB(0,6):FORI=LEN(T$) TO 1 STEP-1:PRINTMID$(T$,I,1):NEXT
 2830MOVE 400,-100:PRINT"PILE DISPLACEMENT mms."
 2840IFA$="M" THEN PROCSmooth ELSE PROCCurve
 2850A$=GET$:IFA$=""THEN 2850
 2860IFA$="D" THEN X%=X%*2:IF X%>200 THEN X%=X%/2:GOTO2700
```

```
2870IFA$="D" THEN 2700
2880IFA$="U" THEN X%=X%/2:IF X%<50  THEN X%=X%*2:GOTO2700
2890IFA$="U" THEN 2700
2900IFA$="L" THEN Y%=Y%*2:GOTO2700
2910IFA$="S" THEN Y%=Y%/2:GOTO2700
2920IFA$="M" THEN 2700
2930IFA$="P"THENVDU2:PRINT:PRINT:PRINT:VDU3:*GDUMP 1 1 3 1 20
2940VDU4
2950VDU23,1,1;0;0;0;
2960ENDPROC
2970:
2980DEFPROCChar
2990VDU23,224,0,56,124,198,130,254,254,0: REM "D" SIDEWAYS
3000VDU23,225,0,130,146,146,146,254,254,0: REM "E" SIDEWAYS
3010VDU23,226,254,254,64,48,64,254,254,0: REM "M" SIDEWAYS
3020VDU23,227,0,6,6,6,6,254,254,0:REM "L" SIDEWAYS
3030VDU23,228,0,126,254,144,144,254,126,0:REM "A" SIDEWAYS
3040VDU23,230,0,124,254,130,130,254,124,0:REM "O"  SIDEWAYS
3050VDU23,234,0,0,130,198,124,56,0,0:    REM "("  SIDEWAYS
3060VDU23,235,0,34,54,28,8,254,254,0:    REM "k"  SIDEWAYS
3070VDU23,236,0,30,62,32,32,62,62,0:    REM "n"  SIDEWAYS
3080VDU23,240,0,0,0,3,3,0,0,0    :    REM "."  SIDEWAYS
3090VDU23,231,0,254,254,28,112,254,254,0: REM "N" SIDEWAYS
3100VDU23,242,0,0,56,124,198,130,0,0:    REM ")"  SIDEWAYS
3110T$=CHR$(226)+CHR$(230)+CHR$(224)+CHR$(225)+CHR$(227)+" "
3120T$=T$+CHR$(227)+CHR$(230)+CHR$(228)+CHR$(224)+" "
3130T$=T$+CHR$(234)+CHR$(231)+CHR$(242)
3140ENDPROC
3150:
3160DEFPROCCurve
3170MOVE0,0
3180FORX=1TOcount
3190DRAWx1(X)*X%,y(X)*Y%
3200NEXT
3201MOVE0,0
3202FORX=1TOcount
3203DRAWx2(X)*X%,y(X)*Y%
3204NEXT
3205MOVE0,0
3206FORX =1 TO count
3207DRAWx3(X)*X%,y(X)*Y%
3208NEXT
3210ENDPROC
3220:
3230DEFPROCPlotmate
3240CLS:PRINT"DO YOU WANT A PLOT OF PROTOTYPE LOAD AGAINST DISPLACEMENT (Y/N)"
3250A$=GET$:IFA$=""THEN3250
3260IFA$="N" THEN 3570
3270IFA$="Y"THEN3300
3280GOTO3250
3290PRINT
3300PRINT"PLEASE INSERT PEN AND PAPER INTO PLOTMATE AND PRESS RETURN WHEN READ
"
3310A$=GET$:IFA$<>CHR$(13) THEN 3310
3320PROCScales
3330*PLTMATE
3340VDU 23,255,0,0,0,0,0,0,0,64
3350VDU29,500;200;
3355GOTO3500:REM TO PLOT CURVE ONLY!
3360MOVE0,0:DRAW0,1600:DRAW2000,1600:DRAW2000,0:DRAW0,0
3370FORX=0TO2000 STEP100:MOVEX,10:DRAWX,0:NEXT
3380FORX=0TO2000 STEP 200:MOVEX-40,-30:VDU5:PRINTSTR$(INT(X*X%/2000)):VDU4:NEX
3390FORX=0TO1600 STEP100:MOVEX,1600:DRAWX,1590:NEXT
3400MOVE1600,1600:DRAW1600,1400:DRAW2000,1400
3410MOVE1700,1520:VDU5:PRINTTN$:VDU4
3420FORY=0TO1600 STEP200:MOVE0,Y:DRAW 10,Y:MOVE-130,Y+15:VDU5:PRINTSTR$(INT(Y*
```

```
%/1600)):VDU4:NEXT
 3430FORY=0TO1600 STEP200:MOVE2000,Y:DRAW 1990,Y:NEXT
 3440MOVE 1200,-70:VDU5:PRINT"PILE ROTATION (degrees)"
 3442MOVE 200,-150:PRINT"FIG.       PILE ROTATION AGAINST MODEL MOMENT":VDU4
 3443GOTO3500
 3450MOVE -250,400:VDU5
 3460VDU23,255,5,6,0,2,0,0,0,64
 3470PRINT"MODEL MOMENT (N.m)"
 3480VDU 23,255,0,0,0,0,0,0,0,64
 3490VDU4
 3495GOTO3550
 3500MOVE0,0
 3505X%=20
 3510FORX=1TO count:
 3520REM   DRAWg*x1(X)*2000/X%,g*g*y(X)*1600/Y% IS CHANGED TO 3525
 3525DRAWx4(X)*2000/X%,g*g*y(X)*1000*1600/g/g/Y%:REM MAYBE!!!!
 3530NEXT
 3535MOVEx4(X-1)*2000/X%+20,g*g*y(X-1)*1000*1600/g/g/Y%:VDU5:PRINTRIGHT$(TN$,2)
VDU4
 3536GOTO3450
 3550*PARK
 3560*OFFMATE
 3570ENDPROC
 3580:
 3590DEFPROCScales
 3600CLS:PRINT"CHOOSE MAXIMUM LOAD IN UNITS OF 800 ";:INPUT Y%
 3610PRINT:PRINT"CHOOSE MAXIMUM DISPLACEMENT IN UNITS OF 200";:INPUTX%
 3620CLS:PRINT"HERE ARE YOUR CHOSEN VALUES:":PRINT
 3630PRINT"         MAXIMUM LOAD ="Y%
 3640PRINT"MAXIMUM DISPLACEMENT ="X%
 3650PRINT:PRINT"ARE THESE OK?"
 3660A$=GET$:IFA$<>"Y"ANDA$<>"N"THEN3660
 3670IFA$="N" THEN 3600
 3680ENDPROC
 3685:
 3690DEFPROCSmooth
 3700FOR X =1 TO count:temp(X)=y(X):NEXT
 3710ZZ=1
 3720IF ZZ>=6 THEN 3790
 3730FORI=3 TO count-2
 3740sload(I)=.6*temp(I)+.15*(temp(I-1)+temp(I+1))+.05*(temp(I-2)+temp(I+2))
 3750NEXTI
 3760sload(1)=temp(1):sload(2)=temp(2):sload(count)=temp(count):sload(count-1):
emp(count-1)
 3770FORX=1TO count:temp(X)=sload(X):NEXT
 3780ZZ=ZZ+1:GOTO3720
 3790MOVE0,0
 3800FORX= 1 TO count
 3810DRAWx(X)*X%,sload(X)*Y%
 3820NEXT
 3830ENDPROC
 3835:
 3840REM ENTER THE FOLLOWING LINES FOR DOTTED PRINT-OUT
 3850REM 965 GOTO1220
 3860REM 1250 REM
 3870REM 3100PLOT 69,x(X)*X%,y(X)*Y%
 3880REM 3430PLOT69,g*x(X)*2000/X%,g*g*y(X)*1600/Y%
 3890REM 1290REM
```

APPENDIX D

D3: PROGRAMME TO PLOT LATERAL FORCE AGAINST LATERAL DISPLACEMENT AT GROUND LEVEL

```
      INTEGER REC(200)
      ND(200)
      REAL R(200),RD(200),Y(200),DIFFD(200),DISD(200),
      REAL DISP(200),X(200),DIFF(200),DIS(200),DISDP(200),
      REAL YP(200),YDP(200),TX(200),MX(200),BX(200),BXD(200)
      REAL XD(200),YD(200),TXD(200),MXD(200),
      CHARACTER RESULT*20,TITLE*15,DATAFILE*20
      PARAMETER(UNDEF=999.999)


C     ********************************************************
C                        NOTATION
C     ********************************************************
C     SPACING BETWEEN TOP AND BOTTOM TRANSDUCER = 40mm
C     G : ARTIFICIAL GRAVITY VALUE
C     E : PULLING HEIGHT
C     N/REC/ND : NUMBER OF DATA
C     PJ: PILE LENGTH
C     BH: HEIGHT OF BOTTOM DISPLACEMENT TRANSDUCER FROM
C     PULLING CABLE
C     H : HEIGHT OF TOP DISPLACEMENT TRANSDUCER FROM GROUND
C     LEVEL
C     R : ANGLE OF ROTATION IN TERM OF RADIAN
C     RD: ANGLE OF ROTATION IN TERM OF RADIAN AT PEAK VALUE
C     X : ANGLE OF PILE ROTATION
C     Y : PULLING FORCE
C     YP: PROTOTYPE PULLING FORCE
C     TX: TOP DISPLACEMENT READING
C     MX: MIDDLE DISPLACEMENT READING
C     BX: BOTTOM DISPLACEMENT READING
C     DIS: DISPLACEMENT AT GROUND LEVEL
C     DISP: PROTOTYPE DISPLACEMENT AT GROUND LEVEL
C     DISMAX: MAXIMUM DISPLACEMENT AT GROUND LEVEL
C     YMAX: MAXIMUM PULLING FORCE
C     YD : PEAK PULLING FORCE VALUE
C     YDP: PROTOTYPE PEAK PULLING FORCE VALUE
C     DISD: DISPLACEMENT AT GROUND LEVEL AT PEAK VALUE
C     DISDP: PROTOTYPE DISPLACEMENT AT GROUND LEVEL AT PEAK
C     VALUE
```

```
C       TXD: TOP DISPLACEMENT READING AT PEAK VALUE
C       MXD: MIDDLE DISPLACEMENT READING AT PEAK VALUE
C       BXD: BOTTOM DISPLACEMENT READING AT PEAK VALUE
C       XEND: END DISPLACEMENT VALUE
C       YEND: END OF PULLING FORCE VALUE
C       YENDP: END OF PROTOTYPE PULLING FORCE VALUE

C       ******************************************************
C               OPENING DATA FILE
C       ******************************************************

        READ(15,*)G
        PRINT *,'ENTER THE NAME OF RESULT FILE WITH PATH'
        READ  '(A)',RESULT
        OPEN(15,FILE=DATAFILE,STATUS='OLD')
        OPEN(14,FILE=RESULT,STATUS='NEW')
        READ(15,'(15A)')TITLE
        READ(15,*)E,BH,N,PJ,XEND,YEND


C*************************************************************************
C               CALCULATION FOR MAXIMUM LOAD AND DISPLACEMENT
C*************************************************************************
        G=50
        YENDS=YEND*G**2
        DISMAX=DISMAXS*G
        YMAX=YMAXS*G**2
                YMAX=0.0
                DISMAX=0.0
        XENDP=XEND*G
        YENDP=YENDS
        TG=E+BH
        H=TG+40

        DO 67 I=1,N
        READ(15,*)REC(I),X(I),Y(I),TX(I),MX(I),BX(I)
        YP(I)=Y(I)*G**2
        R(I)=X(I)*3.142/180
        DIFF(I)=H*TAN(R(I))
        DIS(I)=TX(I)-DIFF(I)
        DISP(I)=DIS(I)*G
                IF(YP(I).GT.YMAX)THEN
                YMAX=YP(I)
                DISMAX=DISP(I)
                ENDIF
```

```
      WRITE(14,*)REC(I),Y(I),DISP(I)
 67   CONTINUE
      WRITE(14,*) 'MAX. LOAD = ',YMAX
      WRITE(14,*) 'MAX. DISP.= ',DISMAX

C*********************************************************************
C                  CALCULATION OF PEAK POINT VALUE
C*********************************************************************

      READ(15,*)L
      DO 68 M=1,L
      READ(15,*)ND(M),XD(M),YD(M),TXD(M),MXD(M),BXD(M)
      YDP(M)=YD(M)*G**2
      RD(M)=XD(M)*3.142/180
      DIFFD(M)=H*TAN(RD(M))
      DISD(M)=TXD(M)-DIFFD(M)
      DISPD(M)=DISD(M)*G
      WRITE(14,*)ND(M),YD(M),DISD(M)
 68   CONTINUE

C     ********************************************************
C           UNIRAS PLOTTING SUBROUTINE
C           SELECT AND CHOOSE OPEN DEVICE
C     ********************************************************

      CALL GROUTE('SELECT HPOSTA4;EXIT')
      CALL GOPEN
      CALL RORIEN(2)

C     ********************************************************
C           INITIALISED PLOTTING AREA
C     ********************************************************

      CALL GRPSIZ(XS,YS)
      CALL GVPORT(XS*.3,YS*.3,XS*.5,YS*.6)
      CALL GWBOX(XS*.5,YS*.6,0.)
      CALL GLIMIT(0.0,XENDP,0.0,YENDP,0.0,0.0)
      CALL GSCALE

C     ********************************************************
C                        PLOT AXIS
C     ********************************************************

      CALL RAXLAS(2)
      CALL RAXDIS(5,1,0)
      CALL RAXDIS(6,1,0)
      CALL RTXEXP(1.5)
```

```
      CALL RAXTEF(6,'TRIP',0)
      CALL RAXTEX(6,-2,'PILE DISPLACEMENT (mm)',UNDEF,UNDEF,3.0)
      CALL RAXLFO(1,0,2,1)
      CALL RAXIS(1,0.0,3.,1)

      CALL RAXTEX(6,-2,'LATERAL FORCE, F (kN)', UNDEF, UNDEF,3.0)
      CALL RAXLFO(4,0,1,1)
      CALL RAXIS(2,0.0,3.,1)
      CALL RTXEXP(1.0)

C     ********************************************************
C                   ENCLOSING THE GRAPH LINE
C     ********************************************************

      CALL GVECT(0.0,YENDP,0)
      CALL GWICOL(0.01,1)
      CALL GVECT(XENDP,YENDP,1)
      CALL GVECT(XENDP,0.0,1)

C     ********************************************************
C             DRAW LINE THROUGH EVERY POINT
C     ********************************************************

      CALL GWICOL(0.1,1)
      CALL GDASH(7)
      CALL GVECT(DISP,YP,N)
      CALL GWICOL(0.35,1)
      CALL GDASH(0)
      CALL GVECT(DISPD,YDP,L)
      CALL RTXANG(0.00)

C     ********************************************************
C             PLOTTING A MAXIMUM LINE
C     ********************************************************

      CALL GVECT(0.0,YMAX,0)
      CALL GDASH(3)
      CALL GVECT(DISMAX,YMAX,1)
      CALL GDASH(3)
      CALL GVECT(DISMAX,0.0,1)
      CALL RTXFON('DUPL',0)
      CALL RTXHEI(2.5)
      CALL RTXJUS(1,2)
      CALL RTX(1,'X',DISMAX,YMAX)
```

```
C       ********************************************************
C               PLOTTING THE TEXT FOR MAXIMUM VALUE
C       ********************************************************

        CALL RTXFON('DUPL',0)
        CALL RTXHEI(2.0)
        CALL RTXJUS(0,4)
        CALL RTX(15,'MAXIMUM FORCE = ', DISMAX/20.0,YMAX+YMAX/20.0)
        CALL RTXNC(YMAX,4)
        CALL RTXC(3, 'kN')
        CALL RTXANG(270.00)
        CALL  RTX(15,  'DISPLACEMENT  =  ',  DISMAX+DISMAX/15,+YMAX-
        YMAX/5)
        CALL RTXNC(DISMAX,2)
        CALL RTXC(3,'mm')
        CALL RTXANG(0.0)

C       ********************************************************
C               REFERENCE TITLE OF THE GRAPH
C       ********************************************************
        CALL GSCAMM
        CALL GWICOL(0.1,1)
        CALL GVECT(0.55*XS,0.9*YS,0)
        CALL GVECT(0.55*XS,0.9*(YS-10.0),1)
        CALL GVECT(0.8*XS,0.9*(YS-10.0),1)
        CALL RTXFON('COMP',0)
        CALL RTXHEI(3.0)
        CALL RTXJUS(0,4)
        CALL RTX(7,'MODEL: ',0.55*(XS+5.0),0.9*(YS-2.0))
        CALL RTXC(8,TITLE)
        CALL GCLOSE
        CLOSE(15)
        CLOSE(14)
999     STOP
        END
```

APPENDIX D

D4 : PROGRAMME TO PLOT MOMENT AT GROUND VERSUS PILE ROTATION

```
      INTEGER REC(200)
      ND(200)
      REAL Y(200),MOM(200),MOMT(200),MOMP(200),MOMTP(200),
      REAL TX(200),X(200),MX(200),BX(200),XD(200),YD(200),
      REAL TXD(200),MXD(200),BXD(200)
      CHARACTER TITLE*15,DATAFILE*20
      PARAMETER(UNDEF=999.999)

C     ********************************************************
C                        NOTATION
C     ********************************************************
C     G : ARTIFICIAL GRAVITY VALUE
C     E : PULLING HEIGHT
C     N/REC/ND : NUMBER OF DATA
C     PJ: PILE LENGTH
C     X : ANGLE OF PILE ROTATION
C     Y : PULLING FORCE
C     TX: TOP DISPLACEMENT READING
C     MX: MIDDLE DISPLACEMENT READING
C     BX: BOTTOM DISPLACEMENT READING
C     MOM: MOMENT AT GROUND LEVEL
C     MOMP: PROTOTYPE MOMENT AT GROUND LEVEL
C     MMAX: MAXIMUM MOMENT AT GROUND LEVEL
C     XMAX: PILE ROTATION AT MAXIMUM MOMENT VALUE
C     MOMT: PEAK MOMENT VALUE
C     MOMTP: PROTOTYPE PEAK MOMENT VALUE
C     XD: PILE ROTATION AT PEAK VALUE
C     YD: PULLING FORCE AT PEAK VALUE
C     TXD: TOP DISPLACEMENT READING AT PEAK VALUE
C     MXD: MIDDLE DISPLACEMENT READING AT PEAK VALUE
C     BXD: BOTTOM DISPLACEMENT READING AT PEAK VALUE
C     MXEND: END ROTATION VALUE
C     MYEND: END OF MOMENT AT GROUND LEVEL VALUE
C     MYENDP: END OF PROTOTYPE MOMENT AT GROUND LEVEL VALUE


C     ********************************************************
C              OPENING DATA FILE
C     ********************************************************
```

```
      PRINT *,'ENTER THE NAME OF RESULT FILE WITH PATH'
      READ  '(A)',RESULT
      OPEN(15,FILE=DATAFILE,STATUS='OLD')
      READ(15,'(15A)')TITLE
      READ(15,*)E,N,PJ,MXEND,MYEND

C*************************************************************************
C                 CALCULATION FOR MAXIMUM MOMENT AND ROTATION
C*************************************************************************
      READ(15,*)G
      MYENDP=MYEND*G**3
            MMAX=0.0
            XMAX=0.0
      DO 67 I=1,N
      READ(15,*)REC(I),X(I),Y(I),TX(I),MX(I),BX(I)
 67   CONTINUE

C*************************************************************************
C                 CALCULATION OF PEAK POINT VALUE
C*************************************************************************

      DO 68 J=1,N
      MOM(J)=Y(J)*E/1000
      MOMP(J)=MOM(J)*G**3
      IF (MOMP(J).GT.MMAX)THEN
      MMAX=MOMP(J)
      XMAX=X(J)
      ENDIF
 68   CONTINUE
      READ(15,*)L
      DO 69 M=1,L
      READ(15,*)ND(M),XD(M),YD(M),TXD(M),MXD(M),BXD(M)
 69   CONTINUE
      DO 70 K=1,L
      MOMT(K)=YD(K)*E/1000
      MOMTP(K)=MOMT(K)*G**3
 70   CONTINUE

C     ********************************************************
C           UNIRAS PLOTTING SUBROUTINE
C           SELECT AND CHOOSE OPEN DEVICE
C     ********************************************************


      CALL GROUTE('SELECT HPOSTA4;EXIT')
      CALL GOPEN
      CALL RORIEN(2)
```

```
C     ********************************************************
C                INITIALISED PLOTTING AREA
C     ********************************************************

      CALL GRPSIZ(XS,YS)
      CALL GVPORT(XS*.3,YS*.3,XS*.5,YS*.6)
      CALL GWBOX(XS*.5,YS*.6,0.)
      CALL GLIMIT(0.0,MXEND,0.0,MYENDP,0.0,0.0)
      CALL GSCALE
C     ********************************************************
C                          PLOT AXIS
C     ********************************************************

      CALL RAXLAS(2)
      CALL RAXDIS(5,1,0)
      CALL RAXDIS(6,1,0)
      CALL RTXEXP(1.5)
      CALL RAXTEF(6,'TRIP',0)
      CALL RAXTEX(6,-2,'PILE ROTATION, θ°',UNDEF,UNDEF,3.0)
      CALL RAXLFO(1,0,2,1)
      CALL RAXIS(1,0.0,3.,1)
      CALL RAXTEX(6,-2,'MOMENT AT GROUND LEVEL, M(kN.m)', UNDEF,
     +UNDEF,3.0)
      CALL RAXLFO(4,0,1,1)
      CALL RAXIS(2,0.0,3.,1)
      CALL RTXEXP(1.0)

C     ********************************************************
C                   ENCLOSING THE GRAPH LINE
C     ********************************************************

      CALL GVECT(0.0,MYENDP,0)
      CALL GWICOL(0.01,1)
      CALL GVECT(MXEND,MYENDP,1)
      CALL GVECT(MXEND,0.0,1)

C     ********************************************************
C           DRAW LINE THROUGH EVERY POINT
C     ********************************************************

      CALL GWICOL(0.1,1)
      CALL GDASH(7)
      CALL GVECT(X,MOMP,N)
      CALL GWICOL(0.35,1)
      CALL GDASH(0)
      CALL GVECT(XD,MOMTP,L)
      CALL RTXANG(0.00)
```

```
C     ********************************************************
C           PLOTTING A MAXIMUM LINE
C     ********************************************************

      CALL GVECT(0.0,MMAX,0)
      CALL GDASH(3)
      CALL GVECT(XMAX,MMAX,1)
      CALL GDASH(3)
      CALL GVECT(XMAX,0.0,1)
      CALL RTXFON('DUPL',0)
      CALL RTXHEI(2.5)
      CALL RTXJUS(1,2)
      CALL RTX(1,'X',XMAX,MMAX)

C     ********************************************************
C           PLOTTING THE TEXT FOR MAXIMUM VALUE
C     ********************************************************

      CALL RTXFON('DUPL',0)
      CALL RTXHEI(2.0)
      CALL RTXJUS(0,4)
      CALL RTX(18,'MAXIMUM MOMENT = ', XMAX/20.0,MMAX+MMAX/20.0)
      CALL RTXNC(MMAX,4)
      CALL RTXC(5, 'kN.m')
      CALL RTXANG(270.00)
      CALL RTX(18, 'ROTATION = ', XMAX+XMAX/15,+MMAX-MMAX/5)
      CALL RTXNC(XMAX,2)
      CALL RTXC(7,'DEGREE')
      CALL RTXANG(0.0)

C     ********************************************************
C           REFERENCE TITLE OF THE GRAPH
C     ********************************************************
      CALL GSCAMM
      CALL GWICOL(0.1,1)
      CALL GVECT(0.55*XS,0.9*YS,0)
      CALL GVECT(0.55*XS,0.9*(YS-10.0),1)
      CALL GVECT(0.8*XS,0.9*(YS-10.0),1)
      CALL RTXFON('COMP',0)
      CALL RTXHEI(3.0)
      CALL RTXJUS(0,4)
      CALL RTX(7,'MODEL: ',0.55*(XS+5.0),0.9*(YS-2.0))
      CALL RTXC(8,TITLE)
      CALL GCLOSE
      CLOSE(15)
999   STOP
      END
```

APPENDIX E

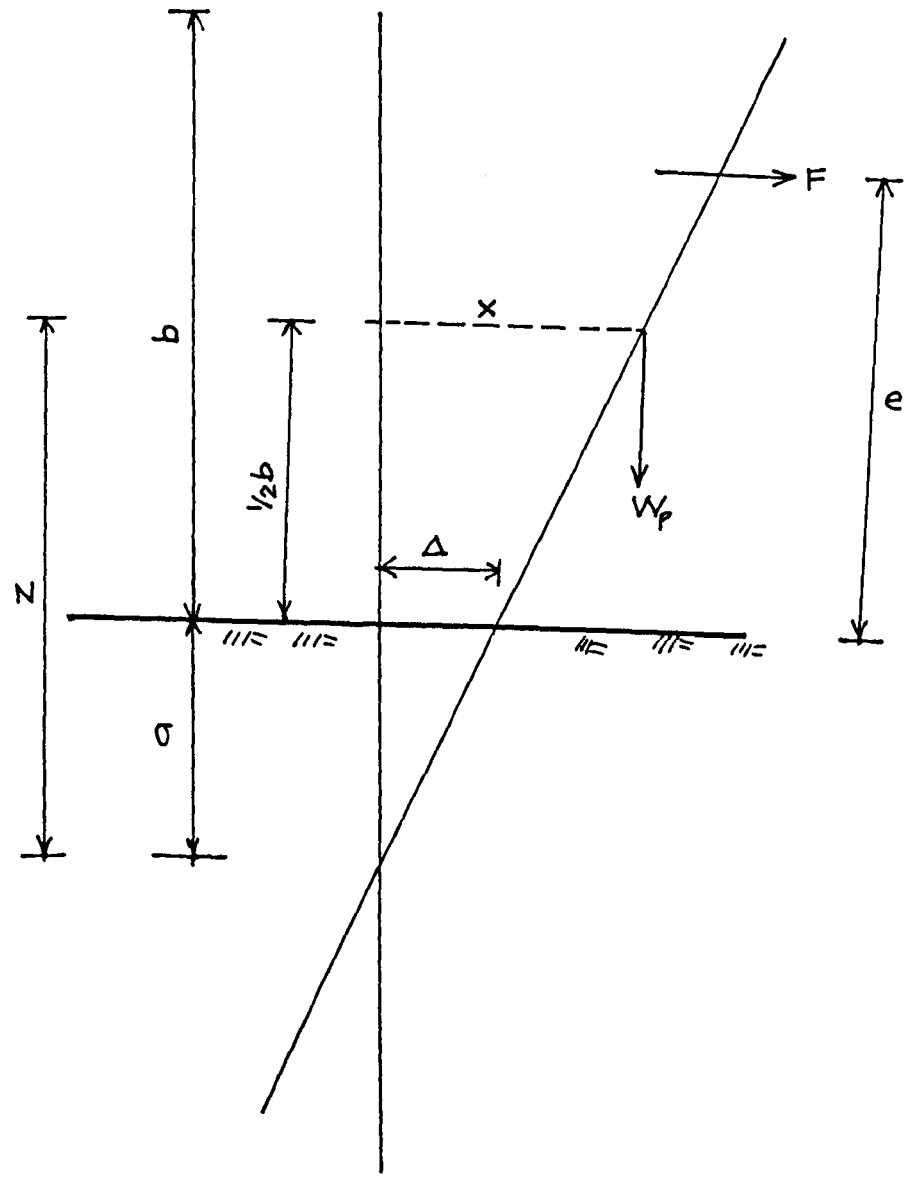

Figure E1 The effect of pulling arm in conventional test for pile with L/D=2.

i) Calculation on the effect of pulling arm in conventional test for pile with e/L=2 and L/D=2. Refering to Figure E1;

Pile length, L=200mm

Pulling height,e=200mm

Pile diameter,D=100mm

F=0.097kN

W_p=0.262kN

Δ=4.68mm

a=113.9mm

b=1700mm

z=963.9mm

Using similar triangle,

4.68/x=113.9/963.9

x=39.61mm

Total moment including the effect of pulling arm weight,

= 0.097(400)/1000 + 0.262(39.61)/1000

= 0.039 + 0.0104

= 0.0494kN.m

% Difference = 0.0104/0.039 x 100

=27%

ii) Calculation on the effect of pulling arm in conventional test for pile with e/L=3 and L/D=2. Refering to Figure E1;

Pile length, L=200mm

Pulling height,e=600mm

Pile diameter,D=100mm

F=0.014kN

W_p=0.262kN

Δ=4.60mm

a=186.58mm

b=1700mm

z=1036.58mm

Using similar triangle,

4.6/x=186.58/1036.58

x=25.56mm

Total moment including the effect of pulling arm weight,

= 0.084(600)/1000 + 0.262(25.56)/1000

= 0.0504 + 0.0067
= 0.0571kN.m

% Difference = 0.0067/0.084 x 100
= 79.9%

iii) Calculation on the effect of pulling arm in conventional test for pile with e/L=4 and L/D=2. Refering to Figure E1;

Pile length, L=200mm

Pulling height,e=800mm

Pile diameter,D=100mm

F=0.066kN

W_p=0.262kN

Δ=4.92mm

a=273.45mm

b=1700mm

z=1123.45mm

Using similar triangle,

4.92/x=273.45/1123.45

x=20.21mm

Total moment including the effect of pulling arm weight,

= 0.066(800)/1000 + 0.262(20.21)/1000

= 0.0528 + 0.0053

= 0.0581kN.m

% Difference = 0.0053/0.053 x 100

= 10%